SYNTHESIS, CHARACTERIZATION, DENSITY FUNCTIONAL THEORY AND BIOLOGICAL EVALUATION OF METAL COMPLEXES OF NEW LIGANDS DERIVED FROM 2-AMINONICOTINALDEHYDE

A THESIS SUBMITTED TO

NATIONAL INSTITUTE OF TECHNOLOGY
WARANGAL

FOR THE DEGREE OF

DOCTOR OF PHILOSOPHY
IN
CHEMISTRY

BY

KONAKANCHI RAMAIAH

(Roll No. 714052)

DEPARTMENT OF CHEMISTRY
NATIONAL INSTITUTE OF TECHNOLOGY WARANGAL
WARANGAL - 506004
TELANGANA, INDIA

JULY 2019

This Dissertation

is Dedicated

to

My Beloved Guide

Prof. K. Laxma Reddy

and

Dr. M. Ramachary

Dr. K. Laxma Reddy
Professor
Department of Chemistry
National Institute of Technology
Warangal - 506 004
Telangana, India

Mobile : +91-9490300457
Email : laxma@nitw.ac.in

CERTIFICATE

This is to certify that the research work presented in this thesis entitled **"Synthesis, Characterization, Density Functional Theory and Biological Evaluation of Metal Complexes of New Ligands Derived from 2-aminonicotinaldehyde"** submitted by **Mr. Konakanchi Ramaiah** for the degree of Doctor of Philosophy in Chemistry, National Institute of Technology, Warangal (Telangana), under my supervision and that the same has not been submitted elsewhere for a degree or diploma.

Date: 17.9.2019
Place:

Prof. K. Laxma Reddy
Thesis Supervisor

ACKNOWLEDGEMENTS

The work presented in this thesis would not have been possible without my close association with many people. I take this opportunity to extend my sincere gratitude and appreciation to all those who made this Ph. D., thesis possible.

It gives me immense pleasure and delight to express my deep sense of gratitude to my research supervisor **Dr. K. Laxma Reddy**, Professor, Department of Chemistry, National Institute of Technology, Warangal for his inspiring and valuable guidance. His unfailing attention, unmitigated encouragement and co-operation have helped me in attaining my goal. It would have been impossible to achieve this goal without his able support and valuable advice. I consider myself fortunate that he has given me a decisive tune, a significant acceleration to my career. I will be thankful to him throughout my lifetime.

I am greatly indebted to **Prof. N. V. Ramana Rao**, Director, National Institute of Technology, Warangal allowing me to submit my research work in the form of a thesis. I express my gratitude to **Prof. T. Srinivasa Rao** and **Prof. G. R. C. Reddy**, former Directors, National Institute of Technology, Warangal for giving me the opportunity to carry out the research work.

My special words of thanks to **Prof. P. V. Srilakshmi,** Head, Department of Chemistry and **Prof. K. V. Gobi, Prof. V. Rajeswar Rao, Prof. B. Rajitha,** former Heads, Department of Chemistry, National Institute of Technology, Warangal for their valuable advice, help and support.

I express my sincere thanks to the Doctoral Scrutiny Committee (DSC) members, **Prof. A. Ramachandraiah, Prof. P. Nageswara Rao,** Department of Chemistry and **Prof. G. V. S. Nageswara Rao**, Department of Metallurgical & Materials Engineering for their valuable suggestions, motivation and care.

I take this opportunity to express thanks to **Prof. B. Venkata Appa Rao**, **Prof. G. V. P. Chandramouli**, **Prof. I. Ajit Kumar Reddy**, **Dr. Vishnu Shanker**, **Dr. Venkatathri Narayanan**, **Dr. D. Kashinath**, **Dr. K. Hari Prasad, Dr. Raghu Chitta, Dr. S. Nagarajan, Dr. M. Raghasudha, Dr. C. Jugun Prakash and Dr. Ravinder Pawar** for their suggestions and encouragement.

Financial assistance from the Government of India, Ministry of Human Resource Development **(MHRD)** in the form of fellowship is gratefully acknowledged.

I thank my research god **Dr. M. Ramachary** for all the chemistry, punctuality, sincerity and humanity I have learned from him. I thank him very much for helping me to grow as a better individual.

I sincerely thank **Dr. K. Shravankumar** and **Dr. J. Prashanth,** Kakatiya University Warangal, for their encouragement and suggestions. I thank all **my Teachers**, right from pre-school to till date for their dedicated efforts in moulding me up to this level.

My heartfelt thanks go to **Dr. J. Haribabu, Mr. K. N. Anees Rahman**, **Mrs. G. Rohini**, National Institute of Technology, Trichy.

My special thanks to **Dr. Y. Narsimha Reddy**, Professor, Department of Pharmacology & Toxicology, Pharmaceutical Sciences, Kakatiya University for evaluating anticancer and antioxidant activity and antimicrobial activity.

I am thankful to **Dr. G. Dhurgaiah** Department of Pharmacology & Toxicology, Pharmaceutical Sciences, Kakatiya University for his interest in the work and kind help getting the compounds assayed for biological activity.

I am sincerely thankful to all my M.Sc. batch mates, seniors and juniors, for their endless love, help, respect and support.

Cheers to my research mates who made my days at the departments memorable, **Mr. M. Saikumar, Mr. T. Sanjeeva, Dr. N. V. Bhart, Mr. V. Sunil Kumar, Dr. B. Thirupaiah, Mrs. N. manjula, Dr. G. Ramesh, Mr. P. Vinay, Dr. M. Venkanna, Mr. T. Dhanunjay Rao, Dr. K. Vimal Kumar, Dr. L. Suresh, Dr. P. Sagar Vijay Kumar, Mr. G. Ambedhkar, Mr. G. Srinath, Mr. G. Sripal Reddy, Mrs. B. Sowmya, Dr. B. Janardhan, N. Satyanarayana, Ms. K. Sujatha, Mr. P. Babji, Mr. Ch. Suman, Mrs. A. Rajini, Mrs. B. Mayuri, Dr. V. Krishnaiah, Dr. V. Ravi Babu, Mr. A. Naveen Reddy, Mr. Ch. Raju, Mr. K. Vijendar reddy, Mr. P. Mahendranath, Dr. B. Rajitha, Dr. M. Satyanarayana, Dr. M. Narsimha Reddy, Dr. P. Sreenu, Dr. K. Koteshwara Reddy, Dr. T. Surender, Dr. T. Ramesh, Dr. G. Srinivasa Rao, Dr. A. Ajay Kumar, Dr. R. Rajkumar, Dr. T. Surendar, Dr. B. Santosh Kumar, Mr. A. Bhargava Sai, Mr. R. Venkatesh, Mr. S. Suresh, Mr. K. Shekar, Mr M. Srikanth, Mr. K. Satish, Mr. J. Parameswara chary, Mrs. Hithavani, Ms. G. Sivaparvathi, Ms. M. Sirisha, Mr. P. Venkatesham, Mrs. B. Sravanthi.**

Above all, I praise my mother **Mrs. K. Dhanamma** and my brother **Mr. K. Kamesh** for providing me the opportunity to carry out the doctoral research and their love and support. I also wish to extend my thankfulness to my family members **Mrs. D. Jyothi, Mr. D. Saidulu, Mrs. K. Sindhura, Mr. B. Nagaraju, Mrs. B. Manjusri, Mr. T. Lingaiah, Mrs. T. Padma, Mr. T. Gopi Kiran, Mrs. T. Navya, Ms. D. Kavya, Mr. D. Srinivas, Mr. T. Karunakar, K. Varshitha, K. Srujana and B. Vishnupriya** for their kindness. Above all I pray and thank my lovable father **Mr. K. Venkateswarlu** for giving me strength for completing my higher studies successfully and dedicate this thesis in his remembrance.

I sincerely appreciate the untiring assistance rendered by my wife **Smt. K. Navya** and son **K. Jishank Varma** for their constant support, cooperation, encouragement, inspiration, love and affection whose blessings made the journey worth effort. I owe everything to them.

Besides these, several people have knowingly or unknowingly helped me for the successful completion of the thesis. I express my apology that I could not mention the names of all of them.

Konakanchi Ramaiah

ABBREVIATIONS

A549	:	Human lung cancer cell line
ALA	:	Alanine
ARG	:	Arginine
ASN	:	Asparagine
ATP	:	Adenosine triphosphate
Calcd.	:	Calculated
$CDCl_3$	:	Deuterated chloroform
CH_3CN	:	Acetonitrile
Conc	:	Concentration
CYS	:	Cysteine
DMF	:	*N*,*N*-Dimethylformamide
DMSO-d_6	:	Deuterated dimethyl sulfoxide
DMSO	:	Dimethyl sulfoxide
DPPH	:	2,2-diphenyl-1-picrylhydrazyl
EtOH	:	Ethanol
FTIR	:	Fourier Transform Infrared Spectroscopy
GLN	:	Glutamine
GLU	:	Glutamate
GLY	:	Glycine
HeLa	:	Human cervical carcinoma cell line
HepG-2	:	Human hepatocellular carcinoma cancer cell line
HEK293	:	Human embryonic kidney 293 cell line
HIS	:	Histidine
HIV	:	Human immunodeficiency virus
IC_{50}	:	Half maximal inhibitory concentration
ILE	:	Isoleucine
LEU	:	Leucine
LYS	:	Lysine
IMR-32	:	Human neuroblastoma cancer cell line
MCF-7	:	Human breast cancer cell line
MeOH	:	Methanol
MET	:	Methionine

MIC	:	Minimum Inhibitory Concentration
mmol	:	milli mole
M.p.	:	Melting point
MTT	:	3-(4,5-dimethylthiazol-2-yl)-2,5-diphenyltetrazolium bromide
ND	:	Not Determined
NMR	:	Nuclear Magnetic Resonance
ORTEP	:	Oak Ridge Thermal Ellipsoid Plot
PDB	:	Protein Data Bank
PHE	:	Phenylalanine
ppm	:	Parts per million
PRO	:	Proline
Raw 264.7	:	Human murine macrophage cancer cell line
SD	:	Standard Deviation
SER	:	Serine
T	:	Temperature
TEA	:	Triethylamine
TGA	:	Thermogravimmetric Analysis
THR	:	Threonine
TMS	:	Tetramethylsilane
UV-Vis	:	Ultra violet-Visible
XRD	:	X-ray Diffraction

NOTATIONS

%	:	Percentage
^{13}C	:	Carbon isotope -13
^{1}H	:	Hydrogen isotope - 1
cm^{-1}	:	Reciprocal centimeter
δ	:	Chemical shift
λ	:	Wavelength
ϑ	:	Frequency
Λ_M	:	Molar conductance
μ_{eff}	:	Effective magnetic moment
°C	:	Degree Celsius
Å	:	Angstrom
bs	:	Broad singlet
cm^{-1}	:	Wave number or per centimeter
d	:	Doublet
dd	:	Doublet of doublet
dt	:	Doublet of triplet
h	:	Hour
Hz	:	Hertz
J	:	Coupling constant
K	:	Kelvin
m	:	Multiplet
max	:	Maximum
mg	:	Milligram
min	:	Minimum
nm	:	Nano meter
q	:	Quartet
s	:	Singlet
t	:	Triplet
µM	:	Micromolar
µg/mL	:	Microgram/milli liter
µL	:	Microliter

CONTENTS

CHAPTER-I

INTRODUCTION

1.1 Introduction to coordination chemistry

The probability of synthesizing a chelating agent showing absolute specificity is, no doubt, remote; however, innovative research has been and is being undertaken towards this end with other functional groups like hydroxyl, acetyl, thiol, etc. several compounds have proved to be potential chelating agents. With ever increasing knowledge of the properties of functional groups and the nature of the donor atoms to the central atom, more selective and more sensitive reagents are required constantly. The involvement of different functional group moieties with the metal ion in different orientations with a specific coordination number in the complexes have occurred. This ensures different electronic probabilities to their biological and DNA binding, docking studies, NLO properties and bacteriostatic, anticancer activities and other physico-chemical properties of these compounds.

Transition metal complexes have been part of the extensive study because of their chemical and physical properties and a wide range of applications in numerous scientific areas [1-3]. The coordination chemistry of transition metals is a complex function which involves numerous variables. Understanding and forecasting the results of the interactions involving transition metal is a prime goal in inorganic chemistry. Metal coordination complex compounds have a vast variety of technological and industrial applications ranging from catalysis and sensors to anticancer drugs. In such compounds, the metal ion has various roles, based on its coordination number, oxidation state, magnetic moment and electronic properties. However, Schiff bases are a dominant class of ligands in coordination chemistry and their complexing ability containing different donor atoms are widely explored [4-6]. The branch of medicinal inorganic chemistry is considered to have evolved with the discovery of anticancer properties of cisplatin. Thus the application of inorganic chemistry to medicine is a rapidly developing field and novel therapeutic and diagnostic of metal complexes are now exercising a positive impact on medicinal practice [7]. With the newly emerging fields of science i.e. genetic engineering, molecular biology, cell biology, nanoscience, biotechnology, magnetic resonance imaging bioinformatics etc., and the recognition of drug receptor theory, drug development programmes have been considerably boosted. The intellectual ability of the chemist plays a pivotal role in the development of new bioactive molecules. The primary task of the chemist is to prepare specific new molecules that can lead more efficiently to useful drug discovery.

Trace quantities of cobalt are essential for living organisms, including humans. Having 0.11 to 0.32 mg per kg of cobalt in soils remarkably enhances the health of grazing animals. Cobalt is a central component of cobalamin vitamin commonly known as vitamin B_{12}. Although cobalt proteins are less common than proteins containing metals like manganese, iron, or zinc, several are known. Most proteins utilize a cofactor based on the corrin cobalt, deduced from vitamin B_{12}, but there are also some proteins in which cobalt is directly coordinated by the protein structure; Methionine aminopeptidase-2 and Nitrile hydrase are two examples [8]. Cobalt compounds are known to have some synergic effect on certain antibiotics notably penicillin and they are electro active species and work as an active pharmaceutical agent in many of the drug molecules. Nickel is used in many industrial and consumer products. It plays numerous roles in the biology of microorganisms and plants [9]. Urease contains nickel as active site and the NiFe-hydrogenases which can characteristically oxidise H_2 are found to have nickel site in addition to iron-sulfur clusters. A nickel-tetrapyrrole coenzyme, F430, is present in the methyl coenzyme M reductase which powers methanogenic archaea. One of the carbon monoxide dehydrogenase enzymes consists of Fe-Ni-S cluster [10]. Other nickel containing enzymes include a class of superoxide dismutase and glyoxalase. Coordination compounds based on nickel ions are also of great interest in the field of catalysis as they are electrochemically active and can exist even in +4 oxidation state. Copper compounds are known in several oxidation states, usually +2, where they often impart blue or green colours to natural minerals such as turquoise and have been used widely as pigments. Copper(II) ion is soluble in water and at low concentration, it exhibits bacteriostatic and fungicidal activity. At lower concentrations, Cu(II) is an essential trace nutrient to all higher plant and animal life. In animals, including humans, it is found widely in tissues, with a concentration in liver, muscle and bone. It functions as a co-factor in various enzymes and in copper-based pigments. A normal human being has copper at a level of about 1.4 to 2.1 mg/kg of body weight. Copper is found in a variety of enzymes, including copper centers of cytochrome c oxidase and the enzyme superoxide dismutase (containing copper and zinc). Redox active copper is used for biological electron transport in addition to its enzymatic roles. Blue copper proteins that participate in electron transport include azurin and plastocyanin. Due to its role in facilitating iron uptake, copper deficiency can very often result in anemia like symptoms. In humans, the symptoms of Wilson's disease are caused by accumulation of copper in body tissues.

Zinc is an essential trace element, necessary for plants [11], animals [12] and microorganism [13]. Zinc is found in nearly 100 specific enzymes, serves as structural ions in transcription factors and is stored and transferred in metallothioneins. It is the second most abundant transition metal in organisms after iron and it is the only metal which appears in all enzyme classes [8]. In proteins, zinc ions are often coordinated to the amino acid side chains of aspartic acid, glutamic acid, cysteine and histidine [14]. In humans, zinc plays ubiquitous biological roles [15].

1.2 General chemistry of metals

1.2.1 Co(II) complexes

The Co(II) ion having an electronic configuration $[Ar]3d^7$ is best known for the formation of complexes with octahedral and tetrahedral geometries [16]. In an octahedral geometry, the ground state can be either $^4T_{1g}$ corresponding to the high spin state $(t_{2g})^5(e_g)^2$ or ^2E_g, corresponding to low spin state $(t_{2g})^6 (e_g)^1$. The complexes with ^2E_g ground term require very high Dq value and only strong field ligands such as cyanides would fulfill this requirement. In tetrahedral geometry, the only possible ground term is $^4A_2$ corresponding to the configuration $(e)^4 (t_2)^3$.

Co(II) forms tetrahedral complexes more readily than any other transitional metal ion, because of the small difference in stability between octahedral and tetrahedral Co(II) complexes. There are many cases where the two geometries with the same ligand are known and may be in equilibrium. Octahedral complexes are usually pale red or purple colour while tetrahedral ones are intense blue in colour.

The electronic spectra of Co(II) in its various geometries are well known and several generalizations can be made from the Orgel and Tanabe-Sugano diagrams. Gaseous Co(II) ion possesses the terms ^4F, ^4P and ^2G and under the influence of a crystal field, the ground term ^4F and the excited term ^4P split into $^4T_{1g}(F)$, $^4T_{2g}(F)$, $^4A_{2g}(F)$ and $^4T_{1g}(P)$, respectively. A schematic diagram of energy level splitting of Co(II) ion in octahedral and tetrahedral fields is given in Fig. 1.1.

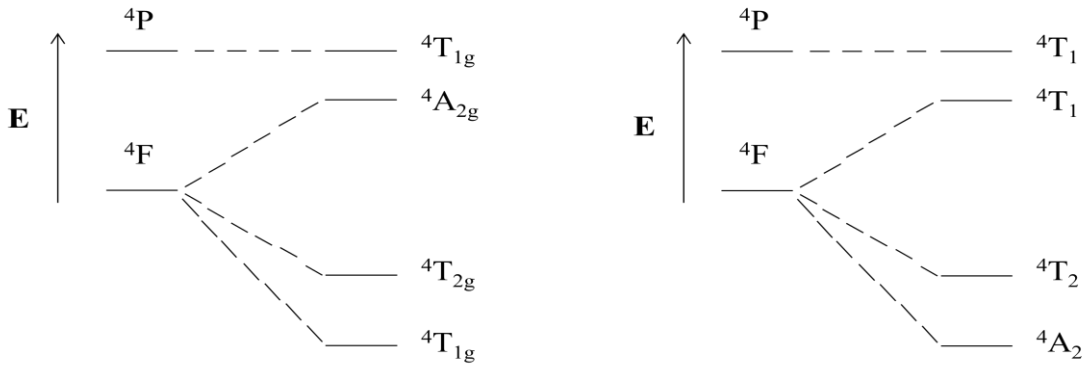

Octahedral complexes **Tetrahedral complexes**

Fig. 1.1 Energy level splitting of Co(II).

Another excited term ^2G located just a little higher than ^4P is also split under the influence of a crystal field, one of the split components being ^2E_g state. As seen from the energy level diagram given by Tanabe and Sugano [17], ^2E_g crosses all the quarter levels on its way down and gives spin-forbidden transitions.

The visible absorption spectrum of octahedral Co(II) complex was explained by Abragam and Pryce [18]. According to them, the spectrum of pink $[Co(H_2O)_6]^{2+}$ shows bands at 8350, 17850 and 20000 cm^{-1} which are assigned to $^4T_{1g}(F) \rightarrow {}^4T_{2g}(F)$, $^4T_{1g}(F) \rightarrow {}^4A_{2g}(F)$ and $^4T_{1g}(F) \rightarrow {}^4T_{1g}(P)$ transitions, respectively. Similar results were reported by Ballhausen and Jorgenson [19] for $[Co(NH_3)_6]^{2+}$ and $[Co(en)_3]^{2+}$ complexes.

Tetrahedral complexes are formed usually with halides, an example being blue $[CoCl_4]^{2-}$. For these complexes the ground term is $^4A_2$ and they also show three bands in the region around 3000-5000, 6000-10000 and 15000-20000 cm^{-1} assignable to $^4A_2(F) \rightarrow {}^4T_2(F)$, $^4A_2(F) \rightarrow {}^4T_1(F)$ and $^4A_2(F) \rightarrow {}^4T_1(P)$, respectively [20]. But in most of the complexes, the first band, the one with lowest energy, has not been observed much.

Square-planar Co(II) complexes are very scarce in literature. A few complexes with this geometry have been reported with bis(salicylal)ethylenediamine, phthalocyanines, porphyrins, etc. [21,22].

1.2.2 Ni(II) complexes

Ni(II) ion with an electronic configuration $[Ar]3d^8$ is well known for the formation of complexes with six coordinate octahedral and four coordinate square-planar

and tetrahedral geometries. Five coordinate complexes of Ni(II) are also known but these are less stable than six and four coordinate complexes.

Octahedral Ni(II) complexes are most common and the ground state of Ni(II) in the coordination is $^3A_{2g}$ corresponding to the configuration $(t_{2g})^6$ $(eg)^2$. These complexes possess Russel-Saunders term ^3F, ^1D, ^3P, ^1G and ^1S in the order of increasing energy. Under the influence of a cubic field the ground term ^3F and excite term ^3P undergoes splitting and transforms into $^3A_{2g}$, $^3T_{2g}$, $^3T_{1g}(F)$ and $^3T_{1g}(P)$. The next excited term ^1G also splits, one of the split components being ^1E_g state which gives spin-forbidden transitions.

The Ni(II) with coordination number six can form complexes of regular or distorted octahedral stereochemistry. In regular octahedral complexes, three spin allowed transitions viz. $^3A_{2g}(F) \rightarrow {}^3T_{2g}(F)$, $^3A_{2g}(F) \rightarrow {}^3T_{1g}(F)$ and $^3A_{2g}(F) \rightarrow {}^3T_{1g}(P)$ are expected and they generally fall within the ranges 7000-13000, 11000-20000 and 19000-27000 cm^{-1}, respectively. In addition, some spin-forbidden transitions are also observed for $[Ni(H_2O)_6]^{2+}$, the three spin allowed transitions in the order given are found at 8500, 13500 and 25300 cm^{-1} and for $[Ni(NH_3)_6]^{2+}$ they are found at 10700, 17500 and 28200 cm^{-1} [23,24]. The energy separation between $^3A_{2g}(F)$ and $^3T_{2g}(F)$ is equal to 10 Dq and the values of 10 Dq in octahedral Ni(II) complexes vary between 6400 and 12700 cm^{-1}, depending on the position of the ligand in the spectrochemical series [25]. In distorted octahedral complexes, more transitions are expected owing to the further splitting of $^3T_{1g}$ and $^3T_{2g}$ states [26,27].

Tetrahedral Ni(II) complexes have the same Russel-Saunders terms as the octahedral ones giving rise to $^3T_1$ ground term. The best example of tetrahedral complexes are Ni(II) halides studied by Furlani and Morpurgo [28], Goodgame et al. [29] and Bostonand Smith et al. [30]. Thus, three bands are observed in the ranges 4000, 7500 and 14000-16000 cm^{-1} which may be assigned respectively to $^3T_1(F) \rightarrow {}^3T_2(F)$ (ϑ_1), $^3T_1(F) \rightarrow {}^3A_2(F)$ (ϑ_2) and $^3T_1(F) \rightarrow {}^3T_{1g}(P)$ (ϑ_3). Also, some spin-forbidden bands are observed [28-30] in the ranges 11000, 11600 and 20000 cm^{-1}, respectively.

The electronic ground state of square-planar Ni(II) complex may be either $(e_g)^4$ $(^1a_{1g})^2$ $(b_{2g})^2$ with a spin-singlet term $^1A_{1g}$ or $(e_g)^4$ $(a_{1g})^2$ $(b_{2g})^1$ $(b_{1g})^1$ with a spin-triplet term $^3A_{2g}$. The relative stability of the $^1A_{1g}$ and $^3A_{2g}$ states is determined by the energy separation (ϑ_1) between d_{xy} and $d_{x^2-y^2}$ orbitals. Ballhausen and Liehr [27] have shown that

low-spin state is more stable, the separation between the two being more than 10000 cm^{-1}. According to Maki [26], the only possible ground state is $^1A_{1g}$ which suggests that all Ni(II) square-planar complexes are diamagnetic. For these complexes, generally one to three bands are observed around 15000, 20000 and 25000 cm^{-1} due to $^1A_{1g}(D) \rightarrow {}^1A_{2g}(G)$, $^1A_{1g}(D) \rightarrow {}^1B_{2g}(G)$ and $^1A_{1g}(D) \rightarrow {}^1E_g(G)$, respectively [26]. Square-planar complexes by the absence of d-d transition below 10000 cm^{-1} in the former as a consequence of large crystal field splitting. Tanabe-Sugano diagram of octahedral Ni(II) complex as shown in Fig. 1.2.

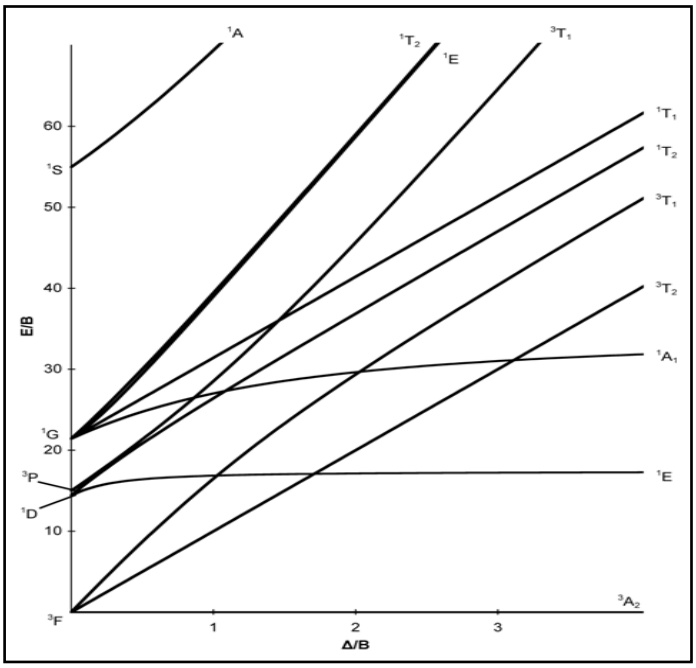

Fig. 1.2 Tanabe-Sugano diagram of octahedral Ni(II) complex.

1.2.3 Cu(II) complexes

The Cu(II) ion having an electronic configuration [Ar]$3d^9$ forms complexes of octahedral, tetrahedral and square-planar geometries with a variety of ligands. It also forms trigonal bipyramidal and square pyramidal complexes, the latter ones being more common [31]. The ground state in octahedral and tetrahedral geometries is orbitally degenerate and since the unsymmetric d^9 configuration is prone to Jahn-Teller distortion, the regular octahedral and the regular tetrahedral complexes of Cu(II) complexes is distorted (elongated) octahedron, involving four short in-plane equatorial bonds and two long axial bonds.

These complexes with octahedral, tetrahedral or square-planar geometry possess only one Russel-Saunders term ^2D and there is no other term in higher energy. This term

splits in octahedral geometry giving ^2E_g ground state and $^2T_{2g}$ excited state and thus only a single transition is expected [32]. But in distorted octahedral or tetragonal complexes ^2E_g will split into two components $^2B_{1g}$, $^2A_{1g}$ and $^2T_{2g}$ into two other components $^2B_{2g}$ and ^2E_g. Therefore, the following three transitions are expected $^2B_{1g} \rightarrow {}^2A_{1g}$, $^2B_{1g} \rightarrow {}^2B_{2g}$ and $^2B_{1g} \rightarrow {}^2E_g$, respectively as shown in Fig. 1.3.

Similar to tetragonal geometry, the ground term in square-planar geometry is $^2B_{1g}$, the excited terms being $^2A_{1g}$, $^2B_{2g}$ and ^2E_g, the three transitions are expected here as well. The d-d bands of square-planar Cu(II) complexes are observed in the range 14000-25000 cm^{-1} [33,34]. However, the electronic spectra provide no much information in distinguishing between planar and tetragonal Cu(II) complexes.

In tetrahedral fields also, the term ^2D will split into two terms giving $^2T_2$ as the ground term and ^2E as the excited term. Crystal field theory predicts again for true tetrahedral complexes only one transition $^2T_2 \rightarrow {}^2E$ which occurs below at 10000 cm^{-1}. In distorted tetrahedral complexes, the ground and excited terms undergo further splitting and as a result, four transitions are expected. However, Sacconi and Ciampolini [35] have reported only three bands at 8500, 13600 and 21000 cm^{-1} in the case of salicylidene aminato Cu(II) complex and assigned them to a pseudo tetrahedral geometry. Octahedral and square-planar Cu(II) complexes have been extensively studied by ESR technique. However, only a few tetrahedral Cu(II) complexes have been subjected to this study. The complete theory for the ESR of Cu(II) complexes have been given by Abraham and Pryce [36] and others [37,38]. Maki and McGarvey [39] and later Kivelson and Neiman derived expressions for the metal-ligand bonding and orbital reduction parameters employing molecular orbital theory.

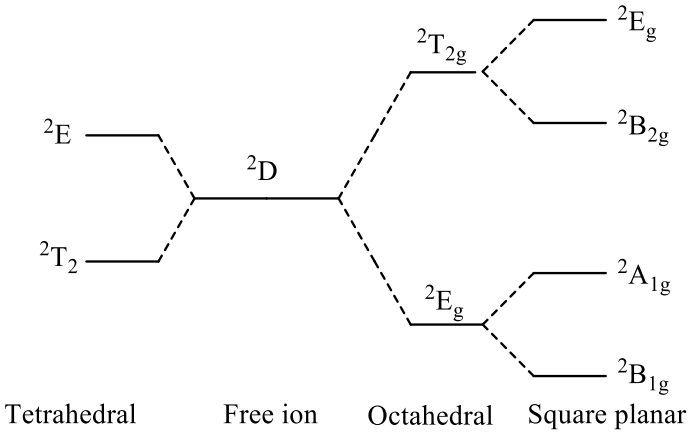

Fig. 1.3 Energy level splitting of Cu(II) complexes.

1.2.4 Zn(II) complexes

Zn(II) ion with the electronic configuration [Ar]$3d^{10}$ forms numerous complexes of tetrahedral e.g. $[Zn(NH_3)_2Cl_2]$, octahedral e.g. $[Zn(Py)_3Cl_2]$ and square pyramidal geometry e.g. aquobis(8-hydroxyquinoline)–Zn(II) stereochemistry and amongst these, the complexes of tetrahedral geometry are predominant. The stereochemical differences of the complexes formed by Zn(II) ion result from the ligand conformation and packing considerations owing to the fact that the ion has a completed d shell (d^{10}) and is, thus, devoid of ligand field stabilization energy effects. Square-planar geometry is less common for Zn(II) complexes; however, a few cases of four coordinate square-planar complexes are known, for example, bis(glycinyl)zinc(II) [40].

Biologically, Zn(II) is one of the most important metal ions and it is an essential constituent of several enzymes e.g. carboxypeptidase. In plants, Zn(II) is a constituent of the enzyme carbonic anhydrase, a catalyst involved in the conversion of carbon dioxide into carbonic acid [41]. Zn(II) also plays an important role in the production of insulin.

1.2.5 Pd(II) complexes

The metal palladium with the electronic configuration [Kr]$4d^8$ forms complexes with various ligands in different oxidation states such as zero, two and four.

Pd(0) generally forms tetrahedral complexes which are diamagnetic. These complexes show a single broad absorption around 25000 cm^{-1}, which may be due to intraligand transition since in a d^{10} system no d-d transition is expected.

Pd(II) mostly forms square-planar complexes which are, as expected, diamagnetic. Pd(II) complexes possessing paramagnetic behaviour are very rare. The electronic ground term for a diamagnetic square-planar Pd(II) complex is $^1A_{1g}$, which is derived from ^1D term symbol. Three peaks are usually observed for Pd(II) square-planar complexes in the visible region around 15000, 20000 and 25000 cm^{-1} which may be assigned to the spin-allowed transitions $^1A_{1g} \rightarrow {}^1A_{2g}$, $^1A_{1g} \rightarrow {}^1B_{1g}$ and $^1A_{1g} \rightarrow {}^1E_g$, respectively [42].

Pd(II) forms octahedral complexes which are also diamagnetic. These show a medium intensity peak at 25000 cm^{-1} due to intraligand transition and a very weak peak due to spin-forbidden $^1A_{1g} \rightarrow {}^1T_{1g}$ transition [43].

1.3 General aspects of the ligand systems used in the present study

The ligand systems used in the present study is the molecule, 2-aminonicotinaldehyde (ANA), a basic unit and the compounds derived from it, so a brief account of the general aspects of these compounds is presented.

1.3.1 2-aminonicotinaldehyde and its derivatives

In recent years, modern coordination chemistry has expanded its horizons to emerging areas of metal organic frameworks [44-47], crystal engineering [48], non-linear optical materials [49-53], therapeutic [54,55], catalytic activity studies [56-58] and other areas of interdisciplinary research. Several classes of ligand architectures have been developed over the ages to suit appropriate applications. One such class of ligands with scarce literature citations are *o*-aminoaldehydes. Historically, *o*-aminoaldehydes have often been employed as important building blocks for several pharmaceutically relevant compounds like naphthyridine derivatives (for Osteoporosis) [59], plant-antitumor agents (Camptothecin-Analogues) [60], antihistamine [61] and pain relieving agents (mGlu5 receptor antagonist) [62], etc., shown in Fig. 1.4.

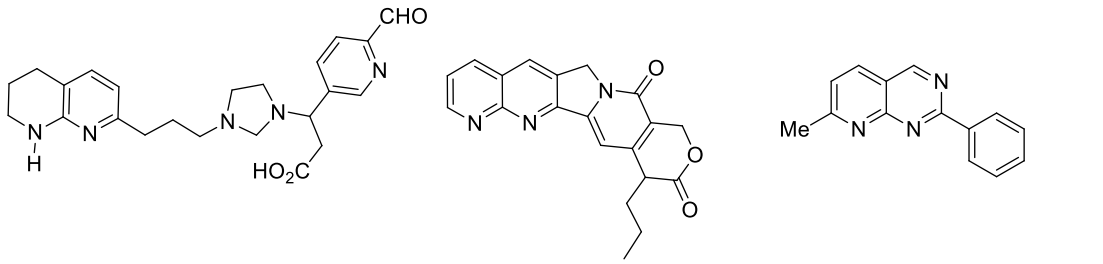

Antagonist | dl-12-Aza-20-deoxycamptothecin | 2-phenyl-6-methylpyrido[2,3-d] pyrimidines

Fig. 1.4 Application of *o*-aminoaldehydes as synthetic building blocks for pharmaceutical applications

2-aminonicotinaldehydes are widely used to prepare other organic compounds in industry and for enabling biological activity in NLO materials and polymers. Similar to *o*-aminobenzaldehyde, 2-aminonicotinaldehyde, though heterocyclic compounds show some aromatic as well as some aliphatic properties, on the whole, the compounds and its derivatives predominantly show aromatic pyridine ring, aldehyde on one hand and amine on the other. An excellent account of these compounds and their applications in different fields are discussed in the literature. These compounds exhibit spectral properties owing to the functional groups present in them. The structural characterization of these

compounds has been established by different analytical techniques so as to select as ligands in the present study.

In the present investigations, we have used 2-aminonicotinaldehyde having aldehyde and amine groups, which condense to form Schiff bases. From a synthetic point of view, ligands like ANA and its Schiff bases have been explored and extensively studied. 2-aminonicotinaldehyde has three coordination sites out of which prominent pyridines ring N atom, N of NH_2 group and O of CHO. Schiff base derivatives are conspicuous in addition to azomethine N atom and other functional group N, O and S donor atoms in the complexes for denticity.

Moreover, the process of coordination/chelation plays a significant role in biological systems [63,64]. Literature studies suggest that the biological activity of many compounds used as drugs is enhanced by chelation with the metal ion [65].

1.4 Use of Schiff bases and their metal complexes

Schiff bases and their metal complexes command significant attention because of their biological activities including antibacterial, antifungal, anti-tumor, nematocide, antiphlogistic antidepressants, anti-carcinogenic and catalytic activity [66,67]. Schiff base metal complexes are also used in different applications such as molecular docking and density functional theory.

1.4.1 Schiff`base metal complexes as catalysts

Schiff`s bases are able to coordinate metals through azomethine nitrogen and there is a wide use of these metal complexes as catalysts. Many Schiff base complexes show excellent catalytic activity in various reactions and in the presence of moisture. Over the past few years, there have been many reports on their applications in homogeneous and heterogeneous catalysis. The high thermal and moisture stabilities of many Schiff base complexes were useful attributes for their application as catalysts in reactions involving high temperatures.

In 1968, Noyori *et al.* [68] developed a Cu(II) Schiff base complex for the metal carbenoid cyclopropanation of styrene, one of the first ligand used for asymmetric catalysis.

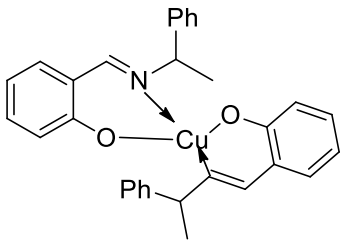

Schiff`s base complexes of metals including Ni(II), Fe(II), Mn(II), Ru(III) Cr(III), etc. have been used as catalysts for epoxidation of olefins and as mono oxygen sources for catalyst to carry out oxygen transfer to the olefins [69,70].

Schiff base transition metal complexes are used as catalyst in several reactions such as oxidation of organic compounds, hydrosilylation of ketones, Henry reaction, aldol reaction, epoxidation of alkenes, reduction of thionyl chloride, reduction reaction of ketones, polymerization reaction, synthesis of bis(indolyl) methanes and Diels-Alder reaction etc.

Mn(II) complex having triazole structure act as a useful catalyst [71] for the Henry reaction and form hydroxy nitroalkanes in good yield. Fe(III), Co(II) and Ru(III) complexes derived from hydroxyl benzaldehyde are used as effective catalysts in oxidation of cyclohexane into cyclohexanol and cyclohexanone in presence of hydrogen peroxide [72].

Fehring *et al.* [73] reported that Schiff base complexes of transition metals were effective catalysts in carrying out asymmetric reduction of dialkyl ketones to alcohols. Catalytic property of dioxomolybdenum(VI) Schiff base complexes for the oxidation of alcohols with H_2O_2 as an oxidant were described by Ngan *et al.*[74].

On observing and making note of the above results, 2-aminonicotinaldehyde containing metal complexes were used as catalyst by using multicomponent reaction.

1.4.2 Multicomponent reaction (MCR)

MCRs are prominent synthetic tools that allow minimum of three components in a one-pot reaction to obtain diverse polyfunctional drug-like scaffolds through the formation of several covalent bonds between carbon-carbon and carbon heteroatoms. In these reactions, most of the starting materials are retained and the isolation of intermediate is not required. The significant advantages of MCRs are high atom economy, efficiency, mild conditions, high convergence or divergence, library generation, the easier progress of the reaction, decreased reaction times, high selectivity, etc. [75-89]. Because

of the variation of substituents, skeleton and stereochemistry, diversity was achieved in MCR approach [90]. Based on the reactivity concept, MCRs can be divided into three different categories. In domino-type MCRs, all reagents have to be present from the very beginning of the process. The subsequent addition of components in a well-defined order without changing the reaction conditions is known as sequential MCR. Finally, the consecutive MCR implements the subsequent addition of reagents by changing the conditions from step to step [91]. The formation of cyanohydrins, imines, first described by Gerhard and Laurent in 1838, can be considered as the first multicomponent reaction. After that, several methods like Strecker synthesis, Hantzsch reaction, Biginelli reaction, Mannich reaction, the Passerini reaction, Ugi reaction etc. were developed [92]. At present using catalyzed MCRs is a common practice to synthesize a variety of heterocycles and heteroatomic organic compounds. In line with these precedents, the use of zinc based catalysts (homogeneous/heterogeneous) and reagents would be a good choice to meet the requirements of green chemistry. We are interested in developing a facile MCR protocol to synthesize pyranopyrazoles or substituted pyridines in view of the imaginative applications in medicinal and materials chemistry.

1.4.3 Theoretical applications

1.4.3.1 Computational chemistry

There are two approaches for designing compounds and understanding their properties in the perspective of applications; a) computational approach and b) experimental approach. Computational science is principally concerned with the numerical calculation of molecular interactions and molecular electronic structures. The term computational chemistry is more often used when a mathematical system is sufficiently well developed for automatic implementation on a computer. Experimental chemistry on the other hand offers analytical expressions for the properties of molecules and their reactions. Two of the important areas of study using computational chemistry are i) Designing new compounds with required properties by molecular modeling, ii) quantum mechanical studies of experimentally synthesized compounds.

Molecular properties such as total energy, charges, surface area volume, reactivity, dipole moment, polarizability, vibrational frequencies or other spectroscopic properties can be predicted. Thus, many experimental chemists are now using computational modeling to gain additional understanding of compounds being examined

in the laboratory. In view of the importance of computational chemistry to generate some of the important properties of novel compounds synthesized in the present investigation.

1.4.3.2 Molecular docking studies

The major application of molecular docking studies is in the design of compounds *in silico* which are targeted against proteins, the binding modes of these compounds (ligands) attaching themselves to active site of a target protein. Thus the compounds which are strongly bound to a protein were treated as lead molecules. In *in vitro* experiments, drugs are discovered by chance in a trial-and-error method by using high-throughput screening of a large number of compounds against a given target. This process is time consuming and highly expensive. On the other hand, if the 3D structure of the compound is known, the molecular docking is a useful tool in the identification of drug candidates by virtual screening of compound databases. The energetically more favourable ligand conformation is suitable for docking. In general, low energy scores represent better protein-ligand bindings [93]. The most commonly used heuristic search algorithms that have been applied to molecular docking are simulated annealing and evolutionary algorithms [94-98].

1.5 Survey of literature on 2-aminonicotinaldehyde and their metal complexes

Metal complexes of Schiff bases have occupied a central role in the development of coordination chemistry. This is manifested by a large number of publications ranging from the purely synthetic to modern physicochemical to biochemically relevant studies of these complexes. A variety of stable compounds containing both transition and non transition metals and multifarious ligands have been synthesized and studied. In many cases, the stereochemistry, electronic structures and properties of these complexes have been reasonably understood.

A detailed literature search on the coordination chemistry of ANA and its Schiff base metal complexes, only a few reports are available. In the following paragraphs are presented survey of literature concerning the synthesis and structural characterization of metal complexes of Schiff bases derived from 2-aminonicotinaldehyde.

Bodige Swamy and Jagannatham Swamy prepared [99] stable metal complexes of Cu(II), Ni(II), Co(II), Zn(II) and Pd(II) with mixed Schiff base ligands derived from 2-aminonicotinaldehyde and benzoic acid hydrazides (Benzoic acid, *p*-toluic acid and *p*-chlorobenzoic). The compounds have been characterized by physicochemical data.

Co(II), Ni(II), Cu(II) and Zn(II) complexes have been assigned for octahedral geometry and square-planar geometry for Pd(II) complexes.

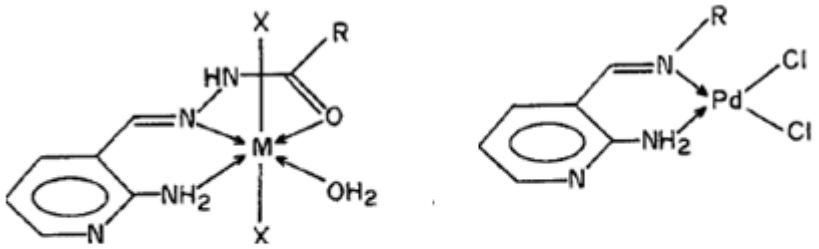

R = Ph or p-MeC_6H_4 or $PClC_6H_4$. X = Cl, Br. M = Co(II), Ni(II), Cu(II) and Zn(II).

Dasharatham *et al.* [100] reported novel compounds of N,N'-bis(2-aminonicotinalidene)-1,2-ethanediamine (**1**), N,N'-bis(2-aminonicotinalidene)-1,2-phenylenediamine (**2**), N,N'-bis(2-aminonicotinalidene)-1,2-phenylenediamine (**3**) and N,N'-bis(2-aminonicotinalidene)-1,3-propanediamine (**4**) and their Co(II) complexes derived from 2-aminonicotinaldehyde. The compounds are characterized by different spectroscopic techniques, and ligand **2** was confirmed by single crystal X-ray data. The ligands act as neutral quadridentate and form square-planar type complexes. All the Cu(II) complexes are stable and non-electrolytes in nature. These complexes also act as potential precursors for the synthesis of macrocyclic compounds.

Khamamkar *et al.* [101] reported the synthesis and characterization of Mn(II), Co(II), Ni(II), Cu(II), Zn(II) and Cd(II) complexes with Schiff base ligand *E*-2-((2-amino pyridine-3-yl) methylene amino)ethane thiol derived from 2-aminonicotinaldehyde and cysteamine. The ligand acts as neutral, bidentate with N and S donor atoms assigned octahedral geometry for Mn(II), Co(II), Cu(II), Zn(II) and Cd(II), Tetrahedral for Ni(II). The antibacterial activity of Co(II) and Ni(II) complexes exhibited potent activity.

Swamy *et al.* [102] carried out the synthesis and characterization of Ni(II), Co(II), Zn(II), Cu(II) and Cd(II) complexes with acetic acid and phenyl acetic acid hydrazones. The compounds were confirmed using different techniques like elemental analysis, electronic, IR, magnetic moment, molar conductance, thermal and ESR spectral studies. The complexes have been assigned for octahedral geometry.

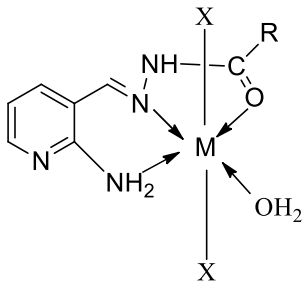

M = Co(II), Ni(II), Cu(II), Zn(II) and Cd(II). X = Cl/Br, R = CH3/ CH_2-C_6H_5.

Jyothi *et al.* [103] described the synthesis and characterization of Co(II), Ni(II), Cu(II) and Zn(II) complexes with Schiff bases obtained by the condensation of 2-aminopyridine-3-carbaldehyde with 1,2-diaminoethane (APMED)/ 1,2-diaminopropane (APMPD)/1,3-diaminopropane (APMP'D)/*trans*-cyclohexane-1,2-diamine. The complexes have been characterized by NMR, IR, Electronic and ESR spectral studies. All the complexes have octahedral geometry holding 0-6 water molecules in the lattice with general molecular formula [$MLCl_2$].n H_2O. These complexes were reported to show excellent non-linear optical properties.

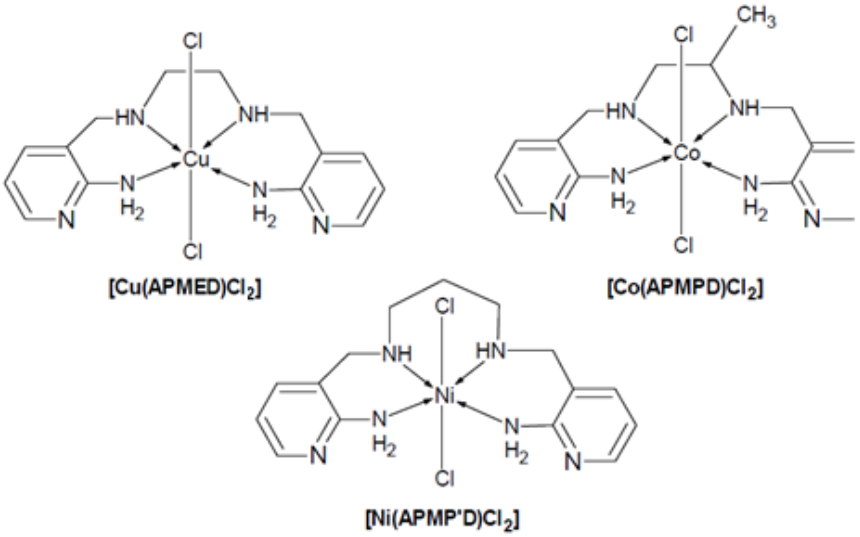

Swamy *et al.* [104] reported that hexadentate ligands derive from 2-aminonicotinaldehyde. The compounds are characterized by elemental analysis and IR spectroscopic techniques.

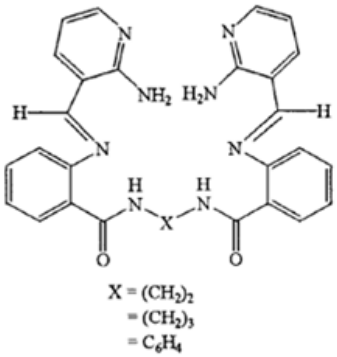

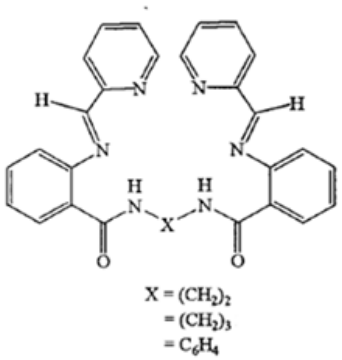

Kalidasan *et al.* [105] have reported new Schiff base complexes [Cp*MCl_2(L)] [where M = Rh, Ir; L1 = 2-amino-3-picoline, L2 = 2-amino-3-nirtopyridine, L3 = 2-amino-3-pyridine carboxyaldehyde and L4 = 2-aminopyridine. The complexes are confirmed by single crystal X-ray diffraction studies.

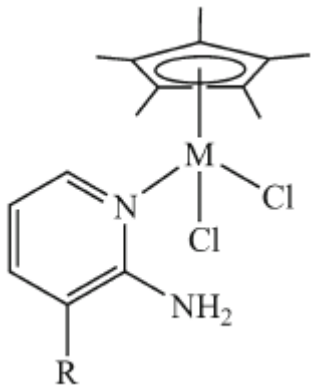

M = Rh (**1**) Ir (**2**)

M = Rh (**3**) Ir (**4**)

M = Rh (**5**) Ir (**6**)

M = Rh (**7**) Ir (**8**)

Majewicz *et al.* [106] described the reaction pyridine analog of 2-aminonicotinaldehyde with cyclic aliphatic diketones (1,3-diketocyclohexane) yields fused polypyridyl ligands which have been extensively used to prepare polymetallic complexes having interesting magnetic properties.

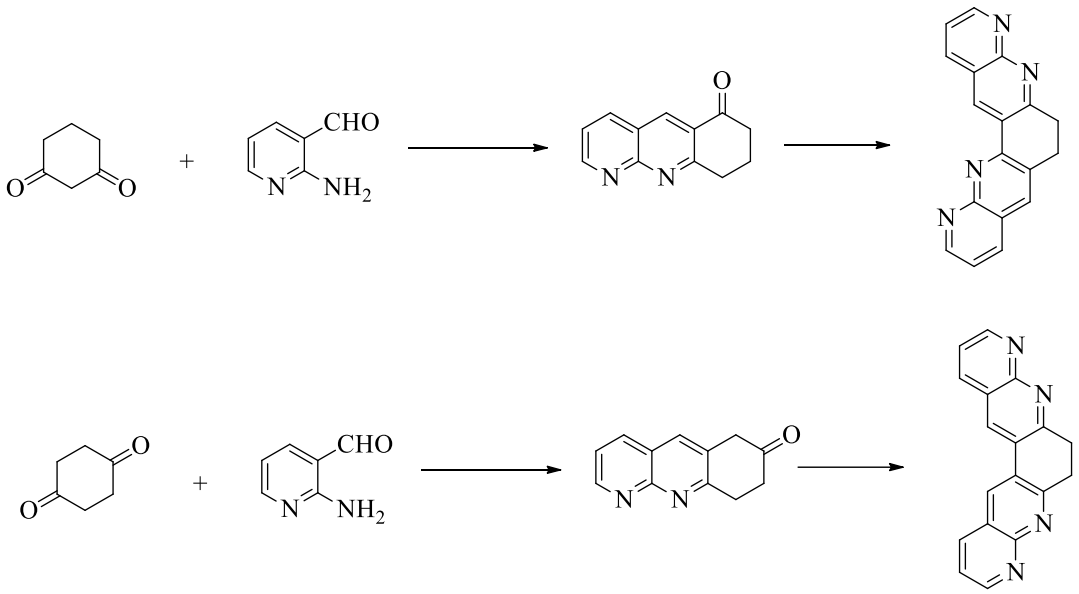

Application of 2-aminonicotinaldehyde for the synthesis of fused polypyridyl ligands

Metal binding affinities of *o*-aminoaldehydes have not been extensively studied. Eichhorn and co-workers have reported Cu(II) complexes of *o*-aminobenzaldehyde. Preliminary spectral characterization revealed a di-copper complex [107].

Equipped with the knowledge of biological and optical importance of ANA, we set out to explore the coordination properties of ANA and ANA containing Schiff base ligands with metals like Co(II), Ni(II), Cu(II), Zn(II), Cd(II) and Pd(II).

1.6 Objectives of the present work

Metal complexes of a wide variety of organic ligands have significantly contributed to the development of modern coordination chemistry. Among the forerunners of organic ligands are heterocyclic compounds and their derivatives, with a particular reference to 2-aminonicotinaldehyde which are generally Schiff bases. These derivatives and their metal complexes have received much attention by researchers mainly because of their synthetic feasibility, bonding variability, structural diversity, catalytic capability and varied bioactivity [108].

2-aminonicotinaldehyde and its Schiff base ligands have acquired a great deal of interest because of their potentially ambidentate nature and pharmacological applications. These ligands bind to a metal ion in a variety of bonding modes along with a monodentate *N*-pyridine ligand in addition to bidentate ligand and these compounds play an important role in biology. Metal complexes of these ligands have exhibited antibacterial, anti-

fungal, anticancer, ROS, antioxidant and anti-inflammatory activities as indicated by recent literature [109-111].

Considering the importance associated with this class of compound, the author has considered it worthwhile to undertake the synthesis, characterization, biological evaluation and theoretic studies of metal complexes by different new 2-aminonicotinaldehyde containing Schiff base ligands. The studies have been also extended by testing the catalytic applications of the metal complexes for the synthesis of fully substituted pyridines and dihydropyrano[2,3-*c*]pyrazoles.

References

[1] S. Niu, M.B. Hall, *Chem. Rev.* **2000**, *100*, 353.

[2] G. Zeng, S. Sakaki, *Inorg. Chem.* **2012**, *51*, 4597.

[3] A.M. Abu-Dief, I.M. Mohamed, *Beni-Seuf. Univ. J. Basic Appl. Sci.* **2015**, *4*, 119.

[4] A. Naik, A. Nevrekar, D.G. Kokare, A. Kotian, V. Komat, V.K. Revankar, *J. Mol. Struct.* **2016**, *1125*, 671.

[5] D.G. Kokare, K. Naik, A. Nevrekar, A. Kotian, V. Komat, V.K. Revankar, *Appl. Organomet. Chem.* **2016**, *30*, 181.

[6] A. Kamath, K. Naik, S.P. Netalkar, D.G. Kokare, V.K. Revankar, *Med. Chem. Res.* **2012**, *22*, 1948.

[7] N.V. Kulkarni, A. Kamath, S. Budagumpi, V.K. Revankar, *J. Mol. Struct.* **2011**, *1006*, 580.

[8] M. Kobayashi, S. Shimizu, *Eur. J. Biochem.* **1992**, *261*, 1.

[9] L. Macomber, R.P. Hausinger, *metallomics* **2013**, *3*, 1153.

[10] P. Amara, J.-M. Mouesca, A. Volbeda, J.C. Frontecilla-Camps, *Inorg. Chem.* **2011**, *50*, 1868.

[11] M.R. Broadley, P.J. White, J.P. Hammond, I. Zelko, A. Lux, *New Phytol.* **2007**, *173*, 677.

[12] A.S. Prasad, *Mol. Med.* **2008**, *14*, 353.

[13] B. Sugarman, L.R. Epps, *J. Med. Microbiol.* **1984**, *18*, 393.

[14] E.G. Brandt, M. Hellgren, T. Brinck, T. Bergman, O. Edholm, *Phys. Chem. Chem. Phys.* **2009**, *11*, 975.

[15] K.M. Hambidge, N.F. Krebs, *Int. J. Nutr.* **2007**, *137*, 1101.

[16] F.A. Cotton, C. Wilkinson, *Advanced Inorganic Chemistry*, 5th Edition, John Wiley & Sons, New York, **1988**.

[17] Y. Tanabe, S. Sugano, *J. Phys. Soc.* **1954**, *9*, 753.

[18] A. Abragam, M.H.L. Pryce, *Proc. R. Soc. Lond. A* **1951**, *206*, 173.

[19] C.J. Ballhausen, C.K. Jorgenson, *Acta. Chem. Scand.* **1955**, *9*, 397.

[20] S.A. AbouEl-Enein, F.A. El-Saied, T.I. Kasher, A.H. El-Wardany, *Spectrochim. Acta A Mol. Biomol. Spectrosc.* **2007**, *67*, 737.

[21] B.N. Figgis, R.S. Nyholm, *J. Chem. Soc.* **1958**, *0*, 338.

[22] P.G. Owston, J.M. Rowe, *J. Chem. Soc.* **1963**, *0*, 3411.

[23] C.K. Jorgenson, *Acta Chem. Scand.* **1962**, *16*, 2017.

[24] C.K. Jorgenson, *Prog. Inorg. Chem.* **1963**, *4*, 73.

[25] R.L. Carlin, *Transit. Met. Chem.* **1968**, *4*, 199.

[26] G. Maki, *J. Chem, Phys.* **1958**, *28*, 651.

[27] C.J. Ballhausen, A.D. Liehr, *J. Am. Chem. Soc.* **1959**, *81*, 538.

[28] C. Furlani, G. Morpurgo, *Z. Phys. Chem.* (Frank Fust) **1961**, *28*, 93.

[29] D.M.L. Goodgame, F.A. Cotton, M. Goodgame, *J. Am. Chem. Soc.* **1961**, *83*, 4161.

[30] G.R. Boston, P. Smith, *J. Am. Chem. Soc.* **1953,** *85*, 1006.

[31] D.P. Graddon, R.H. Schulz, *Aust. J. Chem.* **1965**, *18*, 1731.

[32] C.J. Ballhausen, *Introduction to ligand field theorey*, Mc. Graw-Hill, New York, **1962**, 108.

[33] J.P. Fackler, F.A. Cotton, D.W. Barhum, *Inorg. Chem.* **1963**, *2*, 97.

[34] B.C. Werden, E. Billing, H.B. Gray, *Inorg. Chem.* **1966**, *5*, 78.

[35] L. Sacconi, M. Ciampolini, *J. Chem. Soc.* **1964**, 276.

[36] A. Abragam, M.H.L. Pryce, *Proc. Roy. Soc.* (London) **1951**, *A205*, 135.

[37] B. Bleany, K.D. Bowers, M.H.L. Pryce, *Proc. Roy. Soc.* (London) **1955**, *A228*, 166.

[38] B. Bleany, R.P. Penrose, B.E. Plumpton, *Pryce. Proc. Roy. Soc.* (London) **1949**, *A198*, 406.

[39] A.H. Maki, B.R. McGarvey, *J. Chem. Phys.* **1958**, *29*, 31.

[40] F.A. Cotton, G. Wilkison, *Advanced inorganic chemistry*, 2nd ed. Wiley Eastern Pvt. Ltd. New Delhi, **1966**, 610.

[41] D. Keilen, T. Mann, *Biochem. J.* **1940**, *34*, 1163.

[42] P.D. Harvey, H.B. Gray, *J. Am. Chem. Soc.* **1988**, *110*, 2145.

[43] C. Furlani, M.L. Luciani, *Inorg. Chem.* **1968**, *7*, 1586.

[44] B.F. Abrahams, S.R. Batten, M.J. Grannas, H. Hamit, B.F. Hoskins, R. Robson, *Angew. Chem. Int. Ed.* **1999**, *38*, 1475.

[45] B. Moulton, M.J. Zaworotko, *Chem. Rev.* **2001**, *101*, 1629.

[46] M. Eddaoudi, B. Moler, H. Ji, B. Chen, T.M. Reineke, M. O'Keeffe, O.M. Yaghi, *Acc. Chem. Res.* **2001**, *34*, 319.

[47] H. Li, M. Eddaoudi, M. O' Keeffe, O.M. Yaghi, *Nature* **1999**, *402*, 276.

[48] L. Brammer, *Chem. Soc. Rev.* **2004**, *33*, 476.

[49] P. Metranglo, F. Meyer, T. Pilati, D.M. Proserpio, G.Resnati, *Chem. Eur. J.* **2007**, *13*, 5765.

[50] M.D. Ward, *Coord. Chem. Rev.* **2007**, *251*, 1663.

[51] O.R. Evans, W.B. Lin, *Acc. Chem. Res.* **2002**, *35*, 511.

[52] S. Dibella, *Chem. Soc. Rev.* **2001**, *30*, 355.

[53] B.J. Coe, L.A. Jones, J.A. Harris, B.S. Brunschwig, I. Asselberghs, K. Clays, A. Persoons, J. Garin, J. Orduna, *J. Am. Chem. Soc.* **2004**, *126*, 3880.

[54] N. Shahabadi, S. Kashanian, F. Darabi, *Eur. J. Med. Chem.* **2010**, *45*, 4239.

[55] B. Peng, H. Chao, B. Sun, F. Gao, L.N. Ji, J. Zhang, *Trans. Met. Chem.* **2007**, *32*, 271.

[56] A. Pui, C. Policar, J.P. Mahy, *Inorganica Chim. Acta* **2007**, *360*, 2139.

[57] Division of organic chemistry, Indian Institute of Chemical Technology, Hyderabad, India, *Synthesis* **2008**, *23*, 3787.

[58] C. Lherbet, D. Soupaya, C. Bandoin-Dehoux, C. Andre, C. Blonski, P. Hoffmann, *Tetrahedron Lett.* **2008**, *49*, 5449.

[59] N. Yasuda, Y. Hsiao, M.S. Jensen, N.R. Rivera, C. Yang, K.M. Wells, Y.J. James, M. Palucki, L. Tan, P.G. Dormer, R.P. Volante, D.L. Hughes, P.J. Reider, *J. Org. Chem.* **2004**, 69, 1959.

[60] M.C. Wani, P.E. Ronman, J.T. Lindley, M.E. Wall, *J. Med. Chem.* **1980**, *23*, 554.

[61] M.C. Wani, P.F. Ronman, J.T. Lindley, M.E. Wall, *J. Med. Chem.* **1980**, *23*, 554.

[62] J.A. Wendt, S.D. Deeter, S.E. Bove, C.S. Knauer, R.M. Brooker, C.A. Szafran, R.D. Schwarz, J.J. Kinsorac, K.S. Kilgorec, *Bioorg. Med. Chem. Lett.* **2007**, *17*, 5396.

[63] (a) Z. Baráth, R. Radics, G. Spengler, I. Ocsovszki, M. Kawase, N. Motohashi, Y. Shirataki, A. Shah, J. Molnár, *In Vivo* (Brooklyn), **2006**, *20*, 645; (b) M.P.S. Ishar, G. Singh, S. Singh, K.K. Sreenivasan, G. Singh, *Bioorg. Med. Chem. Lett.* **2006**, *16*, 1366.

[64] (a) A.M.A. Hassan, A.I. Hanafy, M.M. Ali, A.A. Salman, Z.A. El-shafay, Z.H.A. El-wahab, I.A. Salama, *J. Basic. Appl. Chem.* **2012**, *2*, 1; (b) M. Kalanithi, D. Kodimunthiri, M. Rajarajan, P. Tharmaraj, *Spectrochim. Acta A Mol. Biomol. Spectrosc.* **2011**, *82*, 290.

[65] (a) G. Puthilibai, S. Vasudhevan, S. Kutti Rani, G. Rajagopal, *Spectrochim. Acta A Mol. Biomol. Spectrosc.* **2009**, *72*, 796; (b) L.H. Abdel-Rahman, A.M. Abu-Dief, R.M. El-Khatib, S.M. Abdel-Fatah, *J. Photochem. Photobiol. B Biol.* **2016**, *162*, 298; (c) T. Arun, R. Subramanian, N. Raman, *J. Photochem. Photobiol. B Biol.* **2016**, *154*, 67.

[66] S. Ren, R. Wang, K. Komatsu, P. Bonaz-Krause, Y. Zyrianov, C.E. Mckenna, C. Csipke, Z.A. Tokes, E.J. Lien, *J. Med. Chem.*, **2002**, *45*, 410.

[67] S. Kannan, R. Ramesh, Y. Liu, *J. Organomet. Chem*. **2007**, *692*, 3380.

[68] H. Nozaki, H. Takaya, S. Moriuti, R. Noyori, *Tetrahedron* **1968,** *24*, 3655.

[69] P.G. Cozzi, *Chem. Soc. Rev*. **2004,** *33*, 410.

[70] G. In, Y. Kim, J. Choi, *Bull. Korean Chem. Soc.* **2008,** *29*, 969.

[71] G.P. Zhou, Y.H. Hui, N.N. Wan, Q.J. Liu, Z.F. Xie, J.D. Wang, *Chin. Chem. Lett.* **2012,** *23*, 690.

[72] M. Tumer, E. Akgun, S. Toroglu, A. Kayraldiz, L. Donbak, *J. Coord. Chem.* **2008**, *61*, 2935.

[73] V. Fehring, R. Selke, *Angew. Chem. Int. Ed Eng.* **1998**, *37*, 1327.

[74] N.K. Ngan, M.L. Kong, R. Wong, *Polyhedron* **2012,** *33*, 235.

[75] M.R. Nabid, S.J.T Rezaei, R. Ghahremanzadeh, A. Bazgir, *Ultrason. Sonochem.* **2010**, *17*, 159

[76] B.H. Rotstein, S. Zaretsky, V. Rai, A.K. Yudin, *Chem. Rev.* **2014**, *114*, 8323.

[77] A. Dömling, *Chem. Rev.* **2006,** *106*, 17.

[78] W. Chen, X. Peng, L. Zhong, Y. Li, R. Sun, *ACS Sustain. Chem. Eng.* **2015**, *3*, 1366.

[79] C. Liu, M. Shen, B. Lai, A. Taheri, Y. Gu, *ACS Comb. Sci.* **2014**, *16*, 652.

[80] A.N. Muller, I.R. Correa, Jr.H. Prinz, C. Rosenbaum, K. Saxena, H.J. Schwalbe, D. Vestweber, G. Cagna, S. Schunk, O. Schwarz, H. Schiewe, H. Waldmann, *Proc. Natl. Acad. Sci.* **2006,** *103,* 10607.

[81] P. Vincetti, A. Brianza, N. Scalacci, G. Costantino, D. Castagnolo, M. Radi, *Tetrahedron Lett.* **2016,** *57,* 1464.

[82] L. Hai, G. Dou, D. Shi, *J. Comb. Chem.* **2010,** *12,* 633.

[83] A.S. Girli, Y. Deureust, B. Kariuki, D.W. Knight, *Tetrahedron* **2013,** *69,* 69.

[84] J.F.A. Filho, B.C. Lemos, A.S.D. Souza, S. Pinheiro, S.J. Greco, *Tetrahedron* **2017,** *73,* 6977.

[85] T.N. Trinh, A.M. Cluskey, *Tetrahedron Lett.* **2016,** *57,* 3256.

[86] M.S. Reddy, L.R. Chowhan, N.S. Kumar, P. Ramesh, S.B. Mukkamala, *Tetrahedron Lett.* **2018,** *59,* 1366.

[87] Y.H. He, J.F. Cao, R. Li, Y. Xiang, D.C. Yang, Z. Guan, *Tetrahedron* **2015,** *71*, 9299.

[88] M.C. Bellucci, A. Sganappa, M. Sani, A. Volonterio, *Tetrahedron* **2015,** *71,* 7630.

[89] P. Pattnaik, S. Nayak, D.R. Mishra, P. Panda, B.P. Raiguru, N.P. Mishra, S. Mohapatra, N.A. Mallampudi, C.S. Purohit, *Tetrahedron Lett.* **2018,** *59,* 2688.

[90] A.D. Morozova, E.A. Muravyova, V.S. Shishkina, V. Elena, Y.V. Senko, V.A. Chebanova, *J. Heterocyclic Chem.* **2017,** *54,* 932.

[91] L. Levi, T.J.J. Muller, *Chem. Soc. Rev.* **2016,** *45,* 2825.

[92] S. Brauch, S.S.V. Berkela, B. Westermann, *Chem. Soc. Rev.* **2013,** *42,* 4948.

[93] R. Thomsen, M.H. Christensen, *J. Med. Chem.* **2006,** *49,* 3315.

[94] S. Kirkpatrick, C.D. Gelatt, M.P. Vecchi, *Science* **1983**, *220*, 671.

[95] D.S. Goodsell, A.J. Olson, *Proteins* **1990**, *8*, 195.

[96] D.R. Westhead, D.E. Clark, C.W. Murray, *J. Comput. Aided Mol. Des.* **1997**, *11*, 209.

[97] G. Jones, P. Willett, R.C. Glen, A.R. Leach, R. Taylor, *J. Mol. Biol.* **1997**, *267*, 727.

[98] G.M. Morris, D.S. Goodsell, R.S. Halliday, R. Huey, W.E. Hart, R.K. Belew, A.J. Olson, *J. Comput. Chem.* **1998**, *19*, 1639.

[99] B. Swamy, J.R. Swamy, *Transition Met. Chem.* **1991**, *16*, 35.

[100] D. Dasharatham, A. Thirupathaiah, *Int. J. Adv. Pharm. Biol.* Chem. **2012**, *1*, 169.

[101] A. Khamamkar, S. Gajula, V.R. Pallapothula, *Int. J. Pharm. Science. Res.* **2016**, *7*, 3322.

[102] B. Swamy, J.R. Swamy, *Asain J. Chem.* **1991**, *3*, 152.

[103] S. Jyothi, K. Sreedhar, D. Nagaraju, S.J. Swamy, *Can. Chem. Chem.* **2015**, *3*, 368.

[104] S.J. Swamy, K. Suresh, P. Someshwar, D. Nagaraju, *Synth. Commun.* **2004**, *34*, 1847.

[105] M. Kalidasan, S. Forbes, Y. Mozharivskyj, M.R. Kollipara, *J. Chem. Sci.* 2015, *127*, 1135.

[106] T.G. Majewicz, P. Caluwe, *J. Org. Chem.* **1975**, *40*, 3407.

[107] G.L. Eichhorn, R.A. Latif, *J. Am. Chem. Soc.* **1954**, *76*, 5180.

[108] R. Konakanchi, R. Mallela, R. Guda, L.R. Kotha, *Res. Chem. Intermed.* **2018**, *44*, 27.

[109] R. Mallela, R. Konakanchi, R. Guda, N. Munirathinam, D. Gandamalla, N.R. Yellu, L.R. Kotha, *Inorganica Chim. Acta* **2018**, *469*, 66.

[110] R. Konakanchi, J. Haribabu, J. Prashanth, N.V. Bharat, M. Ramachary, D. Gandamalla, R. Karvembu, B.V. Reddy, N.R. Yellu, L.R. Kotha, *Appl. Organomet. Chem.* **2018**, *32*, e4415.

[111] K. Ramaiah, J. Prashanth, J. Haribabu, K.E. Sreekanth, B.V. Reddy, R. Karvembu, K. Laxma Reddy, *J. Mol. Struct.* **2019**, *1175*, 769.

CHAPTER-II

EXPERIMENTAL

2.1 Preparation of the ligands

2.1.1 Synthesis of 2-aminonicotinaldehyde (ANA)

A mixture of nicotinamide (36.5 g) and ammonium sulphamate (52.0 g) was heated in an oil bath at 150 ˚C. After a clear melt was obtained, the temperature was raised slowly to 200 ˚C. The mixture was kept at this temperature for 6 h after which the contents of flask had completely solidified. Water was added and the precipitate obtained was filtered and washed with ether. This was refluxed in 2N HCl for 4 h, made alkaline and extracted with ether. This resulting ether solution was dried over K_2CO_3 and evaporated to give pure 2-aminonicotinaldehyde. It was recrystallized from benzene to give yellow crystals suitable for X-ray diffraction. Yield: 40%. M.p.: 99 ˚C. Anal. Calcd. for $C_6H_6N_2O$ (%): C, 58.95; H, 4.91; N, 22.93. Found: C, 58.80; H, 4.80; N, 22.87. FT-IR (KBr): υ, cm^{-1} 3414 ($\upsilon_{(N-H)}$), 1667 ($\upsilon_{(c=0)}$), 1590 ($\upsilon_{(c=N)\,(Py)}$). ^{1}H NMR (400 MHz, DMSO-*d*$_6$): δ, ppm 9.84 (s, 1H, CHO), 8.24 (d, *J* = 8.0 Hz, 1H, Ar-H), 8.00 (d, *J* = 8.0 Hz, 1H, Ar-H), 7.55 (s, 2H, -NH_2), 6.72-6.75 (m, 1H, Ar-H). ^{13}C NMR (100 MHz, DMSO-*d*$_6$): δ, ppm 194.12 (CHO), 158.70, 155.36, 145.02, 113.44, 112.69 (Aromatic carbons).

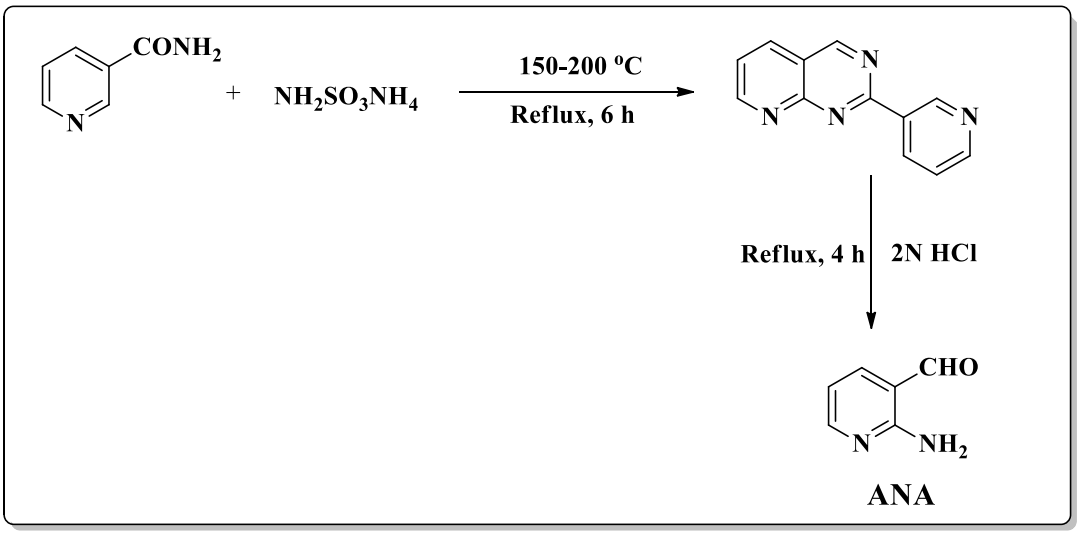

2.1.2 Synthesis of 2-aminonicotinaldehyde *N*-methyl thiosemicarbazone (ANMTSC)

ANMTSC ligand was prepared by refluxing 4-methyl-3-thiosemicarbazide (1.05 g, 10 mmol) with 2-aminonicotinaldehyde (1.22 g, 10 mmol) in 50 mL of methanol for 2 h in the presence of glacial acetic acid (4-5 drops). During this time, yellow coloured compound was obtained, the product was filtered and washed with cold methanol and dried in *vacuum*. The compound was recrystallized in DMF-DCM (1:3) to get pure product. Yield: 90%. M.p.: 245 ˚C. Anal. Calcd. for $C_8H_{11}N_5S$ (%): C, 45.91; H, 5.30; N,

33.47; S, 15.32. Found: C, 45.88; H, 5.28; N, 33.42; S, 15.30. FT-IR (KBr): υ, cm^{-1} 3413, 3315, 3180 (N–H), 1557 (C=N), 1272 (C=S). ^{1}H NMR (400 MHz, DMSO-d_6): δ, ppm 11.23 (s, 1H, NH), 8.38 (q, *J* = 3.6 Hz, 1H, terminal NH), 8.15 (s, 1H, HC=N), 8.00 (d, *J* = 7.3 Hz, 1H, aromatic-H), 7.49 (d, *J* = 7.5 Hz, 1H, aromatic-H), 6.98 (s, 2H, NH_2), 6.66-6.55 (m, 1H, aromatic-H), 3.01 (d, *J* = 3.8 Hz, 3H, terminal CH_3). ^{13}C NMR (100 MHz, DMSO-d_6): δ, ppm 177.5 (C=S), 156.6 (C=N), 149.8, 145.7, 140.8, 112.4, 110.7 (aromatic carbons), 31.6 (methyl carbon).

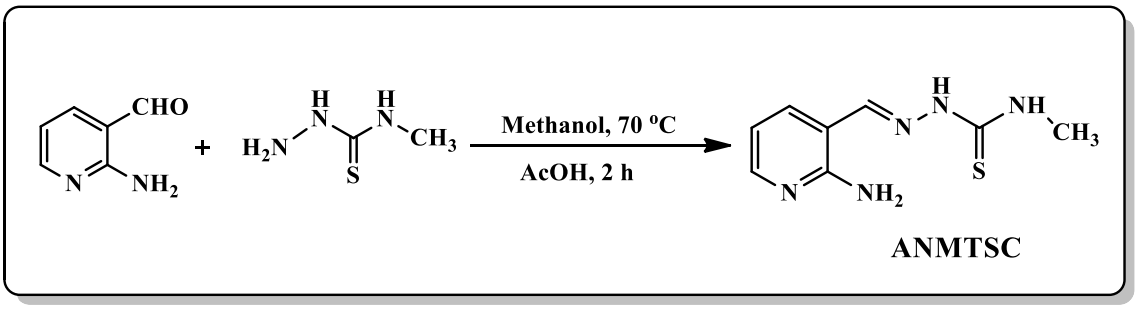

2.1.3 Synthesis of 4-(2-aminopyridin-3-methylene)aminobenzoic acid (ANABZA)

A mixture of 2-aminonicotinaldehyde (1.22 g, 10 mmol) and 4-aminobenzoic acid (1.37 g, 10 mmol) in methanol was stirred for 1 h, to obtain a yellow color precipitate. The product was collected by filtration, washed with methanol and dried in a desiccator over calcium chloride. Yield: 95%. M.p.: 270-272 °C. Anal. Calcd. for $C_{13}H_{11}N_3O_2$ (%): C, 64.72; H, 4.60; N, 17.42. Found: C, 64.65; H, 4.56; N, 17.48. FT-IR (KBr): υ, cm^{-1} 3420 (N–H), 1629 (C=N), 1567 $(C=N)_{py}$, 1701 $(C=O)_{carboxylic\ acid}$. ^{1}H NMR (400 MHz, DMSO-d_6): δ, ppm 12.93 (s, 1H, OH), 8.72 (s, 1H, CH=N), 8.14 (d, *J* = 6.0 Hz, 1H, aromatic-H), 8.00-7.87 (m, 5H, aromatic-H), 7.38 (s, 2H, NH_2), 6.72-6.69 (m, 1H, aromatic-H). ^{13}C NMR (100 MHz, DMSO-d_6): δ, ppm 167.49, 163.88, 158.44, 155.10, 152.18, 143.40, 131.11, 128.37, 121.77, 112.46, 112.34.

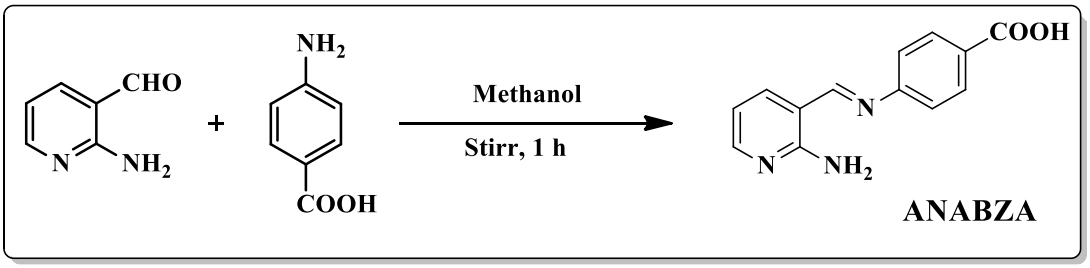

2.1.4 Synthesis of 2-aminonicotinaldehyde benzoxazinonyl acetic acid hydrazone (ABAH)

This compound was prepared in three steps:

(i) (3,4-dihydro-3-oxo-2H-1,4-benzoxazin-2-yl)-acetate

A mixture of 2-aminophenol (5.45 g, 0.05 mol) and maleic anhydride (4.9 g, 0.05 mol) were dissolved in methanol containing 3.25 mL of triethylamine. The contents of the flask were refluxed for 6 h. The solution was removed in *vacuo* and the residual semisolid mass poured into crushed ice while stirring. The compound that separated out was filtered, washed several times with cold water and methanol to give a white compound. Yield: 89%. M.p.: 143-145 °C. Anal. Calcd. for $C_{10}H_8NO_4^-$ (%): C, 58.25; H, 3.91; N, 6.79; O, 31.04. Found: C, 58.02; H, 3.87; N, 6.46; O, 30.94.

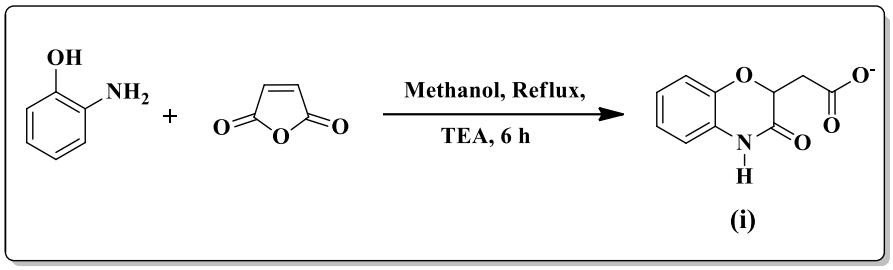

(ii) (3,4-Dihydro-3-oxo-2H-1,4-benzoxazin-2-yl) acetic acid hydrazide

11.05 g (0.05 mol) of compound (**i**) was dissolved in methanol and to this 3.75 mL of hydrazine hydrate was added gradually with stirring. The two solutions were refluxed for 4 h during the course of which 1-2 drops of pyridine was added. The reaction mixture was reduced to half its volume and cooled to get white solid. The product was filtered, washed with water and methanol. Yield: 87%. M.p.: 208-210 °C. Anal. Calcd. for $C_{13}H_{11}N_3O_2$ (%): C, 54.29; H, 5.01; N, 19.00; O, 21.70. Found: C, 54.05; H, 4.90; N, 18.82; O, 21.50.

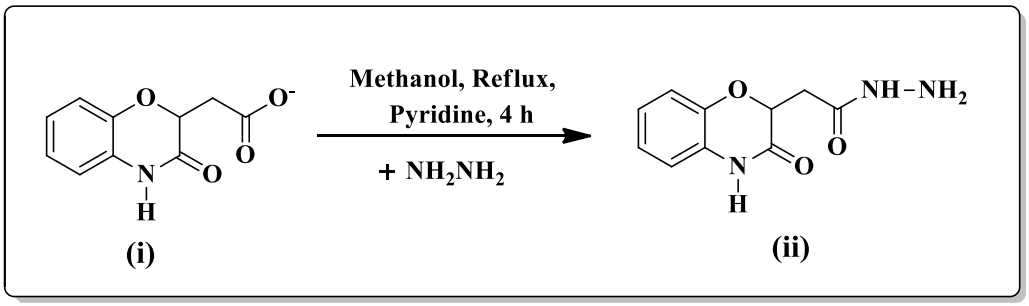

(iii) 2-Aminonicotinaldehyde benzoxazinonyl acetic acid hydrazone (ABAH)

5.52 g (0.025 mol) of compound (**ii**) was taken in a minimum amount of methanol. This was added gradually to another solution containing 3.05 g (0.025 mol) of 2-aminonicotinaldehyde in 10 mL of methanol under stirring in the presence of acetic acid (2 drops). The reaction mixture was refluxed for 3 h when a light yellow compound separated out. This was filtered and washed with methanol to get pure light yellow colored compound. Yield: 87%. M.p.: 257-259 ˚C. Anal. Calcd. for $C_{13}H_{11}N_3O_2$ (%): C, 59.08; H, 4.65; N, 21.53; O, 14.75. Found: C, 59.15; H, 4.62; N, 21.35; O, 14.33. FT-IR (KBr): υ, cm^{-1} 3400 (N–H, free), 3180 (N–H, H-bonded) 1670 (C=O, ring amide), 1610 (C=N), 1570 (C=O, ali.amide). ^{1}H NMR (400 MHz, DMSO): δ ppm 12.13 (s, 1H, cyclic -NH), 11.05 (s, 1H, CO-NH-N), 8.72 (s, 1H, CH=N), 7.39 (s, 2H, NH_2), 6.69-8.10 (M, 7H, aromatic-H), 5.02 (t, 1H, C_2H of benzoxazinone), 2.51 (d, *J* = 6.0 Hz, 2H, -CH_2-CO).

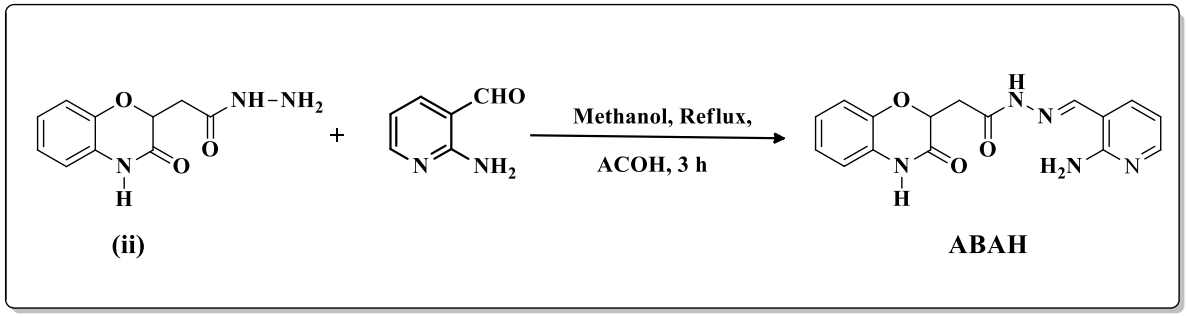

2.2 Preparation of the complexes

In the preparation of all the metal complexes, the metal salt and the ligand were combined in 1:2 mole ratio (the metal being in slight excess of what the ratio required) using required quantities of methanol so as to effect the solubility of the metal salts and the ligands. The general procedure adopted in the preparation of the metal complexes is given metal-wise while other synthetic details are presented in Table 1.

2.2.1 Co(II) complexes

A solution of $Co(OAc)_2{\cdot}4H_2O$/ $CoCl_2.6H_2O$ in methanol was added drop-wise under stirring with methanolic solution of the ligand. The reaction mixture was stirred for few minutes at room temperature followed by refluxing. The resulting colored solid was filtered off, washed with methanol and dried in *vacuum* over fused $CaCl_2$.

2.2.2 Ni(II) complexes

A solution of the ligand in methanol was added slowly with stirring to $Ni(OAc)_2 \cdot 4H_2O$/ $NiCl_2.6H_2O$ in methanol. The mixture was refluxed on a hot water bath. The solid that resulted from refluxing the mixture was filtered and then washed with water, methanol and ether after which it was dried in vacuum over $CaCl_2$.

2.2.3 Cu(II) complexes

The methanolic solution of ligand and methanolic solution containing $Cu(OAc)_2 \cdot H_2O$/ $CuCl_2$ were mixed with constant stirring for a few hours under reflux, and then the precipitate formed was collected by filtration, washed with methanol and dried in a desiccator over calcium chloride.

2.2.4 Zn(II) complexes

$ZnCl_2.4H_2O$ solution in methanol was added slowly under stirring with methanolic solution of the ligand. The solid that separated on refluxing the mixture on a hot water bath was filtered, washed with methanol and ether and dried at *vacuum*.

2.2.4.1 $[Zn(ANA)_2Cl_2]$ complex

^{1}H NMR (400 MHz, DMSO-d_6): δ, ppm 9.89 (s, 2H, -CHO), 8.28 (d, J = 8.0, 2H), 8.00 (d, J = 8.0, 2H), 7.58 (s, 4H, $-NH_2$), 6.73-6.76 (m, 2H). ^{13}C NMR (100 MHz, DMSO-d_6): δ, ppm 194.10, 158.68, 155.31, 145.08, 113.49, 112.69.

2.2.4.2 $[Zn(ANMTSC)_2]$ complex

^{1}H NMR (400 MHz, DMSO-d_6): δ, ppm 8.43 (s, 1H, terminal NH), 8.20 (s, 1H, HC=N), 8.05 (d, J = 7.2 Hz, 1H, aromatic-H), 7.56 (d, J = 6.4 Hz, 1H, aromatic-H), 7.02 (s, 2H, NH_2), 6.67 (s, 1H, aromatic-H), 3.07 (s, 3H, terminal CH_3). ^{13}C NMR (100 MHz, DMSO-d_6): δ, ppm 177.5 (C–S), 156.5 (C=N), 149.8, 145.7, 140.8, 112.4, 110.7 (aromatic carbons), 31.6 (methyl carbon).

2.2.4.3 $[Zn(ANABZA)_2Cl_2]$ complex

^{1}H NMR (400 MHz, DMSO-d_6): δ, ppm 12.07 (s, 1H, OH), 8.74 (s, 1H, CH=N), 8.13-7.91 (m, 6H, aromatic-H), 7.33 (s, 2H, NH_2), 6.72 (s, 1H, aromatic-H). ^{13}C NMR (100 MHz, DMSO-d_6): δ, ppm 166.98, 163.78, 157.30 154.88, 152.08, 142.96, 131.01, 129.01, 121.67, 112.42, 112.31.

2.2.5 Pd(II) complexes

A 0.1 N HCl solution of $PdCl_2$* was treated with an equal volume of methanol added dropwise under stirring with a solution of the ligand in methanol. The mixture was refluxed on a hot water bath. At the end of the reaction excess methanol was removed in vacuum and filtered after cooling to obtain pure product.

[*$PdCl_2$ was dissolved in concentrated hydrochloric acid and diluted with water to 100 mL to give 0.1 N solution with respect to hydrochloric acid].

2.2.5.1 $[Pd(ANA)_2Cl_2]$ complex

^{1}H NMR (400 MHz, DMSO-d_6): δ, ppm 9.86 (s, 2H), 8.25 (d, J = 8.0, 2H), 8.05 (d, J = 8.0, 2H), 7.64 (s, 4H, -NH_2), 6.76-6.79 (m, 2H). ^{13}C NMR (100 MHz, DMSO-d_6): δ, ppm 193.99, 158.15, 154.34, 145.68, 113.91, 112.70.

2.2.5.2 $[Pd(ANMTSC)Cl_2]$ complex

^{1}H NMR (400 MHz, DMSO-d_6): δ, ppm 8.38 (s, 1H, terminal NH), 8.14 (s, 1H, HC=N), 7.99 (d, J = 7.2 Hz, 1H, aromatic-H), 7.51 (d, J = 7.2 Hz, 1H, aromatic-H), 6.97 (s, 2H, NH_2), 6.62 (bs, 1H, aromatic-H), 3.01 (s, 3H, terminal CH_3). ^{13}C NMR (100 MHz, DMSO-d_6): δ, ppm 177.5 (C–S), 156.5, 149.8, 145.6, 140.8, 112.4, 110.8 (aromatic carbons), 31.6 (methyl carbon).

2.2.5.3 $[Pd(ANABZA)Cl_2]$ complex

^{1}H NMR (400 MHz, DMSO-d_6): δ, ppm 12.82 (s, 1H, OH), 8.61 (s, 1H, CH=N), 8.03 (d, J = 6.0 Hz, 1H, aromatic-H), 7.89-7.77 (m, 5H, aromatic-H), 7.28 (s, 2H, NH_2), 6.62-6.59 (m, 1H, aromatic-H). ^{13}C NMR (100 MHz, DMSO-d_6): δ, ppm 167.39, 163.79, 158.44, 155.00, 152.09, 143.30, 131.01, 128.27, 121.68, 112.36, 112.25.

2.2.6 Cd(II) complexes

The solution mixture consisting of $CdCl_2 \cdot H_2O$ and the ligand in methanol was refluxed on hot water bath and cooled when a solid separated. It was filtered, washed with methanol and ether in succession and was dried in vacuum over fused $CaCl_2$.

2.2.6.1 $[Cd(ANA)_2Cl_2]$ complex

^{1}H NMR (400 MHz, DMSO-d_6): δ, ppm 9.85 (s, 2H, -CHO), 8.25 (d, J = 8.0, 2H), 8.01 (d, J = 8.0, 2H), 7.55 (s, 4H, -NH_2), 6.73- 6.76 (m, 2H). ^{13}C NMR (100 MHz, DMSO-d_6): δ, ppm 194.52, 158.70, 155.340, 145.04, 113.47, 112.68.

2.2.6.2 [Cd(ANMTSC)$_2$] complex

^{1}H NMR (400 MHz, DMSO-d_6): δ, ppm 8.19 (s, 1H, terminal NH), 7.93 (d, *J* = 3.6 Hz, 1H, HC=N), 7.75 (d, *J* = 7.6 Hz, 1H, aromatic-H), 7.36 (d, *J* = 6.8 Hz, 1H, aromatic-H), 7.03 (s, 2H, NH_2), 6.57 (t, *J* = 6.4 Hz, 1H, aromatic-H), 3.00 (s, *J* = 3.2 Hz, 3H, terminal CH_3). ^{13}C NMR (100 MHz, DMSO-d_6): δ, ppm 178.0 (C–S), 156.5 (C=N), 148.6, 147.0, 140.2, 112.3, 112.1 (aromatic carbons), 32.8 (methyl carbon).

2.2.6.3 [Cd(ANABZA)Cl$_2$] complex

^{1}H NMR (400 MHz, DMSO-d_6): δ, ppm 12.52 (s, 1H, OH), 8.22 (s, 1H, CH=N), 8.10-7.85 (m, 6H, aromatic-H), 7.85 (s, 2H, NH_2), 6.60 (s, 1H, aromatic-H). ^{13}C NMR (100 MHz, DMSO-d_6): δ, ppm 165.28, 163.11, 155.01 153.63, 150.47, 139.65, 130.01, 127.51, 120.54, 112.83, 110.62.

2.3 Bio assay investigations

2.3.1 *In vitro* antibacterial and antifungal activity

The *in vitro* antimicrobial activity of the ligands and their metal complexes were evaluated against different gram positive bacteria (*Bacillus subtilis* and *Staphylococcus aureus*) and different gram negative bacteria such as (*Proteus vulgaris, Klebsiella pneumoniae*, *Pseudomonas aeruginosa* and *Escherichia coli*) and few fungal strains (*Aspergillus niger*, *Aspergillus flavus*, *Pencillium notatum*, *Curvularia lunata*, *Rhizoctonia bataticola* and *Candida albicans*) by disc diffusion method. By using Whatmann No. 1 paper, 6 mm diameter sterile antibiotic discs were placed over the nutrient agar medium. With the help of micropipette, 100 μg/mL concentrated compounds were transferred to each disc (Initially compounds were dissolved in DMSO). Subsequently bacteria and fungi incubated overnight at 37 ˚C and 25 ˚C, respectively. The zone of inhibition values were calculated in millimeter and distinguished with standard antibiotics. DMSO was used as a negative control whereas Streptomycin 30 μg/disc (standard antibiotic) and standard antifungal drug Ketoconazole/Nystatin (10 μg/disc) were chosen as positive controls. All the experiments were carried out in triplicate and the average zone of inhibition was recorded and minimum inhibitory concentration (MIC) values for the tested compounds as well as standards were measured in μg/mL.

2.3.2 DPPH free radical scavenging activity assay

The free radical scavenging activity of the newly synthesized ligands and their metal complexes were determined using DPPH (1,1-diphenyl-2-picryl hydrazyl) method [1]. According to literature [2], DPPH is a well known radical and a scavenger for other radicals, therefore, DPPH radical was reduced in the presence of antioxidant. In brief 0.2 mM solution of DPPH in 100 mL methanol was prepared. In this 3 mL of methanolic DPPH solution was added to 1 mL of ligands and their metal complexes in DMSO at different concentrations (3 μM, 10 μM, 30 μM, and 100 μM) after which the mixture was shaken vigorously and kept in dark at room temperature. After 30 min the absorbance of the test compounds was measured at 517 nm using UV-Visible spectrophotometer. Methanol was used as blank, ascorbic acid was used as standard while DPPH solution was used as control without the test compounds. The percentage of scavenging activity of DPPH free radical was measured using the following formula.

$$Scavenging\ Activity(\%) = \frac{A_0 - A_1}{A_0}\ X100$$

Here A_0, is the absorbance of DPPH in the absence of an antioxidant and A_1, is the absorbance of DPPH in the presence of an oxidant. In addition, IC_{50} values were calculated for all the compounds.

2.3.3 *In vitro* anticancer activity

The ligands and their metal complexes were evaluated for their *in vitro* anticancer activity against different human cancer cell lines, namely HeLa (cervical), IMR-32 (neuroblastoma), A549 (lung), MCF-7 (breast), COLO-205 (colon), HepG-2 (liver), murine macrophage (Raw 264.7) and HEK293 (embryonic kidney), by comparing them with corresponding activity in the case of the standard drug cisplatin. These cancer cell lines were provided by the National Centre for Cell Sciences (NCCS), Pune, India. Cell viability in the presence of synthesized compounds were measured by MTT (3-(4,5-dimethylthiazol-2-yl)-2,5-diphenyltetrazolium bromide)-microcultured tetrazolium assay [3,4], which is a quantitative colorimetric method for the determination of cell viability. The assessed parameter is the metabolic activity of viable cells. Metabolically active cells reduce pale yellow tetrazolium salt (MTT) to a dark blue formazan, which is insoluble in water. This can be quantified directly, after solubilization with DMSO, as the absorbance of the formazan is related to the number of viable cells. HeLa, IMR-32, A549, MCF-7,

COLO-205, HepG-2 and Raw 264.7 cells were plated into a 96-well plate at a density of 1×10^4 cells/well. Cells were grown overnight in the full medium and then switched to low serum media. 1% DMSO was used as a control. After 48 h of treatment with different concentrations of test compounds, the cells were incubated with MTT (2.5 mg/mL) in the CO_2 chamber for 2 h. The medium was then removed and 100 µL of DMSO was added into each well to dissolve formazan crystals. After thoroughly mixing, the plates were read at 570 nm for optical density, which bears direct correlation with cell quantity. The results were represented as percentage of viability. All the experiments were carried out in triplicate.

2.3.4 *In vivo* anti-inflammatory activity

Male Albino Wister rats of same age of weight around 170-220 g were selected for the present study. They were housed in polypropylene cages. They were acclimatized in the institute animal house with standard diet and water ad libitum after approval by the animal ethical committee. The animal was made to fast 18 h before the start of the experiment.

2.3.4.1 Method

Carrageenan induced rat paw edema method [5] was used to asses anti-inflammatory activity in rats. The animals were divided into three groups (n = 6). Where GP-I as a control, GP-II received a standard, Indomethacin (5 mg/kg) and GP-III was administered test compounds (10 mg/kg) orally. After 30 min, 0.1 mL of 1 % carrageenan suspension in normal saline was injected into the sub plantar region of the left hind paw of each rat to induce edema. The volume measurements were recorded using plethysmograph at intervals of 0, 1, 2, 4, and 6 h. The paw volumes of treated animals were compared with the control group and the % inhibition was calculated using the following equation.

Percentage inhibition (%) = [1− volume in test (mL)/volume in control] × 100.

2.3.5 *In vivo* antidiabetic activity

2.3.5.1 Animals for the investigation

With prior acceptance number from IAEC/32/UCPSc/KU/2015, male Wister rats were bought from Mahaveer agencies, Hyderabad, India and utilized for antidiabetic

studies. In the investigation of antidiabetic study, the male Wister rats weighed around 180-240 g.

2.3.5.2 Induction of diabetes in rats

In order to induce diabetes in rats that were made to fast overnight alloxan monohydrate single intra peritoneal (i.p) injection (150 mg/kg body weight) was given, which was dissolved in saline. It is followed by 0.5 mL of 20% glucose after 3 h of Alloxan and 5% glucose solution ad libitum for next 24 h. After 72 h of alloxan injection, blood samples were taken from retro-orbital plexus of rats and measured for blood glucose levels. Only those rats with blood glucose levels of ≥ 200 mg/dI (diabetic) were chosen for the study.

2.3.6 Reactive oxygen species levels studies

Reactive oxygen species (ROS) play an important role in cancer cell death and apoptosis. In the assay of ROS, 2′,7′-dichlorodihydrofluorescein diacetate (DCFH-DA) which was used as fluorescent probe gets converted to non-fluorescent probe (DCFH) by the action of intracellular esterases [6]. The non-fluorescent substrate gets oxidized by free radicals present in the cells and gives a fluorescent product of DCF. The intensity of DCF formation depends upon the amount of ROS release which indirectly quantifies the intracellular peroxides formation. So ROS measurement (Cat#: STA-342, OxiSelect™) was used to identify ROS levels on a panel of five cell cultures. The test compounds with concentrations of (100 - 3.125 µM) were tested on HeLa, MCF-7, A549 and IMR-32 cancer cell lines for 24 h under good cell culture practice (GCCP). All the cell lines were obtained with job number 1620 from NCCS, Pune, India. All the cell lines were subcultured in serum free medium, Roswell Park Memorial Institute (RPMI) 1640. In brief, 6×10^4 cells per well were transferred into 96 well plates followed by the addition of 100 µL test compounds solution. After this, all the culture plates were incubated in CO_2 incubator (5% CO_2) at 37 °C (MRC.4.11.13, London, UK). The serum-free media of test metal complexes were removed and renewed with 10 µM 2′,7′-dichlorodihydrofluorescein diacetate solution. The cells were washed gently with cold PBS-EDTA 3 times. The emissions were recorded at 488/525 nm excitation and emission wavelength using fluorescence reader (FLx800™, BioTeK Instruments Gen5™ software, USA). For the determination of fluorescence intensity, the following equation was used.

I = Idet – Icom

Here, Idet is the determination of fluorescence intensity and Icom is the fluorescence intensity of the complex.

2.4 Computational details

2.4.1 Density Functional theory

All computations were accomplished by means of Gaussian 09/DFT program package [7]. Beck's three parameter hybrid exchange functional B3 [8] along with Lee-Yang-Parr correlational functional [9], employing the 6-311++G (d,p)/SDD basis set was used for the ligands and their metal complexes analogues. These basic functionals are more accurate and reduce the computational rate and include few relativistic effects in the calculations [10-12].

We calculated the total molecular dipole moment (μ_t) and its components; total molecular Polarizability (α_t) and its components; anisotropy of Polarizability ($\Delta\alpha$); and first order static hyperpolarizability (β_t) using density functional theory based on finite field approach and following Buckingham's definitions [13], in order to understand NLO behaviour of the ligands and their metal complexes.

Molecular electronic properties such as ionization potential (I), electron affinity (A), global hardness (η), chemical potential (μ), global electrophilicity power (ω) of the compounds obtained from frontier molecular orbital energies comprising HOMO (Highest Occupied Molecular Orbital) and LUMO (Lowest Unoccupied Molecular Orbital) using the following expressions [14-17].

$$I = -E_{HOMO};\ A = -E_{LUMO};\ \eta = (-E_{HOMO} + E_{LUMO})/2;\ \mu = (E_{HOMO}+E_{LUMO})/2;\ \text{and}\ \omega = \mu^2/2\,\eta$$

Where, E_{HOMO} and E_{LUMO} are HOMO and LUMO orbital energies, respectively.

To get an idea of various second order interactions between the filled orbitals of one subsystem and vacant orbitals of another subsystem, natural bond orbital (NBO) calculations were made, employing NBO 3.1 program [18], as implemented in the Gaussian 09W program package at the DFT/ B3LYP level using 6-311++G(d,p)/SDD basis set. Such calculations are needed to quantify hyper conjugation (or delocalization). This is achieved by evaluating donor-acceptor interactions using second order perturbation theory analysis of Fock matrix in NBO basis of compounds. The interactions manifest as loss of occupancy from the localized NBO of the idealized Lewis structure into an empty non-Lewis orbital. The stabilization energy associated with the

delocalization is obtained from the equation provided by Reed et al. [18], and Chocholousova et al. [19].

2.4.2 Molecular docking studies

Our aim was to explain the interactive mechanism of ligands and its complexes with the target receptor and to examine the possible binding modes with target EGFR protein receptor and selected molecular docking simulations. EGFR/HER2 plays a major role in cancer and is the main target for cancer inhibitors. Mutations lead to over expression of EGFR/HER2 and it is associated with a number of cancer diseases including squamous-cell carcinoma of the lung (80% of cases), anal cancers [20], glioblastoma (50%) and epithelial tumors of the head and neck (80-100%) [21]. The docking study was carried out on EGFR protein receptor with ligands and metal complexes. Crystallographic structure of EGFR/HER2 (PDB ID: 4hjo/3ppo) was retrieved from RSC protein data bank. EGFR/HER2 protein was cleaned by removing water molecules and ligands present in the UCSF Chimera. The 2D structures of metal complexes were drawn in Chem Draw Ultra 12.0 and 3D structures were fully optimized with small hf/3-21g* [22], basic set by using Gaussian 09.

2.4.3 Molecular docking protocol

To carry out the molecular docking study, AutoDock Tools (ADT) (http://mgltools.scripps.edu) version 1.5.6 and Autodock 4.2 package suite (*http://autodock.scripps.edu/resources/references*) were chosen. In the ADT process, the rigid protein receptor EGFR/HER2 ligands and their complexes were made to interact with each other. Gasteiger charges were added to each atom of protein structure and non-polar hydrogen atoms were merged. For further studies in ADT, PDB structures were converted to PDBQT format while the energy calculations were done using genetic algorithms. Nonpolar hydrogen atoms, Gasteiger partial charges, rotatable bonds and grid box with dimensions 60 × 60 × 60 $Å^3$ created around the EGFR/HER2 protein receptor were assigned with the aid of Autodock tools 1.5.6 and spacing of (Angstrom): 0.3750 Å. The population size and the maximum number of evaluations were 150 and 25,00,000, respectively. Discovery studio 4.1.0 was used to explore the results obtained. The complete process describes the detailed docking studies of EGFR/HER2 inhibitors including binding energies of receptor compound complexes.

Table 2.1 Synthetic details and physical characteristics of the metal complexes

S.No.	Metal salt	Wt. of the metal salt taken (g)	Ligand	Wt. of the ligand taken (g)	Refluxing time (min.)	Colour of the complex
(1)	**(2)**	**(3)**	**(4)**	**(5)**	**(6)**	**(7)**
1	$CoCl_2.6H_2O$	0.238	**ANA**	0.244	180	Brown
2	$NiCl_2.6H_2O$	0.237	″	0.244	180	Reddish brown
3	$CuCl_2$	0.134	″	0.244	120	Brownish-black
4	$ZnCl_2.4H_2O$	0.208	″	0.244	180	Yellow
5	$PdCl_2$	0.177	″	0.244	60	Yellow
6	$CdCl_2 \cdot H_2O$	0.201	″	0.244	120	Pale yellow
7	$Co(OAc)_2 \cdot 4H_2O$	0.249	**ANMTSC**	0.408	240	Brown
8	$Ni(OAc)_2 \cdot 4H_2O$	0.248	″	0.408	180	Reddish brown
9	$Cu(OAc)_2 \cdot H_2O$	0.199	″	0.408	120	Snuff
10	$ZnCl_2.4H_2O$	0.208	″	0.408	60	Light yellow
11	$PdCl_2$	0.177	″	0.408	150	Dark red

(1)	(2)	(3)	(4)	(5)	(6)	(7)
12	$CdCl_2 \cdot H_2O$	0.201	″	0.408	180	Yellow
13	$CoCl_2.6H_2O$	0.238	**ANABZA**	0.482	120	Dark Brown
14	$NiCl_2.6H_2O$	0.237	″	0.482	90	Light green
15	$CuCl_2$	0.134	″	0.482	180	Green
16	$ZnCl_2.4H_2O$	0.208	″	0.482	60	Light yellow
17	$PdCl_2$	0.177	″	0.482	150	Orange
18	$CdCl_2 \cdot H_2O$	0.201	″	0.482	90	Orange red
19	$CoCl_2.6H_2O$	0.238	**ABAH**	0.650	90	Brick red
20	$NiCl_2.6H_2O$	0.237	″	0.650	120	Brown
21	$CuCl_2$	0.134	″	0.650	60	Dark green
22	$ZnCl_2.4H_2O$	0.208	″	0.650	120	Light yellow
23	$PdCl_2$	0.177	″	0.650	120	Brown
24	$CdCl_2 \cdot H_2O$	0.201	″	0.650	150	Greenish yellow

2.5 Description of the Instruments used and the experimental details

The instruments used in the present investigations and the experimental details are presented below

2.5.1 Conductance measurements

The use of conductivity measurements in organic solvents for the characterization of metal complexes has been known for a long time. Several solvents such as acetone, nitromethane, nitrobenzene, methanol, ethanol, acetonitrile, dimethylformamide, dimethylsulphoxide, pyridine, etc. have been tried for the purpose and a solvent with high dielectric constant and low viscosity is usually preferred. The use of a particular solvent for conductivity measurements of a compound is also governed by the solubility of it in that solvent.

The conductance measurements of metal complexes are usually made at a concentration 10^{-3} M. The molar conductance ($\wedge_M$) is obtained by the following equation

$$\text{Molar conductance} = \frac{\text{specific conductance} \times \text{cell constant}}{\text{concentration}} \times 1000$$

Literature survey indicates that dimethylformamide and nitrobenzene are the most extensively used non-aqueous solvents for conductance measurements. Sears and co-workers [23] measured the conductance of a number of 1:1 electrolytes in dimethylformamide at 25 ˚C over a range of concentrations. It is observed that molar conductance values in a particular solvent are different for different electrolyte types and for the same electrolyte type again they are different in different solvents. The expected $\wedge_M$ ranges ($ohm^{-1}.cm^2.mol^{-1}$) for metal complexes of different electrolyte types at 10^{-3} M in some common organic solvents were summarized by Geary [24] and are as follows.

Solvent	Electrolyte type			
	1:1	**1:2**	**1:3**	**1:4**
Nitromethane	75-95	150-180	220-260	290-330
Nitrobenzene	20-30	50-60	70-82	90-100
Acetone	100-140	160-200	270	360
Acetonitrile	120-160	220-300	340-420	500
DMF	65-90	130-170	200-240	300
Methanol	80-115	160-220	290-350	450
Ethanol	35-45	70-90	120	160

A Systronic model-304 cell type CD-10 digital conductivity meter, with a cell calibrated with 0.1 M KCl solution was used.

2.5.2 Magnetic susceptibility measurements

The measurement of magnetic susceptibility constitutes one of the most important methods that enable the chemist to procure information on the structure and bonding in transition metal complexes. Such measurements have indeed contributed much to the characterization of complex compounds with respect to reactivity and the type of metal-ligand bond.

There are two types of magnetism which are of considerable interest in the study of metal complexes: paramagnetism and diamagnetism. Paramagnetism is shown by substances containing one or more unpaired electrons. When a paramagnetic substance is placed in a magnetic field, the atomic or molecular permanent magnets align themselves in the same direction as the applied field and are thus attracted to it. Diamagnetism arises as a result of the interaction of the applied field with closed shell electrons, inducing a magnetic moment which must, therefore, oppose the applied field. The diamagnetic effect is usually several orders of magnitude weaker than the paramagnetic effect and its importance in inorganic systems is primarily a correction term for precise work.

Chemically useful information is obtained by proper interpretation of magnetic moments. The moments are calculated by measuring magnetic susceptibility and these two are related by the following equation:

$$\Psi_m \text{ (corr)} = N\mu 2/3KT$$

Where Ψ_m (corr) = Corrected molar susceptibility

μ = Magnetic moment

N = Avogadro number

K = Boltzman constant

and T = Absolute temperature at which the measurement is made.

On evaluating the constants, the magnetic moment (effective) can be calculated as,

$$\mu_{eff} = 2.84 \sqrt{\Psi m\ (corr)\ .\ T}$$

The magnetic properties of the transition metal complexes can be explained very satisfactorily by ligand field theory. In this theory, the inner orbitals of interest in complex study are partially filled d orbitals. The d orbitals being degenerate in the free ion will be split up in a complex into different energy levels due to the ligand field. The number of unpaired electrons present in the central ion of the complex can be arrived at following an understanding of the nature and extent of splitting along with the possible application of Hund's rule.

The magnetic moment of a transition metal complex is a combination of spin and orbital moments. In many complexes, the ligand field almost completely quenches the orbital contribution and the magnetic moment can be calculated by the following spin-only formula:

$$\mu = \sqrt{\Psi m\ (corr)\ .\ T}$$

Where S is the total spin of the complex, however, in some others, the experimental μ values differ significantly from the simple spin-only values. The deviations are generally due to incomplete quenching of the orbital magnetic moment by the ligand field. In other words, there would be allowances to magnetic moment of a system in terms of orbital motion and spin-orbital coupling.

The magnetic susceptibilities of the complexes were measured using Sherwood scientific auto magnetic susceptibility balance**.** Gouy balance was used to measure the magnetic susceptibilities of the complexes in solid state at room temperature using $Hg[Co(SCN)_4]$ as calibrant. Diamagnetic corrections were calculated from Pascal's constants.

2.5.3 Thermal studies

Thermo gravimetric analysis which involves the measurement of changes in weight as a function of temperature provides information relating to certain physical and chemical phenomena such as vaporization, decomposition, etc. The technique enjoys wide applicability in different branches of chemistry. Studies of inorganic compounds and complexes by this technique are concerned with their stability, decomposition and structure. The data obtained are often useful to determine, along with other things, the stability of compounds at higher temperatures and to investigate further the dependence of thermal stability on the structure of compounds.

The importance of the investigation of thermal stability of complexes has been emphasized by Bowman and Rogers [25]. Several metal complexes with ligands of different types have been studied by this technique [26]. Bottei and Greene [27] employed the decomposition temperatures in the case of metal chelates of chloroanilic acid, rhodizonic acid and tetrahydroxyquinoline as a measure of their thermal stability. Sheshagiri and Rao [28] have worked out the relation between the solution stability and thermal stability in the case of some metal complexes of resacetophenoneoxime and found that both the stabilities might have been much studied [29] for their thermal behaviour.

The thermal stability of complexes has been related to several rezones such as π-electron delocalization, size of the molecule, number and nature of the rings formed, electron density at the reactive centre, etc. [26,29]. Despite good amount of work, considerable difficulty still exists in assigning definite reasons for the increase or decrease in thermal stability of metal complexes with different ligands.

The thermal gravimetric analysis of the metal complexes was performed on NETZSCH STA-2500 Regulus thermo analyzer under nitrogen atmosphere (RT-800 $^{\circ}$C) at the heating rate of 10°C/ min.

2.5.4 Infrared spectra

Infrared spectroscopy is eminently suited for different types of structural investigations because of the ideal wavelength region it covers in the electromagnetic spectrum. This gives considerable information not only to the structural features but also provides finger-prints of molecules. Various groups present in the molecule give rise to characteristic frequencies for the stretching and bending of the bonds. As these

frequencies are altered only slightly by the presence of other groups, they can be used for diagnostic purpose.

Studies on the effect of coordination on the infrared spectra of metal complexes yield valuable information about the bonding present in complexes. Coordination usually results in (a) the appearance of the new bands and splitting of the degenerate modes due to lowering of symmetry and (b) change in the intensity and the frequency of bands. A study of the frequency shifts of ligand with metal together with the presence or absence of certain bands has been made to deduce structural information.

The FT-IR spectra of the ligands and their metal complexes were recorded, in the spectral range of 4000-400cm^{-1}, using Perkin–Elmer 100S spectrophotometer equipped with liquid nitrogen-cooled deuterated triglycine sulphate (DTGS) detector, by diluting the samples in KBr pellet.

2.5.5 Electronic spectra

The study of electron absorption spectra of transition metal complexes has constituted one of the major efforts by both experimentalists and theoreticians to better characterize and understand the nature of the electronic structure and bonding in these compounds [30]. The particular spectrum exhibited by any compound is dependent upon the energy of the d orbitals, their degeneracy and the number of electrons distributed in them; these features, in turn, are controlled by the oxidation state of the metal, the number and the nature of ligands and geometry of the complex.

Four types of electronic transitions may be observed with transition metal complexes:

1. Transition may occur between the split d levels of the central atom, giving rise to d-d or ligand field spectra. The spectral region where these bands occur spans the near infrared, visible and ultraviolet.

2. Transitions may occur from molecular orbitals located primarily on the ligands to non-bonding or anti bonding molecular orbitals located primarily in the central metal atom. Such transitions are called ligand-to-metal charge transfer transitions.

3. metal-to-ligand charge transfer transitions due to electrons being excited from non-bonding or anti bonding orbitals located primarily on the central metal atom to antibonding orbitals located primarily on the ligands.

4. Intra ligand transitions, which involve the transfer of electrons from one ligand orbital to another ligand orbital.

Bands due to charge transfer and intra ligand transitions usually occur in ultraviolet region.

The probabilities or intensities of these transitions are predicted from certain quantum mechanical selection rules called spin selection and Laporte selection rules. The spin selection rule is not completely valid in the presence of spin-orbit coupling. Therefore, spin-forbidden bands do appear in the spectra of many transition metal complexes, but they are generally weaker in magnitude than spin-allowed bands. Similarly, the d-d transitions are forbidden by Laporte selection rules and even if they occur, they do with low intensity. However, there are various factors which are responsible for the breakdown of these selection rules. The most general interpretation of the spectra of transition metal complexes is obtained from the Orgel and Tanabe-Sugano energy level diagrams. Although a detailed analysis of absorption spectra of complexes is difficult and not completely possible, several attempts have been made to relate the absorption spectra to the stereochemistry, magnetic behaviour and stability of the complexes.

The UV-Visible spectra of the ligands and their metal complexes were measured on Perkin-Elmer UV-Visible Lambda-25 double beam spectrophotometer, in the range 200-400 nm, in a solution of DMF using 1cm quartz cell.

2.5.6 ^{1}H NMR and ^{13}C NMR spectra

^{1}H and ^{13}C NMR spectra of the ligands and their complexes were recorded using Bruker Avance HD 400 MHz and 100 MHz NMR instrument, respectively. Solvents used were deuterated dimethylsulfoxide DMSO-d_6 or $CDCl_3$. Tetramethylsilane (TMS) was the internal standard in the measurement of NMR spectra. NMR spectra were recorded at room temperature.

2.5.7 ESR spectra

Electronic spin resonance, a branch of absorption spectroscopy, is the study of interaction between electronic magnetic moments arising from system containing one or more unpaired electrons and an applied magnetic field [31].

ESR studies on Cu(II) complexes are interesting owing to the fact that their ground states are orbitally degenerate in regular geometries and non-degenerate in distorted cases. Since an orbitally degenerate conformation is susceptible to Jahn-Teller distortion, the nature of which is strongly dependant on the way in which the complex tends to be bonded, the study of such confirmation can give insight into the nature of bonds. The majority of Cu(II) complexes give rise to orbitally non-degenerate $d_{x^2-y^2}$ ground state, a substantial number have d_{z^2} ground state and some have d_{xy} ground state.

The Cu(II) ion with a d^9 configuration has an effective spin of S = 1/2 and is associated with spin angular momentum, $m_s = \pm ½$ leading to a doubly degenerate spin state in the absence of a magnetic field. When a magnetic field is applied, the spin degeneracy is resolved. The low energy state has spin magnetic moment aligned with the field and corresponds to the quantum number $m_s = -1/2$ which the high energy state $m_s = +1/2$ has its moment opposed to the field. The energy difference between the two states is given by

$$E = h\vartheta = g\beta H$$

Where, h = Planck's constant

ϑ = Frequency of radiation

g = Lande splitting factor

β = Bohr magneton

H = Field strength.

g is not constant but a tensor quantity. For a free electron, the g value is 2.0023. In metal ions the g value is different from the free electron value. In general, the magnitude of g depends upon the orientation of the unpaired electron containing molecule with respect to the magnetic field. If the paramagnetic species is located in a perfectly cubic crystal site (an octahedral or tetrahedral site), the g value is independent of the orientation of the crystal is said to be isotropic. In a crystal site of lower symmetry, the value depends on the orientation of the crystal and is said to be anisotropic.

Basically, the interpretation of the ESR spectrum of an isolated transition metal ion yields values for two kinds of parameter (1) the spectroscopic splitting factor (g values) which describe the frequencies or energies required to bring about transitions between the different electron spin states and (2) the hyperfine coupling constants which

give a measure of electron spin-nuclear spin interactions. These parameters are affected by the presence of ligands around the central metal ion.

The X-band ESR spectra of the Cu(II) complexes were performed in JOEL X-Band Electron Spin Resonance spectrometer working at room temperature.

2.5.8 Single crystal X-ray diffraction (XRD) measurements

XRD data for the ligands and their metal complexes were collected at 100 K on a Bruker D8 QUEST instrument with an IμS Mo micro source (λ = 0.7107Å) and a PHOTON-100 detector. The data collection was made in the range $2.54^o \leq 2\theta \leq 61.18^o$ (θ is the angle of diffraction), for the index ranges $-8 \leq h \leq 8$; $-10 \leq k \leq 10$; $-17 \leq l \leq 17$. Total number of reflections collected was 13043, with 3259 independent reflections (R_{int} = 0.0231, R_{sigma}= 0.0245). The raw data frames were reduced and corrected for absorption effects using Bruker Apex 3 software suite programs [32]. The structure was solved using intrinsic phasing method [33]. It was further refined with SHELXL [33] program and expanded using Fourier techniques. Anisotropic displacement parameters were included for all non-hydrogen atoms. H atoms bonded to N atoms were located in difference Fourier maps, their positions and isotropic displacement parameters were refined. All H atoms bonded to C atoms were positioned geometrically and treated as riding on their parent C atoms.

2.5.9 Elemental analysis

The analytical data of the ligands and their metal complexes were performed using a Vario EL-III CHNS analyzer.

2.5.10 Melting point

The melting points of the synthesized ligands and their complexes were determined with Stuart SMP 30 melting point apparatus and were uncorrected.

2.5.11 Cancer cell lines and antimicrobial strains

Human breast carcinoma cell line (MCF-7), human colon adenocarcinoma cell line (COLO-205), human alveolar carcinoma cell line (A549), human neuroblastoma cell line (IMR-32) and murine macrophage cell line (Raw 264.7) were obtained. All the cell lines were obtained with job number 1620 from NCCS (National Centre for Cell Science), Pune, India. Cell lines were maintained at 37 °C in a humidified 5% CO_2 incubator (Thermo scientific) using suitable media prescribed in NCCS Protocol. The

gram-positive bacterial strains *Bacillus subtilis* (MTCC 96), *Staphylococcus aureus* (MTCC 121) and *Staphylococcus epidermidis* (MTCC 2639) and gram negative bacterial strains *Klebsiella pneumoniae* (MTCC 109), *Escherichia coli* (MTCC 40), and *Pseudomonas aeruginosa* (MTCC 2453). Standard pathogenic microbial cultures were procured from the Microbial Type Culture Collection and Gene Bank (MTCC), Chandigarh, India, which was recognized by the World Intellectual Property Organization (WIPO).

References

[1] M. Cuendet, K. Hostettmann, O. Potterat, *Helv. Chim. Acta* **1997**, *80*, 1144.

[2] M. Burits, F. Bucar, *Phytother. Res.* **2000**, 14, 323.

[3] P. Shekan, R. Storeng, D. Scudiero, A. Monks, J. Mc Mohan, D. Vistica, J.T. Warren, H. Bokesch, S. Kenncy, M.R. Boyd, *J. Natl. Cancer Inst.* **1990**, *82*, 1107.

[4] A. Monks, D. Scudiero, P. Shekan, R. Shoemaker, K. Pamil, D. Vistica, C. Hose, J. Langley, P.J. Cromise, *J. Natl. Cancer Inst.* **1991**, *83*, 757.

[5] M. Di Rosa, J.P. Giroud, D.A. Willouchby, *J. Pathol.* **1971**, *104*, 15.

[6] C. Fan, J. Chen, Y. Wang, Y. Wong, Y. Zhang, W. Zheng, W. Cao, T. Chen, *Free Radic. Biol. Med.* **2013**, *65*, 305.

[7] M.J. Frisch, G.W. Trucks, H.B. Schlegel, G.E. Scuseria, M.A. Robb, J.R. Cheeseman, G. Scalmani, V. Barone, B. Mennucci, G.A. Petersson, H. Nakatsuji, M. Caricato, X. Li, H.P. Hratchian, A.F. Izmaylov, J. Bloino, G. Zheng, J.L. Sonnenberg, M. Hada, M. Ehara, K. Toyota, R. Fukuda, J. Hasegawa, M. Ishida, T. Nakajima, Y. Honda, O. Kitao, H. Nakai, T. Vreven, J.A. Montgomery, Jr., J.E. Peralta, F. Ogliaro, M. Bearpark, J.J. Heyd, E. Brothers, K.N. Kudin, V.N. Staroverov, R. Kobayashi, J. Normand, K. Raghavachari, A. Rendell, J.C. Burant, S.S. Iyengar, J. Tomasi, M. Cossi, N. Rega, J.M. Millam, M. Klene, J.E. Knox, J.B. Cross, V. Bakken, C. Adamo, J. Jaramillo, R. Gomperts, R.E. Stratmann, O. Yazyev, A.J. Austin, R. Cammi, C. Pomelli, J.W. Ochterski, R.L. Martin, K. Morokuma, V.G. Zakrzewski, G.A. Voth, P. Salvador, J J. Dannenberg, S. Dapprich, A.D. Daniels, Ö. Farkas, J.B. Foresman, J.V. Ortiz, J. Cioslowski, D.J. Fox, *Gaussian 09, Revision B.01,* Gaussian, Inc., Wallingford CT, **2010**.

[8] A.D. Becke, *J. Chem. Phys.* **1993**, *98*, 5648.

[9] C. Lee, W. Yang, R.G. Parr, *Phys. Rev. B* **1988**, *37*, 785.

[10] A. Bergner, M. Dolg, W. Kuechle, H. Stoll, H. Preuss, *Mol. Phys.* **1993**, *80*, 1431.

[11] M. Kaupp, P.V.R. Schleyer, H. Stoll, H. Preuss, *J. Chem. Phys.* **1991**, *94*, 1360.

[12] M. Dolg, H. Stoll, H. Preuss, R.M. Pitzer, *J. Phys. Chem.* **1993**, *97*, 5852.

[13] A.D. Buckingham, *Adv. Chem. Phys.* **1967**, *12*, 107.

[14] G. Gece, *Corros. Sci.* **2008**, 50, 2981.

[15] K. Fukui, *Science* **1982**, *218*, 747.

[16] T.A. Koopmans, *Physica* **1933**, *1*, 104.

[17] R.J. Parr, L.V. Szentpa´ly, S. Liu, *J. Am. Chem. Soc.* **1999**, *121*, 1922.

[18] A.E.L. Read, L.A. Curtiss, F. Weinhold, *Chem. Rev.* **1988**, *88*, 899.

[19] J. Chocholoušová , V. Špirko, P. Hobza, *Phys. Chem. Chem. Phys.* **2004**, *6*, 37.

[20] F. Walker, L. Abramowitz, D. Benabderrahmane, X. Duval, V. Descatoire, D. Hénin, T. Lehy, T.Aparicio, *Hum. Pathol.* **2009**, *40*, 1517.

[21] V. Kumar, A. Abbas, J. Aster. *Robbins basic pathology,* Philadelphia, Elsevier/ Saunders, **2013**, pp. 179.

[22] W.J. Pietro, M.M. Francl, W.J. Hehre, D.J. Defrees, J.A. Pople, J.S. Binkley, *J. Am. Chem. Soc.* **1982**, *104*, 5039.

[23] P.G. Sears, E.D. Wihoit, L.R. Dawson, *J. Chem. Phys.* **1955**, *59*, 373.

[24] W.J. Geary, *Coord. Chem. Rev.* **1971**, *7*, 81.

[25] P.B. Bowman, L.B. Rogers, *J. Inorg. Nucl. Chem.* **1966**, *28*, 2215.

[26] R.S. Bottei, C.P. McEachern, *J. Inorg. Nucl. Chem.* **1970**, *32*, 2653.

[27] R.S. Bottei, D.L. Greene, *J. Inorg. Nucl. Chem.* **1968**, *30*, 1469.

[28] V. Seshagiri, S.B. Rao, *Z. Anal. Chem.* **1972**, *262*, 175.

[29] R. Seshadri Naidu, R. Raghava Naidt, *Indian J. Chem.* **1977**, *15A*, 652.

[30] M. Sutton, *Electronic Spectra of transition Metal Complexes,* Mc Graw-Hill, London, **1968**.

[31] R.S. Drago, *Physical methods in inorganic chemistry,* Affiliated East-West Press Pvt. Ltd, New Delhi, **1968**.

[32] Bruker APEX3, *SAINT and SADABS. Bruker AXS*, Inc., Madison, Wisconsin, USA, **2016**.

[33] G.M. Sheldrick, *Acta Cryst. A* **2015**, *71*, 3.

CHAPTER-III

Co(II), Ni(II), Cu(II), Zn(II), Cd(II) and Pd(II) metal complexes of 2-aminonicotinaldehyde: Synthesis, characterization, density functional theory, biological evaluation and catalytic applications

Pyridine and its derivatives are among the extensively used substructures for food flavorings, medicines, dyes, rubber chemicals, adhesives and agrochemicals [1]. Like pyridine heterocyclic ring, the combinative chemistry tries to produce a group of compounds, which exhibits drug activity [2,3]. Pyridyl aldehydes closely resemble aryl aldehydes largely because a carbonyl group cannot interact mesomerically with the nitrogen atom in the pyridine ring. The exploration of these compounds is of paramount importance as they are extensively employed as intermediates for the pharmaceutical, agro-industry and pharmaceutical ingredient. In recent years, the coordinate chemistry of Schiff bases derived from 2-pyridine-carboxaldehyde has encountered much awareness and since of it possesses both nucleophilicity and electrophilicity [4,5]. Due to a wide range of application in agro-chemistry and pharmacology, many spectroscopists retain the attention on vibrational spectra of substituted pyridines. Pyridine heterocycles are a periodic element in varies large molecules with interesting catalytic, electrochemical and photophysical applications [6-13]. They also perform anesthetic property and hence they are used in the development of drugs for certain brain diseases and for prevention of diabetic neuropathy [14,15].

In view of the aforementioned applications, we selected ANA as the ligand. Theoretically, there are three plausible metal binding sites in ANA. Pyridine N being the most probable electron donor site, others include amine N and aldehyde O. The option of having more than one potential metal binding site makes the investigation of the coordination chemistry of ANA is very challenging. A detailed structural study was done with spectroscopic tools like X-rays, ^{1}H NMR, ^{13}C NMR, FT-IR, UV-Visible, spectral techniques supported by Density Functional Theory (DFT) calculations and molecular docking, along with the evaluation of NLO behaviour to understand metal binding affinity of ANA. In addition, the compounds had been evaluated for *in vitro* antimicrobial, antioxidant, anti-inflammatory and anticancer activities, a comprehensive discussion being featured in the sections that follow.

3.1 Results and discussion

All the complexes are stable at room temperature and are non-hygroscopic. Analytical data showed that metal complexes have 1:2:2 (metal:ANA:chloride) stoichiometry as shown in Table 3.1. The ligand ANA is freely soluble in methanol and ethanol while the complexes are soluble in DMF and DMSO.

Table 3.1 Analytical and molar conductivity data of the ligand and its complexes

Compound	Elemental analyses: Found (Calculated)			
	C	**N**	**H**	**M**
$[Co(ANA)_2Cl_2]$	38.43 (38.49)	14.92 (14.97)	3.17 (3.20)	15.70 (15.75)
$[Ni(ANA)_2Cl_2]$	38.50 (38.52)	14.96 (14.98)	3.20 (3.21)	15.62 (15.69)
$[Cu(ANA)_2Cl_2]$	37.99 (38.02)	14.75 (14.78)	3.12 (3.17)	16.75 (10.77)
$[Zn(ANA)_2Cl_2]$	37.80 (37.85)	14.69 (14.72)	3.15 (3.17)	17.00 (17.18)
$[Cd(ANA)_2Cl_2]$	33.60 (33.69)	12.90 (13.09)	2.58 (2.79)	26.24 (26.30)
$[Pd(ANA)_2Cl_2]$	34.12 (34.15)	13.20 (13.28)	2.80 (2.84)	22.50 (22.54)
ANA	58.80 (58.95)	22.87 (22.93)	48.80 (4.91)	- -

3.1.1 Spectroscopy

The IR spectral and molar conductivity data of ANA and its metal complexes are given in Table 3.2. υ_{N-H} of NH_2 of ANA occurs at 3414 cm^{-1}, the peak at 1667 cm^{-1} is assigned to $\upsilon_{C=O}$ of CHO group and the peak at 1590 cm^{-1} is assigned to stretching frequency of the $\upsilon_{C=N}$ of the pyridine ring. The IR spectra of the complexes are similar to ANA with minor shifts in the position of peaks. In all the spectra of complexes, $\nu_{C=N}$ (py) peak shifted significantly to lower wave number by 30-50 cm^{-1}[16,17] implying that the pyridine nitrogen of ANA is coordinated to metal centre. In the far-IR region, the new peaks observed at 472-421 cm^{-1} and 362-290 cm^{-1} were assigned to υ_{M-N} and υ_{M-Cl}, respectively [18,19]. The molar conductance values of the complexes (10-16 $\Omega^{-1}cm^2mol^{-1}$) are too low to account for any dissociation of the complexes in DMF, indicating that

they are non-electrolytes [20]. This implies that chloride anions associated with these complexes are present inside the coordination sphere.

The electronic absorption studies and magnetic measurements provide quick and reliable information about the geometry of metal complexes. These data can serve as an effective tool to differentiate the geometries of the metal complexes. The electronic spectral bands and magnetic moment values of the metal complexes are listed in Table 3.3. The UV-Visible spectrum of ANA showed two bands at 38461 and 28653 cm^{-1} corresponding to $\pi \rightarrow \pi^*$ and $n \rightarrow \pi^*$ transitions, respectively. The UV-Visible spectrum of Co(II) complex usually showed three bands in the region of 3000-5000, 6000-10000 and 15000-21000 cm^{-1}, which may be assigned to $^4A_2(F) \rightarrow {}^4T_2(F)$, $^4A_2(F) \rightarrow {}^4T_1(F)$ and $^4A_2(F) \rightarrow {}^4T_1(P)$ transitions, respectively. However, in the present case, Co(II) complex showed two bands at 9000 and 20400 cm^{-1} characteristic of tetrahedral geometry [21]. Ni(II) complex was found to be paramagnetic and its absorption spectrum showed two bands at 9500 and 19157 cm^{-1}, which could be assigned to $^3T_1(F) \rightarrow {}^3A_2(F)$ and $^3T_1(F) \rightarrow {}^3T_1(P)$ transitions, respectively are characteristic of tetrahedral geometry [22]. The Cu(II) complex exhibited a band at 24096 cm^{-1} and a shoulder at 12195 cm^{-1}, which may be due to $^2B_{1g} \rightarrow {}^2B_{2g}$ and $^2B_{1g} \rightarrow {}^2E_g$ transitions, respectively which is characteristic of square-planar geometry [23]. Pd(II) complex exhibited two bands at 22540 and 31750 cm^{-1}, which may be assigned to $^1A_{1g} \rightarrow {}^1E_g$ and charge transfer transitions which are characteristic of square-planar geometry [24]. No d-d transitions are expected for Zn(II) and Cd(II) complexes, because of d^{10} electronic configuration. Based on single crystal XRD, IR, UV-Visible and other analytical data, tetrahedral geometry has been proposed [25].

Square-planar Cu(II) complexes showed magnetic moment values in the range of 1.8-2.1 B.M. These values are somewhat greater than the spin-only value of 1.73 B.M. and this is due to the spin-orbit coupling followed by lowering of symmetry [26]. In the present study, magnetic moment value of Cu(II) complex is 2.01 B.M. which supports a square-planar geometry around the metal ion [27]. The magnetic moment of Co(II) complex is 4.71 B.M. which suggests high spin tetrahedral geometry [28]. Ni(II) complex is also paramagnetic and the magnetic moment is found to be 2.91 B.M. in good agreement with tetrahedral geometry [29]. Pd(II), Zn(II) and Cd(II) complexes are diamagnetic in nature and based on this, square- planar and tetrahedral geometry have been proposed [30]. Electron Spin Resonance spectrum of Cu(II) complex was recorded

in solid state at room temperature. The solid state spectrum of Cu(II) complex is shown in Fig. 3.1. The solid state spectrum of Cu(II) complex is anisotropic and showed two peaks, one corresponding to $g_{\parallel}$ and the other to $g_{\perp}$. The observed $g_{\parallel}$ and $g_{\perp}$ values are 2.14, 2.08, respectively. The $g_{\parallel}$ value of the complex is less than 2.3 indicating covalent character of the metal-ligand bond [31]. Further, the, $g_{\parallel} > g_{\perp} > 2.0023$, pointing out that the metal ion contains unpaired electron predominantly lies in $d_{x^2-y^2}$ orbital, with square-planar geometry around Cu(II) ion [32]. The geometric parameter G is calculated using the equation

$$G = \frac{g_{\parallel} - 2.0023}{g_{\perp} - 2.0023}$$

According to Hathaway and Billing [33], if the value of G is greater than 4, it indicates that the exchange interaction between Cu(II) centers in the solid state is negligible. Whereas, its value is less than 4 considerable exchange interactions exist in the solid complex. The value for the exchange interaction parameter G for the present Cu(II) complex is 1.77 which is less than 4 indicating there is a spin exchange interacting between Cu(II) ions in the solid state. The thermograms of complexes were heated from 25-800 °C under nitrogen atmosphere. The Co(II) complex is thermally stable up to 225 °C and above this temperature up to 585 °C, it records a weight loss in a continuous manner that corresponds to two molecules of ANA. The resulting moiety is stable for up to 680 °C above which it shows a weight loss, the final product corresponding to CoO as residue. The Ni(II) complex is stable up to 340 °C above which it loses weight continuously up to 550 °C to give NiO as the final product. In Cu(II) complex, a weight loss has been observed in the range of 180-425 °C that amounts to one molecule of ANA. The residue that results appears to be stable up to 480 °C. Thereafter, the thermogram records another weight loss in the range 480-750 °C that corresponds to the loss of remaining ligand moiety. The horizontal line observed over 750 °C corresponds to CuO. Zn(II) complex decomposed gradually leading to the loss of organic ligands from 230-345 °C, continuously to retain ZnO as residue. In case of Cd(II) complex, decomposition started from 218-360 °C for the loss of organic moieties to retain CdO as residue, whereas in case of Pd(II), the complex shows a horizontal line up to 300 °C and above which it starts losing weight in a continuous manner up to 750 °C, which corresponds to PdO. The ^{1}H NMR spectrum of ligand showed the signals at 9.84 (s, 1H, CHO), 8.24 (d, *J* = 8.0 Hz, 1H), 8.00 (d, *J* = 8.0 Hz, 1H), 7.55 (s, 2H, -NH_2), 6.72-6.75 (m, 1H). ^{13}C NMR spectrum

of ANA exhibits signals from 112.69 to 194.12 ppm. The signal at 194.12 is assigned to aldehyde carbon while the peaks at 155.36 and 112.69 ppm are due to quaternary carbons and the peaks at 113.44, 145.02 and 158.70 ppm are for the remaining carbons. These peaks in the spectra of complexes which appeared with positive coordination induced shifts indicate pyridine N of ANA was involved in bonding with metal ions. The ^{1}H and ^{13}C NMR spectra of ANA and its metal complexes are represented in Fig. 3.2.

Table 3.2 IR (cm^{-1}) and molar conductivity data of the compounds

Compound	ν_{N-H}	$\nu_{C=O}$	$\nu_{C=N(py)}$	ν_{M-N}	ν_{M-Cl}	Molar cond. ($\Omega^{-1}cm^2mol^{-1}$)
Co(II)	3420	1664	1512	451	296	15
Ni(II)	3408	1668	1542	472	362	12
Cu(II)	3413	1660	1542	421	290	10
Zn(II)	3412	1675	1564	472	362	11
Cd(II)	3409	1661	1566	446	303	16
Pd(II)	3417	1666	1550	446	303	13
ANA	3414	1667	1590	------	-----	-----

Table 3.3 Electronic spectral data, ligand field parameters and magnetic data of the complexes

Complexes	Frequencies (cm^{-1})	Assignments	μ_{eff} (B.M.)	Geometry
Co(II)	9000	$^4A_2(F) \rightarrow {}^4T_1(F)$	4.71	Tetrahedral
	20400	$^4A_2(F) \rightarrow {}^4T_1(P)$		
Ni(II)	9500	$^3T_1(F) \rightarrow {}^3A_2(F)$	2.91	Tetrahedral
	19157	$^3T_1(F) \rightarrow {}^3T_1(P)$		

Cu(II)	12195 24096	$^2B_{1g} \rightarrow {}^2E_g$ $^2B_{1g} \rightarrow {}^2B_{2g}$	2.01	Square-planar
Zn(II)	-	-	Diamagnetic	Tetrahedral
Cd(II)	-	-	Diamagnetic	Tetrahedral
Pd(II)	22540 31750	$^1A_{1g} \rightarrow {}^1E_g$ Charge transfer	Diamagnetic	Square-planar

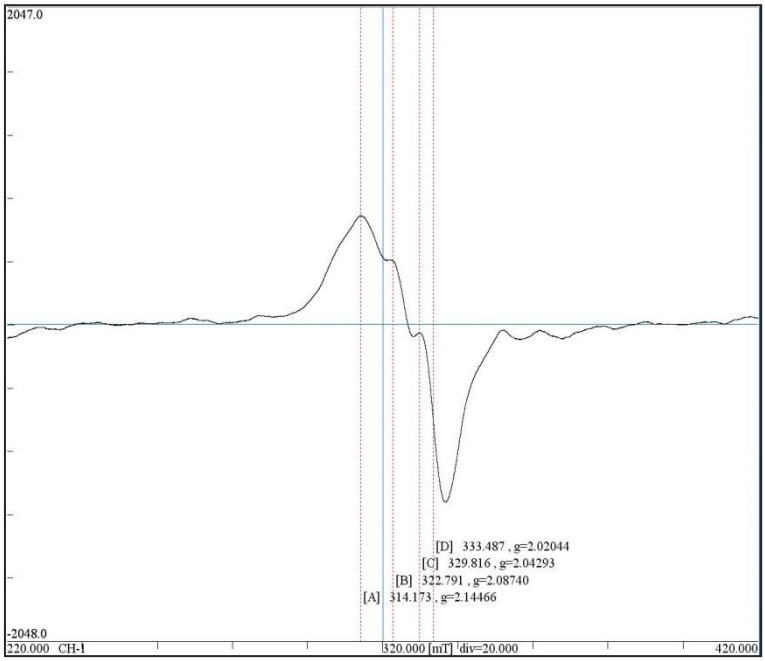

Fig. 3.1. ESR spectrum of Cu(II) complex.

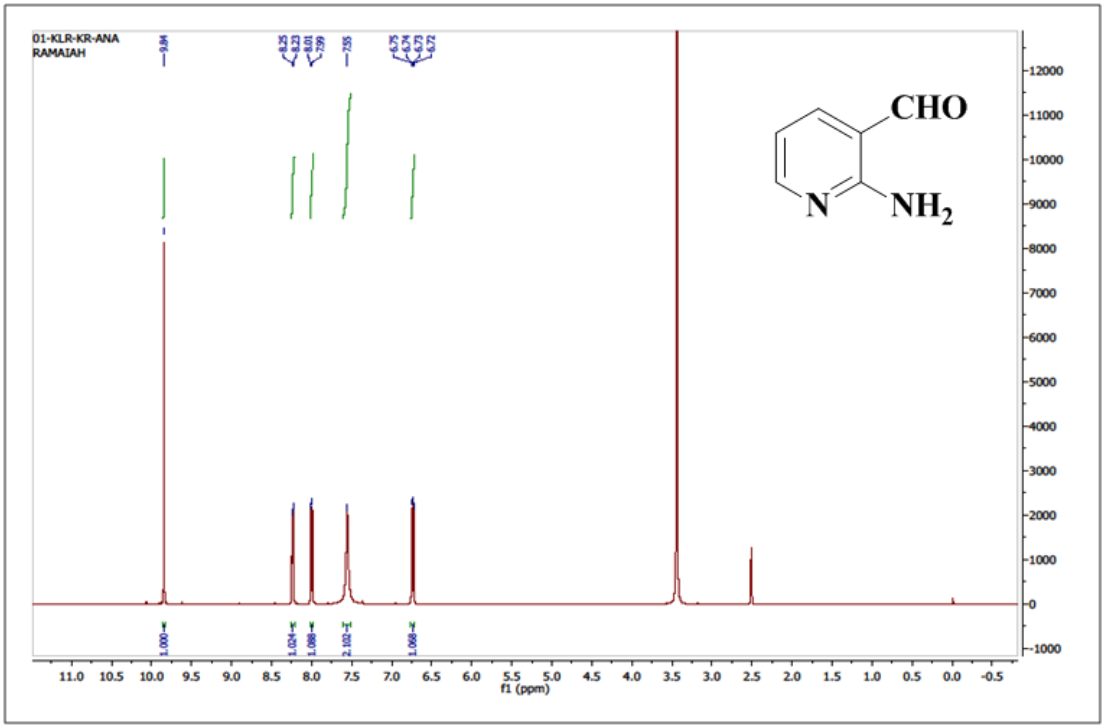

(a)

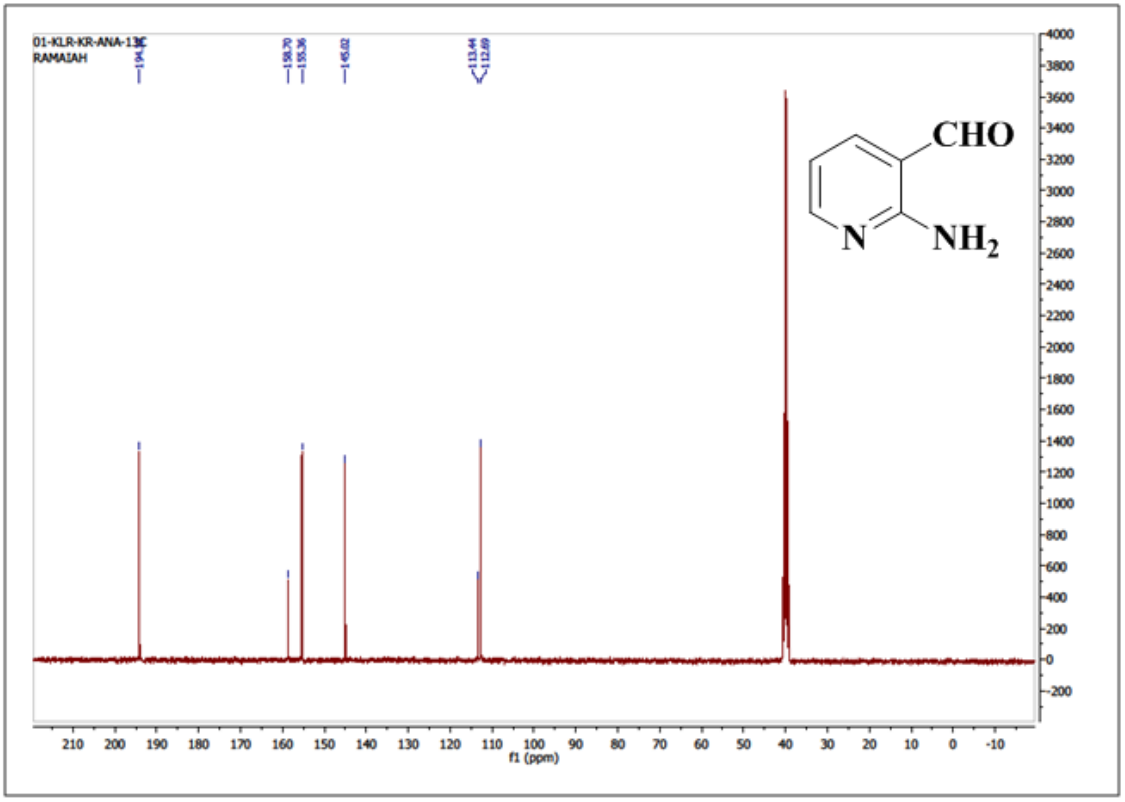

(b)

(a) ^{1}H NMR and **(b)** ^{13}C NMR spectrum of ANA.

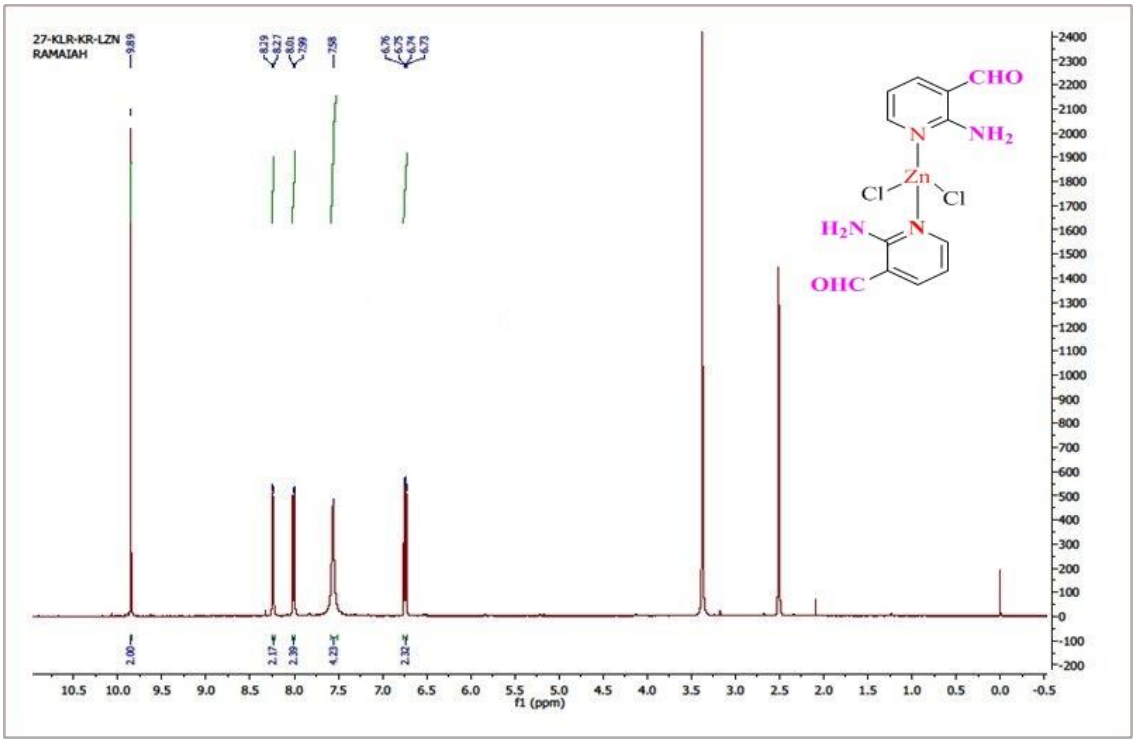

(c)

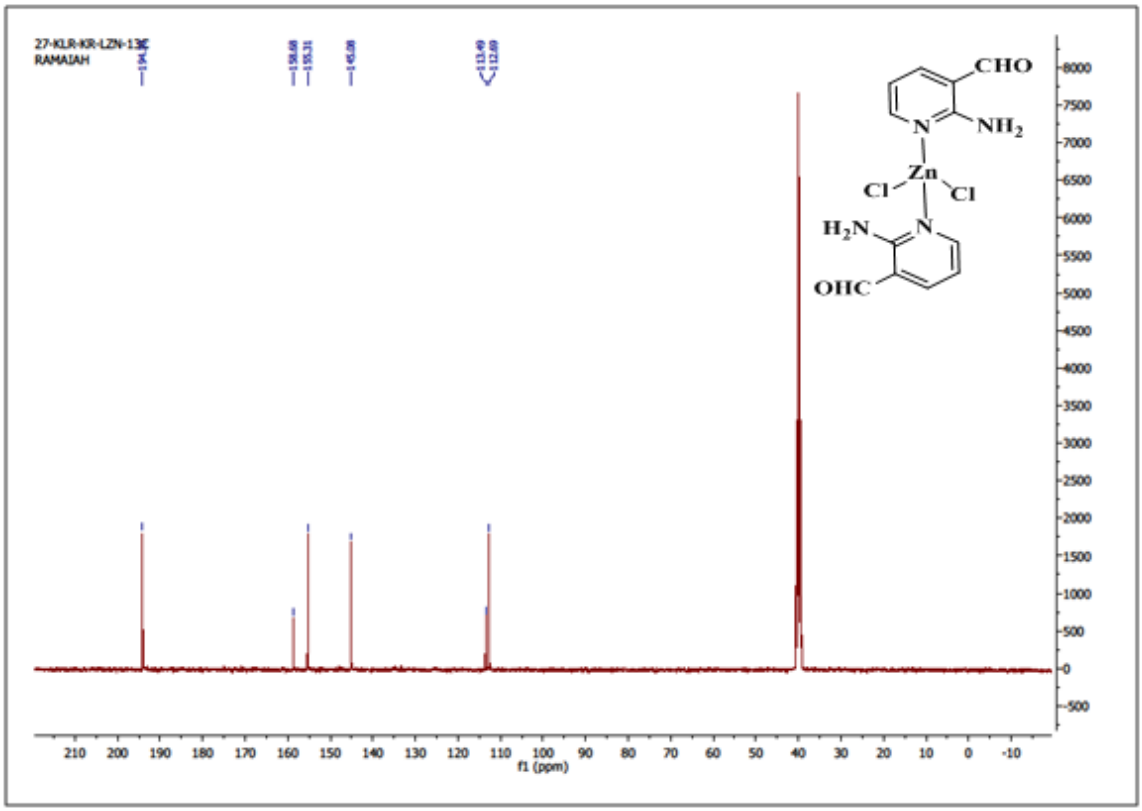

(d)

(c) ^{1}H NMR and **(d)** ^{13}C NMR spectrum of Zn(II) complex.

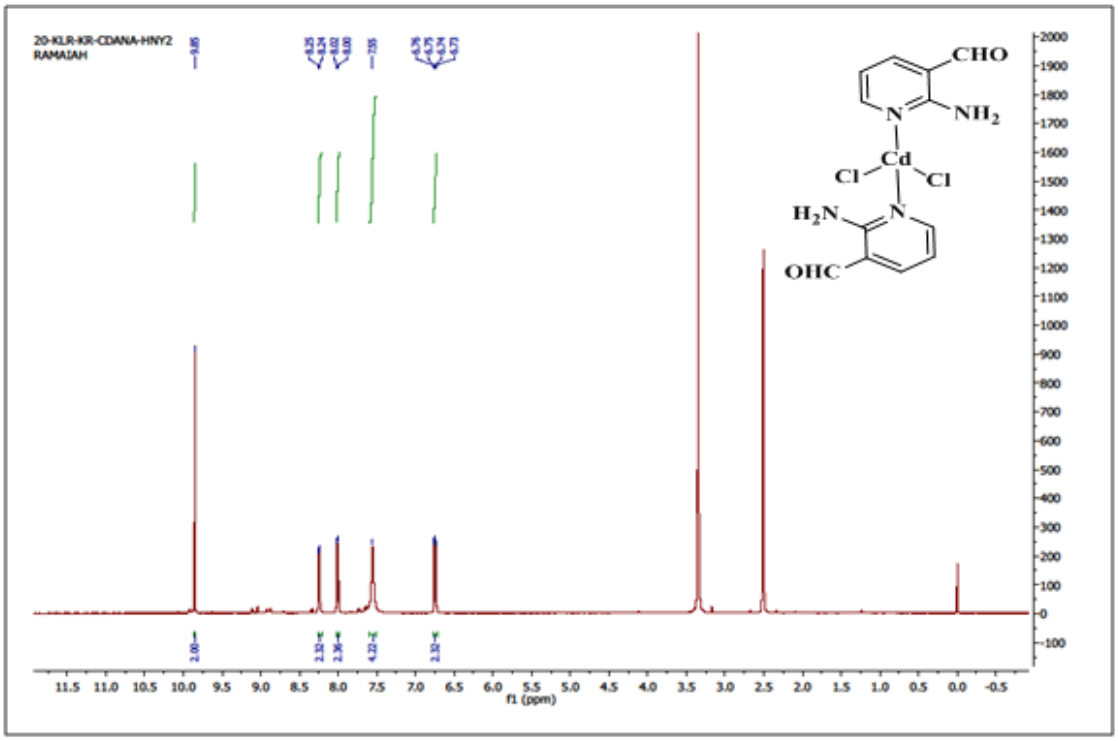

(e)

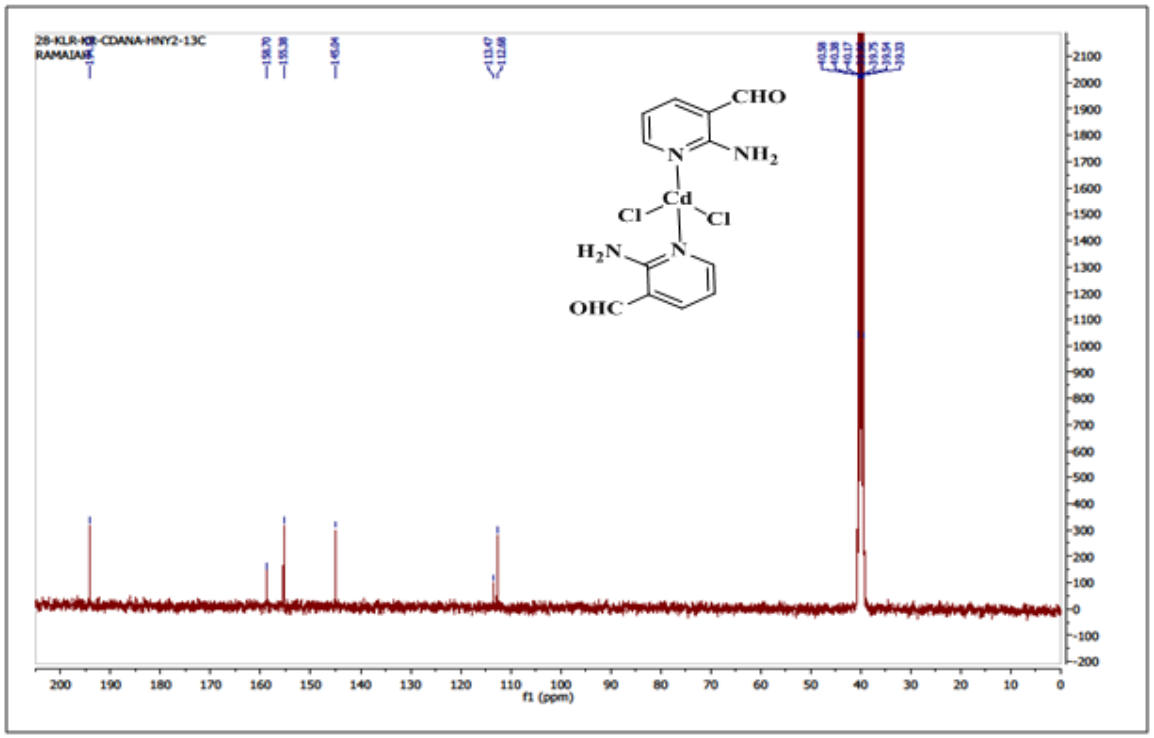

(f)

(e) ^{1}H NMR and **(f)** ^{13}C NMR spectrum of Cd(II) complex.

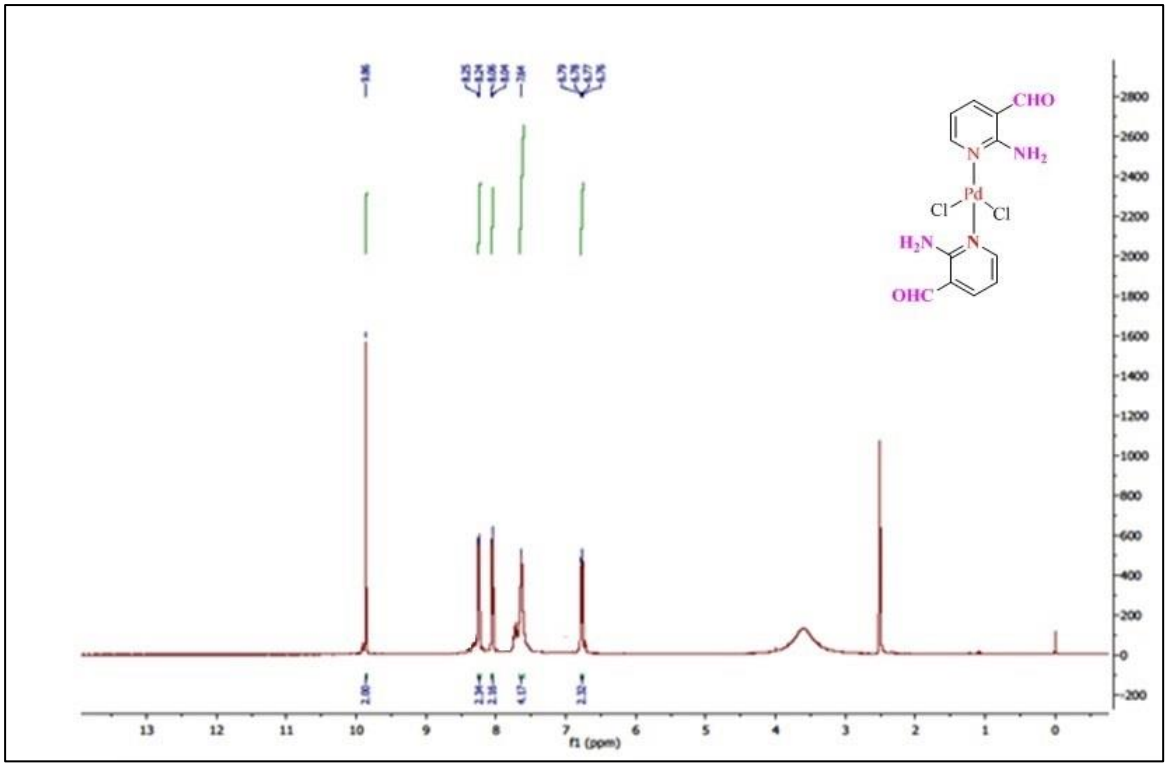

(g)

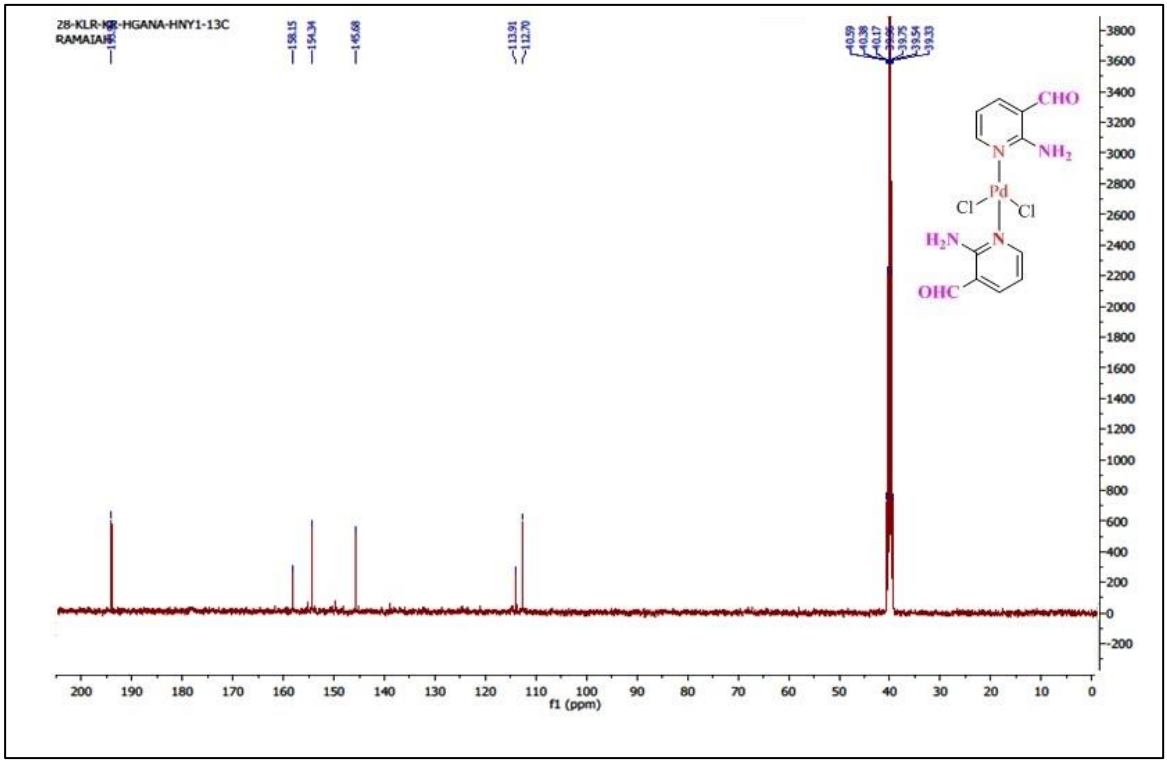

(h)

(g) ^{1}H NMR and **(h)** ^{13}C NMR spectrum of Pd(II) complex.

Fig. 3.2 ^{1}H NMR and ^{13}C NMR Spectra of ANA and its metal complexes

3.1.2 Crystal structure of ANA and its Zn(II) complex

3.1.2.1 ANA

The ligand ANA crystallized in the monoclinic system with a space group $P2_1/c$ with Z = 8. The crystallographic parameters are listed in Table 3.4 and the H-bonding data is listed in Table 3.5. In the crystal structure, an asymmetric unit consists of two molecules of ANA, labeled separately as A and B, which has intramolecular classical N-H…..O

H-bonding occurs between one of the hydrogens of the amine group and the oxygen atom of aldehyde group forming a six membered ring Fig. 3.3. It is intriguing to note that intermolecular H-bonding between N-H…..N of the molecules gives rise to two types of primary molecular pattern N4-H4b…..N3 interactions in the dimeric unit (BB*) at the inversion centre of molecules B and N2-H2b…..N1 interaction monomer unit of the molecules A, leading to herring bone stacking pattern of molecules along b axis Fig. 3.4-a,b. Further, the non-classical weak hydrogen bond interactions between pyridine ring C-H…..N units (BB*/B*B), give rise to a different herring bone stacking pattern of dimeric units Fig. 3.4-c. In addition, the aldehydic hydrogen H12, the pyridine ring hydrogen H9 of dimers BB* and H4 of molecules A involved in intermolecular non-classical C-H…..O H-bonding with oxygen atom as trifurcated acceptor O1 [34], of molecule A is shown in Fig. 3.5. The pyridine ring hydrogen H3 of molecule A is also involved in intermolecular weak H-bonding with aldehydic oxygen atom O2 of molecule B, extending the stacking of molecules on 2D structure Fig. 3.6. Offset π-π stacking interactions established between the aromatic pyridine rings of dimeric units BB* (distance between centroids 3.955 A^o) reinforce crystal structure cohesion in molecular packing within the crystal lattice [35,36]. In a nutshell, the 3D supramolecular stacking pattern of ANA consists of classical and non-classical H-bonding network for its 3D-architecture as depicted in Fig. 3.7.

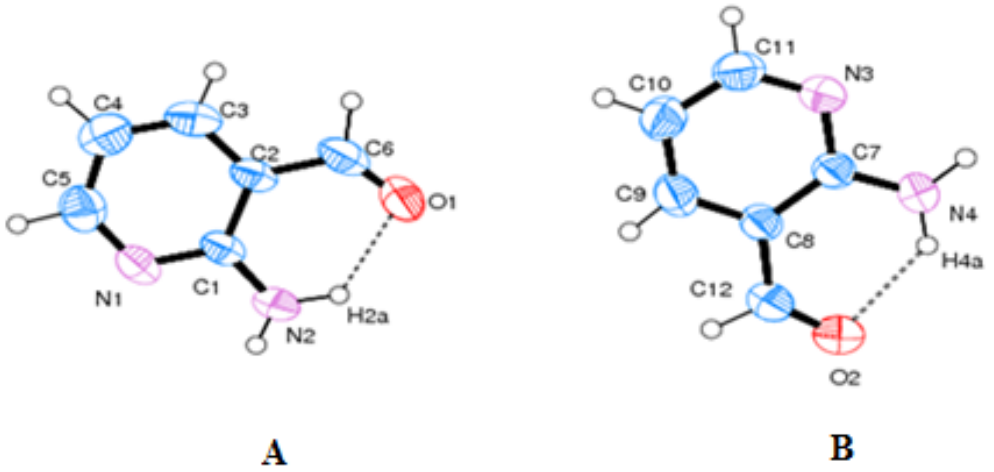

Fig. 3.3 ORTEP diagram of ligand up to 50% probability showing intramolecular N-H---O hydrogen bonds.

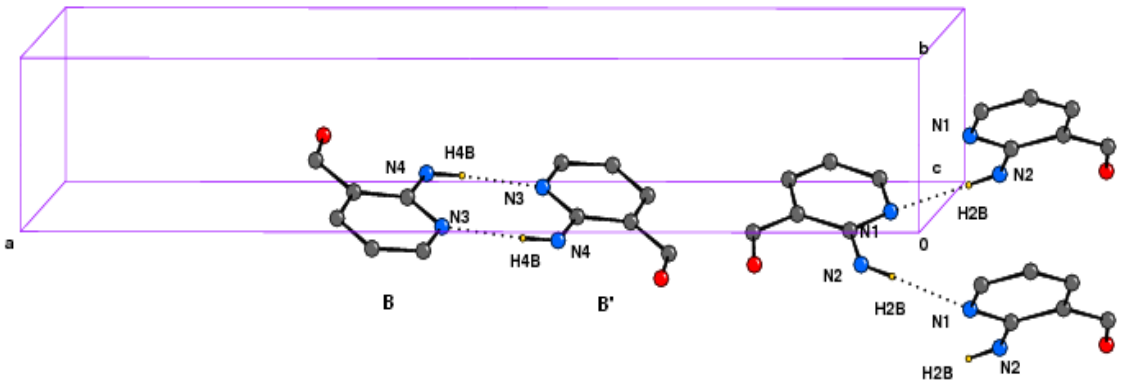

(a)

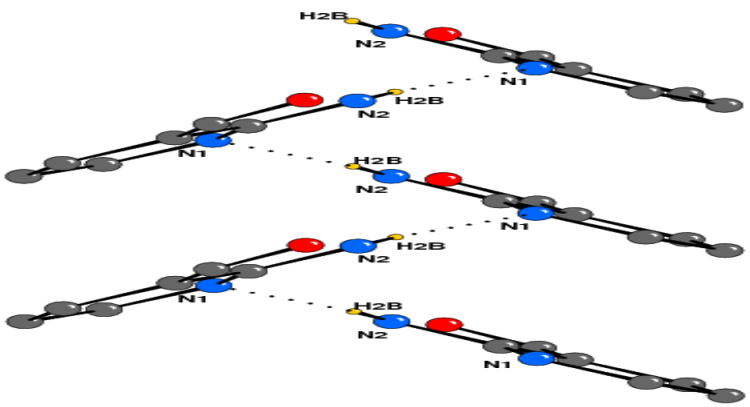

(b)

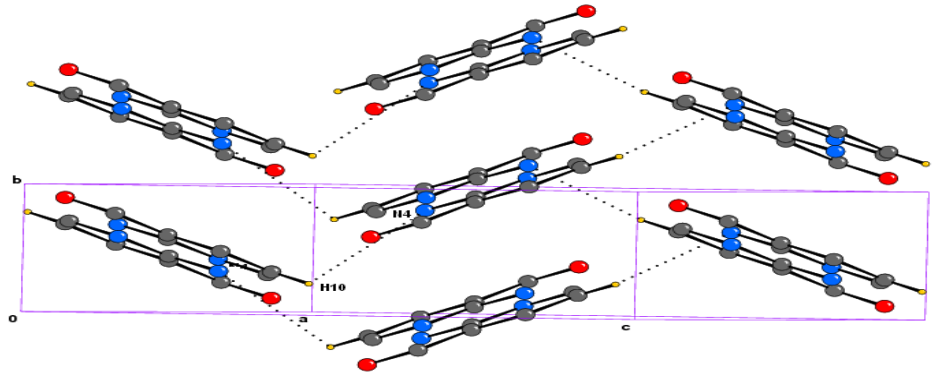

(c)

Fig.3.4-a-c (a) Intermolecular interactions of ANA, intermolecular hydrogen bonding depicting dimer formation of B and herring bone pattern formation A, (**b**) Herring bone stacking pattern of molecule A along b axis, (**c**) Herring bone pattern of dimeric units of molecules B.

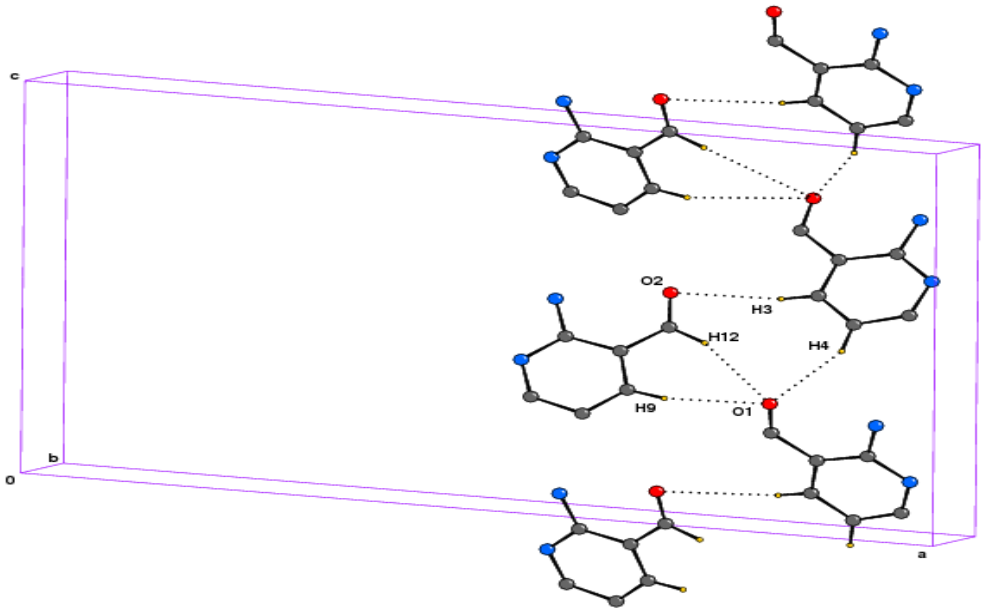

Fig. 3.5 Intermolecular weak hydrogen bonding between the molecules A and B.

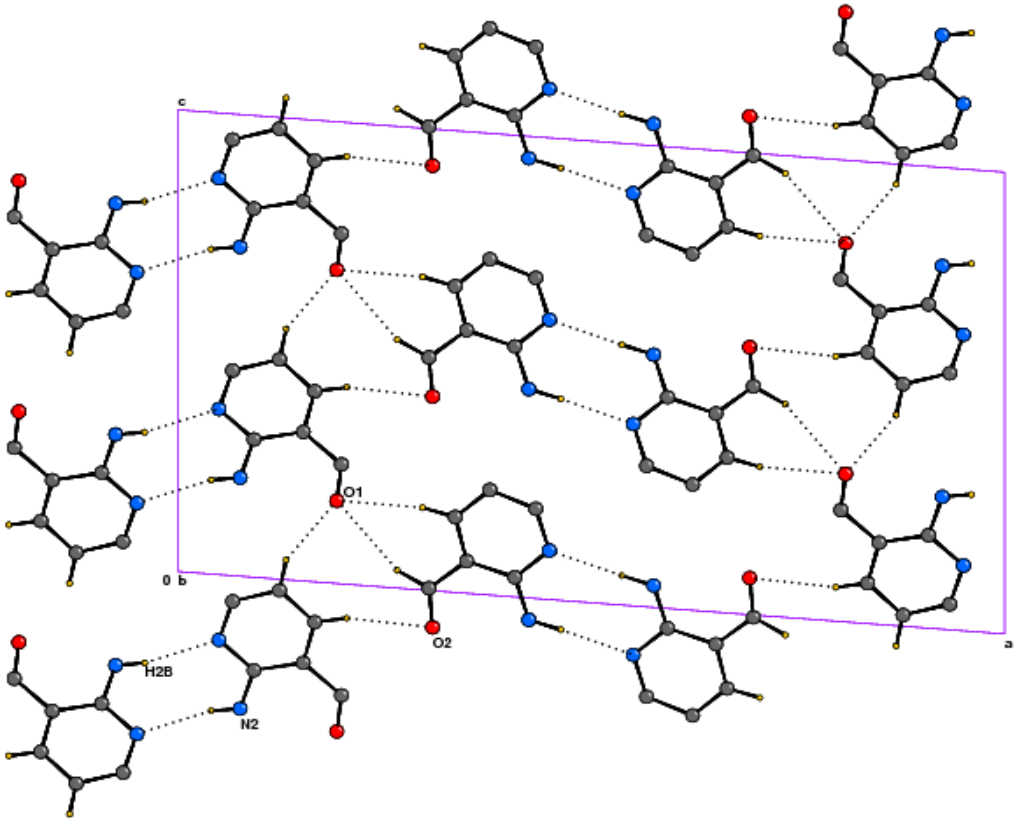

Fig. 3.6 2D stacking pattern diagram depicting the intermolecular H-bonding.

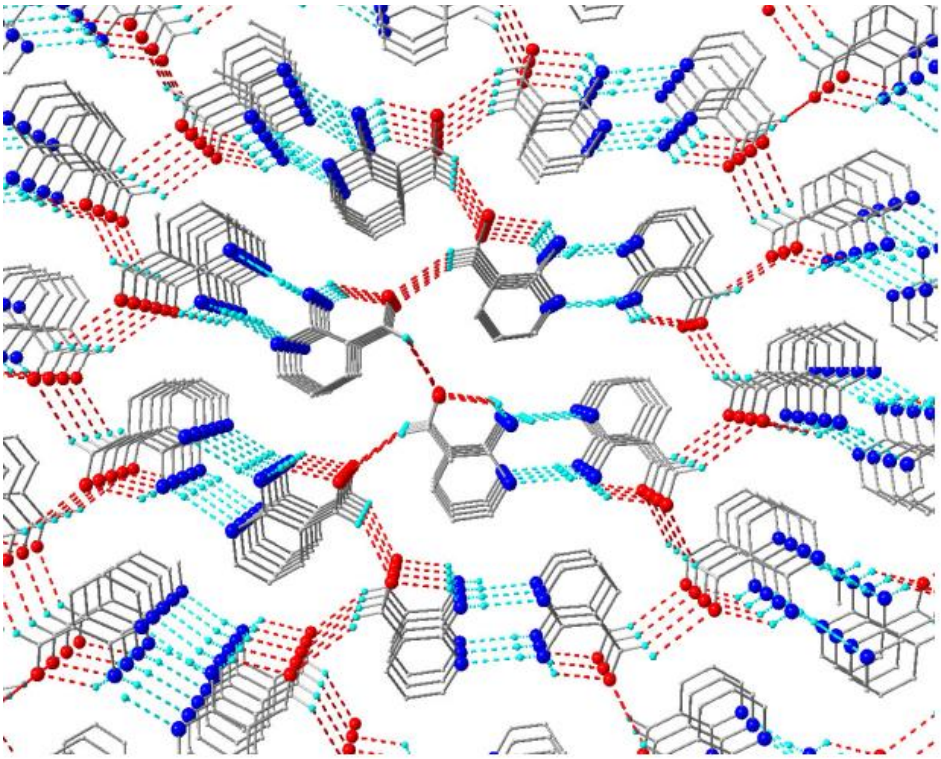

Fig. 3.7 3D-crystal structure of ANA.

3.1.2.2 $[Zn(ANA)_2Cl_2]$ complex

Zn(II) complex crystallized in the triclinic system with *P*-1 space group with Z= 2. The crystallographic data are listed in Table 3.4, and details of H-bonding data are listed in Table 3.5. The coordination environment around the zinc atom is a distorted tetrahedral with two sites occupied by the pyridine nitrogen atom of ANA, labeled separately as A and B, while the remaining two sites are occupied by chloride ions Cl1, Cl2. The ORTEP diagram of Zn(II) complex is shown in Fig. 3.8, while the selected interatomic distances and bond angles are listed in Table 3.6. From the data, it is observed that both classical and non-classical H-bonding interactions are also present in Zn(II) complex. The intramolecular H-bonding N-H….O as observed in the crystal structure of ANA is retained in the structure of the complex. In addition, non-classical intramolecular hydrogen bonds as N-H….Cl occurring as N4-H4b···Cl2 and N2-H2···Cl1 are found in the complex molecule as shown in Fig. 3.8. As observed in the free ligand, Zn(II) complex shows the presence of non-classical intermolecular hydrogen bonds. One of the chloride ligands is involved in the intermolecular non-classical pyridine ring C10-H10….Cl2 hydrogen bond interaction giving rise to a 1-D array of the complex which is shown in Fig. 3.9. The oxygen atom O1 of aldehyde group of ligand A in the complex molecule acts as a bifurcated acceptor for the pyridine ring hydrogens H4 and H5, while H3 hydrogen and aldehyde hydrogen H6 of the ligand "A" in the same complex molecule take part in non-classical intermolecular weak H-bonding with bifurcated acceptor oxygen atom O2 of ligand, which runs parallel along c axis and is shown in Fig. 3.10. Thus, in a 3D crystal structure, one ANA ligand in the complex is involved in two kinds of bifurcated intermolecular weak H-bonding through the oxygen atom of the aldehydic group. The 2D network of these non-classical hydrogen bonds is depicted in Fig. 3.11. It is interesting to note that both ANA and Zn(II) complex invoke classical and non-classical H-bonding arrays resulting in 3D architecture for supramolecular stacking pattern of molecules Fig. 3.12.

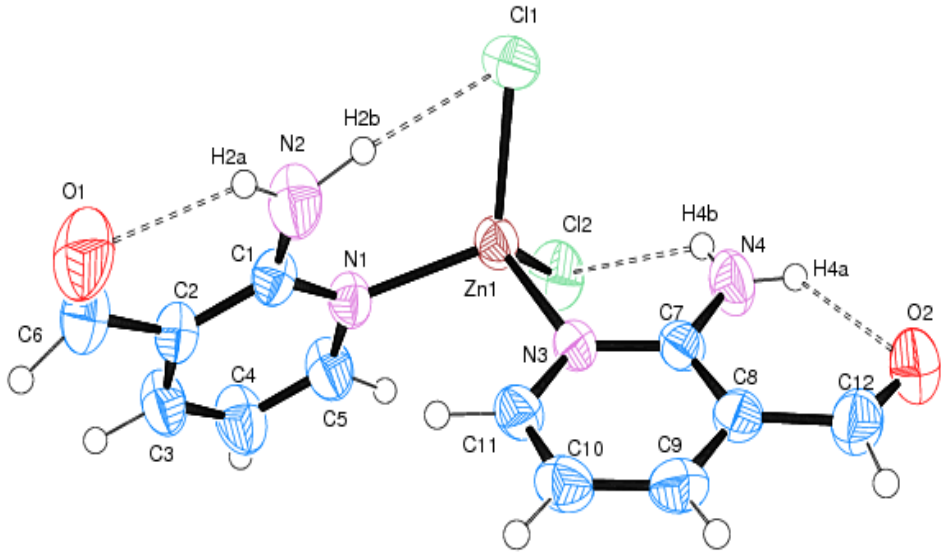

Fig. 3.8 ORTEP diagram of Zn(II) complex depicting intramolecular hydrogen bonding (3D- structure).

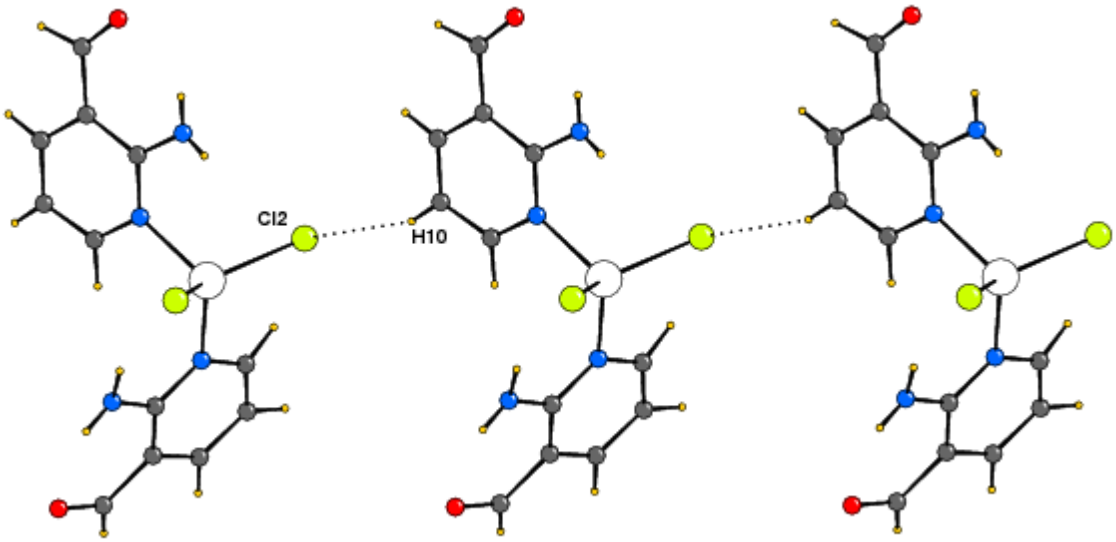

Fig. 3.9 Intermolecular weak hydrogen-bonding showing one-dimensional array of molecules.

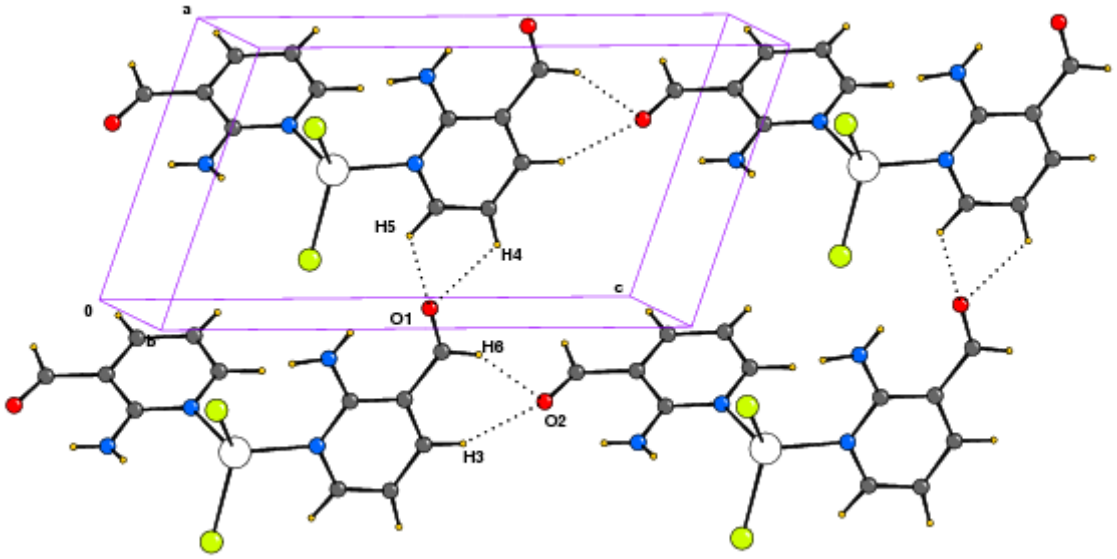

Fig. 3.10 Aromatic C-H ···O weak hydrogen-bonding pattern shown within unit cell.

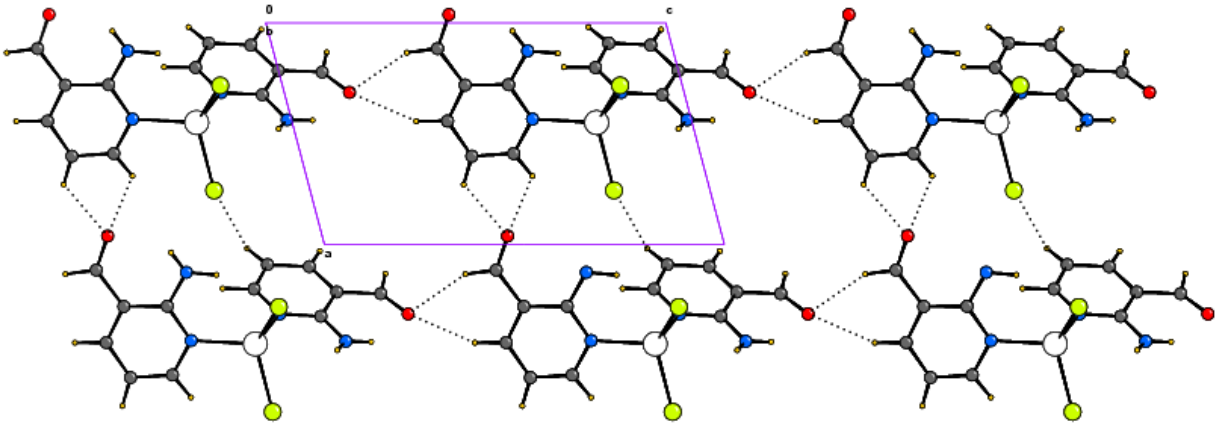

Fig. 3.11 2D-packing diagram of molecules of Zn(II) complex depicting intermolecular weak H-bonds.

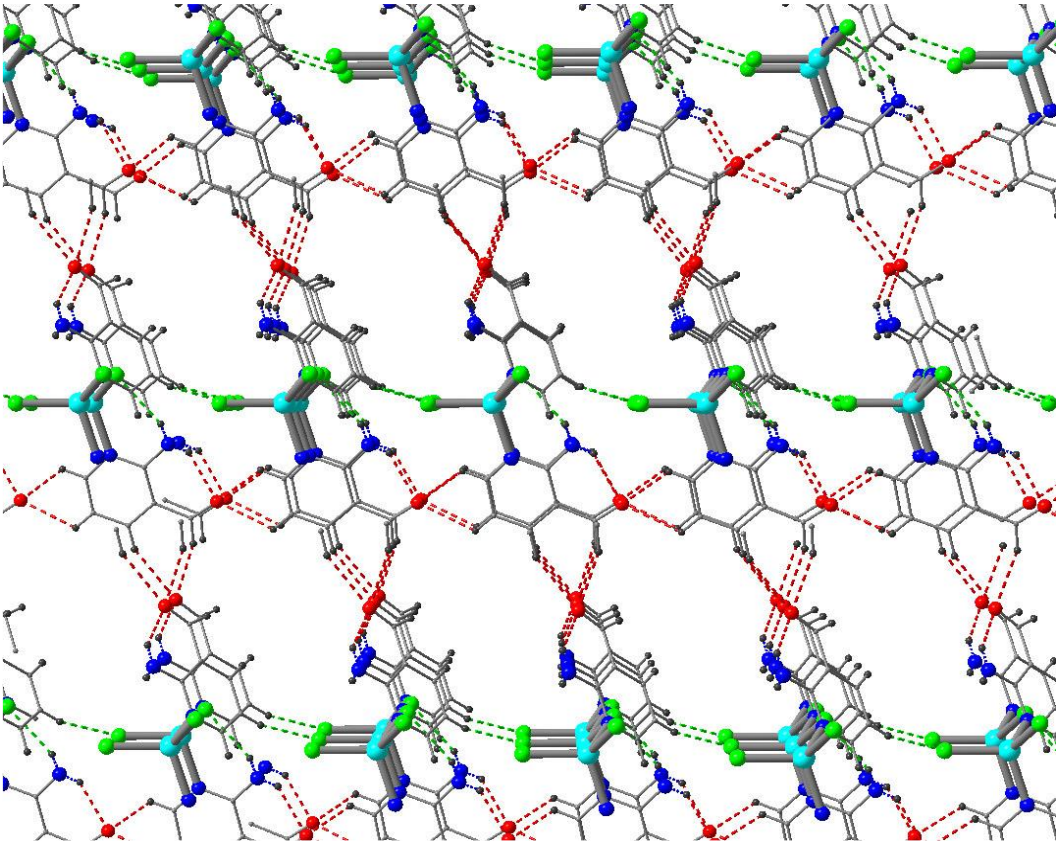

Fig. 3.12 3D-Stacking pattern of Zn(II) complex.

Table 3.4 Crystallographic data of ANA and Zn(II) complex

Compound	**ANA**	**Zn(II) complex**
Empirical formula	$C_6H_6N_2O$	$C_{12}H_{12}Cl_2N_4O_2Zn$
Formula weight	122.13	380.53
Wavelength (Å)	0.71073	0.71073
Crystal system	Monoclinic	Triclinic
Space group	P 2_1/c	P-1
a (Å)	22.8474 (14)	7.8835(2)
b (Å)	3.9552 (2)	8.5122(2)
c (Å)	13.1652 (8)	12.7829(3)
α (°)	90	84.604(1)
β (°)	94.465 (4)	74.250(1)
γ(°)	90	67.617(1)
Volume ($Å^3$)	1186.1 (1)	763.36(3)
Z	8	2

$D_{calc.}$ ($M_g m^{-3}$)	1.368	1.656
Temperature (K)	296	296
Absorption coefficient (mm^{-1})	0.097	1.966
F(000)	512	384
Crystal size (mm^3)	0.23 x 0.20 x 0.18	0.30 x 0.25 x 0.13
θ range for data collection (°)	0.89-25.99	1.7-32.0
Reflections collected / unique	12978/2321	14034/5468
Completeness to θ	25.99, 100%	32,100%
Independent reflections *[R_{int}]*	0.1902	0.0596
Max./ min. transmission	0.9827/0.9779	0.7841/0.5891
Data / parameters	2321/212	5468/238
Goodness-of-fit on F^2	0.881	0.987
Final *R* indices [I>2σ(I)]	[a]R_1 = 0.0497	[a]R_1 = 0.0348
	[b,c]wR_2 = 0.1071	[b,c]wR_2 = 0.0911
R indices(all data)	[a]R_1 = 0.0733	[a]R_1 = 0.0496
	[b,c]wR_2 = 0.1152	[b,c]wR_2 = 0.0970
Extinction coefficient	0.044 (4)	-
Largest diff. peak and hole ($e_{Å}^{-3}$)	0.235 and -0.235	0.771 and -0.469

[a]$R_1 = \sum(\left| F_O \right| - \left| F_C \right|) / \sum \left| F_O \right|$. [b]$wR_2 = \{\sum [w (F_O^2 - F_C^2)^2] / \sum [w(F_O^2)^2]\}^{1/2}$

[c]$w = 1/[\sigma^2(F_O^2)+(aP)^2+bP]$ with $P = [F_o^2+2F_c^2]/3$,

(a = 0.0333 and b = 0.000 for ANA, a = 0.0534 and b = 0.000 for Zn(II) complex)

Table 3.5 Hydrogen-bond parameters of ligand (ANA) and Zn(II) complex

Compound	D-H…A	D-H	D···A	H····A	<D-H····A	Symmetry code
ANA	N2-H2a···O1	1.00(2)	2.745(2)	2.02(2)	127(2)	*x, y, z*
	N4-H4a···O2	0.97(2)	2.781(2)	2.06(3)	130(2)	*x, y, z*
	C3-H3 ····O2	0.91(2)	3.662(2)	2.79(2)	158(2)	*x, y-1, z+1*
	C4-H4····O1	0.98(2)	3.538(3)	2.61(2)	154(2)	*x, -y+1/2, z+1/2*
	C10-H10····N4	0.96(2)	3.666(2)	2.88(2)	138(1)	*x, -y+1/2, z+1/2*
	C9-H9····O1	0.94(2)	3.472(2)	2.57(2)	159(2)	*x, -y+1/2+1, z-1/2*
	C12-H12···O1	1.01(2)	3.558(3)	2.59(2)	159(2)	*x,-y+1/2+1, z-1/2*
	N4H4b····N3	0.92(2)	3.073(2)	2.14(2)	176(2)	*-x+1, -y+1, -z*
	N2-H2b…N1	0.84(2)	3.082(2)	2.25 (2)	167(2)	*-x, y+1/2, -z=1/2+1*
Zn(II)	N2-H2b···· C11	1.02(3)	2.769(3)	2.12(2)	136(2)	*x, y, z*
	N2-H2a····O1	0.81(3)	3.359(2)	2.37(3)	159(2)	*x, y, z*
	N4-H4a····O2	0.81(2)	2.739(3)	2.13(2)	131(2)	*x, y, z*
	N4-H4b····Cl2	0.70(2)	3.438(2)	2.90(2)	136(3)	*x, y, z*
	C5-H5····O1	0.97(3)	3.279(3)	2.64(2)	123(2)	*x-1, y, z*
	C4-H4····O1	0.97(3)	3.247(4)	2.57(3)	126(3)	*x-1, y, z*
	C3-H3····O2	1.01(2)	3.389(3)	2.43(2)	156(2)	*x, y, z+1*
	C6-H6····O2	1.09(2)	3.546(3)	2.51(2)	156(2)	*x, y, z+1*
	C10-H10····Cl2	0.94(2)	3.634(2)	2.73(2)	160(2)	*x+1, y-1, z*

Table 3.6 Selected bond lengths (Å) and bond angles (°) for Zn(II) complex

Bond	Length	Bond	Angle
Zn-Cl1	2.2316(6)	Cl1-Zn-Cl2	117(1)
Zn-Cl2	2.2342(6)	Cl1-Zn-N1	113(1)
Zn-N1	2.0528(1)	Cl1-Zn-N3	105(1)
Zn-N3	2.0553(1)	Cl2-Zn-N1	107(1)
		Cl2-Zn-N3	109(1)
		N1-Zn-N3	106(1)

3.2 DFT studies

3.2.1 Molecular geometry

The optimized geometric structures for the ligand and its metal complexes were performed with DFT/B3LYP employing 6-311G++(d,p)/SDD basis set resulting in minimum energy for C_1 point group symmetry for the complexes with minimum optimization. The energy of the compounds are -3136.870070 Hartree [Co(II)], -3262.65187 Hartree [Ni(II)],

-3394.802234 Hartree [Cu(II)], -3516.405300 Hartree [Zn(II)], -1922.1703745 Hartree [Cd(II)], -1882.277588 Hartree [Pd(II)] and -417.094083 Hartree [ANA], respectively, and the optimized structures are presented in Fig. 3.13. The geometrical parameters such as bond distances, bond angles and dihedral angles of ligand ANA and its metal complexes are reported in Table 3.7.

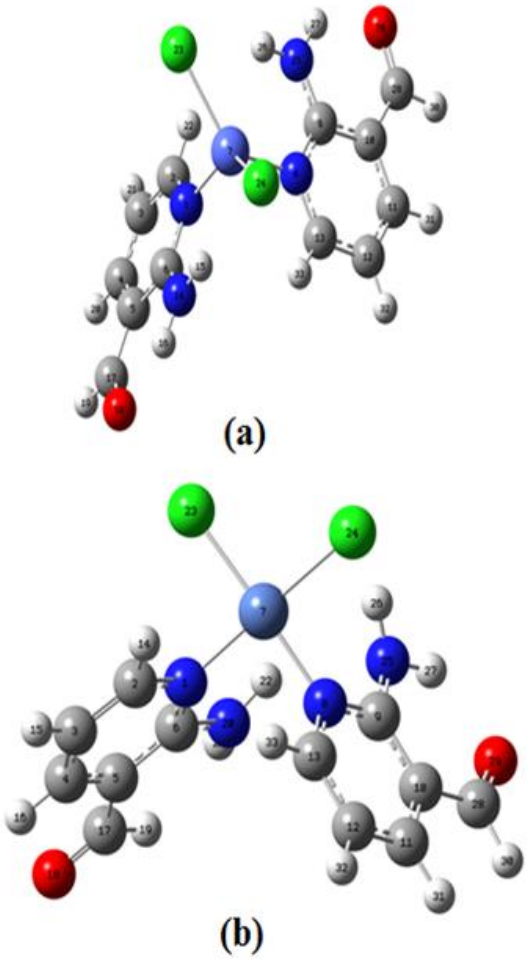

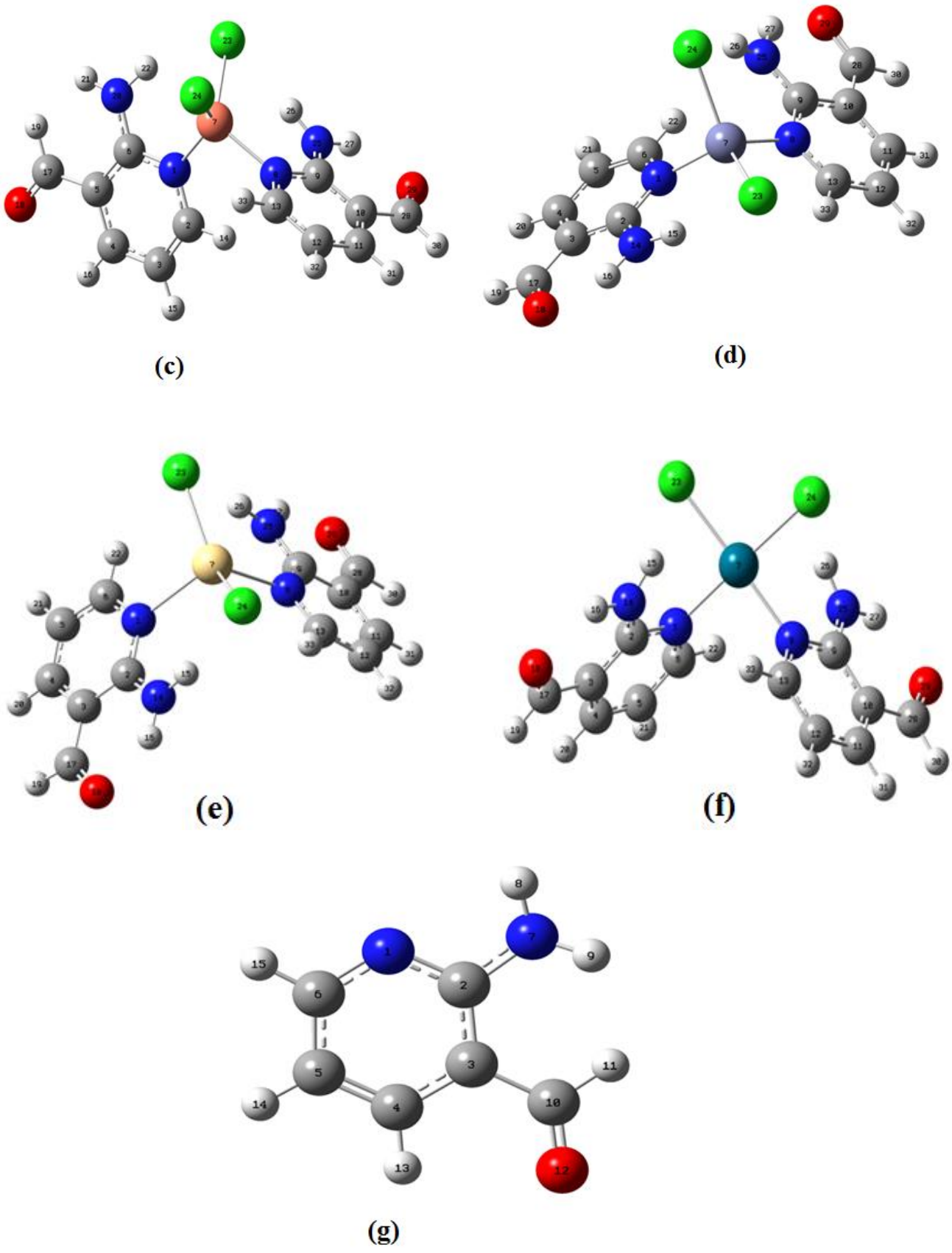

Fig. 3.13 Optimized molecular structures and numbering of atoms of **(a)** Co(II), **(b)** Ni(II), **(c)** Cu(II), **(d)** Zn(II), **(e)** Cd(II), **(f)** Pd(II) and **(g)** ANA.

Table 3.7 Selected bond lengths and bond angles of the Ni(II), Cu(II), Co(II), Cd(II), and Pd(II) complexes

Ni(II)				Cu(II)			
Bond length	**Value (Å)**	**Bond angle**	**Value (Å)**	**Bond length**	**Value (Å)**	**Bond angle**	**Value (Å)**
N1–C2	1.34797	N1–C2–C3	123.49397	N1–C2	1.34694	N1–C2–C3	124.29379
C2–C3	1.38569	C2–C3–C4	117.74394	C2–C3	1.38538	C2–C3–C4	117.53157
C3–C4	1.38996	C3–C4–C5	120.36352	C3–C4	1.39076	C3–C4–C5	120.37914
C4–C5	1.39458	C4–C5–C6	118.64506	C4–C5	1.39251	C4–C5–C6	118.87156
C5–C6	1.42481	C5–C6–N1	120.27344	C5–C6	1.42899	C5–C6–N1	120.17383
C6–N1	1.35839	C6–N1–C2	119.42251	C6–N1	1.36920	C6–N1–C2	118.73498
N1–Ni7	1.91494	C6–N1–Ni7	124.28809	N1–Cu7	2.02057	C6–N1– Cu7	121.50259
Ni7–N8	1.92336	N1–Ni7–N8	89.78835	Cu7–N8	2.03733	N1–Cu 7–N8	100.42745
N8–C9	1.36200	N8–C9–C10	120.31710	N8–C9	1.36529	N8–C9–C10	120.06766
C9–C10	1.42685	C9–C10–C11	118.72239	C9–C10	1.43584	C9–C10–C11	118.72239
C10–C11	1.39489	C10–C11–C12	120.22315	C10–C11	1.39355	C10–C11–C12	118.52042
C11–C12	1.39058	C11–C12–C13	117.67835	C11–C12	1.39203	C11–C12–C13	117.62409
C12–C13	1.38812	C12–C13–N8	123.85918	C12–C13	1.38825	C12–C13–N8	123.83399
C13–N8	1.34385	C13–N8–C9	119.13498	C13–N8	1.34638	C13–N8–C9	119.30992
C2–H14	1.08344	N1–C2–H14	115.28292	C2–H14	1.08302	N1–C2–H14	115.19340
C3–H15	1.08297	C2–C3–H15	120.21324	C3–H15	1.08299	C2–C3–H15	120.34108
C4–H16	1.08533	C3–C4–H16	122.11776	C4–H16	1.08555	C3–C4–H16	122.12549
C5–C17	1.47719	C4–C5–C17	118.30726	C5–C17	1.47846	C4–C5–C17	117.97288
C17–O18	1.21693	C5–C17–O18	123.59726	C17–O18	1.21701	C5–C17–O18	123.43197
C17–H19	1.11044	C5–C17–H19	116.87584	C17–H19	1.10986	C5–C17–H19	117.09124
C6–N20	1.35722	O18–C17–H19	119.52197	C6–N20	1.34844	O18–C17–H19	119.47618
N20–H21	1.00610	C6–N20–H21	120.06685	N20–H21	1.00614	C6–N20–H21	119.70090
N20–H22	1.01234	C6–N20–H22	118.58897	N20–H22	1.02196	C6–N20–H22	117.94652
Ni7–Cl23	2.17820	H21–N20–H22	116.27146	Cu7–Cl23	2.30964	H21–N20–H22	116.50581
Ni7–Cl24	2.19935	N1–Ni7–Cl23	87.97416	Cu7–Cl24	2.20097	N1–Cu7–Cl23	100.10784
C9–N25	1.35487	Cl23–Ni7–Cl24	93.25197	C9–N25	1.33906	Cl23–Cu7–Cl24	108.13611

N25–H26	1.02273	Cl24–Ni7–N8	89.15803	N25–H26	1.01969	Cl24–Cu7–N8	98.99417
N25–H27	1.01745	N8–C9–N25	117.38983	N25–H27	1.01582	N8–C9–N25	118.79160
C10–C28	1.46719	C9–N25–H26	113.91940	C10–C28	1.46287	C9–N25–H26	120.25019
C28–O29	1.22372	C9–N25–H27	114.35883	C28–O29	1.22558	C9–N25–H27	116.52157
C28–H30	1.10917	H26–N25–H27	117.75295	C28–H30	1.10928	H26–N25–H27	120.56574
C11–H31	1.08723	C9–C10–C28	122.01158	C11–H31	1.08763	C9–C10–C28	122.01852
C12–H32	1.08282	C10–C28–O29	125.64082	C12–H32	1.08274	C10–C28–O29	125.66547
C13–H33	1.08417	C10–C28–H30	114.20672	C13–H33	1.08532	C10–C28–H30	114.28075
		C10–C11–H31	120.15208			C10–C11–H31	118.74175
		C11–C12–H32	119.00132			C11–C12–H32	122.08575
		C12–C13–H33	122.03159			C12–C13–H33	121.36682
		C3–C2–H14	121.21893			C3–C2–H14	115.19340
		C4–C3–H15	122.03369			C4–C3–H15	120.34108
		C5–C4–H16	117.51806			C5–C4–H16	117.48988
		C6–C5–C17	123.04345			C6–C5–C17	123.15502
		N1–C6–N20	116.95816			N1–C6–N20	116.93598
		C2–N1–Ni7	116.20153			C2–N1–Cu7	119.01442
		C13–N8–Ni7	119.03245			C13–N8–Cu7	119.52953
		N8–C13–H33	115.59106			N8–C13–H33	114.78726

Co(II)				Pd(II)				Cd (II)			
Bond length	**Value (Å)**	**Bond angle**	**Value (Å)**	**Bond length**	**Value (Å)**	**Bond angle**	**Value (Å)**	**Bond length**	**Value (Å)**	**Bond angle**	**Value (Å)**
N1–C2	1.37883	N1–C2–C3	119.55759	N1–C2	1.38065	N1–C2–C3	119.57098	N1–C2	1.37976	N1–C2–C3	119.81508
C2–C3	1.43613	C2–C3–C4	118.83649	C2–C3	1.44442	C2–C3–C4	118.87668	C2–C3	1.44802	C2–C3–C4	118.68220
C3–C4	1.39918	C3–C4–C5	120.58057	C3–C4	1.40631	C3–C4–C5	120.45339	C3–C4	1.40727	C3–C4–C5	120.55953
C4–C5	1.39445	C4–C5–C6	118.06898	C4–C5	1.40352	C4–C5–C6	117.86766	C4–C5	1.40318	C4–C5–C6	117.80304
C5–C6	1.39149	C5–C6–N1	123.18717	C5–C6	1.40071	C5–C6–N1	123.33680	C5–C6	1.40230	C5–C6–N1	123.50735
C6–N1	1.35549	C6–N1–Co7	120.75474	C6–N1	1.35889	C6–N1–C2	119.82760	C6–N1	1.36057	C6–N1–C2	119.58834
N1–Co7	1.92958	N1–Co7–N8	93.34945	N1–Pd7	2.08508	C6–N1– Pd7	117.95543	N1–Cd7	2.33864	C6–N1– Cd7	114.47750
Co7–N8	1.92958	Co7–N8–C9	119.45783	Pd7–N8	2.08501	N1–Pd7–N8	90.06329	Cd7–N8	2.33864	N1–Cd7–N8	104.72770
N8–C9	1.37883	N8–C9–C10	119.55759	N8–C9	1.38063	N8–C9–C10	119.57196	N8–C9	1.37976	N8–C9–C10	119.81508
C9–C10	1.43613	C9–C10–C11	118.83649	C9–C10	1.44441	C9–C10–C11	118.87580	C9–C10	1.44802	C9–C10–C11	118.68220
C10–C11	1.39918	C10–C11–C12	120.58057	C10–C11	1.40631	C10–C11–C12	120.45347	C10–C11	1.40727	C10–C11–C12	120.55953
C11–C12	1.39445	C11–C12–C13	118.06898	C11–C12	1.40352	C11–C12–C13	117.86792	C11–C12	1.40318	C11–C12–C13	117.80304
C12–C13	1.39149	C12–C13–N8	123.18717	C12–C13	1.40071	C12–C13–N8	123.33571	C12–C13	1.40230	C12–C13–N8	123.50735
C13–N8	1.35549	C13–N8–C9	119.75911	C13–N8	1.35888	C13–N8–C9	119.82862	C13–N8	1.36057	C13–N8–C9	119.58834
C2–N14	1.34533	C2–N14–H15	121.72945	C2–N14	1.35235	N1–C2–N14	118.80467	C2–N14	1.35196	N1–C2–N14	119.23144
N14–H15	1.01866	C2–N14–H16	117.44584	N14–H15	1.01859	C2–N14–H15	118.76446	N14–H15	1.02277	C2–N14–H15	121.39250
N14–H16	1.01683	C3–C17–O18	125.24863	N14–H16	1.01951	C2–N14–H16	117.80877	N14–H16	1.01971	C2–N14–H16	117.54009

C3–H17	1.45646	C3–C17–H19	115.26484	C3–C17	1.46572	C2–C3–C17	121.76102	C3–C17	1.46358	C2–C3–C17	121.99676
C17–O18	1.25241	C3–C4–H20	118.81759	C17–O18	1.25880	C3–C17–O18	125.05423	C17–O18	1.26026	C3–C17–O18	125.15389
C17–H19	1.10203	C4–C5–H21	121.80199	C17–H19	1.10503	C3–C17–H19	115.06689	C17–H19	1.10519	C3–C17–H19	115.10550
C4–H20	1.08625	C5–C6–H22	121.30291	C4–H20	1.08832	C3–C4–H20	119.07271	C4–H20	1.08863	C3–C4–H20	118.99070
C5–H21	1.08163	N1–Co7–Cl23	95.36804	C5–H21	1.08324	C4–C5–H21	122.12208	C5–H21	1.08320	C4–C5–H21	122.14121
C6–H22	1.08127	N1–Co7–Cl24	129.24570	C6–H22	1.08436	C5–C6–H22	120.94297	C6–H22	1.08652	C5–C6–H22	121.10681
Co7–Cl23	2.31441	N8–C9–N25	119.10482	Pd7–Cl23	2.36323	N1–Pd7–Cl23	88.96285	Cd7–Cl23	2.47770	N1–Cd7–Cl23	99.82128
Co7–Cl24	2.31441	C9–N25–H26	121.72945	Pd7–Cl24	2.36321	N1–Pd7–Cl24	178.50680	Cd7–Cl24	2.47770	N1–Cd7–Cl24	105.44238
C9–N25	1.34533	C9–N25–H27	117.44584	C9–N25	1.35237	N8–C9–O25	118.80229	C9–N25	1.35196	N8–C9–O25	119.23144
N25–H26	1.01866	C9–C10–C28	121.73888	N25–H26	1.01952	C9–O25–H26	117.80782	N25–H26	1.02277	C9–O25–H26	121.39250
N25–H27	1.01683	C10–C28–O29	125.24863	N25–H27	1.01857	C9–O25–H27	118.76414	N25–H27	1.01971	C9–O25–H27	117.54009
C10–C28	1.45646	C10–C28–H30	115.26484	C10–C28	1.46572	C9–C10–H28	121.76192	C10–C28	1.46358	C9–C10–C28	121.99676
C28–O29	1.25241	C10–C11–H31	118.81759	C28–O29	1.25881	C10-C28-O29	125.05424	C28–O29	1.26026	C10-C28-O29	125.15389
C28–H30	1.10203	C11–C12–H32	121.80199	C28–H30	1.10503	C10–C28–H30	115.06702	C28–H30	1.10519	C10–C28–H30	115.10550
C11–H31	1.08625	C12–C13–H33	121.30291	C11–H31	1.08832	C10-C11-H31	119.07286	C11–H31	1.08863	C10-C11-H31	118.99070
C12–H32	1.08163	-	-	C12–H32	1.08324	C11–C12–H32	122.12178	C12–H32	1.08320	C11–C12–H32	122.14121
C13–H33	1.08127	-	-	C13–H33	1.08436	C12–C13–H33	120.94438	C13–H33	1.08652	C12–C13–H33	121.10681

3.2.2 NLO properties

The large values of first order hyperpolarizabilities of molecules imply that they are high potential candidates for non-linear optical (NLO) property, which finds generous applications in the fields of engineering, physics and chemistry. The hyperpolarizability, polarizability and dipole moment are characteristic properties of molecules in the presence of applied electric field [37-39]. The first order hyperpolarizability is a third rank tensor, which has 27 components, represented by a 3 x 3 x 3 matrix. These 27 components get reduced to 10 components due to Kleinman symmetry [40], which are characterized as β_{xxx}, β_{xxy}, β_{xyy}, β_{yyy}, β_{xxz}, β_{xyz}, β_{yyz}, β_{xzz}, β_{yzz} and β_{zzz}. They can be deliberate using the following equation [41]

$$\beta_i = \beta_{iii} + (1/3) \sum_{i \neq j} (\beta_{ijj} + \beta_{jij} + \beta_{jji})$$

The total static dipole moment μ_t, the anisotropy of polarizability $\Delta\alpha$, the isotropic (or average) linear polarizability α_t and the mean first order hyperpolarizability β_t, employing the x, y and z components are defined as:

$$\mu_t = (\mu_x^2 + \mu_y^2 + \mu_z^2)^{1/2}$$

$$\Delta\alpha = 2^{-1/2} [(\alpha_{xx} - \alpha_{yy})^2 + (\alpha_{yy} - \alpha_{zz})^2 + (\alpha_{zz} - \alpha_{xx})^2 + 6\alpha_{xx}^2]^{1/2}$$

$$\alpha_t = (\alpha_{xx} + \alpha_{yy} + \alpha_{zz})/3$$

$$\beta_t = (\beta_x^2 + \beta_y^2 + \beta_z^2)^{1/2}$$

Hence, the first order hyperpolarizability and its constituents; the total molecular polarizability (α_t) and its elements; the total molecular dipole moment (μ_t) and calculated to determine the NLO behaviour of the complexes and the results are reported in Table 3.8.

The direction of charge delocalization is theoretically calculated by β component. The observed first hyperpolarizability values along β_{zzz} direction indicate that the complexes are acceptable for developing the crystals along this direction in NLO applications. The calculated electronic dipole moment values were found to be 11.5846 [Co(II)], 10.0277 [(Ni(II)], 7.8673 [(Cu(II)], 10.6475 [(Zn(II)], 8.0237 [(Cd(II)] and 12.8373 [Pd(II)] Debye, respectively. The first hyperpolarizability values of the complexes are found to be 22.590×10^{-30} [Co(II)], 16.518×10^{-30} [(Ni(II)], 9.256×10^{-30} [(Cu(II)], 7.271×10^{-30} [(Zn(II)], 6.795×10^{-30} [Cd(II)] and 14.490×10^{-30} cm^5/esu

[(Pd(II)], respectively. The large value of hyper polarizability indicates the NLO property of the system, which is interlinked with the intra-molecular charge transfer.

Table 3.8 Values of dipole moment μ_t (in Debye) and first order hyperpolarizability β_t (in 10^{-30} cm^5/e.s.u) of Co(II), Ni(II), Cu(II), Zn(II), Cd(II) and Pd(II) metal complexes

Type of component	**Co (II)**	**Ni(II)**	**Cu(II)**	**Zn(II)**	**Cd(II)**	**Pd(II)**
β_{xxx}	-----	-138.34363	396.20978	-80.20083	-----	-0.25571
β_{xxy}	-----	-697.07944	-107.76313	473.45250	-----	-828.55048
β_{xyy}	-----	17.41297	-123.94889	142.88101	-----	0.07014
β_{yyy}	-----	-975.20715	-630.73276	370.58285	-----	-610.62142
β_{xxz}	-601.54585	76.68435	72.12951	370.58285	-197.30207	-0.04140
β_{xyz}	-109.28478	–122.25993	36.17691	-423.30895	178.34002	-57.49727
β_{yyz}	-1072.97703	105.77613	164.62764	66.39342	-355.25481	-0.03405
β_{xzz}	-----	-7.38930	-169.47095	128.00036	-----	0.144615
β_{yzz}	-----	–188.22568	-307.48620	-22.18342	-----	-238.0176
β_{zzz}	-942.64606	239.74554	-445.08562	150.98381	-234.11614	0.35382
β_t	22.590×10^{-30} cm^5/e.s.u	16.518×10^{-30} cm^5/e.s.u	9.256×10^{-30} cm^5/e.s.u	7.271×10^{-30} cm^5/e.s.u	6.795×10^{-30} cm^5/e.s.u	14.490×10^{-30} cm^5/e.s.u
μ_x	-----	–0.0285	-2.1695	2.3945	-----	0.0023
μ_y	-----	–9.0708	-6.8587	6.6655	-----	-12.8373
μz	-11.5846	4.27449	-3.1854	-7.9506	-8.0237	0.0036
μ_t	11.5846	10.0277	7.8673	10.6475	8.0237	12.8373
α_{xx}	205.75401	234.48152	260.20054	231.34036	240.91342	279.97943
α_{xy}	-24.70522	–362020	18.68605	23.32278	-25.6077	-0.02352
α_{yy}	244.55917	217.97303	197.90762	192.1428	217.63905	223.29787
α_{xz}	-----	-4.29959	17.94660	-3.11494	-----	-25.06125
α_{yz}	-----	4.58804	2.34623	24.3365	-----	0.00692
α_{zz}	172.23036	180.88416	181.76819	131.83487	171.9118	184.88500
α_t	207.25	211.1103	213.28666	185.12312	210.150	229.38400

3.2.3 Frontier Molecular Orbitals

HOMO-LUMO energy gap can be used to determine the chemical reactivity of the compounds. The HOMO-LUMO energy gap can play a vital role in the determination of stability and reactivity of the molecules [42]. LUMO and HOMO are the two different important molecular orbitals. HOMO refers to ability to donate electron, while LUMO to the ability to accept an electron. Using HOMO, LUMO orbital energies, the electron affinity (A), chemical potential (μ), ionization energy (I), global electrophilicity power (ω) and global hardness (η) [43-45] were calculated.

The computed HOMO, LUMO energies and frontier energy gap at B3LYP/6-31G (d,p)/SDD, level for the complexes are shown in Fig. 3.14 and Table 3.9. From the results, we predict that chemical potential values of the compounds are negative and the frontier molecular gap is very small. Hence the complexes under investigation are most stable and polarizable.

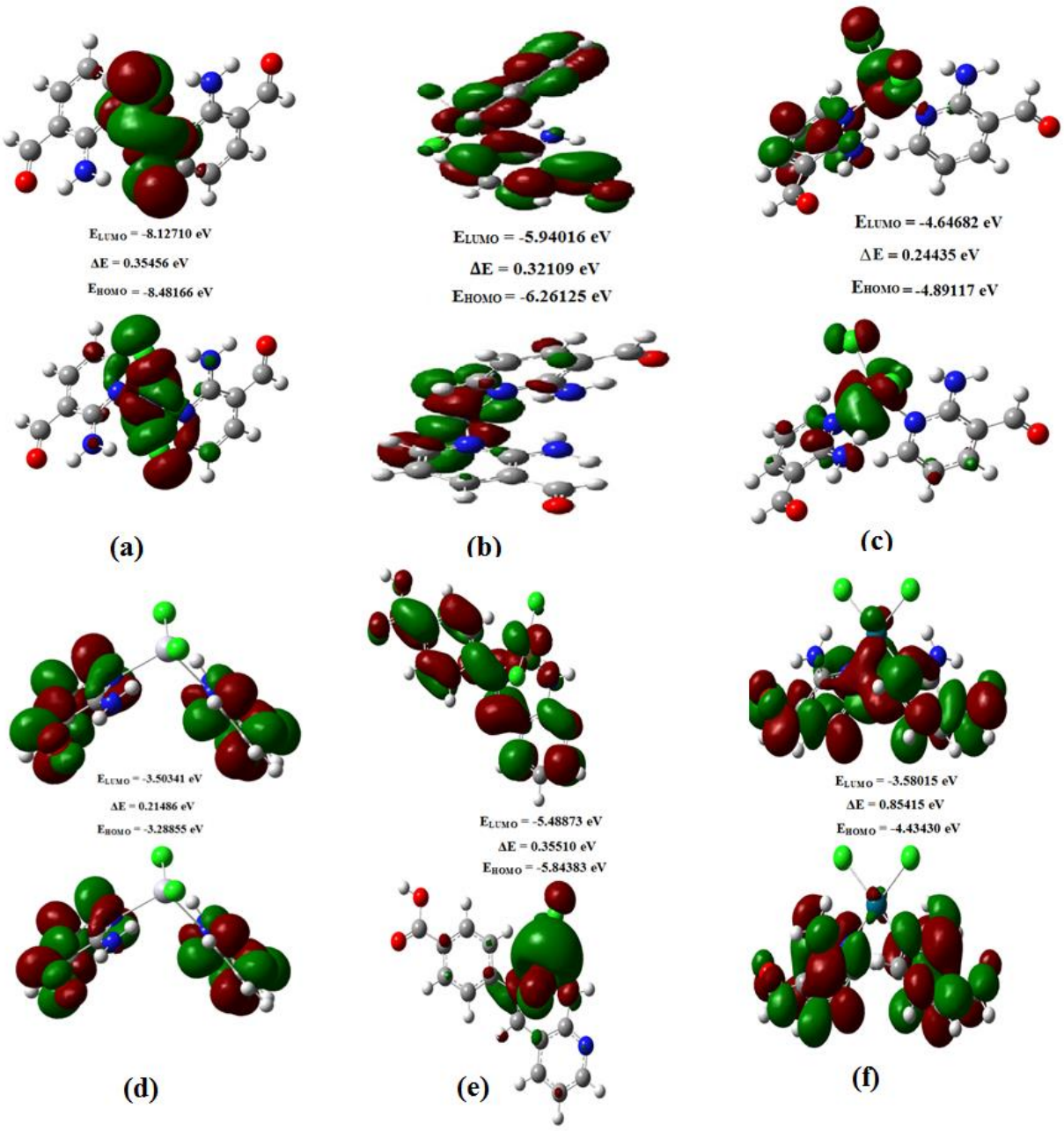

Fig. 3.14 Frontier molecular orbital energy gap of **(a)** Co(II), **(b)** Ni(II), **(c)** Cu(II), **(d)** Zn(II), **(e)** Cd(II) and **(f)** Pd(II) complexes.

Table 3.9 Frontier molecular orbital parameters of metal complexes values present (**eV**)

Frontier molecular orbital parameter	Co(II)	Ni(II)	Cu(II)	Zn(II)	Cd(II)	Pd(II)
HOMO energy	-8.48166	-6.26125	-4.89117	-3.50341	-5.84383	-4.43430
LUMO energy	- 8.12710	–5.94016	-4.64682	-3.28855	-5.48873	-3.58015
Frontier molecular orbital	**0.35456**	**0.32109**	**0.24435**	**0.21486**	**0.35510**	**0.85415**
Ionization energy (**I**)	8.48166	6.26125	4.89117	3.50341	5.84383	4.43430
Electron affinity (**A**)	8.12710	5.94016	4.64682	3.28855	5.48873	3.58015
Global hardness (**η**)	0.17728	0.16054	0.12217	0.10743	0.17755	0.42707
Chemical potential (**μ**)	**-8.30438**	**-6.10068**	**-4.76899**	**-3.39598**	**-5.66628**	**-4.00722**
Global electrophilicity power (**ω**)	194.50246	115.91900	93.08037	53.67532	90.41602	18.79980

3.3 Biological evaluation

The biological activity of a compound is attributed to the results of interlinked chemical reactions or the observed manifestation of interference with a delicately balanced system of interdependent chemical and physical process.

Metals, upon which most of the life processes depend, at times share the characteristics of a two-edged sword by being beneficial to living systems on one hand and being toxic on the other. Metals, when present in optimum quantities, serve vital functions in biological systems, but the same in excessive amounts turn toxic and even lethal. In fact, the metal ion that has gained access to the circulation in sufficient amounts and is not excreted readily is toxic to an extent depending on metal itself. These metals which cannot be metabolized persist in living body and exert their toxic effects by combining with one or more reactive groups essential for normal physiological functions.

The metal binding substances (ligands) which function by chelation, have furnished many useful drugs and other substances of value in checking the toxicity of metals. The chelating compounds called metal antagonists are designed specifically to compete with the endogenous bio-chemicals for the metals and thereby prevent or reverse toxic effects and enhance excretion of the metals.

8-hydroxyquinoline, a well known analytical reagent and a ligand is found to have antibacterial activity and it has been proposed that the antibacterial action of this compound is due to its chelating trace metal ions, which are essential for the bacterial growth and bacterial function. Detailed studies have shown that 8-hydroxyquinoline when complexed with Fe(III), in 1:1 molar ratio, is highly effective and that the ligand and Fe(III) are both inactive when separated from each other. It has been suggested that 1:3 [Fe(III): 8-hydroxyquinoline] complex alone is capable of penetrating the cell membrane. Presumably, once the 1:3 complexes are inside the cell, they break down the more effective coordinatively unsaturated and charged 1:2 and 1:1 complex which bind too strongly to the membrane. It appears that the metal which increases the liposolubility of 8-hydroxyquinoline is necessary for the entry of this ligand molecule into the cell [46,47]

Certain metal chelates are active at low concentration against a range of bacteria, fungi and viruses. Thus, the organism Staphylococcus pyrogens, found in wound infections, is very resistant to many standard antibiotics but it succumbs dramatically to the complexes $[Fe(Me_4phen)_3]^{2+}$and $[Ru(Me_4phen)_2(acac)]^{+}$.

Different mechanisms have been put forth to explain the phenomenon. These include, amongst others, the transfer of the metal from the complex to the affected site where it exerts its toxic effect and the ligand rendering the metal ion fat soluble, thus making it act within the cell and the metal complex inactivating a virus by occupying sites on its surface which would normally be utilized in the initiation of the infection of the host cell.

The metal-ligand interaction in a biological environment assumes importance in that the metal may considerably influence the reactivity of the ligand by:

1. Changing the electron distribution in the ligand.

2. Masking a chemically active centre of the ligand.

3. Assembling the ligand molecules into a particular stereochemical form, and

4. Providing a conducting pathway for electron addition or removal.

3.3.1 Antibacterial activity

The *in vitro* antibacterial activity of the compounds were evaluated against two gram positive (*S. aureus* and *S. epidermidis*) and three gram negative (*K. pneumoniae, E. coli* and *P. vulgaris*) bacterial strains, and the results are illustrated in Table 3.10. It is

evident from Table 3.10 that ligand ANA doesn't show any activity against the tested strains, while Co(II) and Cu(II) complexes exhibited potent activity against *P. vulgaris* with MIC = 5.62 and 5.24 µg/mL, respectively. Cu(II) complex showed outstanding activity than the standard drug Streptomycin against *S. epidermidis* with MIC value of 10.51 µg/mL. The Co(II) and Zn(II) complexes registered promising inhibition against *S. aureus* with MIC = 12.5 and 12.5 µg/mL, respectively. The remaining compounds showed moderate to poor activity against the strains.

Table 3.10 Antibacterial activity of the compounds [MIC (µg/mL)]

Compound	*S. aureus*	*S. epidermidis*	*K. pneumoniae*	*E. coli*	*P. vulgaris*
Co(II)	12.5	25	25	50	**5.62**
Ni(II)	50	100	>100	50	>100
Cu(II)	25	**10.51**	25	25	**5.24**
Zn(II)	12.5	25	25	25	>100
Cd(II)	100	50	>100	>100	25
Pd(II)	100	50	>100	50	25
ANA	>100	>100	>100	>100	>100
Metal chlorides	NA	NA	NA	NA	NA
Streptomycin	6.25	12.5	12.5	6.25	3.25

NA: no activity

3.3.2 Antifungal activity

ANA and its metal complexes were investigated for their *in vitro* antifungal activity against few fungal strains such as *A. niger* and *P. notatum* and compared to standard drug Ketoconazole with minimum inhibitory concentration (MIC) values. The results of antifungal activity in MIC values of the tested compounds are presented in Table 3.11 and the results revealed that Cu(II) complex against *A. niger and P. notatum* and Co(II) complex against *A. niger* exhibited significant activity with MIC = 6.25, 6.25 and 6.25 µg/mL, respectively compared to reference control Ketoconazole. Zn(II) complex exhibited moderate activity against *A. niger and P. notatum* with MIC = 12.5 and 12.5 µg/mL. The remaining compounds showed poor activity against the tested strains.

Table 3.11 Antifungal activity of the compounds [MIC (µg/mL)]

Compound	*A. niger*	*P. notatum*
Co(II)	6.25	12.5
Ni(II)	50	50
Cu(II)	6.25	6.25
Zn(II)	12.5	12.5
Cd(II)	>100	>100
Pd(II)	50	50
ANA	>100	>100
Metal chlorides	NA	NA
Ketoconazole	3.12	3.12

NA- no activity

3.3.3 Antioxidant activity

The IC_{50} values of the ligand and its metal complexes are given in Table 3.12; by increasing the concentration of the compounds the scavenging activity also increases. The DPPH assay of the metal complexes was calculated as percentage inhibition (Fig. 3.15)**.** From the results, it is shown that the scavenging effect of the free ligand (IC_{50} =20.60 ± 1.38 µM) is significantly lower compared to metal complexes. The antioxidant activity of Zn(II) complex showed potent activity with IC_{50} value of 10.14 ± 2.50 µM. Ni(II) complex exerts significant activity with IC_{50} value of 11.39 ± 1.26 µM compared to standard drug. Cu(II), Pd(II) and Cd(II) complexes showed moderate activity while the remaining compounds exhibited poor activity. According to IC_{50} values, the scavenging activity order of the ligand and its metal complexes are Zn(II) > Ni(II) > Cu(II) > Pd(II) > Cd(II) > Co(II) > ANA.

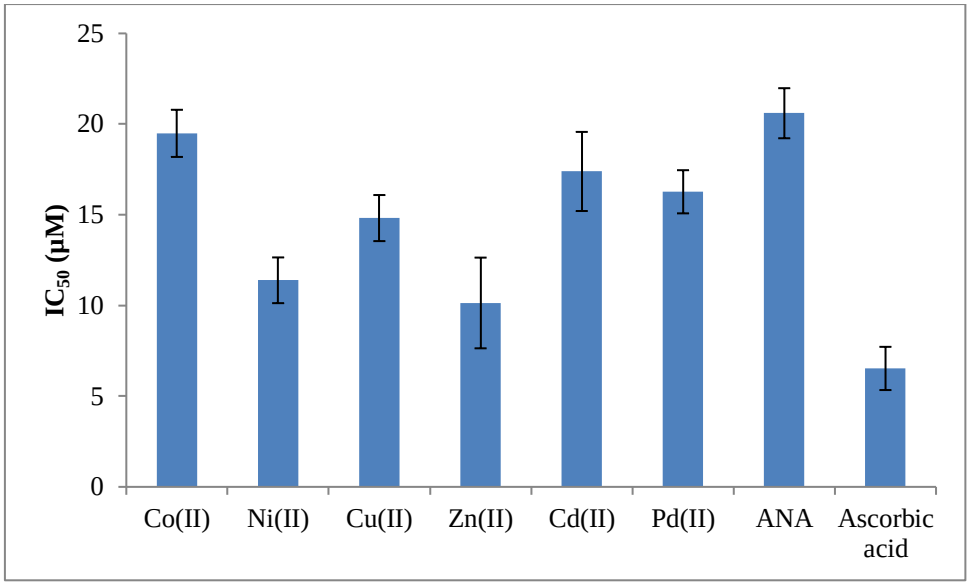

Fig. 3.15 Radical scavenging activity of ligand and metal complexes in terms of IC_{50} value (50% inhibition)

Table 3.12 IC_{50} (µM) values of DPPH scavenging activity of ligand and its metal complexes

Compound	IC_{50}
Co(II)	19.49 ± 1.30
Ni(II)	11.39 ± 1.26
Cu(II)	14.82 ± 1.27
Zn(II)	10.14 ± 2.50
Cd(II)	17.39 ± 2.18
Pd(II)	16.27 ± 1.19
ANA	20.60 ± 1.38
Ascorbic acid	6.53 ± 1.19

3.3.4 *In vitro* cytotoxicity investigations

A comparison of *in vitro* percentage cell viability for human carcinoma cell lines HepG-2 (hepatocellular carcinoma), IMR-32 (neuroblastoma) and Raw 264.7 (murine macrophage) at IC_{50} values of compounds and standard drug cisplatin (CP) are listed in Table 3.13. This data is used to generate survival curves for three carcinoma cell lines under investigation by plotting percentage cell viability vs percentage concentration graphs, which appear in Fig. 3.16. The effectiveness of the new compounds against

carcinoma cell lines is usually evaluated using a quantity known as the response parameter IC_{50} and comparing it with standard drug CP. IC_{50} is the concentration of the compounds or drug at which the cell viability gets inhibited by 50%. From the results, Zn(II) complex exhibited potent activity against IMR-32, HepG-2 and Raw 264.7 cell lines with IC_{50} values of 18.13 ± 0.31, 11.63 ± 0.43 and 5.39 ± 1.03 µM, respectively. The corresponding quantity for CP is 11.67 ± 0.35, 7.65 ± 1.03 and 3.58 ± 1.04 µM. Ni(II) complex showed good activity against IMR-32, HepG-2 with IC_{50} values of 20.51 ± 1.23 and 13.37 ± 1.12 µM. Cd(II) and Cu(II) complexes against IMR-32, Ni(II) complex against Raw 264.7 exhibited moderate activity with IC_{50} values of 41.69 ± 0.62, 45.12 ± 1.53 and 13.26 ± 0.19 µM, respectively. The remaining compounds Co(II), Pd(II) and ANA showed poor activity with IC_{50} values ranging from 43.21 ± 0.27 to 89.54 ± 0.15 µM. The potent Zn(II) and Ni(II) complexes were also examined in normal cell line against HEK293 with IC_{50} values of 30.34 ± 1.72and 43.98 ± 1.58 µM. The results seemed to suggest that the potent compounds are nontoxic.

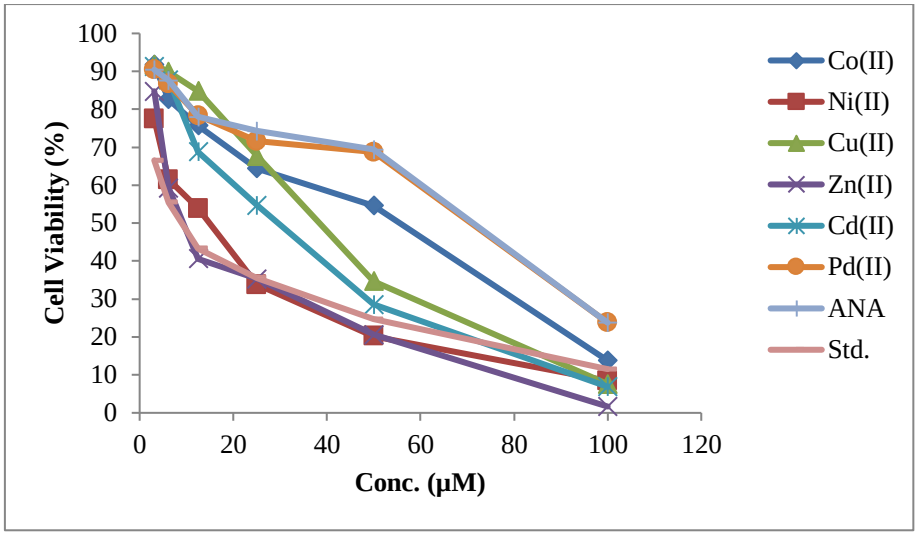

(a)

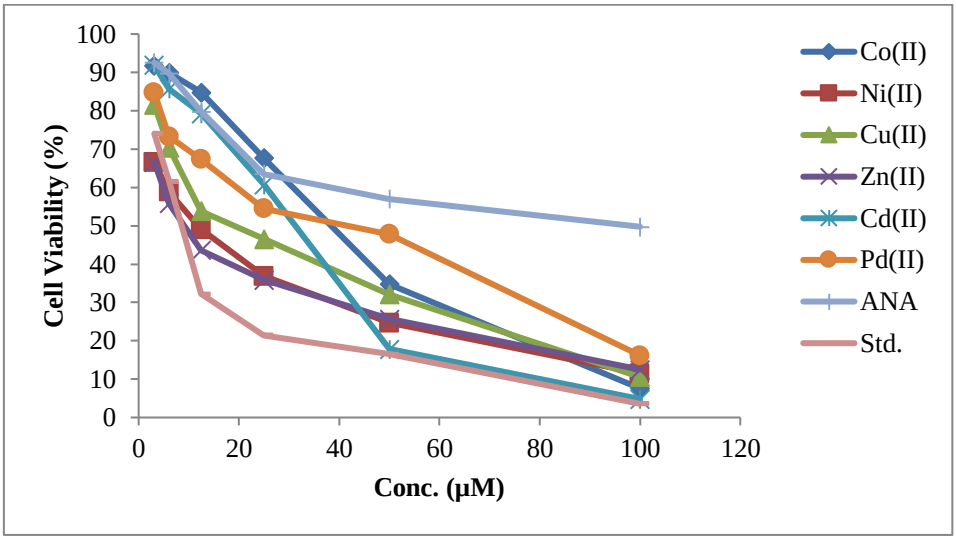

(b)

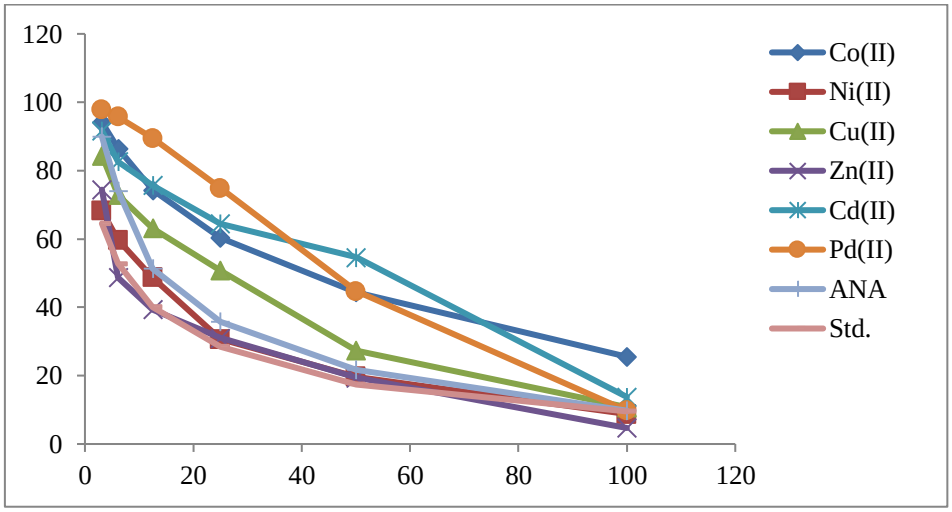

(c)

Fig. 3.16 Survival curves of cell lines **(a)** IMR-32, **(b)** HepG-2 and **(c)** Raw 264.7.

Table 3.13 Cytotoxic activities of newly synthesized compounds on human cancer cell lines IMR-32, HepG-2 and Raw 264.7 [*in vitro* (IC_{50} μM)][a]

Compound	IMR-32	HepG-2	Raw 264.7	HEK 293
Co(II)	51.76 ± 1.26	49.68 ± 1.12	55.43 ± 1.53	ND
Ni(II)	20.51 ± 1.23	13.37 ± 1.12	13.26 ± 0.19	43.98 ± 1.58
Cu(II)	45.12 ± 1.53	32.55 ± 0.48	35.38 ± 1.23	ND
Zn(II)	18.13 ± 0.31	11.63 ± 0.43	5.39 ± 1.03	30.34 ± 1.72
Cd(II)	41.69 ± 0.62	38.43 ± 0.11	50.81 ± 1.03	ND
Pd(II)	64.49 ± 1.15	43.21 ± 0.27	53.18 ± 1.34	ND
ANA	65.12 ± 1.02	89.54 ± 0.15	26.35 ± 1.04	ND
cisplatin	11.67 ± 0.35	7.65 ± 1.03	3.58 ± 1.04	ND

[a]values are expressed as mean ± SEM. ND stands for not determine

3.3.5 *In vivo* anti-inflammatory activity

Carrageenan induced rat paw edema method [48] was used to asses anti-inflammatory activity in rats. The animals were divided into three groups (n = 6). Where GP-I as a control, GP-II has received a standard, Indomethacin (5 mg/kg) and GP-III was administered with test compounds (10 mg/kg) orally. After 30 min, 0.1 mL of 1 % carrageenan suspension in normal saline was injected into the sub plantar region of the left hind paw of each rat to induce edema. The activity was measured with the help of plethysmographic method at different intervals (0, 1, 2, 4, and 6 h) (Fig. 3.17), the results of which are listed in Table 3.14. Compared to all complexes, Cu(II) and Zn(II) complexes have shown better activity at different time intervals 1 h, 2 h and 6 h.

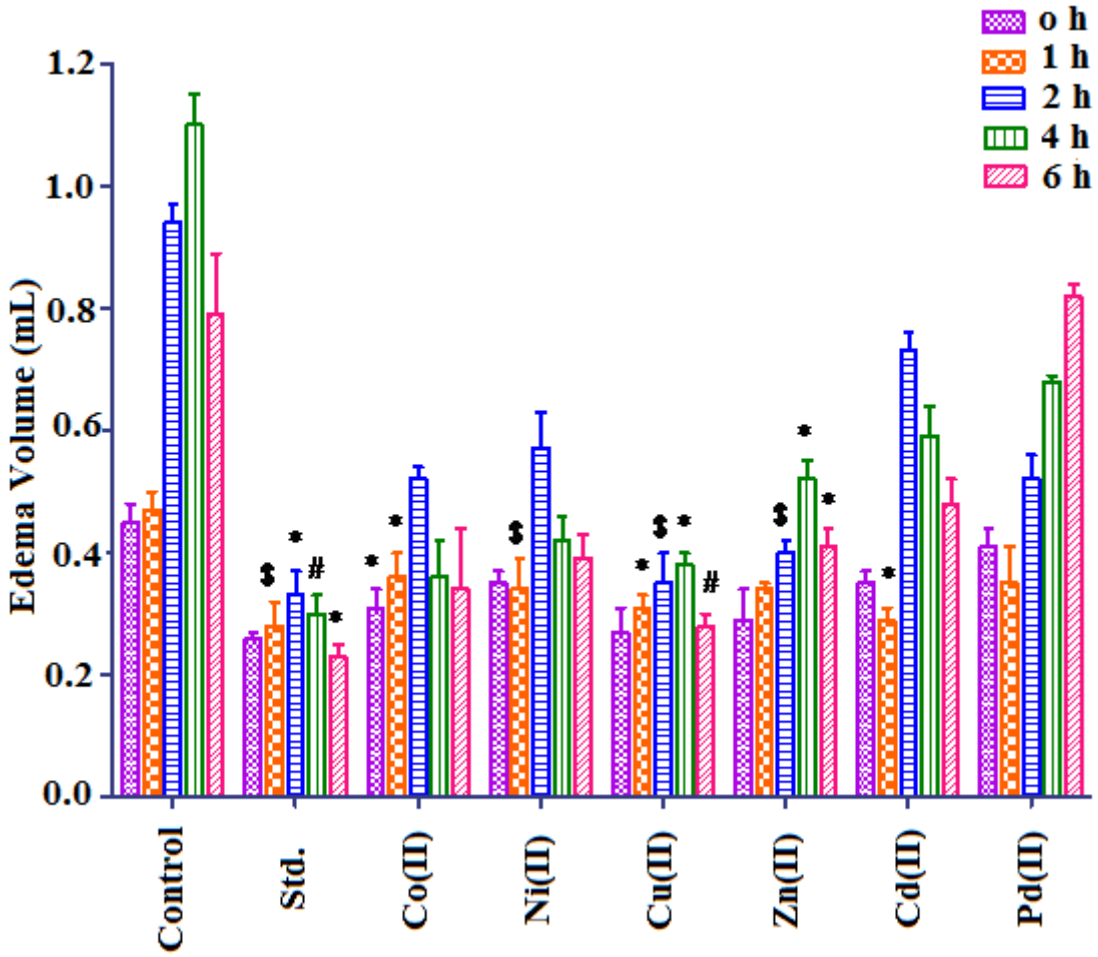

Fig. 3.17 The data are expressed as mean ± SD. The level of significance were assigned as $^{*}p < 0.05$, $^{\$}p < 0.01$, $^{\#}p < 0.001$ compared to standard using unifactorial analysis of variance (ANOVA) followed by Dunnett's multiple comparison test

Table 3.14 Anti-inflammatory activity screening by rat paw edema method

Compound	0 h	1 h	2 h	4 h	6 h
Control	0.45 ± 0.05	0.47 ± 0.02	0.94 ± 0.03	1.10 ± 0.06	0.79 ± 0.05
Standard	0.26 ± 0.01	0.28 ± 0.04	0.33 ± 0.08	0.30 ± 0.03	0.23 ± 0.02
Co(II)	0.31 ± 0.03	0.36 ± 0.09	0.52 ± 0.02	0.36 ± 0.06	0.34 ± 0.10
Ni(II)	0.35 ± 0.02	0.41 ± 0.04	0.57 ± 0.06	0.51 ± 0.04	0.37 ± 0.07
Cu(II)	0.28 ± 0.04	0.31 ± 0.02	0.35 ± 0.05	0.38 ± 0.02	0.28 ± 0.08
Zn(II)	0.29 ± 0.05	0.34 ± 0.01	0.40 ± 0.02	0.52 ± 0.03	0.41 ± 0.03
Cd(II)	0.35 ± 0.08	0.29 ± 0.02	0.73 ± 0.03	0.59 ± 0.05	0.48 ± 0.07
Pd(II)	0.41 ± 0.03	0.35 ± 0.07	0.52 ± 0.04	0.68 ± 0.01	0.82 ± 0.02

3.4 Molecular Docking

The ANA and its metal complexes Co(II), Ni(II), Cu(II), Zn(II), Cd(II) and Pd(II) bind strongly to the EGFR protein receptor by showing their minimum binding energies of -4.23 (ANA), -4.36, -4.64, -4.88, -5.79, -5.13, and -4.46 kcal/mol, respectively. When compared to the ligand, metal complexes interacted more effectively with the protein receptor, assuming that the ligand ANA in the complexes shows inclination to orient for the formation of grid protein. These binding energies in molecular docking studies strongly recommend *in vitro* anticancer activity results. The results are represented in Table 3.15 and Fig. 3.18. The docking results revealed that Zn(II) and Cd(II) complexes showed the least binding energies compared to other metal complexes against receptors EGFR with their binding energies of -5.79 and -5.13 kcal/mol. Hence EGFR was taken as the target protein receptors for an insightful and deep discussion into Zn(II) and Cd(II) complexes.

In Zn(II) complex, seven hydrogen bonds were observed between the ligands of metal complexes and EGFR protein receptor. Two hydrogen bonds, one with LYS721 and O-atom of the carbonyl group and the other with N atom of NH_2 group of one ANA having bond distances of 2.19 A° and 1.81 A° and bond angles of 132.27°, 139.32° in the complex were formed, One hydrogen bond with Arg817 and O-atom of carbonyl group having a bond distance 2.35 A° and a bond angle 117.14° was formed while another hydrogen bond was formed between ASN818 amino acid and hydrogen atom of NH_2 group with a bond distance of 2.34 A°, bond angle of 128.68° while the remaining three hydrogen bonds were formed with ASP831 amino acids. In that, two hydrogen atoms of NH_2 group were involved in bonding with bond distances of 2.05 A° and 2.72 A°, and bond angles of 105.86° and 98.12°, respectively, while another hydrogen bond was formed with hydrogen atoms of $–NH_2$ group of second ANA of the Zn(II) complex, with a bond distance of 1.93 A° and the bond angle of 135.44°. Among these hydrogen bonding interactions, Zn(II) complex forms some hydrophobic interactions with ARG817, ASN818, ASP831 and LYS721 amino acids.

In Cd(II) complex, two hydrogen bonds were formed when the ligand in the complex interacted strongly with protein receptor. One hydrogen bond was formed with ASP813 amino acid by interacting with H-atom of NH_2 group with a bond distance of 2.48 A° and bond angle of 124.53°, while another strong hydrogen bond was formed between ARG817 and N-atom of amine group with a bond distance of 2.15 A° and bond angle of 147.76°.

Besides these interactions, the complex had hydrophobic interactions with the following amino acids: ARG817 (2.89 A°), ASP813 (2.48 A°), LEU834, ALA835, ALA834, ALA698 and LYS851 amino acids.

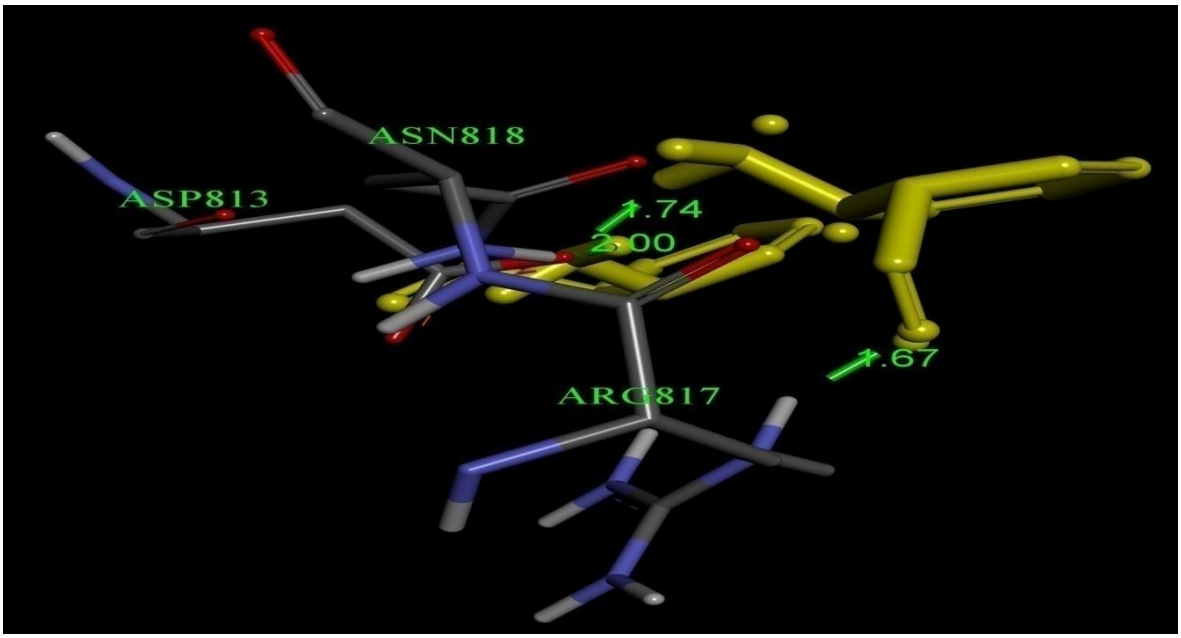

(a)

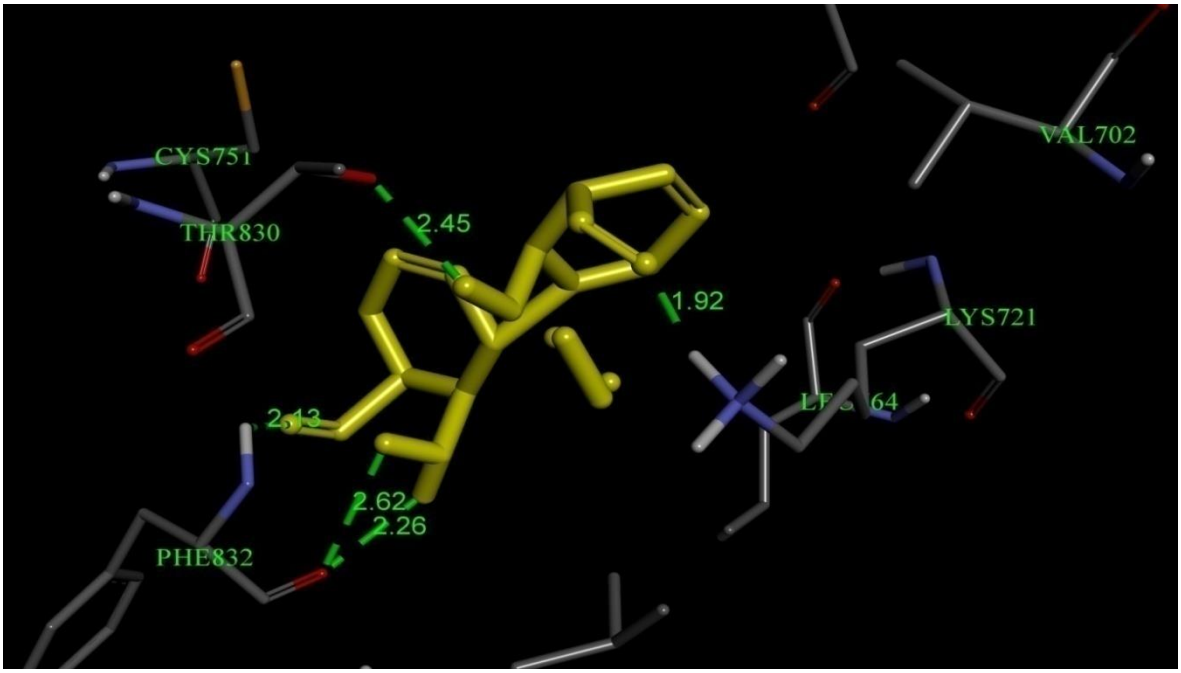

(b)

Fig. 3.18a-b The best docking pose and interactions of **(a)** Co(II) and (**b**) Ni(II) complexes.

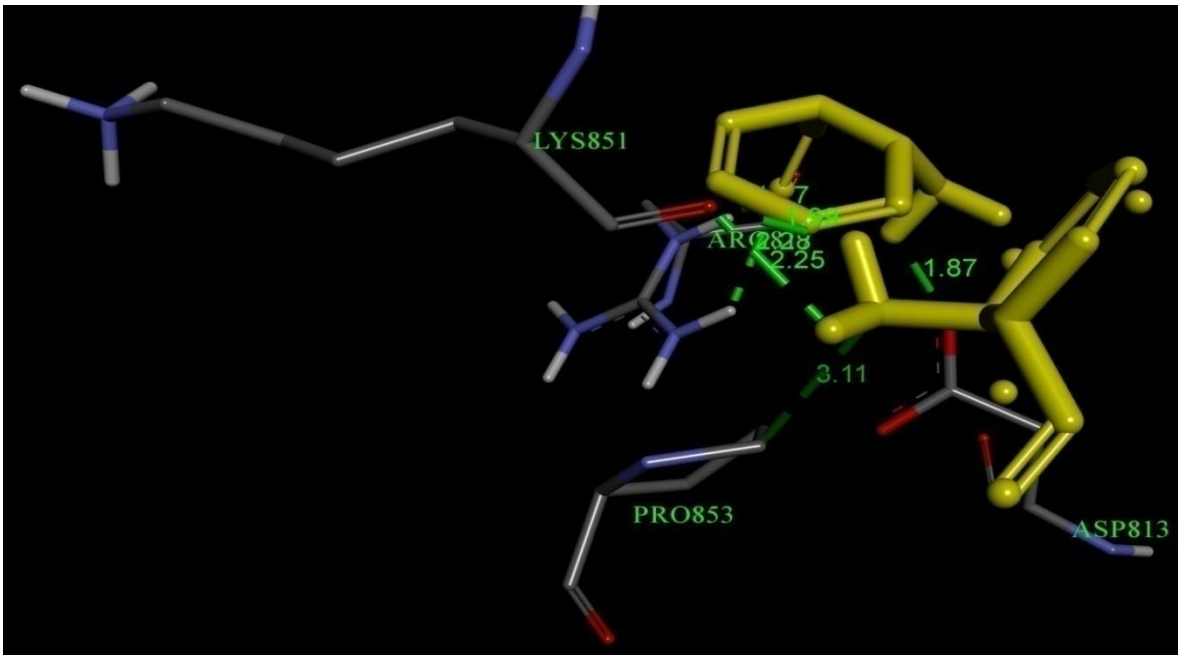

(c)

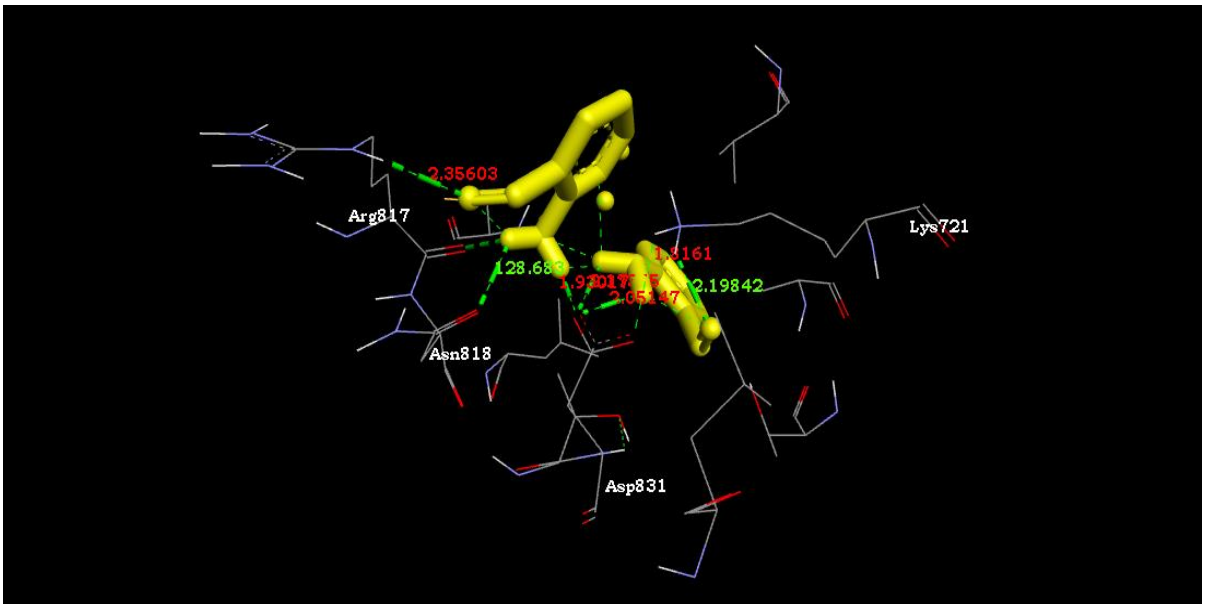

(d)

Fig. 3.18c-d The best docking pose and interactions of **(c)** Cu(II) and (**d**) Zn(II) complexes.

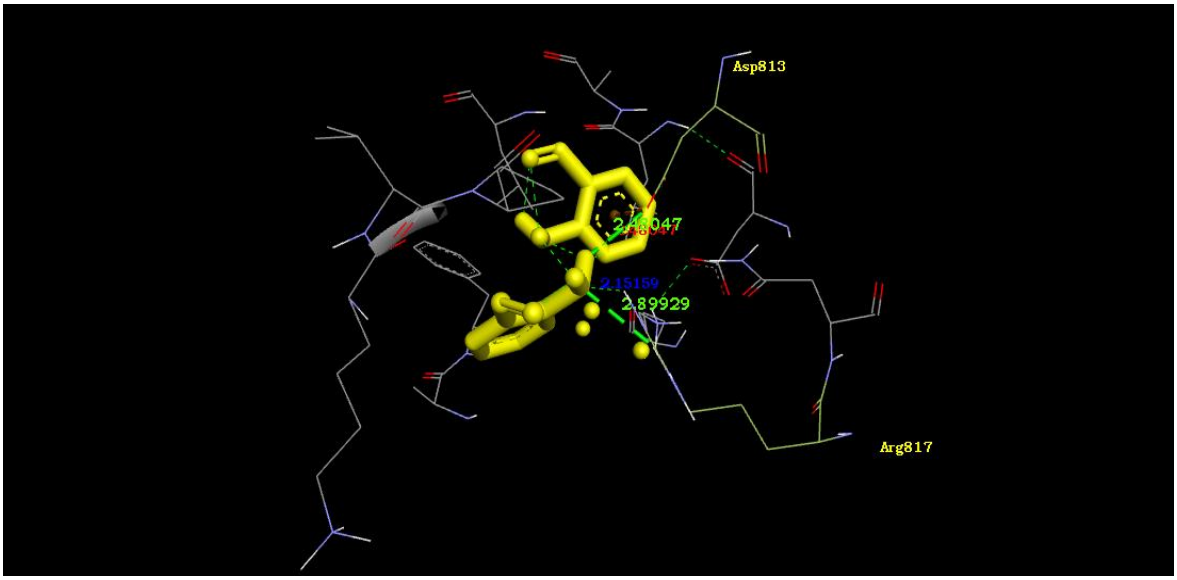

(e)

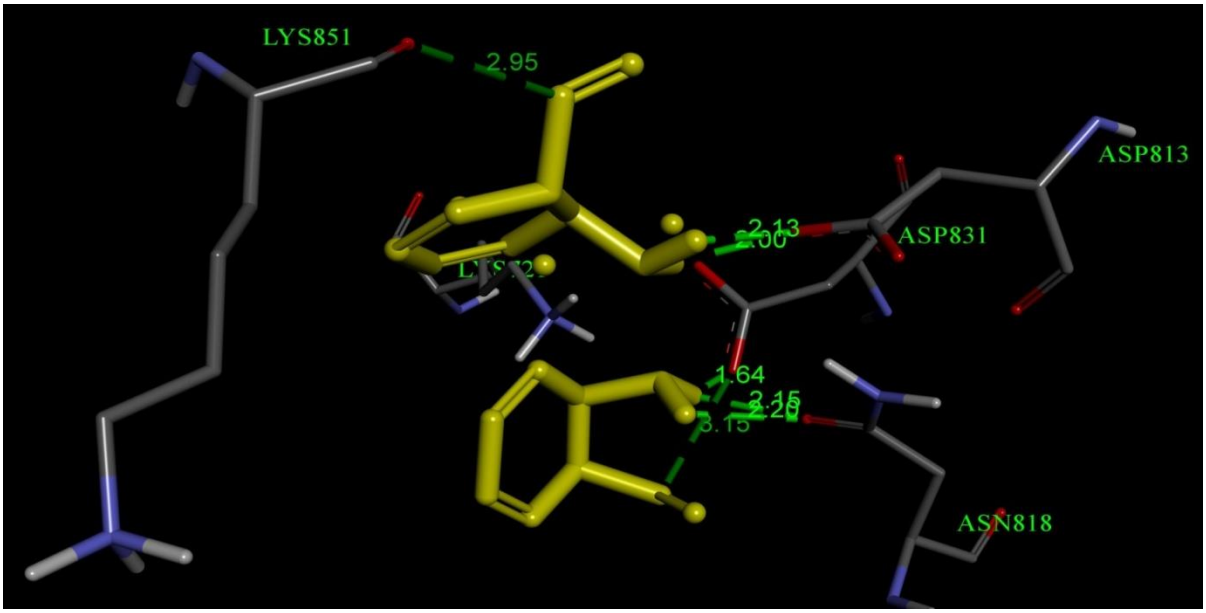

(f)

Fig. 3.18e-f The best docking pose and interactions of **(e)** Cd(II) and (**f**) Pd(II) complexes.

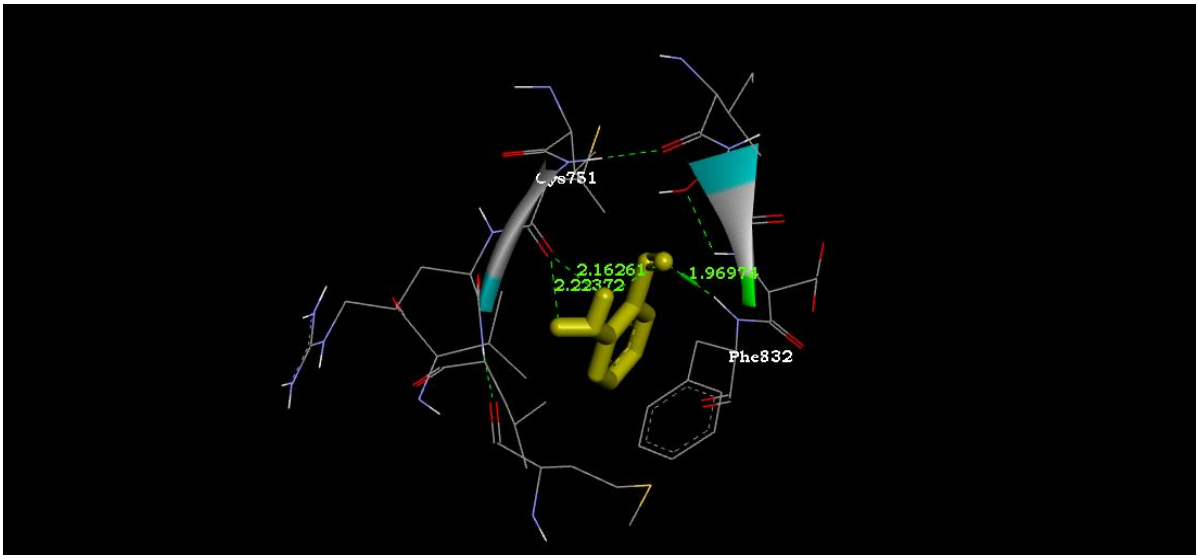

(g)

Fig. 3.18g The best docking pose and interactions of **(g)** ANA.

Table 3.15 Binding energies of metal complexes with EGFR protein receptor (PDB ID: 4hjo)

Compound	Binding energy (kcal/mol)	No. of H-bonds	Residues	Bond distances (A°)	Bond angles (°)
Co(II)	-4.36	3	ARG817, ASP813	1.67, 1.74, 2.00	144.19, 127.15, 133.84
Ni(II)	-4.64	5	LYS721, PHE832, THR830	1.92 2.13, 2.26, 2.62 2.45	166.60 111.24, 116.65, 93.19 116.28
Cu(II)	-4.88	5	ARG817, LYS851, ASP813	1.77, 2.28 1.99, 2.25 1.87	149.60, 131.35 95.19, 111.92 115.86
Zn(II)	-5.79	7	LYS721, ARG817, ASN818 ASP831	2.19, 1.81 2.35 2.05, 2.72, 1.93 2.34	132.27, 139.32 117.14 105.86, 98.12 135.44 128.68
Cd(II)	-5.13	2	ASP813 ARG817	2.48 2.15	124.53 147.76
Pd(II)	-4.46	5	ASP813 ASP818	2.00, 2.13 2.15, 2.20	108.90, 100.29 100.92, 98.08
ANA	-4.23	3	PHE832, CYS751	1.96 2.22, 2.16	149.19 96.97, 100.81

3.5 Catalytic applications in MCR

The catalytic activity of Zn(II) complex was investigated by employing it as a catalyst in the synthesis of fully substituted pyridines and dihydropyrano[2,3-*c*]pyrazoles. Zn(II) complexes have several advantages, which can be justified as follows. Zinc is one of the highly abundant, cheap and low toxic metals in the periodic table. It can be easily separated or extracted in high purity from the corresponding minerals than many other metals. The biological relevance of zinc makes it an essential trace element to regulate enzymatic function of both animal and plant kingdom. Besides, at present, the current

research in 'green chemistry' is focusing on the use of cheap and low toxic metals as catalysts or stoichiometric reagents to develop environmentally sustainable protocols in organic synthesis and pharmaceutical synthesis [49]. In line with these precedents, the use of zinc based catalysts (homogeneous/heterogeneous) and reagents would be a good choice to meet the requirements of green chemistry [49b,50].

Since the discovery of first organometallic diethyl zinc, a variety of catalytic and stoichiometric reagent applications of zinc compounds have been found in organic synthesis. For instance, the use of zinc in Negishi coupling, Reformatskii and Fukuyama reactions has been recognized as breakthrough reactions of organic synthesis [51,52]. However, as compared to other metals, the use of zinc compounds in organic synthesis is still at a developing stage due to its position in the periodic table that placed zinc between transition elements and main group elements. The filled d-orbital electronic configuration provides different chemistry to zinc than those of other d-block elements and more related chemistry to main group elements, which is quite simple and predictable. However, recent trends in green chemistry have strongly recommended the development of cheaper and low toxic zinc based organic transformations of C-C as well as C-heteroatom bond forming reactions for sustainable environment [49c,53].

The concept of multicomponent reaction (MCR) is one type of modern perspective emerged in green chemistry, wherein three or more than three components reacts in one-pot through sequential reactions and provide the desired product on a selective basis by reducing the waste. MCRs are indeed cost-effective, time-saving and environmentally benign as compared to step-by-step reactions of traditional organic synthesis in achieving the desired final product. A majority of MCRs require multifunctional catalyst to control the selectivity in the sequential reactions. At present, catalyzed MCRs are common practice to synthesize a variety of heterocycles and heteroatomic organic compounds [54].

We are interested in developing a facile MCR protocol to synthesize highly substituted pyridines and pyranopyrazole in view of their exciting applications in medicinal and materials chemistry. The use of a variety of homogeneous and heterogeneous catalysts has been reported previously to synthesize various densely substituted pyridines *via* traditional organic synthesis or MCR synthesis [55,56a,56b]

In this regard, $Zn(ANA)_2Cl_2$ complex was chosen as a catalyst for the synthesis of a variety of fully substituted pyridines and dihydropyrano[2,3-*c*]pyrazoles.

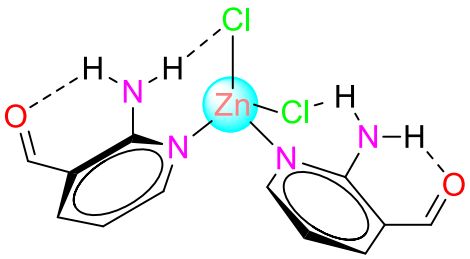

$[Zn(ANA)_2Cl_2]$ complex

3.5.1 Synthesis of fully substituted pyridines

Initially, we chose to investigate a four component sequential one-pot reaction between malononitrile, ketone and ammonium acetate as partners to aromatic aldehydes to form a variety of fully substituted pyridines in environmentally friendly solvent ethanol (Scheme 1) under RT conditions. It is a matter of interest that the green aspect is connected not only with the use of water as reaction medium but also with the possibility to use other green solvents such as ethanol to improve yields and selectivity.

$Zn(ANA)_2Cl_2$ complex was prepared on mixing freshly prepared solutions of ANA dissolved in 20 mL ethanol and $ZnCl_2.4H_2O$ dissolved in 10 mL ethanol, at reflux temperature for about 3 h. At the end of the reaction, excess ethanol was removed in vacuum and filtered after cooling to obtain pure $Zn(ANA)_2Cl_2$ complex. Further, by using $[Zn(ANA)_2Cl_2]$ complex, the studies were extended to explore the catalytic ability of Zinc in MCR. It is worth noting that previously there were very few reports in the literature on the catalytic MCR synthesis of fully substituted pyridines. However, there was no information about the use of zinc catalysts in the MCR synthesis of fully substituted pyridines.

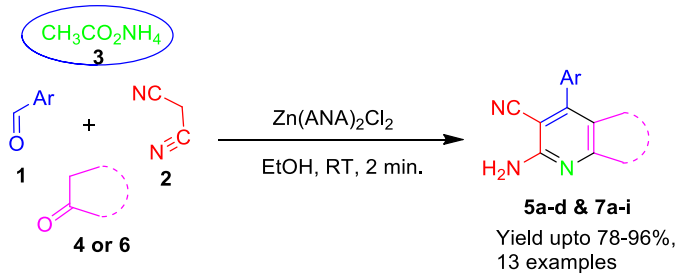

Scheme 1 Synthesis of fully substituted pyridines

Initially we chose to probe a four-component sequential one-pot reaction (MCR) between benzaldehyde (**1a)** malononitrile (**2**), ammonium acetate (**3**) and 2-butanone **(4)** (acyclic ketone) in ethanol in the presence of different zinc salts and a $Zn(ANA)_2Cl_2$ complex for the synthesis of substituted pyridine **5a**. The details of the reaction and the results are given in Table 3.16.

Table 3.16 Optimization of reaction parameters for the synthesis of **5a**[a].

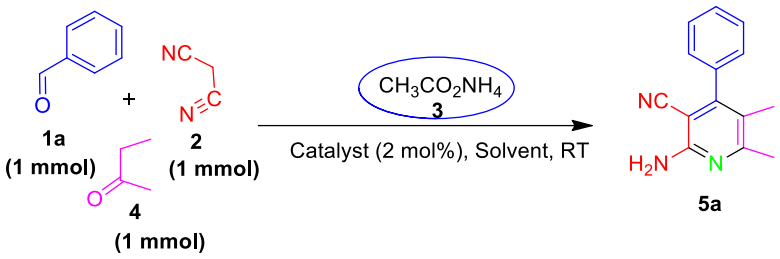

Entry	Catalyst	Solvent	Temperature[b]	Yield (%)[c]
1	No Catalyst	EtOH	RT	--
2	$Zn(OAc)_2$	EtOH	RT	24
3	$Zn(OTf)_2$	EtOH	RT	36
4	$ZnCl_2$	EtOH	RT	35
5	$Zn(NO_3)_2$	EtOH	RT	30
6	$ZnBr_2$	EtOH	RT	32
7	$Zn(BF_4)_2$	EtOH	RT	35
8	ZnI_2	EtOH	RT	35
9	$CuCl_2$	EtOH	RT	28
10	$CuBr_2$	EtOH	RT	26
11	$Zn(ANA)_2Cl_2$	EtOH	RT	92
12	$Zn(ANA)_2Cl_2$	THF	RT	22

13	$Zn(ANA)_2Cl_2$	CH_3CN	RT	18
14	$Zn(ANA)_2Cl_2$	DCM	RT	20
15	$Zn(ANA)_2Cl_2$	Dioxane	RT	Trace
16	$Zn(ANA)_2Cl_2$	Benzene	RT	Trace

[a]All the reactions were carried out by using benzaldehyde **1a** (1 mmol), malononitrile **2** (1 mmol), ammonium acetate (**3**) and 2-butanone **(4)** (1 mmol) in water at room temperature to synthesize the compound **5a**. [b] Progress of the reaction was monitored by TLC. [c] Isolated yields.

The intended MCR was not observed in the absence of catalyst under RT conditions in ethanol (Table 3.16, entry 1). Later, we investigated the above MCR in the presence of different zinc salts including $Zn(OAc)_2$, $Zn(OTf)_2$, $ZnCl_2$, $Zn(NO_3)_2$, $ZnBr_2$, $Zn(BF_4)_2$, ZnI_2 (Table 3.16, entries 2-8) and copper salts $CuCl_2$ and $CuBr_2$ as catalysts (Table 3.16, entries 9, 10) under RT conditions. However, it was noticed that the simple zinc salts and copper salts did not facilitate the intended MCR under RT. In this situation, when $Zn(ANA)_2Cl_2$ was employed as a catalyst, there was a dramatic acceleration in the proposed MCR at RT which yielded the expected/desired substituted pyridine **5a** selectively just in 2 minutes in good yield (92%, Table 3.16, entry 11). It is also important to note that the above $Zn(ANA)_2Cl_2$ catalyzed reaction was observed to be sluggish and non-selective in non-protic solvents, THF, CH_3CN, DCM, Dioxane, Benzene (Table 3.16, entries 12-16). This information outlines that the choice of solvent is also one of the key factors in this catalyzed MCR.

Table 3.17 Recyclability studies of the catalyst

S. No.	**Cycle No.**	**Reaction time (min.)[a]**	**Yield (%)[b]**
1	1	2	92
2	2	2	92
3	3	4	90
4	4	6	83
5	5	6	82

[a] Reaction progress was monitored by TLC, [b] Isolated yield

Literature reveals that there were few similar MCR strategies (malononitrile, ketone, ammonium acetate and aromatic aldehyde) developed with or without catalysts [56,57]. However, except the one that uses Ag(I)-NHC catalysts [56a], the remaining methodologies reported the requirement of refluxing or microwave conditions and longer reaction times [57]. Our results indicate the efficiency of zinc catalyst ($Zn(ANA)_2Cl_2$) in catalyzing MCR at just RT conditions to produce **5a** to meet the requirements of green catalysis. The solid product of **5a** obtained in our work was further identified and quantified on the basis of its analytical and spectral data Using the above optimized conditions ($Zn(ANA)_2Cl_2$, 2 mol%, 2 min, RT, ethanol) for four-component MCR, we extended substrate scope to synthesize some diverse fully substituted pyridines. We have used various structurally different aldehydes (**1b-g**), acyclic ketones (**4**) and cyclic ketones (**6a-c**)) in the MCR to study the electronic effects. The results are summarized in Scheme 2. The results indicate that $Zn(ANA)_2Cl_2$ is highly efficient in facilitating the MCRs of Scheme 2 and providing good yields in short reaction times. The substrates of MCR bearing electron donating or electron-withdrawing groups on the aromatic ring proceeded smoothly and formed the corresponding fully substituted pyridines in good yields.

Structures of the substituted pyridines (**5a-d** & **7a-i**, Scheme 2) were established on the basis of elemental analysis and spectral data (^1H and ^{13}C NMR).

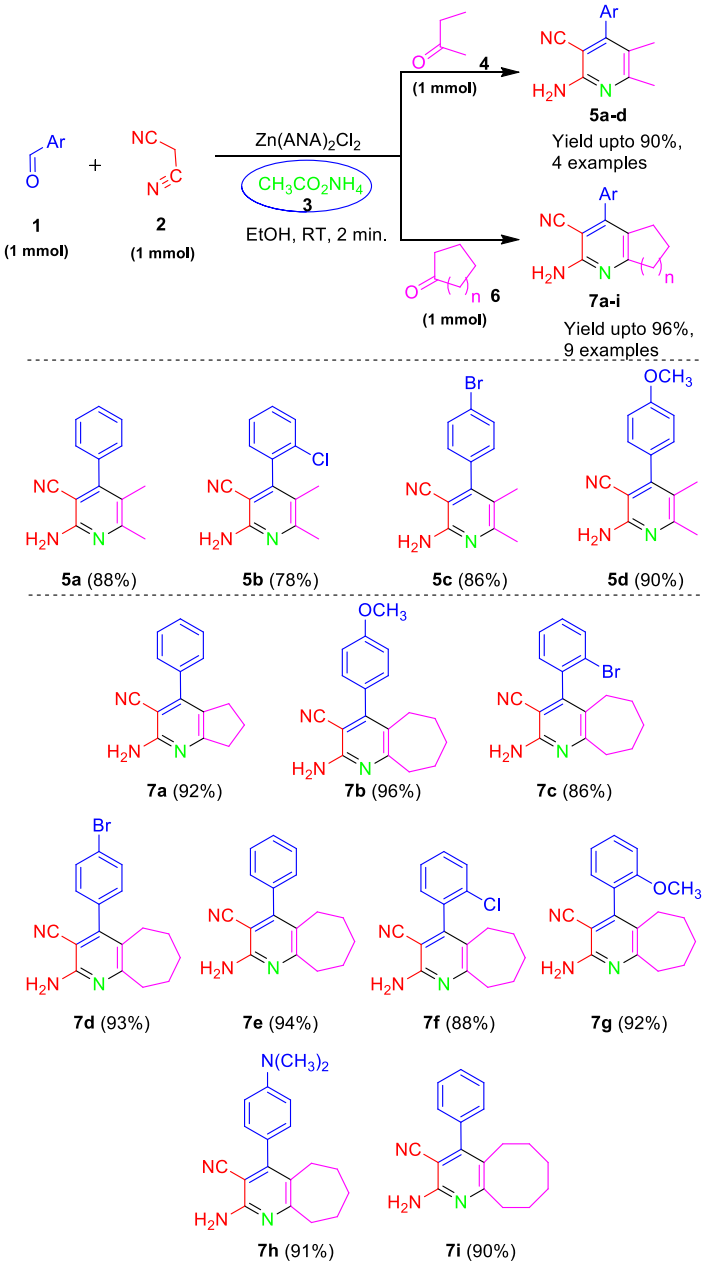

Scheme 2 Synthesized fully substituted pyridine derivatives

Finally, based on the results obtained in our work and previous reports concerning the MCR synthesis of fully substituted pyridines including control experiments, a plausible mechanism has been deduced in Scheme 3. The reaction may proceed *via* forming enamine (**A**) the condensed product of ketone and ammonium acetate, then activated by $Zn(ANA)_2Cl_2$, which then reacts with alkylidenemalononitrile (**B**) (Knoevenagel condensed product of aldehyde with malononitrile) to give intermediate (**C**) (Michael adduct). The Michael adduct then undergoes cycloaddition and isomerization to give 1,4-dihydropyridine (**D**). The subsequent oxidative aromatization of

1,4-dihydropyridine (**D**) under air atmosphere will produce the desired fully substituted pyridines (**5a-d & 7a-i**) as shown in Scheme 3.

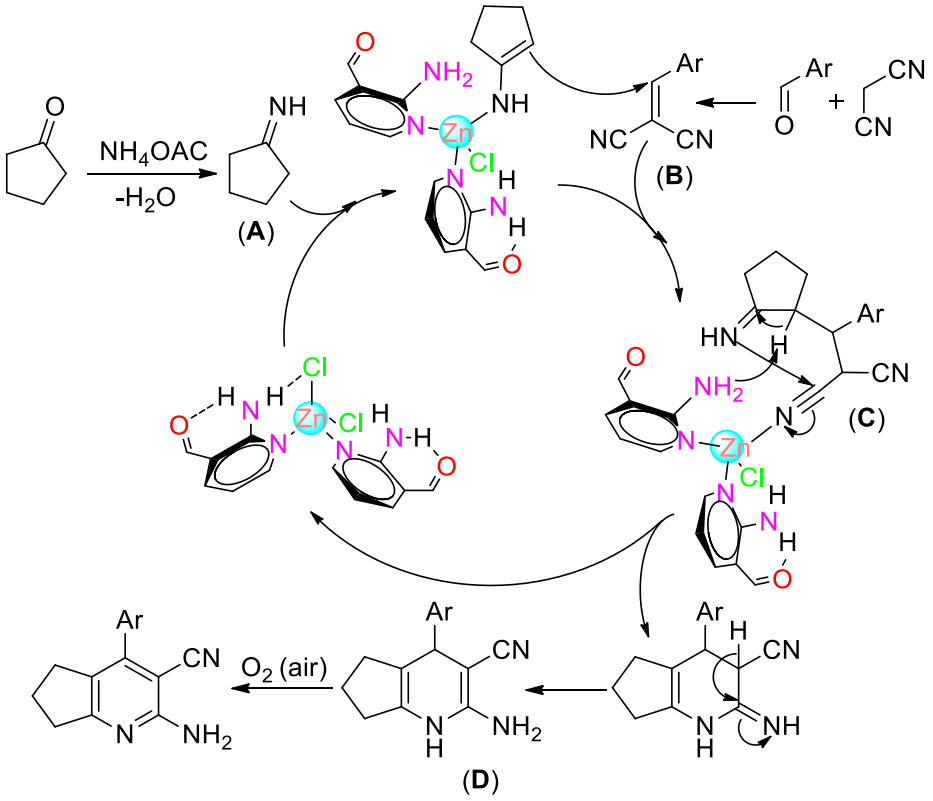

Scheme 3 A plausible mechanism for the formation fully substituted pyridines

3.5.2 Synthesis of substituted dihydropyrano[2,3-c]pyrazoles

In preliminary experiments, the three-component sequential one-pot reaction (MCR) between benzaldehyde (**8a**), malononitrile (**9**), and 3-methyl-1-phenyl-2-pyrazoline-5-one (**10**), in water as a solvent at room temperature, and the scope of a variety of potential catalyst materials. The details of the reaction and the results are given in Table 3.18. There was no MCR sequence observed without any catalyst (Table 3.18, entry 1). Later, the above MCR was investigated in the presence of different zinc and copper salts including $Zn(BF_4)_2$, $Zn(OTf)_2$, $ZnBr_2$, $Zn(NO_3)_2$, (Table 3.18, entries 2-5) and copper salts $Cu(OAc)_2$ and $CuBr_2$ as catalysts (Table 3.18, entries 6,7) at RT conditions. However, when 5 mol% of $Zn(ANA)_2Cl_2$ was employed as catalyst, product **11a** (Scheme 4) formed with a yield 79% in 12 min. (Table 3.18, entry 8). After that, the same reaction was carried out by using 10, 15 and 20 mol % of $Zn(ANA)_2Cl_2$ catalyst, the results were impressive producing the substituted dihydropyrano[2,3-c]pyrazoles (**11a**) selectively and at room temperature in good yields at different times (Table 3.18, entries 8-11). The catalyst with 10 mol% was the best catalyst in water resulting in high yields with low

reaction time (Table 3.18, entry 9). Continuing the work, we have also investigated the above MCR to get the optimized reaction condition, the reaction further proceeded with 10 mol% of $Zn(ANA)_2Cl_2$ catalyst for 30 min. (Table 3.18, entry 12) without any increase yields. There was also no progress in the above MCR when carried out at different temperatures (Table3.18, entries 13,14). The catalyzed MCRs of present study in water are found to be slightly exothermic in the beginning as observed in other works. It is also important to note that the above catalyzed reaction was observed to be sluggish and non-selective in non-protic solvents; THF, CH_3CN, and CH_2Cl_2 and finally ended up with a mixture of products. This information outlines that the choice of solvent is also one of the key factors in the catalyzed MCR.

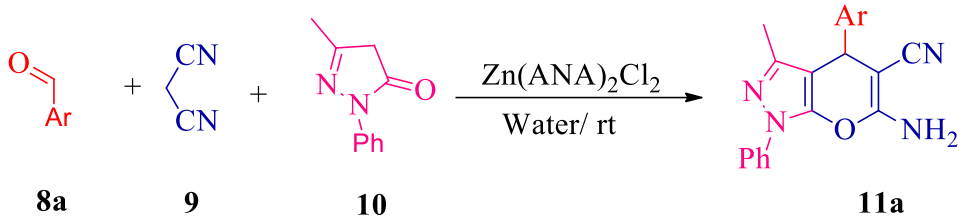

8a **9** **10** **11a**

Scheme 4 The synthetic pathway of compounds **11a**

Table 3.18 Optimization of reaction conditions for the synthesis **11a**[a]

Entry	Catalyst (mol%)	Temperature (˚C)	Time[b]	Yield (%)[c]
1	No Catalyst	rt	60 min.	Trace
2	$Zn(BF4)_2$	rt	45 min.	40
3	$Zn(OTf)_2$	rt	45 min.	35
4	$ZnBr_2$	rt	30 min.	25
5	$Zn(NO_3)_2$	rt	30 min.	35
6	$Cu(OAc)_2$	rt	30 min.	Trace
7	$CuBr_2$	rt	30 min.	Trace
8	$Zn(ANA)_2Cl_2$ (5 mol%)	rt	12 min.	79
9	$Zn(ANA)_2Cl_2$ (10 mol%)	rt	5 min.	88
10	$Zn(ANA)_2Cl_2$ (15 mol%)	rt	8 min.	85
11	$Zn(ANA)_2Cl_2$ (20 mol%)	rt	7 min.	85
12	$Zn(ANA)_2Cl_2$ (10 mol%)	rt	10 min.	88

13	$Zn(ANA)_2Cl_2$ (10 mol%)	60	5 min.	83
14	$Zn(ANA)_2Cl_2$ (10 mol%)	80	5 min.	80

[a] All the reactions were carried out by using benzaldehyde **8a** (1 mmol), malononitrile **9** (1 mmol) and 3-methyl-1-phenyl-2-pyrazoline-5-one **10** (1 mmol) in water at room temperature to synthesize the compound **11a**. [b] Progress of the reaction was monitored by TLC. [c] Isolated yields.

In order to recycle $Zn(ANA)_2Cl_2$, the reaction mixture was filtered and the residue was quenched two times with ethyl acetate to separate the crude product after the first catalytic run. The water layers dried and were reused for the next catalytic runs. It has been noticed that up to four successive catalytic yields of dihydropyrano[2,3-c]pyrazoles are almost in the close range (entries 1-4 of Table 3.18) and there was no considerable agglomeration of $Zn(ANA)_2Cl_2$. However, the yields were slowly reduced from the fifth cycle (entry 5 of Table 3.18) due to increase in operation time. This is attributed to the decrease of multi-component activity of the catalyst due to the percentage of catalyst and metal deposition, which inhibits the activity of active sites of the catalyst. The recyclability studies of the catalyst and the derivatives of the compounds (**11a-l**) are shown in Table 3.18 and 3.19.

Table 3.19 Recyclability studies of the catalyst ($Zn(ANA)_2Cl_2$ complex)

S. No.	Cycle No.	Reaction time (min.)[a]	Yield (%)[b]
1	1	5	86
2	2	5	86
3	3	8	85
4	4	8	85
5	5	10	80

[a] Reaction progress was monitored by TLC, [b] Isolated yield

Table 3.20 Time and yields for the formation of dihyhdropyrano[2,3-c]pyrazoles **11a-l**

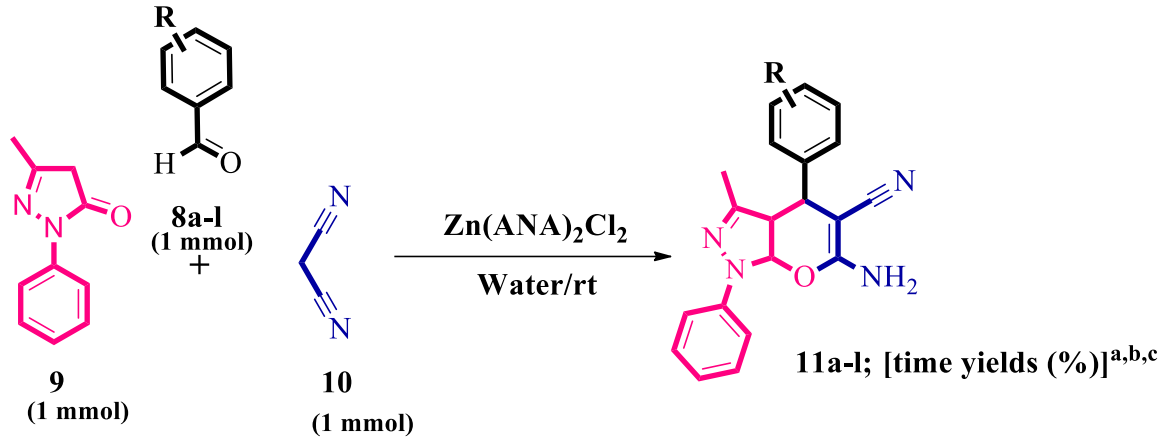

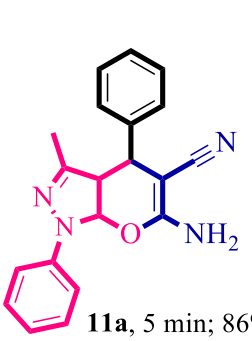

11a, 5 min; 86%

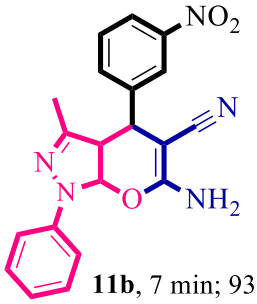

11b, 7 min; 93%

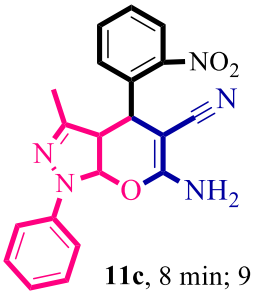

11c, 8 min; 91%

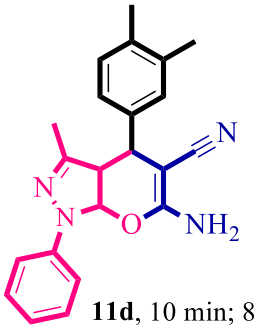

11d, 10 min; 85%

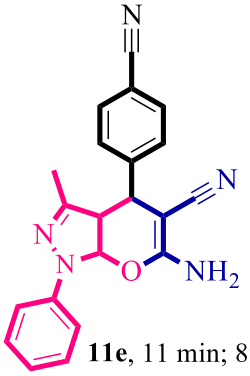

11e, 11 min; 89%

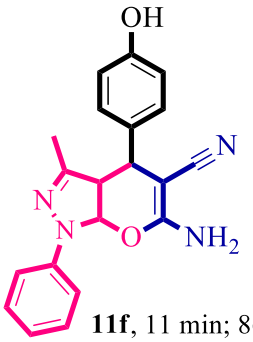

11f, 11 min; 86%

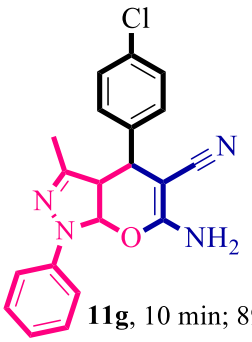

11g, 10 min; 89%

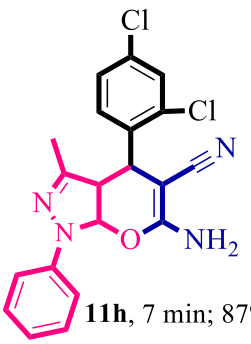

11h, 7 min; 87%

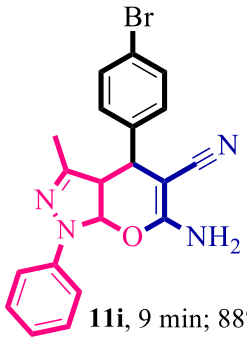

11i, 9 min; 88%

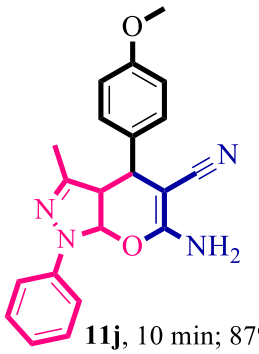

11j, 10 min; 87%

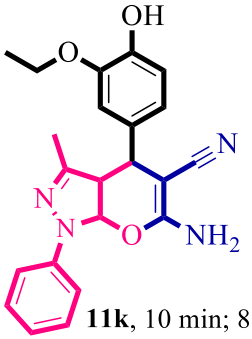

11k, 10 min; 85%

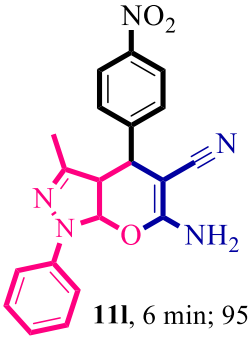

11l, 6 min; 95%

[a] All the reactions were carried out by using aromatic aldehydes **8a-l**, 3-methyl-1-phenyl-2-pyrazoline-5-one **9** and malononitrile **10** as starting material in water with the $Zn(ANA)_2Cl_2$ complex as catalyst. [b] Progress of the reaction was monitored by TLC. [c] Isolated yields (%).

Employing the same reaction conditions for the synthesis of **11a** (RT, $Zn(ANA)_2Cl_2$ (10 mol%, 5 min, water), we investigated the scope of the reaction with a variety of structurally different aldehydes (**8b-l**) in combination with malononitrile (**9**) and 3-methyl-1-phenyl-2-pyrazoline-5-one (**10**) for the three component condensation reaction. The results are depicted in Table 3.19. The substrates of MCR bearing electron donating or electron-withdrawing groups on the aromatic ring proceeded smoothly and formed the corresponding substituted dihydropyrano[2,3-c]pyrazoles in good yields (85-95%) under the chosen conditions. This reaction was considered as a green reaction because of its mild reaction condition, use of environmentally benign solvent and reusable catalyst.

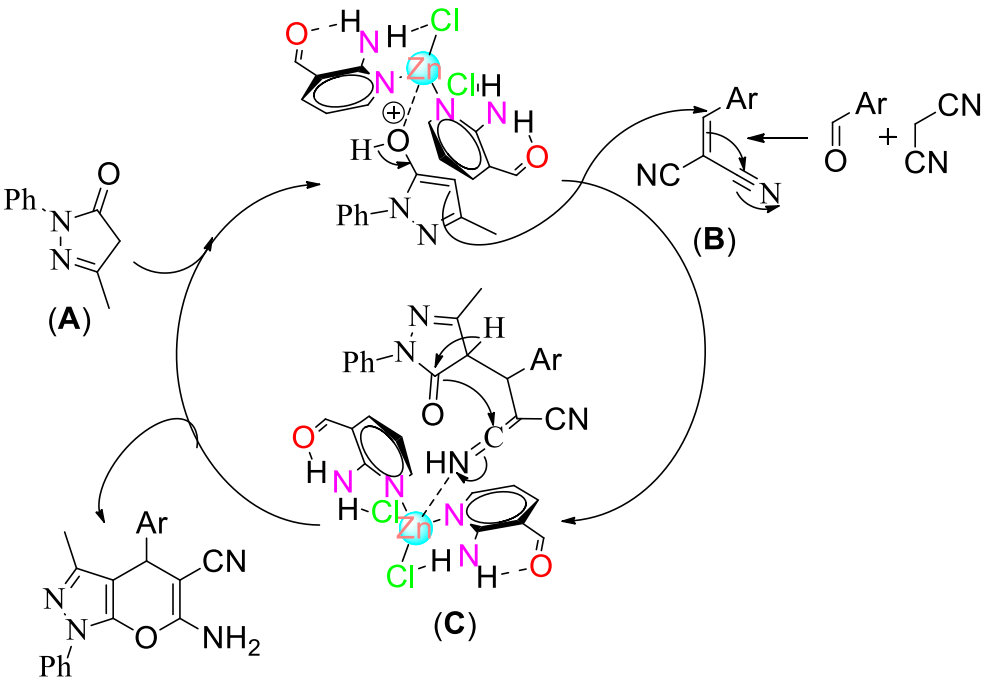

Scheme 5 Possible mechanism for the formation of Pyranopyrazole *via* catalyzed by $Zn(ANA)_2Cl_2$

Based on previous reports and current results in the MCR synthesis of Pyranopyrazole, a plausible mechanism is proposed and depicted in Scheme 5 which involves a domino Michael addition-tautomerism-*O*-cyclization sequence of reactions. The reaction may proceed *via* forming chelation between phenylmethylpyrazolone and $Zn(ANA)_2Cl_2$ complex (A) and which then reacts with alkylidenemalononitrile (B) (Knoevenagel condensed product of aldehyde with malononitrile) to give intermediate (C) (Michael adduct). The Michael adduct then undergoes *O*-cyclization to give Pyranopyrazoles.

3.6.1 General procedure for the synthesis of pyridines (5a-d & 7a-i)

Aromatic aldehydes (**1**) (1 mmol) and malononitrile (1 mmol) was dissolved in EtOH (10 mL) and added the ethanolic solution of cyclic ketone/ethyl methyl ketone (**2a-c** or **2d**) (1.2 mmol), ammonium acetate (1.2 mmol) and catalyst $Zn(ANA)_2Cl_2$ (2 mol%) were stirred over a period of 2 min. at room temperature. Complete consumption of starting material as judged by TLC and GC analysis. The reaction mass was filtered and washed with ethanol to obtained off-white solid crude product which was subjected to recrystalization in hot ethyl acetate to afford pure products (**5a-d** & **7a-i**).

3.6.2 Spectral data of Pyridine compounds (5a-d & 7a-i)

2-Amino-5,6-dimethyl-4-phenyl-nicotinonitrile (5a)

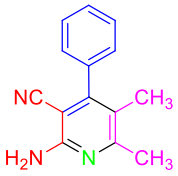

The product was obtained as off-white solid. Yield: 88%. M.p.: 240-241 ˚C. ^{1}H NMR (400 MHz, $CDCl_3$): δ, ppm 1.95 (s, 3H, CH_3), 2.44 (s, 3H, CH_3), 5.05 (s, 2H, NH_2), 7.23-7.50 (m, 5H). ^{13}C NMR (100 MHz, $CDCl_3$): δ, ppm 15.30, 23.72, 89.72, 116.80, 119.69, 128.33, 128.64, 128.77, 136.79, 153.86, 157.23, 161.57. Anal. Calcd. (%) for $C_{14}H_{13}N_3$: C, 75.31; H, 5.87; N, 18.82. Found: C, 75.37; H, 5.89; N 18.78.

2-Amino-4-(2-chloro-phenyl)-5,6-dimethyl-nicotinonitrile (5b)

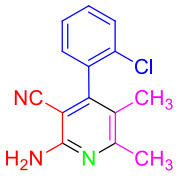

The product was obtained as off-white solid. Yield: 78%. M.p.: 251-252 ˚C. ^{1}H NMR (400 MHz, $CDCl_3$): δ, ppm 1.88 (s, 3H, CH_3), 2.46 (s, 3H, CH_3), 5.03 (s, 2H, NH_2), 7.17-7.53 (m, 4H). ^{13}C NMR (100 MHz, $CDCl_3$): δ, ppm 14.89, 23.66, 116.20, 120.43, 127.0, 127.22, 129.81, 129.94, 130.16, 130.30, 132.45, 151.14, 157.13, 161.71. Anal. Calcd. (%) for $C_{14}H_{12}ClN_3$: C, 65.25; H, 4.69; N, 16.30. Found: C, 65.29; H, 4.74; N, 16.36.

2-Amino-4-(4-bromo-phenyl)-5,6-dimethyl-nicotinonitrile (5c)

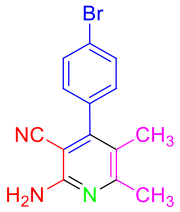

The product was obtained as off-white solid. Yield: 86%. M.p.: 265-266 °C. ^{1}H NMR (400 MHz, $CDCl_3$): δ, ppm 1.94 (s, 3H, CH_3), 2.44 (s, 3H, CH_3), 5.02 (s, 2H, NH_2), 7.11 (d, *J* = 8.2 Hz, 2H), 7.63 (d, *J* = 8.1 Hz, 2H). ^{13}C NMR (100 MHz, $CDCl_3$): δ, ppm 15.3, 23.79, 89.94, 112.48, 119.53, 129.72, 130.07, 131.98, 132.12, 153. 68, 157.23, 161.92. Anal. Calcd. (%) for $C_{14}H_{12}BrN_3$: C, 55.65; H, 4.0; N, 13.91. Found: C, 55.57; H, 4.04; N, 13.87.

2-Amino-4-(4-methoxy-phenyl)-5,6-dimethyl-nicotinonitrile (5d)

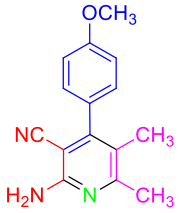

The product was obtained as off-white solid. Yield: 90%. M.p.: 276-277 °C. ^{1}H NMR (400 MHz, $CDCl_3$): δ, ppm 1.97 (s, 3H, CH_3), 2.44 (s, 3H, CH_3), 3.86 (s, 3H, OCH_3), 5.0 (s, 2H, NH_2), 6.98 (d, *J* = 8.5 Hz, 2H), 7.17 (d, *J* = 8.5 Hz, 2H). ^{13}C NMR (100 MHz, $CDCl_3$): δ, ppm 15.36, 23.78, 55.29, 89.94, 114.05, 119.95, 128.90, 129.58, 129.81, 153.68, 157.25, 159.89, 161.46. Anal. Calcd. (%) for $C_{15}H_{15}N_3O$: C, 71.13; H, 5.97; N, 16.59. Found: C, 71.18; H, 5.99; N, 16.64.

2-Amino-4-phenyl-6,7-dihydro-5*H*-cyclopenta[b]pyridine-3-carbonitrile (7a)

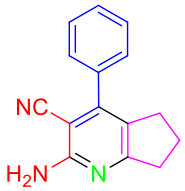

The product was obtained as off-white solid. Yield: 92%. M.p.: 220-221 °C. ^{1}H NMR (400 MHz, $CDCl_3$): δ, ppm 1.90-1.98 (m, 2H), 2.60 (t, *J* = 7.3 Hz, 2H), 2.80 (t, *J* = 7.6 Hz, 2H), 6.66 (s, 2H, NH_2), 7.42-7.51 (m, 5H). ^{13}C NMR (100 MHz, $CDCl_3$): δ, ppm 22.22, 28.78, 34.50, 85.52, 117.39, 123.02, 128.24, 128.49, 128.92, 135.92, 149.16,

160.99, 169.64. Anal. Calcd. (%) for $C_{15}H_{13}N_3$: C, 76.57; H, 5.57; N, 17.86. Found. C, 76.59; H, 5.58; N, 17.89.

2-Amino-4-(4-methoxy-phenyl)-6,7,8,9-tetrahydro-5*H*-cyclohepta[b]pyridine-3-carbonitrile (**7b**)

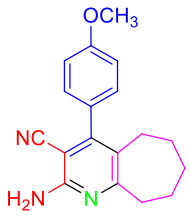

The product was obtained as off-white solid. Yield: 96%. M.p.: 223-224 ˚C. ^{1}H NMR (400 MHz, $CDCl_3$): δ, ppm 1.48-1.53 (m, 2H), 1.70-1.84 (m, 4H), 2.49 (t, *J* = 5.4 Hz, 2H), 2.91 (t, *J* = 5.4 Hz, 2H), 3.85 (s, 3H, OCH_3), 5.07 (s, 2H, NH_2), 6.98 (d, *J* = 8.6, 2H), 7.15 (d, *J* = 8.6, 2H). ^{13}C NMR (100 MHz, $CDCl_3$): δ, ppm 26.20, 28.06, 28.91, 32.0, 39.69, 55.28, 89.59, 114.03, 117.21, 126.69, 128.97, 129.82, 152.94, 157.24, 159.82, 167.86. Anal. Calcd. (%) for $C_{18}H_{19}N_3O$: C, 73.69; H, 6.53; N, 14.32. Found: C, 73.72; H, 6.55; N, 14.39.

2-Amino-4-(2-bromo-phenyl)-6,7,8,9-tetrahydro-5*H*-cyclohepta[b]pyridine-3-carbonitrile (7c)

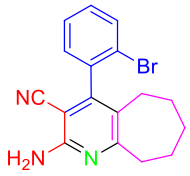

The product was obtained as off-white solid. Yield: 86%. M.p.: 261-262 ˚C. ^{1}H NMR (400 MHz, $CDCl_3$): δ, ppm 1.38-3.0 (m, 10H), 5.14 (s, 2H, NH_2), 7.14-7.70 (m, 4H). ^{13}C NMR (100 MHz, $CDCl_3$): δ, ppm 26.11, 27.54, 29.27, 32.01, 39.80, 89.17, 116.28, 122.30, 126.58, 127.71, 129.79, 130.29, 133.03, 137.91, 151.86, 157.13, 168.14. Anal. Calcd. (%) for $C_{17}H_{16}BrN_3$: C, 59.66; H, 4.71; N, 12.28. Found: C, 59.69; H, 4.76; N, 12.32.

2-Amino-4-(4-bromo-phenyl)-6,7,8,9-tetrahydro-5*H*-cyclohepta[b]pyridine-3-carbonitrile (7d)

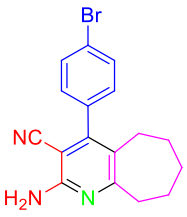

The product was obtained as off-white solid. Yield: 93%. M.p.: 236-237 °C. ^{1}H NMR (400 MHz, $CDCl_3$): δ, ppm 1.48-1.51 (m, 2H), 1.70-1.84 (m, 4H), 2.44 (t, *J* = 5.4 Hz, 2H), 2.92 (t, *J* = 5.4 Hz, 2H), 5.14 (s, 2H, NH_2), 7.10 (d, *J* = 8.3, 2H), 7.60 (d, *J* = 8.3, 2H). ^{13}C NMR (100 MHz, $CDCl_3$): δ, ppm 26.14, 27.99, 28.97, 31.92, 39.67, 88.90, 116.76, 123.13, 126.26, 130.10, 131.93, 135.68, 151.73, 157.26, 168.25. Anal. Calcd. (%) for $C_{17}H_{16}BrN_3$: C, 59.66; H, 4.71; N, 12.28. Found: C 59.74, H 4.68, N 12.35.

2-Amino-4-phenyl-6,7,8,9-tetrahydro-5*H*-cyclohepta[b]pyridine-3-carbonitrile (7e)

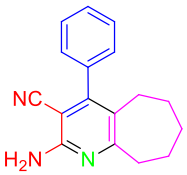

The product was obtained as off-white solid. Yield: 94%. M.p.: 227-228 °C. ^{1}H NMR (400 MHz, $CDCl_3$): δ, ppm 1.47-1.52 (m, 2H), 1.69-1.82 (m, 4H), 2.46 (t, *J* = 5.4 Hz, 2H), 2.92 (t, *J* = 5.5 Hz, 2H), 5.11 (s, 2H, NH_2), 7.21-7.49 (m, 5H). ^{13}C NMR (100 MHz, $CDCl_3$): δ, ppm 26.18, 28.03, 28.97, 31.98, 39.67, 89.33, 116.94, 126.42, 128.38, 128.60, 128.68, 136.85, 153.11, 157.22, 167.96. Anal. Calcd. (%) for $C_{17}H_{17}N_3$: C, 77.54; H, 6.51; N, 15.96. Found: C, 77.62; H, 6.49; N, 15.98.

2-Amino-4-(2-chloro-phenyl)-6,7,8,9-tetrahydro-5*H*-cyclohepta[b]pyridine-3-carbonitrile (7f)

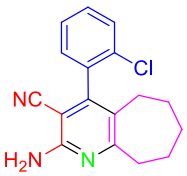

The product was obtained as off-white solid. Yield: 88%. M.p.: 273-274 °C. ^{1}H NMR (400 MHz, $CDCl_3$): δ, ppm 1.39-2.96 (m, 10H), 5.18 (s, 2H, NH_2), 7.15-7.52 (m, 4H). ^{13}C NMR (100 MHz, $CDCl_3$): δ, ppm 26.11, 27.57, 29.27, 32.01, 39.77, 89.24, 116.34,

126.78, 127.12, 129.87, 129.91, 130.20, 132.58, 135.81, 150.33, 157.21, 168.07. Anal. Calcd. (%) for $C_{17}H_{16}ClN_3$: C, 68.57; H, 5.42; N, 14.11. Found: C, 68.65; H, 5.46; N, 14.09.

2-Amino-4-(2-methoxy-phenyl)-6,7,8,9-tetrahydro-5*H*-cyclohepta[b]pyridine-3-carbonitrile (7g)

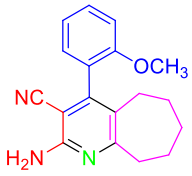

The product was obtained as off-white solid. Yield: 92%. M.p.: 244-245 ˚C. ^{1}H NMR (400 MHz, $CDCl_3$): δ, ppm 1.42-2.94 (m, 10H), 3.78 (s, 3H, OCH_3), 5.03 (m, 2H, NH_2), 6.99-7.43 (m, 4H). ^{13}C NMR (100 MHz, $CDCl_3$): δ, ppm 26.18, 27.65, 29.40, 32.13, 39.76, 55.46, 90.08, 111.11, 117.03, 120.74, 125.59, 127.36, 130.0, 130.39, 150.33, 156.11, 157.16, 167.37. Anal calcd. (%) for $C_{18}H_{19}N_3O$: C, 73.69; H, 6.53; N, 14.32. Found: C, 73.62; H, 6.56; N, 14.30.

2-Amino-4-(4-dimethylamino-phenyl)-6,7,8,9-tetrahydro-5*H*-cyclohepta[b]pyridine-3-carbonitrile (7h)

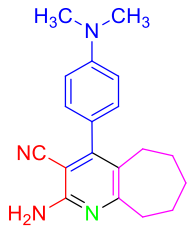

The product was obtained as light yellow solid. Yield: 91%. M.p.: 230-231 ˚C. ^{1}H NMR (400 MHz, $CDCl_3$): δ, ppm 1.52-1.81 (m, 6H), 2.56 (t, J = 5.3 Hz, 2H), 2.91 (t, J = 5.4 Hz, 2H), 3.01 (s, 6H, $N(CH_3)_2$), 4.96 (s, 2H, NH_2), 6.76 (d, J = 8.6 Hz, 2H), 7.11 (d, J = 8.6 Hz, 2H). ^{13}C NMR (100 MHz, $CDCl_3$): δ, ppm 26.25, 28.15, 28.90, 32.06, 39.73, 40.26, 88.90, 111.77, 123.13, 124.04, 126.79, 129.63, 135.68, 150.42, 153.68, 157.28, 167.58. Anal. Calcd. (%) for $C_{19}H_{22}N_4$: C, 74.48; H, 7.24; N, 18.29. Found: C, 74.56; H, 7.28; N, 18.32.

2-Amino-4-phenyl-5,6,7,8,9,10-hexahydro-cycloocta[b]pyridine-3-carbonitrile (7i)

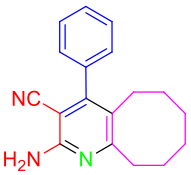

The product was obtained as off-white solid. Yield: 90%. M.p.: 234-235 °C. ^{1}H NMR (400 MHz, $CDCl_3$): δ, ppm 1.27-1.38 (m, 6H), 1.68 (s, 2H), 2.38-2.80 (m, 4H), 6.58 (s, 2H, NH_2), 7.23-7.51 (m, 5H). ^{13}C NMR (100 MHz, $CDCl_3$): δ, ppm 25.26, 25.76, 26.01, 30.01, 30.56, 34.87, 88.35, 116.59, 121.64, 127.91, 128.29, 128.40, 137.14, 153.75, 158.21, 165.19. Anal. Calcd. (%) for $C_{18}H_{19}N_3$: C, 77.95; H, 6.90; N, 15.15. Found: C 77.98; H 6.92; N, 15.18.

Spectra of pyridine compounds (**5a-d** & **7a-i**)

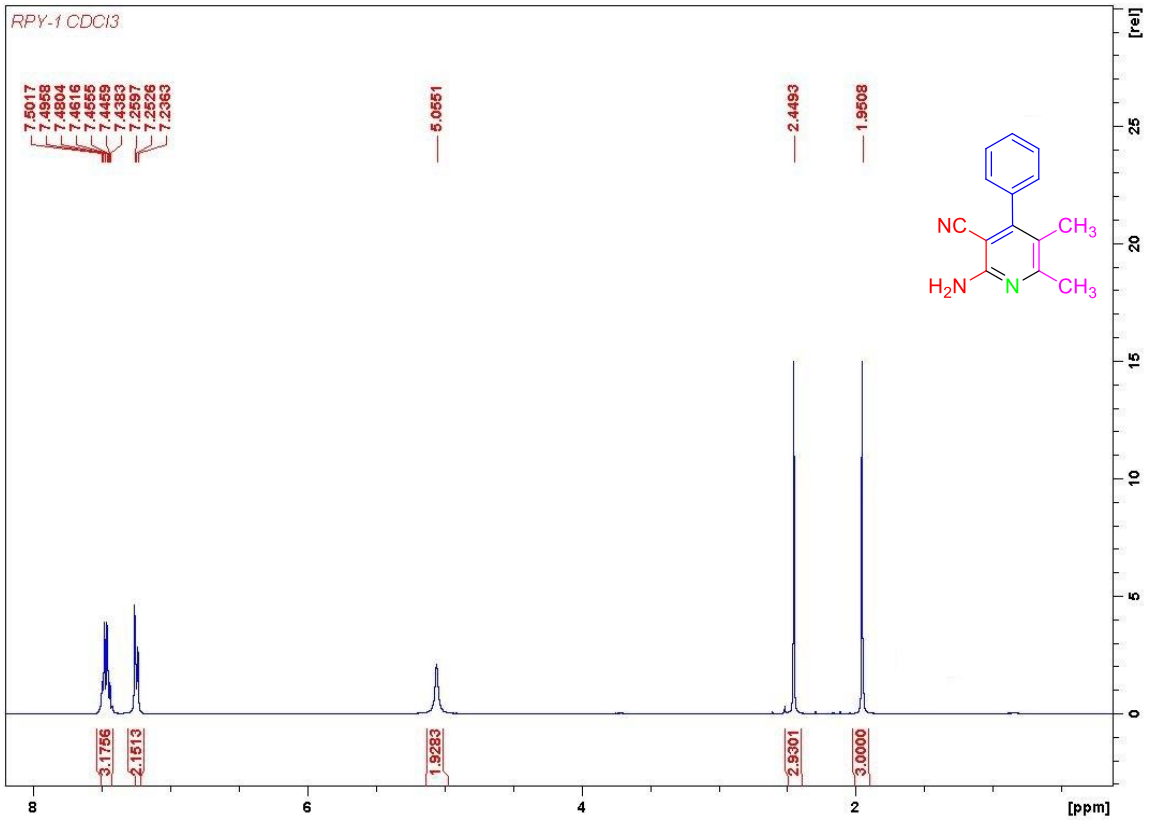

^{1}H NMR spectrum of pyridine compound **5a.**

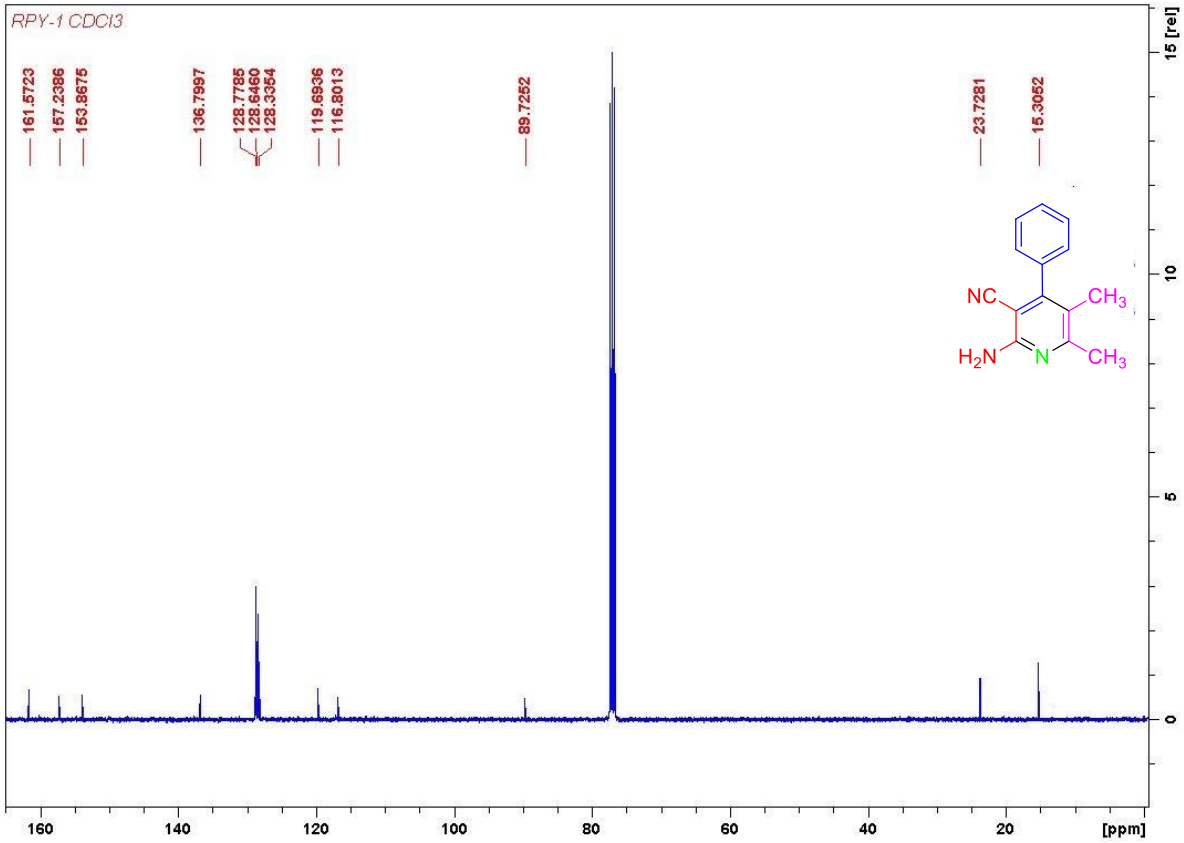

^{13}C NMR spectrum of pyridine compound **5a.**

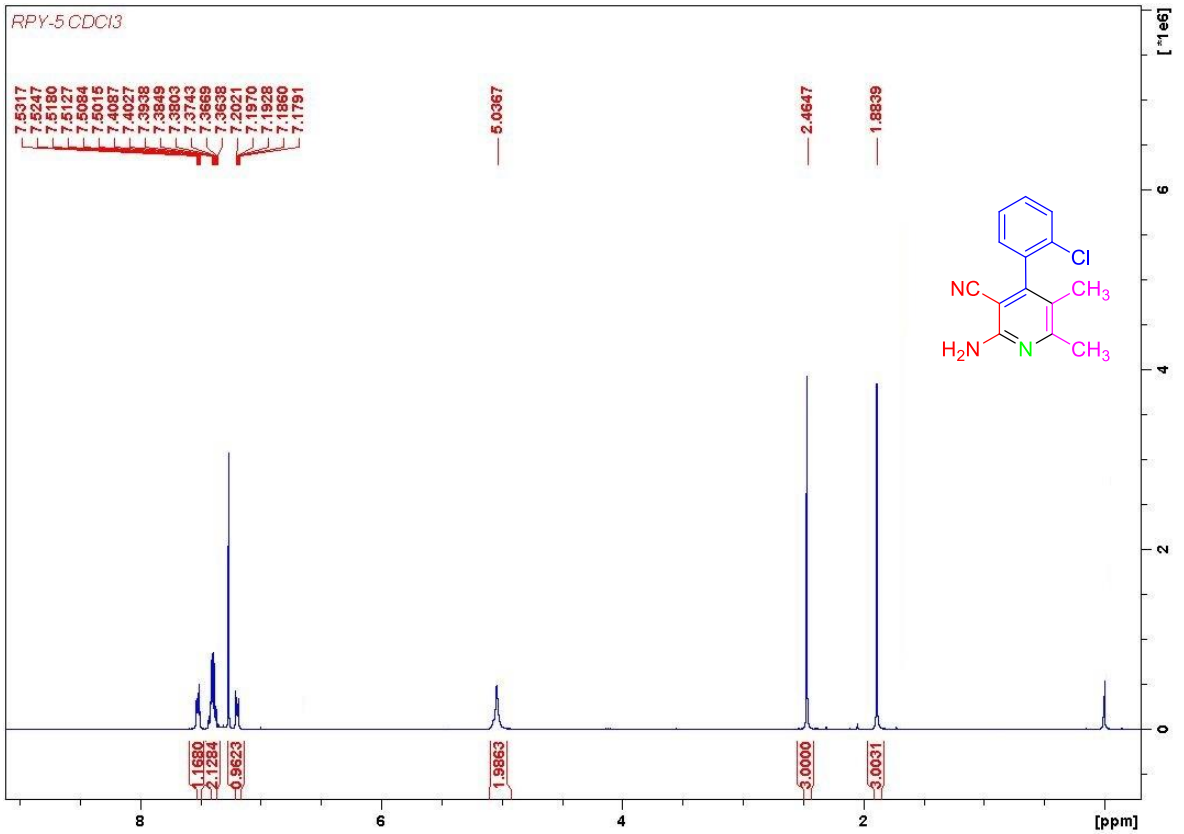

^{1}H NMR spectrum of pyridine compound **5b.**

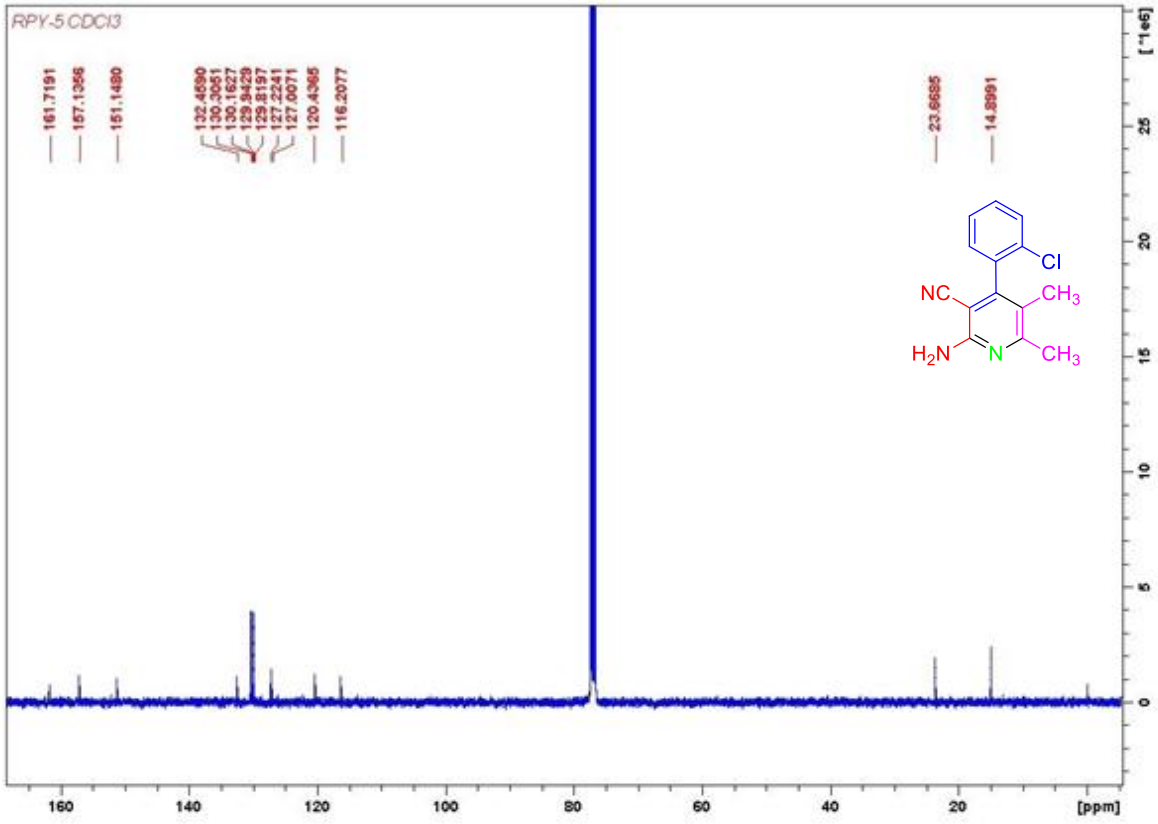

^{13}C NMR spectrum of pyridine compound **5b.**

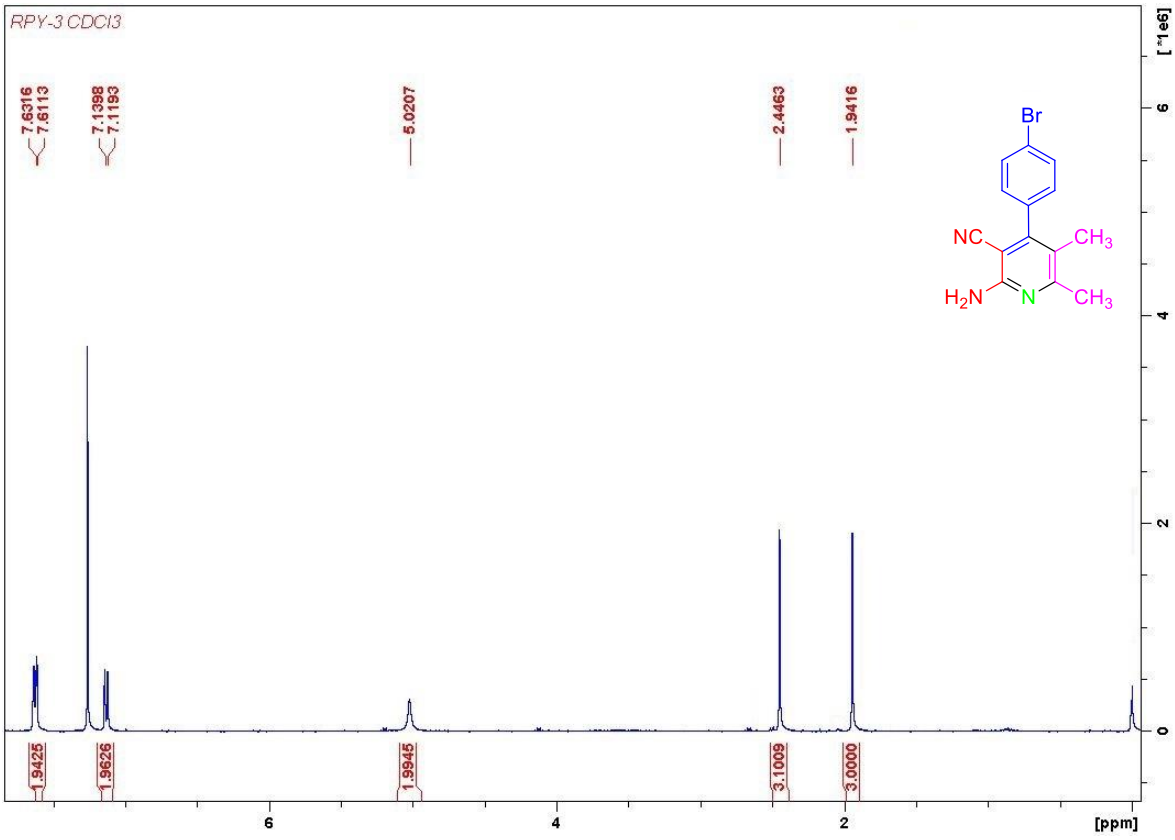

^{1}H NMR spectrum of pyridine compound **5c.**

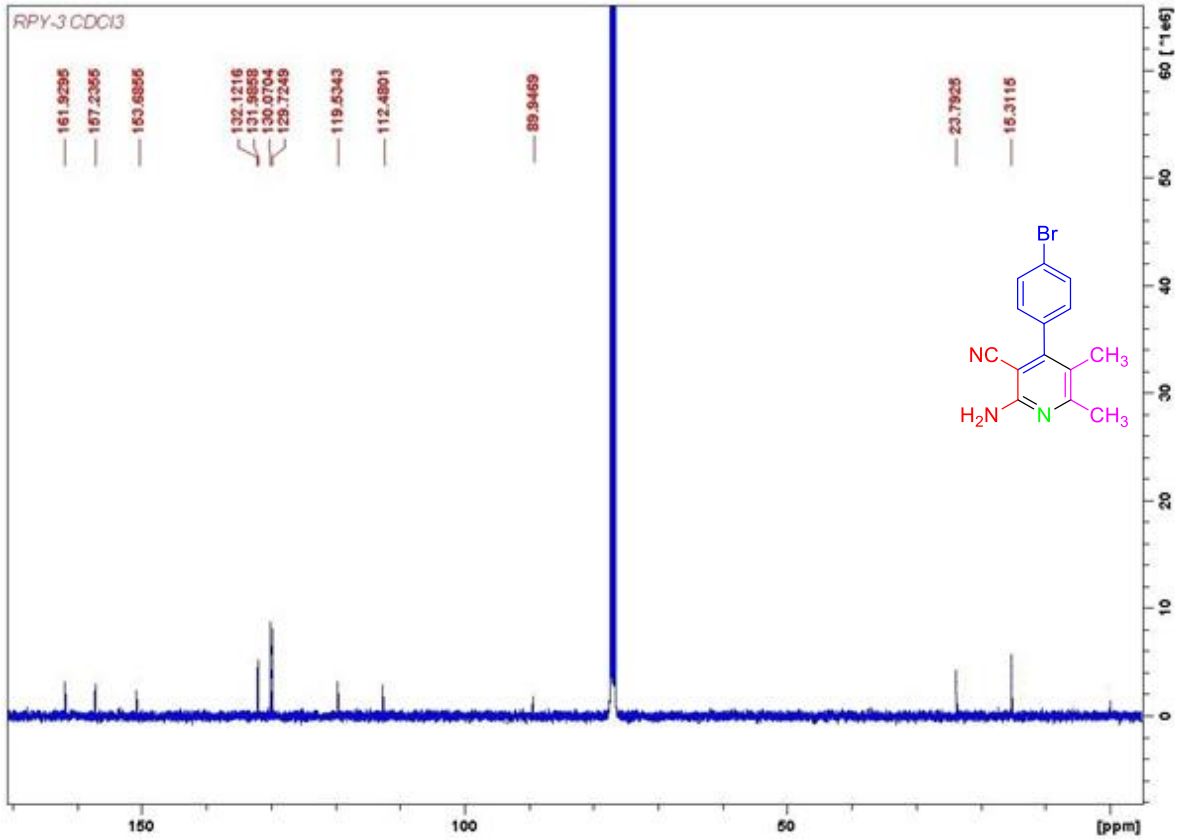

^{13}C NMR spectrum of pyridine compound **5c.**

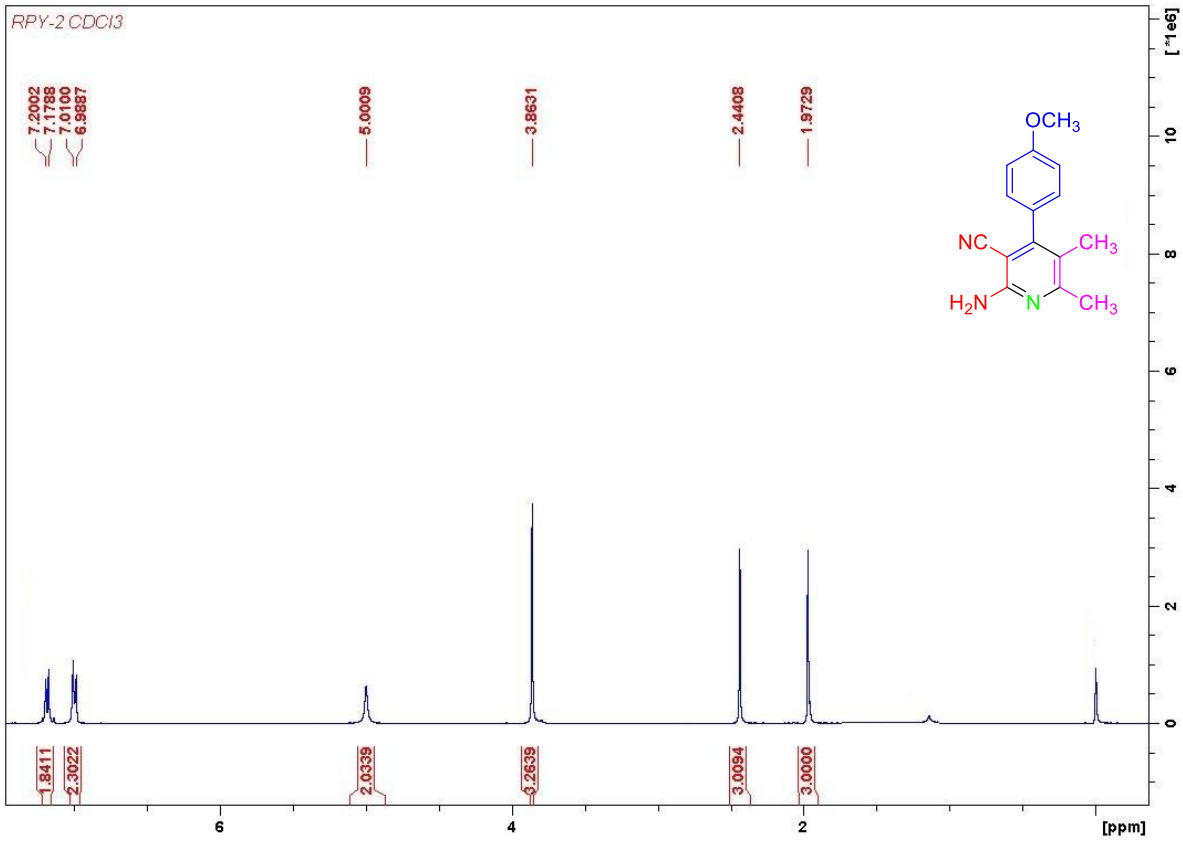

^{1}H NMR spectrum of pyridine compound **5d.**

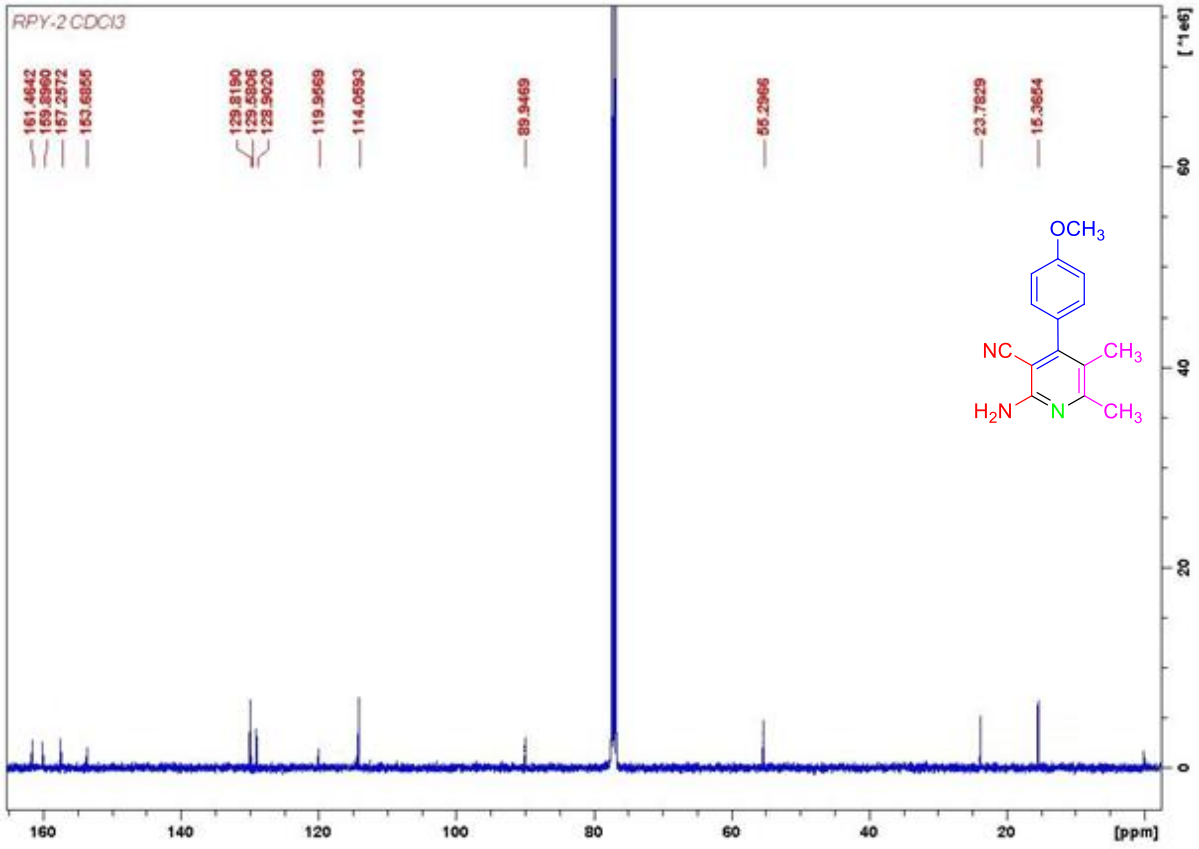

^{13}C NMR spectrum of pyridine compound **5d.**

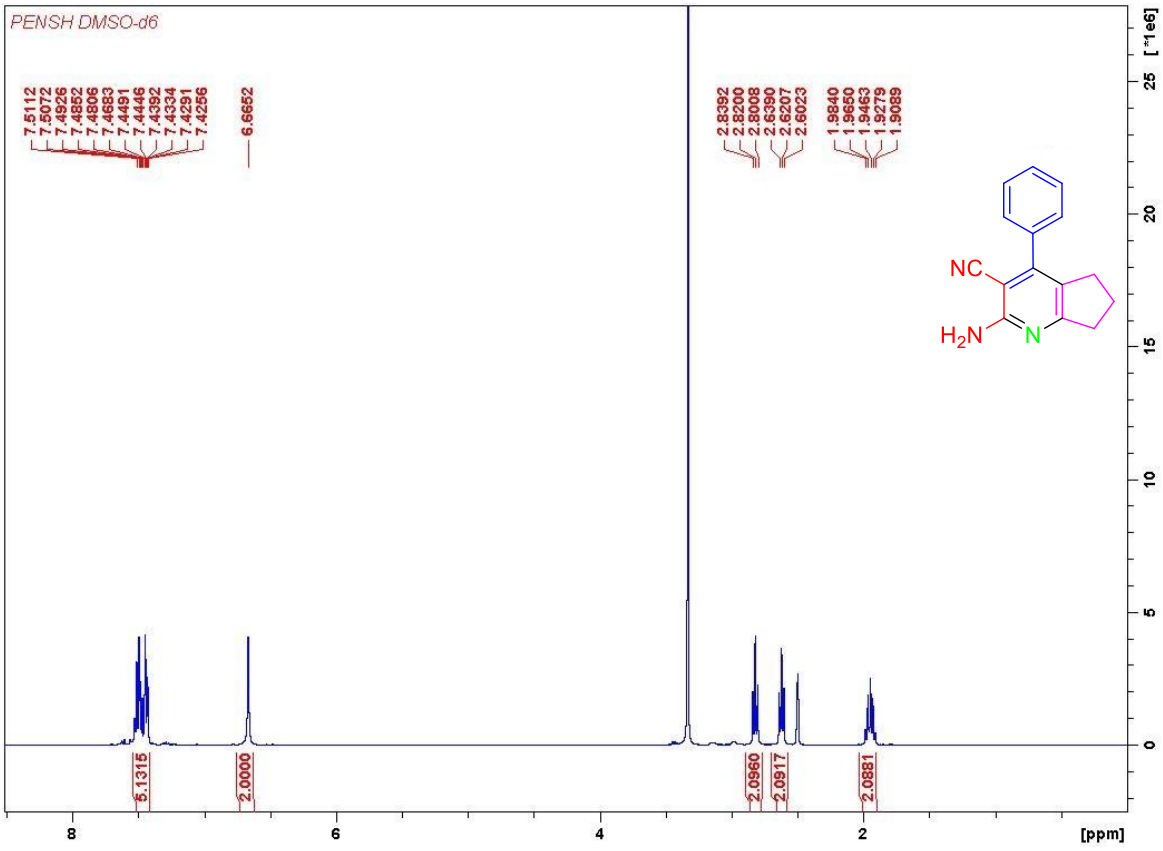

^{1}H NMR spectrum of pyridine compound **7a.**

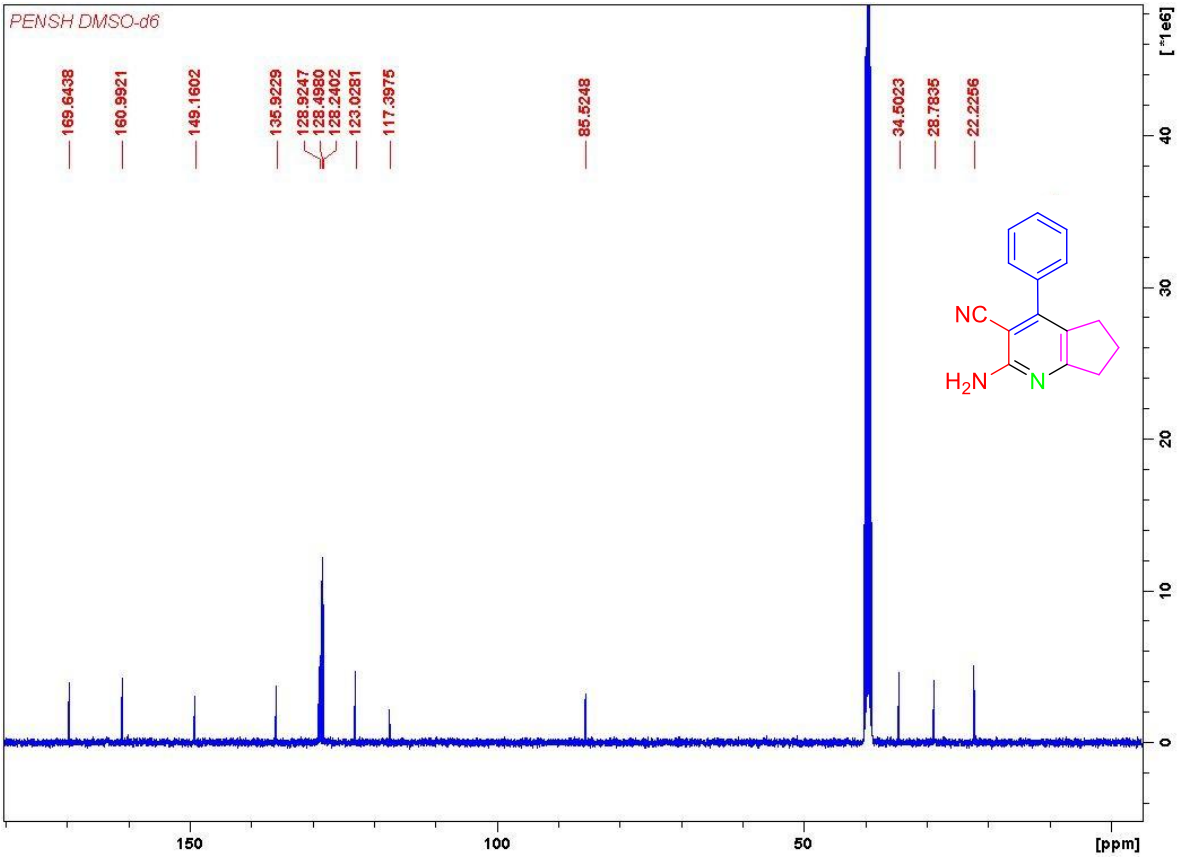

^{13}C NMR spectrum of pyridine compound **7a.**

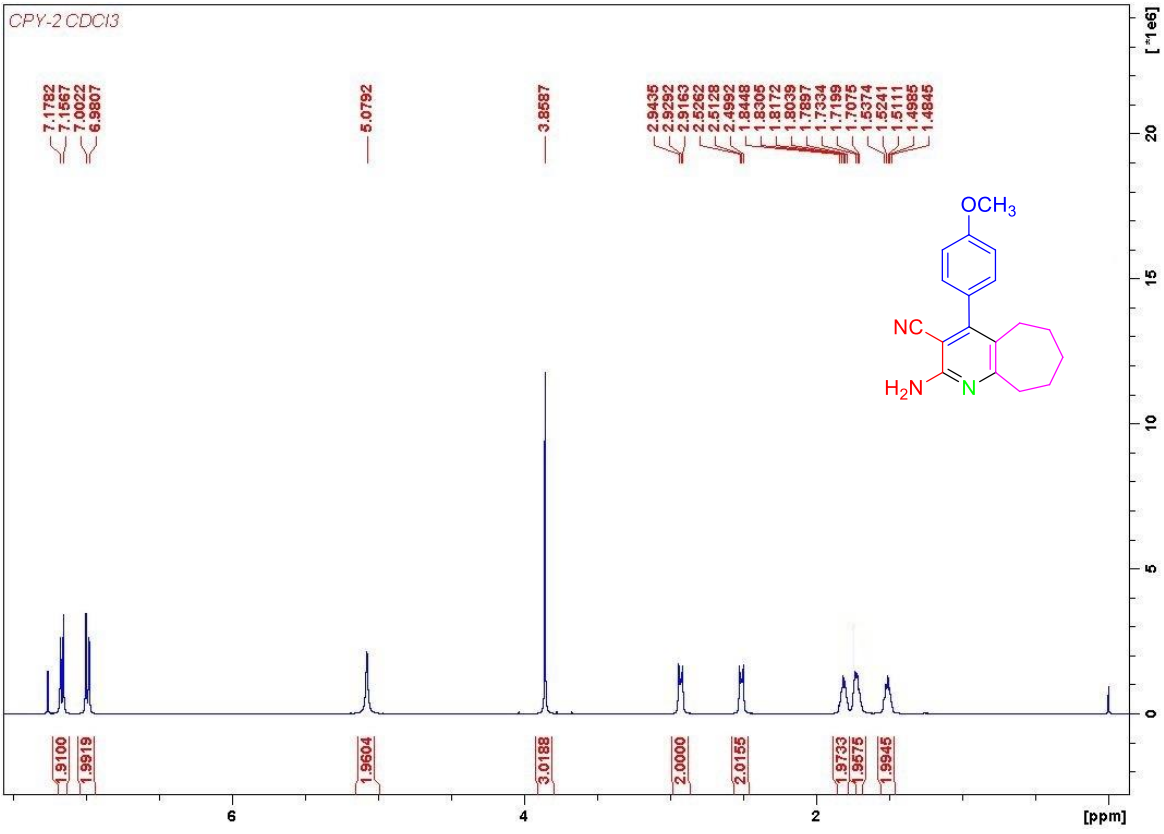

^{1}H NMR spectrum of pyridine compound **7b.**

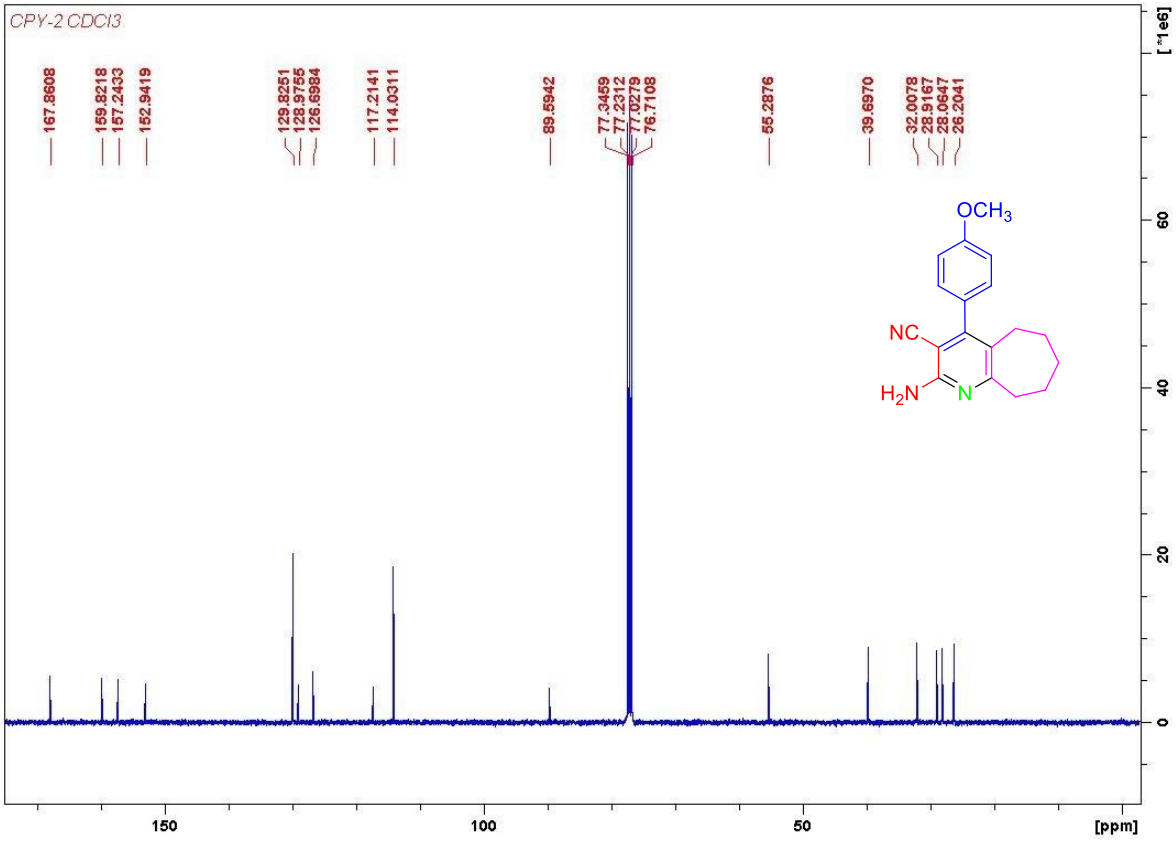

^{13}C NMR spectrum of pyridine compound **7b.**

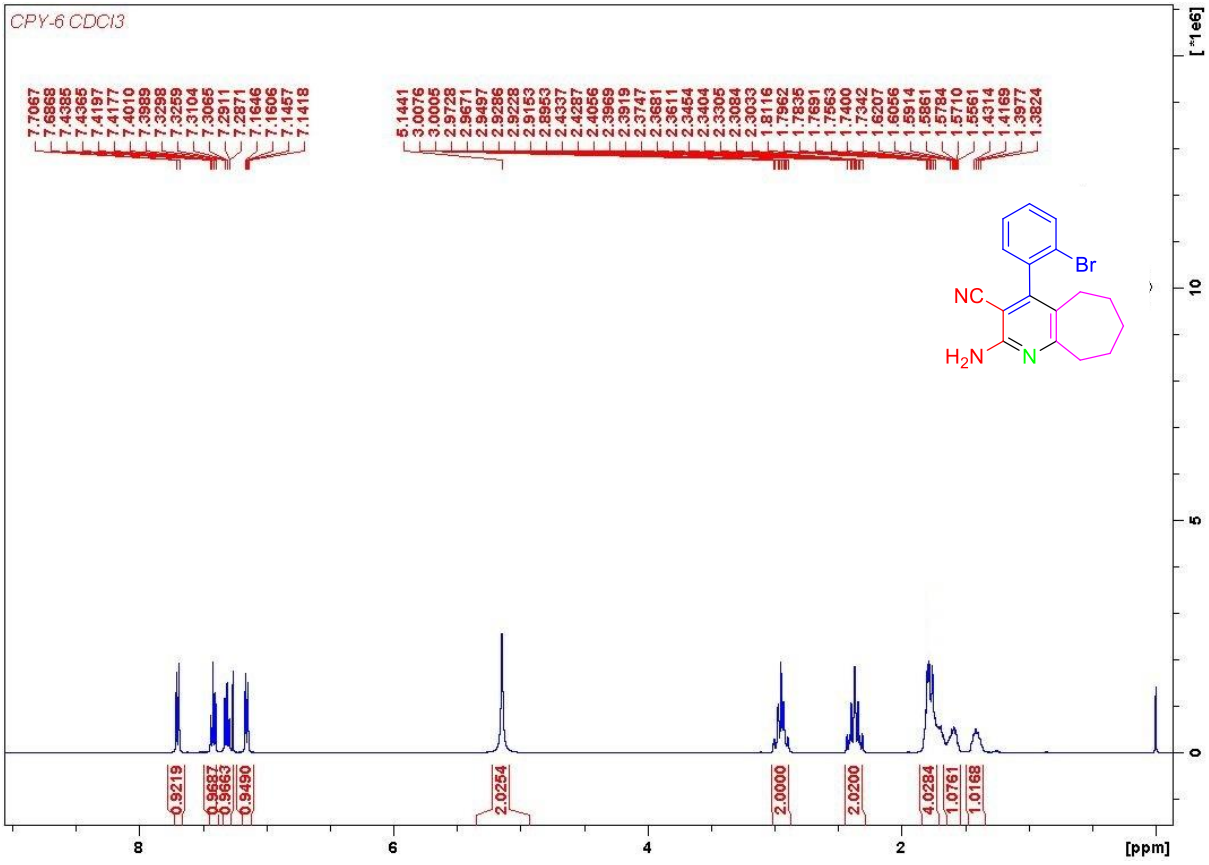

^{1}H NMR spectrum of pyridine compound **7c.**

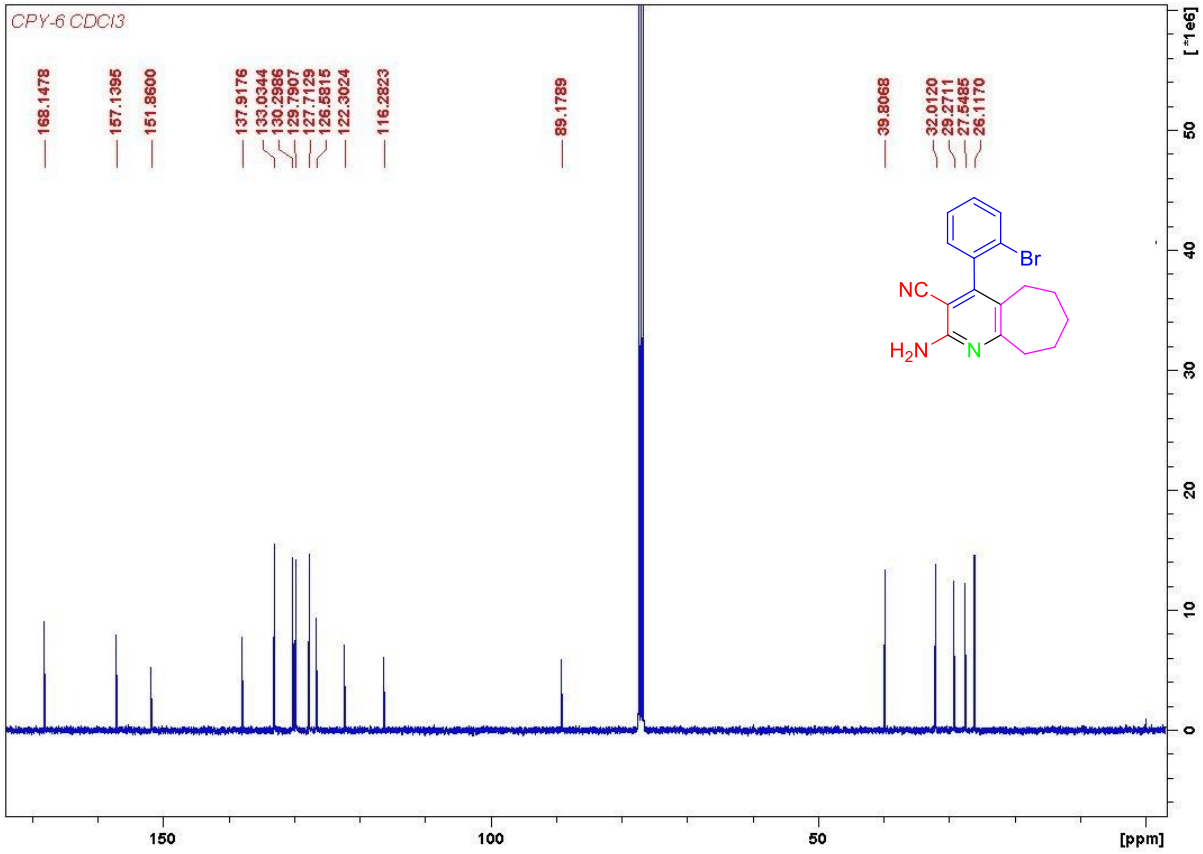

^{13}C NMR spectrum of pyridine compound **7c.**

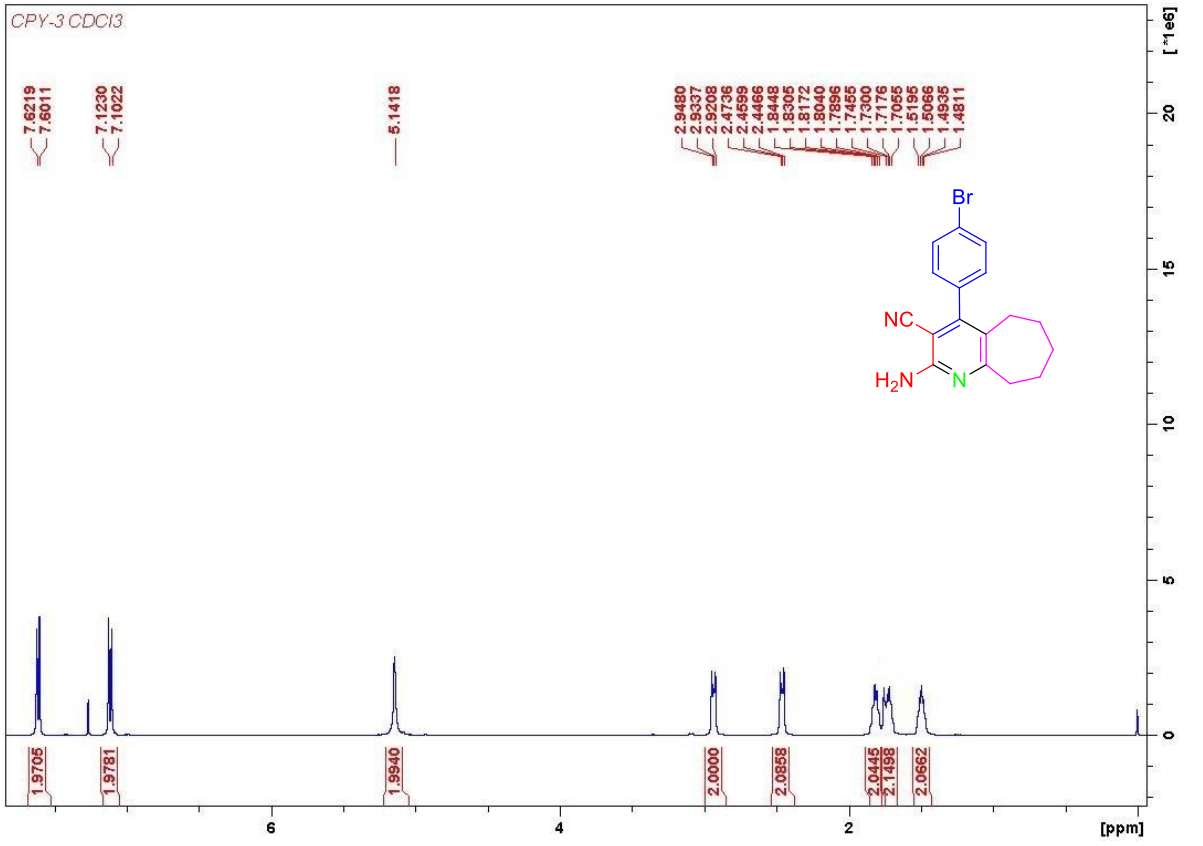

^{1}H NMR spectrum of pyridine compound **7d.**

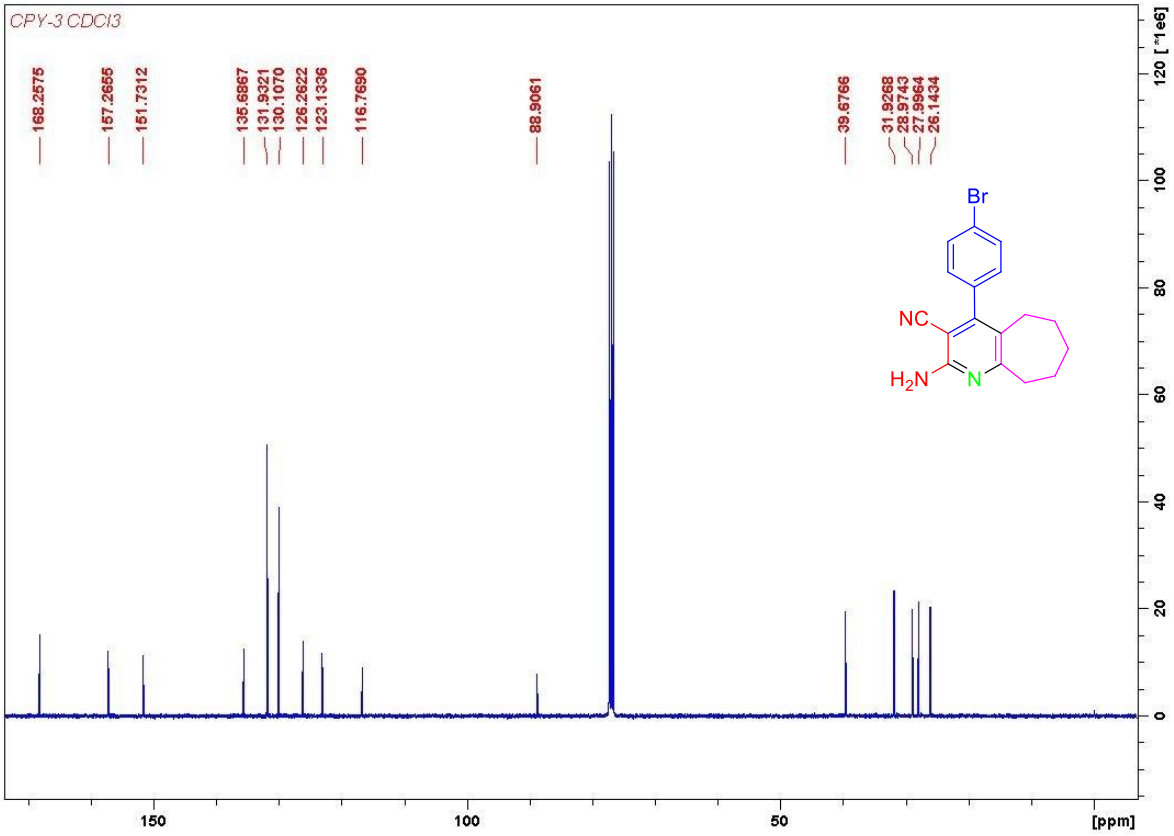

^{13}C NMR spectrum of pyridine compound **7d.**

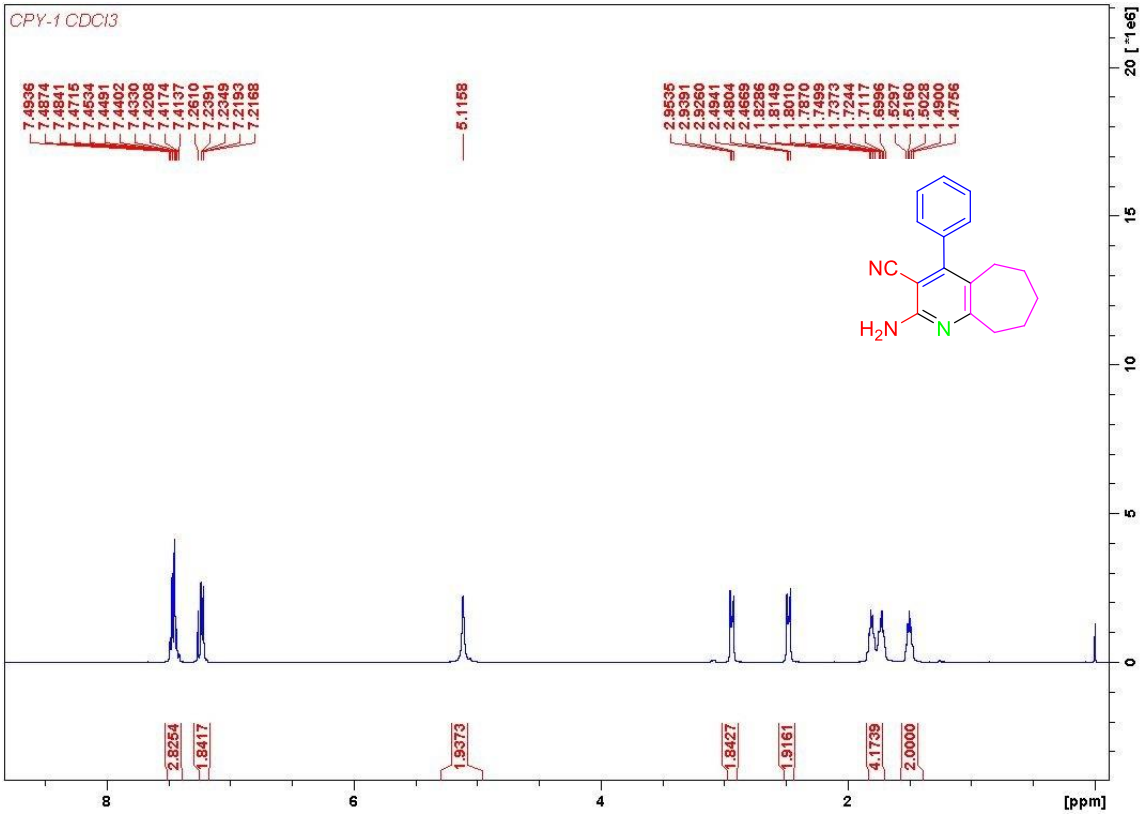

^{1}H NMR spectrum of pyridine compound **7e.**

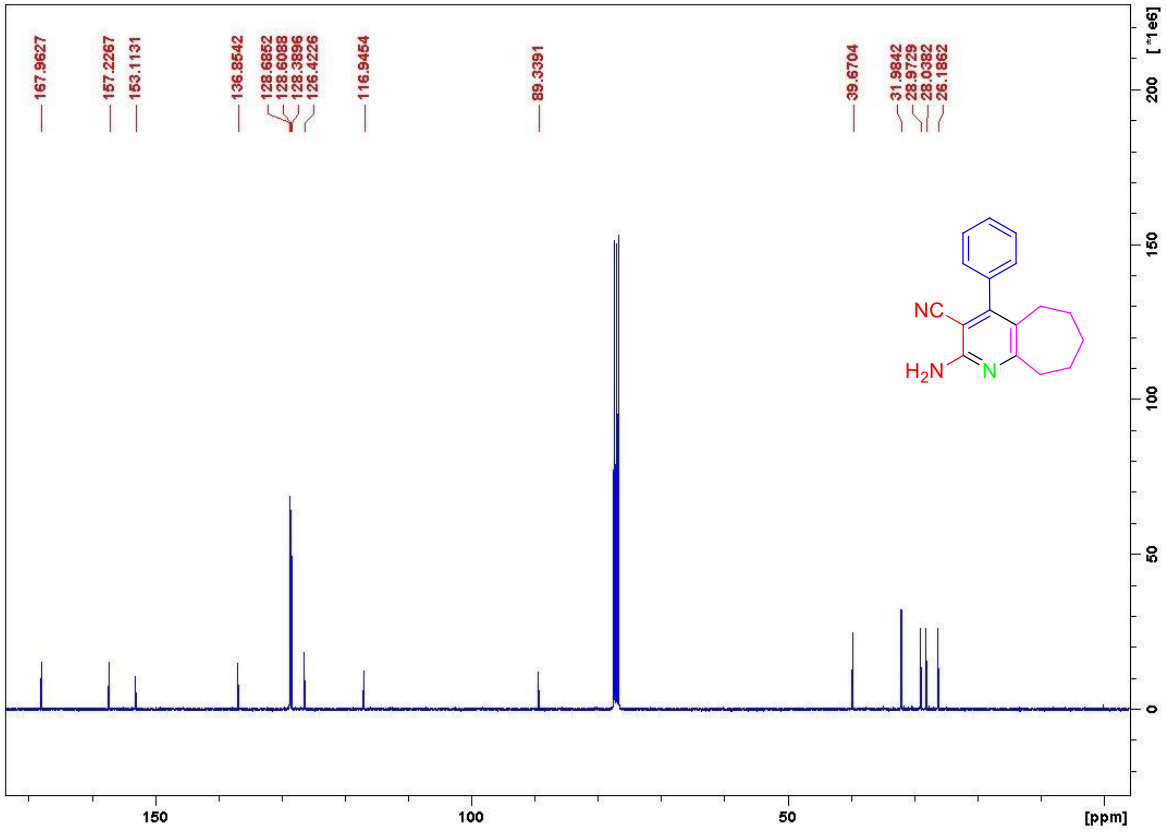

^{13}C NMR spectrum of pyridine compound **7e.**

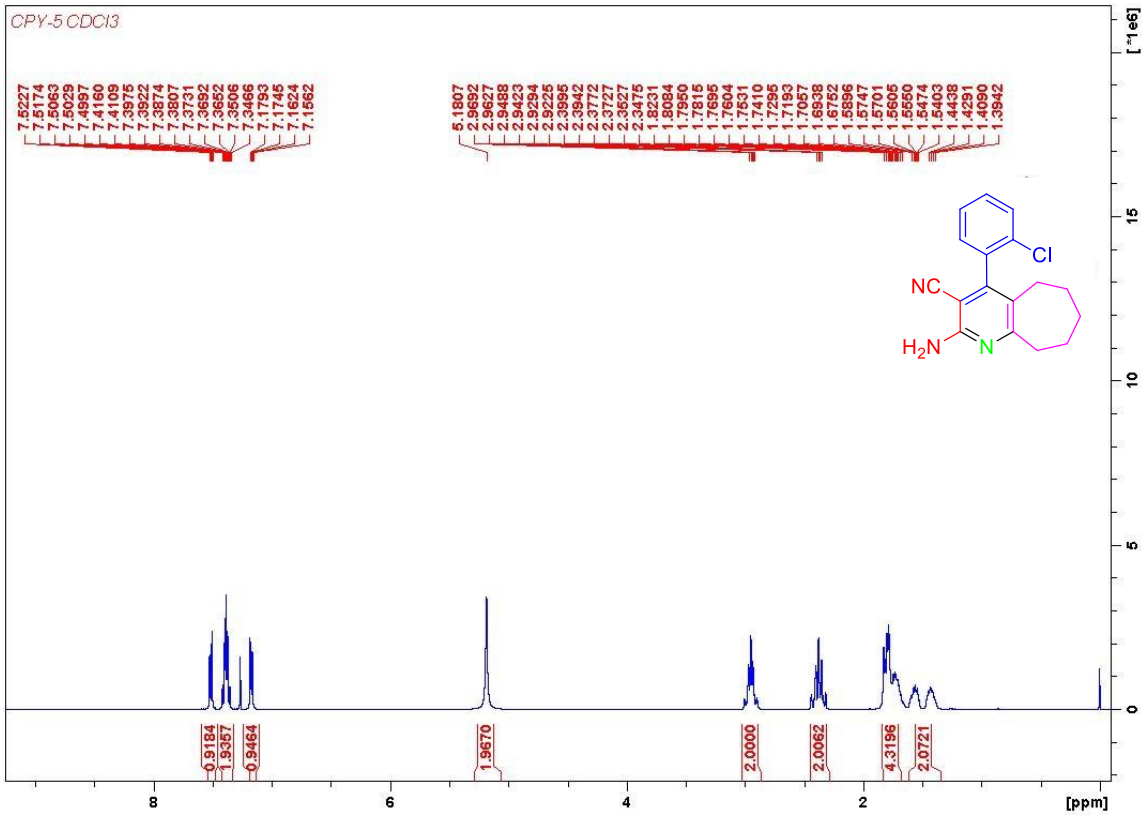

^{1}H NMR spectrum of pyridine compound **7f.**

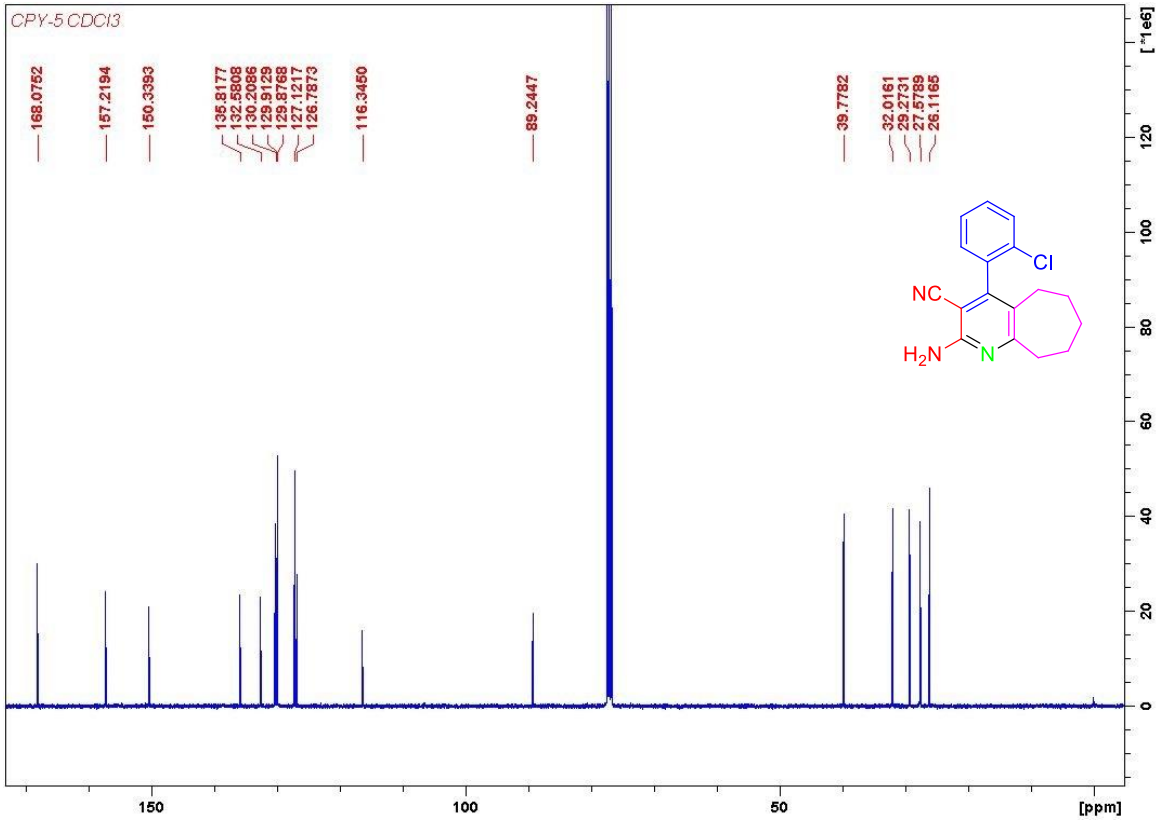

^{13}C NMR spectrum of pyridine compound **7f.**

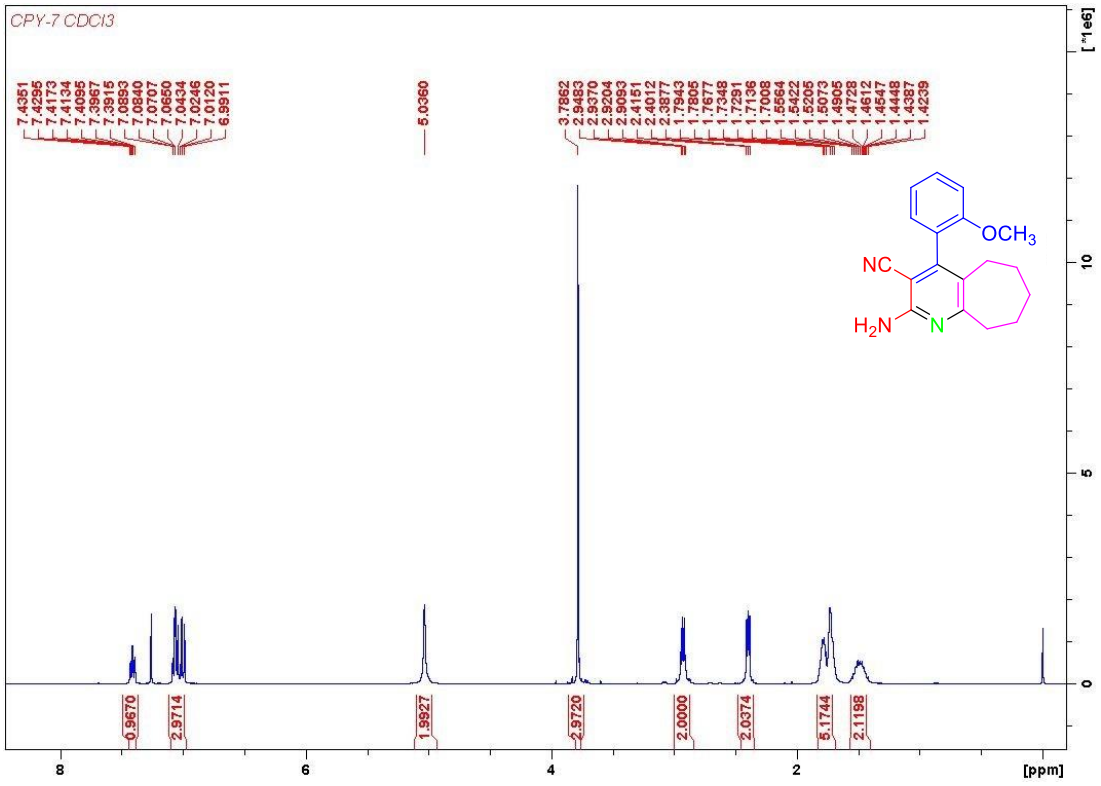

^{1}H NMR spectrum of pyridine compound **7g.**

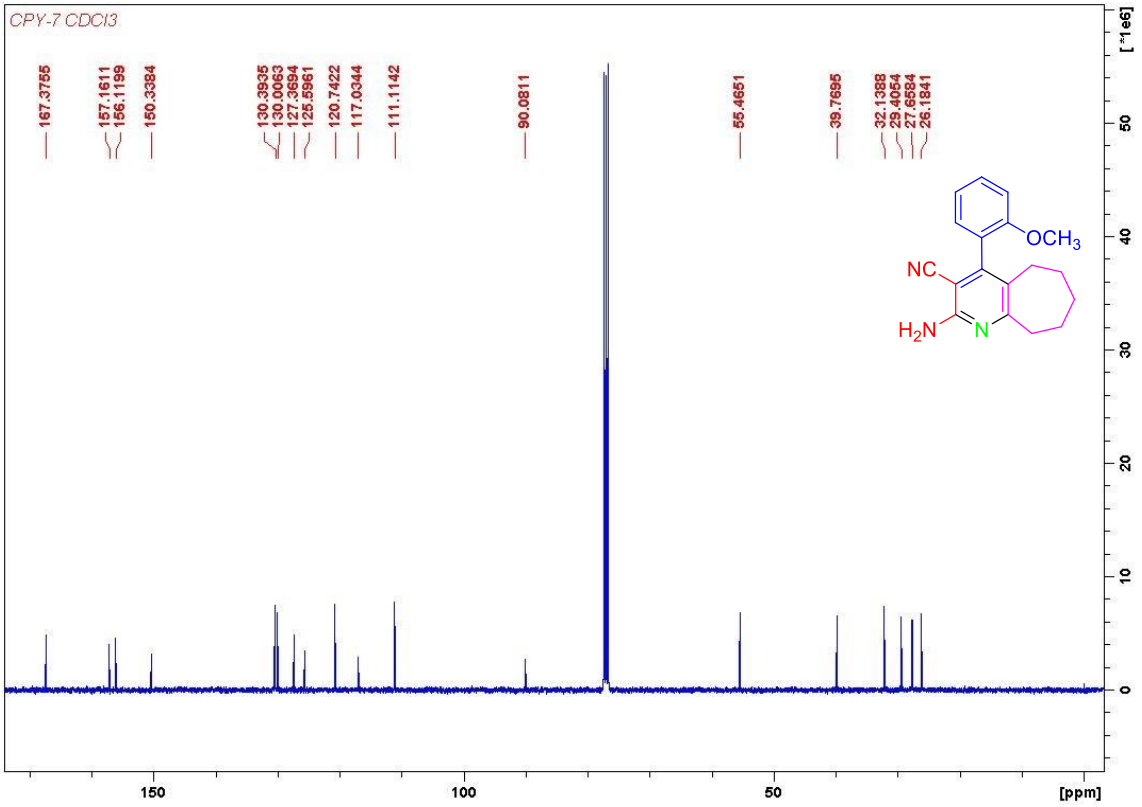

^{13}C NMR spectrum of pyridine compound **7g.**

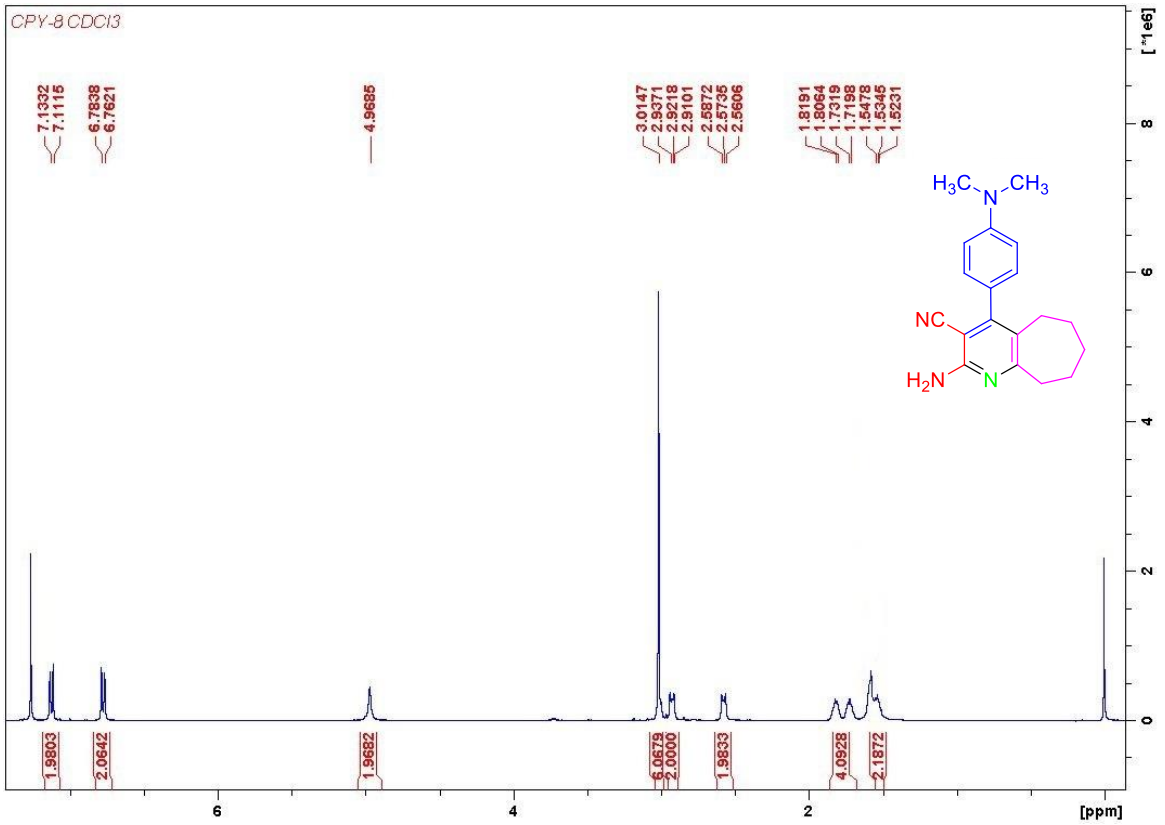

^{1}H NMR spectrum of pyridine compound **7h.**

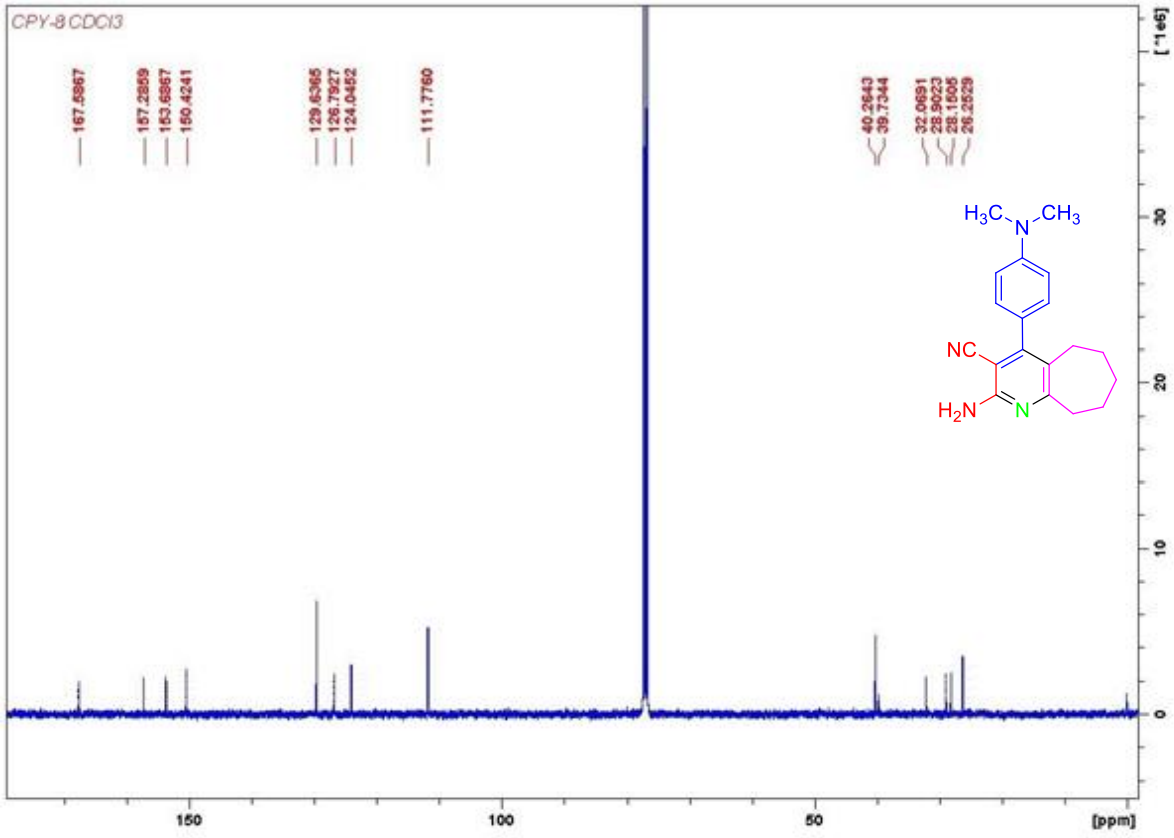

^{13}C NMR spectrum of pyridine compound **7h.**

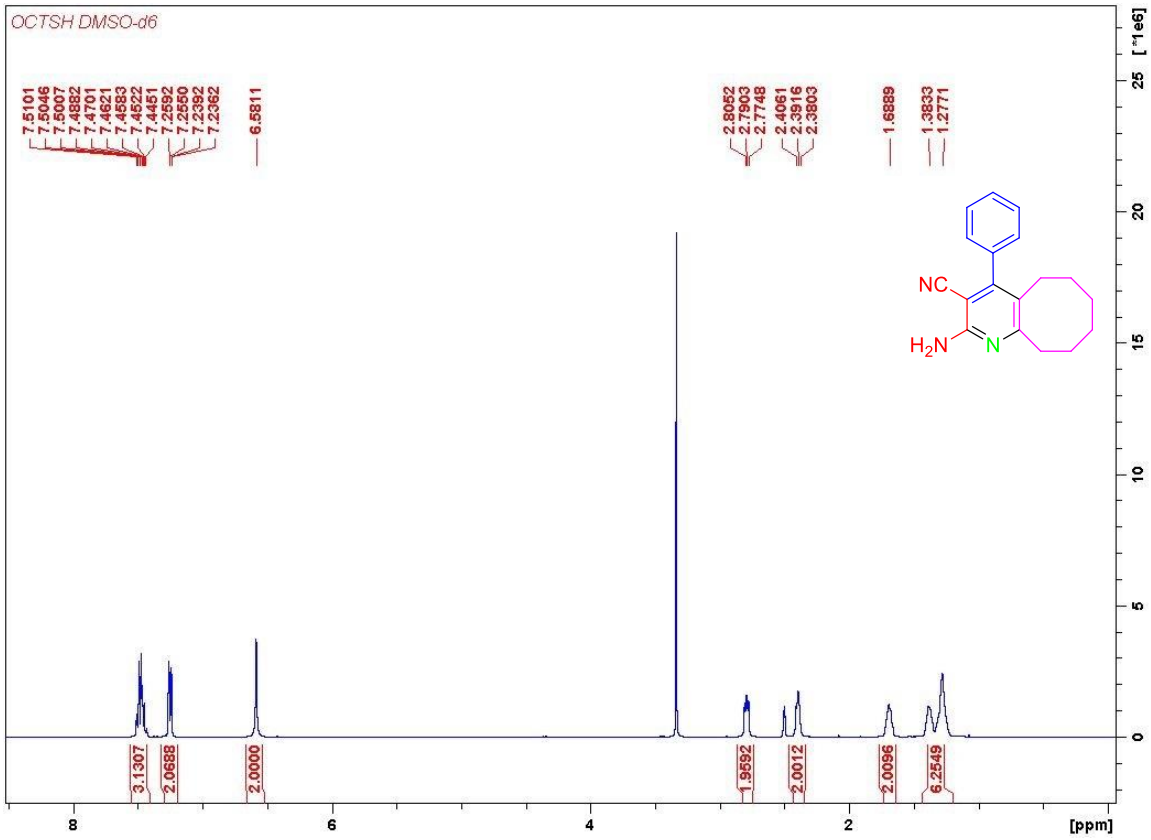

^{1}H NMR spectrum of pyridine compound 7**i.**

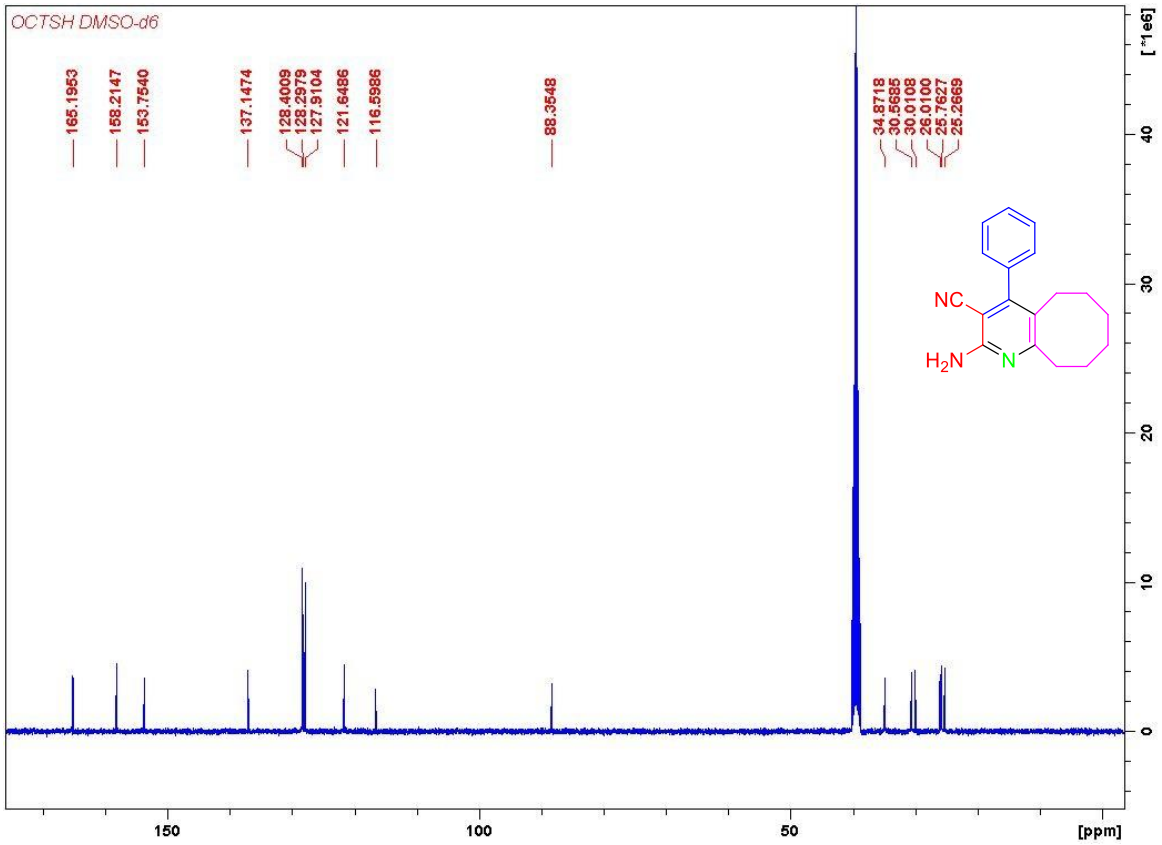

^{13}C NMR spectrum of pyridine compound **7i.**

3.6.3 General procedure for the synthesis of the dihydropyrano[2,3-c]pyrazoles (11a-l)

A mixture of aromatic aldehydes (1 mmol), malononitrile (1 mmol) and 3-methyl-1-phenyl-2-pyrazoline-5-one (1 mmol) was stirred in water at room temperature in the presence of 10 mol% of $Zn(ANA)_2Cl_2$ complex for appropriate time to produce dihydropyrano[2,3-c]pyrazoles. Reaction progress was monitored by TLC. After completion of the reaction, the product was filtered. The residue was washed with ethyl acetate. Ethyl acetate was evaporated under vacuum and the obtained solid was purified by recrystalization process in ethyl acetate.

3.6.4 Spectral data of the compounds 11a-l

6-amino-3-methyl-1,4-diphenyl-1,4-dihydropyrano[2,3-c]pyrazole-5-carbonitrile (11a)

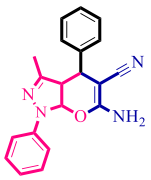

Colour: White solid. M.p.: 168-170 °C. ^{1}H NMR (400 MHz, DMSO-d_6): δ, ppm 1.79 (s, 3H, CH_3), 4.89 (s, 1H), 7.22-7.36 (m, 8H), 7.5 (d, 2H, J = 7.6 Hz), 7.8 (d, 2H, J = 7.6 Hz). ^{13}C

NMR (100 MHz, DMSO-d_6): δ, ppm 159.90, 145.75, 144.36, 144.08, 138.02, 129.80, 129.00, 128.25, 127.52, 126.63, 120.43, 99.11, 58.68, 37.23, 13.03. Anal. Calcd. for $C_{20}H_{16}N_4O$: C, 73.15; H, 4.91; N, 17.06. Found: C, 73.37; H, 4.98; N, 17.29.

6-amino-3-methyl-4-(3-nitrophenyl)-1-phenyl-1,4-dihydropyrano[2,3-c]pyrazole-5-carbonitrile (11b)

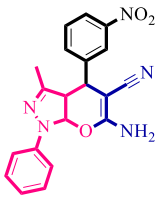

Colour: White solid. M.p.: 187-189 °C. ^{1}H NMR (400 MHz, DMSO-d_6): δ, ppm 1.81 (s, 3H), 4.99 (s, 1H), 7.34 (t, 1H, *J* = 7.2 Hz), 7.42 (s, 2H), 7.51 (t, 2H, *J* = 7.6 Hz), 7.69 (t, 1H, *J* = 8.4 Hz), 7.79- 7.82 (m,3H), 8.17 (bs, 2H). ^{13}C NMR (100 MHz, DMSO-d_6): δ, ppm 160.23, 148.42, 146.45, 145.63, 144.50, 137.91, 135.25, 130.76, 129.80, 129.39, 126.77, 122.76, 122.73, 120.58, 120.28, 98.13, 57.53, 36.67, 13.08. Anal. Calcd. (%) for $C_{20}H_{15}N_5O_3$: C, 64.34; H, 4.05; N, 18.76. Found: C, 64.59; H, 4.11; N, 18.49.

6-amino-3-methyl-4-(2-nitrophenyl)-1-phenyl-1,4-dihydropyrano[2,3-c]pyrazole-5-carbonitrile (11c)

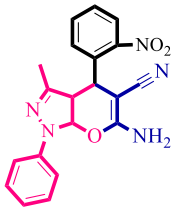

Colour: White solid. M.p.: 156-158 °C. ^{1}H NMR (400 MHz, DMSO-d_6): δ, ppm 1.76 (s, 3H), 5.21 (s, 1H), 7.32-7.39 (m, 3H), 7.49-7.56 (m, 4H), 7.7 (t, 1H, *J* = 7.6 Hz), 7.8 (d, 2H, *J* = 8.00 Hz), 7.91 (d, 1H, *J* = 8.00 Hz). ^{13}C NMR (100 MHz, DMSO-d_6): δ, ppm 160.26, 149.75, 147.25, 145.36, 144.83, 138.18, 137.89, 137.17, 133.89, 132.12, 129.82, 129.11, 126.82, 124.19, 120.59, 119.96, 97.78, 57.28, 32.38, 12.75. Anal. Calcd. (%) for $C_{20}H_{15}N_5O_3$: C, 64.34; H, 4.05; N, 18.76. Found: C, 64.02; H, 4.15; N, 18.98.

6-amino-4-(3,4-dimethylphenyl)-3-methyl-1-phenyl-1,4-dihydropyrano[2,3-c]pyrazole-5-carbonitrile (11d)

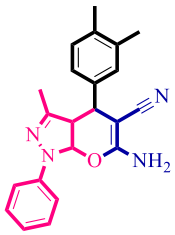

Colour: White solid. M.p.: 150-151 °C. ^{1}H NMR (400 MHz, DMSO-d_6): δ, ppm 1.82 (s, 3H), 3.72 (s, 3H), 3.74 (s,3H), 4.64 (s, 1H), 6.75-6.93 (m, 3H), 7.17 (s, 2H) 7.32 (t, 1H, *J* = 7.2 Hz), 7.49 (t, 2H, *J* = 7.6 Hz), 7.79 (d, 2H, *J* = 8.00 Hz). ^{13}C NMR (100 MHz, DMSO-d_6): δ, ppm 159.80, 149.09, 148.28, 145.86, 144.27, 138.07, 136.52, 129.79, 126.57, 120.55, 120.35, 112.26, 112.03, 99.18, 58.90, 56.04, 55.93, 36.65, 13.15. Anal. Calcd. (%) for $C_{22}H_{20}N_4O$: C, 74.14; H, 5.66; N, 15.72. Found: C, 74.39; H, 5.75; N, 15.51.

6-amino-4-(4-cyanophenyl)-3-methyl-1-phenyl-1,4-dihydropyrano[2,3-c]pyrazole-5-carbonitrile (11e)

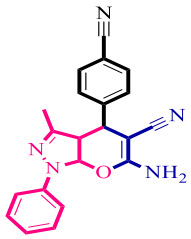

Colour: White solid. M.p.: 198-200 °C. ^{1}H NMR (400 MHz, DMSO-d_6): δ, ppm 1.79 (s, 3H), 4.85 (s, 1H), 7.34 (t, 1H, *J* = 7.2 Hz), 7.39 (s, 2H), 7.49-7.52 (m, 4H), 7.80-7.86(m, 4H). ^{13}C NMR (100 MHz, DMSO-d_6): δ, ppm 160.17, 149.66, 145.59, 144.50, 137.92, 133.11, 129.79, 129.43, 126.75, 120.57, 120.25, 119.24, 110.43, 98.11, 57.50, 37.13, 13.01. Anal. Calcd. (%) for $C_{21}H_{15}N_5O$: C, 71.38; H, 4.28; N, 19.82. Found: C, 71.62; H, 4.34; N, 19.69.

6-amino-4-(4-hydroxyphenyl)-3-methyl-1-phenyl-1,4-dihydropyrano[2,3-c]pyrazole-5-carbonitrile (11f)

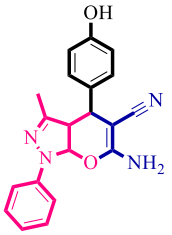

Colour: White solid. M.p.: 205-207 °C. ^{1}H NMR (400 MHz, DMSO-d_6): δ, ppm 1.81 (s, 3H), 4.57 (s, 1H), 6.76 (s, 2H), 7.06 (s, 2H), 7.17 (s, 2H), 7.31(s, 1H), 7.49 (s,2H), 7.80 (s,2H), 9.39 (s,1H). ^{13}C NMR (100 MHz, DMSO-d_6): δ, ppm 159.67, 156.77, 145.84, 144.24, 138.07, 134.41, 129.78, 129.26, 126.52, 120.62, 120.33, 115.70, 99.50, 59.27, 36.50, 19.03. Anal. Calcd. (%) for $C_{20}H_{16}N_4O_2$: C, 69.76; H, 4.68; N, 16.27. Found: C, 69.91; H, 4.75; N, 16.11.

6-amino-4-(4-chlorophenyl)-3-methyl-1-phenyl-1,4-dihydropyrano[2,3-c]pyrazole-5-carbonitrile (11g)

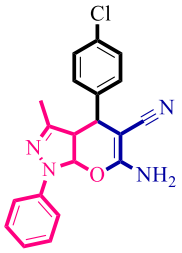

Colour: Pale yellow solid. M.p.: 176-178 °C. ^{1}H NMR (400 MHz, DMSO-d_6): δ, ppm 1.82 (s, 3H), 4.73 (s, 1H), 7.27-7.34 (m, 5H), 7.42 (d, 2H, *J* = 8.00 Hz), 7.5 (t, 2H, *J* = 7.2 Hz), 7.8 (d, 2H, *J* = 7.6 Hz). ^{13}C NMR (100 MHz, DMSO-d_6): δ, ppm 159.95, 145.67, 144.40, 143.14, 137.97, 132.06, 130.18, 129.80, 129.01, 126.69, 120.50, 120.34, 98.66, 58.24, 36.56, 13.04. Anal. Calcd. (%) for $C_{20}H_{15}ClN_4O$: C, 66.21; H, 4.17; N, 15.44. Found: C, 66.43; H, 4.10; N, 15.19.

6-amino-4-(2,4-dichlorophenyl)-3-methyl-1-phenyl-1,4-dihydropyrano[2,3-c]pyrazole-5-carbonitrile (11h)

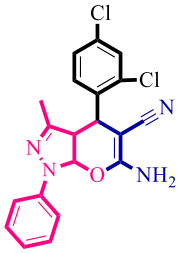

Colour: White solid. M.p.: 183-185 °C. ^{1}H NMR (400 MHz, DMSO-d_6): δ, ppm 1.78 (s, 3H), 5.16 (s, 1H), 7.32 (d, 1H), 7.36 (s, 2H,), 7.39-7.63 (m, 5H,), 7.78-7.80 (d, 2H). ^{13}C NMR (100 MHz, DMSO-d_6): δ, ppm 160.42, 145.30, 144.75, 139.74, 137.90, 133.55, 133.02, 132.97, 30.54, 129.82, 129.43, 128.59, 126.78, 120.53, 120.01, 97.76, 56.62, 34.02, 12.82. Anal. Calcd. (%) for $C_{20}H_{14}Cl_2N_4O$: C, 60.47; H, 3.55; N, 14.10. Found: C, 60.69; H, 3.49; N, 14.39.

6-amino-4-(4-bromophenyl)-3-methyl-1-phenyl-1,4-dihydropyrano[2,3-c]pyrazole-5-carbonitrile (11i)

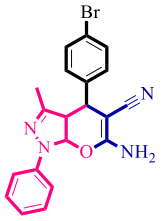

Colour: White solid. M.p.: 182-184 °C. ^{1}H NMR (400 MHz, DMSO-d_6): δ, ppm 1.8 (s, 3H), 4.72 (s, 1H), 7.23-7.34 (m, 5H), 7.48-7.6 (m, 4H), 7.79 (d, 2H, *J* = 8.00 Hz). ^{13}C

NMR (100 MHz, DMSO-d_6): δ, ppm 159.95, 145.67, 144.40, 143.56, 137.96, 131.93, 130.54, 129.80, 126.69, 120.60, 120.49, 120.34, 98.59, 58.16, 36.62, 13.05. Anal. Calcd. (%) for $C_{22}H_{21}N_5O$: C, 71.14; H, 5.70; N, 18.85. Found: C, 71.35; H, 5.75; N, 18.63.

6-amino-4-(4-methoxyphenyl)-3-methyl-1-phenyl-1,4-dihydropyrano[2,3-c]pyrazole-5-carbonitrile (11j)

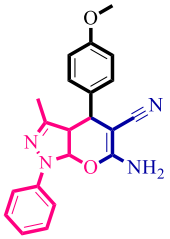

Colour: White solid. M.p.: 172-174 °C. ^{1}H NMR (400 MHz, DMSO-d_6): δ, ppm 1.79 (s, 3H), 3.75 (s, 3H), 4.63 (s,1H), 6.91 (d, 1H, *J* = 8.4 HZ), 7.16-7.18 (m, 3H), 7.31 (t, 1H, *J* = 7.2 Hz), 7.38 (t, 1H, *J* = 7.6 Hz), 7.49 (t, 2H, *J* = 7.6 Hz), 7.79 (d, 3H, *J* = 8.4 Hz). Anal. Calcd. (%) for $C_{21}H_{18}N_4O_2$: C, 70.38; H, 5.06; N, 15.63. Found: C, 69.69; H, 5.85; N, 6.19.

6-amino-4-(3-ethoxy-4-hydroxyphenyl)-3-methyl-1-phenyl-1,4-dihydropyrano[2,3-c]pyrazole-5-carbonitrile (11k)

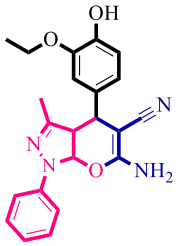

Colour: White solid. M.p.: 167-169 °C. ^{1}H NMR (400 MHz, DMSO-d_6): δ, ppm 1.30 (t, 3H, *J* = 6.8 Hz), 1.82 (s, 3H), 3.96-4.01 (m, 2H), 4.56 (s, 1H), 6.61-7.13 (m, 5H), 7.31 (t, 1H, *J* = 7.2 Hz), 7.49 (t, 2H, *J* = 7.6 Hz) 7.79 (d, 2H, *J* = 8.4 Hz), 8.83 (s, 1H). ^{13}C NMR (100 MHz, DMSO-d_6): δ, ppm 159.69, 146.91, 146.30, 145.87, 144.23, 138.09, 134.97, 129.79, 126.53, 120.66, 120.57, 120.31, 116.09, 113.96, 99.36, 64.44, 59.15, 36.79, 15.18, 13.13. Anal. Calcd. (%) for $C_{22}H_{20}N_4O_3$: C, 68.03; H, 5.19; N, 14.42. Found: C, 69.69; H, 5.85; N, 6.19.

6-amino-3-methyl-4-(4-nitrophenyl)-1-phenyl-1,4-dihydropyrano[2,3-c]pyrazole-5-carbonitrile (11l)

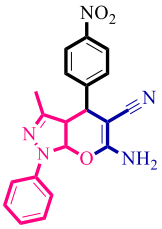

Colour: White solid. M.p.: 191-193 °C. ^{1}H NMR (400 MHz, DMSO-d_6): δ, ppm 1.82 (s, 3H), 4.94 (s, 1H), 7.44-7.6 (m, 7H), 7.83 (bs, 2H), 8.25 (bs, 2H). ^{13}C NMR (100 MHz, DMSO-d_6): δ, ppm 160.20, 151.66, 147.08, 145.62, 144.48, 137.91, 129.79, 129.68, 126.76, 124.36, 120.54, 120.23, 98.05, 57.38, 36.90, 13.03. Anal. Calcd. (%) for $C_{20}H_{15}N_5O_3$: C, 64.34; H, 4.05; N, 18.76. Found: C, 64.61; H, 3.97; N, 18.98.

Spectra of substituted dihydropyrano[2,3-c]pyrazoles compounds (11a-l)

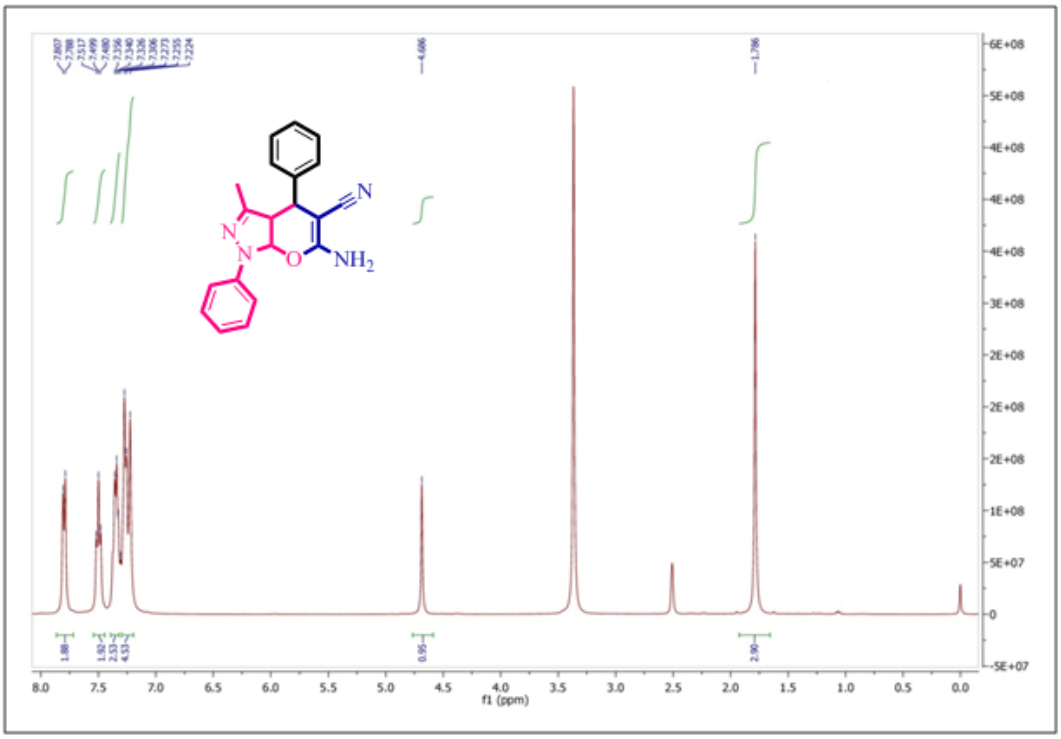

^{1}H NMR spectrum of compound **11a.**

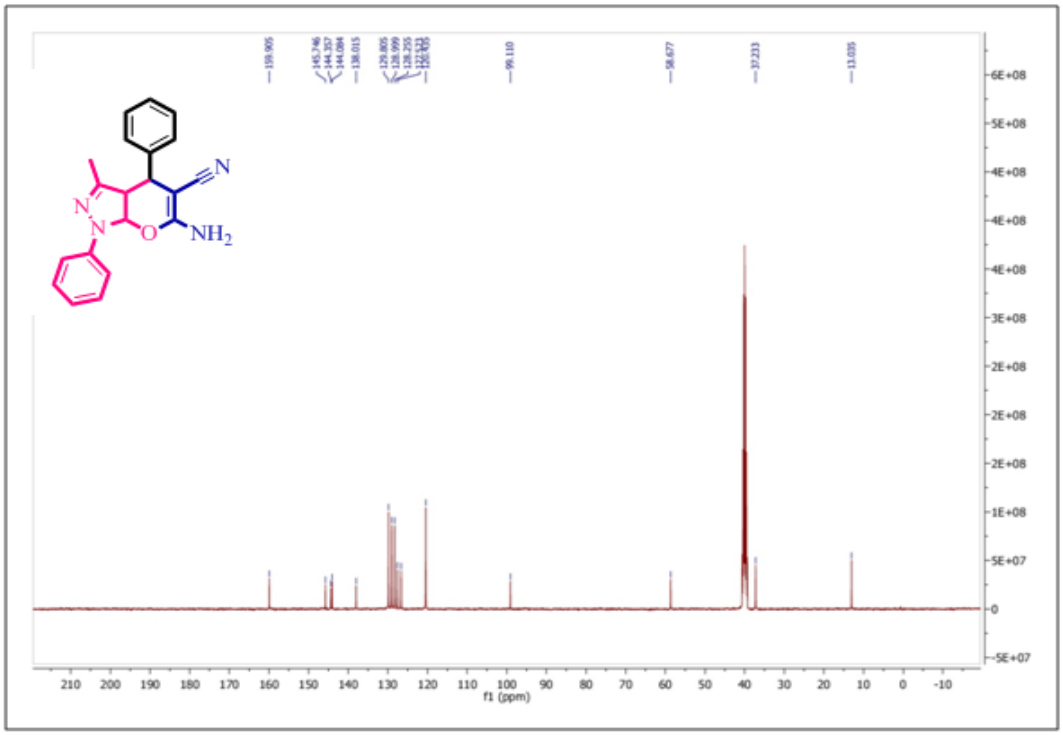

^{13}C NMR spectrum of the compound **11a.**

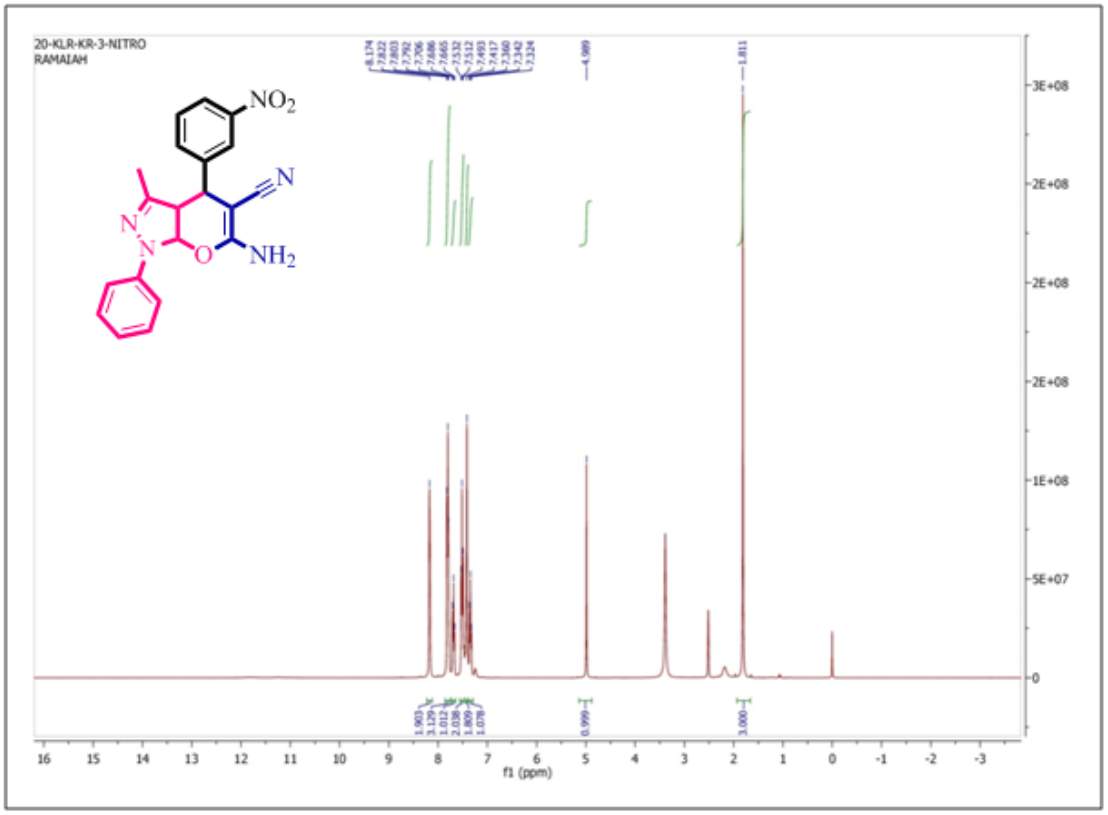

^{1}H NMR spectrum of compound **11b.**

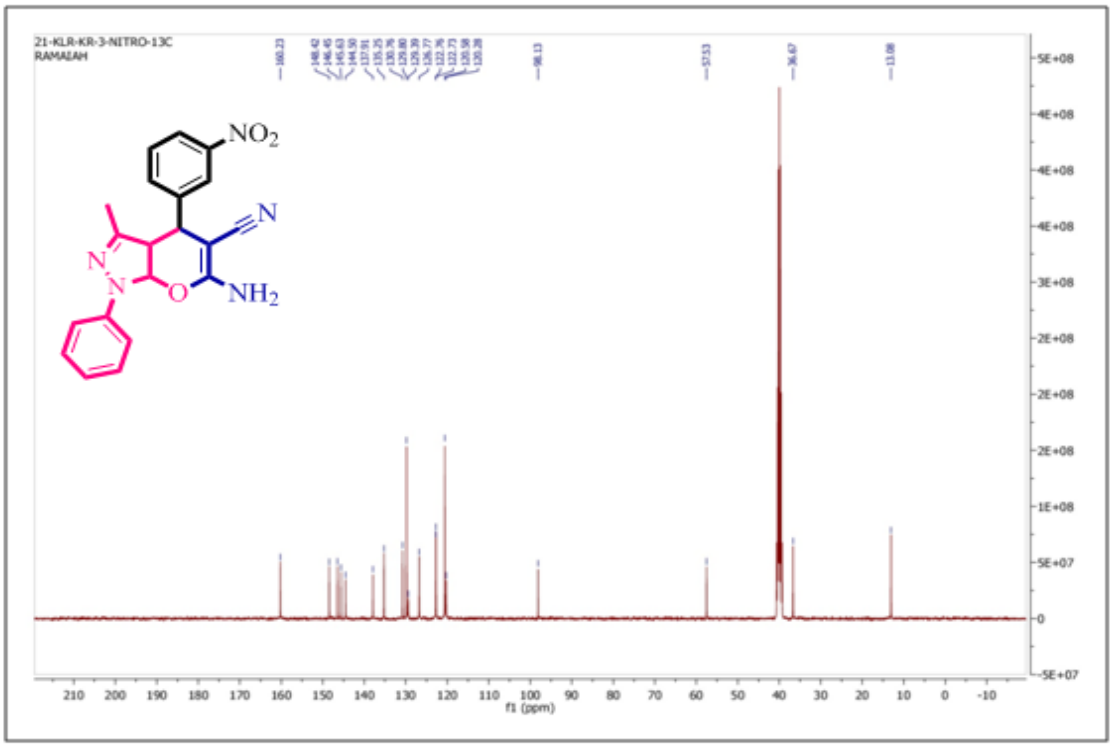

^{13}C NMR spectrum of compound **11b.**

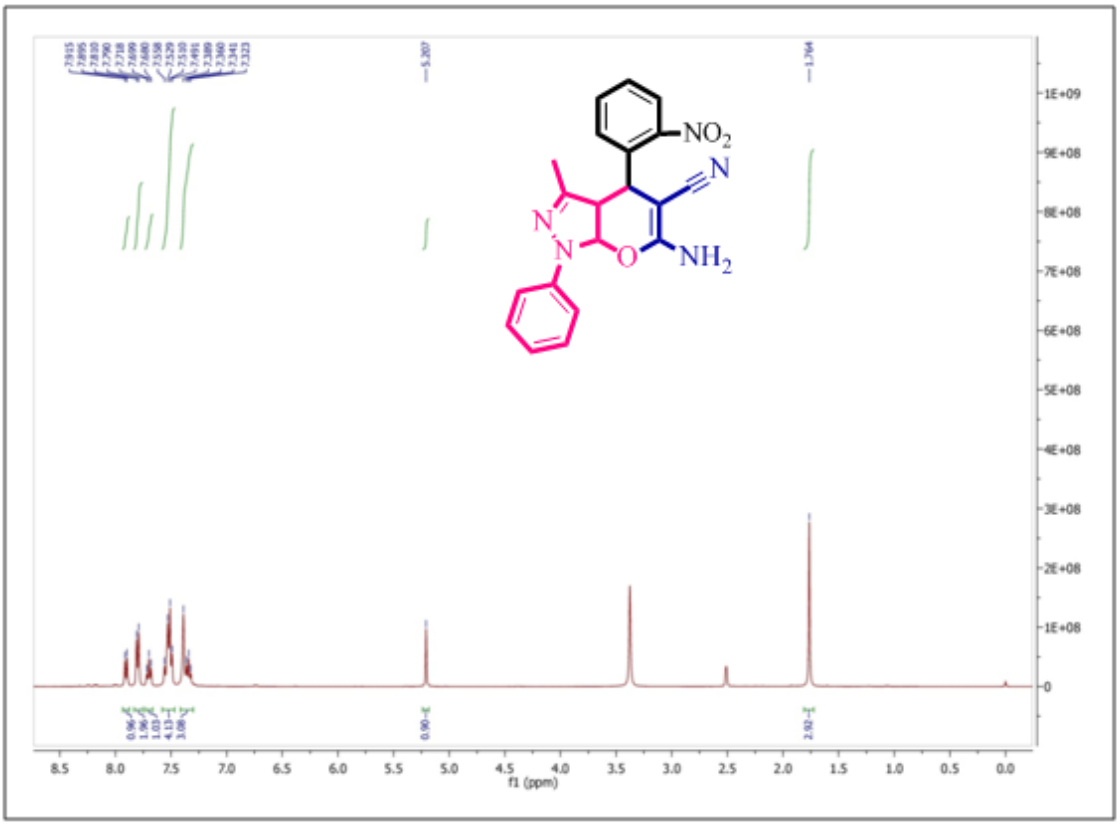

^{1}H NMR spectrum of compound **11c.**

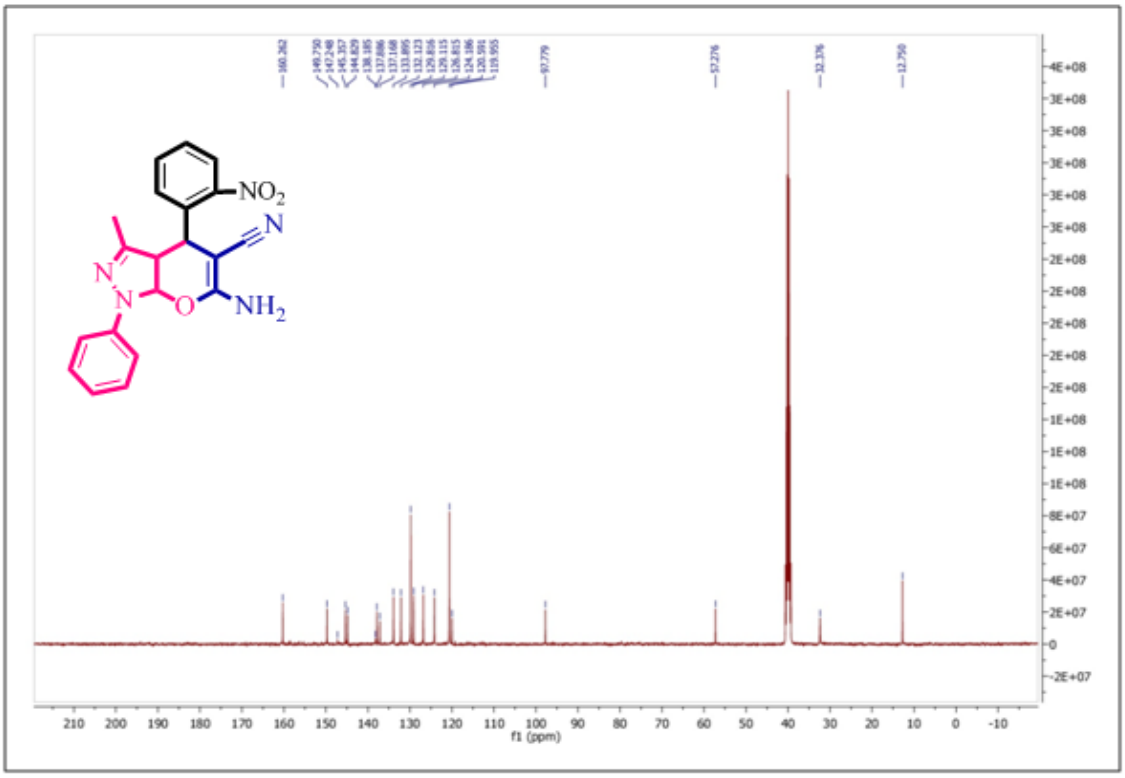

^{13}C NMR spectrum of the compound **11c.**

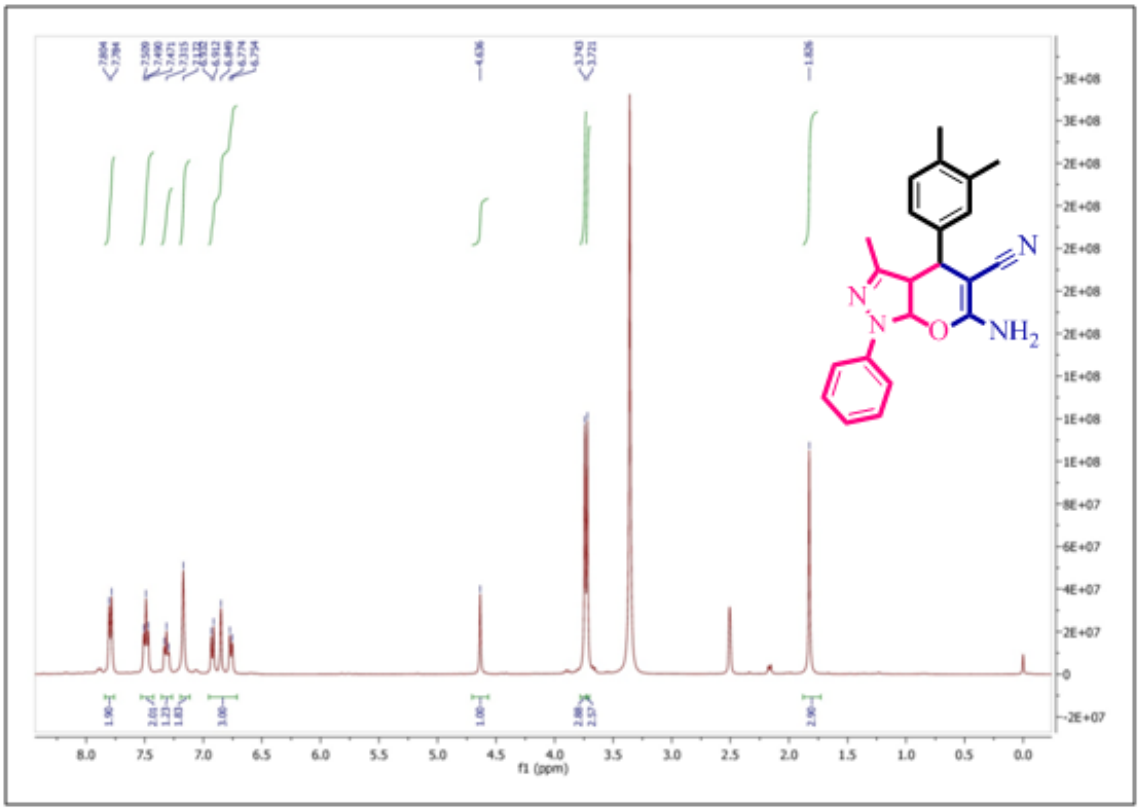

^{1}H NMR spectrum of compound **11d.**

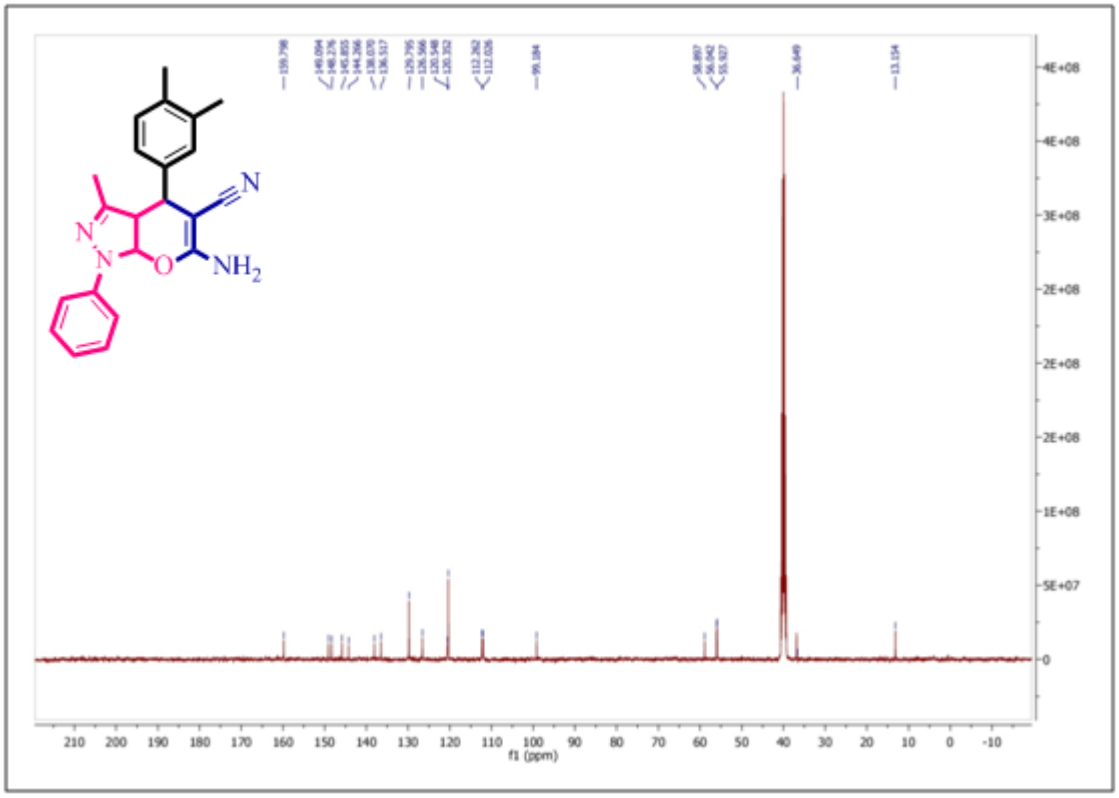

^{13}C NMR spectrum of the compound **11d.**

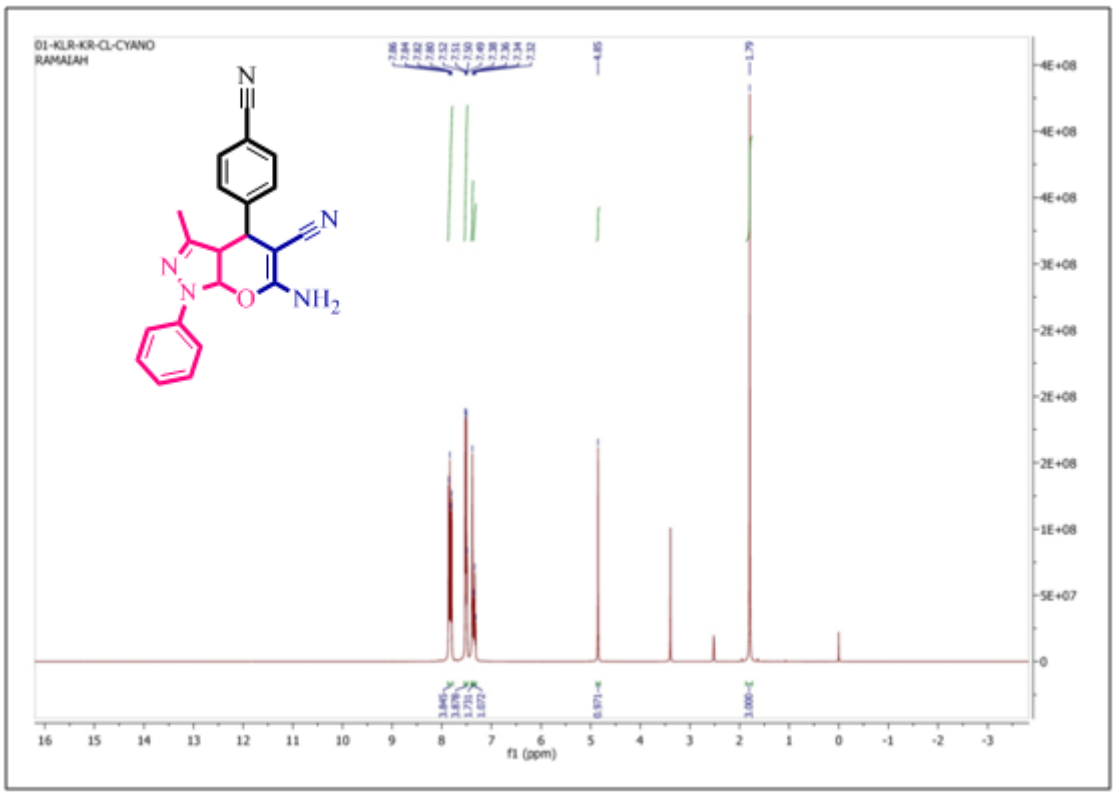

^{1}H NMR spectrum of the compound **11e.**

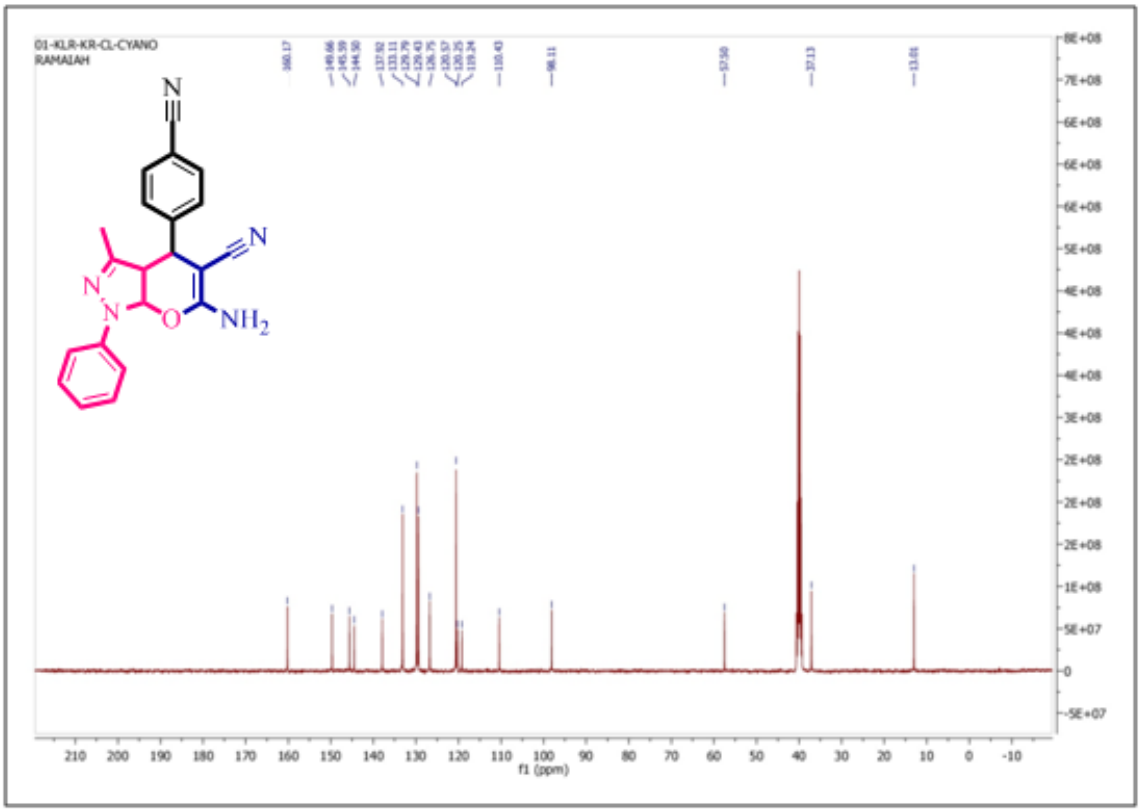

^{13}C NMR spectrum of the compound **11e.**

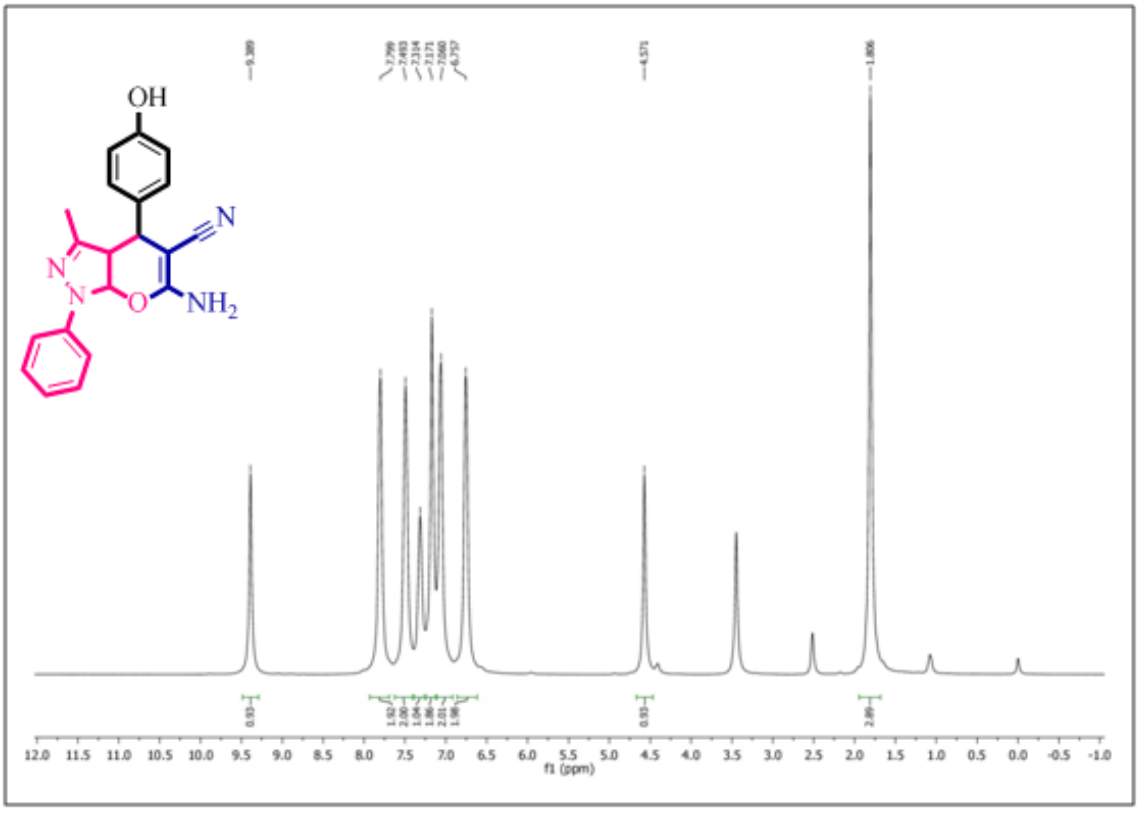

^{1}H NMR spectrum of the compound **11f.**

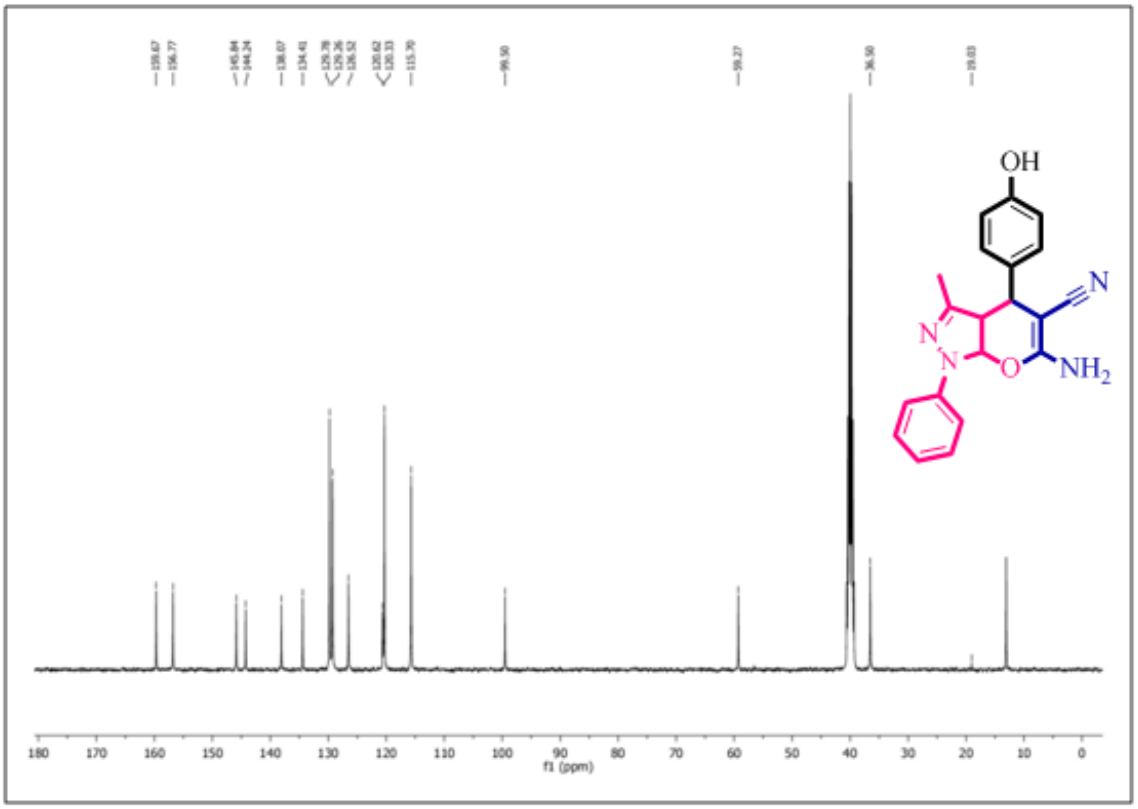

^{13}C NMR spectrum of the compound **11f.**

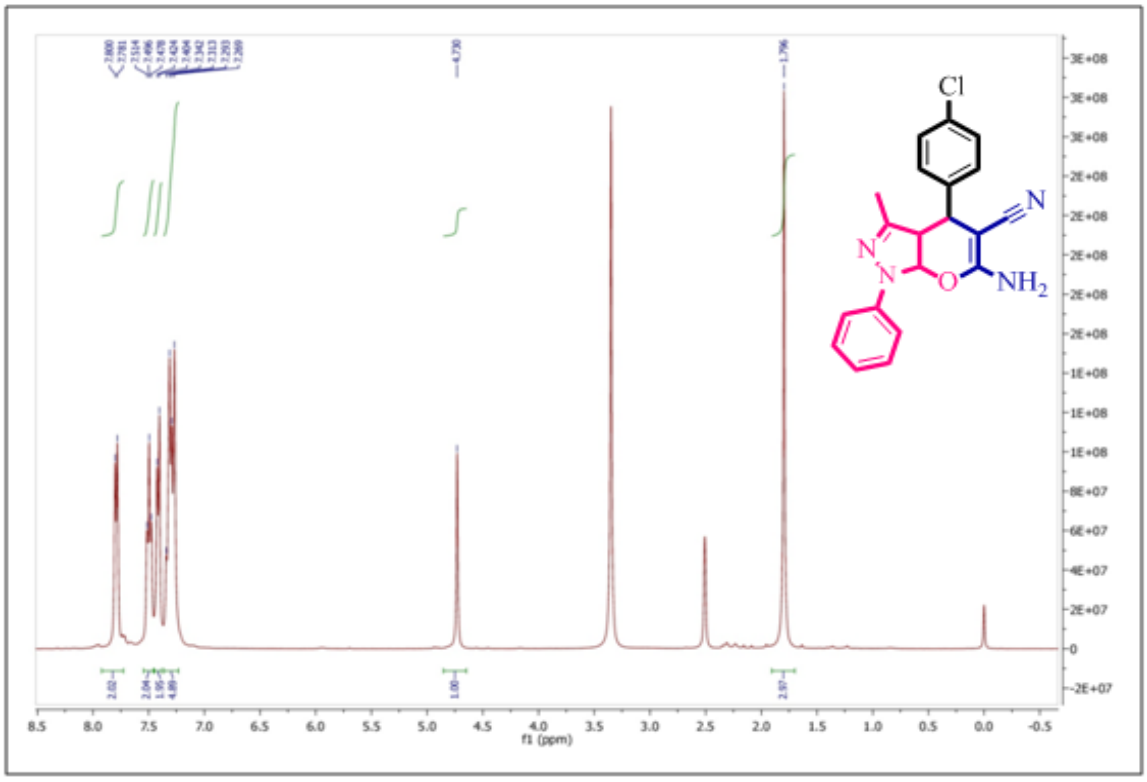

^{1}H NMR spectrum of compound **11g.**

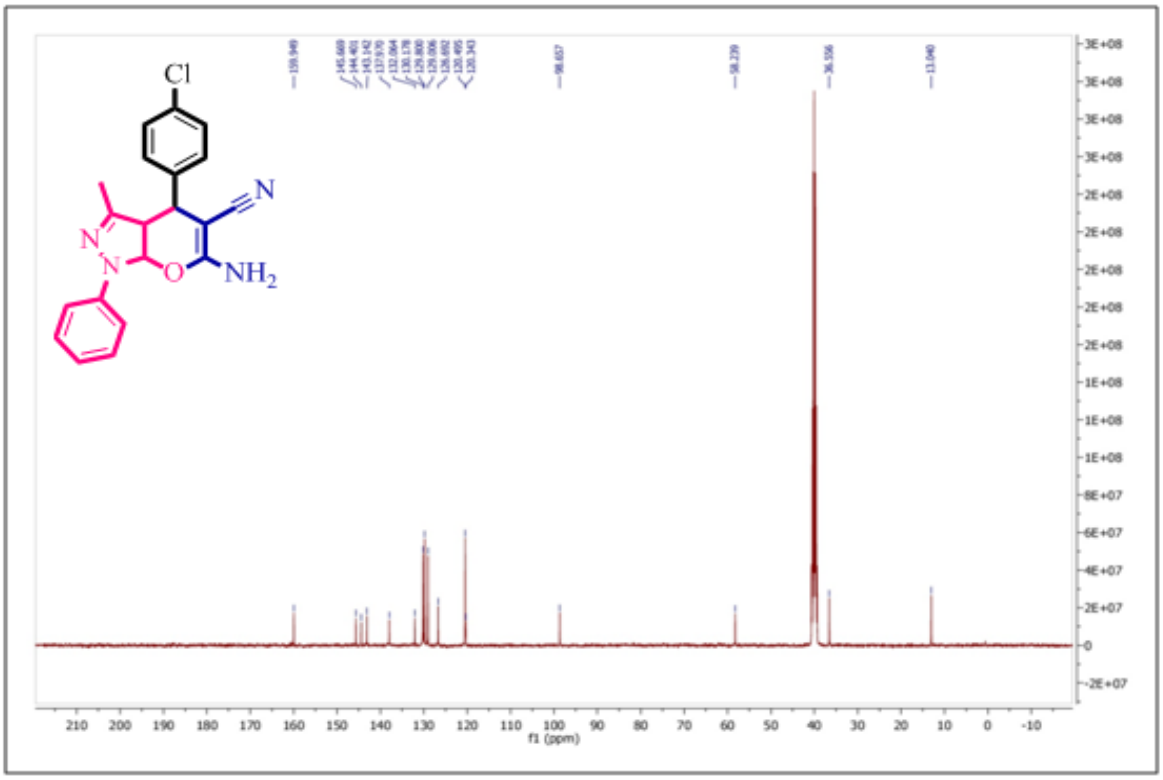

^{13}C NMR spectrum of the compound **11g.**

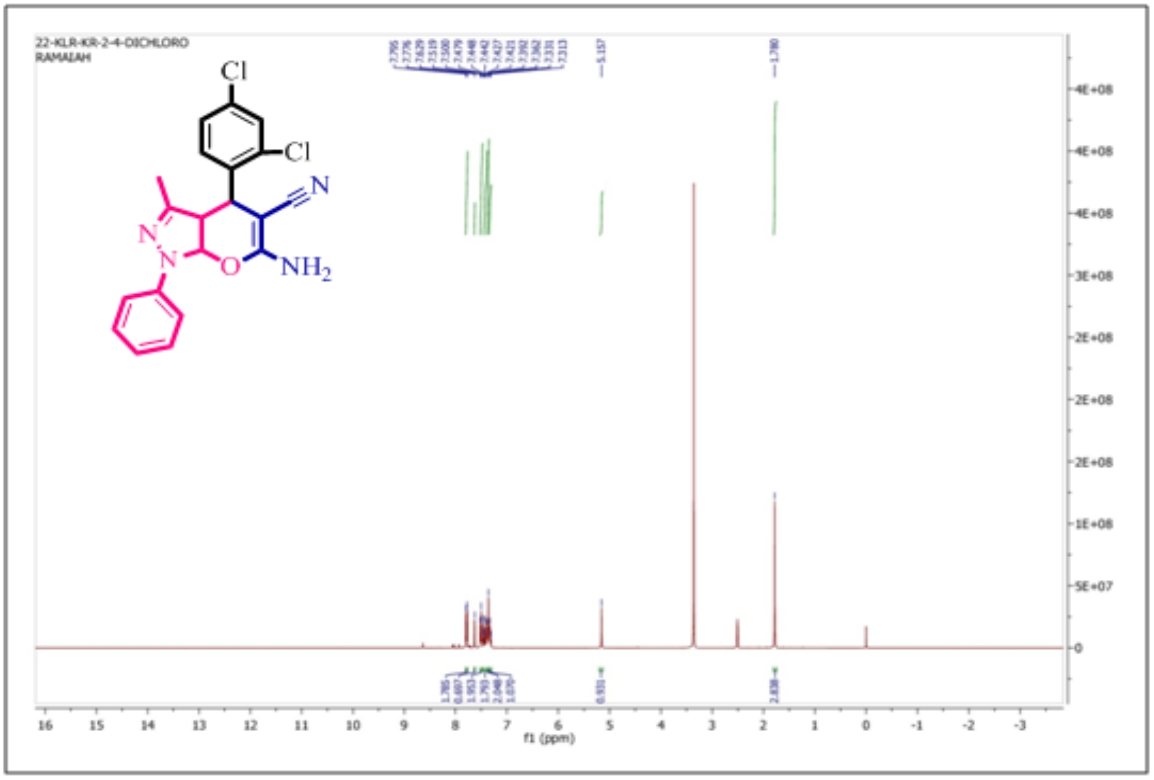

^{1}H NMR spectrum of the compound **11h.**

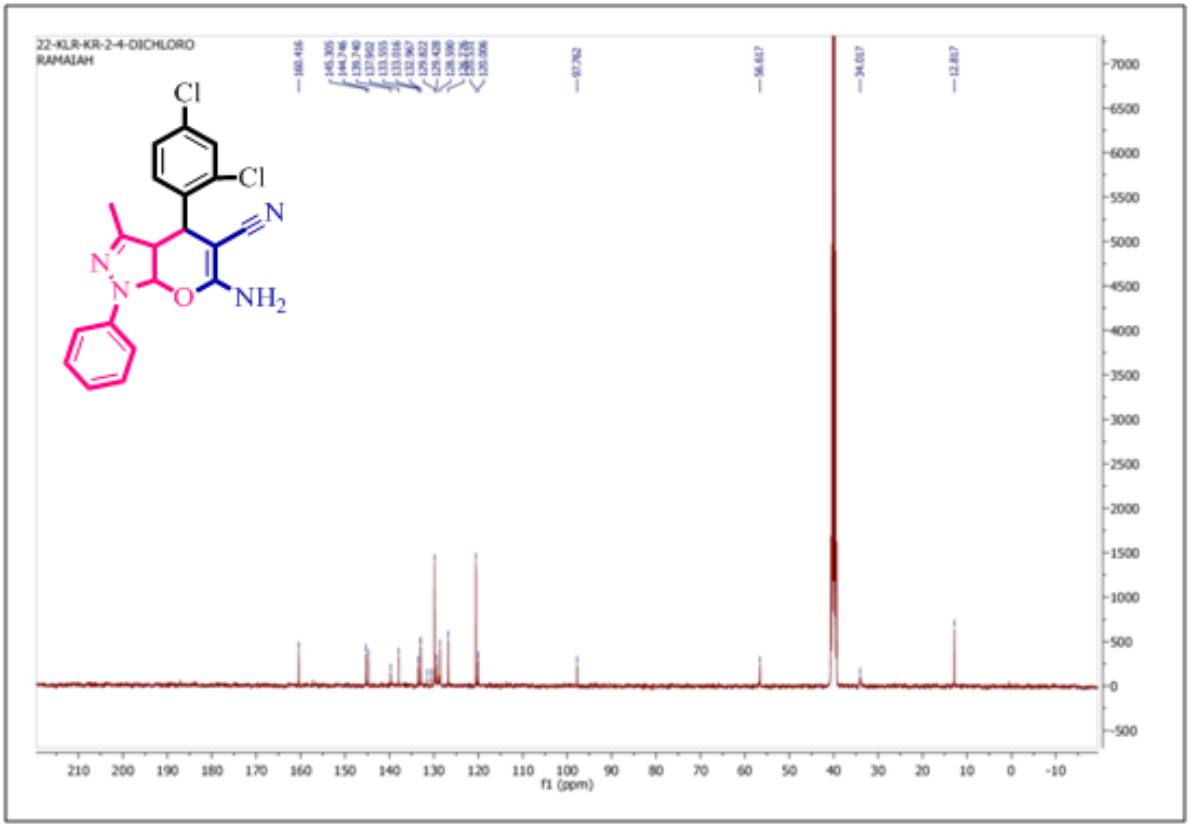

^{13}C NMR spectrum of the compound **11h.**

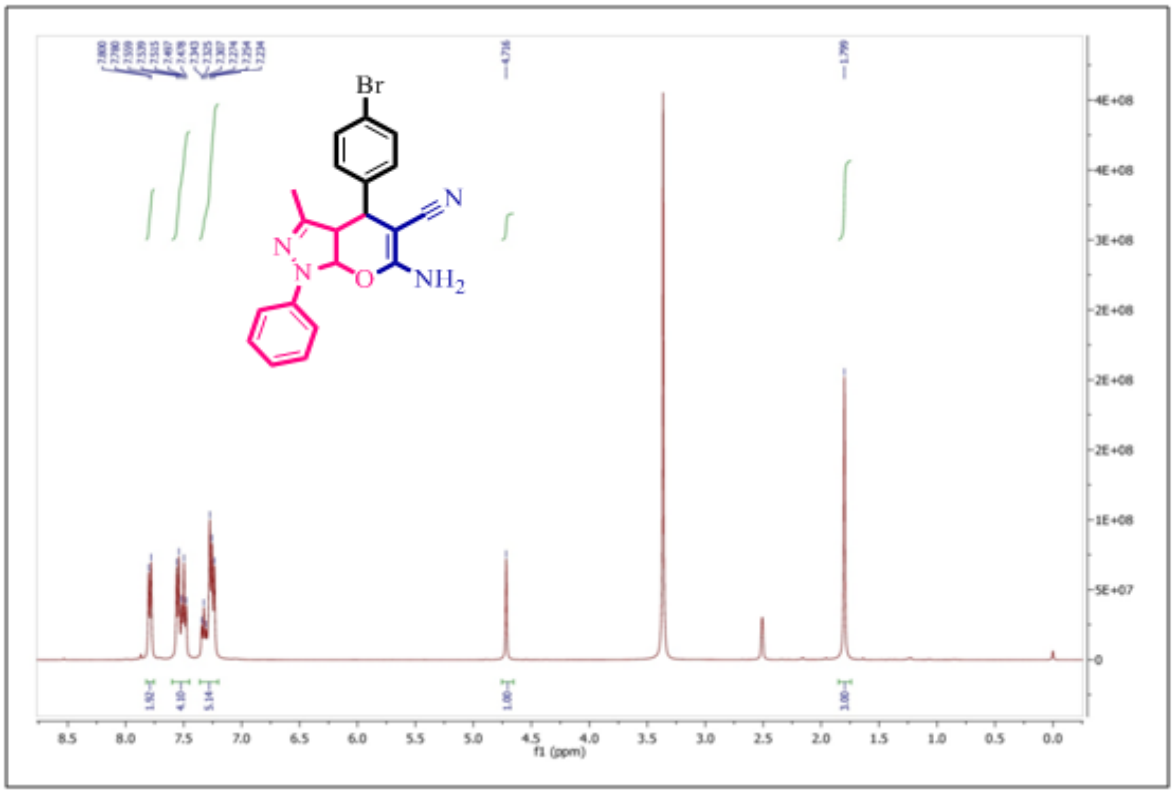

^{1}H NMR spectrum of compound **11i.**

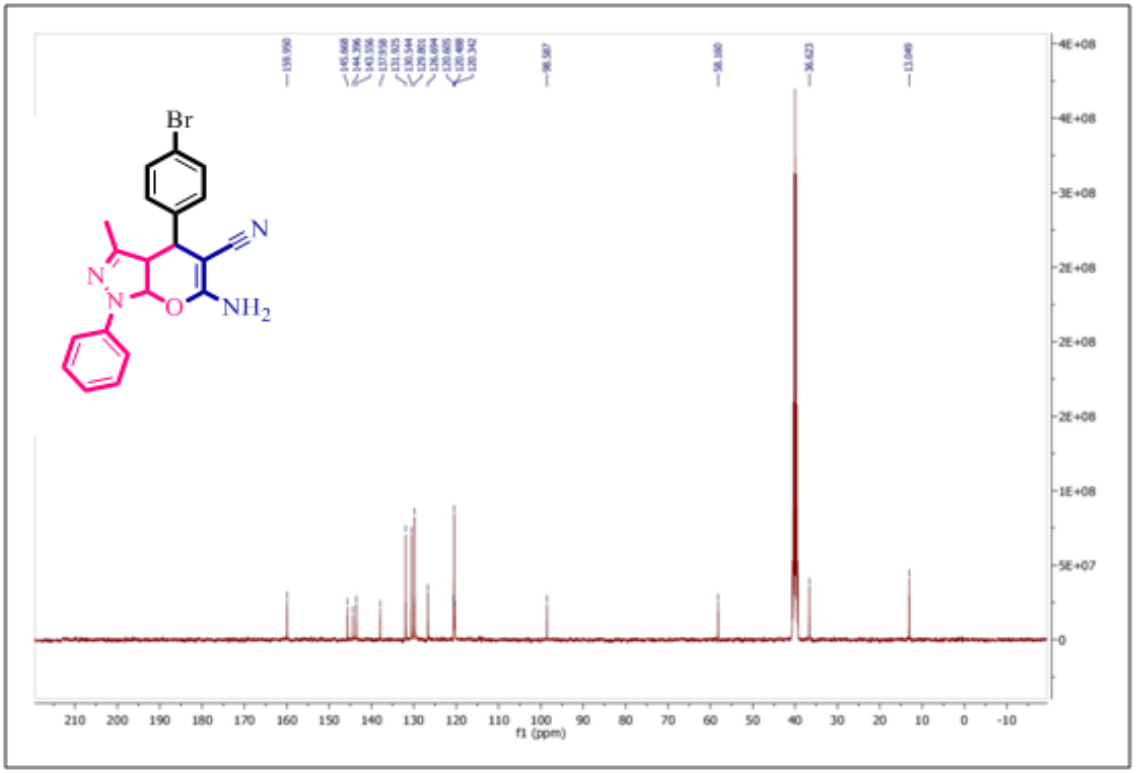

^{13}C NMR spectrum of the compound **11i.**

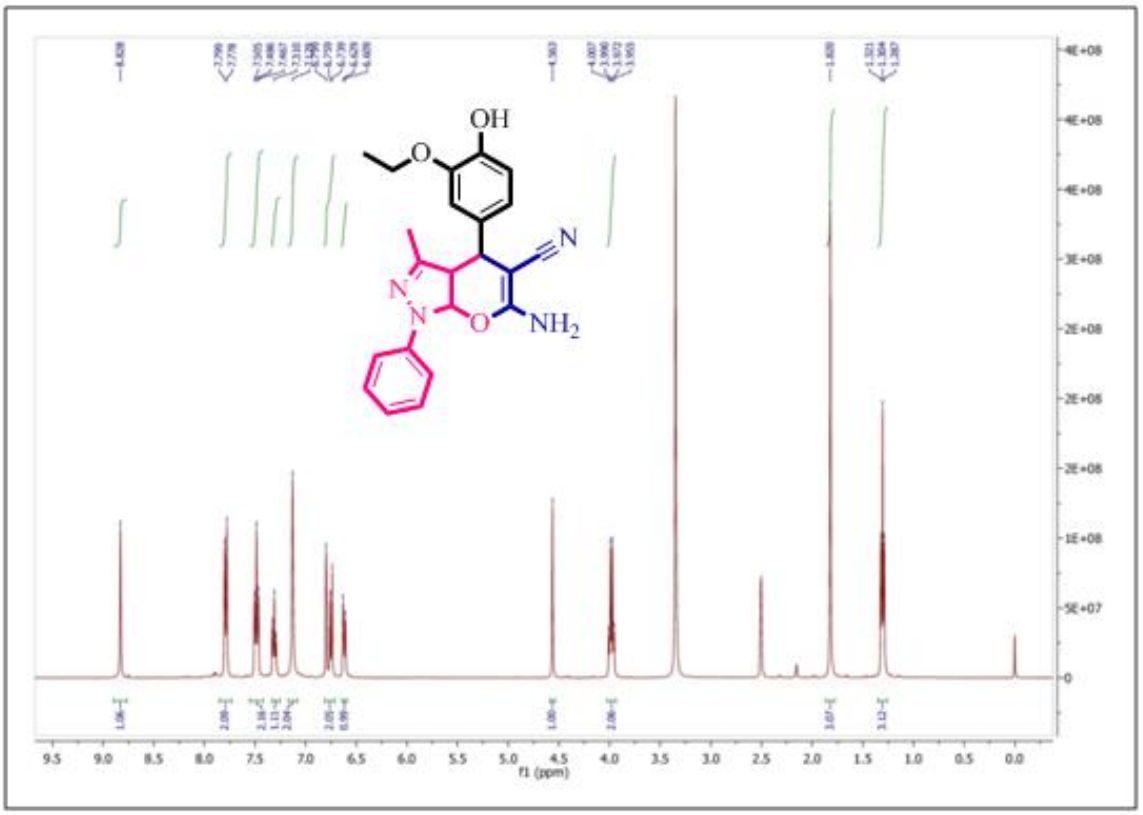

^{1}H NMR spectrum of the compound **11k.**

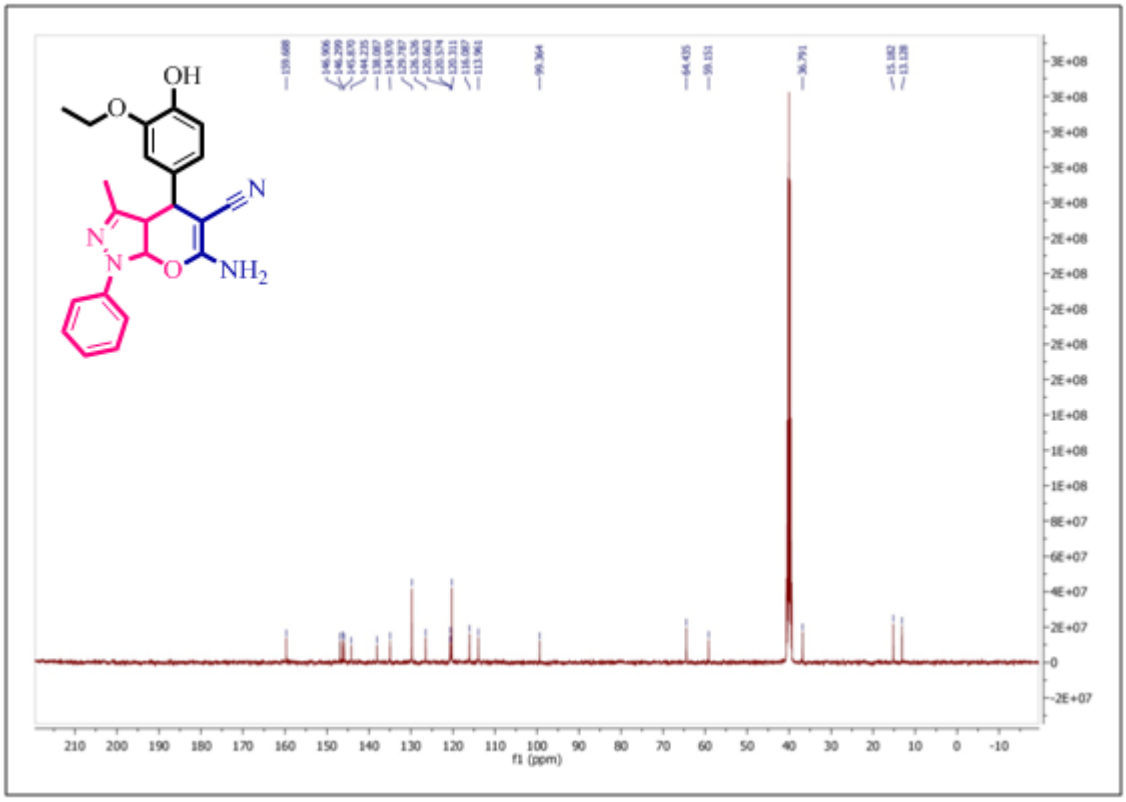

^{13}CNMR spectrum of the compound **11k.**

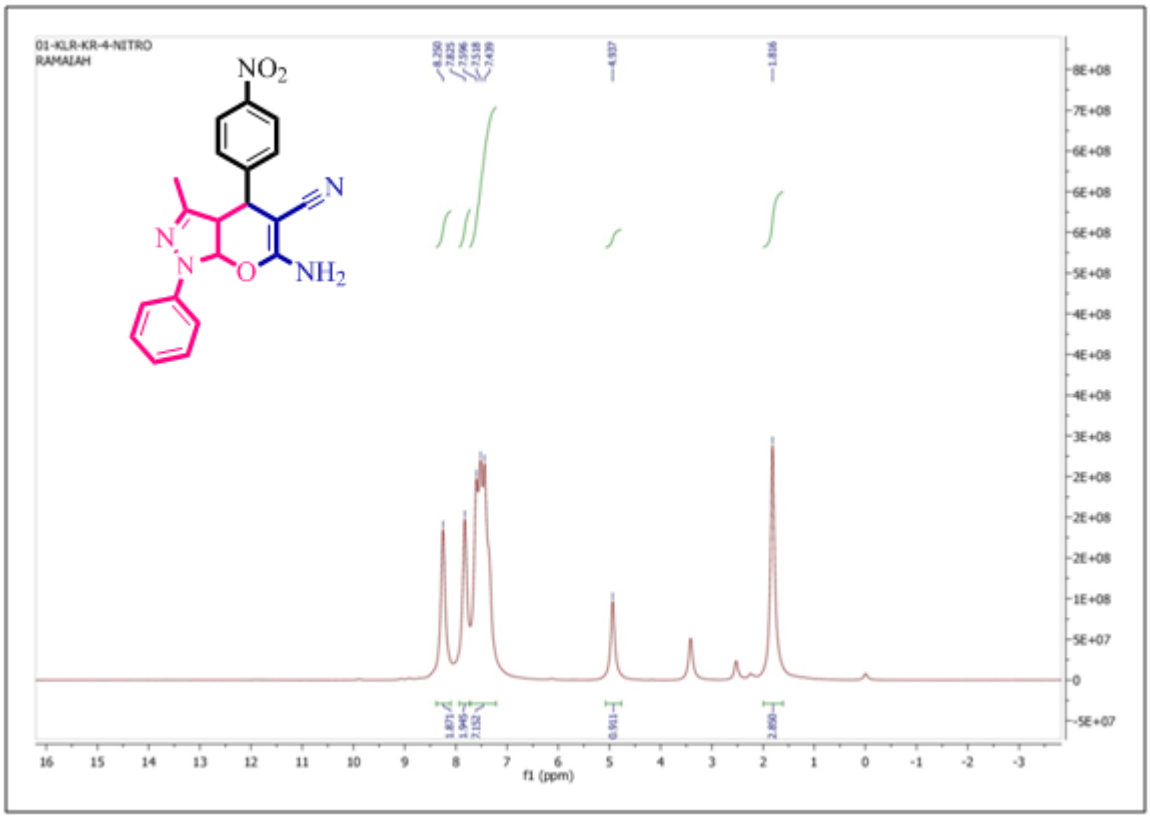

^{1}H NMR spectrum of the compound **11l.**

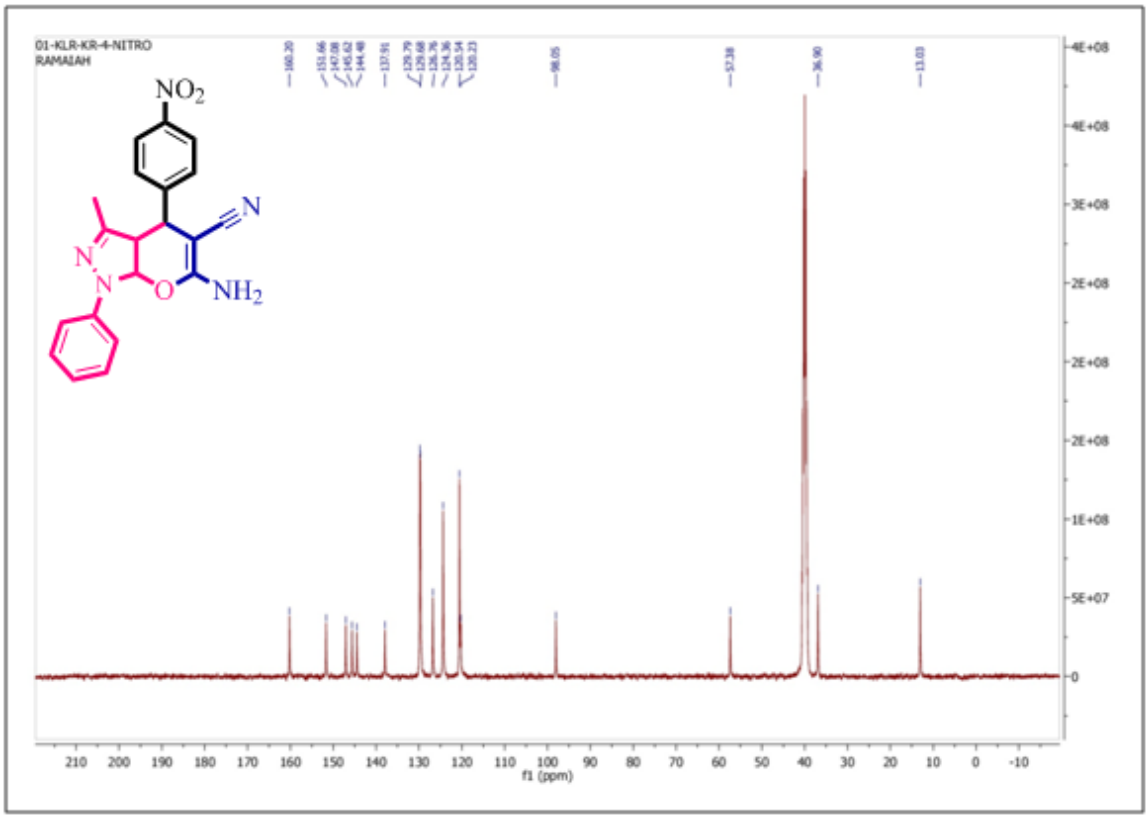

^{13}C NMR spectrum of the compound **11l.**

4. Conclusions

We have, for the first time, demonstrated the coordinating behaviour of ANA with metals Co(II), Ni(II), Cu(II), Zn(II), Cd(II) and Pd(II). The ligand and its metal complexes have been characterized by a variety of spectroscopic techniques. The single crystal X-ray structure of ANA and its corresponding Zn(II) complex have shown their ability to form strong as well as weak H-bonding interaction which may have implications in crystal engineering. The related single crystal X-ray structures of Zn(II) complex of 2-aminopyridine and 3-pyridine aldehyde revealed their ability to form 1-dimensional and 2-dimensional structures, respectively. The presence of both aldehyde and amine group helps ANA to have a 3-D structure. Based on spectral data, it was apparent that Pd(II) and Cu(II) complexes show square-planar geometry, whereas Co(II), Ni(II), Zn(II) and Cd(II) complexes showed tetrahedral geometry with $[M(N)_2(Cl)_2]$ coordination sphere. The ANA acts as mono dentate ligand towards the metal ions through N atom of pyridine ring, orienting the aldehyde and amine potential functional groups of the ligand in the metal complexes. In DFT studies, all the complexes showed excellent nonlinear optical properties. In addition, the biological evaluation results

revealed that Co(II) and Pd(II) complexes have shown significant antimicrobial activity against the tested microorganisms. The scavenging activity of Zn(II) complex showed potent activity with IC_{50} value of 10.14 ± 2.50 µM compared to standard ascorbic acid. Zn(II) complex exhibited significant anticancer activity against IMR-32, HepG-2 and Raw 264.7 cell lines compared to cisplatin as the reference control. Furthermore, the molecular docking analysis against EGFR protein receptor, Zn(II) complex showed the lowest binding energy of -5.79 kcal/mol. The molecular docking results strongly correlate with experimental *in vitro* anticancer activity results. In order to extend this work, we have demonstrated the usefulness of a cheaper, low toxic and environmentally benign zinc metal complex, $Zn(ANA)_2Cl_2$ as a catalyst in the to produce a variety of fully substituted pyridines and dihydropyrano[2,3-c]pyrazoles in good yields via MCR approach. The significant advantages of these protocols include readily available substrates, short reaction time, easy workup, and no column chromatographic purification (without any tedious work-up or purification). These advantages made this methodology facile and appropriate to create diverse libraries. The presence of reactive −CN and $-NH_2$ groups at 5 and 6 positions, respectively, renders these compounds ready for further transformations into more complex heterocycles.

References

[1] A.F. Pozharskii, A.T. Soldatenkov, A.R. Katritzky, John Wiley and Sons, UK, **1997**.

[2] G.W. Bemis, M.A. Murcko, *J. Med. Chem.* **1996**, *39*, 2887.

[3] J. Xu, J. Stevenson, *J. Chem. Inf. Sci. Comput. Sci.* **2000**, *40*, 1177.

[4] Z.F. Chem, Y.Z. Tang, H. Liang, H.K. Fun, K.B. Yu, *J. Coord. Chem.* **2006**, *59*, 207.

[5] G.S. Sreeletha, *Asian J. Chem.* **2005**, *17*, 1073.

[6] F. Zucchi, G. Trabanelli, N.A. Gonzalez, *Ach-Models Chem.* **1995**, *132*, 4579.

[7] B.T. Khan, S.R.A. Khan, K. Annapoorna, *Indian J. Chem. A* **1995**, *34A*, 878.

[8] M.E. Lizarraga, R. Navarro, E.P. Urriolabeitia, *J. Org. Met. Chem.* **1997**, *542*, 51.

[9] A.S. Georgopoulou, S. Ulvenlund, D.M.P. Mingos, I. Baxter, D.J. Williams, *J. Chem. Soc.* **1999**, *4*, 547.

[10] W. Liaw, N. Lee, C. Chen, C. Lee, G. Lee, S. Peng, *J. Am. Chem. Soc.* **2000**, *122*, 488.

[11] P.J. Trotter, P.A. White, *J. Appl. Spectrosc.* **1978**, *32*, 323.

[12] K.Y. Rajpure, C.H. Bhosale, *J. Mater. Chem. Phys.* **2000**, *64*, 70.

[13] S. Licht, *Sol. Energy Mater. Sol. Cells* **1995**, *38*, 305.

[14] J.M. Altenburger, G.Y. Lassalle, M. Matrougui, D. Galtier, J.C. Jetha, Z. Bocskei, C.N. Berry, C. Lunven, J. Lorrain, J.P. Herault, P. Schaeffer, S.E. O'Connor, J.M. Herbert, *Bioorg. Med. Chem.* **2004**, *12*, 1713.

[15] H. Camp, J. Perk, *Hand Book of American Chemical Society*, **2000**, pp. 31.

[16] K. Nakamoto, *Infrared and Raman spectra of Inorganic and Coordination compounds*, 5th Edn, Wiley-Interscience, New York, **1997**

[17] M. Sandstrom, I. Perssan, *Acta Chem. Scand.* **1990**, *44*, 653.

[18] K. Nakamoto, *Infrared spectra of Inorganic and Coordination compounds*, Wiley and Sons, New York, **1986**, pp. 212.

[19] K. Nakamoto, *Infrared and Raman spectra of Inorganic and Coordination Compounds*, 5th Edn, Wiley-Interscience, New York, **1997**, pp. 86.

[20] W.J. Geary, *Coord. Chem. Rev.* **1971**, *7*, 81.

[21] D.M.A. El–Aziz, S.E.H. Etaiw, E.A. Ali, *J. Mol. Struct.* **2013,** *487*, 1048.

[22] S.E.H. Etaiw, D.M.A. El–Aziz, E.H.A. El–Zaher, E.A. Ali, *Spectrochim. Acta A* **2011**, 79, 1331.

[23] S. Sobha, R. Mahalakshmi, N. Raman, *Spectrochim. Acta A 2012*, *92*, 175.

[24] Y. Li, Z.Y. Yang, *J. Fluoresc.* **2010**, 20, 329.

[25] D.M.L. Goodgame, M. Goodgame, F.A. Cotton, *J. Am. Chem. Soc.* **1961**, *83*, 4161.

[26] D. Banerje, *Coordination Chemistry*, Tata McGraw–Hill Publisher, London, **1993**.

[27] R. Selwin Joseyphus, M. Sivasankaran Nair, *Arabian J. Chem.* **2010**, *3*, 195.

[28] S.B. Kalia, K. Lumba, G. Kaushal, M. Sharma, *Indian J. Chem. A* **2007**, *46*, 1233.

[29] V.K. Naveen, S.K. Gurunath, B. Srinivasa, K. Vidyanand, K.J. Revankar, *J. Coord. Chem.* **2010**, *63*, 3301.

[30] O.A.M. Ali, *Spectrochim. Acta A* **2014**, *132*, 52.

[31] D. Kivelson, R. Nieman, *J. Chem Phys.* **1961**, *35*, 149.

[32] D. Arish, M. Sivankaran Nair, *J. Mol. Struct.* **2010**, *983*, 112.

[33] (a) B.J. Hathaway, D.E. Billing, *Coord. Chem. Rev.* **1970**, *5*, 143; (b) B.J. Hathaway**,** *Struct. Bond.* (Berlin) **1984**, *57*, 55.

[34] G.A. Jeffrey, *An introduction to Hydrogen bonding*, Oxford University press**, 1997**.

[35] Z.T. Zhang, Q.Y. wang, *J. Chem. Cryst.* **2005**, *35*, 989.

[36] C. Janiak. *J. Chem. Soc. Dalton Trans.* **2000**, *31*, 3885.

[37] P.N. Prasad, D.J. Williams, *Introduction to Nonlinear Optical Effects in Molecules and Polymers*, Wiley, New York, **1991**.

[38] F. Meyers, S.R. Marder, B.M. Pierce, J.L. Bredas, *J. Am. Chem. Soc.* **1994**, *116*, 10703.

[39] A. Hinchliffe, R.W. Munn, John Wiley and Sons Ltd, Chichester, **1985**.

[40] D.A. Kleinman, *Phys. Rev.* **1962**, *126*, 1977.

[41] R. Zhang, B. Du, G. Sun, Y.X. Sun, *Spectrochim. Acta A* **2010**, *75*, 1115.

[42] G. Gece, *Corros. Sci.* **2008**, *50*, 2981.

[43] K. Fukui, *Science* **1982**, *218*, 747.

[44] T.A. Koopmans, *Physica* **1933**, *1*, 104.

[45] R.J. Parr, L.V. Szentpaly, S. Liu, *J. Am. Chem. Soc.* **1999**, *121*, 1922.

[46] A. Albert, S.D. Goldacre, R.J. Goldacre, B.G. Balfour, *Brit. J. Exptl. Pathol.* **1947**, *28*, 69.

[47] A. Albert, *Soc. Gen. Microbiol.* **1958**, *8*, 112.

[48] M. Di Rosa, J.P. Giroud, D.A. Willouchby, *J. Pathol.* **1971**, 104, 15.

[49] Reviews on zinc catalysis: a) X.-F. Wu, *Chem. Asian J.* **2012**, *7*, 2502; b) S. Enthaler, *ACS Catal.* **2013**, *3*, 150; c) X.-F. Wu, H. Neumann, *Adv. Synth. Catal.* **2012**, *354*, 3141; d) S, Enthaler, X.-F. Wu, *Zinc Catalysis: Applications in Organic Synthesis*, Wiley, V.C.H, Weinheim, **2015**; e) M.J. González, L.A. López, R. Vicente, *Tetrahedron Lett.* **2015**, *56*, 1600.

[50] a) E. Altman, G.D. Stefanidis, T. Gerven Van, A. Stankiewicz, *Ind. Eng. Chem. Res.* **2012**, *51*, 1612; b) I.D. Hosein, C.M. Liddell, *Langmuir* **2007**, *23*, 2892; c) F. Shin-ichiro, Y. Yuki, A. Masahiko, *J. Catal.* **2013**, *297*, 137; d) M.E. Cucciolito, M. Lega, V. Papa, F. Ruffo, *Catal. Lett.* **2016**, *146*, 1113; e) K. Wilson, A. Renson, J.H. Clark. *Catal. Lett.* **1999**, *61*, 51.

[51] a) L. Marie-France, B. Damien, C. Janine, *Org. Lett*. **2005**, *7*, 171; b) S. Thapa, A.S. Vangala, R. Giri, *Synthesis* **2016**, *48*, 504.

[52] a) W.A. Herrmann, *Synthetic Methods of Organometallic and Inorganic Chemistry: Catalysis*, **2002**; b) P. Knochel, P. Jones, *Organozinc reagents: A practical approach*, Oxford University Press, Oxford, **1999**; c) S. Sase, M. Jaric, A. Metzger, V. Malakhov, P. Knochel, *J. Org. Chem.* **2008**, *73*, 7380; d) N. Hadei, E.A.B. Kantchev, C.J. O'Brien, M.G. Organ, *Org. Lett.* **2005**, *7*, 3805; e) C. Han, S.L. Buchwald. *J. Am. Chem. Soc.* **2009**, *131*, 7532; f) H. Diana, M.H. Jeffrey, G. Robert, K. Paul, *ACS Catal.* **2016**, *6*, 1540; g) M. Sailer, K.I. Dumichi, J.L. Sorensen, *Synthesis* **2015**, *47*, 79; h) C. Wolf, M. Moskowitz, *J. Org. Chem.* **2011**, *76*, 6372; i) S. Toshiaki, S. Masahiko, *Tetrahedron Lett.* **2001**, *42*, 429.

[53] A. Krasovskiy, C. Duplais, B.H. Lipshutz, *J. Am. Chem. Soc.* **2009**, *131*, 15592.

[54] a) X. Zhang, X. Xu, G. Chen, W. Yi, *Org. Lett.* **2016**, *18*, 4864; b) J.J. Chu, B.L. Hu, Z.Y. Liao, X.G. Zhang, *J. Org. Chem.* **2016**, *81*, 8647; c) X.Q. Mou, Z. Xu, L.L. Xu, S.H. Wang, B.H. Zhang, D. Zhang, J. Wang, W.T. Liu, W. Bao, *Org. Lett.* **2016**, *18*, 4032; d) X. Zhang, W. Liu, R. Sun, X. Xu, Z. Wang, Y. Yan, *Synlett* **2016**, *27*, 1563; e) P. Patil, J. Zhang, K. Kurpiewska, J. Kalinowska-Tłuścik, A. Dömling, *Synthesis* **2016**, *48*, 1122; f) S. Chandrasekhar, V. Patro, L.N. Chavan, R. Chegondi, R. Grée, *Tetrahedron Lett*. **2014**, *55*, 5932; g) G. Brahmachari, S. Das, *Tetrahedron Lett.* **2012**, *53*, 1479.

[55] a) L. Zheng, J. Ju, Y. Bin, R. Hua, *J. Org. Chem.* **2012**, *77*, 5794; b) C. Wang, X. Li, F. Wu, B. Wan, *Angew. Chem. Int. Ed.* **2011**, *50*, 7162; c) X. Xin, Y. Wang, S. Kumar, X. Liu, Y. Lin, D. Dong, *Org. Biomol. Chem*. **2010**, *8*, 3078; d) B. Jiang, J. Hao, X. Wang, F. Shi, S.J. Tu, *J. Comb. Chem.* **2009**, *11*, 846; e) F. Zhou, X. Liu, N. Zhang, Y. Liang, R. Zhang, X. Xin, D. Dong, *Org. Lett.* **2013**, *15*, 5786; f) F. Sha, L. Wu, X. Huang, *J. Org. Chem.* **2012**, *77*, 3754; g) S. Yamamoto, K. Okamoto, M. Murakoso, Y. Kuninobu, K. Takai, *Org. Lett.* **2012**, *14*, 3182; h) C. Wang, D. Wang, F. Xu, B. Pan, B. Wan, *J. Org. Chem.* **2013**, *78*, 3065; i) P. Thirumurugan, P.T. Perumal, *Tetrahedron* **2009**, *65*, 7620; j) V.P.A. Raja, G. Tenti, S. Perumal, J.C. Men´endez, *Chem. Commun.* **2014**, *50*, 12270; k) Y. Hao, X.P. Xu, T. Chen, L.L. Zhao, S.J. Ji, *Org. Biomol. Chem.* **2012**, *10*, 724; l) J. Hu,

Z. Deng, X. Zhang, F. Zhang, H. Zheng, *Org. Biomol. Chem*. **2014**, *12*, 4885; m) K. Shekarrao, P.P. Kaishap, S. Gogoi, R.C. Boruah, *RSC Adv*. **2014**, *4*, 14013; Heterogenous-catalyzed, pyridine synthesis: (n) L. Abahmane, A. Knauer, U. Ritter, J.M. Köhler, G.A. Groß, *Chem. Eng. Technol.* **2009**, *32*, 1799; (o) V.H.S.B. Sandeep, M. Suresh, K.G. Kranthi, B.J. Sreekanth, *Arab. J. Chem. (In press);* (p) S. Sebenzile, M. Suresh, E.V.Z. Werner, B.J. Sreekantha. *Ind. Eng. Chem. Res.* **2017**, *56*, 11372.

[56] a) K. Shravankumar, P. Ramakanth, M.S.V. Suresh Chandra, B.J. Sreekantha, *RSC Adv*. **2015**, *5*, 105446; b) P. Ramakanth, M. Suresh, M. Vashen, E.V.Z. Werner, B.J. Sreekanth, *Tetrahedron Lett*. **2014**, *55*, 4006; c) J. Tang, L. Wang, Y. Yao, L. Zhang, W. Wang, *Tetrahedron Lett.* **2011**, *52*, 509; d) R. Pagadala, S. Maddila, V.D.B.C. Dasireddy, S.B. Jonnalagadda, *Catal. Commun.* **2014**, *45*, 148; e) R. Pagadala, S. Maddila, S. Rana, S.B. Jonnalagadda, *RSC Adv*. **2014**, *4*, 6602; f) R. Pagadala, S. Maddila, S.B. Jonnalagadda, *Ultrason. Sonochem*. **2014**, *21*, 472.

[57] a) D.C. Mungra, M.P. Patel, R.G. Patel, *ARKIVOC* **2009**, *xiv*, 64; b) F. Shi, S. Tu, F. Fang, T. Li, *ARKIVOC* **2005**, *i*, 137.

CHAPTER-IV

Synthesis, structural, biological evaluation and DFT studies of Co(II), Ni(II), Cu(II), Zn(II), Cd(II) and Pd(II) complexes bearing heterocyclic thiosemicarbazone ligand

Thiosemicarbazones have an extensive set of N and S donor atoms which have proved their indispensability in coordination chemistry. These ligands are popular due to their great versatility, which is exhibited by their ability to exist in two forms (thione-thiol) and the capacity to bind metal ions in the anionic or neutral form, behaving as monodentate or bidentate ligand [1–6]. These compounds have been explored for their inhibitory action on the DNA enzyme Ribonucleotide diphosphate reductase, as well as their selectivity toward hormone-responsive cancers [7]. Owing to these properties, a number of compounds, both organic and metal-organics, have been derived from thiosemicarbazones and these have many structural and medicinal applications [8]. They have been found to be very active against insects, tuberculosis, influenza, leprosy, bacterial and viral infections, rheumatism, psoriasis, coccidiosis and trypanosomiasis [9–12]. The metal complexes of semicarbazones and thiosemicarbazones have provoked substantial interest because of their industrial and biological importance and many of these compounds have been reported to have expansive spectrum of therapeutic properties [13].

Through decades, metal ions have been continuously establishing themselves in the biological systems and also have proved important to humans in varying levels [14]. Introduction of metal complexes into the biological system can be approved for either therapeutic or diagnostic purposes. Metal ions in the form of complexes enrich their medicinal applications because of their geometrical orientation ascribed chelation ability [15–21].

In the present chapter, we describe the synthesis, characterization and theoretical studies of new heterocyclic appended thiosemicarbazone ligand and their corresponding metal complexes. Further, the new compounds are investigated for their *in vitro* antimicrobial, antioxidant, anticancer, ROS and *in vivo* antidiabetic activities. Interestingly, these complexes exhibit potential biological properties, which are discussed in detail in this chapter.

4.1 Results and discussion

2-aminonicotinaldehyde *N*-methyl thiosemicarbazone (ANMTSC) and its metal complexes are non-hygroscopic and stable under ordinary conditions. Upon heating, the complexes decompose without melting. The ligand is soluble in methanol, ethanol, DMF and DMSO while the complexes are soluble in DMF and DMSO and insoluble in

methanol, ethanol, chloroform, dichloromethane etc. Analytical and molar conductivity data of the complexes are present in Table 4.1. The molar conductance of the complexes (10^{-3} M DMF solution) is in the range of 08-22 $\Omega^{-1}cm^2mol^{-1}$ suggesting that metal complexes are non-electrolytes.

Table 4.1 Analytical and molar conductivity data for the ligand and its complexes

Compound	**Elemental analyses: Found (Calculated)**				
	C	**N**	**H**	**S**	**Molar Cond. ($\Omega^{-1}cm^2mol^{-1}$)**
$[Co(ANMTSC)_2(H_2O)_2]$	37.54 (37.57)	27.33 (27.38)	4.69 (4.73)	12.50 (12.54)	11
$[Ni(ANMTSC)_2(H_2O)_2]$	37.57 (37.59)	27.34 (27.40)	4.69 (4.73)	12.48 (12.54)	13
$[Cu(ANMTSC)_2(H_2O)_2]$	37.19 (37.24)	27.10 (27.14)	4.66 (4.69)	12.39 (12.43)	18
$[Zn(ANMTSC)_2]$	39.85 (39.88)	29.02 (29.07)	4.16 (4.18)	13.26 (13.31)	08
$[Cd(ANMTSC)_2]$	36.29 (36.33)	26.45 (26.48)	3.78 (3.81)	12.09 (12.12)	10
$[Pd(ANMTSC)Cl_2]$	24.65 (24.92)	18.01 (18.16)	2.59 (2.61)	8.23 (8.32)	22
ANMTSC	45.88 (45.91)	33.42 (33.47)	5.28 (5.30)	15.30 (15.32)	- -

4.1.1 Spectroscopy

The difference between the infrared spectrum of the ANMTSC ligand and its corresponding metal(II) [Co(II), Ni(II), Cu(II), Zn(II), Cd(II) and Pd(II)] complexes have given basic evidence for the coordination mode of the complexes. The IR data of the newly synthesized ligand and its complexes are depicted in Table 4.2 and shown in Fig. 4.1 (a-c). The azomethine (C=N), thiocarbonyl (C=S) and $(C=N)_{(py)}$ groups of the ligand were shown stretching frequencies at 1557, 1272 and 1582 cm^{-1}, respectively. On

coordination with metal ions, the azomethine and thiocarbonyl stretching frequencies shifted to lower frequencies (1518-1537 and 1227-1250 cm^{-1}) while the $(C=N)_{(py)}$ stretching frequency remains unchanged, which clearly implies that the ligand coordinates with metal ions through azomethine nitrogen and thiocarbonyl sulphur donor atoms (NS^{-}), respectively [22,23]. The IR spectrum of the ligand displayed a band of around 3413, 3315 and 3180 cm^{-1}, which are assigned to pyridine attached NH, terminal NH and thiocarbonyl attached NH groups, respectively. After complexation, stretching frequency of the thiocarbonyl group adjacent to –NH disappeared while the other two bands were unaltered, which strongly pointed to the ligand coordination with all the metal(II) ions in the deprotonated thiol form [24]. The electronic spectral frequencies and magnetic data observed for the complexes [Co(II), Ni(II), Cu(II), Zn(II), Pd(II) and Cd(II)] along with ligand field parameters have been calculated for Co(II) and Ni(II) complexes and the results are represented in Table 4.3. The UV-Visible spectra of the Co(II) complex showed four band frequencies at 8890, 17240, 20000 and 28570 cm^{-1}, respectively, the first three assignable corresponding to $^4T_{1g}(F) \rightarrow {}^4T_{2g}(F)$ (ϑ_1), $^4T_{1g}(F) \rightarrow {}^4A_{2g}(F)$ (ϑ_2) and $^4T_{1g}(F) \rightarrow {}^4T_{2g}(P)$ (ϑ_3) transitions of octahedral geometry [25] and the last band due to charge transfer; this was also further supported by $\vartheta_2 / \vartheta_1$ which lies in the range of 1.80-2.20 for octahedral geometry [26]. The ligand field parameters have been calculated using the equation [27].

$$10\ Dq = 1/3\ (2\ \vartheta_2 - \vartheta_3\ ) + 5B$$

$$B = \frac{\vartheta 3 + \vartheta 2 - 3\ \vartheta 1}{15}$$

The B value was calculated and found to be 705 cm^{-1}. The experimental B value is lower than the free ion value B' [971 cm^{-1} for Co(II)] which gives information about the overlapping of orbitals and d-orbital delocalization. This is in accordance with the observation made by Jorgenson [28], the ligand which coordinate with sulphur donor atom has a low value of B and causes very pronounced nephelauxetic effect. The nephelauxetic effect suggests that the lower the value of β, greater the extent of covalence. For Co(II) complex, β value is less than one indicating the covalent character of the metal-ligand bond. Ni(II) complex reveal bands around 9900, 16390 and 25970 cm^{-1} corresponding to $^3A_{2g}(F) \rightarrow {}^3T_{2g}(F)$ (ϑ_1), $^3A_{2g}(F) \rightarrow {}^3T_{1g}(F)$ (ϑ_2) and $^3A_{2g}(F) \rightarrow {}^3T_{1g}(P)$ (ϑ_3) transitions, respectively, which are characteristic of octahedral geometry [29,30], also further supported by $\vartheta_2 / \vartheta_1$ being equal to 1.66. This value is lower than $\vartheta_2 / \vartheta_1$ value

of 1.80 observed for regular octahedral $[Ni(H_2O)_6]^{2+}$ complex. The lowering of value in the present case may be attributed to the asymmetric environment around Ni(II) of the complex. The B value [27] for the complex is 854 cm^{-1}. This value is lower than the free ion value B' [1030 cm^{-1} for Ni(II)] which gives information about the overlapping of orbitals and d-orbital delocalization. However, the Cu(II) complex shows a broad peak at 16000 cm^{-1}, attributed to $^2B_{1g} \rightarrow {}^2A_{1g}$, $^2B_{1g} \rightarrow {}^2B_{2g}$ and $^2B_{1g} \rightarrow {}^2E_g$ transitions, respectively and characteristic of tetragonal or distorted octahedral geometry [31-34] and these bands overlap to give one broad absorption peak in the spectrum of Cu(II) complex [35]. The Pd(II) complex show three peaks at 16850 cm^{-1} ($^1A_{1g} \rightarrow {}^1A_{2g}$), 20400 cm^{-1} ($^1A_{1g} \rightarrow {}^1B_{1g}$) and 24350 cm^{-1} ($^1A_{1g} \rightarrow {}^1E_g$), these transitions being characteristic of square-planar geometry [23]. The electronic spectra of Zn(II) and Cd(II) complexes do not show any d → d transition, which may be due to d^{10} electronic configuration [36]. It has been reported that tetrahedral is the most favoured one and it is confirmed from analytical data [37].

The Co(II) and Ni(II) complexes exhibited magnetic moment values of 4.98 B.M. and 3.28 B.M. which might be attributed to the octahedral geometries around Co(II) [38] and Ni(II) [26]. The Cu(II) complex showed a magnetic moment of 1.81 B.M. This value is close to spin-only value with a slight allowance for a magnetic moment from spin-orbit coupling, suggesting tetragonal geometry around Cu(II) [39,40]. Zn(II), Pd(II) and Cd(II) complexes are diamagnetic in nature [41].

ESR spectroscopy was performed to determine the existence of unpaired electrons. In the present study, ESR spectrum of Cu(II) complex was performed at room temperature in solid state and the recorded spectrum is shown in Fig. 4.2 and the ESR parameters are represented in Table 4.4. From the spectral data, the g values obtained for Cu(II) complex indicates that $g_{\parallel}$ (2.25) > $g_{\perp}$ (2.06) > 2.0023, and so the unpaired electron lies predominantly in $d_{x^2-y^2}$ orbital, a characteristic feature of tetragonal or distorted octahedral geometry [42].

From the axial spectra, the g–values were connected with exchange interaction coupling constant (G). The nature of the ligand was also determined using the following expression

$$G = \frac{g_{\parallel} - 2.0023}{g_{\perp} - 2.0023}$$

As reported by Karlin and Zubieta (Eds.) [43], if G > 4, the exchange interaction was insignificant due to local tetragonal axes that were aligned parallel. If G < 4, the exchange interaction was reasonable and the local tetragonal axes were misaligned. The G value (4.29) observed for Cu(II) complex was found to be more than four, indicating that there was no exchange interaction in solid state as suggested.

$A_{\parallel}$- The parallel component of copper hyperfine splitting has also been obtained for the complex from its well resolved $g_{\parallel}$ components and values are given in Table 3.9. It was assumed that Cu(II) free ion spin-orbit coupling constant, λ_0 = –828 cm^{-1}, the orbital reduction parameters, $K^2{}_{\parallel}$ and $K^2{}_{\perp}$ have been calculated by correlating electronic and ESR spectral data by the following expression [44,45].

$$g_{\parallel} = 2.0023 - \frac{8\ K^2{}_{\parallel}\ \lambda 0}{\Delta E(2\mathrm{B1g} \rightarrow 2\mathrm{B2g})}$$

$$g_{\perp} = 2.0023 - \frac{2\ K^2{}_{\perp}\ \lambda 0}{\Delta E(2\mathrm{B1g} \rightarrow 2\mathrm{B2g})}$$

Hathaway and Billing [46,47] have pointed out that $K^2{}_{\parallel} < K^2{}_{\perp}$ for in-plane pi-bonding and $K^2{}_{\parallel} > K^2{}_{\perp}$ out of plane pi-bonding, in the present case while the observed value is $K^2{}_{\parallel} > K^2{}_{\perp}$, which implies that the present complex was supposed to be out of plane pi-bonded. Further, the spin-orbit coupling constant also has been evaluated using the equation,

$$g_{\parallel} = 2.0023 - \frac{8\lambda}{\Delta E}$$

From the results, the λ value for Cu(II) complex (–495 cm^{-1}) is lower than free ion value suggesting the significant mixing of the ground and excited terms.

In ^{1}H NMR spectra of the ligand, the thiocarbonyl attached N–H and terminal N–H protons showed signals of around 11.23 and 8.38 ppm, respectively. In the complexes [Zn(II), Pd(II) and Cd(II)] thiocarbonyl attached N–H proton signals disappeared, which clearly indicates coordination of the ligand in the anionic form after deprotonation and the terminal N–H proton appeared at 8.19-8.43 ppm. The signal azomethine CH proton appeared at 8.15 ppm and the same proton occurred in the complexes around 7.93-8.20 ppm. The signals due to the protons of NH_2 attached to the pyridine ring were observed at 6.98 ppm as the singlet, whereas, in the complexes, NH_2 appeared in the region at 6.97-7.02 ppm. The aromatic protons of ligand and complexes

(pyridine ring and terminal phenyl) appeared in the range of 8.05-6.55 ppm. ^{13}C NMR spectrum of the ligand displayed resonances due to C=S and C=N carbons at 177.5 and 156.6 ppm, respectively. Conversely, in the spectra of Zn(II), Pd(II) and Cd(II) complexes, C–S, and C=N chemical shifts appeared around 178.7-175.2 ppm and 147.2–141.1 ppm, respectively. Chemical shift of all other protons and carbons was observed in the expected regions as shown Fig.s 4.3-4.6.

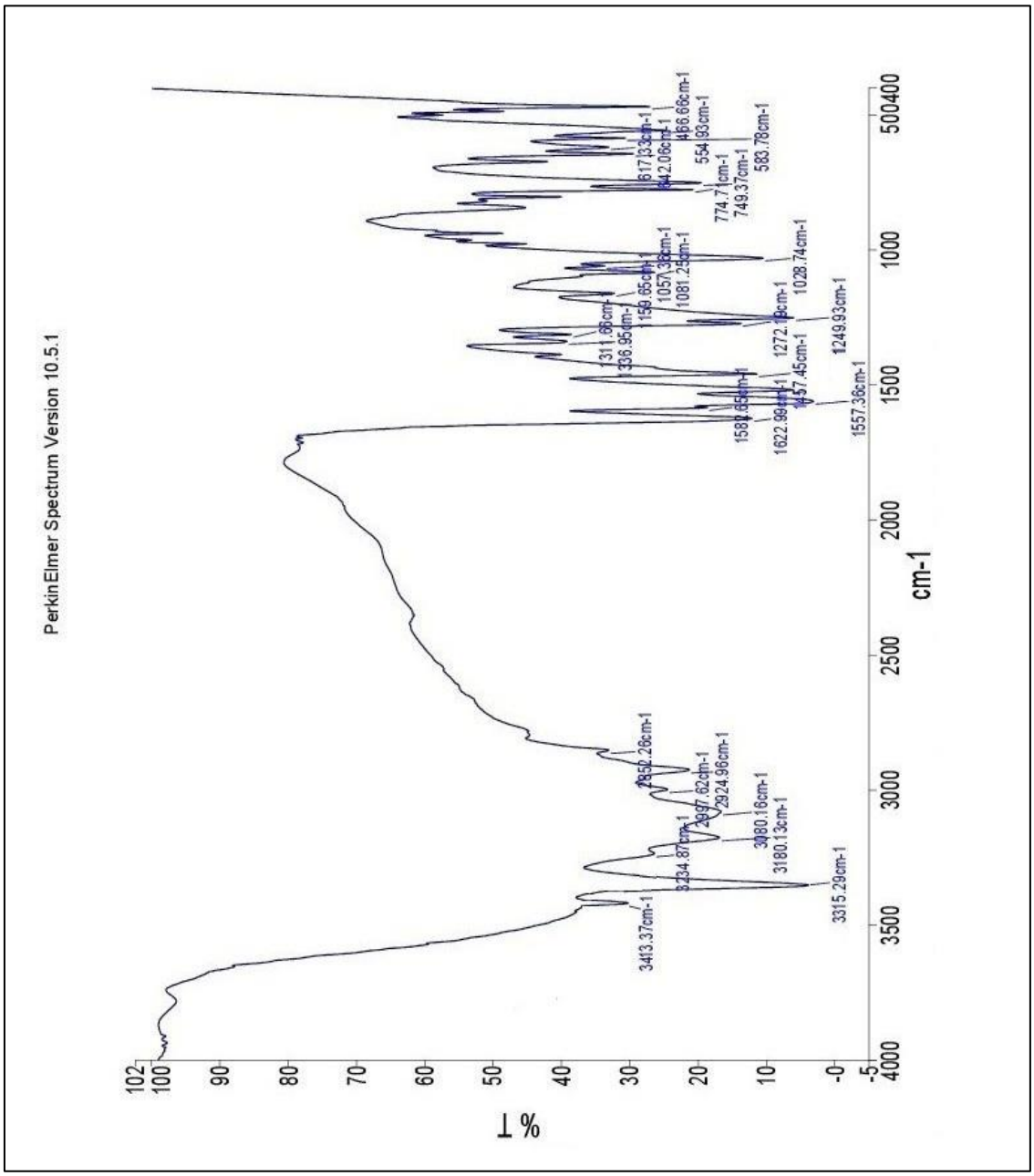

(a)

Fig. 4.1(a) FT-IR spectrum of ANMTSC.

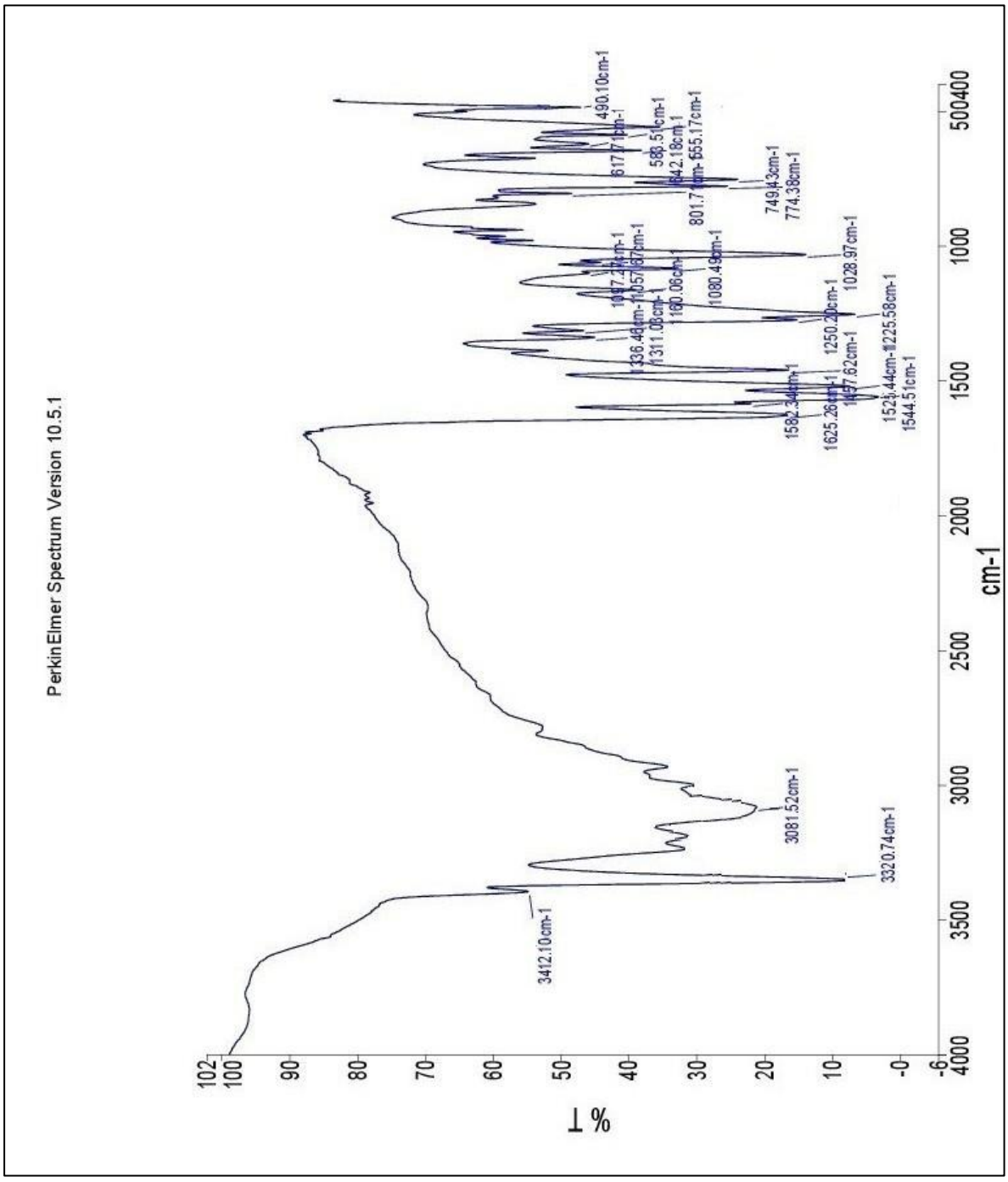

(b)

Fig. 4.1(b) FT-IR spectrum of Zn(II) complex.

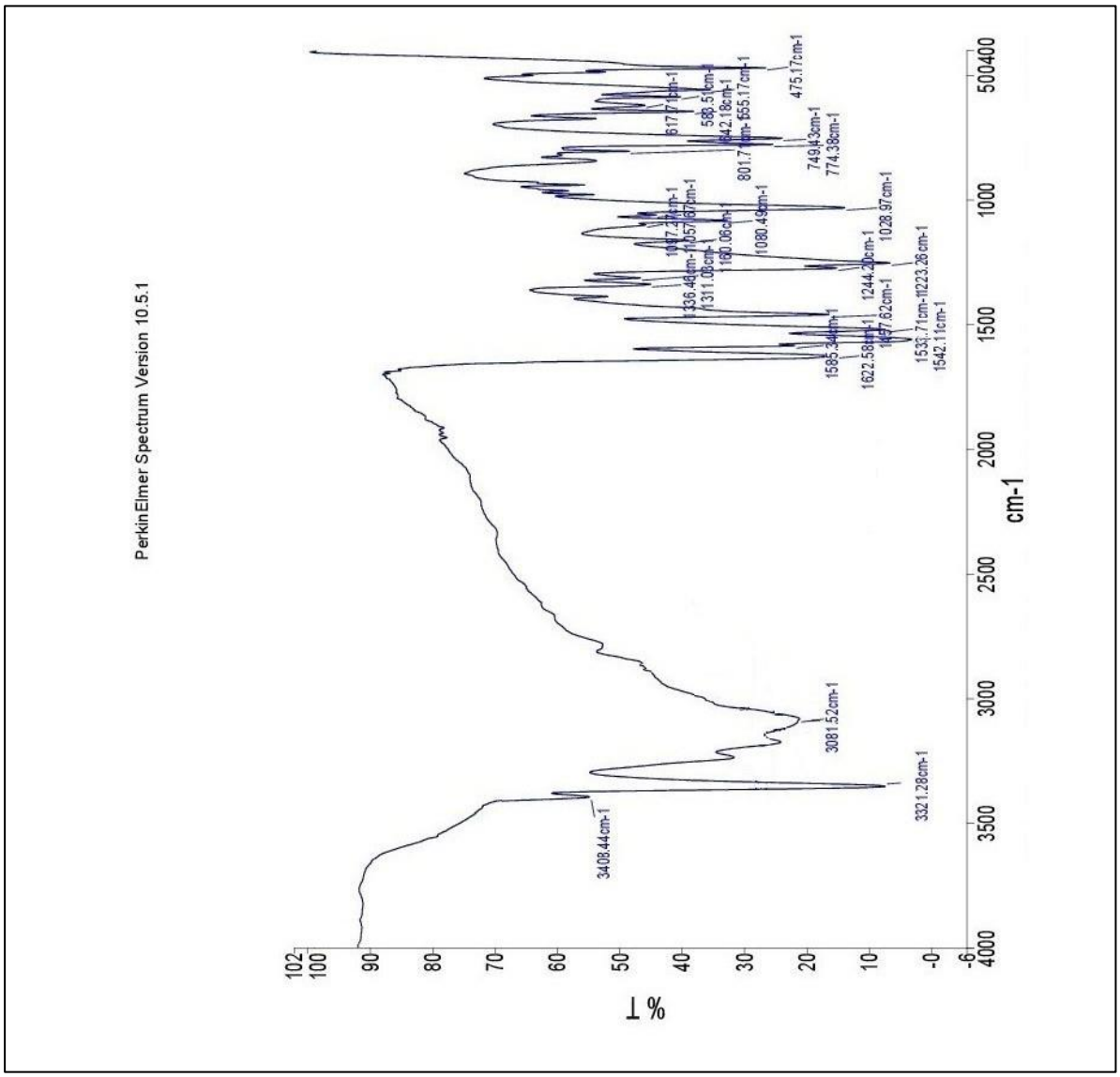

(c)

Fig. 4.1 (c) FT-IR spectrum of Cd(II) complex.

Table 4.2 The important infrared frequencies (in cm^{-1}) of ligand and its complexes

Compound	**υ(N–H)**	**υ(OH)**	**υ(C=N) (Azomethine)**	**υ(C=N)(py)**	**υ(N=C)**	**υ(C=S)**	**υ(M–N)**	**υ(M–O)**	**υ(M–S)**
Co(II)	3419, 3309	3470	1520	1583	1565	1227	480	421	325
Ni(II)	3410, 3310	3446	1518	1580	1509	1238	480	445	320
Cu(II)	3409, 3316	3451	1537	1578	1506	1250	490	418	326
Zn(II)	3412, 3320	-	1525	1582	1544	1250	490	-	320
Cd(II)	3408, 3321	-	1533	1585	1542	1224	475	-	320
Pd(II)	3411, 3321	-	1515	1579	1546	1231	450	-	335
ANMTSC	3413, 3315, 3180	-	1557	1582	-	1272	-	-	-

Table 4.3 Electronic spectral data, ligand field parameters and magnetic moments of the complexes

Complexes	Frequencies (cm^{-1})	Assignments	μ_{eff} (B.M.)	$\vartheta_2 / \vartheta_1$	10 Dq (cm^{-1})	B (cm^{-1})	β	Geometry
Co(II)	8890	$^4T_{1g}(F) \rightarrow {}^4T_{2g}(F)$ (υ_1)						
	17240	$^4T_{1g}(F) \rightarrow {}^4A_{2g}(F)$ (υ_2)	4.98	1.94	8350	705	0.73	Octahedral
	20000	$^4T_{1g}(F) \rightarrow {}^4T_{2g}(P)$ (υ_3)						
	28570	Charge Transfer						
	9900	$^3A_{2g}(F) \rightarrow {}^3T_{2g}(F)$ (υ_1)						
Ni(II)	16390	$^3A_{2g}(F) \rightarrow {}^3T_{1g}(F)$ (υ_2)						
	25970	$^3A_{2g}(F) \rightarrow {}^3T_{1g}(P)$ (υ_3)	3.28	1.66	9880	854	0.82	Octahedral
Cu(II)	16000	$^2B_{1g} \rightarrow {}^2A_{1g}$ $^2B_{1g} \rightarrow {}^2B_{2g}$ $^2B_{1g} \rightarrow {}^2E_g$	1.81	-	-	-	-	Tetragonal (or) Distorted octahedral
Zn(II)	-	-	Diamagnetic	-	-	-	-	Tetrahedral
Cd(II)	-	-	Diamagnetic	-	-	-	-	Tetrahedral
Pd(II)	16850	$^1A_{1g} \rightarrow {}^1A_{2g}$	Diamagnetic	-	-	-	-	Square-planar
	20400	$^1A_{1g} \rightarrow {}^1B_{1g}$						
	24350	$^1A_{1g} \rightarrow 1E_g$						

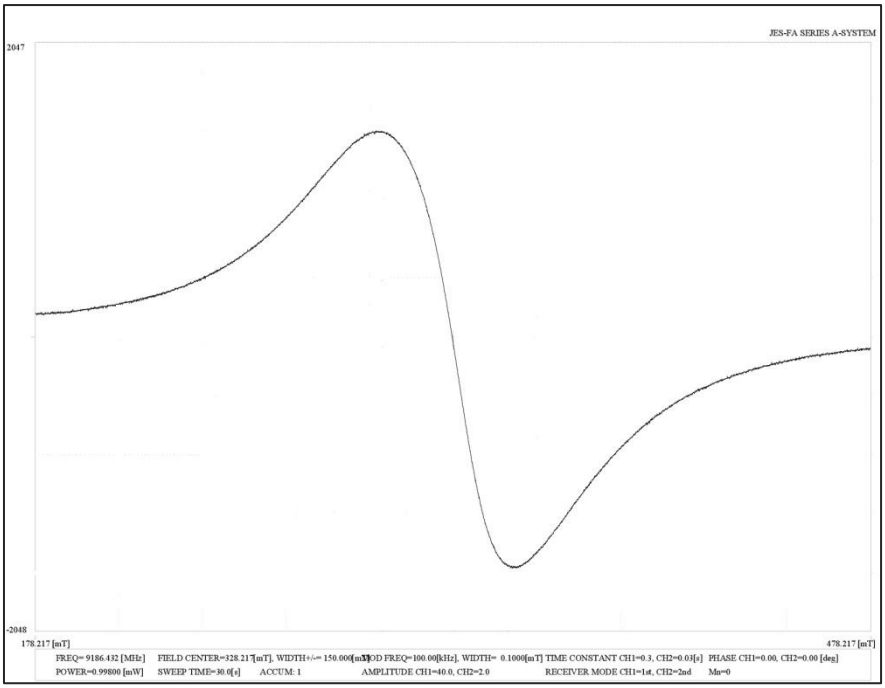

Fig. 4.2 ESR spectrum of Cu(II) complex.

Table 4.4 ESR parameters of Cu(II) complex

Complex	$g_{\parallel}$	$g_{\perp}$	**|g|**	**G**	$A_{\parallel}\times10^{5}$ **(cm^{-1})**	$K^2{}_{\parallel}$	$K^2{}_{\perp}$	**-λ (cm^{-1})**
Cu(II)	2.25	2.06	2.12	4.29	605	0.598	0.557	495

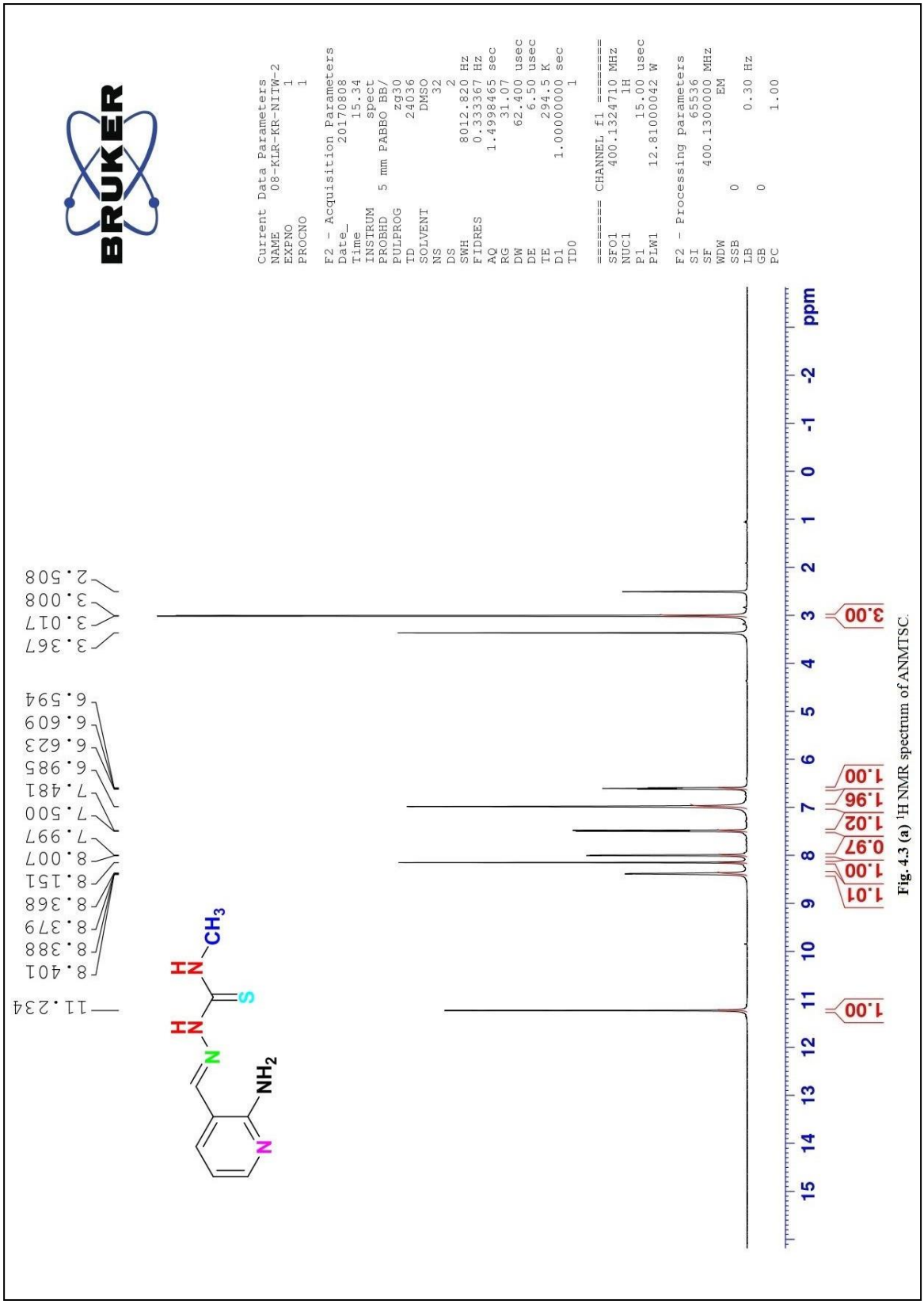

Fig. 4.3 (a) ^{1}H NMR spectrum of ANMTSC.

(a)

Fig. 4.3 (a) ^{1}H NMR spectrum of ANMTSC.

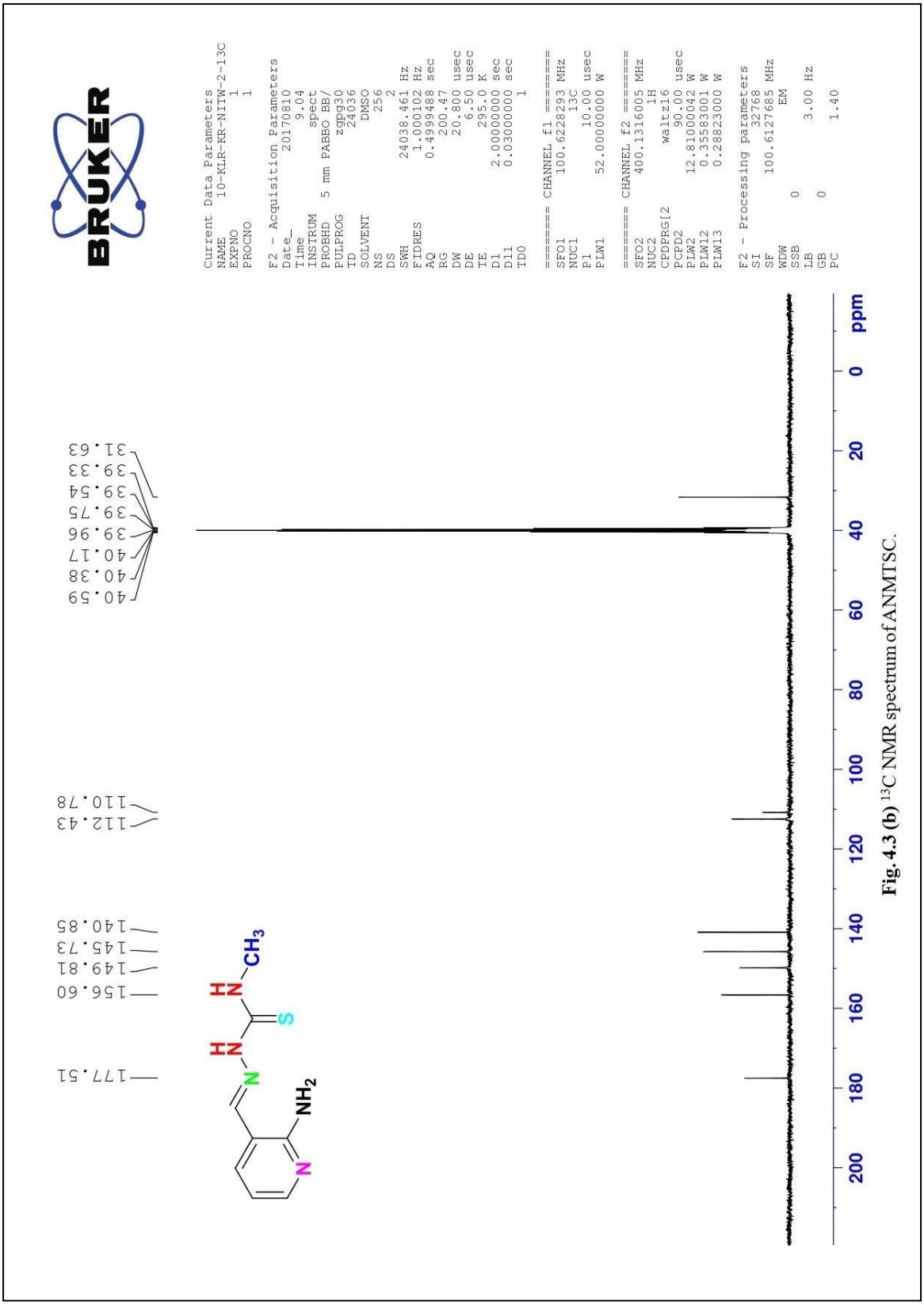

Fig. 4.3 (b) ^{13}C NMR spectrum of ANMTSC.

(b)

Fig. 4.3 (b) ^{13}C NMR spectrum of ANMTSC.

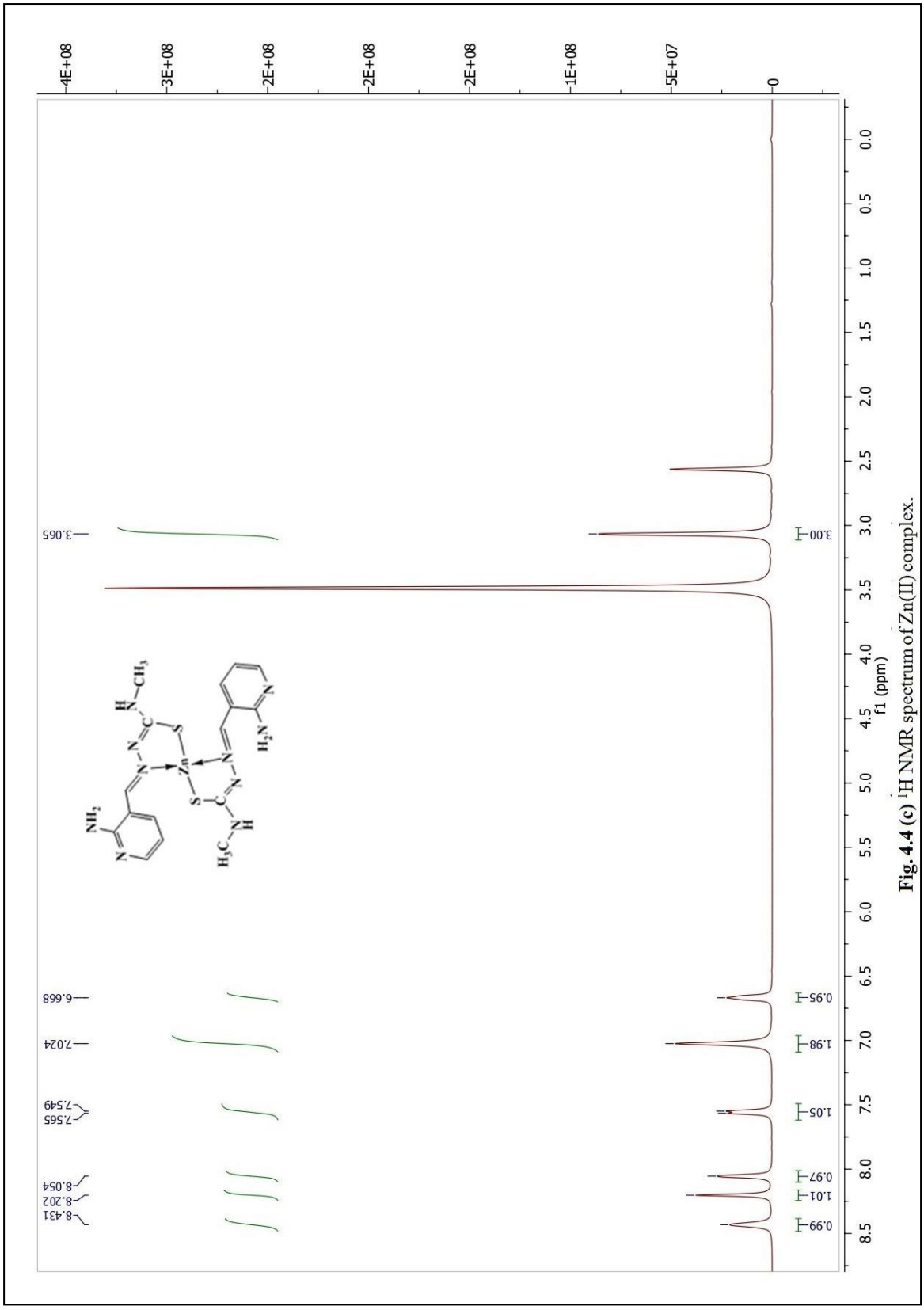

Fig. 4.4 (c) ^{1}H NMR spectrum of Zn(II) complex.

(c)

Fig. 4.4 (c) ^{1}H NMR spectrum of Zn(II) complex.

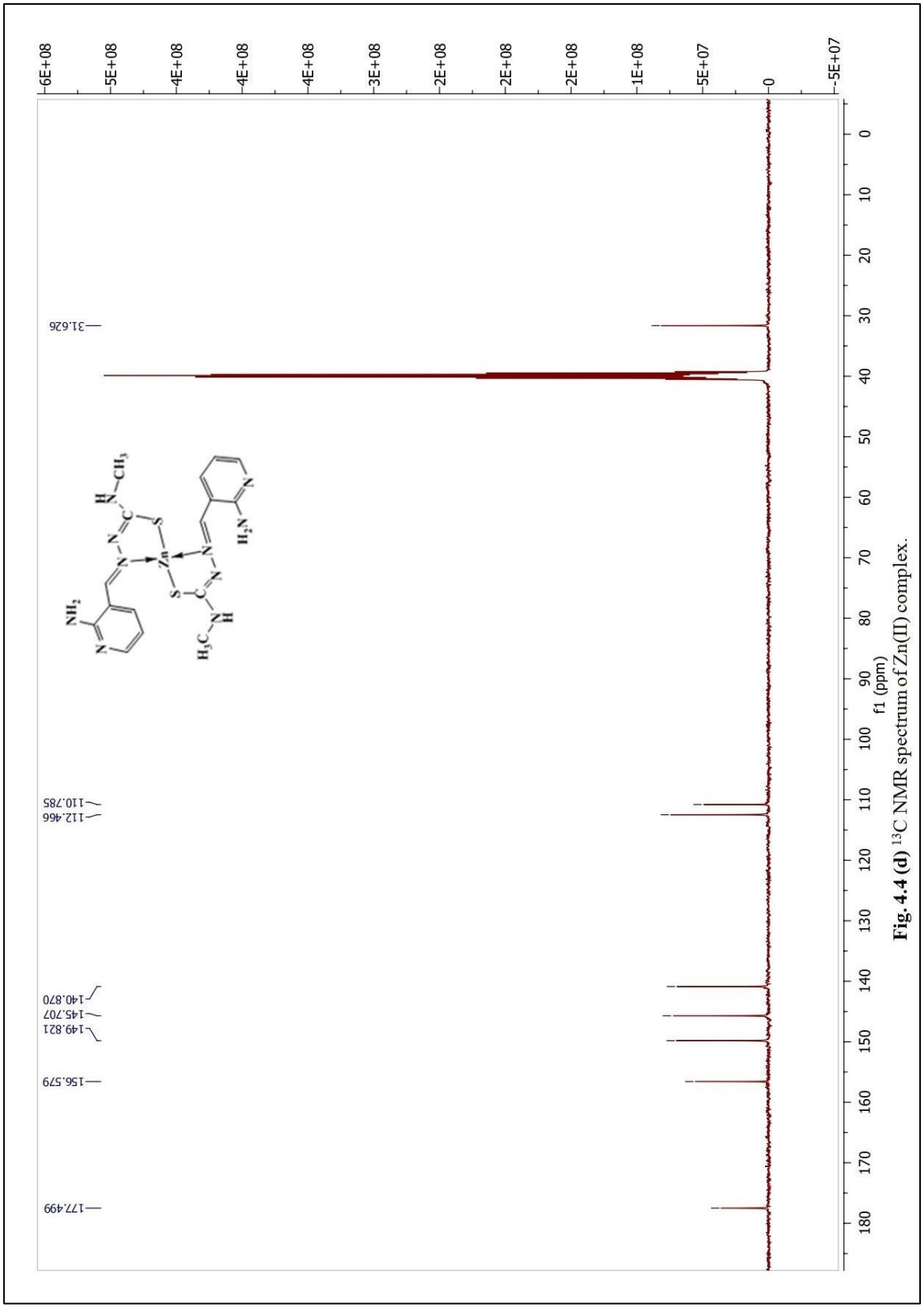

Fig. 4.4 (d) ^{13}C NMR spectrum of Zn(II) complex.

(d)

Fig. 4.4 (d) ^{13}C NMR spectrum of Zn(II) complex.

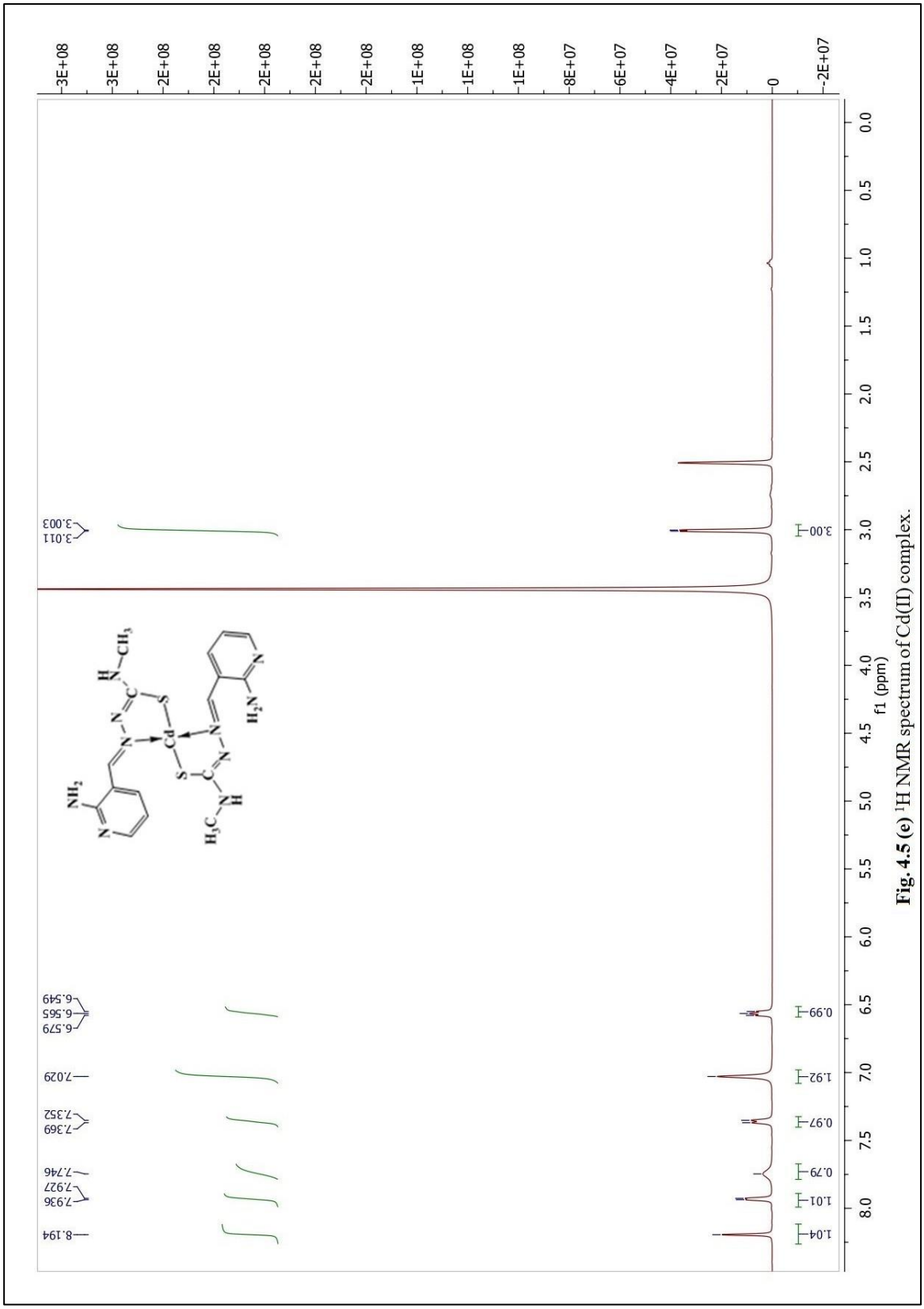

Fig. 4.5 (e) ^{1}H NMR spectrum of Cd(II) complex.

(e)

Fig. 4.5 (e) ^{1}H NMR spectrum of Cd(II) complex.

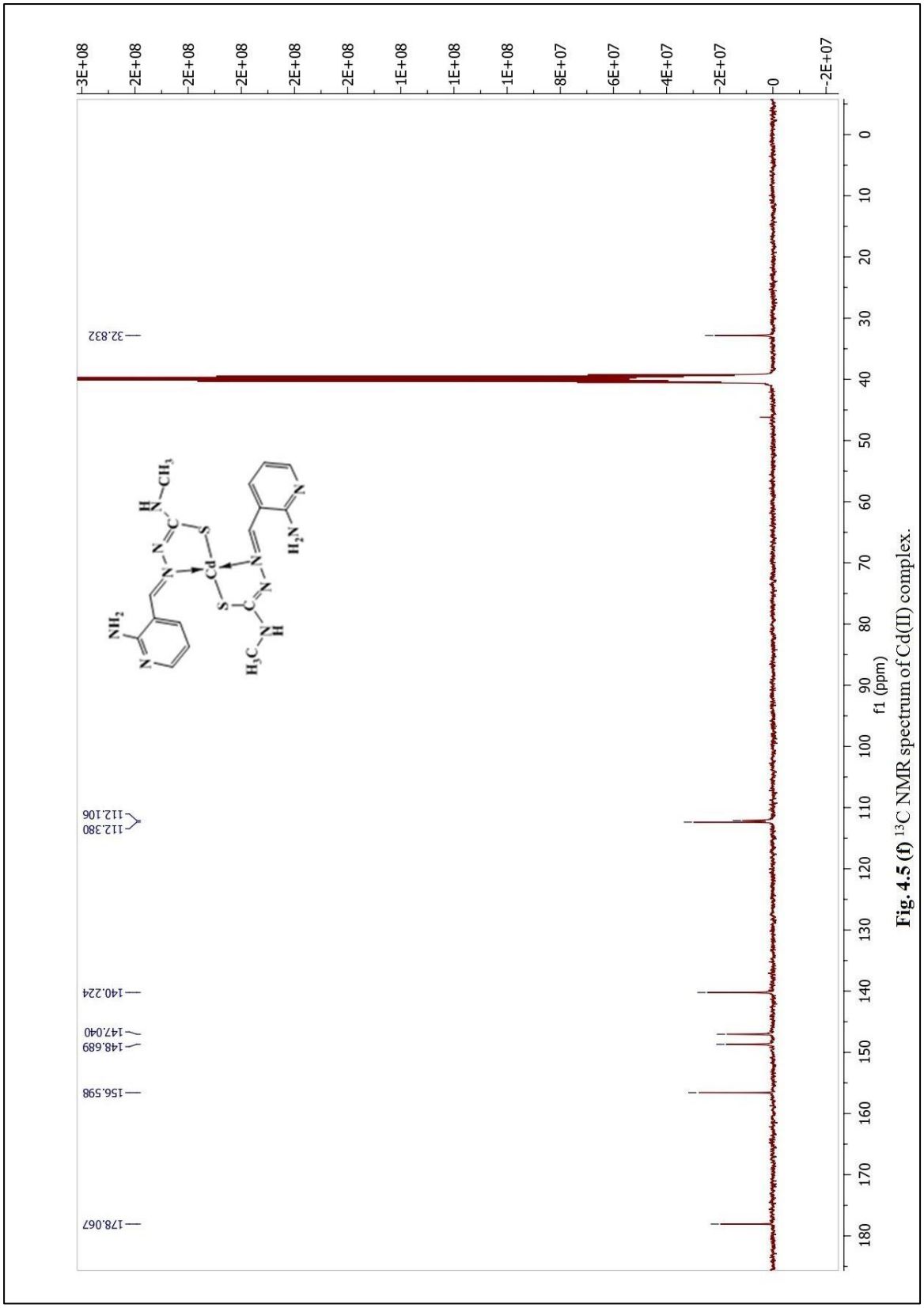

Fig. 4.5 (f) ^{13}C NMR spectrum of Cd(II) complex.

(f)

Fig. 4.5 (f) ^{13}C NMR spectrum of Cd(II) complex.

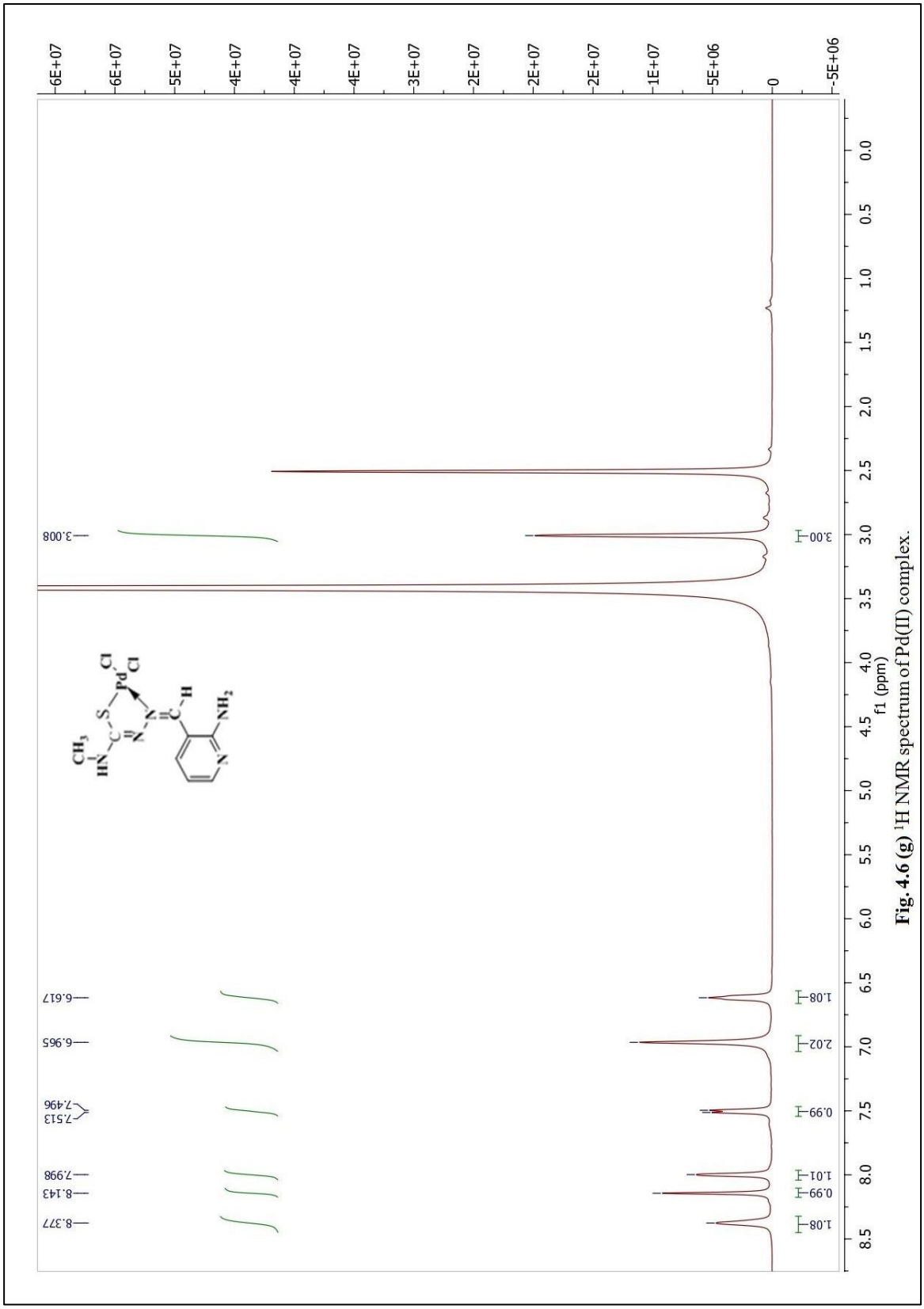

Fig. 4.6 (g) ^{1}H NMR spectrum of Pd(II) complex.

(g)

Fig. 4.6 (g) ^{1}H NMR spectrum of Pd(II) complex.

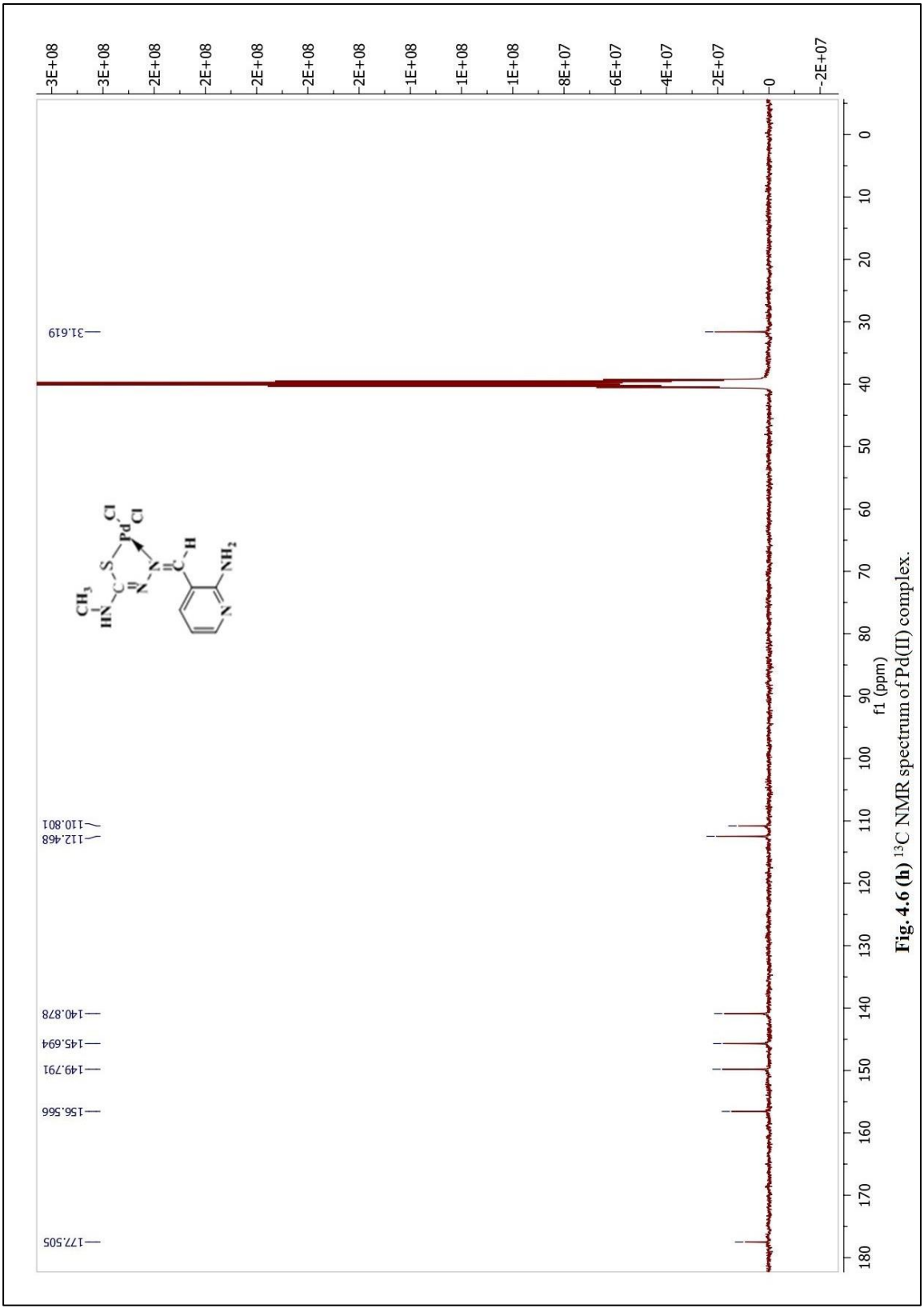

Fig. 4.6 (h) ^{13}C NMR spectrum of Pd(II) complex.

(h)

Fig. 4.6 (h) ^{13}C NMR spectrum of Pd(II) complex.

4.1.2 X-ray analysis

X-ray analysis of single crystal of ANMTSC compound under investigation showed that it belongs to monoclinic crystal system, with space group $P2_1/n$ having four molecules per unit cell (i.e. Z = 4). The dimensions of the unit cell are a = 6.1537(3) Å, b = 22.0194(12) Å, c = 7.2700(4) Å, α = 90°, β= 92.149(2)°, γ = 90°, with volume V = 984.40(9) $Å^3$, at temperature T = 296(2) K, calculated density D being 1.412 g cm^{-3} (M = 223.3 g mol^{-1}), with absorption coefficient μ, for Mo K_α line, as 0.296 mm^{-1}. Refinement of full-matrix least-squares method on F^2 converged with goodness-of- fit 1.175. R indices (all data) has come out to be R1 = 0.0633 and wR2 = 0.1493. Final R indices [I > 2 sigma (I] are R1 = 0.0592 and wR2 = 0.1467.

A view of ANMTSC showing atom-labeling scheme appears in Fig. 4.7. Experimental molecular structure parameters comprising crystal data, bond lengths, bond angles, dihedral angles and intra-molecular hydrogen bond are presented in Tables 4.5-4.6. The crystal data for ANMTSC is available as supplementary material from CCDC (Cambridge Crystallographic Data Centre) 1576355, free of charge, at www.ccdc.cam.ac.uk/centre/retrieving.html (or CCDC, 12 Union Road, Cambridge CB2 1EZ, UK; fax: 44(0) 1223336033; email: deposit@ccdc.com.ac.uk)

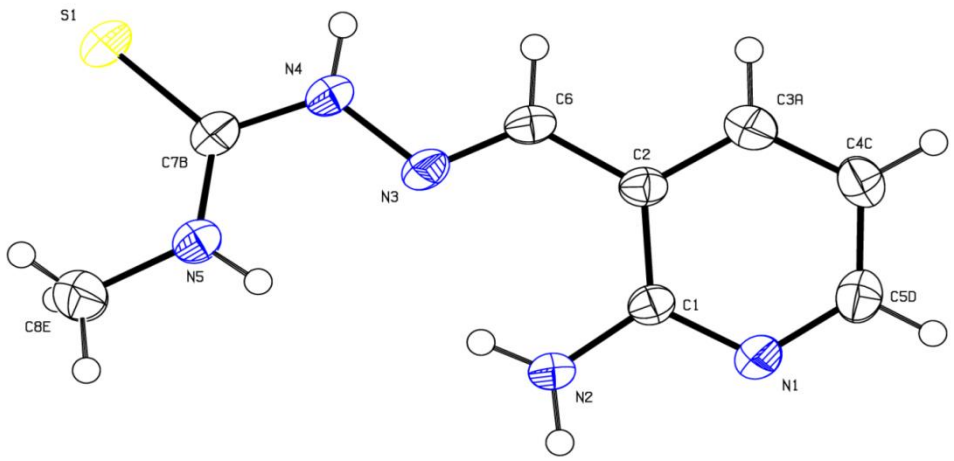

Fig. 4.7 Oak Ridge Thermal ellipsoid (50%) plot (ORTEP) of ligand ANMTSC.

Table 4.5 Crystallographic data and refinement parameters for ligand ANMTSC

	ANMTSC
Empirical formula	$C_8H_{11}N_5S$
Formula weight	209.28
Temperature (K)	296(2)
Wavelength (Å)	0.71073
Crystal system	Monoclinic
Space group	$P2_1/n$
Unit cell dimensions	
a (Å)	6.1537(3)
b (Å)	22.0194(12)
c (Å)	7.2700(4)
α (°)	90
β (°)	92.149(2)
γ (°)	90
Volume ($Å^3$)	984.40(9)
Z	4
Density (calculated) Mg/m^3	1.412
Absorption coefficient (mm^{-1})	0.296
F(000)	440
Theta range for data collection (°)	2.95 to 26.39
Index ranges	–7< = h< = 7, –27< = k < = 27, –9 < = l < = 9
Reflections Collected	17520
Independent Reflections	1997 (0.0375)
Completeness to theta (%)	99.0
Refinement Method	Full-matrix least-squares on F^2
Data / restraints /Parameters	1997 / 0 / 128

Goodness-of-fit on F^2	1.175
Final R indices [I>2sigma(*I*)]	R1 = 0.0592, wR2 = 0.1467
R indices (all data)	R1 = 0.0633, wR2 = 0.1493
Largest diff. Peakand hole (e.Å^{-3})	0.389 and –0.405

Table 4.6 Selected bond lengths (Å) and angles (°) of ANMTSC

	ANMTSC
S(1)−C(7B)	1.683(3)
N(3)−C(6)	1.277(4)
N(3)−N(4)	1.384(3)
N(2)−C(1)	1.360(3)
N(4)−C(7B)	1.353(4)
N(1)−C(1)	1.341(3)
C(6)−N(3)−N(4)	115.1(2)
C(7B)−N(4)−N(3)	120.4(2)
N(3)−N(4)−H(4)	119.8
N(1)−C(1)−N(2)	116.0(2)
N(5)−C(7B)−N(4)	117.2(2)
N(5)−C(7B)−S(1)	123.9(2)
N(4)−C(7B)−S(1)	118.9(2)

4.2 DFT computations

4.2.1 Molecular geometry

Obtaining the optimized structures with minimum energy is the initial prerequisite for carrying out computations to determine the characteristics of any molecule. So, the complexes under investigation were subjected to meticulous conformational study around free rotation bonds. The optimized structures corresponding to minimum on the potential energy surface were determined for each of the six complexes by solving self-consistent field equation iteratively. On geometry optimization, the global minimum energy was

found to be –2264.12440 Hartree, –2289.27901 Hartree, –2315.681002 Hartree, –2191.94083 Hartree, –2132.55260 Hartree and –2092.658898 Hartree, respectively for Co(II), Ni(II), Cu(II), Zn(II), Cd(II) and Pd(II) complexes, respectively. The optimized structures of these complexes are shown in Fig. 4.8 along with the numbering of atoms and the geometrical parameters like bond lengths and bond angles are given in Table 4.7.

Based on the results of DFT computations, all the complexes assume C1 point group symmetry. Each of the Co(II), Ni(II) and Cu(II) complexes consists of 55 atoms and 159 fundamental vibrations are observed. Zn(II), Cd(II) and Pd(II) complexes consist of 49 atoms each and 141 fundamental vibrations are observed. All the vibrations of C1 point group symmetry belong to a species which are active in both infrared absorption and Raman scattering.

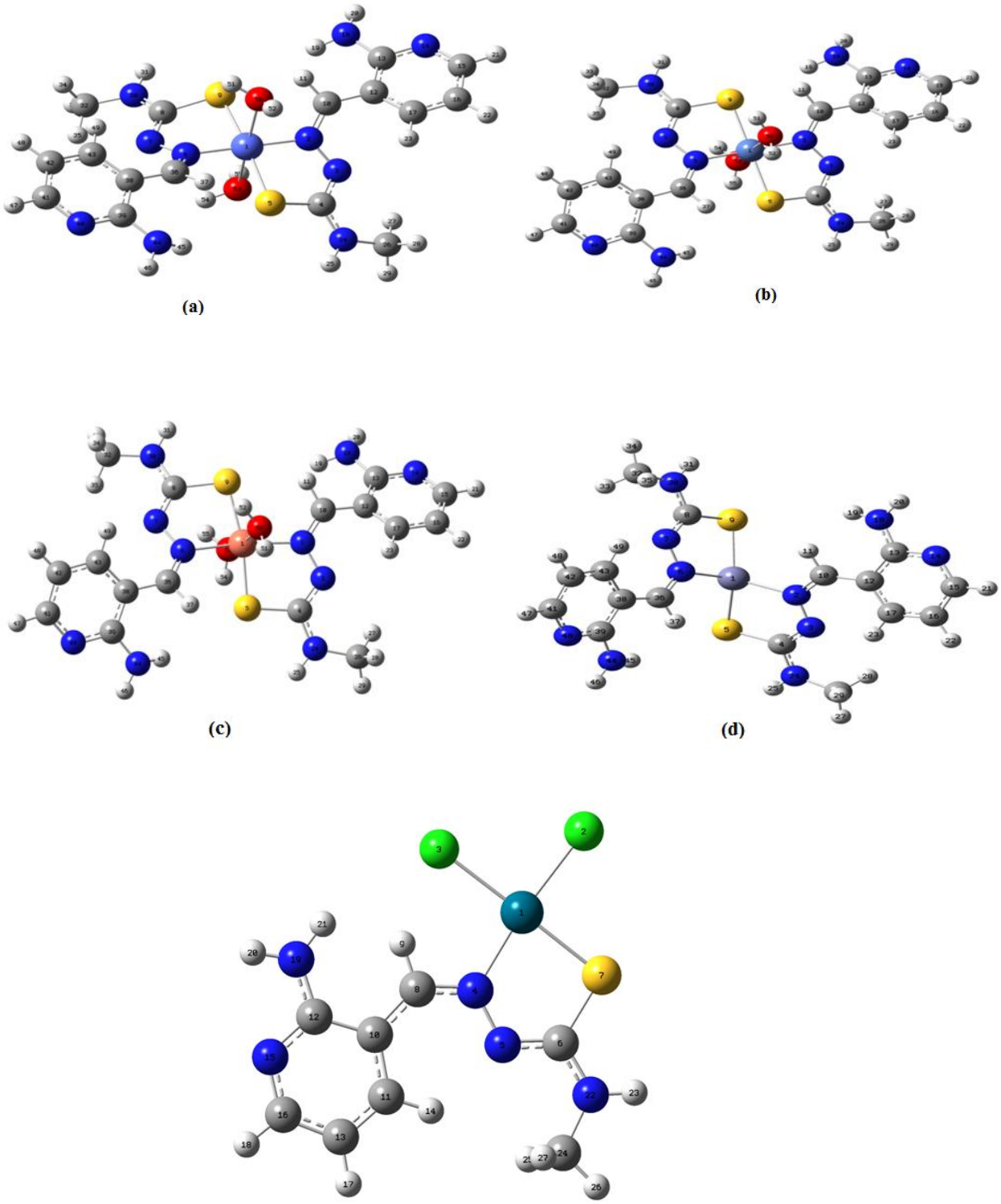

Fig. 4.8 Optimized structures along with atomic numbering of **(a)** Co(II), **(b)** Ni(II), **(c)** Cu(II), **(d)** Zn(II), **(e)** Cd(II) and **(f)** Pd(II) complexes.

Table 4.7 Selected bond lengths and bond angles of metal complexes

Co(II)		Ni(II)		Cu(II)	
Bond length	**Value (Å)**	**Bond length**	**Value (Å)**	**Bond length**	**Value (Å)**
N6–Co1	1.885	N6–Ni1	1.866	N6–Cu1	2.104
N2–Co1	1.886	N2–Ni2	1.865	N2–Cu1	2.039
Co1–S9	2.176	Ni1–S9	2.232	Cu1–S9	2.138
Co1–S5	2.171	Ni1–S5	2.222	Cu1–S5	2.172
N6–N7	1.386	N6–N7	1.376	N6–N7	1.382
N7–C8	1.351	N7–N8	1.351	N7–C8	1.340
C8–S9	1.767	C8–S9	1.759	C8–S9	1.763
N2–N3	1.386	N2–N3	1.377	N2–N3	1.381
N3–C4	1.349	N3–C4	1.353	N3–C4	1.338
C4–S5	1.772	C4–S5	1.760	C4–S5	1.765
N6–C36	1.317	N6–C36	1.310	N6–C36	1.311
N2–C10	1.316	N2–C10	1.309	N2–C10	1.311
Co1–O50	2.146	Ni1–O50	2.410	Cu1–O50	1.992
Co1–O53	2.128	Ni1–O53	2.423	Cu1–O53	1.988
O50–H51	0.985	O50–H51	0.953	O50–H51	0.981
O50–H52	0.984	O50–H52	0.954	O50–H52	0.989
O53–H54	0.994	O53–H54	0.954	O53–H54	0.991
O53–H55	0.997	O53–H55	0.954	O53–H55	0.984
Bond angle	Value (°)	Bond angle	Value (°)	Bond angle	Value (°)
N6–Co1–N2	178.37	N6–Ni1–N2	177.89	N6–Cu1–N2	172.39
S9–Co1–S5	170.88	S9–Ni1–S5	167.69	S9–Cu1vS5	168.35
N6–Co1–S5	93.50	N6–Ni1–S5	92.57	N6–Cu1–S5	87.83
S9-Co1-N2	95.83	S9–Ni1–N2	92.93	S9–Cu1–N2	101.39
N6–Co1–S9	85.17	N6–Ni1–S9	87.57	N6–Cu1–S9	87.83
N2–Co1–S5	85.68	N2–Ni1–S5	87.63	N2–Cu1–S5	86.53
Co1–N6–N7	118.92	Ni1–N6–N7	117.73	Cu1–N6–N7	115.32
N6–N7–C8	112.89	N6–N7–C8	114.81	N6–N7–C8	113.76
N7–C8–S9	118.86	N7–C8–S9	121.02	N7–C8–S9	122.92
C8–S9–Co1	94.98	C8–S9–Ni1	91.65	C8–S9–Cu1	97.24
Co1–N2–N3	120.04	Ni1–N2–N3	117.18	Cu1–N2–N3	118.22
N2–N3–C4	113.43	N2–N3–C4	114.61	N2–N3–C4	114.79
N3–C4–S5	118.75	N3–C4–S5	120.55	N3–C4–S5	123.00

C4–S5–Co1	95.49	C4–S5–Ni1	91.72	C4–S5–Cu1	97.23
Co1–N6–C36	123.20	Ni1–N6–C36	124.03	Cu1–N6–C36	126.90
Co1–N2–C10	122.37	Ni1–N2–C10	124.12	Cu1–N2–C10	124.73
N6–Co1–O50	94.06	N6–Ni1–O50	86.02	N6–Cu1–O50	89.74
N6–Co1–O53	89.72	N6–Ni1–O53	87.12	N6–Cu1–O53	94.59
N2–Co1–O50	84.96	N2–Ni1–O50	93.70	N2–Cu1–O50	86.88
N2–Co1–O53	91.37	N2–Ni1–O53	93.14	N2–Cu1–O53	89.83
Co1–O50–H51	115.21	Ni1–O50–H51	118.92	Cu1–O50–H51	119.98
Co1–O50–H52	112.13	Ni1–O50–H52	118.49	Cu1–O50–H52	117.18
Co1–O53–H54	111.29	Ni1–O53–H54	117.85	Cu1–O53–H54	118.15
Co1–O53–H55	105.60	Ni1–O53–H55	117.98	Cu1–O53–H55	119.12
H51–O50–H52	105.29	H51–O50–H52	107.50	H51–O50–H52	104.98
H54vO53–H55	103.56	H54–O53–H55	107.34	H54–O53–H55	104.78

Zn(II)		**Cd(II)**		**Pd(II)**	
Bond length	**Value (Å)**	**Bond length**	**Value (Å)**	**Bond length**	**Value (Å)**
Zn1–N2	2.054	Cd1–N2	2.292	Pd1-N4	2.07745
Zn1–N6	2.058	Cd1–N6	2.296	N4-N5	1.38457
Zn1–S9	2.346	Cd1–S9	2.528	N5-C6	1.33846
Zn1–S5	2.343	Cd1–S5	2.526	C6-S7	1.81240
S9–C8	1.820	S5–C4	1.828	Pd1-S7	2.32439
C8–N7	1.338	N2–N3	1.390	Pd1-Cl2	2.33692
N7–N6	1.392	N3–C4	1.335	Pd1-Cl3	2.38802
C36–N6	1.318	N6–N7	1.388	N4-C8	1.33637
N2–N3	1.394	N7–C8	1.337	C5-N22	1.36084
N3–C4	1.336	S9–C8	1.826	Bond angle	Value (°)
C4–S5	1.822	N6–C36	1.319	Pd1-S7-C6	95.97359
C10–N2	1.318	N2–C10	1.319	S7-C6-N5	123.51906
Bond angle	Value (°)	Bond angle	Value (°)	C6-N5-N4	115.34143
N6–Zn1–N2	119.24	N6–Cd1–N2	122.67	N5-N4-Pd1	121.43770
S9–Zn1–S5	142.22	S9–Cd1–S5	154.21	N4-Pd1-S7	83.72811
N6–Zn1–S5	112.02	N6–Cd1–S5	111.93	Cl2-Pd1-Cl3	91.07298
S9–Zn1–N2	112.20	N2–Cd1–S9	112.33	N4-Pd1-Cl3	95.41259
N6–Zn1–S9	87.08	N6–Cd1–S9	80.53	S7-Pd1-Cl2	89.78632
N2–Zn1–S5	87.29	N2–Cd1–S5	80.73	Pd1-N4-C8	120.17843
Zn1–N6–N7	118.71	Cd1–C6–C36	120.61	N5-N4-C8	118.38385

N6–N7–C8	115.09	Cd1–C6–C7	119.43	S7-C6-N22	117.64068
N7–C8–S9	127.42	N6–N7–C8	116.69	N5-C6-N22	118.84026
C8–S9–Zn1	91.59	N7–C8–S9	129.36	Pd1-N4	2.07745
Zn1–N6–C36	121.18	C8–S9–Cd1	94.00	N4-N5	1.38457
Zn1–N2–N3	118.58	Cd1–N2–N3	119.30	N5-C6	1.33846
N2–N3-C4	115.09	N2–N3–C4	116.72	C6-S7	1.81240
N3–C4-S5	127.48	N3–C4–S5	129.38	Pd1-S7	2.32439
C4–S5–Zn1	91.45	C4–S5–Cd1	93.84	Pd1-Cl2	2.33692
Zn1–N2–C10	121.24	Cd1–N2–C10	120.68	Pd1-Cl3	2.38802

4.2.2 Frontier molecular orbitals

The Co(II), Ni(II), Cu(II), Zn(II), Cd(II) and Pd(II) complexes were thought to have frontier orbitals which are simply HOMO and LUMO. These frontier molecular orbitals are considered when evaluating the kinetic characteristics of reactants and reactions. At distances greater than typical bond lengths, the maximum orbital overlap is between frontier molecular orbitals, which are likely to be the main initial interactions as reactants approach. They were used to find frontier electron density for predicting the most probable reactive position in π-electron systems. The gap between HOMO and LUMO exemplifies the chemical stability of a molecule. A small gap designates significant degree of intermolecular charge transfer from electron-donor groups to efficient electron-accepter groups through π-conjugated path [48].

The energies of HOMO, LUMO and frontier molecular orbital gap at DFT/B3LYP/SDD level of theory for complexes are depicted in Fig. 4.9. The frontier molecular orbital parameters of the compounds are presented in Table 4.8. The frontier molecular orbital energy gap of Co(II), Ni(II), Cu(II), Zn(II), Cd(II) and Pd(II) complexes were evaluated as 1.28926, 1.52708, 0.75674, 1.95565, 2.12083 and 0.14748 eV, respectively. It can be noticed that the frontier molecular orbital gap is small and hence, the complexes under investigation are more stable and polarizable. From the results, the frontier orbitals energy gap is found to be in the order Cd(II) > Zn(II) > Ni(II) > Co(II) > Cu(II) > Pd(II). The same order is followed for determining chemical potential (μ) values for the complexes. Based on the frontier orbital energies and chemical potential values, the Cd(II) complex has greater chemical reactivity and chemical stability, whereas Pd(II) complex has lower chemical reactivity and chemical stability.

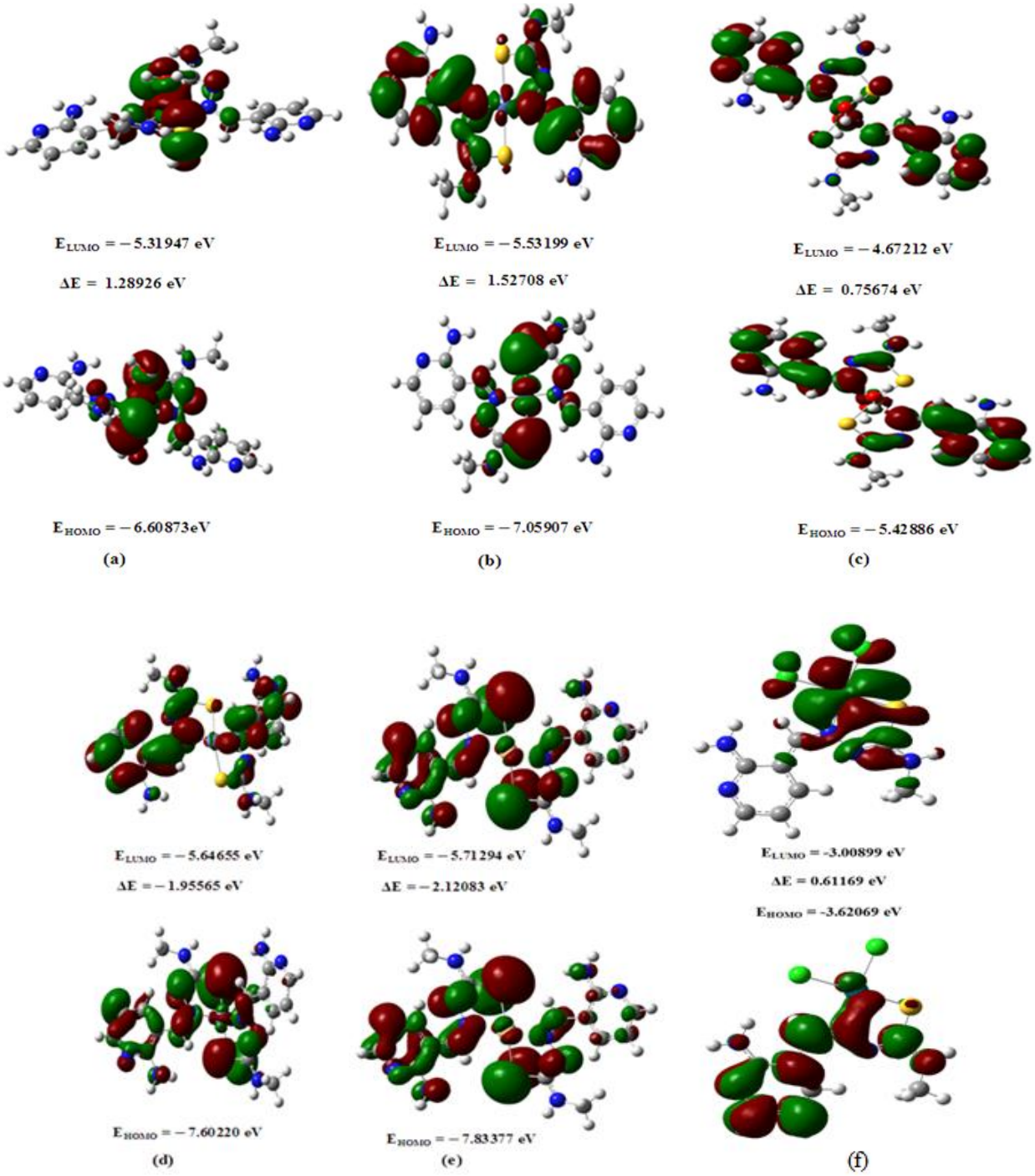

Fig. 4.9 Frontier molecular orbitals of **(a)** Co(II), **(b)** Ni(II), **(c)** Cu(II), **(d)** Zn(II), **(e)** Cd(II) and **(f)** Pd(II) metal complexes.

Table 4.8 Frontier molecular orbital parameters of complexes (in **eV**)

Frontier molecular orbital parameter	Co(II)	Ni(II)	Cu(II)	Zn(II)	Cd(II)	Pd(II)
HOMO energy	-6.60873	-7.05903	-5.42886	-7.60220	-7.83377	-3.62069
LUMO energy	-5.31947	-5.53199	-4.67212	-5.64655	5.71294	-3.00899
Frontier molecular orbital energy gap	1.28926	1.52708	0.75674	1.95565	2.12083	0.61169
ionization energy (I)	6.60873	7.05903	5.42886	7.60220	7.83377	3.62069
Electron affinity (A)	5.31947	5.53199	4.67212	5.64655	5.71294	3.00899
Global hardness (η)	0.64463	0.76354	0.37837	0.97782	1.06041	0.30584
Chemical potential (μ)	-5.96410	-6.29553	-5.05049	-6.62434	-6.77335	-3.31784
Global electrophilicity power (ω)	27.59112	25.95390	33.73645	22.43768	21.63234	17.96360

4.3 Biological evaluations

4.3.1 *In vitro* antimicrobial activity

The antimicrobial activity of the newly synthesized ligand and its metal complexes were evaluated against certain human sensitive pathogenic two gram-positive and two gram-negative bacteria (*Staphylococcus aureus, Bacillus subtilis, Escherichia coli* and *Klebsiella pneumoniae*) and two fungal strains (*Pencillium notatum* and *Aspergillus niger*) by disc diffusion method. The antimicrobial activity results of the synthesized compounds as well as standard drugs are summarized in Tables 4.9 and 4.10. From the results, it was observed that the ligand does not show any activity against tested microorganisms. In all the cases the activity of complexes increases with increasing concentration of the test samples and standards [69]. In our investigation, it was observed that Cd(II) complex showed excellent antibacterial activity against the tested strains *S. aureus* (MIC: 1.562 μg/mL), *B. subtilis* (MIC: 3.125 μg/mL), *K. pneumoniae* (MIC: 3.125 μg/mL) and *E. coli* (MIC: 1.562 μg/mL), respectively and the Cu(II) complex displayed good activity against *S. aureus* (MIC: 6.25 μg/mL), *B. subtilis* (MIC: 12.5 μg/mL) and *E. coli* (MIC: 6.25 μg/mL) compared to streptomycin standard drug. Complexes Ni(II) and

Pd(II) exhibited moderate activity against *S. aureus* and *K. pneumoniae* with MIC values of 12.5 µg/mL and 6.25 µg/mL, respectively. In the antifungal activity, the Cd(II) complex showed excellent activity against *P. notatum* compared to standard drug with MIC value of 3.125 µg/mL. The complexes Ni(II**)** and Cd(II) showed potent activity against *A. niger* with MIC values of 6.25 and 6.25 µg/mL, respectively. However, the other complexes showed poor activity against the tested microorganisms.

Table 4.9 MIC values of antibacterial activity of the compounds (µg/mL)

Compound	***S. aureus***	***B. subtilis***	***K. pneumoniae***	***E. coli***
Co(II)	50	>100	50	>100
Ni(II)	12.5	50	>100	>100
Cu(II)	6.25	12.5	25	6.25
Zn(II)	>100	>100	50	>100
Cd(II)	**1.562**	3.125	3.125	**1.562**
Pd(II)	50	50	6.25	>100
ANMTSC	>100	>100	>100	>100
Streptomycin	3.125	6.25	1.562	3.125

Table 4.10 MIC values of antifungal activity of compounds (µg/mL)

Compound	***A. niger***	***P. notatum***
Co(II)	50	50
Ni(II)	6.25	6.25
Cu(II)	25	25
Zn(II)	50	>100
Cd(II)	6.25	**3.125**
Pd(II)	25	>100
ANMTSC	50	>100
Ketoconazole	3.125	3.125

4.3.2 *In vitro* antioxidant property

The scavenging activity of the ligand and its metal complexes were extensively studied by DPPH (1,1-Diphenyl-2-picryl-hydrazyl) method [49] and the values are indicated in terms of IC_{50}. DPPH is an established radical and is utilized to scavenge other radicals. DPPH radical shows deep violet colour in solution and has strong absorption at 517 nm. When the DPPH radical is paired off with the free radical scavenger, the colour of the solution vanishes. DPPH becomes colourless or pale yellow when neutralized and the resulting decolorization corresponds to the number of electrons paired up. From Fig. 4.10 and Table 4.11 which represents the IC_{50} values of the newly synthesized compounds, it is clear that these synthesized compounds showed impressive scavenging activity compared to ascorbic acid (standard). Importantly, Co(II) and Zn(II) complexes exhibited the most potent scavenging activity with IC_{50} values of 11.17 ± 1.92 µM and 10.79 ± 0.85 µM, respectively and also Ni(II) and Pd(II) complexes showed moderate scavenging ability with IC_{50} values of 18.43 ± 1.30 µM and 20.31 ± 1.92 µM compared to standard drug ascorbic acid. The other complexes Cu(II) and Cd(II) exhibited poor antioxidant activity with IC_{50} values of 34.96 ± 1.82 µM and 26.08 ± 1.03 µM, respectively and ANMTSC ligand showed least (IC_{50} = 38.79 ± 1.03 µM) activity. Based on IC_{50} values the order of activity is Zn > Co(II) > Ni(II) > Pd(II) > Cd(II) > Cu(II) > ANMTSC.

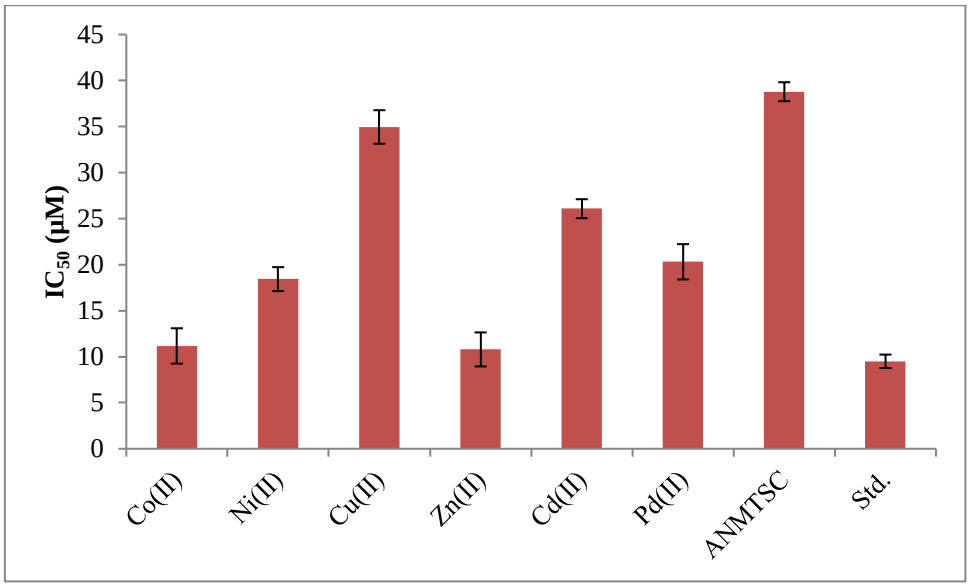

Fig. 4.10 Antioxidant activity of ANMTSC and its metal complexes.

Table 4.11 IC_{50} values of DPPH scavenging activity of ligand ANMTSC and its complexes

Compound	IC_{50} (µM)
Co(II)	**11.17 ± 1.92**
Ni(II)	18.43 ± 1.30
Cu(II)	34.96 ± 1.82
Zn(II)	**10.79 ± 0.85**
Cd(II)	26.08 ± 1.03
Pd(II)	20.31 ± 1.92
ANMTSC	38.79 ± 1.03
Ascorbic acid	**9.50 ± 0.73**

4.3.3 *In vivo* blood glucose level test

In vivo blood glucose level test has been carried out to screen antidiabetic property of the compounds. Diabetes induced rats were divided into nine (group II-X) groups and each group consisted of six rats other than group I and group II. These two were employed as normal control and diabetic control, group III had metformin as standard and the groups IV-X were employed as test groups. The standard and the prepared compounds were served orally at 20 mg/kg. After treatment, blood samples were taken from all the groups on 1st day, 7th day and 14th day and then blood glucose levels were recorded by using glucometer. The antidiabetic activity of the test compounds are shown in Fig. 4.11 and blood glucose test results are summarized in Table 4.12, where one can see that compared to the standard drug Metformin, Zn(II) and Pd(II) complexes showed good antidiabetic activity compared to other complexes and free ligand.

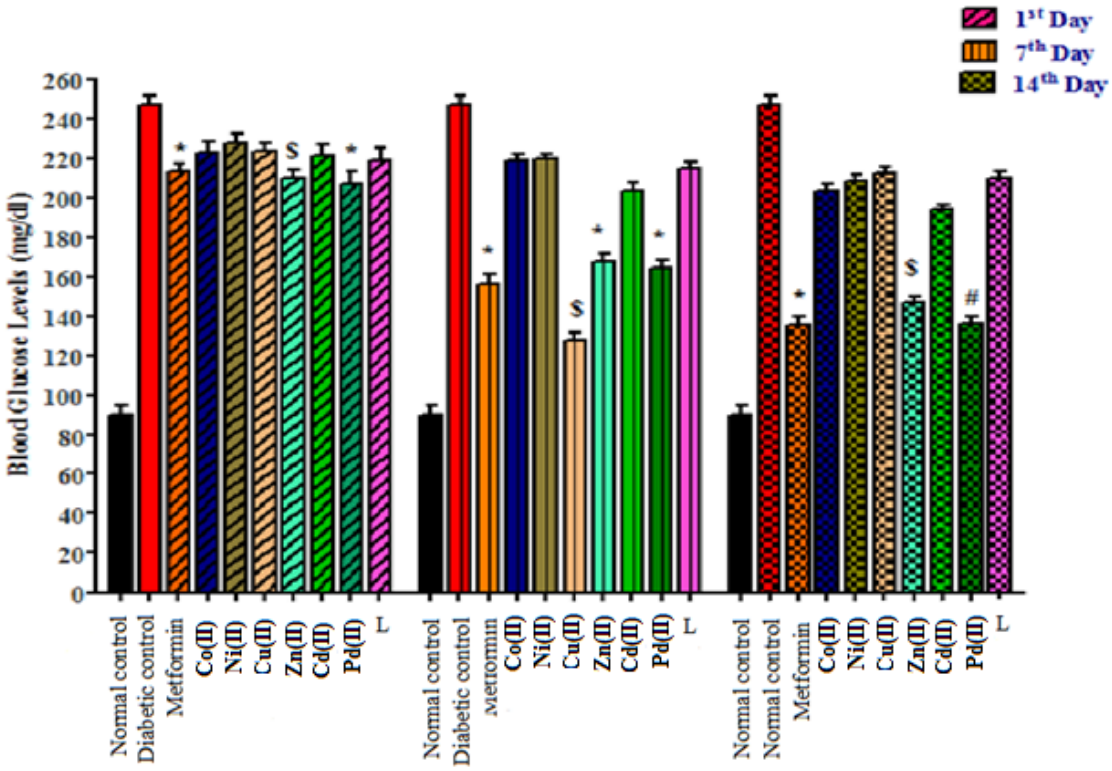

Fig. 4.11 Antidiabetic activity of the ANMTSC and its metal complexes (20 mg/Kg).

Table 4.12 Effect of prepared compounds on fasting blood glucose levels in alloxan induced diabetic rats in sub acute study (14 days study)

Group	Dose (mg/kg b.w.)	Fasting blood glucose level (mg/dl)		
		1st Day	7th Day	14th Day
I	Normal control	90.70 ± 4.62	90.70 ± 4.83	90.70 ± 4.52
II	Diabetic control	246.00 ± 5.37	246.00 ± 5.37	246.00 ± 5.37
III	Metformin 20 mg/Kg	213.26 ± 4.27	156.53 ± 4.62	135.93 ± 4.20
IV	Co(II) 20 mg/Kg	223.00 ± 5.14	219.20 ± 3.28	203.47 ± 3.25
V	Ni(II) 20 mg/Kg	227.41 ± 4.68	219.30 ± 3.19	208.50 ± 3.29
VI	Cu(II) 20 mg/Kg	223.96 ± 6.61	217.83 ± 4.38	212.36 ± 3.27

VII	Zn(II) 20 mg/Kg	210.41 ± 4.03	168.20 ± 4.29	147.40 ± 3.50
VIII	Cd(II) 20 mg/Kg	221.51 ± 5.59	204.10 ± 3.40	194.30 ± 2.10
IX	Hg(II) 20mg/Kg	206.63 ± 3.20	168.20 ± 4.29	139.37 ± 4.15
X	ANMTSC 20 mg/Kg	219.00 ± 6.50	214.83 ± 3.20	210.36 ± 3.20

4.3.4 *In vitro* cytotoxicity

To explore the cytotoxic effects of the synthesized compounds, an MTT assay was carried out by using cisplatin as a reference drug. As shown in Fig. 4.12 survival curves have been drawn for MCF-7, HeLa, A549 and IMR-32 cancer cell lines. IC_{50} values of the tested compounds are summarized in Table 4.13. All the compounds have shown potent to moderate activity against all the tested cell lines when compared to the standard drug. The results showed that Co(II) and Zn(II) complexes displayed most potential cytotoxic property against four panel cell lines with IC_{50} values of 15.27 ± 0.10 µM and 10.28 ± 0.69 µM against HeLa; 9.91 ± 0.37 µM and 9.80. ± 0.83 µM against MCF-7; 12.57 ± 0.36 µM and 11.08 ± 0.57 µM against A549, and 13.92 ± 0.58 µM and 10.41 ± 0.60 µM against IMR-32, respectively. Besides, the Cd(II) complex showed moderate activity against HeLa and IMR-32 with IC_{50} values of 20.15 ± 0.69 µM and 22.78 ± 0.25 µM, respectively. The remaining compounds exhibited reasonable cytotoxic property with the IC_{50} values ranging from 30.23 ± 0.18 µM to 48.20 ± 0.91 µM for the four cell lines.

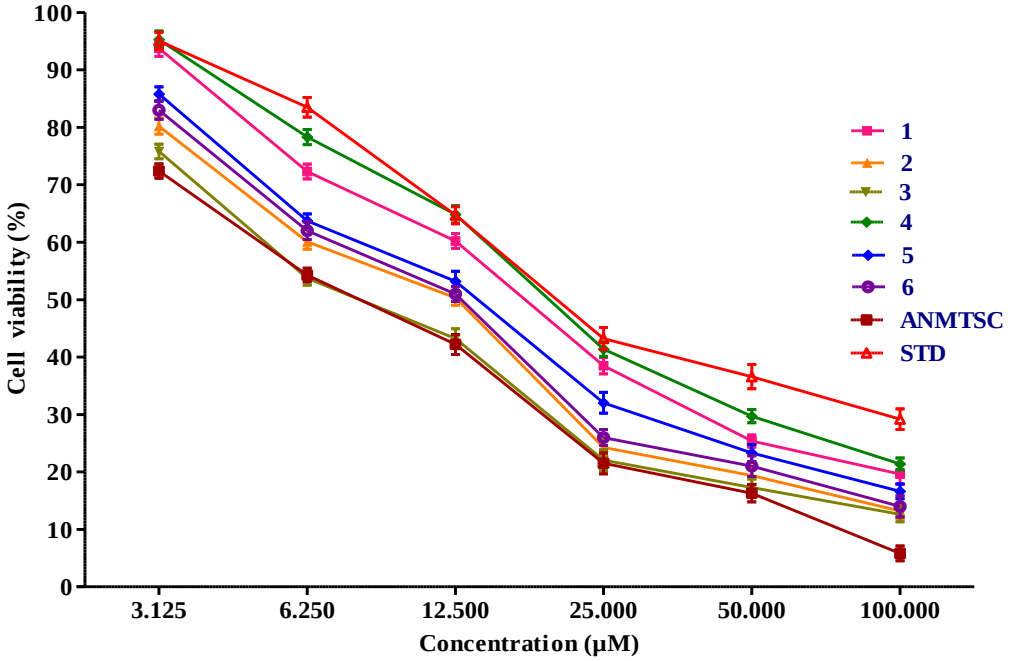
Cell viability (%)
100
90
80
70
60
50
40
30
20
10
0
3.125
6.250
12.500
25.000
50.000
100.000
Concentration (µM)
1
2
3
4
5
6
ANMTSC
STD

(a)

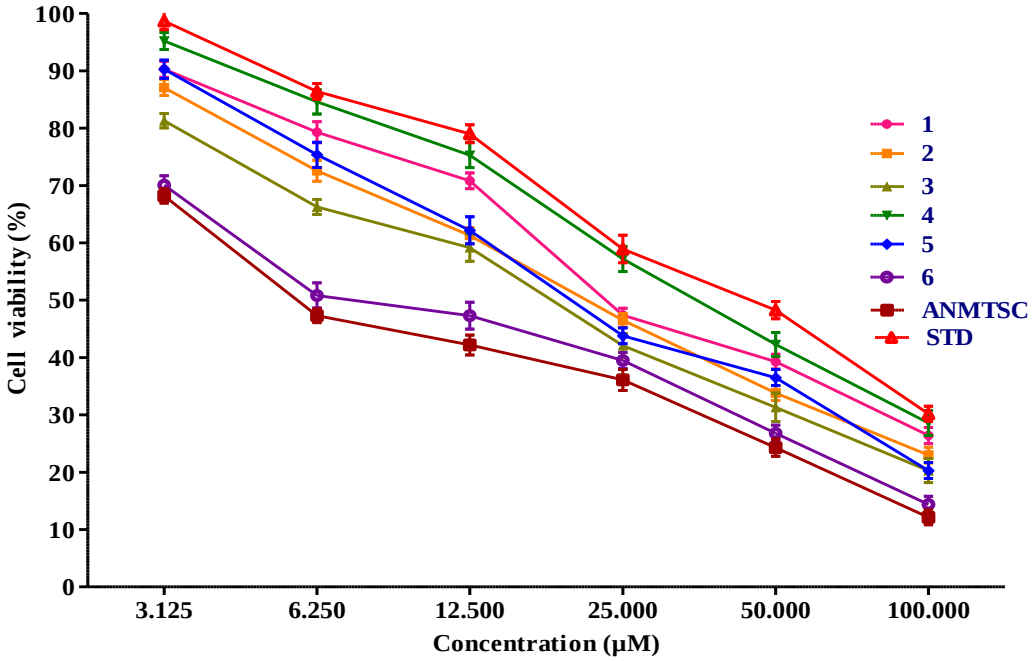
Cell viability (%)
100
90
80
70
60
50
40
30
20
10
0
3.125
6.250
12.500
25.000
50.000
100.000
Concentration (µM)
1
2
3
4
5
6
ANMTSC
STD

(b)

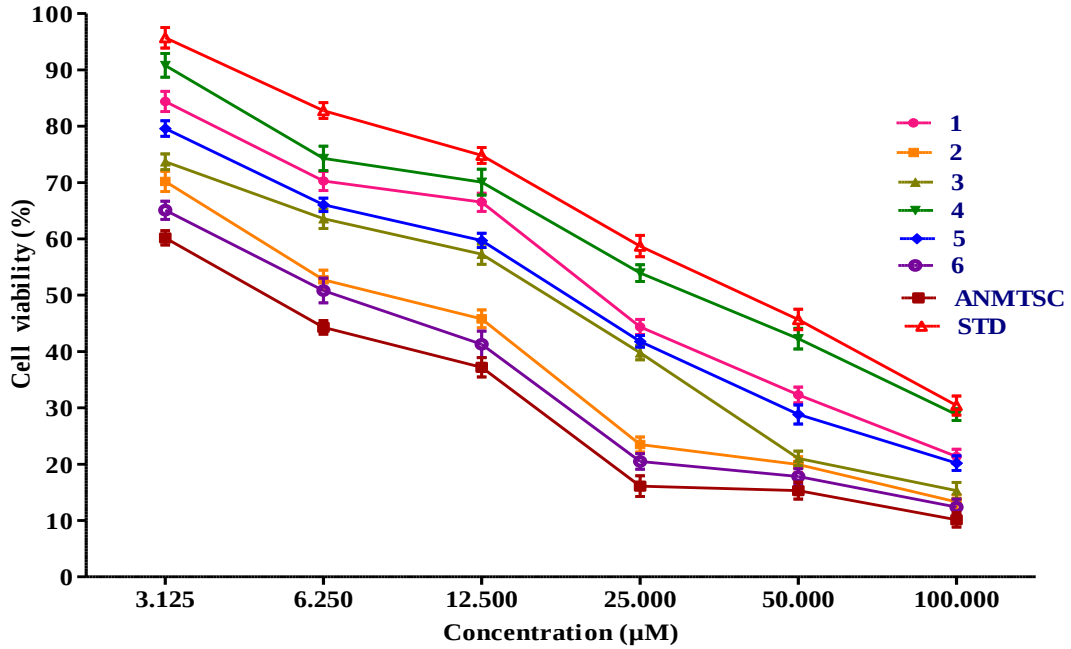
Cell viability (%)
100
90
80
70
60
50
40
30
20
10
0
3.125
6.250
12.500
25.000
50.000
100.000
Concentration (µM)
1
2
3
4
5
6
ANMTSC
STD

(c)

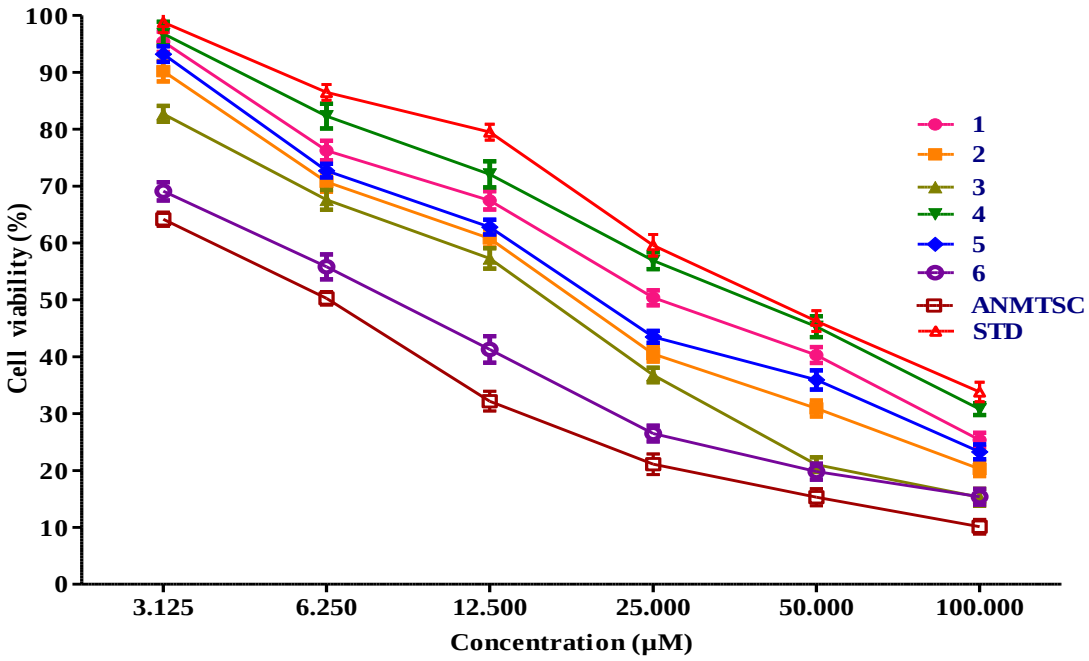
Cell viability (%)
100
90
80
70
60
50
40
30
20
10
0
3.125
6.250
12.500
25.000
50.000
100.000
Concentration (µM)
1
2
3
4
5
6
ANMTSC
STD

(d)

Fig. 4.12 Survival curves of **(a)** HeLa, **(b)** MCF-7, **(c)** A549 and **(d)** IMR-32 of the compounds. [In graphs, 1 = Co(II), 2 = Ni(II), 3 = Cu(II), 4 = Zn(II), 5 = Cd(II), and 6 = Pd(II) complexes].

Table 4.13 IC_{50} (µM) values of anticancer activity of ANMTSC and its metal complexes

Compound	HeLa	MCF-7	A549	IMR-32	HEK 293
Co(II)	**15.27 ± 0.10**	**9.91 ± 0.37**	**12.57 ± 0.36**	**13.92 ± 0.58**	ND
Ni(II)	41.94 ± 0.91	32.75 ± 0.47	40.58 ± 0.62	32.49 ± 0.21	ND
Cu(II)	45.38 ± 0.60	42.90 ± 0.61	39.52 ± 0.25	43.10 ± 0.15	ND
Zn(II)	**10.28 ± 0.69**	**9.80 ± 0.83**	**11.08 ± 0.57**	**10.41 ± 0.60**	**56.82 ± 0.32**
Cd(II)	20.15 ± 0.69	30.23 ± 0.18	29.83 ± 0.57	22.78 ± 0.25	ND
Pd(II)	33.47 ± 0.13	40.01 ± 0.86	44.29 ± 0.31	38.22 ± 0.53	ND
ANMTSC	48.20 ± 0.91	45.35 ± 0.32	41.60 ± 0.70	46.81 ± 0.42	ND
Cisplatin	4.83 ± 0.17	6.24 ± 0.16	5.32 ± 0.24	4.39 ± 0.40	ND

Values are expressed as mean ± SEM. ND stands for not determine

4.3.5 Reactive oxygen species (ROS)

ROS has a predominant role in cell death through cellular senescence paving because of which there is a demand for therapeutic drugs that may prevent oxidative stress induced neuro degeneration. It was highly possible that the pro-oxidant effect is responsible for the apoptotic activity of these extracts. ROS has key signaling molecules to modulate cell death [50]. Accumulating evidence indicates that when high levels of ROS were produced by cancer injected cells, it led to a state of increased basal oxidative stress. The increased production of ROS in cancer cells was observed in *in vitro* studies [51]. Ahmad et al. demonstrated that naringenin leads to cell death in cancer cells *via* inducing ROS generation [52]. We therefore investigated the effectiveness of methanolic extract in generation of ROS. It was found that exposure of all four cancer cells to these extracts dramatically enhanced generation of intracellular ROS at different levels in a dose dependent manner in all cell lines. The results of ROS generation effect of methanolic extract on cancer cell lines HeLa, MCF-7, A549 and IMR-32 are shown in Fig. 4.13. The results showed that the methanolic extract significantly increased the ROS production in all the cell cultures.

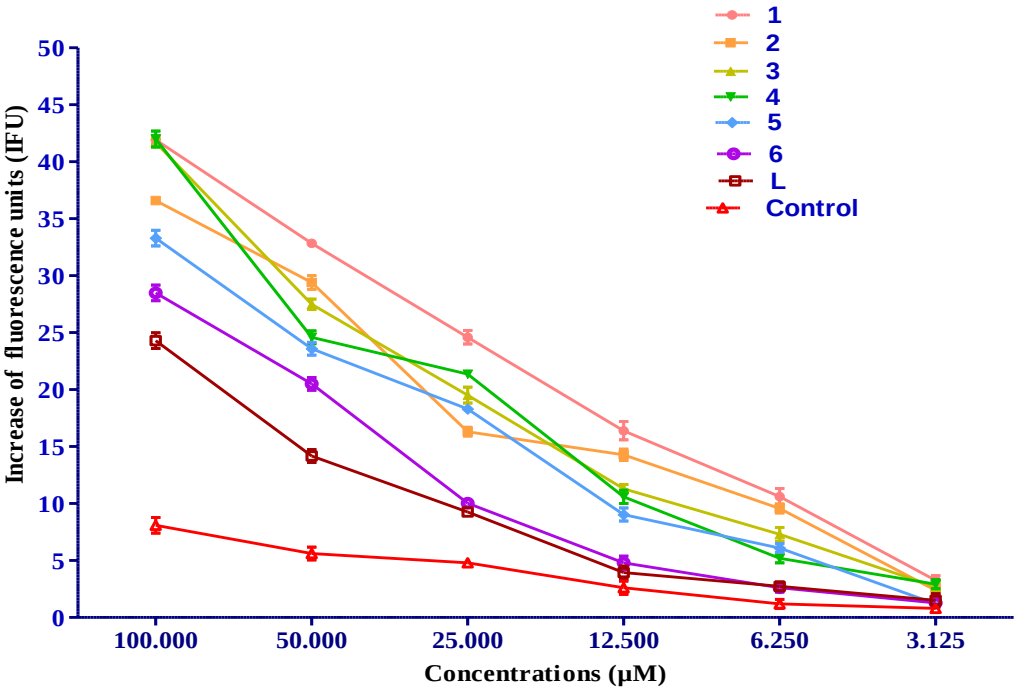
1
2
3
4
5
6
L
Control
Increase of fluorescence units (IFU)
0
5
10
15
20
25
30
35
40
45
50
100.000
50.000
25.000
12.500
6.250
3.125
Concentrations (µM)

(a)

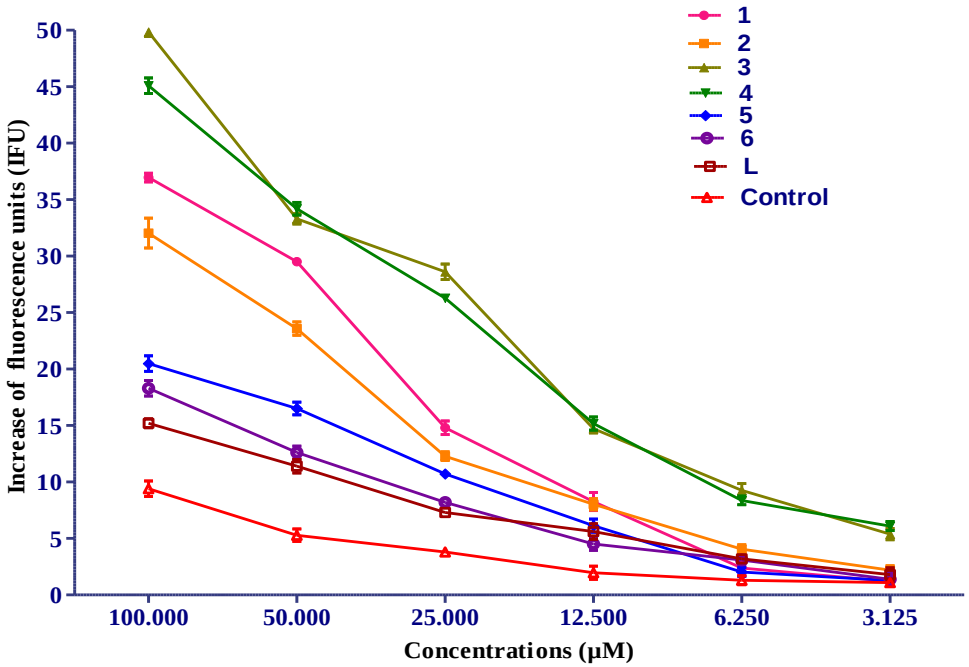
1
2
3
4
5
6
L
Control
Increase of fluorescence units (IFU)
0
5
10
15
20
25
30
35
40
45
50
100.000
50.000
25.000
12.500
6.250
3.125
Concentrations (µM)

(b)

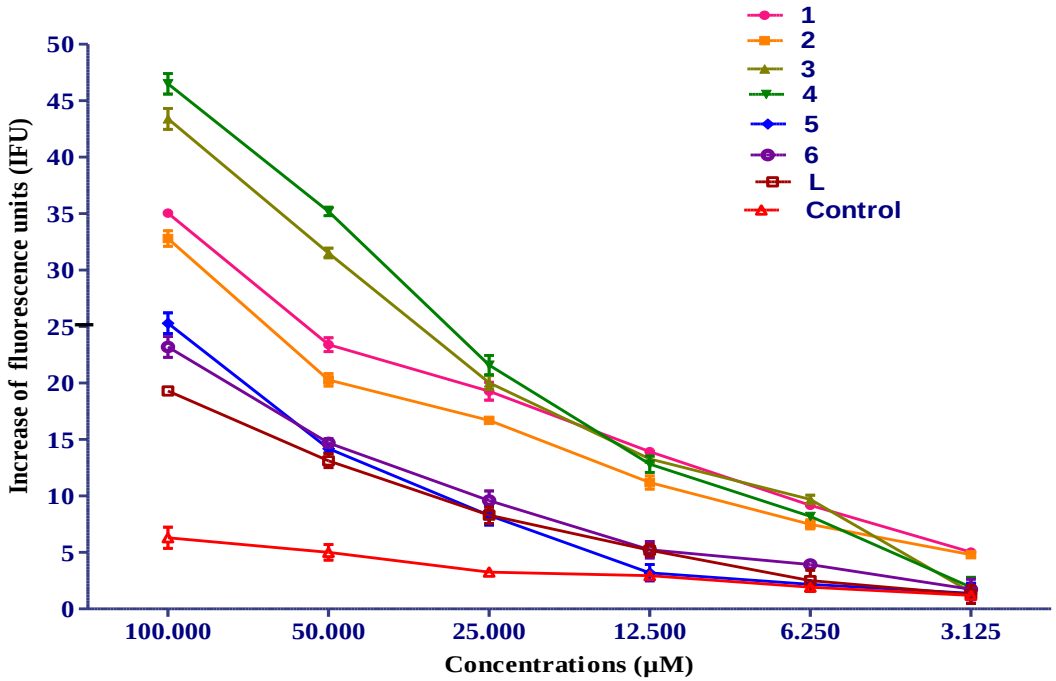
1
2
3
4
5
6
L
Control
Increase of fluorescence units (IFU)
50
45
40
35
30
25
20
15
10
5
0
100.000
50.000
25.000
12.500
6.250
3.125
Concentrations (µM)

(c)

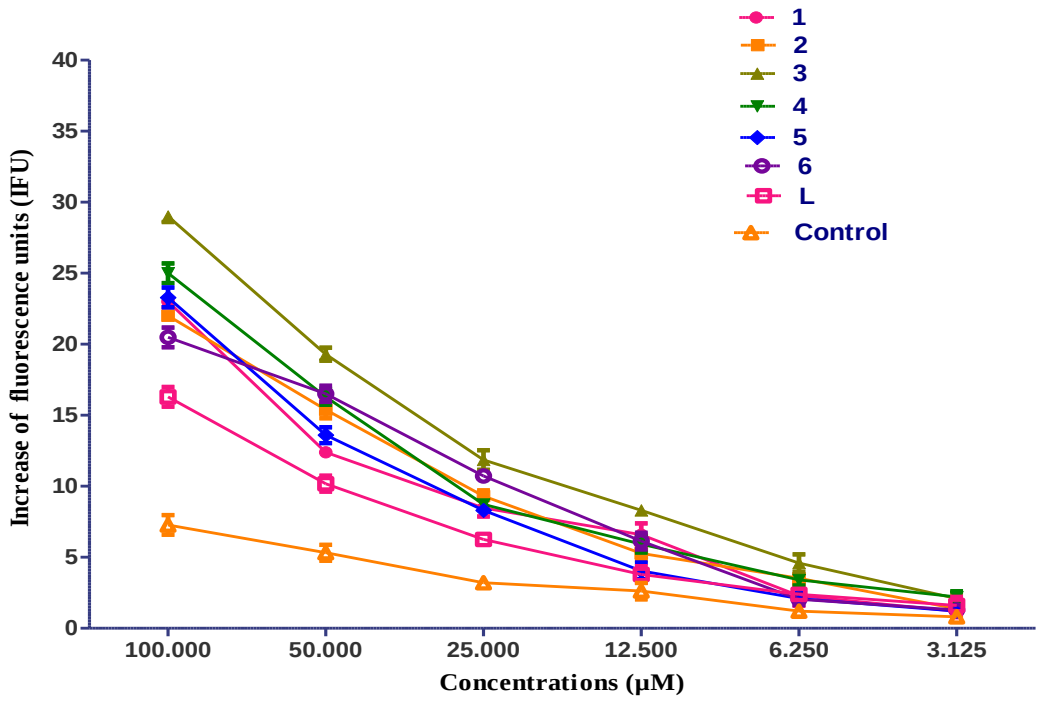
1
2
3
4
5
6
L
Control
Increase of fluorescence units (IFU)
40
35
30
25
20
15
10
5
0
100.000
50.000
25.000
12.500
6.250
3.125
Concentrations (µM)

(d)

Fig. 4.13 Relative ROS intra-cellar release on human cancer [**(a)** HeLa, **(b)** MCF-7, **(c)** A549, and **(d)** IMR-32] cell lines exposed to ligand ANMTSC and its complexes with the concentrations (100-3.25 µM) for 24 h. [1 = Co(II), 2 = Ni(II), 3 = Cu(II), 4 = Zn(II), 5 = Cd(II), 6 = Pd(II) complexes and L = ANMTSC].

4.4 *In silico* molecular docking studies

The *in silico* molecular docking analysis of the ligand and its metal complexes against epidermal growth factor (EGFR) was carried out to verify the relation between *in vitro* anticancer activity results and binding affinities of the inhibitors by using AutoDock programme. Docking results revealed that ligand and its metal complexes were strongly bound to the receptors of EGFR protein by exhibiting the best ligand pose binding energy values i.e., –3.97 (ANMTSC), –5.91 [Co(II)], –5.19 [Ni(II)], –4.51 [Cu(II)], –6.81 [Zn(II)], –5.75 [Cd(II)] and –5.80 [Pd(II)] kcal/mol, respectively. The efficient interactions of the complexes with the protein when compared with free ligand with protein may be due to their orientation in the grid of the protein. The *in silico* molecular docking studies of the ligand and its complexes showed that all synthesized compounds interact with amino acid residues of the EGFR protein receptor by forming hydrogen bonds. Among all the complexes, Zn(II) complex showed the lowest binding energy (–6.81 kcal/mol) with EGFR protein receptor. Five hydrogen bonds were observed between Zn(II) complex and EGFR protein receptor. Two hydrogen bonds were formed with residue ARG817 with bond distances of 2.33 Å and 2.10 Å, while the remaining three hydrogen bonds with LYS851, ASN818 and ASP831 residues had bond distances of 1.99 Å, 2.22 Å and 1.79 Å, respectively. Along with these hydrogen bonds, there was a hydrophobic interaction with ARG817. When compared with ligand the other complexes Co(II), NI(II), Cu(II), Cd(II) and Pd(II) exhibited good binding energies with EGFR protein receptor. The binding energies, number of hydrogen bond(s), their bond lengths and residues responsible for the hydrogen bonds are shown in Table 4.14. The best confirmation of ligand and complexes were visualized and shown in Fig. 4.14. In conclusion, the docking results strongly support the *in vitro* anticancer activity results.

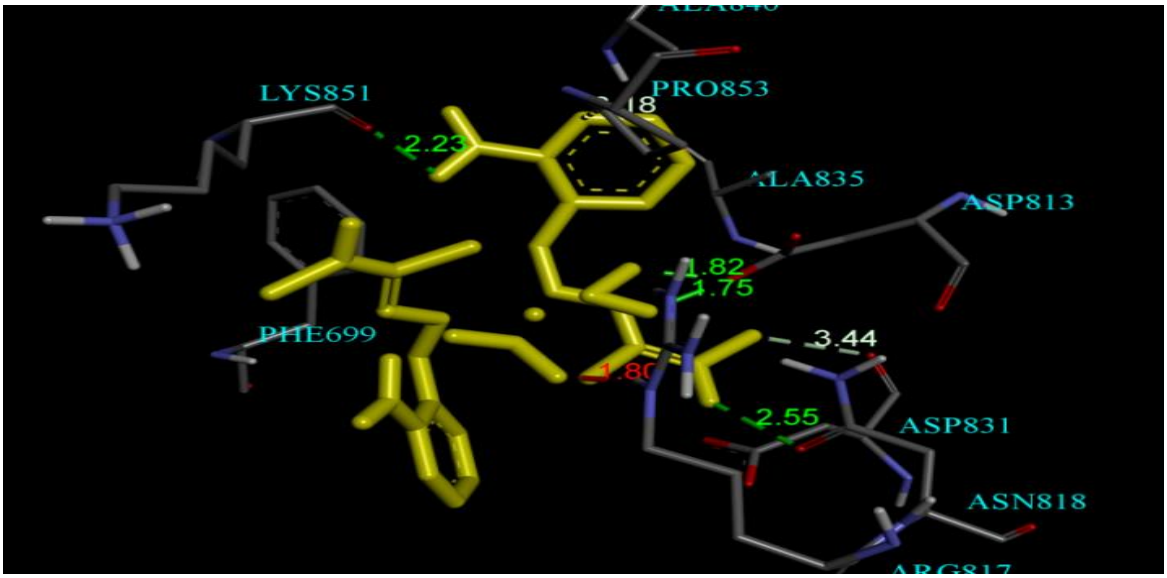

(a)

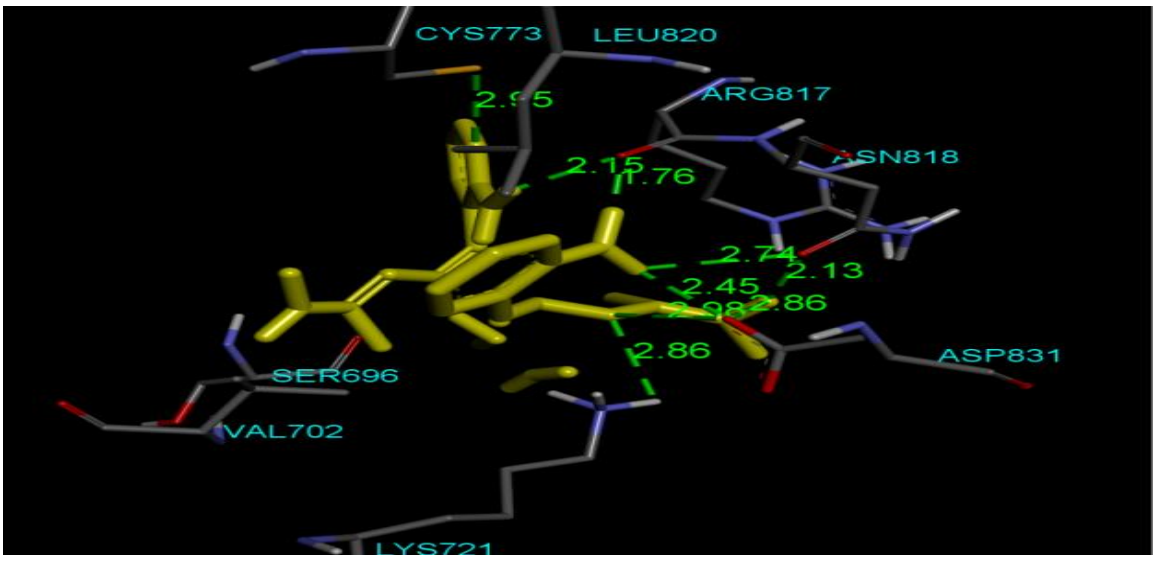

(b)

Fig. 4.14a-b docking interactions of **(a)** Co(II) complex, **(b)** Ni(II) complex.

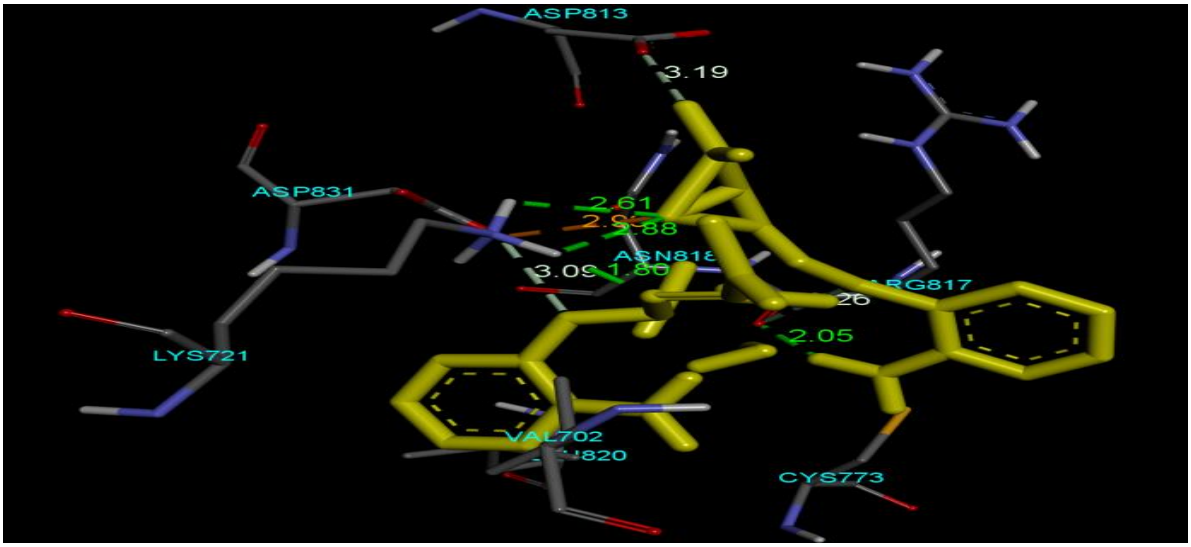

(c)

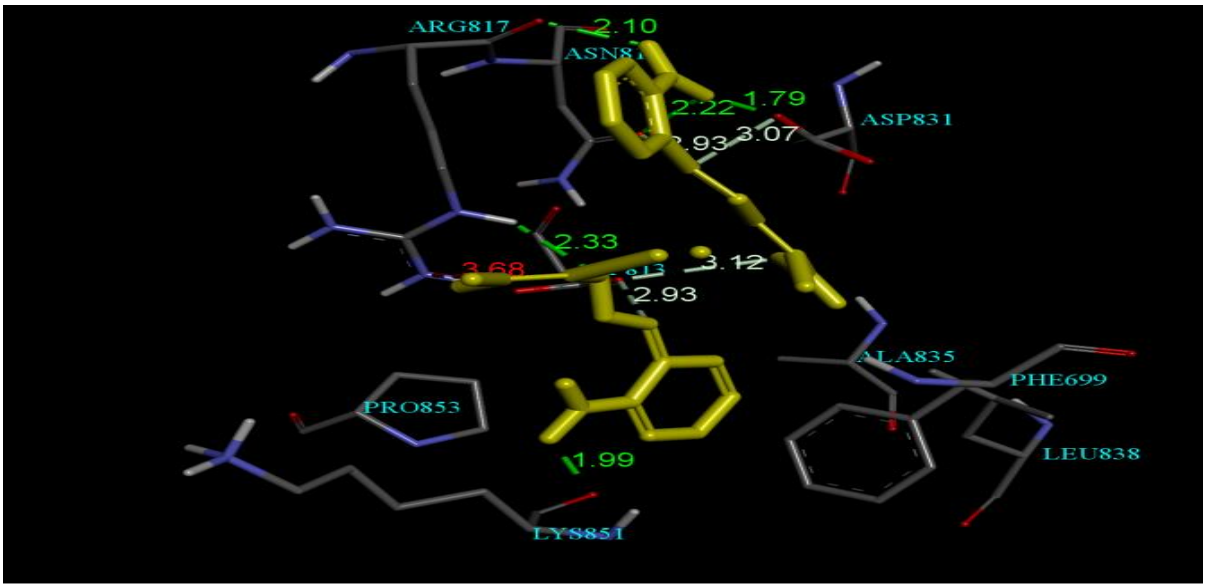

(d)

Fig. 4.14c-d docking interactions of **(c)** Cu(II) complex, **(d)** Zn(II) complex.

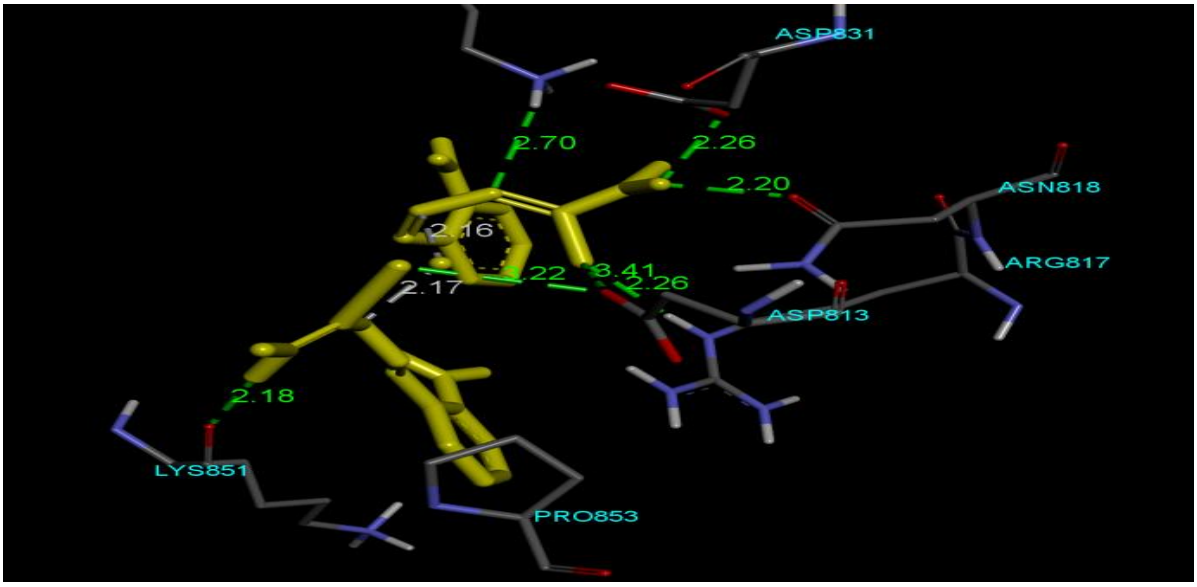

(e)

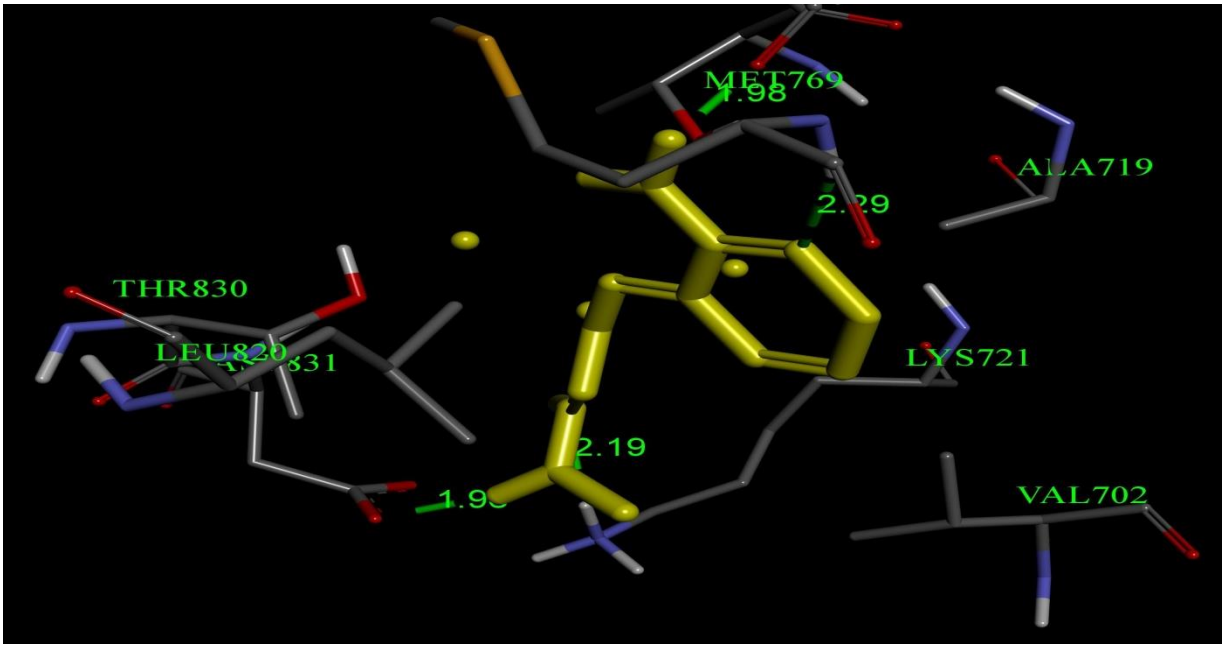

(f)

Fig. 4.14e-f docking interactions of **(e)** Cd(II) complex, **(f)** Pd(II) complex.

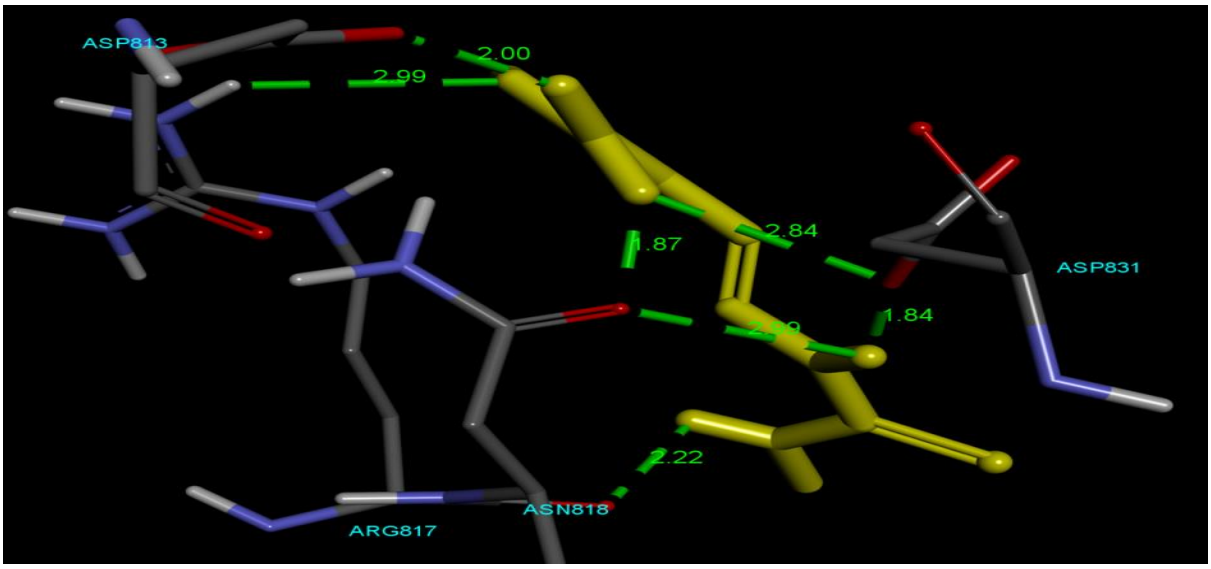

(g)

Fig. 4.14g docking interactions of **(g)** ANMTSC to the binding sites of target protein EGFR (PDB ID: 4hjo).

Table 4.14 Binding energy, bond length, hydrogen bonds and residues involved in hydrogen bonding of ligand and its complexes inhibitors against EGFR receptor

Compound	Binding energy (kcal/mol)	No. of hydrogen bonds	Residues involved in hydrogen bonding	Bond length (Å)
Co(II)	–5.91	4	ASP813	1.82, 1.75
			LYS851	2.23
			ASN818	2.55
Ni(II)	–5.19	10	LYS721	2.86
			CYS773	2.95
			ASP831	2.96, 2.45, 2.86
			ARG817	1.76, 2.15
			ASN818	2.74, 2.13
			SER676	2.25
Cu(II)	–4.51	5	LYS721	2.61, 1.80, 2.88
			ASN818	2.35
			ARG817	2.05
Zn(II)	–6.81	5	ARG817	2.33, 2.10
			LYS851	1.99
			ASN818	2.22
			ASP831	1.79
Cd(II)	–5.75	7	LYS721	2.70
			ARG817	2.26
			ASP813	3.21, 3.41
			LYS851	2.18
			ASN818	2.20

			ASP831	2.26
Pd(II)	–6.16	4	GLN767	2.19, 2.93
			ASP831	1.90
			LYS721	2.29
			MET769	1.98
ANMTSC	–3.97	7	ARG817	2.99, 2.22
			ASN818	2.99, 1.87
			ASP831	1.84, 2.84
			ASP813	2.00

4.5 Conclusions

The present chapter dealt with synthesis and characterization of new ANMTSC ligand and its corresponding Co(II), Ni(II), Cu(II), Zn(II, Cd(II) and Pd(II) complexes. The molecular structure of the ligand was determined by XRD. The ligand acts as monobasic, bidentate coordination towards metal ion and coordinates through imine nitrogen and thiocarbonyl sulphur atoms, which was confirmed by various spectroscopic tools. Based on Spectral data and theoretical studies Co(II) and Ni(II) complexes have octahedral geometry, Cu(II), Pd(II) complexes have distorted octahedral, square-planar and while the complexes Zn(II) and Cd(II) are tetrahedral geometry. The ESR parameters of the Cu(II) complex confirm that the metal-ligand bonds are covalent out of plane pi-bonds. In biological applications, Co(II) and Zn(II) complexes were found to be most potent antioxidant agents with IC_{50} values of 11.17 ± 1.92 µM and 10.79 ± 1.85 µM, compared to the reference drug ascorbic acid as well as Co(II) and Zn(II) complexes displayed excellent anticancer activity with IC_{50} values of 15.27 ± 0.10 µM, 10.28 ± 0.69 µM (for HeLa), 9.91 ± 0.37 µM, 9.80 ± 0.83 µM (for MCF-7), 12.57 ± 0.36 µM, 11.08 ± 0.57 µM (for A549) and 13.92 ± 0.58 µM, 10.41 ± 0.60 µM (for IMR-32) cell lines. The Cu(II) and Zn(II) complexes showed notable reduction in blood glucose level. Furthermore, the Cd(II) complex exhibited excellent antibacterial activity against two gram positive and two gram negative bacteria such as *B. subtilis, S. aureus, K. pneumonia*e and *E. coli*. The Ni(II) and Cd(II) complexes exhibited most promising

antifungal activity. In future, these encouraging results would prove useful in designing and developing new drugs that combat cancer.

References

[1] S. Padhyé, G.B. Kauffman, *Coord. Chem. Rev.* **1985**, *63*, 127.

[2] D.X. West, A.E. Liberta, S.B. Padhye, R.C. Chikate, P.B. Sonawane, A.S. Kumbhar, R.G. Yerande, *Coord. Chem. Rev.* **1993**, *123*, 49.

[3] A. Berkessel, G. Hermann, O. Rauch, M. Büchner, A. Jacobi, G. Huttner, *Chem. Ber.* **1996**, *129*, 1421.

[4] J.S. Casas, M.S. García-Tasende, J. Sordo, *Coord. Chem. Rev.* **2000**, *209*, 197.

[5] T.S. Lobana, P. Kumari, R.J. Butcher, T. Akitsu, Y. Aritake, J. Perles, F.J. Fernandez, M.C. Vega, *J. Organomet. Chem.* **2012**, *701*, 17.

[6] C. Gan, J. Cui, S. Su, Q. Lin, L. Jia, L. Fan, Y. Huang, *Steroids* **2014**, *87*, 99.

[7] S. Tardito, L. Marchio, *Curr. Med. Chem.* **2009**, *16*, 1325.

[8] İ. Kizilcikli, Y.D. Kurt, B. Akkurt, A.Y. Genel, S. Birteksöz, G. Ötük, B. Ülküseven, *Folia Microbiol. (Praha).* **2007**, *52*, 15.

[9] P.I.da S. Maia, F.R. Pavan, C.Q.F. Leite, S.S. Lemos, G.F.de Sousa, A.A. Batista, O. R. Nascimento, J. Ellena, E.E. Castellano, E. Niquet, et al. *Polyhedron* **2009**, *28*, 398.

[10] T.A. Yousef, G.M. Abu El-Reash, O.A. El-Gammal, R.A. Bedier, *J. Mol. Struct.* **2013**, *1035*, 307.

[11] M.M. Aly, Y.A. Mohamed, K.A.M. El-Bayouki, W.M. Basyouni, S.Y. Abbas, *Eur. J. Med. Chem.* **2010**, *45*, 3365.

[12] R. Acharyya, S.-M. Peng, G.-H. Lee, S. Bhattacharya, *Inorg. Chem.* **2003**, *42*, 7378.

[13] R. Prabhakaran, S.V. Renukadevi, R. Karvembu, R. Huang, J. Mautz, G. Huttner, R. Subashkumar, K. Natarajan, *Eur. J. Med. Chem.* **2008**, *43*, 268.

[14] S. Hossain, C.M. Zakaria, Kudrat-E-Zahan, *Asian J. Res. Chem.* **2017**, *10*, 6.

[15] S. Halder, S.-M. Peng, G.-H. Lee, T. Chatterjee, A. Mukherjee, S. Dutta, U. Sanyal, S. Bhattacharya, *New J. Chem.* **2008**, *32*, 105.

[16] D. Kovala-Demertzi, M.A. Demertzis, J.R. Miller, C.S. Frampton, J.P. Jasinski, D.X. West, *J. Inorg. Biochem.* **2002**, *92*, 137.

[17] P.I.da S. Maia, A.G.de A. Fernandes, J.J.N. Silva, A.D. Andricopulo, S.S. Lemos, E.S. Lang, U. Abram, V.M. Deflon, *J. Inorg. Biochem.* **2010**, *104*, 1276.

[18] A.I. Matesanz, P. Souza, *J. Inorg. Biochem.* **2007**, *101*, 245.

[19] A.I. Matesanz, C. Hernández, A. Rodríguez, P. Souza, *J. Inorg. Biochem.* **2011**, *105*, 1613.

[20] L. Otero, M. Vieites, L. Boiani, A. Denicola, C. Rigol, L. Opazo, C. Olea-Azar, J.D. Maya, A. Morello, R.L. Krauth-Siegel, et al. *J. Med. Chem.* **2006**, *49*, 3322.

[21] K. Husain, M. Abid, A. Azam, *Eur. J. Med. Chem.* **2007**, *42*, 1300.

[22] B. Wang, Z.-Y. Yang, P. Crewdson, D. Wang, *J. Inorg. Biochem.* **2007**, *101*, 1492.

[23] B. Wang, Z.-Y. Yang, D. Qin, Z.-N. Chen, *J. Photochem. Photobiol. A Chem.* **2008**, *194*, 49.

[24] M. Muralisankar, S.M. Basheer, J. Haribabu, N.S.P. Bhuvanesh, R. Karvembu, A. Sreekanth, *Inorganica Chim. Acta* **2017**, *466*, 61.

[25] R.A. Walton, R.W. Matthews, *Inorg. Chem.* **1971**, *10*, 1433.

[26] P.S.N. Reddy, B.V. Agarwala, *Synth. React. Inorg. Met. Chem.* **1987**, *17*, 585.

[27] A.B.P. Lever, *J. Chem. Educ.* **1968**, *45*, 711.

[28] C.K. Jørgensen, U. Persmark, S.E. Rasmussen, A. Block-Bolten, J.M. Toguri, H. Flood, *Acta Chem. Scand.* **1962**, *16*, 2017.

[29] L. Carlin, *Local Environ.* **2000**, *5*, 231.

[30] L. Rehab, A. L.K. Abdul, L.W.A. Jaafar, *Baghdad Sci. J.* **2017**, *14*, 13.

[31] G. Basu, R.L. Belford, R.E. Dickerson, *Inorg. Chem.* **1962**, *1*, 438.

[32] A. Chakravorty, S. Basu, *J. Inorg. Nucl. Chem.* **1961**, *17*, 55.

[33] R. Williams, *J. Chem. Phys.* **1957**, *26*, 1186.

[34] Atkins, Shiver, *Inorg. Chem.* Elsevier, **2013**.

[35] Y. Nishida, S. Kida, *Coord. Chem. Rev.* **1979**, *27*, 275.

[36] M. Lavanya, M. Jagadeesh, J. Haribabu, R. Karvembu, H.K. Rashmi, P. Uma

Maheswari Devi, A. Varada Reddy, *Inorganica Chim. Acta* **2018**, *469*, 76.

[37] D.M.L. Goodgame, M. Goodgame, F.A. Cotton, *J. Am. Chem. Soc.* **1961**, *83*, 4161.

[38] K.K. Verma, **2011**, *9*, 229.

[39] E.M. Gouge, J.F. Geldard, *Inorg. Chem.* **1978**, *17*, 270.

[40] P. Kavitha, M. Saritha, K. Laxma Reddy, *Spectrochim. Acta Mol. Biomol. Spectrosc.* **2013**, *102*, 159.

[41] O.A.M. Ali, *Spectrochim. Acta Mol. Biomol. Spectrosc.* **2014**, *132*, 52.

[42] S.M. Abdallah, G.G. Mohamed, M.A. Zayed, M.S.A. El-Ela, *Spectrochim. Acta Mol. Biomol. Spectrosc.* **2009**, *73*, 833.

[43] R. Kumar, S. Obrai, A.K. Jassal, M.S. Hundal, J. Mitra, S. Sharma, *J. Coord. Chem.* **2015**, *68*, 2130.

[44] R.C. Chikate, A.R. Belapure, S.B. Padhye, D.X. West, *Polyhedron* **2005**, *24*, 889.

[45] D.R. Eaton, K. Zaw, *Coord. Chem. Rev.* **1971**, *7*, 197.

[46] C.C. Reviews, W. Park, *Chem. Rev.* **1970**, *5*, 143.

[47] B.J. Hathaway, *in Complex Chem, Springer Berlin Heidelberg*, Berlin, Heidelberg, **1984**, pp. 55.

[48] L. Sinha, O. Prasad, V. Narayan, S.R. Shukla, *Mol. Simul.* **2011**, *37*, 153.

[49] M. Tagashira, Y. Ohtake, *Planta Med.* **1998**, *64*, 555.

[50] C.-C. Wu, S. B. Bratton, *Antioxid. Redox Signal.* **2013**, *19*, 546.

[51] B. Halliwell, *Biochem. J.* **2007**, *401*, 1.

[52] M.S. Ahamad, S. Siddiqui, A. Jafri, S. Ahmad, M. Afzal, M. Arshad, *PLoS One* **2014**, *9*, e110003.

CHAPTER-V

Complexation of 2-aminonicotinaldehyde benzoxazinonyl acetic acid hydrazone with Co(II), Ni(II), Cu(II), Zn(II), Cd(II) and Pd(II) ions: Synthesis, structural investigation, DFT and biological evaluations

Hydrazones are azomethines that are characterized by the presence of the triatomic grouping R1R2C=NNH_2 [1]. Hydrozones and their derivatives command an eminent position amongst organic compounds because of their analytical and industrial potential and biological activities including antimicrobial, anticonvulsant, antitubercular, analgesic, antiplatelet, anti-inflammatory, anti-proliferative, antitumoral and anti-parasitic activities [2-6]. They are also used in plasticizers, polymerization initiators, stabilizers for polymers, antioxidants, etc. [7]. According to an insightful biological view, many of the hydrazones are physiologically active and possess application in the treatment of numerous dreaded diseases; they show hypotensive action, spasmolytic activity and activity against leukemia, sarcomas and other malignant neoplasms [8,9]. Further, they act as acaricides, herbicides, antibacterial agents, plant growth regulators, nematocides, rodenticides and insecticides [10,11,9].

Over the years, the role of these compounds in the field of coordination chemistry has emerged in new dimensions because of the fact that they exhibit different ligational behaviour towards various metal ions and novel structural features manifest in the metal complexes [12-16]. Hydrazones have a wide range of applications in synthetic chemistry for the preparation of novel structurally diversified compounds, for the identification and isolation of carbonyl compounds in analytical chemistry and for the detection and determination of several metal ions. They also find applications as indicators and spot test reagents [17-19]. Furthermore, it has been recently proven that hydrazones together with pyridoxal isonicotinoyl hydrazone (PIH) analogues are powerful iron chelators *in vivo* and *in vitro* and can be of value for the treatment of iron overload [20]. Metal complexes of hydrazones have proved to have potential applications as catalysts [21], molecular sensors [22] and luminescent probes [23].

Despite the fact that these compounds have been endowed with different types of biological activity, the detailed chemistry of their action remains obscure. In order to gain more mechanistic aspects, coordination chemists have been showing great interest and effort in the synthesis and structural elucidation of metal complexes obtained from these ligands, and these studies would throw light on these properties in which the ligands are known for. Partaking of the interest in this regard, we have synthesized the metal complexes of 2-aminonicotinaldehyde benzoxazinonyl acetic acid hydrazone and obtained their structural characterization based on physico-chemical data. These studies have been explored by the biological screening of the ligand and its metal complexes and compared with data from theoretical studies (DFT and molecular docking).

5.1 Results and discussion

The ligand, 2-aminonicotinaldehyde benzoxazinonyl acetic acid hydrazone (ABAH) and its metal complexes are stable at room temperature and are non-hygroscopic. They decompose without melting, on heating. The ligand is soluble in methanol, ethanol, dimethyl sulfoxide and dimethylformamide. In the case of complexes, they are soluble in dimethyl sulfoxide and dimethylformamide. The analytical data of the compounds are presented in Table 5.1. It is clear from the table that the theoretical values calculated for the composition shown of each of the complexes are in good agreement with experimental values. The conductance measurements of the metal complexes in DMF solution were made at 10^{-3} mol.dm^{-3} concentrations. All the complexes show only residual molar conductance values (12-19 ohm^{-1} cm^2 mol^{-1}) so they could be considered non-electrolytes in this solvent. This implies that two chloride molecules associated with the complexes are present inside the coordination sphere.

Table 5.1 Analytical, molar conductance and physical parameters for the ligand and its metal complexes

Molecular formula	Elemental analyses: Found (Calculated)				
	C	N	H	M	Molar Cond. (ohm^{-1}cm^{2}mol^{-1})
$[Co(ABAH)_2Cl_2]$	49.35	17.96	3.99	7.68	14
	(49.24)	(17.95)	(3.87)	(7.55)	
$[Ni(ABAH)_2Cl_2]$	49.39	18.01	3.90	7.62	17
	(49.26)	(17.95)	(3.88)	(7.52)	
$[Cu(ABAH)_2Cl_2]$	49.03	17.98	3.99	8.15	13
	(48.95)	(17.84)	(3.85)	(8.09)	
$[Zn(ABAH)Cl_2]$	41.72	15.19	3.36	14.27	19
	(41.63)	(15.17)	(3.28)	(14.16)	
$[Cd(ABAH)Cl_2]$	37.82	13.81	3.05	22.28	15
	(37.78)	(13.77)	(2.97)	(22.10)	
$[Pd(ABAH)Cl_2]$	38.31	13.99	3.10	21.32	12
	(38.23)	(13.93)	(3.01)	(21.17)	
ABAH	59.15	21.65	4.68	---	---
	(59.07)	(21.53)	(4.65)		

5.1.1 Spectroscopy

The important absorption frequencies of ABAH and its metal complexes are given in Table 5.2. Ligand ABAH exhibited medium or small bands at 3400 and 3200 cm^{-1} which is attributed to free N-H stretching [24] and H-bonded ring N-H stretching [25]. A strong band at 1670 cm^{-1} is due to C=O of ring amide [26]. All these vibrational bands remain unshifted in the complexes suggesting non-involvement of these groups in coordination. However, the ligand display a medium intensity bands at 1580 cm^{-1} and 1610 cm^{-1} corresponding to C=O of aliphatic amide [27] and C=N of azomethine; these bands suffers considerable (about 40-50 cm^{-1}) lower shift in the complexes, implying the coordination through oxygen of aliphatic amide and nitrogen of azomethine groups. ABAH which had a band at 3320 cm^{-1} due to $\upsilon(NH_2)$ remains unshifted in the complexes [28]. The bands that appear around 480-500 cm^{-1}, 370-390 cm^{-1} and 280-300 cm^{-1} in the complexes have been assignable to υ(M–O), υ(M–N) and υ(M–Cl) vibrations, respectively [29-31]. From the above discussion, it may be concluded that the ligand act as neutral, bidentate coordinating through oxygen of aliphatic amide and nitrogen of azomethine groups. The UV-Visible spectral data of the complexes and their assignments along with the corresponding ligand field parameters are presented in Table 5.3. The electronic spectra of the ligand exhibit strong bands at 36000 cm^{-1} ($\pi^* \leftarrow \pi$) and 33000 cm^{-1} ($\pi^* \leftarrow$ n) transitions, respectively. Co(II) complex displays three bands around 8500, 17000 and 20000 cm^{-1} which may be assigned to spin-allowed transitions $^4T_{2g}(F) \leftarrow {}^4T_{1g}(F)\,(\vartheta_1)$, $^4A_{2g}(F) \leftarrow {}^4T_{1g}(F)\,(\vartheta_2)$ and $^4T_{1g}(P) \leftarrow {}^4T_{1g}(F)$, respectively, which is characteristic of octahedral geometry [32,33]. Ni(II) complex shows three peaks that appeared at 9280, 14550 and 25600 cm^{-1}. These have been assigned, respectively, to the transitions $^3T_{2g}(F) \leftarrow {}^3A_{2g}(F)$, $^3T_{1g}(F) \leftarrow {}^3A_{2g}(F)$ and $^3T_{1g}(P) \leftarrow {}^3A_{2g}(F)$ of octahedral geometry [34]. The octahedral geometry of Co(II) and Ni(II) complexes are further supported by the ratio of $\vartheta_2 / \vartheta_1$ values (2.04, 1.57). Various ligand field parameters viz., Racah inter-electronic repulsion parameter (B), ligand field splitting energy (10 Dq) and nephelauxetic effect (β) have been calculated. The values of B (870 and 821 cm^{-1}) for Co(II) and Ni(II) complexes are found to be lower than free ion value of 971 cm^{-1}, which is an indication of orbital overlap and delocalization of d orbitals. The nephelauxetic effect of Jorgenson [35] is derived in terms of parameter β which is the ratio of B and B′. It has been argued that the decrease in the value of β is a measure of covalency. β (0.77 and 0.797) values observed for the Co(II) and Ni(II) complexes are less than one suggesting a considerable amount of covalent character of the metal-ligand bands. The Cu(II) complex reveals a peak at 18351

cm^{-1} ($^2B_{2g} \leftarrow {}^2B_{1g}$) and a shoulder on the lower energy side at 13825 cm^{-1} ($^2E_g \leftarrow {}^2B_{1g}$), respectively to indicate distorted octahedral geometry [36]. Zn(II) and Cd(II) complexes show no d-d bands as in the case with a d^{10} system, however, and the peak at 30500 cm^{-1} is due to charge transfer. Tetrahedral geometry has been proposed based on spectroscopic techniques [28]. The Pd(II) complex shows three peaks at 14560 cm^{-1} ($^1A_{2g} \leftarrow {}^1A_{1g}$), 16700 cm^{-1} ($^1B_{1g} \leftarrow {}^1A_{1g}$) and 24870 cm^{-1} ($^1E_g \leftarrow {}^1A_{1g}$), respectively these transitions are characteristic of square-planar geometry [31]. Further, the band at 28500 cm^{-1} is due to charge transfer. Further, $\vartheta_2 / \vartheta_1$ value observed for the complex is 1.15 which also supports the square-planar geometry. The experimental magnetic moment data were obtained at room temperature and the results are listed in Table 2. The magnetic moment values found for Co(II) and Ni(II) complexes are 4.21 and 3.23 B.M, respectively indicate that they are paramagnetic with magnetic moments usually observed for octahedral complexes [37,38]. The magnetic moment value of Cu(II) complex is found as 1.81 B.M. The value is close to spin-only value with a slight allowance for magnetic moment from spin-orbit coupling. The magnetic moment value suggests either square-planar or distorted octahedral geometry around Cu(II) complex [36]. Zn(II), Cd(II) and Pd(II) complexes are diamagnetic in nature.

The EPR spectrum of Cu(II) complex has been obtained in solid state and the geometrical parameters were determined. The results are listed in Table 5.4 and EPR spectrum is shown in Fig. 5.1. The EPR spectrum of Cu(II) complex is anisotropic and shows two peaks, one of intense absorption at high field and the other of less intensity at low field. Following Kneubuhl's method [39], the g values: $g_{\parallel}$ and $g_{\perp}$ have been calculated. From these values, g_{ave} has been calculated using the equation.

$$g_{ave} = 1/3\ (g_{\parallel} + g_{\perp})$$

The g value of Cu(II) complex can be used to derive the ground state [40]. In tetragonally elongated octahedral complexes, $g_{\parallel} > g_{\perp} > 2$ with $d_{x^2-y^2}$ orbital have unpaired electron. In a tetragonally compressed octahedron, on other hand, the unpaired electron lies in d_{z^2} orbital with $g_{\perp} > g_{\parallel} = 2$. The experimental g values for the Cu(II) complex are $g_{\parallel} = 2.19$ and $g_{\perp} = 2.05$ indicating that $g_{\parallel} > g_{\perp} > 2$, suggesting elongated distorted octahedral geometry and that the unpaired electron lies in $d_{x^2-y^2}$ orbital [41].The EPR isotropic parameters $g_{ave} = 2.10$, $A_{ave} = 71$, other parameters follow the order $A_{\parallel} = 158\ cm^{-1} > A_{\perp,} = 28\ cm^{-1}$ under investigation of Cu(II) complex.

The metal-ligand σ-bonding parameter (α^2), in plane π-bonding parameter (β^2) and γ^2 out of plane π-bonding for the complexes have been obtained using the simplified equations [42].

$$\alpha^2 = (A_{\parallel}/0.036) + (g_{\parallel} - 2.0027) + 3/7\,(g_{\perp} - 2.0027) + 0.04$$

$$\beta^2 = (g_{\parallel} - 2.0027)E / (-8\,\alpha^2) \text{ and}$$

$$\gamma^2 = (g_{\parallel} - 2.0027)E / (-2\lambda\alpha^2)$$

Where, $\lambda = -828\ cm^{-1}$ for free copper ion and E is electronic transition energy. A value of $\alpha^2 = 0.5$ indicates 100% covalent nature, while $\alpha^2 = 1$ indicates complete ionic character. The α^2 and γ^2 parameters are similarly a measure of covalency in the in-plane and out-of plane π-bonding, respectively. β^2 or $\gamma^2 = 1$ indicates total ionic character and β^2 and $\gamma^2 = 0.5$ corresponds to a total covalent character. The observed α^2 value for the Cu(II) complex is 0.69 indicative of strong/appreciable in-plane σ-bonding. The β^2 and γ^2 values are 0.61 and 0.77, respectively which suggest appreciable/moderate in-plane and out-of-plane π-bonding. This is further confirmed by orbital reduction parameters $r_{\parallel}$ and $r_{\perp}$, which are calculated using the expressions, $r_{\parallel} = \alpha^2\beta^2$ and $r_{\perp} = \alpha^2\gamma^2$, for in-plane π-bonding $r_{\parallel} < r_{\perp}$ and for out-of-plane π-bonding $r_{\perp} < r_{\parallel}$. The observed $r_{\parallel}$ and $r_{\perp}$ values are 0.53 and 0.66, respectively, revealing that the present complex is in-plane π-bonded type. Further, λ (spin-orbit coupling constant) value for the present complex is ($-322\ cm^{-1}$) which is less than the free ion value ($\lambda_0 = -828\ cm^{-1}$) indicating considerable mixing of ground and excited terms. ^{1}H NMR spectrum of the ligand ABAH show the signals at 8.72, 7.39 ppm corresponding to azomethine and NH_2 protons, respectively, the ^{1}H NMR spectrum as shown in Fig. 5.2

Table 5.2 Infrared absorption frequencies (cm^{-1}) of ligand and its complexes.

Compound	**υ(N–H) (free)**	**υ(N–H) (H-bonded)**	**υ(C=O) (ring amide)**	**υ(C=N)**	**υ(C=O) (ali.amide)**	**υ(M–Cl)**	**υ(M–N)**
Co(II)	3398	3200	1673	1590	1568	300	379
Ni(II)	3403	3205	1670	1580	1541	291	390
Cu(II)	3397	3203	1673	1572	1530	287	384
Zn(II)	3400	3195	1665	1591	1555	280	389
Cd(II)	3401	3208	1675	1588	1560	295	370
Pd(II)	3406	3200	1669	1542	1545	284	385
ABAH	3400	3200	1670	1610	1580	-	-

Table 5.3 Electronic spectral data, ligand field parameters and magnetic data of the complexes

Complexes	Frequencies (cm^{-1})	Assignments	μ_{eff} (B.M.)	$\vartheta_2 / \vartheta_1$	10 DQ (cm^{-1})	B (cm^{-1})	β	Geometry
Co(II)	8500 17000 20000	$^4T_{2g}(F) \leftarrow {}^4T_{1g}(F)$ (υ_1) $^4A_{2g}(F) \leftarrow {}^4T_{1g}(F)$ (υ_2) $^4T_{1g}(P) \leftarrow {}^4T_{1g}(F)$ (υ_3)	4.21	2.04	9300	870	0.77	Octahedral
Ni(II)	9280 14550 25600	$^3T_{2g}(F) \leftarrow {}^3A_{2g}(F)$ (υ_1) $^3T_{1g}(F) \leftarrow {}^3A_{2g}(F)$ (υ_2) $^3T_{1g}(P) \leftarrow {}^3A_{2g}(F)$ (υ_3)	3.23	1.57	9280	821	0.797	Octahedral
Cu(II)	18351 13825	$^2B_{2g} \leftarrow {}^2B_{1g}$ $^2E_g \leftarrow {}^2B_{1g}$	1.81	-	-	-	-	Distorted octahedral
Zn(II)	-	-	Diamagnetic	-	-	-		Tetrahedral
Cd(II)	-	-	Diamagnetic	-	-	-	-	Tetrahedral
Pd(II)	14560 16700 24870	$^1A_{2g} \leftarrow {}^1A_{1g}$ $^1B_{1g} \leftarrow {}^1A_{1g}$ $^1E_g \leftarrow {}^1A_{1g}$	Diamagnetic	1.15	-	-		Square-planar

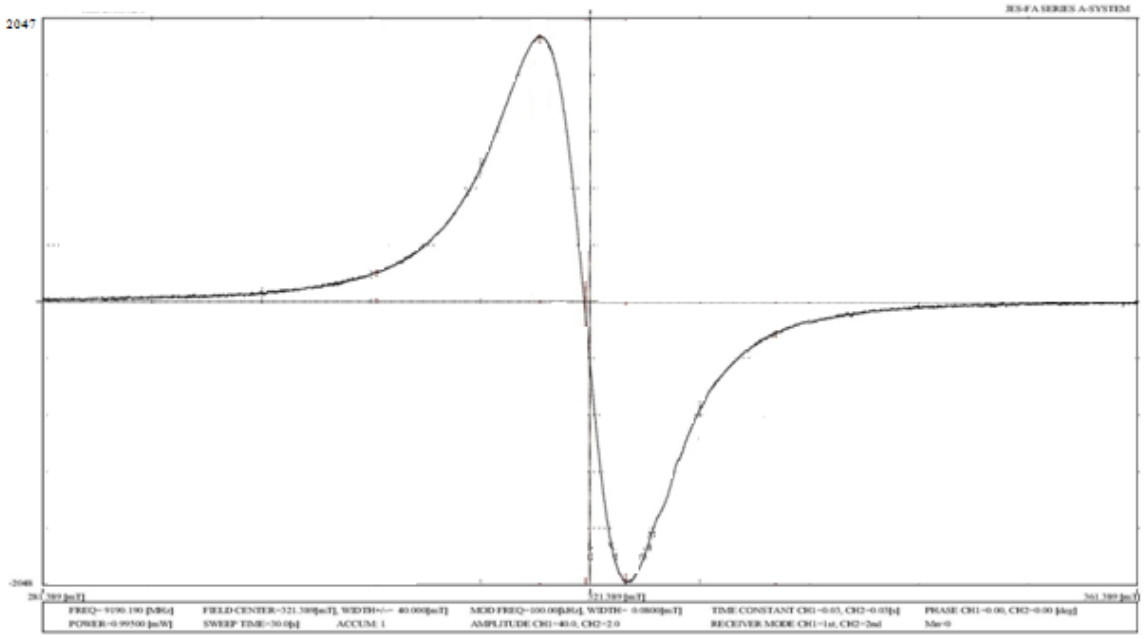

Fig. 5.1 ESR spectrum of Cu(II) complex.

Table 5.4 ESR spectral data of Cu(II) complex

Complex	$g_{\parallel}$	$g_{\perp}$	**|g|**	**G**	$A_{\parallel}\times10^{4}$ **(cm^{-1})**	$A_{\perp}\times10^{4}$ **(cm^{-1})**	$A_{ave}\times10^{4}$ **(cm^{-1})**	$K^2{}_{\parallel}$	$K^2{}_{\perp}$	α^2	β^2	γ^2	**-λ (cm^{-1})**
Cu(II)	2.19	2.05	2.10	4.56	158	28	71	0.53	0.66	0.69	0.61	0.77	322

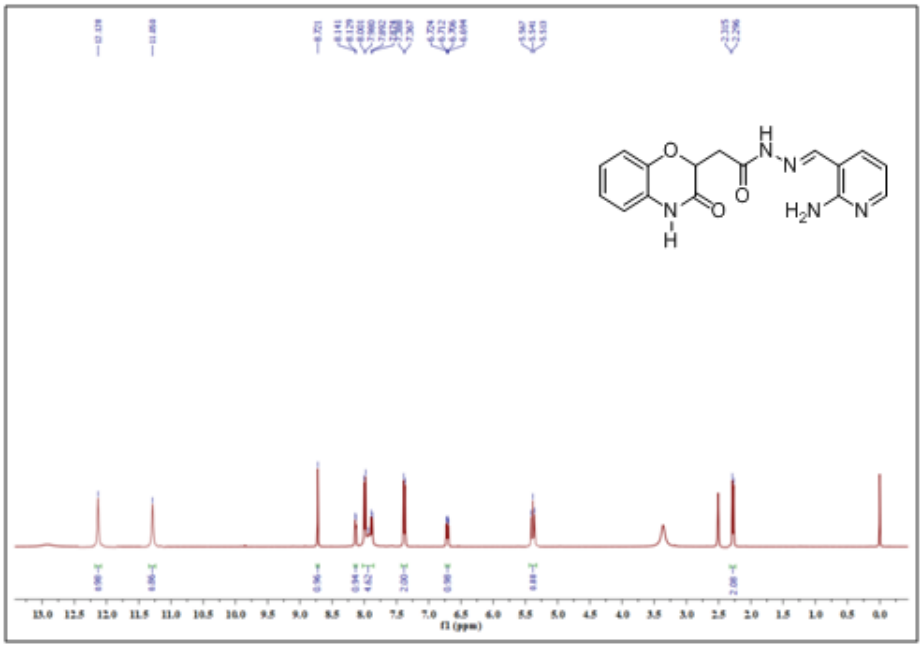

Fig. 5.2 ^{1}H NMR spectrum of ABAH.

5.2 DFT studies

5.2.1 Quantum chemical calculations

DFT geometric optimization and frequency calculations were performed for ligand and its metal complexes analogues with Gaussian o9W software package. DFT/B3LYP functional was used, with 6-311++G(d,p) basis set for the ligand and SDD basis set for its metal complexes analogues. The optimized geometric structure was obtained by solving self-consistent field equations iteratively; on geometry optimization, the global minimum was found to be -1118.48456 Hartree, -3302.38148 Hartree, -3327.45035 Hartree, -3353.84579 Hartree, -2265.016902 Hartree, -2205.65174 Hartree and -2166.385111 Hartree, respectively for the ligand [ABAH], Co(II), Ni(II), Cu(II), Zn(II), Cd(II) and Pd(II) complexes**,** respectively as shown in Fig. 5.3 along with numbering of atoms. The selected structural parameters of metal complexes moiety are listed in Tables 5.5-5.6.

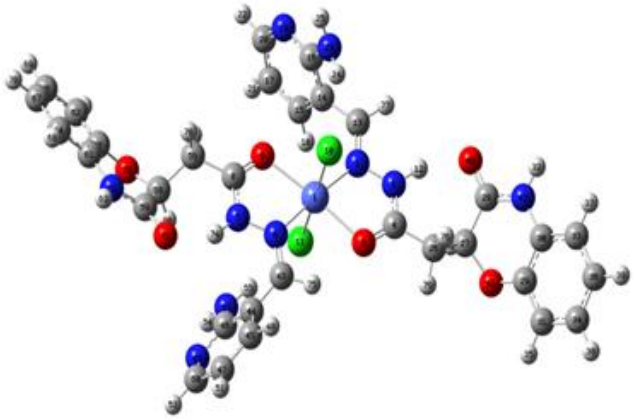

1

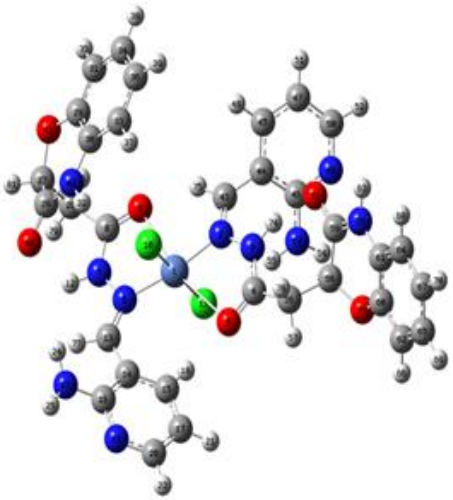

2

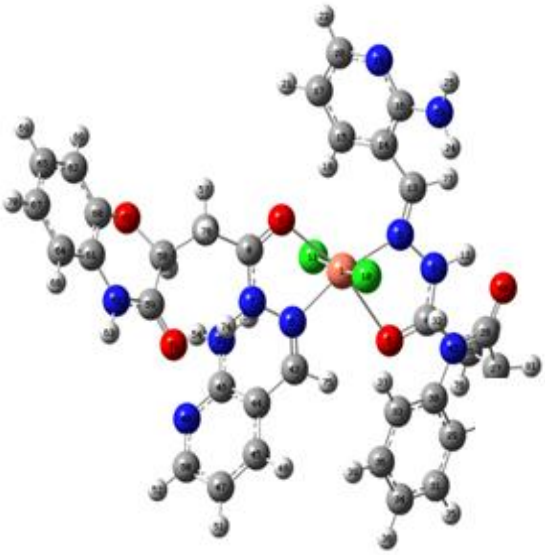

3

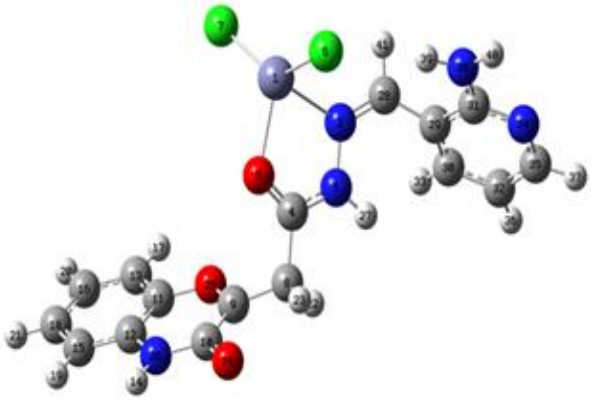

4

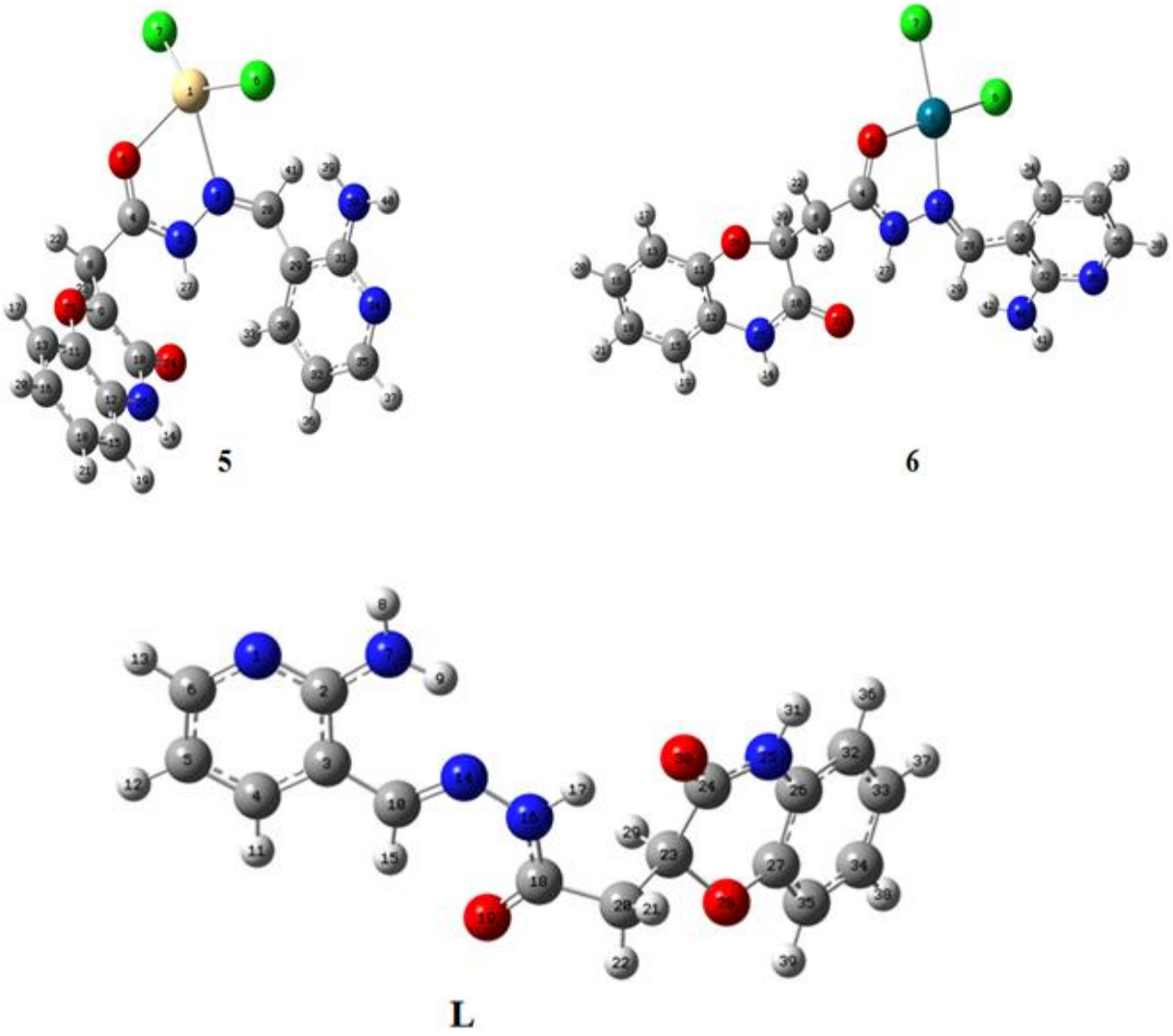

Fig. 5.3 Optimized structures along with atomic numbering of **(1)** Co(II), **(2)** Ni(II), **(3)** Cu(II), **(4)** Zn(II), **(5)** Cd(II), **(6)** Pd(II) complexes and **(L)** ligand ABAH.

Table 5.5 Optimized geometrical parameters of ABAH

Bond length	Value (Å)	Bond angle	Value (°)	Dihedral angle	Value (°)
N1-C2	1.34513	N1-C2-C3	122.23334	N1-C2-C3-C4	-0.03486
C2-C3	1.43237	C2-C3-C4	116.71720	C2-C3-C4-C5	0.01351
C3-C4	1.39894	C3-C4-C5	120.91889	C3-C4-C5-C6	0.01561
C4-C5	1.38845	C4-C5-C6	117.35560	C4-C5-C6-N1	-0.02791
C5-C6	1.39432	C5-C6-N1	124.08309	C5-C6-N1-C2	0.00783
C6-N1	1.33047	C6-N1-C2	118.69186	C6-N1-C2-C3	0.02464
C2-N7	1.35430	N1-C2-N7	116.30118	C6-N1-C2-N7	179.96341
N7-H8	1.00646	C2-N7-H8	117.82053	N1-C2-N7-H8	0.71071
N7-H9	1.01096	C2-N7-H9	119.52392	C3-C2-N7-H9	-0.69436
C4-H11	1.08548	C2-C3-C10	125.08561	N1-C2-C3-C10	179.98475
C5-H12	1.08224	C3-C4-H11	118.68348	C2-C3-C4-H11	179.98606
C6-H13	1.08706	C4-C5-H12	121.74842	C3-C4-C5-H12	-179.99779
C3-C10	1.45429	C5-C6-H13	120.31703	C4-C5-C6-H13	179.96528
C10-H15	1.08563	C3-C10-H15	116.59647	C2-C3-C10-C14	0.06411
C10-N14	1.29288	C3-C10-N14	121.98407	C2-C3-C10-H15	-179.75617
N14-N16	1.37490	C10-N14-N16	121.13199	C10-N14-N16-H17	179.22030
N16-H17	1.01588	N14-N16-C18	130.31933	N14-N16-C18-O19	-3.39324
N16-C18	1.36801	N14-N16-H17	112.47546	N16-C18-C20-H21	50.26262
C18-O19	1.22258	C16-C18-O19	124.95813	N16-C18-C20-H22	167.73142
C18-C20	1.53551	C18-C20-H21	110.83130	C18-C20-C23-H29	-31.85257
C20-H21	1.09252	C18-C20-H22	105.58833	C23-C24-N25-C26	-4.86049
C20-H22	1.08885	C18-C20-C23	114.44761	C24-N25-C26-C27	-15.16143
C20-C23	1.53108	C20-C23-H29	110.27047	N25-C26-C27-O28	0.06165
C23-H29	1.10036	C23-C24-N25	113.90780	C26-C27-O28-C23	34.90445
C23-C24	1.53699	C24-N25-C26	123.52389	C27-O28-C23-C24	-52.71870
C24-N25	1.36039	N25-C26-C27	117.34413	O28-C23-C24-N25	37.47006
N25-C26	1.40851	C26-C27-O28	119.42768	O28-C23-C24-O30	-144.08026
C26-C27	1.39922	C27-O28-C23	114.93083	C23-C24-N25-H31	176.87852
C27-O28	1.37190	C23-C24-O30	123.38382	C26-C32-C33-C34	0.36500
O28-C23	1.43989	C24-N25-H31	116.55310	C32-C33-C34-C35	0.38073
C24-O30	1.22314	C26-C32-C33	119.65950	C33-C34-C35-C27	-0.41863

N25-H31	1.01191	C32-C33-C34	120.16261	C34-C35-C27-C26	-0.28689
C26-C32	1.39328	C33-C34-C35	120.29960	C35-C27-C26-C32	1.03303
C32-C33	1.39307	C34-C35-C27	119.51842	C27-C26-C32-C33	-1.06612
C33-C34	1.39455	C26-C32-H36	119.72221	C27-C26-C32-H36	179.57133
C34-C35	1.39402	C32-C33-H37	119.58977	C26-C32-C33-H37	-179.69785
C35-C27	1.38908	C33-C34-H38	120.12153	C32-C33-C34-H38	179.90616
C32-H36	1.08483	C34-C35-H39	121.65770	C33-C34-C35-H39	179.89845
C33-H37	1.08314	H8-N7-H9	122.64114		
C34-H38	1.08330	H22-C20-H21	108.64436		
C35-H39	1.08309	C18-N16-H17	116.57489		

Table 5.6 Selected bond lengths and bond angles for Co(II), Ni(II), Cu(II), Zn(II), Cd(II) and Pd(II) metal complexes

Co(II)		**Ni(II)**		**Cu(II)**	
Bond length	**Value (Å)**	**Bond length**	**Value (Å)**	**Bond length**	**Value (Å)**
Co1-N2	1.96700	Ni1-N2	1.90613	Cu1-N2	2.03563
N2-N3	1.40783	N2-N3	1.39281	N2-N3	1.40420
N3-C4	1.36457	N3-C4	1.38010	N3-C4	1.37912
C4-O5	1.26431	C4-O5	1.25075	C4-O5	1.25587
O5-Co1	2.18181	O5-Ni1	2.75488	O5-Cu1	2.46677
Co1-N6	1.95279	Ni1-N6	1.91606	Cu1-N6	2.01839
N6-N7	1.39666	N6-N7	1.41067	N6-N7	1.39201
N7-C8	1.37063	N7-C8	1.38283	N7-C8	1.37647
C8-O9	1.26120	C8-O9	1.25132	C8-O9	1.25655
O9-Co1	2.19545	O9-Ni1	2.66682	O9-Cu1	2.39896
Co1-Cll0	2.41605	Ni1-Cll0	2.29613	Cu1-Cll0	2.40301
Co1-Cll1	2.42988	Ni1-Cll1	2.29998	Cu1-Cll1	2.40223
Bond angle		Bond angle	Value (°)	Bond angle	Value (°)
Co1-N2-N3	111.67601	Ni1-N2-N3	123.20445	Cu1-N2-N3	113.66698
N2-N3-C4	118.08106	N2-N3-C4	121.80949	N2-N3-C4	122.19491
N3-C4-O5	121.13196	N3-C4-O5	123.65760	N3-C4-O5	122.46485
C4-O5- Co1	108.46798	C4-O5- Ni1	98.86249	C4-O5-Cu1	104.67763
O5- Co1-N2	80.50202	O5- Ni1-N2	71.59047	O5-Cu1-N2	76.41801
Co1-N6-N7	114.07006	Ni1-N6-N7	115.34109	Cu1-N6-N7	116.53631
N6-N7-C8	116.70499	N6-N7-C8	125.32655	N6-N7-C8	118.71720
N7-C8-O9	120.87079	N7-C8-O9	124.34791	N7-C8-O9	122.20583

C8-O9- Co1	109.00847	C8-O9- Ni1	97.49504	C8-O9-Cu1	106.99758
O9- Co1-N6	79.20737	O9-Ni1-N6	76.94309	O9-Cu1-N6	75.47416
N2- Co1-Cl10	85.90685	N2-Ni1-Cl10	91.56020	N2-Cu1-Cl10	87.74648
N6-Co1-Cl11	86.67042	N6-Ni1-Cl11	91.84646	N6-Cu1-Cl11	86.91021
Cl10- Co1-Cl11	177.74106	Cl10- Ni1-Cl11	174.30404	Cl10-Cu1-Cl11	173.36792
Zn(II)		**Cd(II)**		**Pd(II)**	
Bond length	**Value (Å)**	**Bond length**	**Value (Å)**	**Bond length**	**Value (Å)**
Zn1-N2	2.19616	Cd1-N2	2.41874	Pd1-N2	2.11364
N2-N3	1.39748	N2-N3	1.39920	N2-N3	1.42282
N3-C4	1.37808	N3-C4	1.36964	N3-C4	1.35440
C4-O5	1.26353	C4-O5	1.26730	C4-O5	1.27943
O5-Zn1	2.12242	O5-Cd1	2.35427	O5-Pd1	2.11035
Zn1-Cl6	2.26930	Cd1-Cl6	2.47211	Pd1-Cl6	2.34662
Zn1-Cl7	2.20493	Cd1-Cl7	2.40437	Pd1-Cl7	2.32503
Bond angle	Value (°)	Bond angle	Value (°)	Bond angle	Value (°)
Zn1-N2-N3	110.73586	Cd1-N2-N3	113.73211	Pd1-N2-N3	107.08793
N2-N3-C4	116.55300	N2-N3-C4	116.84399	N2-N3-C4	118.42460
N3-C4-O5	120.43418	N3-C4-O5	122.70827	N3-C4-O5	120.75528
C4-O5-Zn1	116.36444	C4-O5- Cd1	117.88031	C4-O5- Pd1	111.62828
O5- Zn1-N2	75.61134	O5-Cd1-N2	68.70678	O5- Pd1-N2	79.17102
O5- Zn1-Cl7	111.32731	O5-Cd1-Cl7	107.12498	O5-Pd1-Cl7	91.77773
N2- Zn1-Cl6	92.23720	N2-Cd1-Cl6	88.04614	N2- Pd1-Cl6	98.28401
Cl6-Zn1-Cl7	133.48557	Cl6-Cd1-Cl7	137.40857	Cl6- Pd1-Cl7	90.50886

5.2.2 Molecular Electrostatic Surface Potential

The molecular electrostatic surface potential **(**MESP) provides the electrons and nuclei of a molecule made in the surrounding region are well built as a guide to the elucidation and forecast of molecular reactive behavior. It is through this potential V(r) is given by

$$V(r) = \sum_A \frac{Z_A}{|R_A - r|} - \int \frac{\rho(r')}{|r' - r|} dr'$$

Where ρ(r') is the electronic density function of the molecule and Z_A is the charge on nucleus A, located at R_A; for studying both nucleophilic and electrophilic character V(r) is a useful tool which can be determined either computationally or experimentally by diffraction methods [43-45]. The different values of electro static potential are characterized by different

colors; blue color represents positive electrostatic potential, green represents the region of zero potential, yellow represents slight electron negative and red represents the maximum negative regions of electrostatic potential. The potential increases from red to blue in the order: red < orange < yellow < green < blue [46,47]. The various regions on the surface of the molecule which denotes electrophilic and nucleophilic regions are shown by red and blue colors, respectively. Any region there which has no electrostatic potential would be represented by green color. The MESP of the compounds are represented in Fig. 5.4.

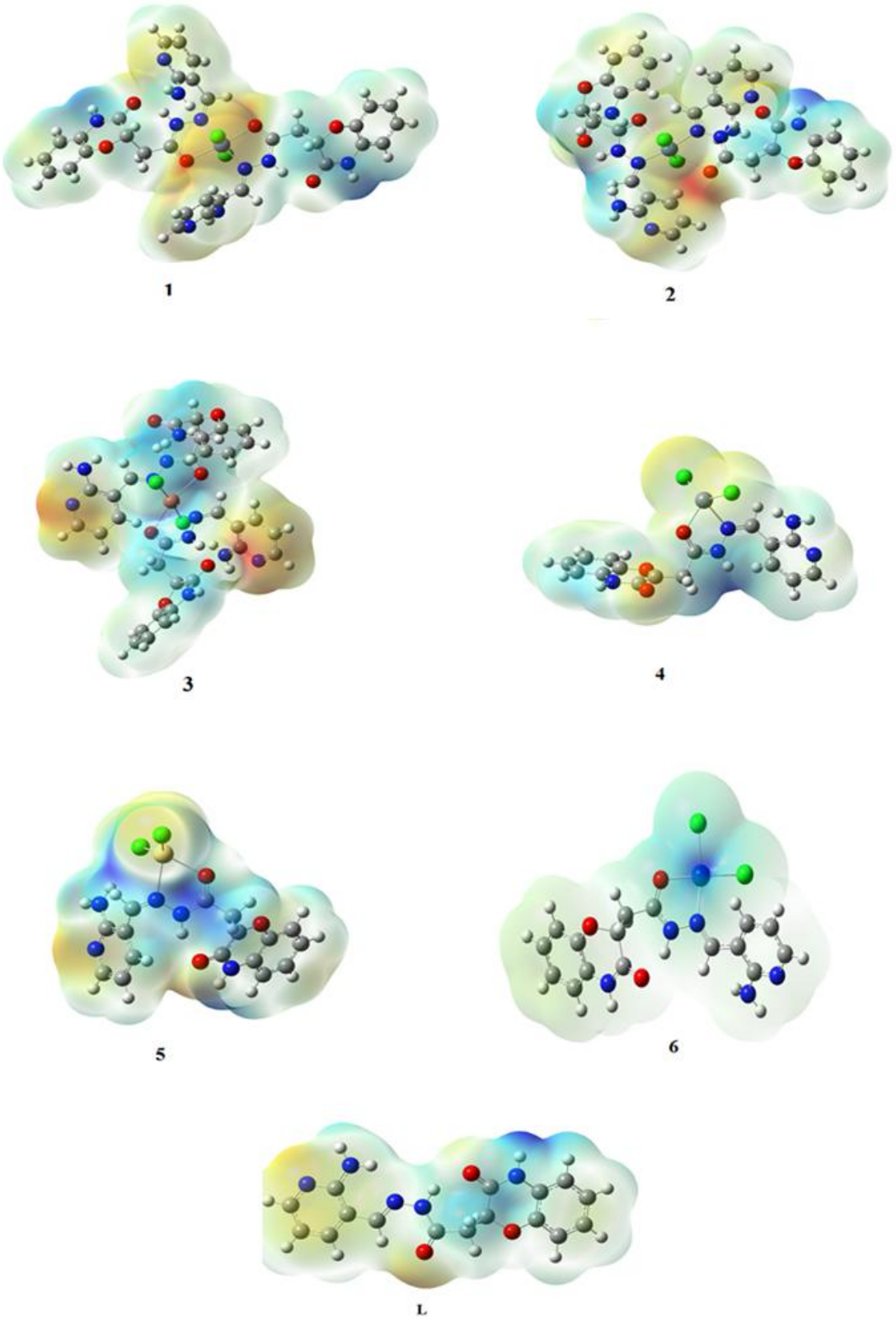

Fig. 5.4 Total electron density mapped with electrostatic potential surface of **(1)** Co(II), **(2)** Ni(II), **(3)** Cu(II), **(4)** Zn(II), **(5)** Cd(II), **(6)** Pd(II) complexes and **(L)** ligand ABAH.

5.2.3 Non-linear optical (NLO) behaviour

As the electromagnetic radiation passes through a non-linear optical (NLO) material, it interacts with the material. As a result, it experiences a change in frequency, amplitude, phase or other propagation characteristics giving rise to new fields [48]. This property of NLO materials has been extensively exploited in the fields of telecommunications, signal processing and optical inter-connections. They play a key role in providing important functions such as frequency shifting, optical logic, optical switching and optical memory [49-52]. The value of first order hyperpolarizability is a measure of NLO behaviour. Hence, DFT has been used extensively to investigate organic NLO materials [53-57]. The NLO parameters such as total molecular dipole moment (μ_t) and its components; total molecular polarizability (α_t) and its components; anisotropy of polarizability ($\Delta\alpha$); and first order static hyperpolarizability (β_t) were calculated using DFT approach and the results are available in Table 5.7. It is usual practice to determine the NLO behaviour of given compounds by comparing its total molecular dipole moment and mean first order hyperpolarizability with the corresponding values of urea, which are 1.3732 Debye and 0.3728 x 10^{-30} cm^5/esu, respectively. For ABAH, the value of μ_t is 4.2890 Debye and that of β_t is 6.094 × 10^{-30} cm^5/e.s.u. Thus μ_t and β_t for ABAH are 3.1 and 16 times that of corresponding values for Urea. Similarly, for metal complexes, the values of μ_t and β_t are 4.8978 Debye and 10.551 × 10^{-30} cm^5/e.s.u [for Co(II)], 6.5745 Debye and 8.679 × 10^{-30} cm^5/e.s.u [for Ni(II)], 4.1649 Debye and 9.510 × 10^{-30} cm^5/e.s.u [for Cu(II)], 14.7174 Debye and 7.596 × 10^{-30} cm^5/e.s.u [for Zn(II)], 16.4889 Debye and 9.051 × 10^{-30} cm^5/e.s.u [for Cd(II)] and 18.5557 Debye and 10.090 × 10^{-30} cm^5/e.s.u [for Pd(II)], respectively. From the above results, it is observed that μ_t and β_t values for the complexes are greater than that for free ligand; hence all the compounds exhibit NLO properties. The values of hyperpolarizability are a measure of NLO activity of the molecular system. It is associated with intra-molecular charge transfer that is attributed to electron cloud movement through π - conjugated framework of electrons [58]. Hence the ligand and its metal complexes are a strong candidate for the development of new NLO materials based on the values of the dipole moment and first order hyperpolarizability.

Table 5.7 The values of dipole moment μ_t (in Debye); polarizability α_t and first order hyperpolarizability β_t (in 10^{-30}cm^5/e.s.u) of ABAH and its metal complexes

Type of component	ABAH	CO(II)	Ni(II)	Cu(II)	Zn(II)	Cd(II)	Pd(II)
β_{xxx}	-143.7662	-381.2124	-294.7664	-340.4875	825.5725	-326.5225	-322.4513
β_{xxy}	-518.2514	-54.7218	76.0487	-44.7029	306.2312	239.2630	-617.3580
β_{xyy}	-144.6968	-631.2433	-446.8517	-533.6427	-112.6181	156.7480	-211.160
β_{yyy}	-23.0129	-702.0125	-833.8649	-755.1356	-378.9437	-832.8282	1301.425
β_{xxz}	93.9004	72.9021	54.6869	88.8929	394.0927	-485.1925	-144.9417
β_{xyz}	-86.8808	181.2015	194.0196	199.3795	-99.0628	-27.4418	-130.1204
β_{yyz}	33.0995	-25.6157	41.1576	-16.5179	-195.9680	-186.3256	-428.6618
β_{xzz}	21.0968	21.6218	28.9043	54.5423	266.6312	10.1696	-69.8450
β_{yzz}	-39.4006	71.7215	51.4309	66.1717	-153.8917	44.7092	-29.2302
β_{zzz}	171.2565	-10.2128	-45.5366	-29.3968	-120.2824	206.6175	-168.3470
β_t	6.094×10^{-30} cm^5/e.s.u	10.551×10^{-30} cm^5/e.s.u	8.679×10^{-30} cm^5/e.s.u	9.510×10^{-30} cm^5/e.s.u	7.596×10^{-30} cm^5/e.s.u	9.051×10^{-30} cm^5/e.s.u	10.090×10^{-30} cm^5/e.s.u
μ_x	4.2659	3.1047	4.6764	2.9897	-2.5198	15.8442	-14.1573
μ_y	-0.3761	0.9535	-3.0431	2.5898	14.2351	4.1345	11.8918
μz	-0.2366	-3.6661	-3.4777	1.3043	-2.7618	-1.9369	-1.5709
μ_t	4.2890 Debye	4.8978 Debye	6.5745 Debye	4.1649 Debye	14.7174 Debye	16.4889 Debye	18.5557 Debye
α_{xx}	388.3676	543.009	532.5798	531.0093	358.7237	323.6439	422.1275
α_{xy}	10.5918	46.3210	22.6376	35.3227	-55.5303	11.8591	9.6547
α_{yy}	232.4213	608.2541	609.6395	611.3923	220.3510	315.4715	326.5448
α_{xz}	0.7363	-35.1102	-19.5505	-15.0936	30.1800	28.7107	-17.5980
α_{yz}	-9.4129	-24.2251	-9.5223	-8.3043	-7.3043	-1.7895	21.2325
α_{zz}	158.4662	351.9541	344.2411	345.0263	231.2670	205.644	160.1821
α_t	259.7491	505.0814	495.4862	495.8091	270.1100	281.5833	302.9466
$<\Delta\alpha>$	203.2692	231.4479	236.4726	236.6458	133.2140	114.1344	229.5906

5.2.4 Frontier molecular orbitals

The Frontier orbitals HOMO and LUMO are the important factors in quantum chemistry as these determine the way a molecule interacts with other species. The frontier orbital gap is used as an indicator for chemical reactivity and chemical stability of the molecule. Generally, a molecule with a small frontier orbital gap is readily polarizable and normally exhibits high chemical reactivity and low kinetic stability [59-61]. The results are presented in Table 5.8 and Fig. 5.5. From the observed quantum chemical calculations, frontier orbitals energy gap was found in the order of ABAH > Zn(II) > Ni(II) > Co(II) > Cd(II) > Pd(II) > Cu(II). A molecule with a lower frontier orbital gap is generally associated with chemical reactivity and low kinetic stability. The frontier molecular orbital gap of metal complexes are small compared to ligand; hence metal complexes are more polarizable than ligand. It is seen from Table 5.8, that the chemical potential of the compounds is negative, which signifies that the compounds are stable.

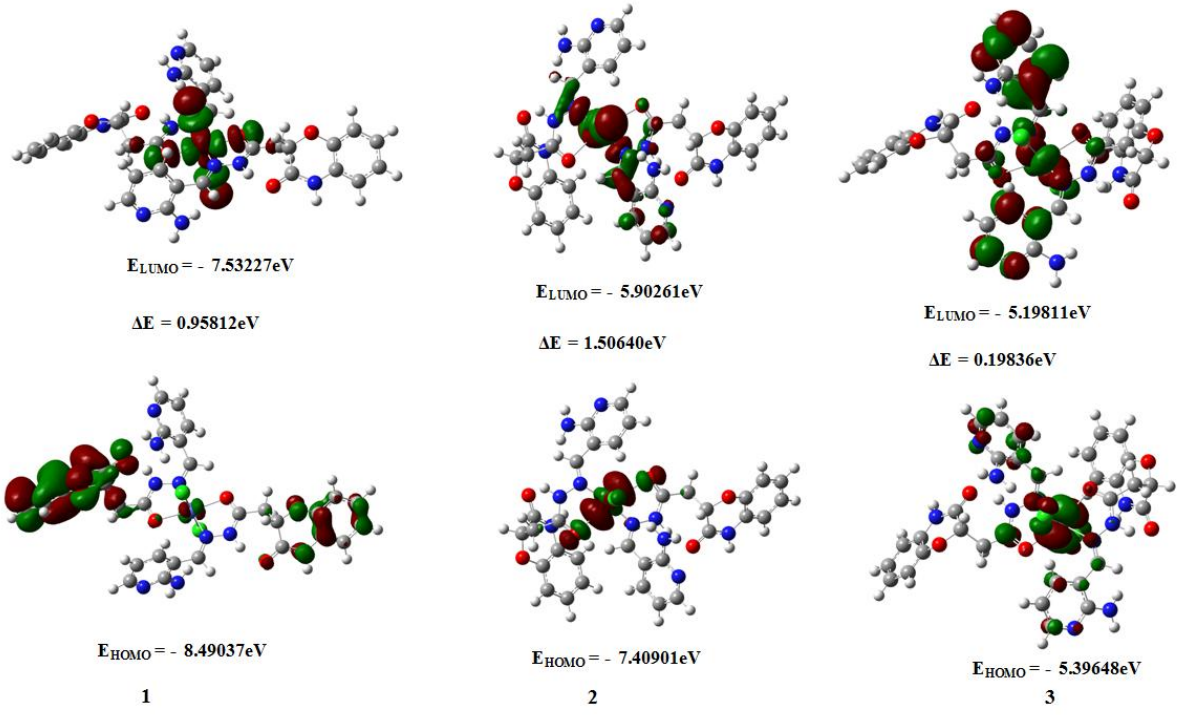

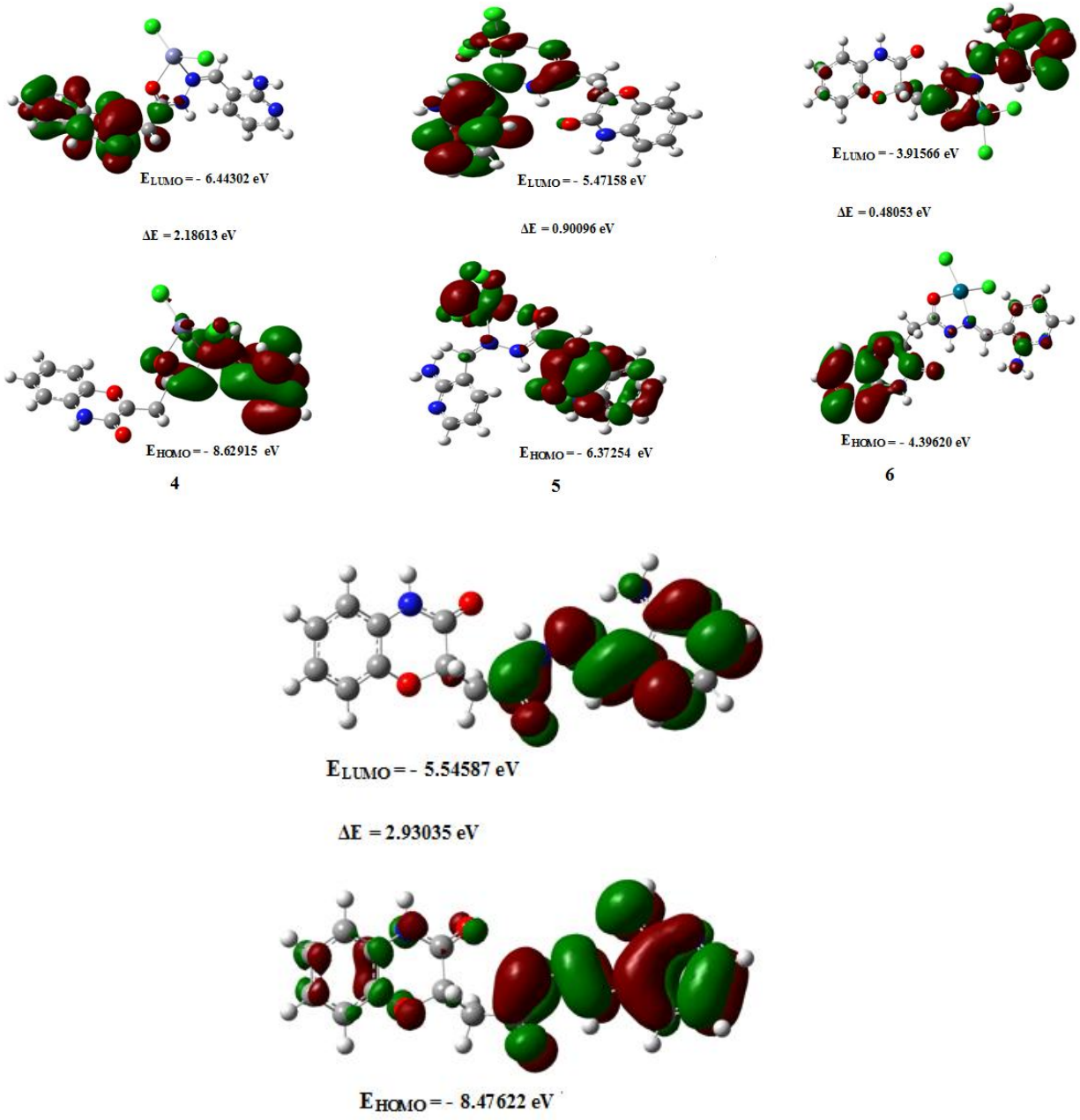

Fig. 5.5 Frontier molecular orbital's of **(1)** Co(II), **(2)** Ni(II), **(3)** Cu(II), **(4)** Zn(II), **(5)** Cd(II), **(6)** Pd(II) complexes and **(7)** ligand ABAH.

Table 5.8 Frontier molecular orbital parameters of ligand and its metal complexes, values are expressed in (**eV**)

Frontier molecular Orbital parameter	**ABAH**	**Co(II)**	**Ni(II)**	**Cu(II)**	**Zn(II)**	**Cd(II)**	**Pd(II)**
HOMO energy	-8.47622	-8.49037	-7.40901	-5.39648	-8.62915	-6.37254	-4.39620
LUMO energy	-5.54587	-7.53227	-5.90261	-5.19811	-6.44302	-5.47158	-3.91566
Frontier molecular orbital energy gap	2.93035	0.95812	1.50640	0.19836	2.18613	0.90096	0.48053
Ionization energy (I)	8.47622	8.49037	7.40901	5.39648	8.62915	6.37254	4.39620
Electron affinity (A)	5.54587	7.53227	5.90261	5.19811	6.44302	5.47158	3.91566
Global hardness (η)	1.46517	0.47906	0.75320	0.09918	1.09306	0.45048	0.24026
Chemical potential (μ)	-7.01101	-8.01132	-6.65581	-5.29729	-7.53660	-5.92206	-4.15593
Global lectrophilicity power (ω)	16.77419	66.98664	29.40772	141.400	25.98036	38.92602	35.94261

5.3 Biological evaluations

5.3.1 Antimicrobial activity

The synthesized compounds have been assessed for their *in vitro* antimicrobial activity against both gram-negative (G^-) bacteria [*Pseudomonas aeruginosa, Klebsiella pneumoniae* and *Escherichia coli*] and gram-positive (G^+) bacteria [*Bacillus subtilis, Staphylococcus aureus* and *Staphylococcus epidermidis*] and different fungal strains [*Aspergillus niger, Aspergillus flavus, Curvularia lunata, Rhizoctonia bataticola* and *Candida albicans*] via the disc approach through the use of Streptomycin and Nystatin as reference controls. The minimum inhibitory concentrations (MICs) for all the tested compounds have been suggested in μg/mL, and the outcomes are illustrated in Table 5.9 and Table 5.10. It's far obvious from the tables that the synthesized compounds exerted significant *in vitro* antimicrobial activity against almost all the tested bacterial and fungal strains. Among the tested compounds, Co(II) complex observed to be efficient and exhibited equipotent inhibitory efficacy and broader antibacterial activity than that of the reference drug. The Co(II) complex showed excellent activity than the standard drug Streptomycin against *E. coli* with MIC values of 2.68 μg/mL, and most potent activity against gram-positive and gram-negative bacterial strains such as *S. aureus, B. subtilis, S. epidermidis, K.*

pneumoniae and *P. aeruginosa* with MIC values of 3.15, 7.46, 3.88, 5.62 and 8.57 µg/mL, respectively compared to standard drug. Cd(II) complex exhibited a broad spectrum of activity against *S. aureus* (MIC = 3.64 µg/mL), *B. subtilis* (MIC = 9.37 µg/mL), *S. epidermidis* (MIC = 4.70 µg/mL), *K. pneumoniae* (MIC = 6.55 µg/mL), *E. coli* (MIC = 3.18 µg/mL), and *P. aeruginosa* (MIC = 14.06 µg/mL), respectively. Zn(II) complex against *S. aureus* (MIC = 6.28 µg/mL) and *E. coli* (MIC = 5.16 µg/mL), Pd(II) complex against *K. pneumoniae* (MIC = 9.58 µg/mL) showed modest activity, while the rest of the compounds [ABAH, Ni(II) and Cu(II)] exhibited marginal activity against the microorganisms tested. The antifungal activity of the complexes, Co(II) complex against *A. flavus* and Zn(II) complex against *C. albicans* was potent with MIC values of 4.67 and 10.99 µg/mL, respectively compared to positive control Nystatin. In addition, Co(II) complex reported good activity against *A. niger* (MIC = 9.12 µg/mL), *C. lunata* (MIC = 8.61 µg/mL) and *C. albicans* (MIC = 13.85 µg/mL), while Zn(II) complex also showed good activity against *A. niger* (MIC = 9.59 µg/mL) and *A. flavus* (MIC = 5.73 µg/mL), respectively. The remaining compounds exhibited poor activity against the tested fungi strains.

From the results it is apparent that the metal complexes exert more antimicrobial activity than the ligand, indicating that the metals are actually in action. It is assumed that the role of a ligand associated with the metal ion in a complex is to make the metal ion fat soluble. It may be expected that the capability of a ligand that forms negative ion upon deprotonation in making the metal ion fat soluble is more owing to the fact that such a ligand would perfectly neutralize the positive charge on metal ion and make the complex neutral as a whole. Once the complex makes its way across the cell membrane, depending on the environment there, it undergoes dissociation releasing the metal ion and enabling it to exert its toxic effect.

Table 5.9 MIC of the synthesized compounds against the growth of bacteria (µg/mL)

Compound	*S. aureus*	*B. subtilis*	*S. epidermidis*	*E. coli*	*K. pneumoniae*	*P. aeruginosa*
Co(II)	3.15	7.46	3.88	2.68	5.62	8.57
Ni(II)	>100	14.83	49.07	18.57	>100	56.38
Cu(II)	45.66	>100	71.06	45.44	56.83	>100
Zn(II)	6.28	11.35	9.34	5.16	18.39	11.26
Cd(II)	3.64	9.37	4.70	3.18	6.55	14.06
Pd(II)	>100	>100	50	24.40	9.58	42.01
ABAH	>100	50	68.57	>100	78.66	88.24
Streptomycin	**2.14**	**5.33**	**2.65**	**2.71**	**4.66**	**6.49**

Table 5.10 MIC of the synthesized compounds against the growth of bacteria (µg/mL)

Compound	*A. niger*	*A. flavus*	*C. lunata*	*R. bataticola*	*C. albicans*
Co(II)	9.12	4.67	8.61	>100	13.85
Ni(II)	>100	15.63	>100	50	61.53
Cu(II)	21.86	45.99	>100	>100	36.22
Zn(II)	9.59	5.73	22.56	50	10.99
Cd(II)	45.53	11.30	50	50	16.15
Pd(II)	50	17.96	>100	45.87	75.63
ABAH	50	71.12	>100	83.62	80.94
Nystatin	5.85	3.62	5.13	4.73	8.63

5.3.2 Antioxidant activity

The antioxidant activity of the new compounds was investigated for their antioxidant ability and this was carried out using DPPH (1,1-diphenyl-2-picrylhydrazyl) method where ascorbic acid was chosen as a reference drug. The ligand and its metal complexes were performed in triplicate and the standard deviation was calculated. The activity results are expressed in terms of IC_{50}. IC_{50} (µM) values were given in Table 5.11 and Fig. 5.6. From the evaluation of antioxidant activity, Ni(II) complex exhibited potent activity as observed in IC_{50} value of 18.35 ± 0.28 µM; this IC_{50} value of Ni(II) complex is close to reference ascorbic acid IC_{50}. Cu(II) complex showed good activity at an IC_{50} value of 20.17 ± 1.28 µM, while moderate activity was observed for other complexes with IC_{50} values of 28.09 ± 0.55

µM [Co(II)], 39.40 ± 1.13 µM [Zn(II)], 35.16 ± 1.26 µM [Cd(II)], 50.83 ± 0.27 µM [Pd(II)] and 50.91 ± 0.18 µM [ABAH], respectively. The above experimental results investigated that the order of activity of the compounds was: Ni(II) > Cu(II) > Co(II) > Cd(II) > Zn(II) > Pd(II) > ABAH.

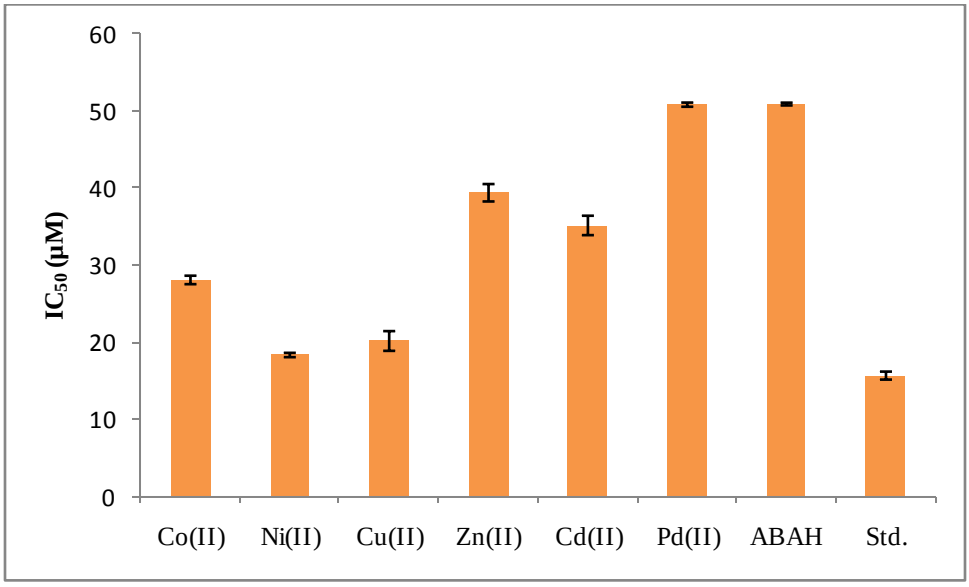

Fig. 5.6 Scavenging activity of the ligand and its complexes

Table 5.11 DPPH scavenging capacities (IC_{50}, μM) of ligand and its metal complexes

Compounds	**IC_{50} (µM)**
Co(II)	28.09 ± 0.55
Ni(II)	**18.35 ± 0.28**
Cu(II)	20.17 ± 1.28
Zn(II)	39.40 ± 1.13
Cd(II)	35.16 ± 1.26
Pd(II)	50.83 ± 0.27
ABAH	50.91 ± 0.18
Ascorbic acid	15.68 ± 0.52

5.3.3 Cytotoxic activity

The cytotoxicity of the compounds was carried out against different human cancer cell lines MCF-7 (breast), HeLa (cervical), A549 (lung), HepG-2 (liver), IMR-32 (neuroblastoma) and HEK293 (embryonic kidney) using MTT-microcultured tetrazolium assay. The relationship between surviving fraction and drug concentration was plotted to obtain the survival curve of MCF-7, HeLa, A549, HepG2 and IMR-32 are shown in Fig 5.7. The IC_{50} values for compounds are represented in Table 5.12. From the cytotoxic activity results, Ni(II) complex exhibited equal level of anticancer activity compared to cisplatin with IC_{50} values of 8.60 ± 0.15 µM (IMR-32), 4.17 ± 0.13 µM (HeLa), 4.92 ± 0.21 µM (MCF-7), 7.72 ± 0.24 µM (A549), 3.01 ± 1.13 µM (HepG-2), respectively. The Cu(II) complex showed a broad spectrum of activity at IC_{50} values of 10.46 ± 1.01 µM, 5.70 ± 1.12 µM, 6.44 ± 0.41 µM, 12.35 ± 1.17 µM and 3.96 ± 0.61 µM against IMR-32, HeLa, MCF-7, A549 and HepG-2, respectively. Zn(II) complex against IMR-32 (IC_{50} = 17.55 ± 0.22 µM), Co(II) complex against MCF-7 (IC_{50} = 7.62 ± 0.19 µM), and HepG-2 (IC_{50} = 5.14 ± 1.06 µM) exhibited high activity. The remaining compounds showed moderate to poor activity with IC_{50} values ranging from 20.56 ± 0.43 µM to 78.69 ± 0.83 µM. The potent complexes Ni(II) and Cu(II) are also tested anticancer activity against normal cell line HEK293 with IC_{50} values of 91.84 ± 0.26 µM and 85.67 ± 0.13 µM, respectively indicate that the potent complexes are nontoxic.

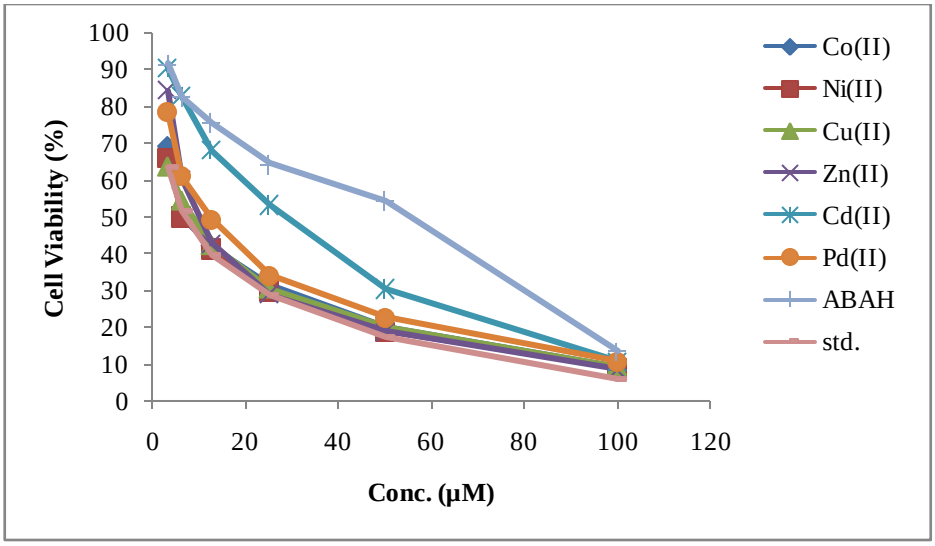
Cell Viability (%)
Conc. (µM)
Co(II)
Ni(II)
Cu(II)
Zn(II)
Cd(II)
Pd(II)
ABAH
std.

(A)

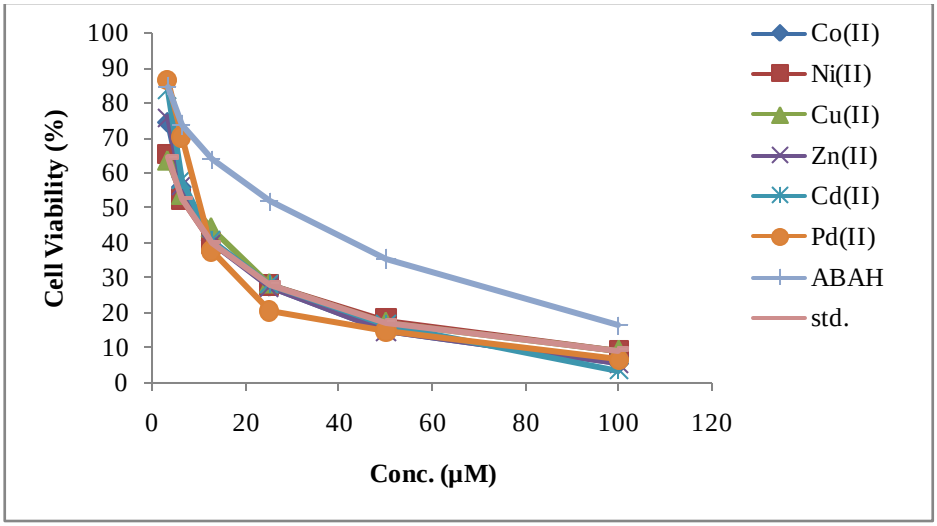
Cell Viability (%)
Conc. (µM)
Co(II)
Ni(II)
Cu(II)
Zn(II)
Cd(II)
Pd(II)
ABAH
std.

(B)

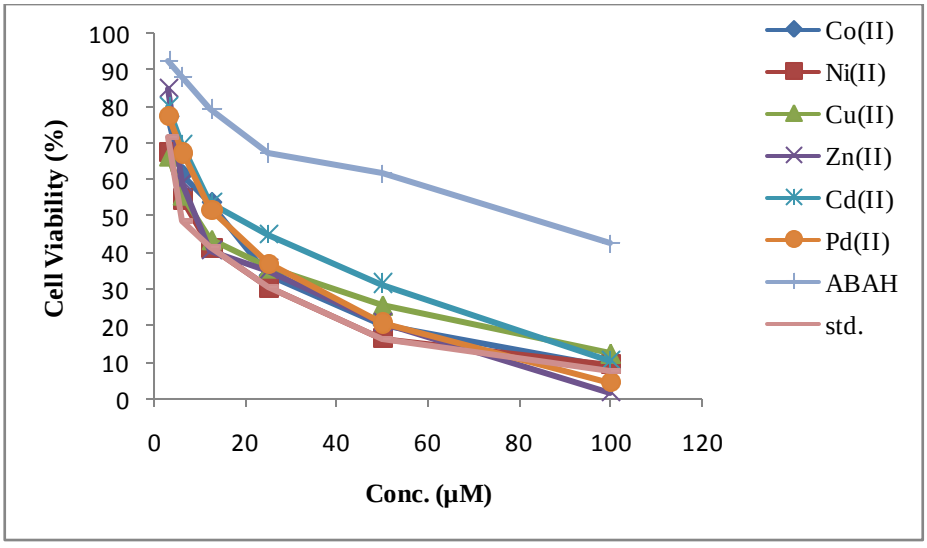
Cell Viability (%)
Conc. (µM)
Co(II)
Ni(II)
Cu(II)
Zn(II)
Cd(II)
Pd(II)
ABAH
std.

(C)

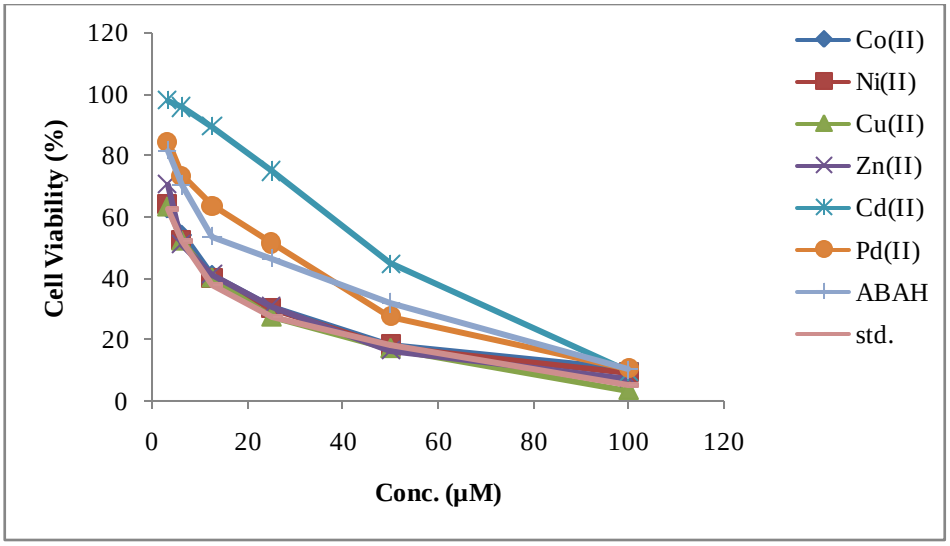

(D)

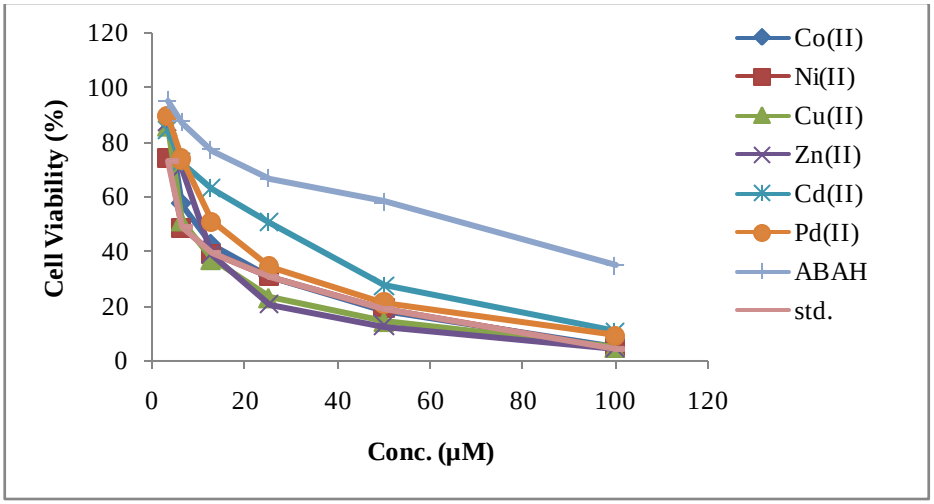

(E)

Fig. 5.7 Effect of the complexes against **(A)** MCF-7, **(B)** HeLa, **(C)** A549, **(D)** HepG-2 and **(E)** IMR-32 cancer cells

Table 5.12 Anticancer activity of the compounds and standard cisplatin against human cancer cell lines

Compound	IMR-32	HeLa	MCF-7	A549	HepG-2	HEK 293
Co(II)	19.28 ± 0.25	10.35 ± 0.44	7.62 ± 0.19	21.05 ± 1.11	5.14 ± 1.06	ND
Ni(II)	**8.60 ± 0.15**	**4.17 ± 0.13**	**4.92 ± 0.21**	**7.72 ± 0.24**	**3.01 ± 1.13**	**91.84 ± 0.26**
Cu(II)	10.46 ± 1.01	5.70 ± 1.12	6.44 ± 0.41	12.35 ± 1.17	3.96 ± 0.61	**85.67 ± 0.13**
Zn(II)	17.55 ± 0.22	10.88 ± 0.23	17.84 ± 0.24	18.65 ± 0.33	7.58 ± 0.25	ND
Cd(II)	35.02 ± 0.28	15.46 ± 0.15	40.41 ± 1.26	30.16 ± 1.03	52.75 ± 0.81	ND
Pd(II)	28.37 ± 0.38	17.23 ± 1.04	20.56 ± 0.43	22.93 ± 0.52	35.70 ± 0.12	ND
ABAH	68.13 ± 1.04	39.53 ± 0.32	51.28 ± 0.15	78.69 ± 0.83	31.18 ± 1.24	ND
Cisplatin	8.14 ± 0.31	3.58 ± 0.12	3.26 ± 1.03	7.11 ± 0.25	2.29 ± 0.14	ND

Values are expressed in mean ± SD of three replicates. ND stands for not determine

5.3.4 Molecular docking

The *in silico* molecular docking analysis of the ligand ABAH and its metal complexes against human epidermal growth receptor (HER2) and epidermal growth factor receptor (EGFR) was carried out to verify the relation between *in vitro* antiproliferative activity results and binding affinities of the inhibitors using AutoDock program. HER2 contained the trans membrane tyrosine kinase receptor. It can regulate normal cell growth and is useful in its development also. It can dimerize without any ligand. The receptor dimerization leads to autophosphorylation and results in cell-cycle progression *via* delocalization and degradation of cell-cycle inhibitor p27Kip1, angiogenesis, cell differentiation, invasion, proliferation, etc. HER2 is also associated with breast, ovarian and gastric cancers. Hence, without dimerization HER2 becomes inactive [62]. EGFR contains an intracellular tyrosine kinase domain and extracellular ligand binding domain. They are stabilized by disulphide structures. Its overexpression leads to tumor, non-small-cell lung cancer (NSCLC) because it plays a major role in signal transduction pathways accompanied with cell growth, differentiation, survival [63,64]. Hence, HER2 and EGFR are the best biological targets for the discovery and development of dual inhibitors [65].

The comparative molecular docking studies of the complexes and the ligand with the protein receptors HER2 and EGFR (Table 5.13) obviously suggest that the affinity of target

compounds towards protein receptor HER2 is better than that of protein receptor EGFR. Hence HER2 was taken as target protein receptor for the discussion. Docking studies revealed that the complexes Ni(II) and Cu(II) exhibited least binding energies i.e. −10.11 kcal/mol and −10.68 kcal/mol, respectively against HER2.

Besides, Ni(II) complex exhibited ten hydrogen bonds; one strong hydrogen bond between the amine group of 2-aminopyridyl ring and amino acid residue ASP855 with a bond length of 1.88 Å, one strong hydrogen bond between the –NH group of oxazinone ring and amino acid residue ALA722 with a bond length 2.13 Å, one hydrogen bond between –O-atom of oxazinone ring with amino acid residue ARG841 with a bond length 2.16 Å, one hydrogen bond between carbonyl oxygen atom of oxazinone ring and amino acid residue LYS745 with a bond length 2.17 Å, one hydrogen bond between –NH group of imine moiety with amino acid residue ASN842 with a bond length 2.63 Å, two hydrogen bonds between carbonyl oxygen adjacent to imine moiety and amino acid residue LYS745 with a bond length 2.97 Å and 3.05 Å, respectively, one hydrogen bond between –CH group of 2-aminopyridyl ring with amino acid residue CYS797 with a bond length 3.23 Å and one hydrogen bond between 2-aminopyridyl ring and amino acid residue CYS797 with a bond length 3.83 Å. The phenyl ring in the benzoxazinone ring interacts with the amino acid residues PHE723, LEU844, LEU718 and ALA743; the pyridyl ring interacts with amino acid residues VAL726 and LYS745 through hydrophobic interactions. In addition to this, there was an electrostatic interaction between the –NH group of imine moiety with the amino acid residue ASP855.

The Cu(II) complex exhibited five hydrogen bonds; one hydrogen bond between amine group of 2-aminopyridine ring and amino acid residue ASN842 with a bond length 1.96 Å, one hydrogen bond between carbonyl oxygen of oxazinone ring and amino acid residue LYS745 with a bond length 1.96 Å, one hydrogen bond between amine group of 2-aminopyridyl ring and amino acid residue ASP855 with a bond length 1.98 Å and one carbon-hydrogen bond between –NH group of oxazinone ring and amino acid residue ASP855 with a bond length 2.02 Å, and one hydrogen bond between –CH group of 2-amino pyridine ring and amino acid residue of ALA722. The phenyl ring interacts with the amino acid residues LEU718 and LEU777 and the pyridyl ring interacts with amino acid residues LEU718, LEU844 AND ALA743 through hydrophobic interactions. The molecular docking results for ligand ABAH and its complexes against HER2 and EGFR are shown in Table

5.13. The hydrogen bonding interactions and hydrophobic interactions of Ni(II) and Cu(II) complexes are shown in Fig.s 5.8-5.21.

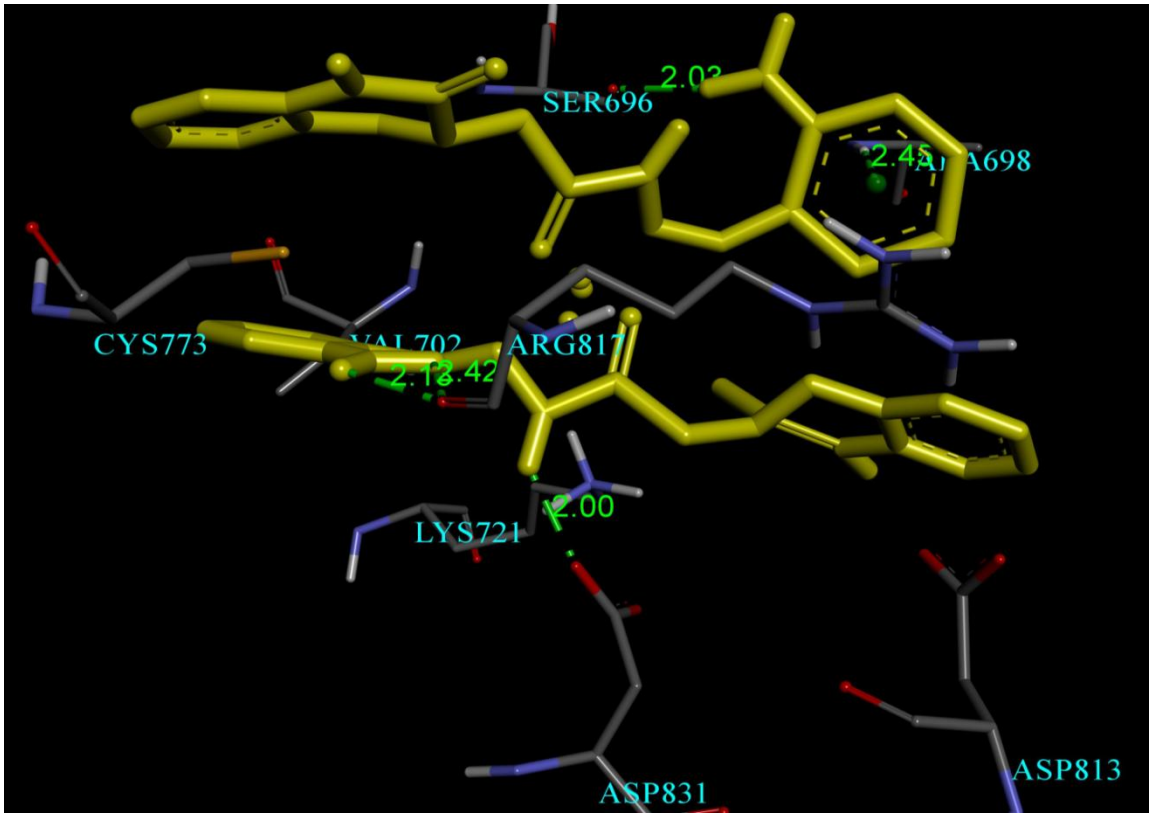

a)

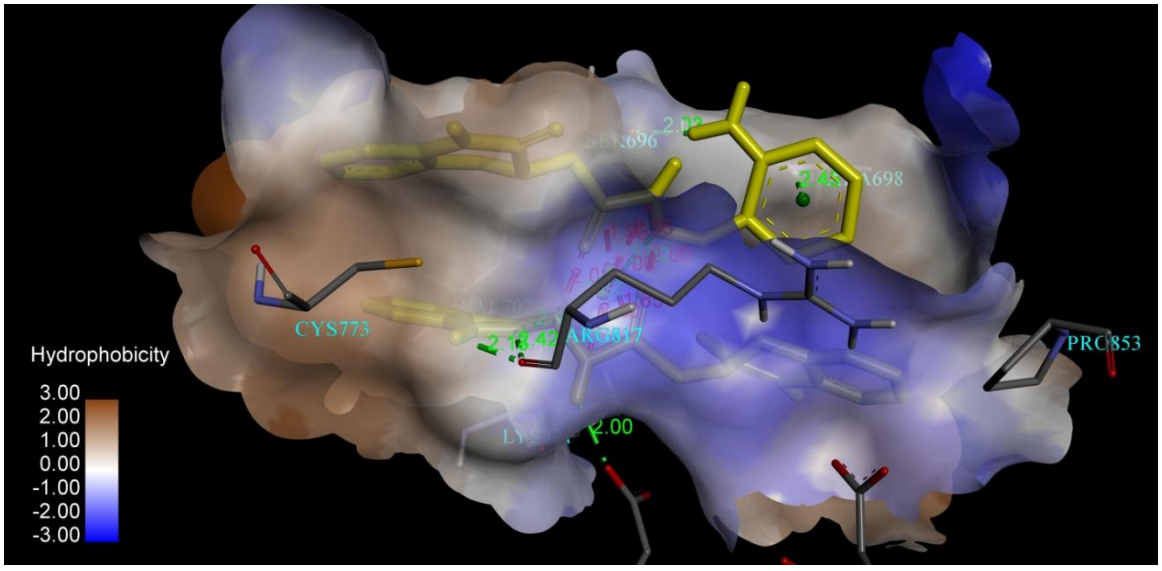

b)

Fig. 5.8 The best docking pose of the Co(II) complex with EGFR, **a)** hydrogen bond interaction, **b)** hydrophobic interactions.

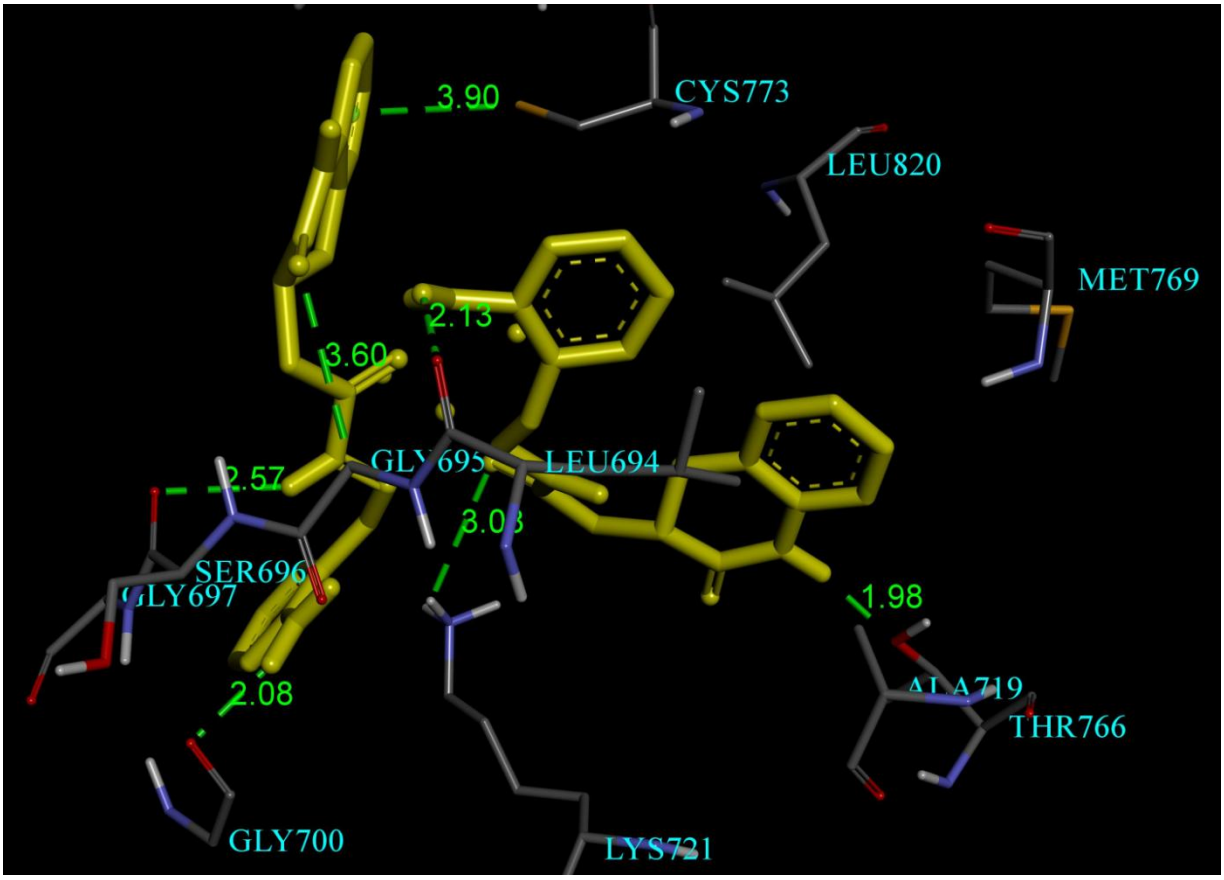

c)

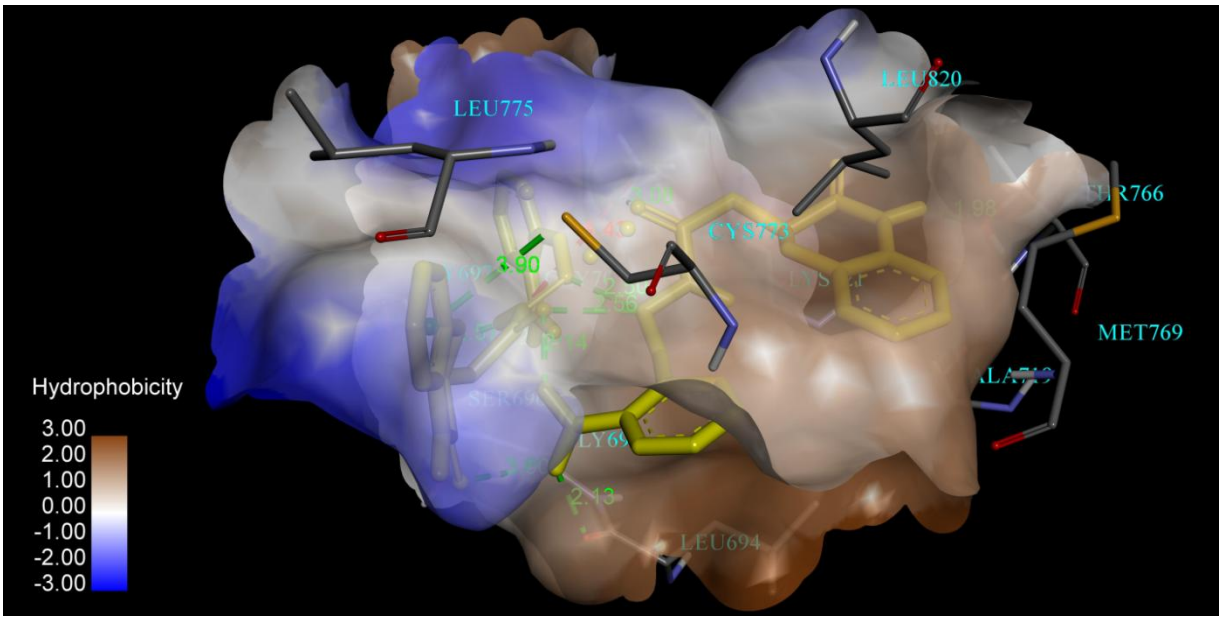

d)

Fig. 5.9 The best docking pose of the Ni(II) complex with EGFR, **c)** hydrogen bond interaction, **d)** hydrophobic interactions.

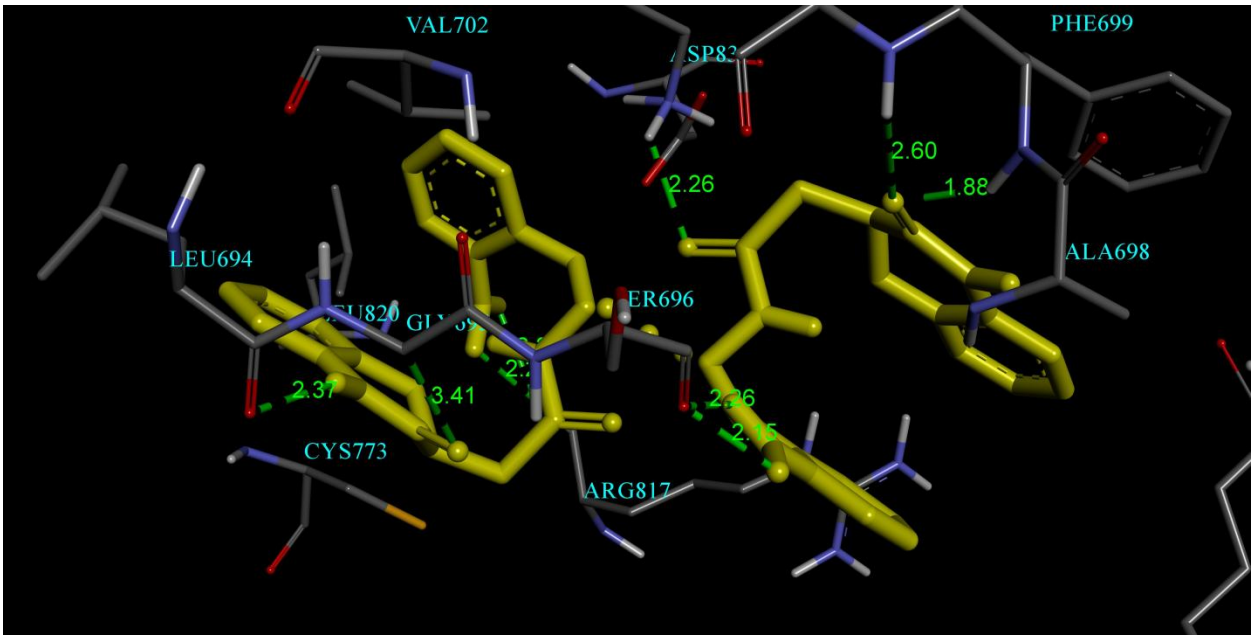

e)

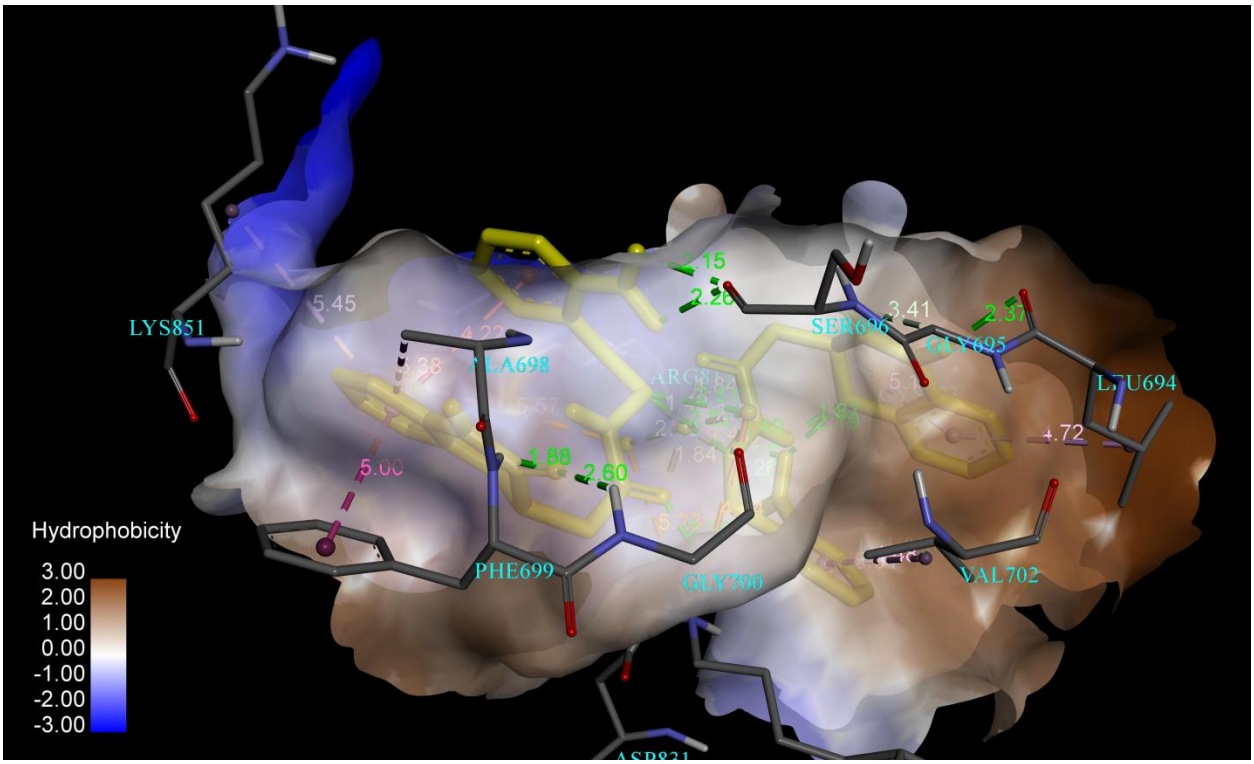

f)

Fig. 5.10 The best docking pose of the Cu(II) complex with EGFR, **e)** hydrogen bond interaction, **f)** hydrophobic interactions.

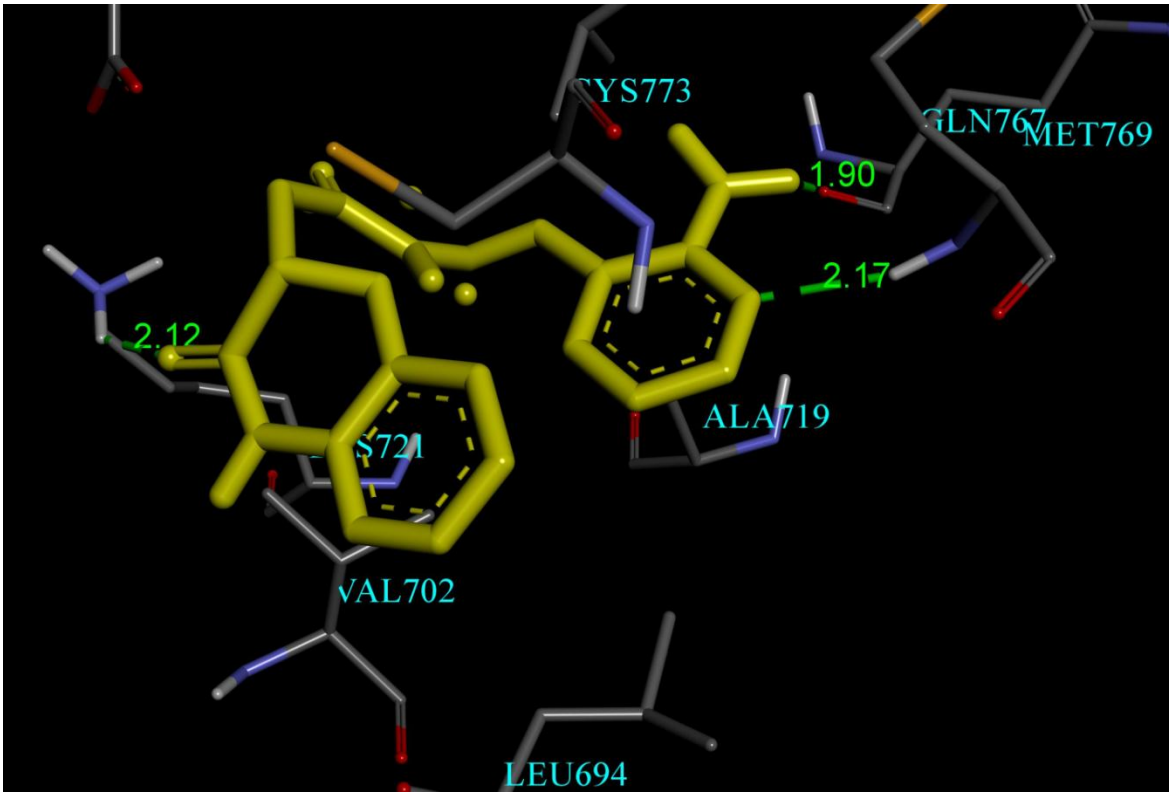

g)

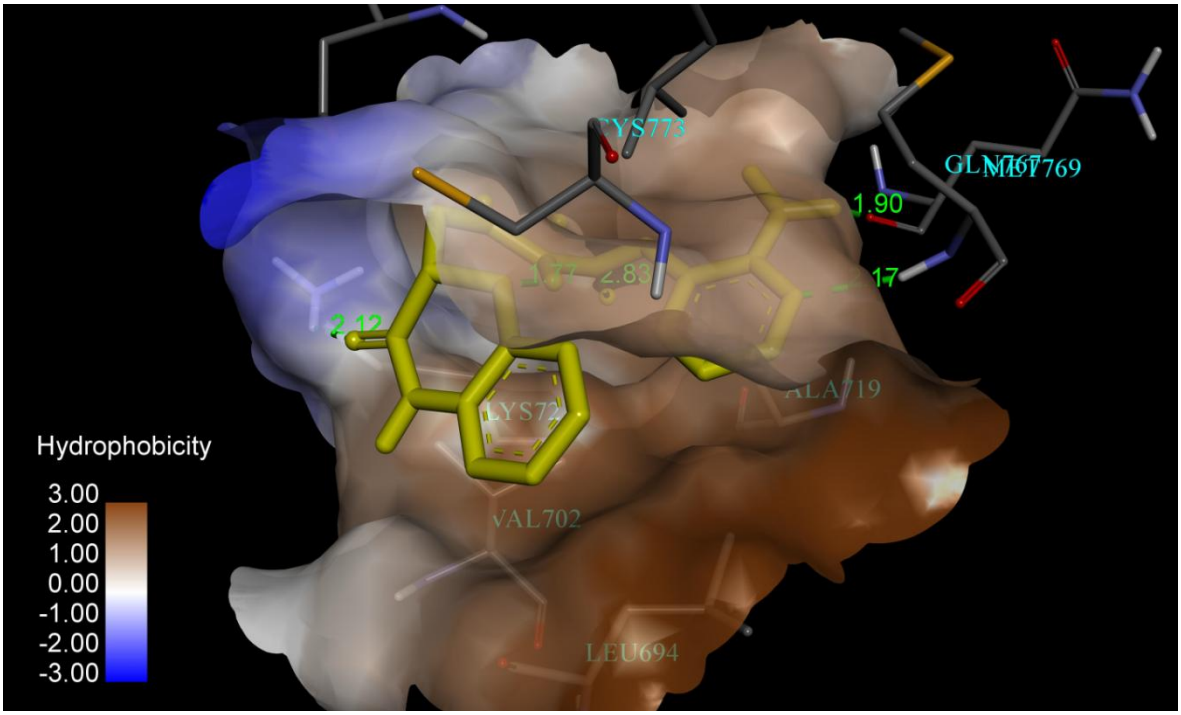

h)

Fig. 5.11 The best docking pose of the Zn(II) complex with EGFR, **g)** hydrogen bond interaction, **h)** hydrophobic interactions.

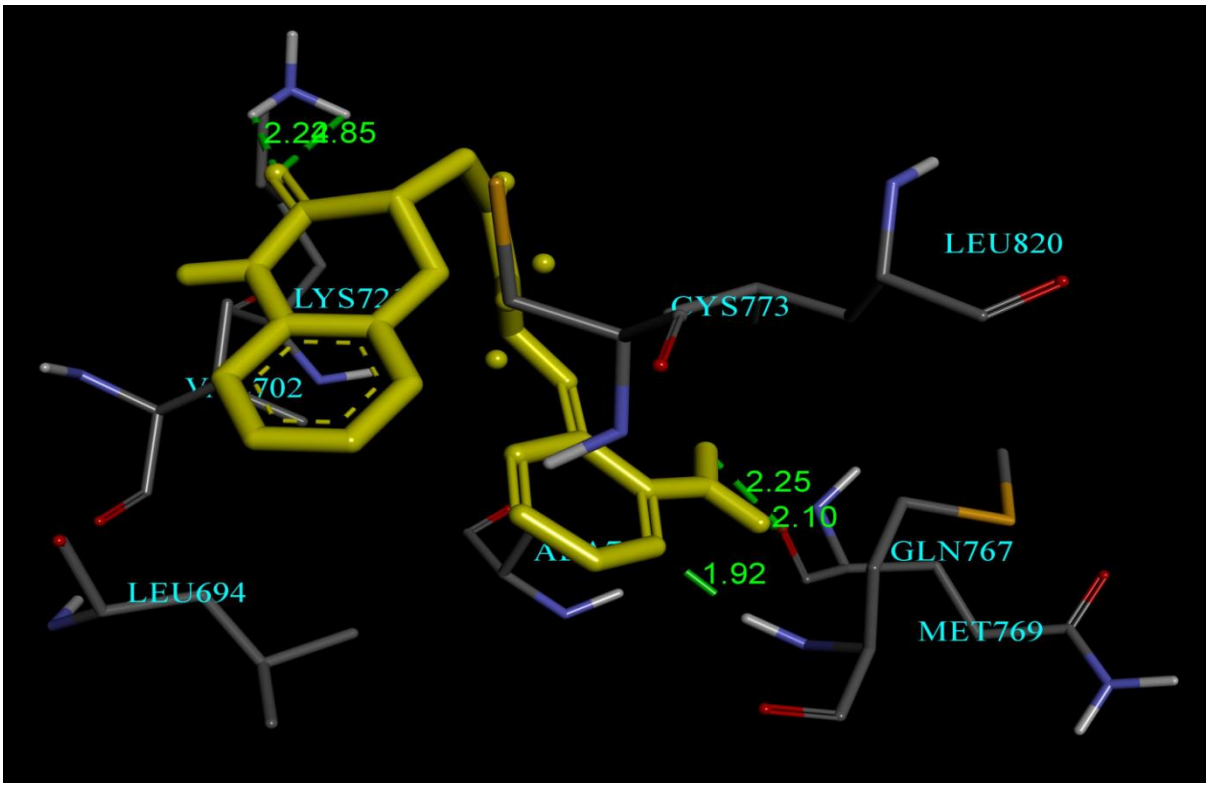

i)

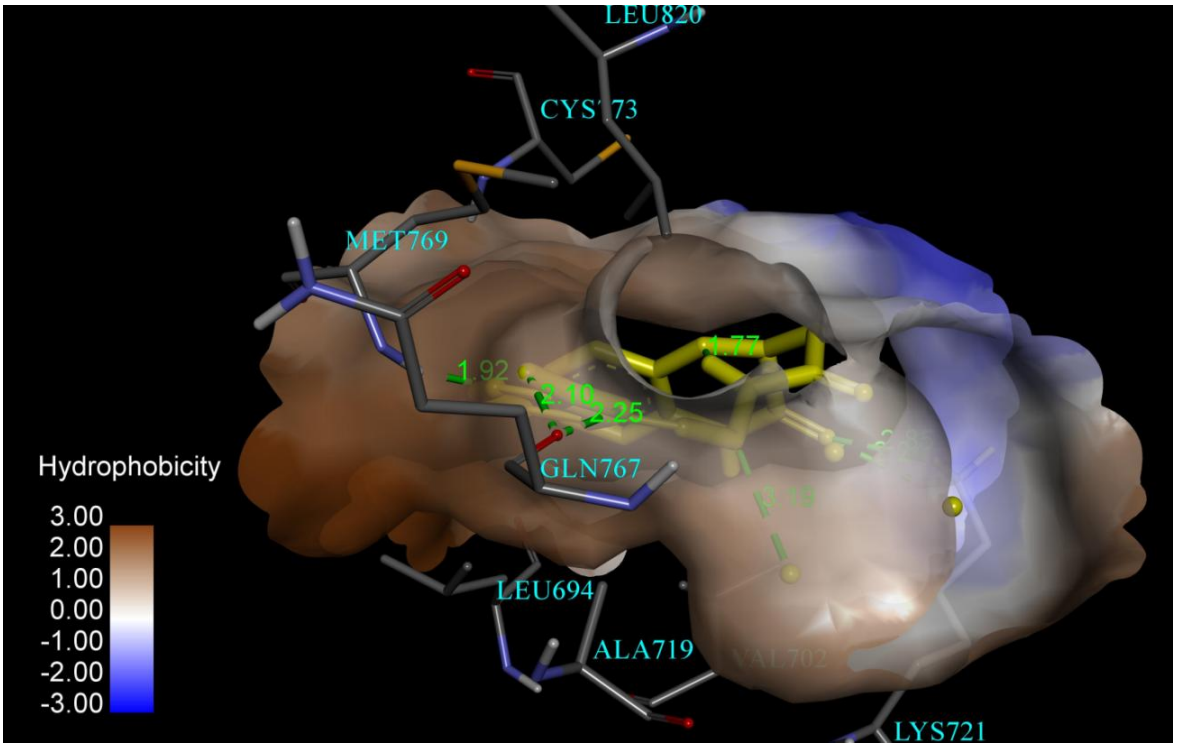

j)

Fig. 5.12 The best docking pose of the Cd(II) complex with EGFR, **i)** hydrogen bond interaction, **j)** hydrophobic interactions.

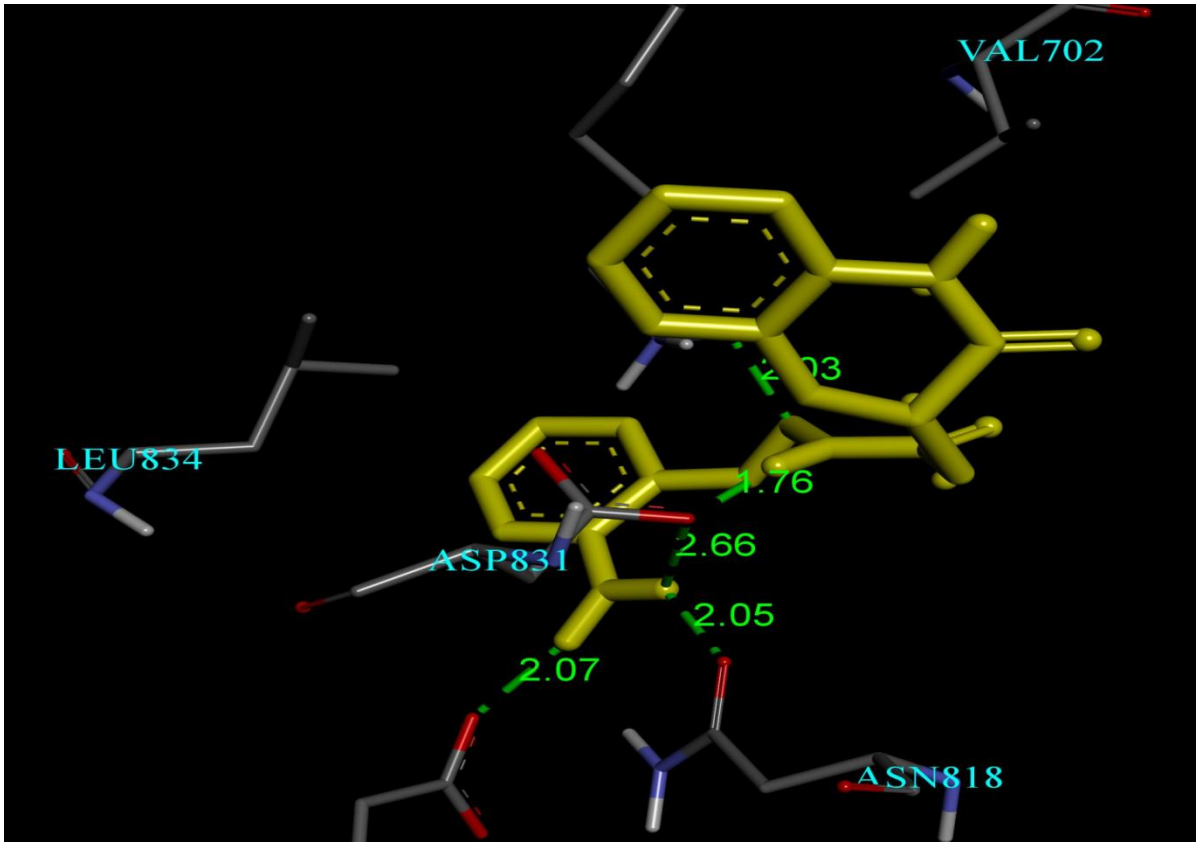

k)

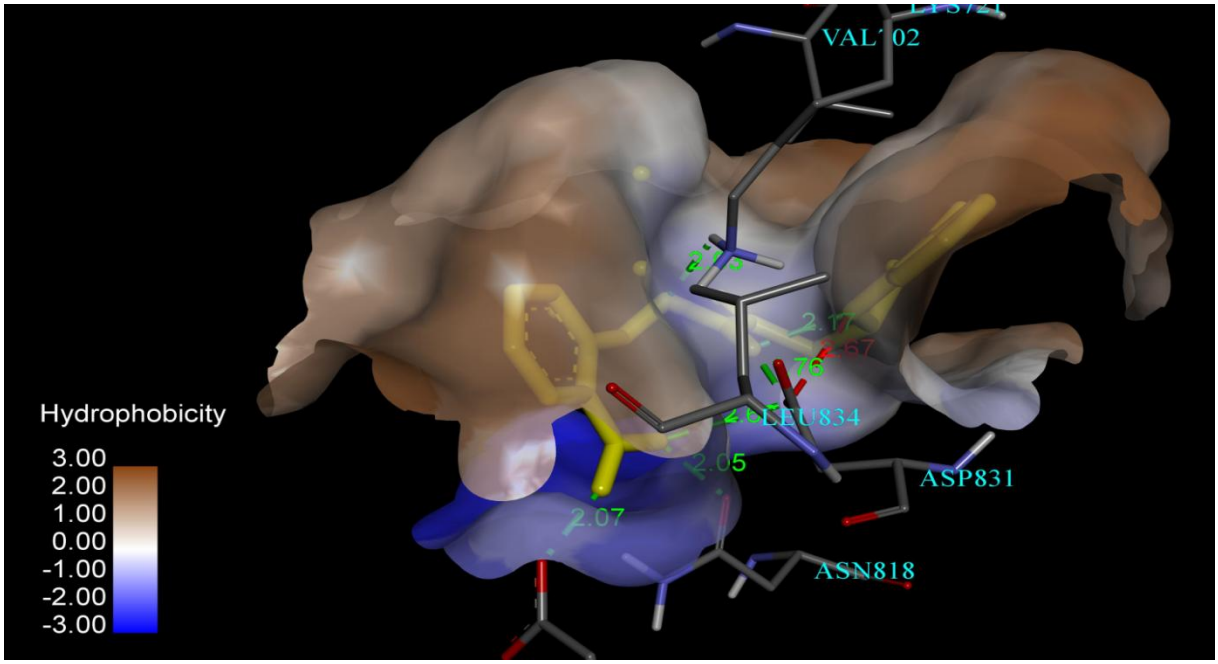

l)

Fig. 5.13 The best docking pose of the Pd(II) complex with EGFR, **k)** hydrogen bond interaction, **l)** hydrophobic interactions.

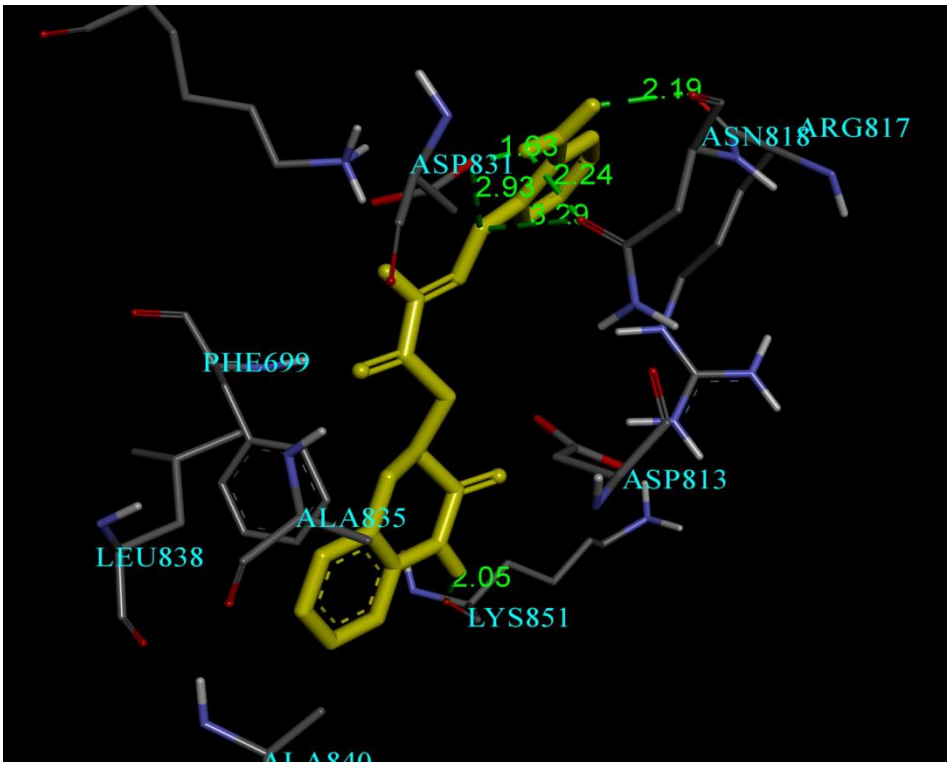

m)

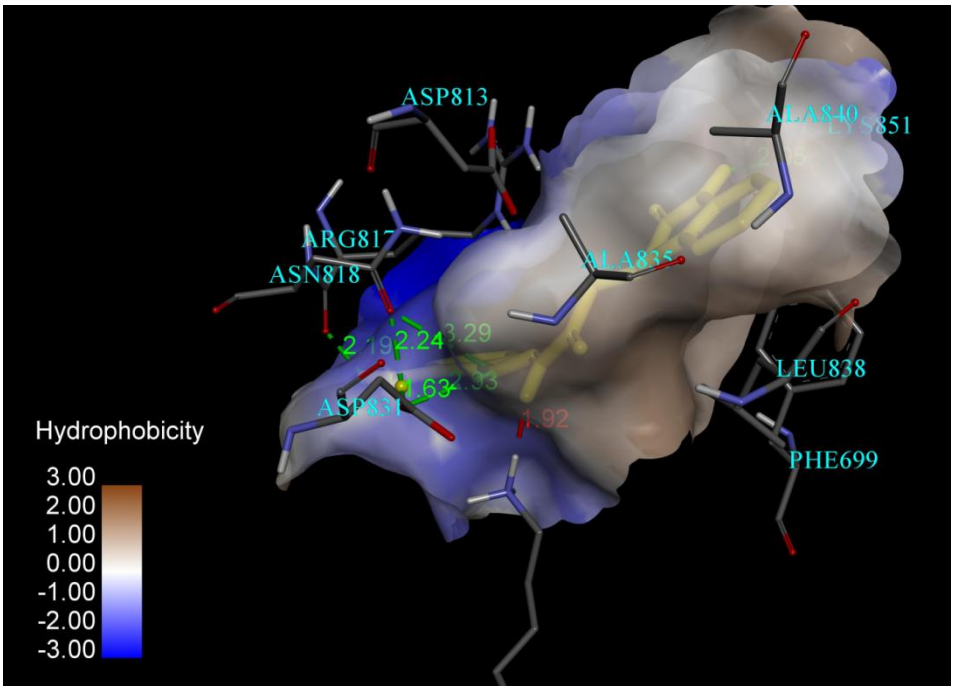

n)

Fig. 5.14 The best docking pose of the ligand ABAH with EGFR, **m)** hydrogen bond interaction, **n)** hydrophobic interactions.

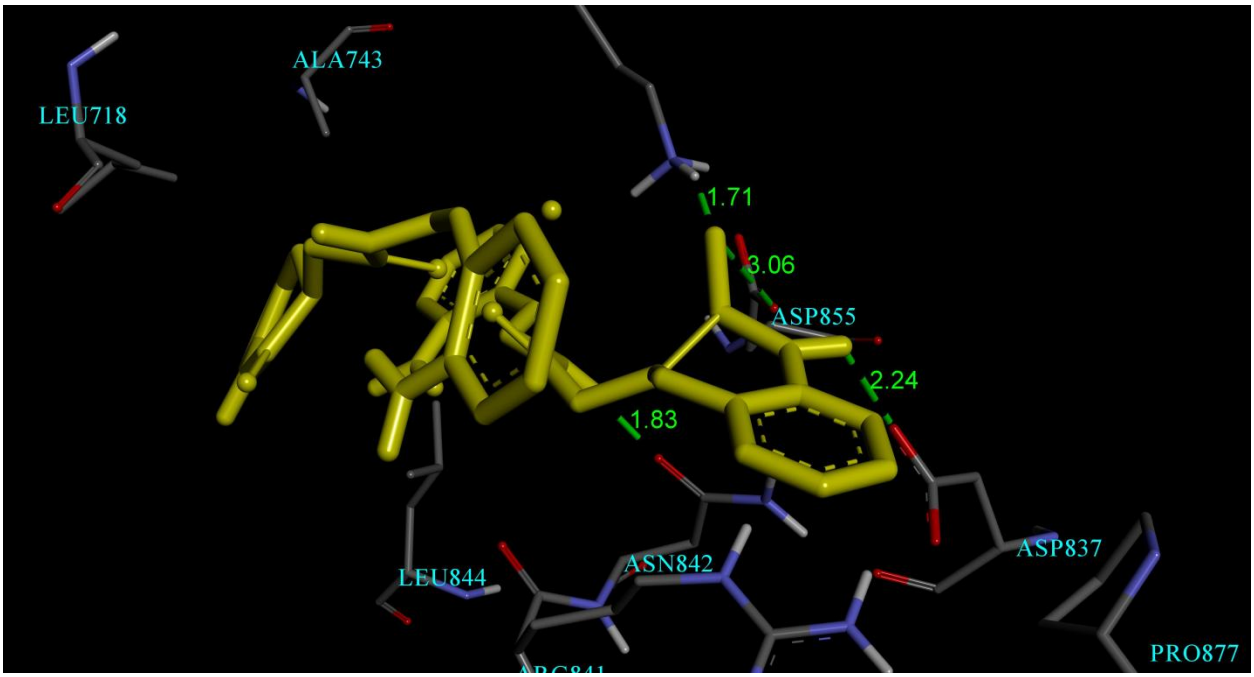

o)

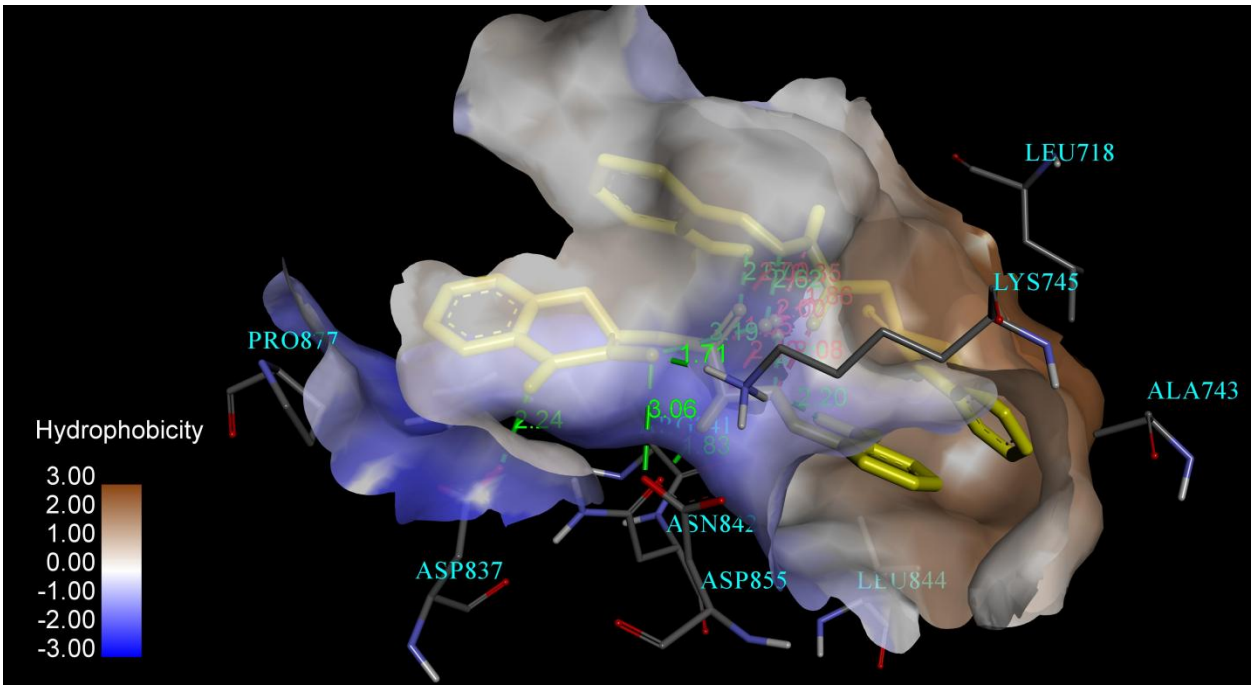

p)

Fig. 5.15 The best docking pose of the Co(II) complex with HER2, **o)** hydrogen bond interaction, **p)** hydrophobic interactions.

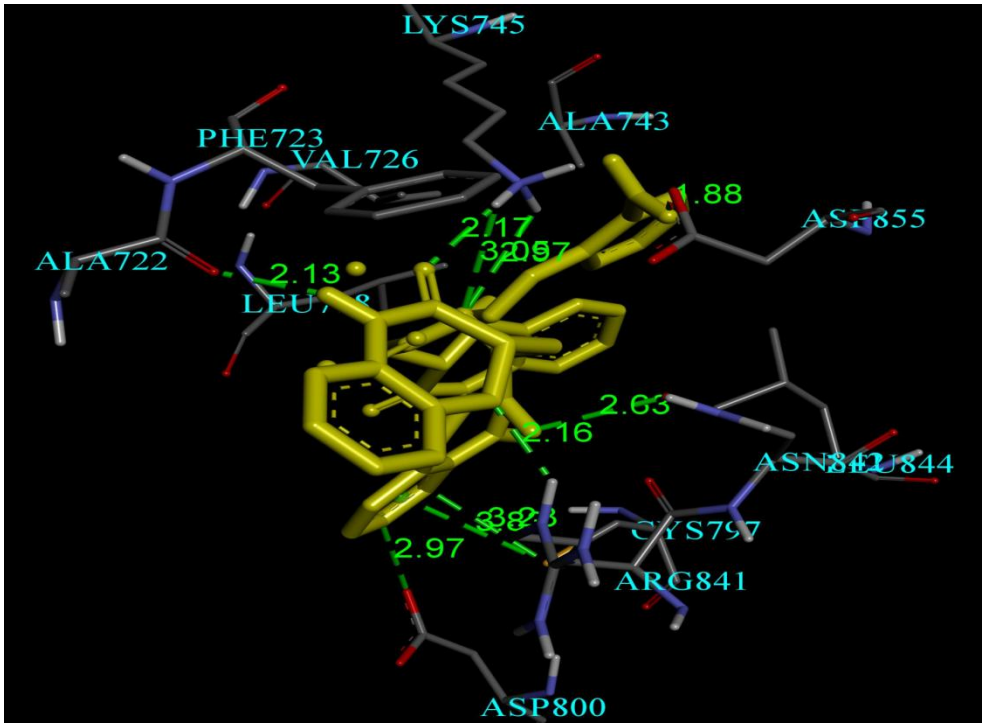

q)

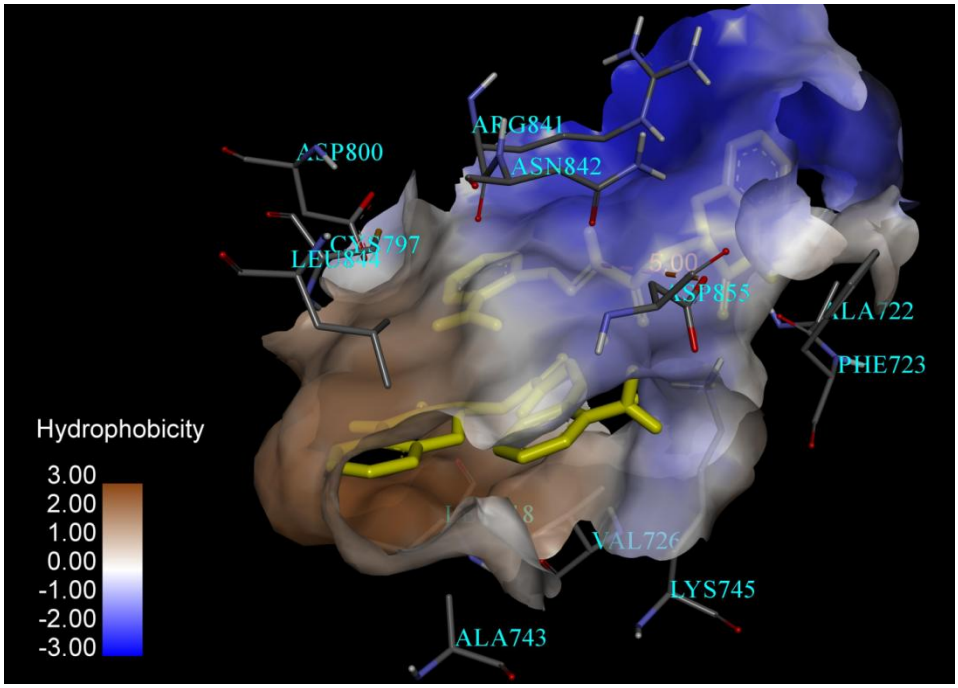

r)

Fig. 5.16 The best docking pose of the Ni(II) complex with HER2, **q)** hydrogen bond interaction, **r)** hydrophobic interactions.

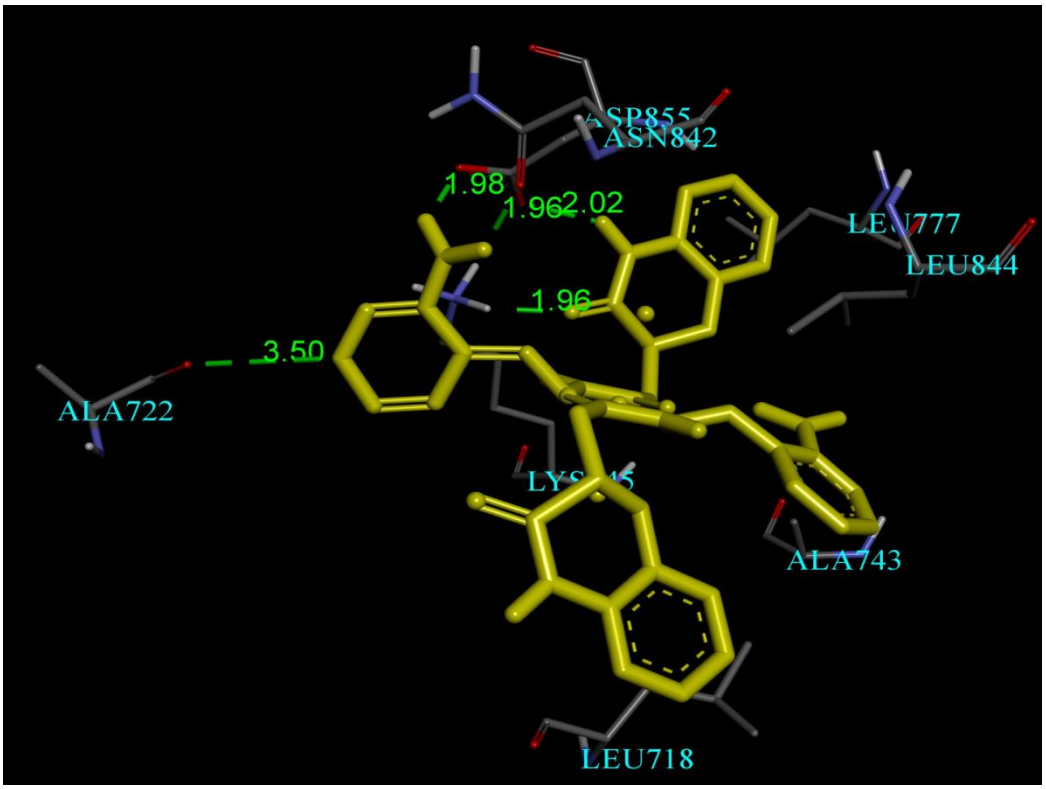

s)

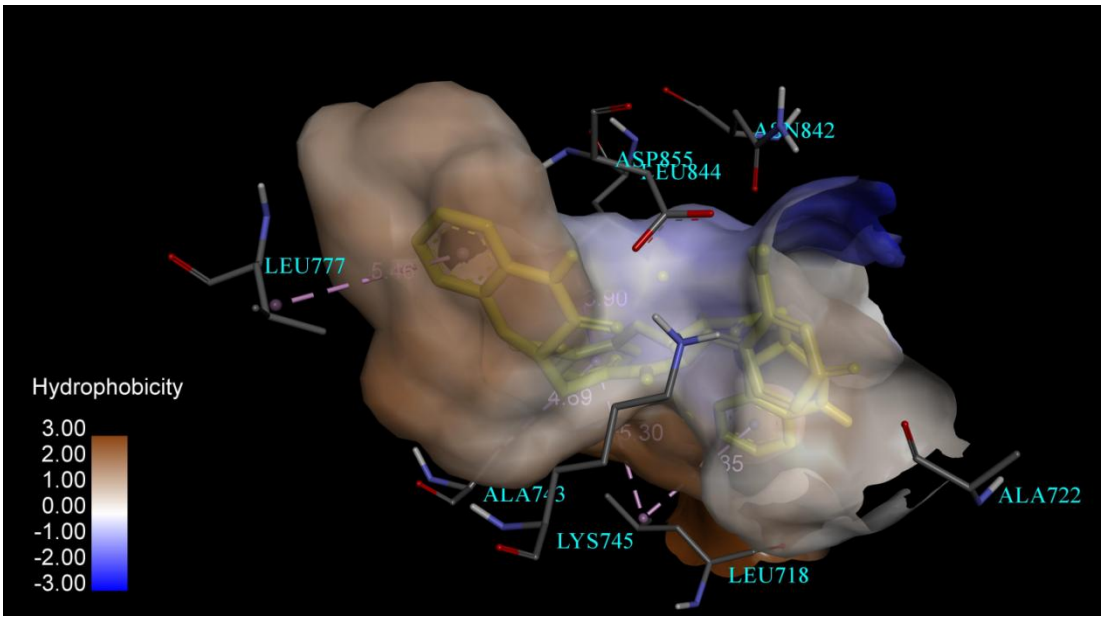

t)

Fig. 5.17 The best docking pose of the Cu(II) complex with HER2, **s)** hydrogen bond interaction**, t)** hydrophobic interactions.

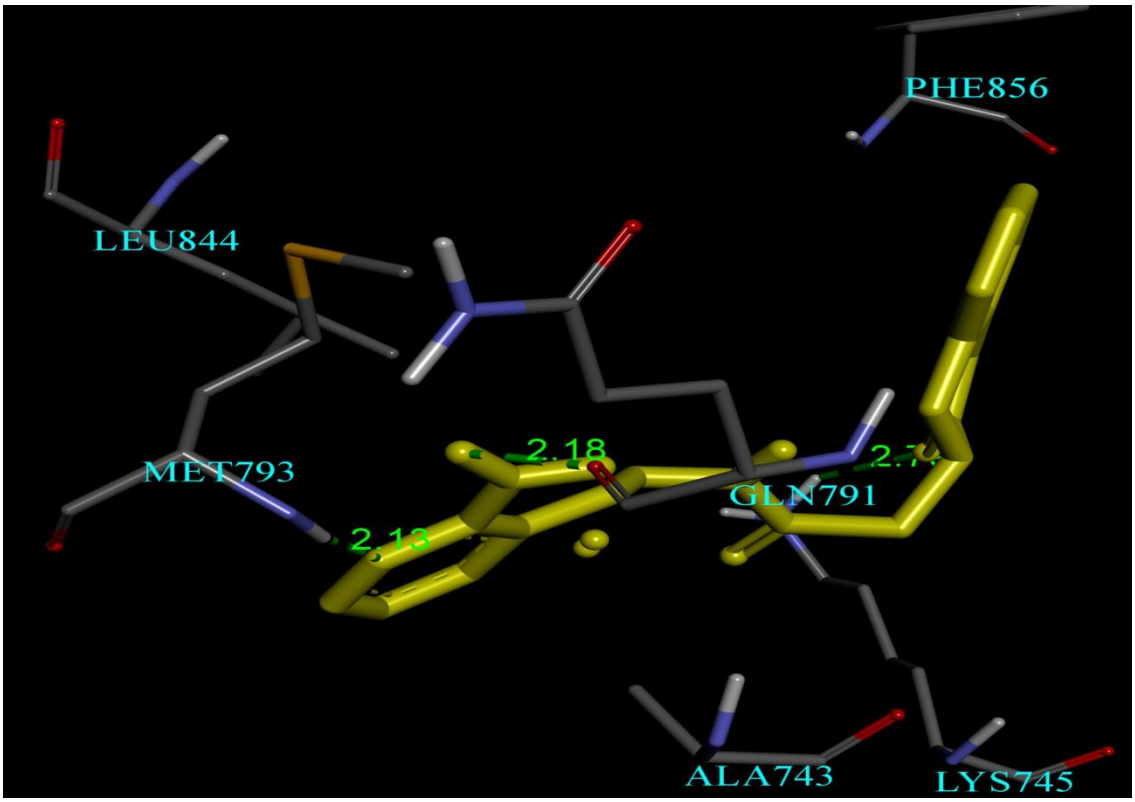

u)

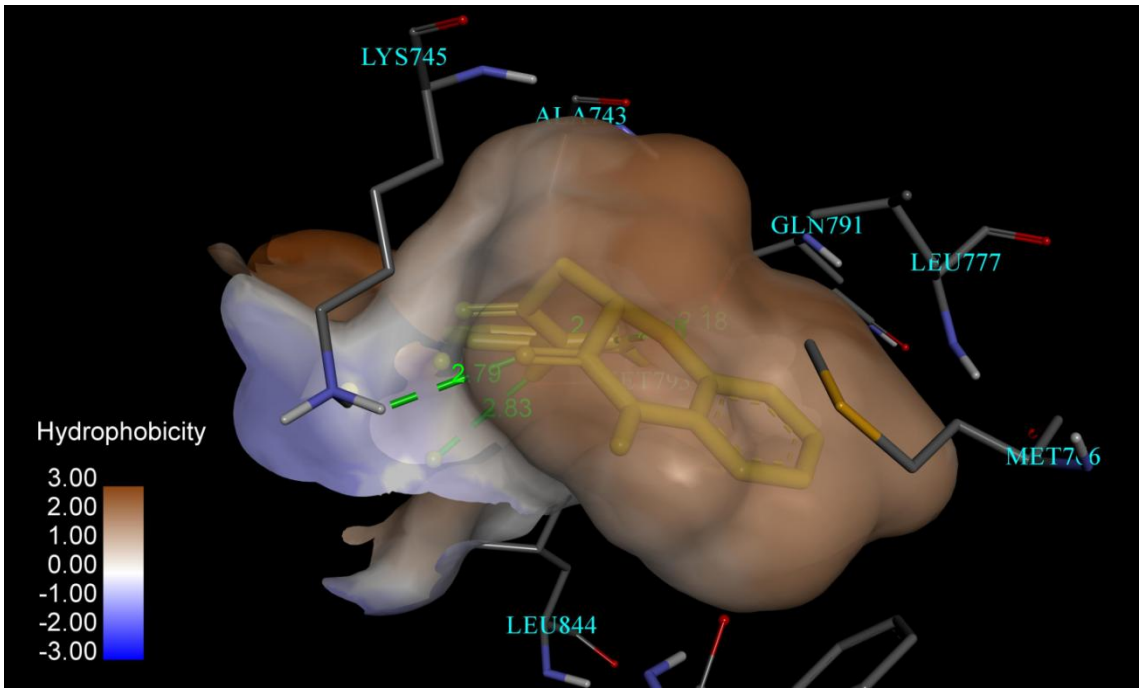

v)

Fig. 5.18 The best docking pose of the Zn(II) complex with HER2, **u)** hydrogen bond interaction**, v)** hydrophobic interactions.

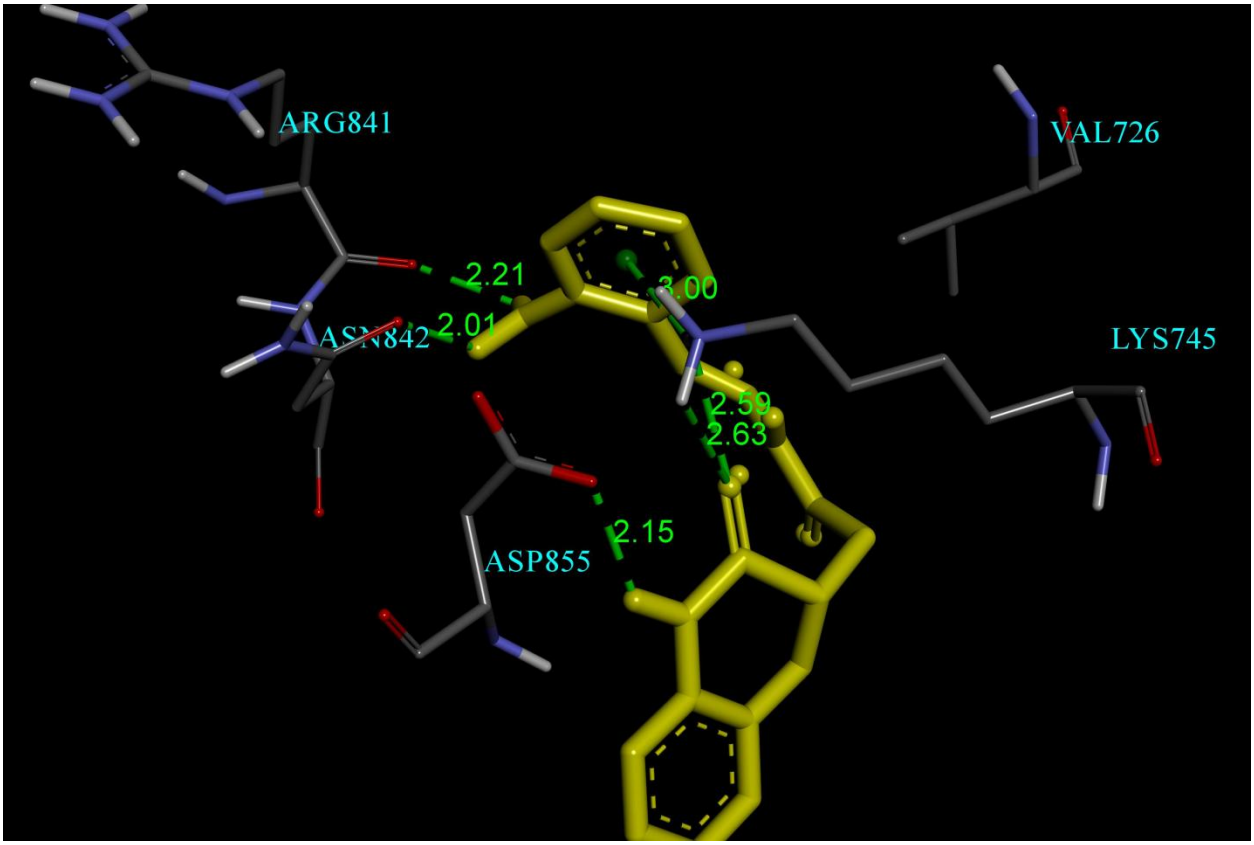

w)

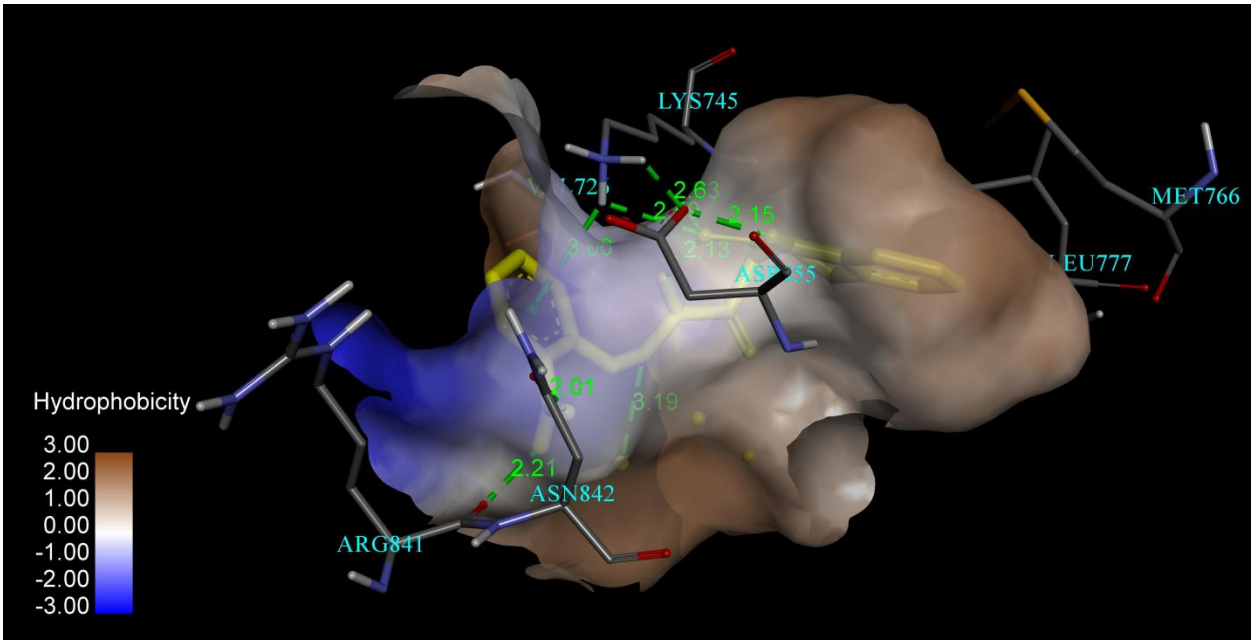

x)

Fig. 5.19 The best docking pose of the Cd(II) complex with HER2, **w)** hydrogen bond interaction, **x)** hydrophobic interactions.

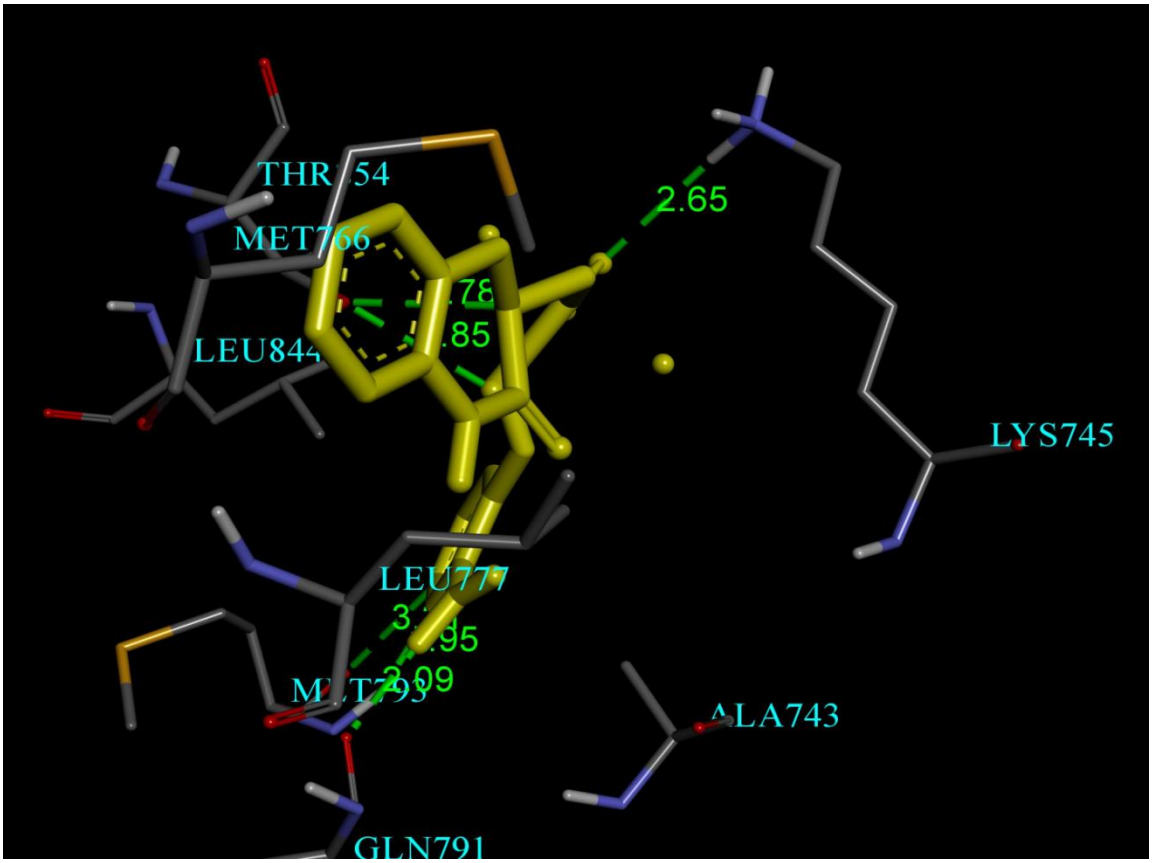

y)

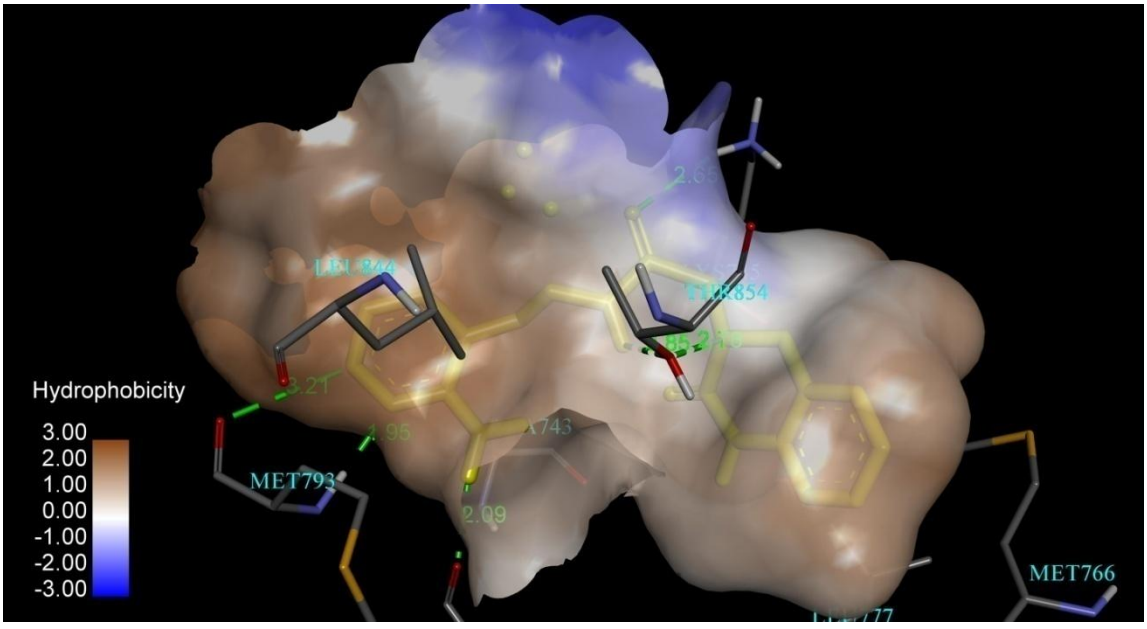

z)

Fig. 5.20 The best docking pose of the pd-complex with HER2, **y)** hydrogen bond interaction, **z)** hydrophobic interactions.

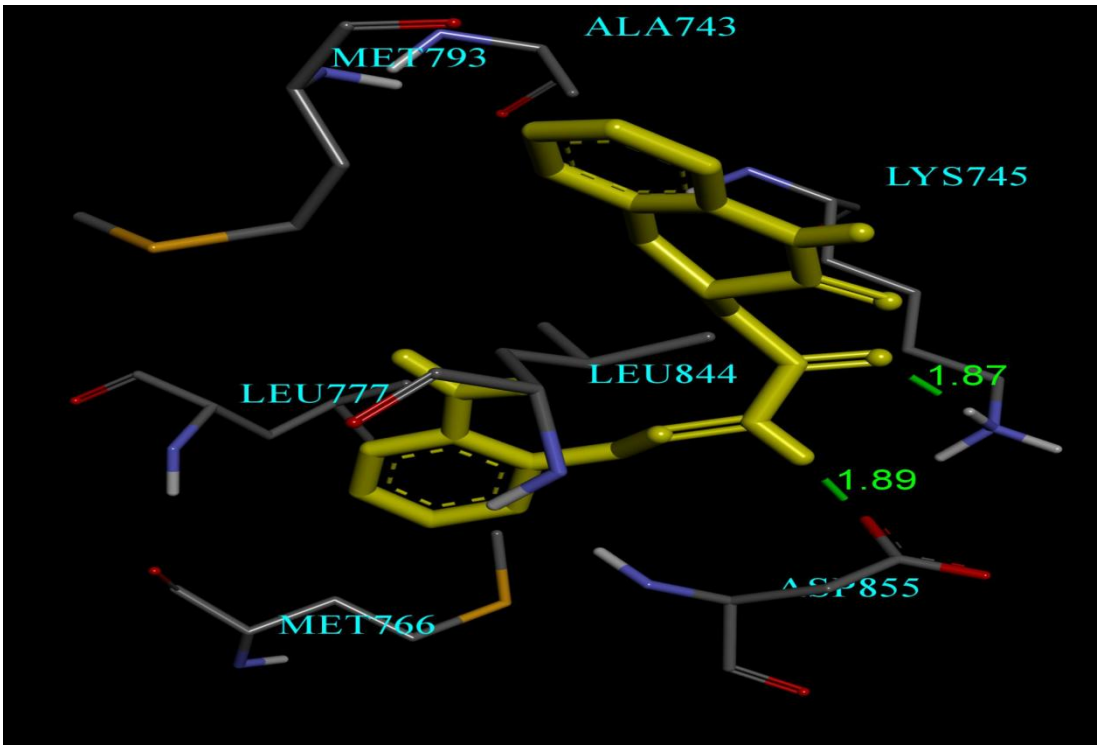

1)

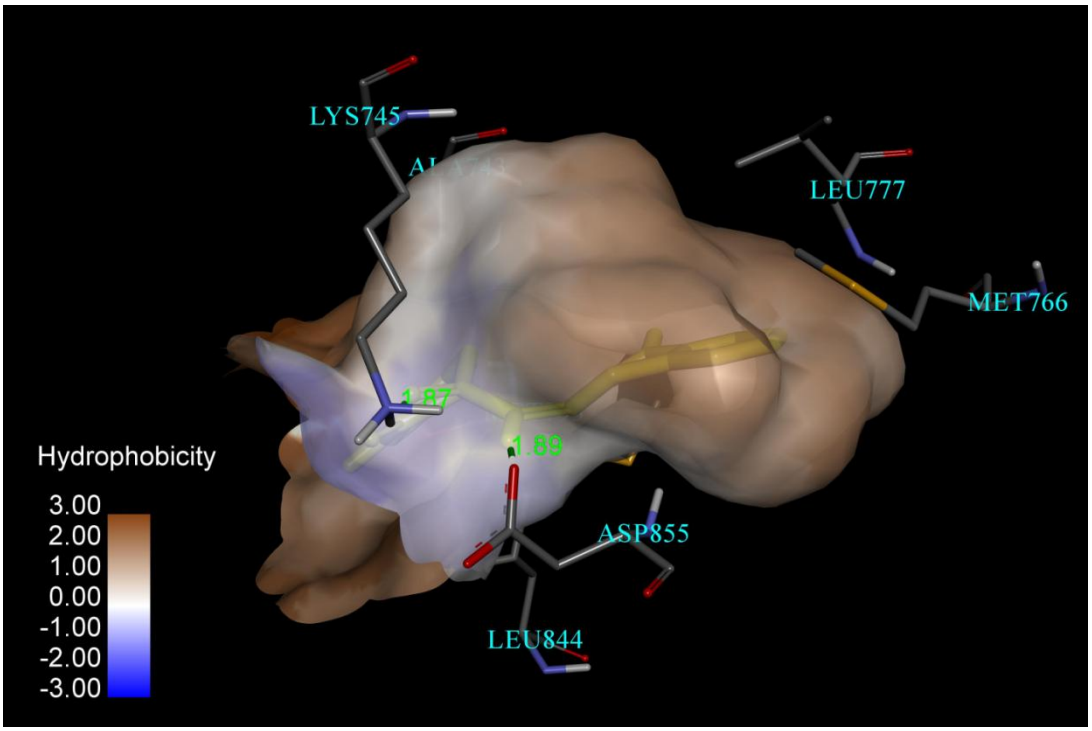

2)

Fig. 5.21 The best docking pose of the ligand ABAH with HER2**, 1)** hydrogen bond interaction, **2)** hydrophobic interactions.

Table 5.13 Binding energies of ligand and its metal complexes against protein receptors **HER 2** and **EGFR**

HER2 (PDB ID: 3POZ)					EGFR (PDB ID: 4HJO)			
Compound	**Binding energy (kcal/mol)**	**No. of Hydrogen bonds**	**Amino acid residues involved in the hydrogen bonding**	**Hydrogen bond length (Å)**	**Binding energy (kcal/mol)**	**No. of Hydrogen bonds**	**Amino acid residues involved in the hydrogen bonding**	**Hydrogen bond length (Å)**
Co(II)	-9.56	4	LYS745, ASN842, ASP837, ASP855	1.71, 1.83, 2.24, 3.06	-8.29	5	ASP831, SER696, ARG817, ALA698	2.00, 2.03,2.13, 2.42,2.44
Ni(II)	**-10.11**	**10**	**ASP855, ALA722, ARG841, LYS745, ASN842, CYS797**	**1.88, 2.13, 2.16, 2.17, 2.63, 2.97, 2.97, 3.05, 3.23, 3.83**	**-9.85**	**7**	**THR766, GLY700, LEU694, SER696, LYS721, GLY695, CYS773**	**1.98, 2.08, 2.13, 2.57, 3.08, 3.60, 3.90**
Cu(II)	**-10.68**	**5**	**LYS745, ASN842, ASP855, ALA722**	**1.96, 1.96, 1.98, 2.02, 3.50**	**-8.85**	**9**	**PHE699, SER696, LYS721, ARG817, LEU694, GLY700, GLY695**	**1.88, 2.15, 2.26, 2.26, 2.26, 2.26, 2.37, 2.60, 3.41**
Zn(II)	-9.21	3	LYS745, MET793, GLN791	2.13, 2.18, 2.79	-7.75	3	LYS721, MET769, GLN767	1.90, 2.12, 2.17
Pd(II)	-8.70	6	LYS745, ASN842, THR854, GLN791, MET793	1.95, 2.09, 2.65, 2.85, 2.78, 3.21	-7.28	5	ASP831, LYS721, ASN818, ASP813	1.76, 2.03, 2.05, 2.07, 2.66
Cd(II)	-8.46	6	ASN842, ASP855, ARG841, LYS745	2.01, 2.15, 2.21, 2.59, 2.63, 3.00	-8.15	5	MET769, GLN767, LYS721	1.92, 2.01, 2.24, 2.25, 2.84
ABAH	-7.89	2	ASP855, LYS745	1.87, 1.89	-7.07	6	ASP831, LYS851, ARG817, ASN818	1.63, 2.05, 2.19, 2.24, 2.93, 3.29

5.4 Conclusions

We have synthesized novel metal complexes of 2-aminonicotinaldehyde benzoxazinonyl acetic acid hydrazone. The compounds have been structurally characterized by different physico-chemical techniques with an aim to evaluate their antioxidant, antimicrobial and cytotoxic activities as well as for purposes of DFT calculations and docking studies. The analytical data indicate 1:2 (M:L) stoichiometry in the case of Co(II), Ni(II) and Cu(II) complexes and 1:1 stoichiometry in Zn(II), Cd(II) and Pd(II) complexes; each complex further being associated with a corresponding number of anions such as chlorides. All the complexes are non-electrolytes in DMF. The ligand ABAH reacts with metal complexes in a neutral, bidentate fashion, the coordinating atoms being oxygen of aliphatic amide group and nitrogen of azomethine group. The Co(II), Ni(II) and Cu((II) complexes are paramagnetic to the extent of three, two and one unpaired electrons, respectively, while complexes of Zn(II), Cd(II) and Pd(II) are diamagnetic. Based on the spectral and DFT data the geometry of the complexes as proposed as octahedral for Co(II) and Ni(II) complexes, distorted octahedral for Cu(II) complex, tetrahedral for Zn(II) and Cd(II) complexes and square-planar for Pd(II) complex. The evaluation of ESR parameters from the ESR spectrum of Cu(II) complex indicates that the M-L bonds are covalent and out of plane π-bonded. DFT studies revealed that the ligand and its metal complexes are good precursors for the development of new NLO materials. The antimicrobial activity of the complexes Co(II) and Cd(II) showed broad and excellent antimicrobial activities against G^+, G^- and fungal strains comparable to that of standard antimicrobial agents. The antioxidant activity of the complexes Ni(II) and Cu(II) was excellent with IC_{50} values of 18.35 ± 0.28 µM and 20.17 ± 1.28 µM, respectively compared to ascorbic acid as a positive control. With regard to anticancer activity, Ni(II) and Cu(II) complexes exhibited potent activity against IMR-32, HeLa, MCF-7, A549 and HepG-2 cell lines compared to standard drug cisplatin. These *in vitro* anticancer studies were further supported by molecular docking. Primarily based on the above outcomes, the synthesized compounds could be potential precursors for further development of novel antimicrobial and anticancer agents.

References

[1] M.A. Malik, O.A. Dar, P. Gull, M.Y. Wani, A.A. Hashmi, *Med. Chem. Commun.* **2018**, *9*, 409.

[2] S. Rollas, S.G. Küçükgüzel, *Molecules* **2007**, *12*, 1910.

[3] P. Vicini, M. Incerti, I.A. Doytchinova, P. La Colla, B. Busonera, R. Loddo, *Eur. J. Med. Chem*. **2006**, *41*, 624.

[4] H.J.C. Bezerra-Netto, D.I. Lacerda, A.L.P. Miranda, H.M. Alves, E.J. Barreiro, C.A.M. Fraga, *Bioorg. Med. Chem*. **2006**, *4*, 7924.

[5] P. Kumar, B. Narasimhan, *Mini-Rev. Med. Chem*. **2013**, *13*, 971.

[6] D.A. Green, W.E. Antholine, S.J. Wong, D.R. Richardson, C.R. Chitambar, *Clin. Can. Res.* **2001**, *7*, 3574.

[7] B. Lakshmi, K.N. Shivananda, G.A. Prakash, A.M. Isloor, K.N. Mahendra, *Bull. Korean Chem. Soc.* **2012**, *33*, 473.

[8] Ng.Ph. Buu-Hoï, Ng.D. Xuong, Ng.H. Nam, F. Binon, R. Royer, *J. Chem. Soc.* **1953**, *0*, 1358.

[9] Y.P. Kitaev, B.I. Buzykin, T.V. Troepol'skaya, *Russ. Chem. Rev*. **1970**, *39*, 441.

[10] M.W. moon, E.G. Gemrich, G. Kaugars, *J. Agr. Food. Chem*. **1972**, *20*, 888.

[11] J.G. Pecca, J. Dobrecky, S.M. Albonico, *J. Pharm. Sci.* **1971**, *60*, 650.

[12] D. Demertzi, D. Nicholls, *Inorganica Chim. Acta* **1983**, *73*, 37.

[13] B. Singh, R.N. Singh, R.C. Aggarwal, *Synth. React. Inorg. Met. Org. Chem*. **1984**, *14*, 815.

[14] I.P. Ferreira, E.D.L. Piló, A.A. Recio-Despaigne, J.G. Da Silva, J.P. Ramos, L.B. Marques, P.H.D.M. Prazeres, J.A. Takahashi, E.M. Souza-Fagundes, W. Rocha, H. Beraldo, *Bioorg. Med. Chem*. **2016**, *24*, 2988.

[15] A.A.R. Despaigne, J.G. Da Silva, A.C.M. Do Carmo, O.E. Piro, E.E. Castellano, H. Beraldo, *J. Mol. Struct*. **2009**, *920*, 97.

[16] D. Kasimbi, K.H. Reddy, N. Devanna, *Asian. J. Chem*. **2019**, *31*, 1289.

[17] A.V. Kurnoskin, N.P. Cheremisinoff, P.N. Cheremisinoff, *Handbook of applied polymer processing technology*, New York, Marcel Dekker, **1996**, 703.

[18] A.V. Kurnoskin, *J. Macro. Sci.-Rev. Macro. Chem. Phys.* **1996**, *36*, 457.

[19] A.V.J. Kurnoskin, *Macro. Sci.-Rev. Macro. Chem Phys.* **1995**, *35*, 419.

[20] R. Aich, F. Tran-Van, F. Goubard, L. Beouch, A. Michaleviciute, J.V. Grazulevicius, B. Ratier, C. Chevrot, *Thin Solid Films* **2008**, *516*, 7260.

[21] O. Pouralimardan, A.-C. Chamayou, C. Janiak, H. Hosseini-Monfared, *Inorganica Chim. Acta* **2007**, *360*, 1599.

[22] M. Bakir, O. Green, W.H. Mulder, *J. Mol. Struct*. **2008**, *873*, 17.

[23] C. Basu, S. Chowdhury, R. Banerjee, H.S. Evans, S. Mukherjee, *Polyhedron* **2007**, *26*, 3617.

[24] R. Konakanchi, J. Haribabu, J. Prashanth, N.V. Bharat, M. Ramachary, D. Gandamalla, R. Karvembu, B. Venkatram Reddy, N.R. Yellu, L.R. Kotha *Appl. Organomet. Chem.* **2018**, *32*, e4415.

[25] J. Haribabu, K. Jeyalakshmi,a Y. Arun, N.S.P. Bhuvanesh, P.T. Perumal, R. Karvembu, *RSC Adv.* **2015**, *5*, 46031.

[26] Y. Jayamma, V. Malla Reddy, *Indian J. Pharm. Sci.* **1993**, *55*, 132.

[27] T.R. Rao, M. Sahay, R.C. Aggarwal, *Indian J. Chem.* **1984**, *23A*, 214.

[28] R. Mallela, R. Konakanchi, R. Guda, N. Munirathinam, D. Gandamalla, N.R. Yellu, L.R. Kotha, *Inorganica Chim. Acta* **2018**, *469*, 66.

[29] S. Chandra, A.K. Sharma, *Spectrochim. Acta A* **2009**, *72*, 851.

[30] J.R. Ferraro, *Low Frequency Vibrations of Inorganic and Coordination Compounds*, Plenum Press, New York, **1971**.

[31] R. Konakanchi, R. Mallela, R. Guda, L.R. Kotha, *Res. Chem. Intermed.* **2018**, *44*, 27.

[32] W.J. Geary, *Coord. Chem. Rev.* **1971**, *7*, 81.

[33] N.H. Kolhe, S.S. Jadhav, *Res. Chem. Intermed.* **2019,** *45*, 973.

[34] A.B.P. Lever, *Inorganic Electronic Spectroscopy, 1st ed.*, Elsevier, Amsterdam, **1968**.

[35] C.K. Jørgensen, U. Persmark, S.E. Rasmussen, A. Block-Bolten, J.M. Toguri, H. Flood, *Acta Chem. Scand.* **1962**, *16*, 2017.

[36] T. Manjuraj, G. Krishnamurthy, D. Yadav, H.S. Bodke, H.S. Bhojya Naik, A. Kumar, *J. Mol. Struct.* **2018**, *1171*, 481.

[37] D.N. Sathyanarayana, *electronic absorption spectroscopy and related technique*, University Press (India), Hyderabad, **2001**.

[38] P.P. Dholakiya, M.N. Patel, *Syn. React. Inorg. Met. Org. Nano-Met. Chem.* **2002**, *32*, 819.

[39] F.K. Kneubuhl, *J. Chem. Phys.* **1960**, *33*, 1074.

[40] K.N. Aneesrahman, K. Ramaiah, G. Rohini, G.P. Stefy, N.S.P. Bhuvanesh, A. Sreekanth, *Inorganica Chim. Acta* **2019**, *492*, 131.

[41] V.P. Singh, A. Katiyar, *Pestic. Biochem. Phys.* **2008**, 92, 8.

[42] N. Raman, A. Sakthivel, N. Pravin, *Spectrochim. Acta A* **2014**, *125*, 2007.

[43] M. Arivazhagan, S. Jeyavijayan, *Spectrochim. Acta A* **2011**, *79*, 376.

[44] P. Politzer, D.G. Truhlar (Eds.), Plenum Press, New York, **1981**.

[45] E. Scrocco Tomasi, *J. Adv. Quantum Chem.* **1978**, *11*, 115.

[46] P. Politzer, K.C. Daiker, in: B.M. Deb (Ed.), Van Nostrand Reinhold, New York, **1981**, pp. 294.

[47] V. Balachandran, A. Lakshmi, A. Janaki, *J. Mol. Struct*. **2012**, *1013*, 75.

[48] Y-X. Sun, Q-L. Hao, W-X. Wei, Z-X. Yu, L-D. Lu, X. Wang, Y-S. Wang, *J. Mol. Struct*. *Theochem*. **2009**, *904*, 74.

[49] C. Andraud, T. Brotin, C. Garcia, F. Pelle, P. Goldner, B. Bigot, A. Collet, *J. Am*. *Chem*. *Soc*. **1994**, *116*, 2094.

[50] V.M. Geskin, C. Lambert, J-L. Bre´das, *J. Am*. *Chem*. *Soc*. **2003**, *125*, 15651.

[51] M. Nakano, H. Fujita, M. Takahata, K. Yamaguchi, *J. Am*. *Chem*. *Soc*. **2002**, *124*, 9648.

[52] D. Sajan, H. Joe, V.S. Jayakumar, J. Zaleski, *J. Mol. Struct*. **2006**, *785*, 43.

[53] Y-X. Sun, Q-L. Hao, Z-X. Yu, W-X. Wei, L-D. Lu, X. Wang, *Mol. Phys*. **2009**, *107*, 223.

[54] A.B. Ahmed, H. Feki, Y. Abid, H. Boughzala, C. Minot, A. Mlayah, *J. Mol. Struct*. **2009**, 920, 1.

[55] J.P. Abraham, D. Sajan, V. Shettigar, S.M. Dharmaprakash, I. Neˇmec, I.H. Joe, V.S. Jayakumar, *J. Mol. Sruct*. **2009**, *917*, 27.

[56] S.G. Sagdinc, A. Esme, *Spectrochim*. *Acta A* **2010**, *75*, 1370.

[57] A.B. Ahmed, H. Feki, Y. Abid, H. Boughzala, C. Minot, *Spectrochim*. *Acta A* **2010**, *75*, 293.

[58] M. Arivazhagan, S. Jeyavijayan, *Spectrochim*. *Acta A* **2011**, *79*, 376.

[59] L. Sinha, O. Prasad, V. Naryan, S.R. Shukla, *J. Mol. Simul*. **2011**, *37*, 153.

[60] D.F.V. Lewis, C. Ioannides, D.V. Parke, *Xenobiotica* **1994**, *24*, 401.

[61] D. Kosar, C. Albayrak, *Spectrochim*. *Acta A* **2011**, *78*, 160.

[62] S. Rampogu, M. Son, A. Baek, C. Park, R. Mukthar Rana, A. Zeb, S. Parameswaran, K. W. Lee, *Comput*. *Biol. Chem*. **2018**, *74*, 327.

[63] W. Liu, J-F. Ning, Q-W. Meng, J. Hu, Y-B. Zhao, C. Liu, L. Cai, *Drug Des. Dev*. *Ther*. **2015**, *9*, 3837.

[64] R.B. Ferreira, M.E. Law, S.C. Jahn, B.J. Davis, C.D. Heldermon, M. Reinhard, R.K. Castellano, B.K. Law, *Oncotarget* **2015**, *6*, 10445.

[65] R.M. de Angelo, M.O. Almeida, H. de Paula, K.M. Honorio, *Int*. *J. Mol. Sci*. **2018**, *19*, 3728.

CHAPTER-VI

Synthesis, characterization, theoretical investigation and biological screening of metal(II) complexes of derived from 4-(2-aminopyridin-3-methylene)aminobenzoic acid

2-aminonicotinaldehyde, which is structurally comparable to 2-aminobenzaldehyde and salicylaldehyde has been little investigated as a precursor for the synthesis of Schiff bases and their metal complexes. A number of reviews on Schiff base metal complexes derived from salicylaldehyde and 2-aminobenzaldehyde have been reported [1-6]. 2-aminonicotinaldehyde should form similar Schiff bases and also form complexes with several metal ions [7-10]. 2-aminonicotinaldehyde containing Schiff base ligands and their metal complexes are well recognized for their use in a variety of biological applications such as antibacterial, antimalarial, antitubercular, antifungal, antioxidant, anti-inflammatory and anticancer activities [11-15].

In particular, cancer is one of the most staggering and death causing diseases in the world which involves abnormal cell proliferation in the body [16-18]. On the one hand cisplatin and its derivatives, and on the other hand, a large number of metal complexes have been introduced in the treatment of a variety of cancers [19,20]. However, it was observed that there are several drawbacks regarding the use of complexes, which includes limiting efficiency, clinical usage and side effects [19]. Excitingly, a large number of metal complexes have been evaluated to design the molecules for high selectivity, maximum efficancy and minimum toxicity.

In view of the aforementioned biological importance of the metal complexes and Schiff bases, we present here, novel metal complexes of Co(II), Cu(II), Ni(II), Zn(II), Cd(II) and Pd(II) with Schiff base in a single molecular framework and their potential *in vitro* anticancer, antioxidant, antimicrobial activities and *in silico* studies (DFT and molecular docking).

6.1 Results and discussion

The new ligand, 4-(2-aminopyridin-3-methylene)aminobenzoic acid and its metal(II) complexes are stable at room temperature and non-hygroscopic. However, at higher temperatures, the ligand undergoes melting while the complexes decompose without melting. The ligand is soluble in MeOH, EtOH, $CHCl_3$, DMF, and DMSO and the complexes are only soluble in dimethyl sulfoxide and dimethylformamide. The authenticities of the synthesized compounds were ascertained using various spectroscopic methods and elemental analysis. The theoretical percent values of the elements in the complexes have been calculated for the formulations given in Table 6.1 to indicate that experimental values agree, within the experimental error, with calculated values.

Table 6.1 Analytical, molar conductance and physical parameters for the ligand and its metal complexes

Molecular formula	Elemental analyses: Found (Calculated)				
	C	**N**	**H**	**M**	**Molar Cond. ($ohm^{-1} cm^2 mol^{-1}$)**
$[Co(ANABZA)_2Cl_2]$	50.93 (51.00)	13.66 (13.72)	3.65 (3.62)	9.69 (9.62)	12
$[Ni(ANABZA)_2Cl_2]$	50.97 (51.02)	13.67 (13.73)	3.58 (3.62)	9.52 (9.59)	16
$[Cu(ANABZA)_2Cl_2]$	50.58 (50.62)	13.59 (13.62)	3.55 (3.59)	10.25 (10.30)	19
$[Zn(ANABZA)_2Cl_2]$	50.41 (50.47)	13.54 (13.58)	3.55 (3.58)	10.50 (10.57)	15
$[Pd(ANABZA)Cl_2]$	37.37 (37.30)	10.09 (10.04)	2.59 (2.65)	25.31 (25.42)	11
$[Cd(ANABZA)Cl_2]$	36.91 (36.78)	9.98 (9.90)	2.64 (2.61)	(26.59) (26.48)	16

6.1.1 Spectroscopic characterization

The positions of the selected characteristic IR bands unambiguously unveiled the formation of new ligand 4-(2-aminopyridin-3-methylene)aminobenzoic acid and its metal complexes. The important absorption frequencies are presented in Table 6.2. The ligand showed the strong band at 1629 cm^{-1} due to υ(C=N), on the other hand, this band was lowered by 20-30 cm^{-1} in the complexes pointing to the fact that the nitrogen of this group is involved in binding with the metal ion [21-25].The amine group nitrogen of the ligand showed the band at 3420 cm^{-1} due to $\upsilon(NH_2)$ has been found at lower frequencies by (3401-3371 cm^{-1}) in the complexes, this kind of shift suggested that amine nitrogen is bonded to the metal [26,27]. The carboxylic acid (C=O) and $(C=N)_{py}$ stretching frequencies of the ligand occurred at 1701 and 1567 cm^{-1}. These bands do not undergo any perceptible shifts in the metal complexes suggesting that there are no interactions

between oxygen and nitrogen of these groups. The aforementioned results proved that the ligand coordinate with metal ions through amine nitrogen atom and azomethine nitrogen. In the complexes, the other peaks observed in the region of 478-520 cm^{-1} and 275-321 cm^{-1} correspond to υ(M–N) and υ(M–Cl), respectively. The conductance measurements of the metal complexes in DMF solution were made at 10^{-3} $mol.dm^{-3}$ concentrations. All the complexes show only residual molar conductance values (11-19 ohm^{-1} cm^2 mol^{-1}) and hence they may be considered non-electrolytes [28,29]. This implies that both the two chloride anions associated with these complexes are present inside the coordination sphere. The electronic and magnetic data are given in Table 6.3. The UV-Visible spectrum of the ligand exhibited bands at 30390 cm^{-1} and 33245 cm^{-1} corresponding to n $\rightarrow \pi^*$ and $\pi \rightarrow \pi^*$ transitions, respectively. The electronic spectra of Co(II) complex exhibits three bands around 9000 cm^{-1} [$^4T_{1g}(F) \rightarrow {}^4T_{2g}(F)$ (ϑ_1)], 18500 cm^{-1} [$^4T_{1g}(F) \rightarrow {}^4A_{2g}(F)$ (ϑ_2)] and 20400 cm^{-1} attributable to [$^4T_{1g}(F) \rightarrow {}^4T_{1g}(P)$ (ϑ_3)], respectively, characteristic of octahedral geometry [30,31]. The octahedral geometry of Co(II) complex also supports ϑ_2/ϑ_1 (2.02) values [32]. The Racah interelectronic repulsion parameter (B) value for Co(II) complex was found to be 756 cm^{-1} which is lower than the free ion value (B^1= 971 cm^{-1}) indicating a good overlap of the orbitals involved [33]. Further, the nephelauxetic effect parameter ($\beta = B/B^1$) value (0.78) is less than one suggesting that M-L bonds are covalent in character. The Ni(II) complex exhibits three peaks in the regions 9800, 15900 and 25800 cm^{-1}. These peaks have been attributed, respectively to the transitions $^3A_{2g}(F) \rightarrow {}^3T_{2g}(F)$, $^3A_{2g}(F) \rightarrow {}^3T_{1g}(F)$ and $^3A_{2g}(F) \rightarrow {}^3T_{1g}(P)$ of octahedral geometry [34-36]. The value ϑ_2/ϑ_1 (1.61) further supports octahedral geometry. The values of B (820 cm^{-1}) and β (0.80) observed for Ni(II) complex is indicative of the orbital overlap and M-L bonds are covalent in character [32]. The Cu(II) complex reveals a peak at 18351 cm^{-1} ($^2B_{1g} \rightarrow {}^2B_{2g}$) and a shoulder on the lower energy side at 13825 cm^{-1} ($^2B_{1g} \rightarrow {}^2E_g$), respectively indicates the distorted octahedral geometry around Cu(II) ion [37]. Zn(II) and Cd(II) complexes show no bands in the visible region as expected for d^{10} system and have a peak at around 28500 cm^{-1} due to charge transfer. The complexes have been assigned octahedral geometry for [Zn(II)] and tetrahedral geometry for [Cd(II)] [38,39] in conformity with analytical, conductance and infrared spectral data. Pd(II) complex shows three peaks at 18700 ($^1A_{1g} \rightarrow {}^1A_{2g}$), 21500 ($^1A_{1g} \rightarrow {}^1B_{1g}$) and 24850 cm^{-1} ($^1A_{1g} \rightarrow {}^1E_g$) where these transitions are characteristic of square-planar geometry [40]. Further, the band at 28000 cm^{-1} is due to charge transfer. Further, the ϑ_2/ϑ_1 value

observed for the complex is 1.14 which also supports the square-planar geometry [41]. The experimental magnetic moment (μ_{eff}) values for Co(II) and Ni(II) complexes are 4.95, 3.22 B.M. respectively, these values also suggest octahedral arrangement [42-47]. The magnetic moment value of Cu(II) complex is observed at 1.90 B.M, which indicates distorted octahedral geometry [48]. The complexes Zn(II), Cd(II) and Pd(II) are diamagnetic. The ESR studies are performed in order to identify the number of unpaired electrons and the type of bonds between ligand and metal ion of Cu(II) complexes. The EPR parameters are listed in Table 6.4 and Fig. 6.1. The ESR spectrum of Cu(II) complex in solid state was recorded at room temperature and shows two bands, one of small intensity towards low field and another one of large intensity towards high field. Based on these bands, the values of $g_{\parallel}$ and $g_{\perp}$ have been calculated [49]. From the results, $g_{\parallel}$ = 2.24 and the other to $g_{\perp} = 2.05$. i.e. $g_{\parallel} > g_{\perp}$, pointing out that metal ion contains an unpaired electron in its $d_{x^2-y^2}$ orbital, and suggests a tetragonal distortion around Cu(II) ions [50]. Kivelson and Neimann [51] showed that $g_{\parallel} > 2.3$ for ionic environment and < 2.3 for covalent compounds. The data presented in Table 6.4 showed that $g_{\parallel}$ obtained for present complex is less than 2.3 indicating the covalent character of M-L band. According to Hathaway and Billing [52], if G value is larger than 4, the exchange interaction is negligible, whereas if its value is less than 4 there is considerable interaction in solid complexes. In the present case, G is found to be greater than 4, thus ruling out solid state exchange interactions between copper centers. Further comparison of $K^2_{\parallel}$ and $K^2_{\perp}$, the observed $K^2_{\parallel}$ value is (0.603) greater than the value of $K^2_{\perp}$(0.484) indicate out of plane pi-bonded [33] complex. The spin-orbit coupling constant (λ) was calculated using the relation.

$$g_{\parallel} = [2 - (8\,\lambda/10\,Dq)]$$

The λ value for Cu(II) complex which is –499 cm^{-1} was found to be much lower than free ion value λ_0 (–828 cm^{-1}) which also supports covalent character of M-L bond. The ^1H and ^{13}C NMR spectra of the ligand and its metal complexes are shown in Fig.s 6.2-6.4. In ^1H NMR spectra of the ligand, the carboxylic acid attached to O-H proton showed a signal at 12.93 ppm. In the complexes, the O-H proton showed the signals around 12.82-12.07 ppm. The signal for azomethine CH proton appeared at 8.72 ppm. The signal due to the proton of NH_2 attached to the pyridine ring was observed at 7.38 ppm as a singlet. In the spectra of complexes, the azomethine CH and NH_2 protons

appeared in the range of 8.74-8.61 ppm (CH=N) and 7.33-7.28 ppm (NH_2), respectively. ^{13}C NMR spectra of the ligand showed chemical shift values at 167.49, 163.88 and 158.44 ppm due to carboxylic acid (C=O), (C=N) and (C-NH_2), respectively. The aromatic carbons were observed in the range 158.44-112.34 ppm, respectively.

Table 6.2 Infrared absorption frequencies (cm^{-1}) of ligand and its complexes

Compound	**υ(N–H)**	**υ(C=N) azomethine**	**υ(C=N) (py)**	**υ(C=O) carboxylic acid**	**υ(M–Cl)**	**υ(M–N)**
Co(II)	3371	1604	1564	1699	321	493
Ni(II)	3389	1663	1569	1704	275	520
Cu(II)	3390	1590	1562	1703	284	501
Zn(II)	3384	1592	1571	1697	315	481
Pd(II)	3401	1608	1570	1705	292	478
Cd(II)	3395	1618	1563	1705	283	490
ANABZA	3420	1629	1567	1701	-	-

Table 6.3 Electronic spectral data, ligand field parameters and magnetic data of the complexes

Complexes	Frequencies (cm^{-1})	Assignments	μ_{eff} (B.M.)	$\vartheta_2 / \vartheta_1$	10 Dq (cm^{-1})	B (cm^{-1})	β	Geometry
Co(II)	9000	$^4T_{1g}(F) \rightarrow {}^4T_{2g}(F)$ (υ_1)	4.95	2.02	9250	756	0.78	Octahedral
	18500	$^4T_{1g}(F) \rightarrow {}^4A_{2g}(F)$ (υ_2)						
	20400	$^4T_{1g}(F) \rightarrow {}^4T_{1g}(P)$ (υ_3)						
Ni(II)	9800	$^3A_{2g}(F) \rightarrow {}^3T_{2g}(F)$ (υ_1)	3.22	1.61	9800	820	0.80	Octahedral
	15900	$^3A_{2g}(F) \rightarrow {}^3T_{1g}(F)$ (υ_2)						
	25800	$^3A_{2g}(F) \rightarrow {}^3T_{1g}(P)$ (υ_3)						
Cu(II)	13825	$^2B_{1g} \rightarrow {}^2E_g$	1.90	-	-	-	-	Distorted
	18351	$^2B_{1g} \rightarrow {}^2B_{2g}$						octahedral
Zn(II)	-	-	Diamagnetic	-	-	-		Octahedral
Pd(II)	18700	$^1A_{1g} \rightarrow {}^1A_{2g}$	Diamagnetic	1.14	-	-	-	Square-planar
	21500	$^1A_{1g} \rightarrow {}^1B_{1g}$						
	24855	$^1A_{1g} \rightarrow {}^1E_g$						
	28000	Charge transfer						
Cd(II)	-	-	Diamagnetic	-	-	-		Tetrahedral

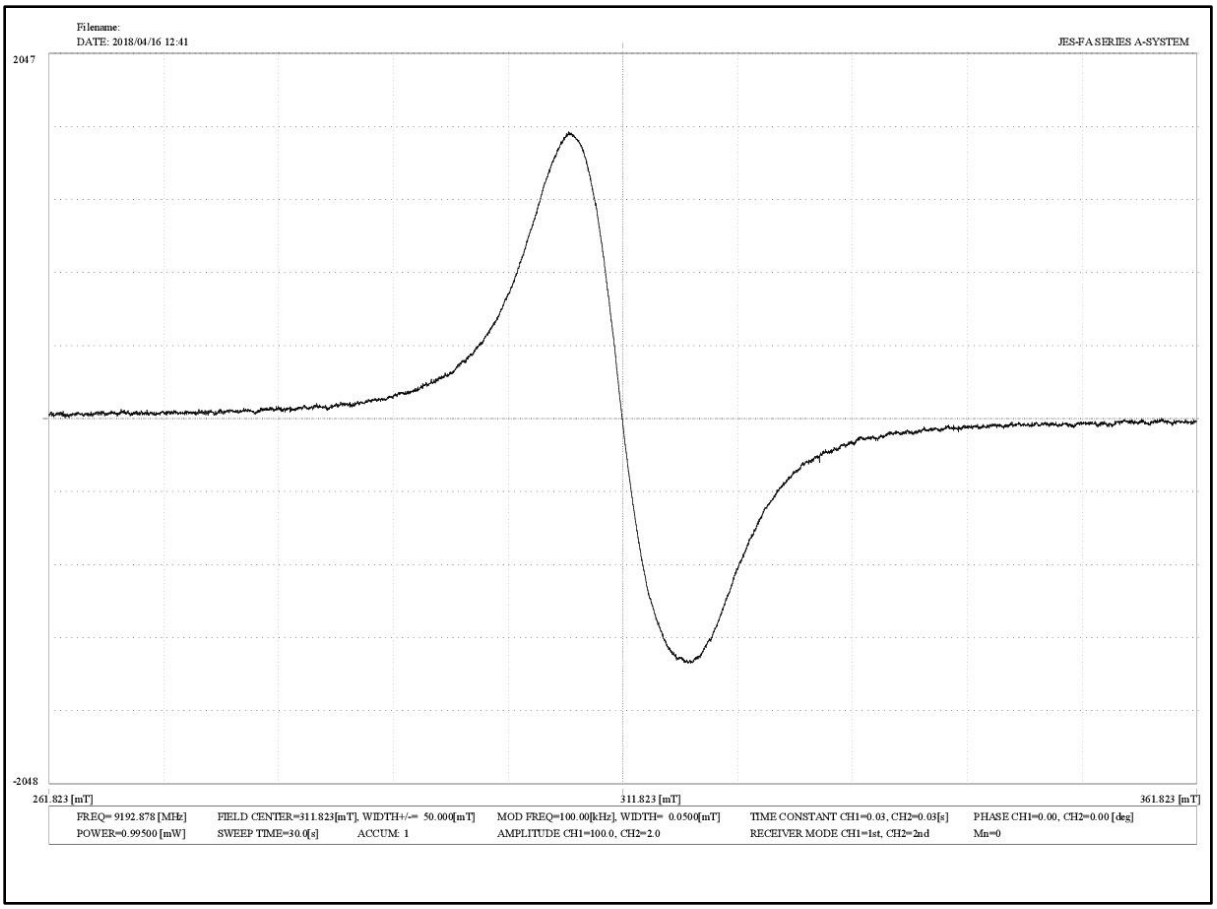

Fig. 6.1 ESR spectrum of Cu(II) complex.

Table 6.4 ESR spectral data of Cu(II) complex

Complex	$g_{\parallel}$	$g_{\perp}$	**|g|**	**G**	$A_{\parallel} \times 10^5$ **(cm^{-1})**	$K^2_{\parallel}$	$K^2_{\perp}$	**-λ (cm^{-1})**
Cu(II)	2.22	2.05	2.11	4.56	465	0.534	0.468	442

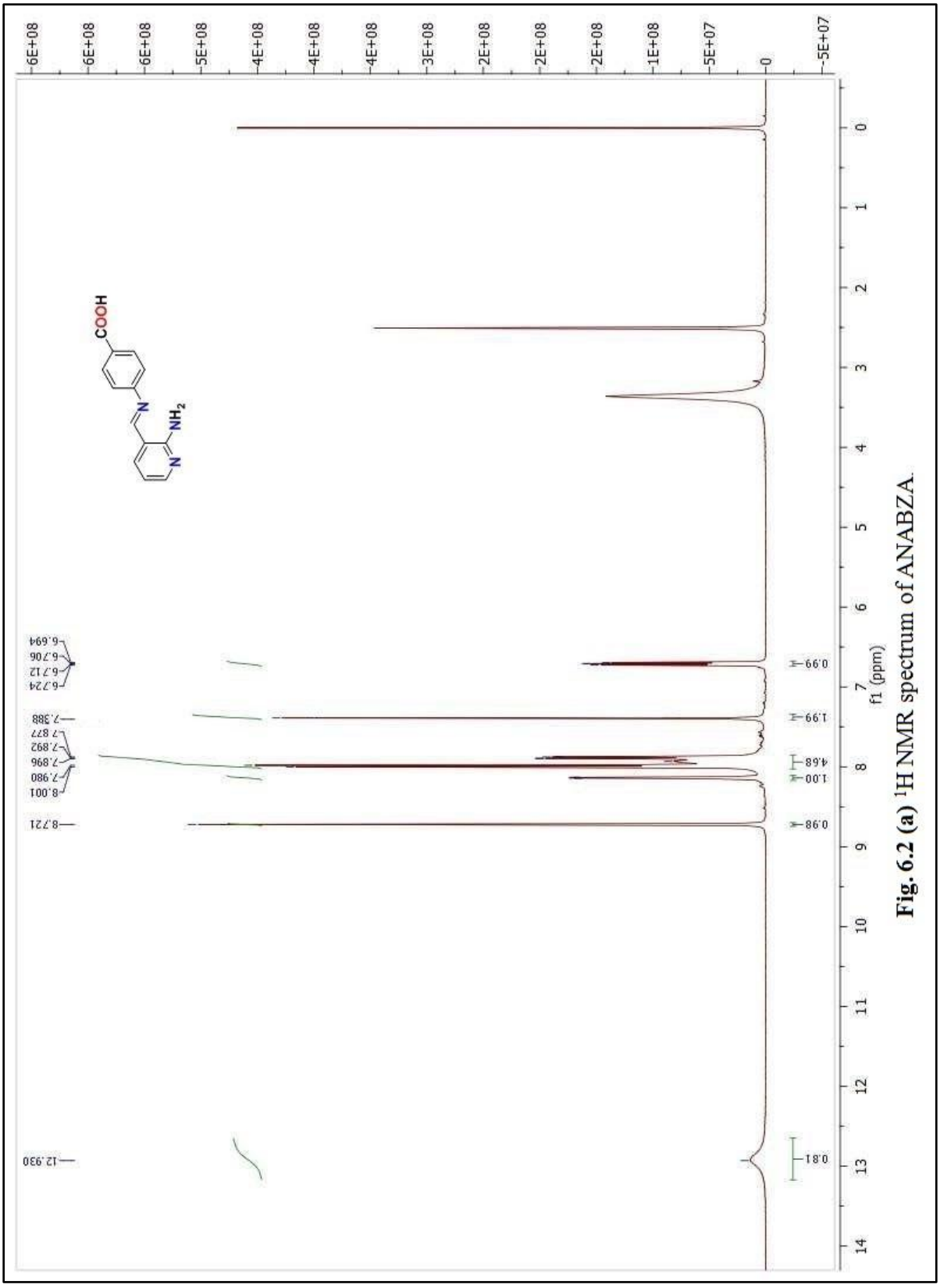

Fig. 6.2 (a) ^{1}H NMR spectrum of ANABZA.

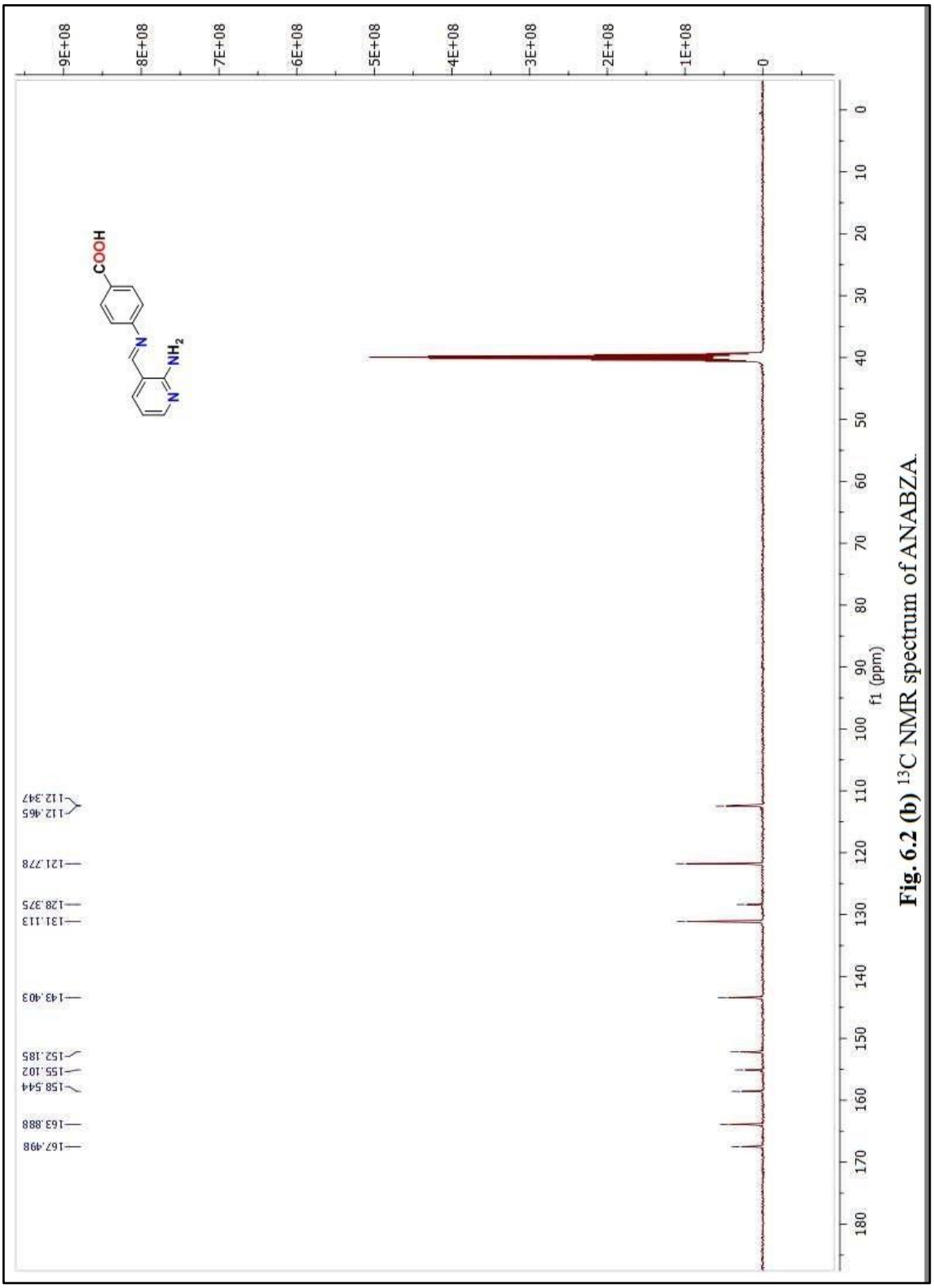

Fig. 6.2 (b) ^{13}C NMR spectrum of ANABZA.

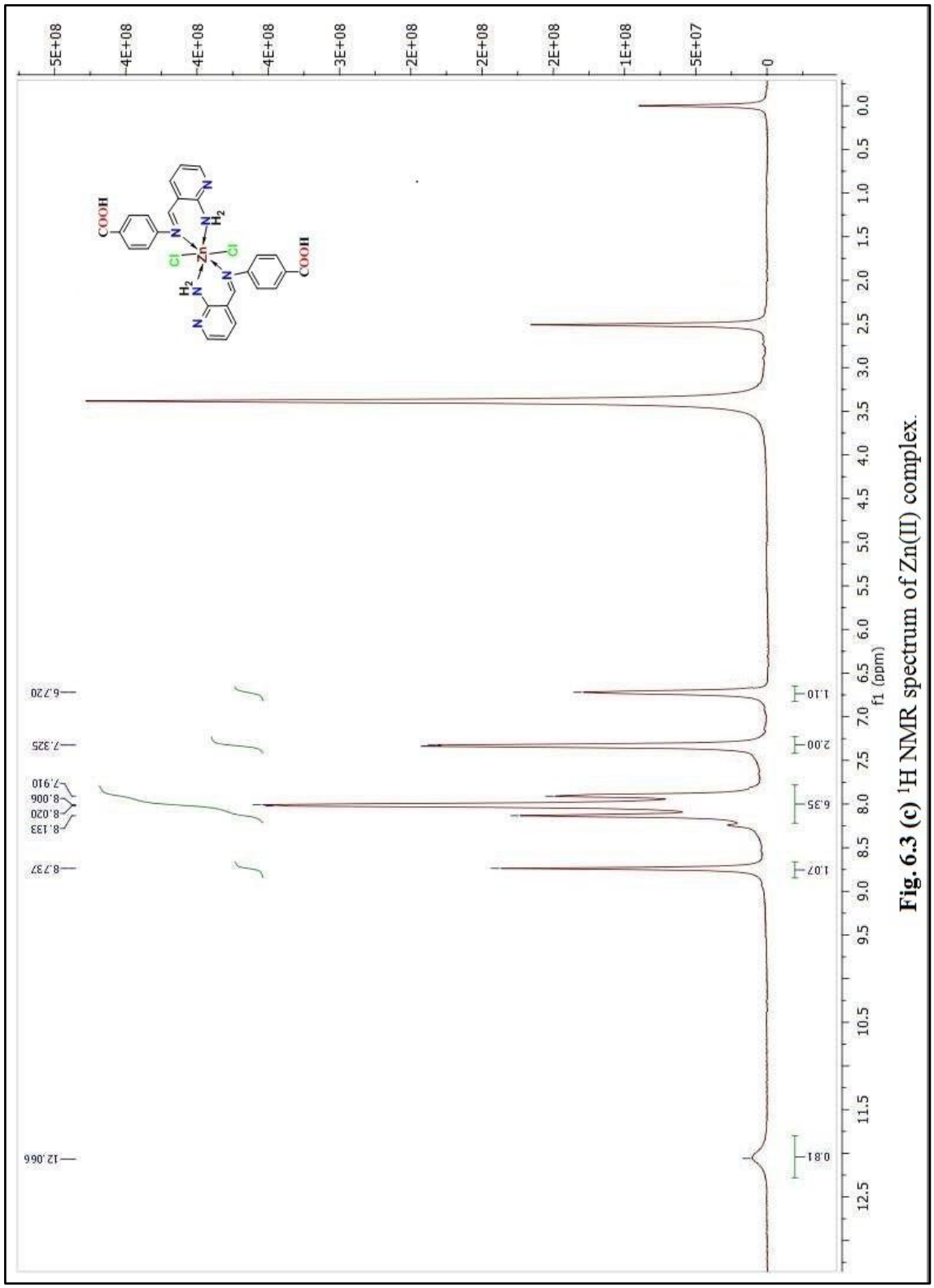

Fig. 6.3 (c) ^{1}H NMR spectrum of Zn(II) complex.

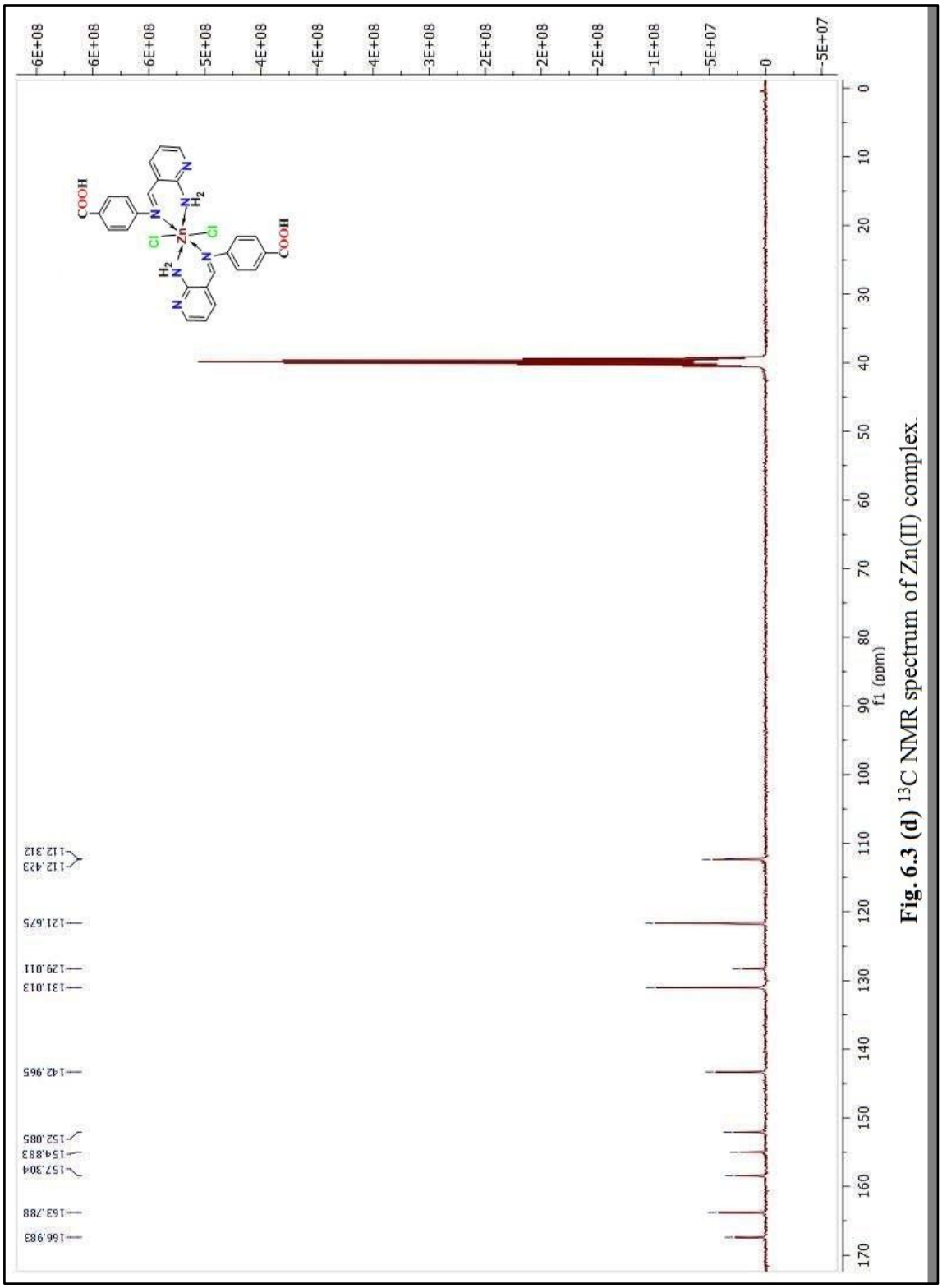

Fig. 6.3 (d) ^{13}C NMR spectrum of Zn(II) complex.

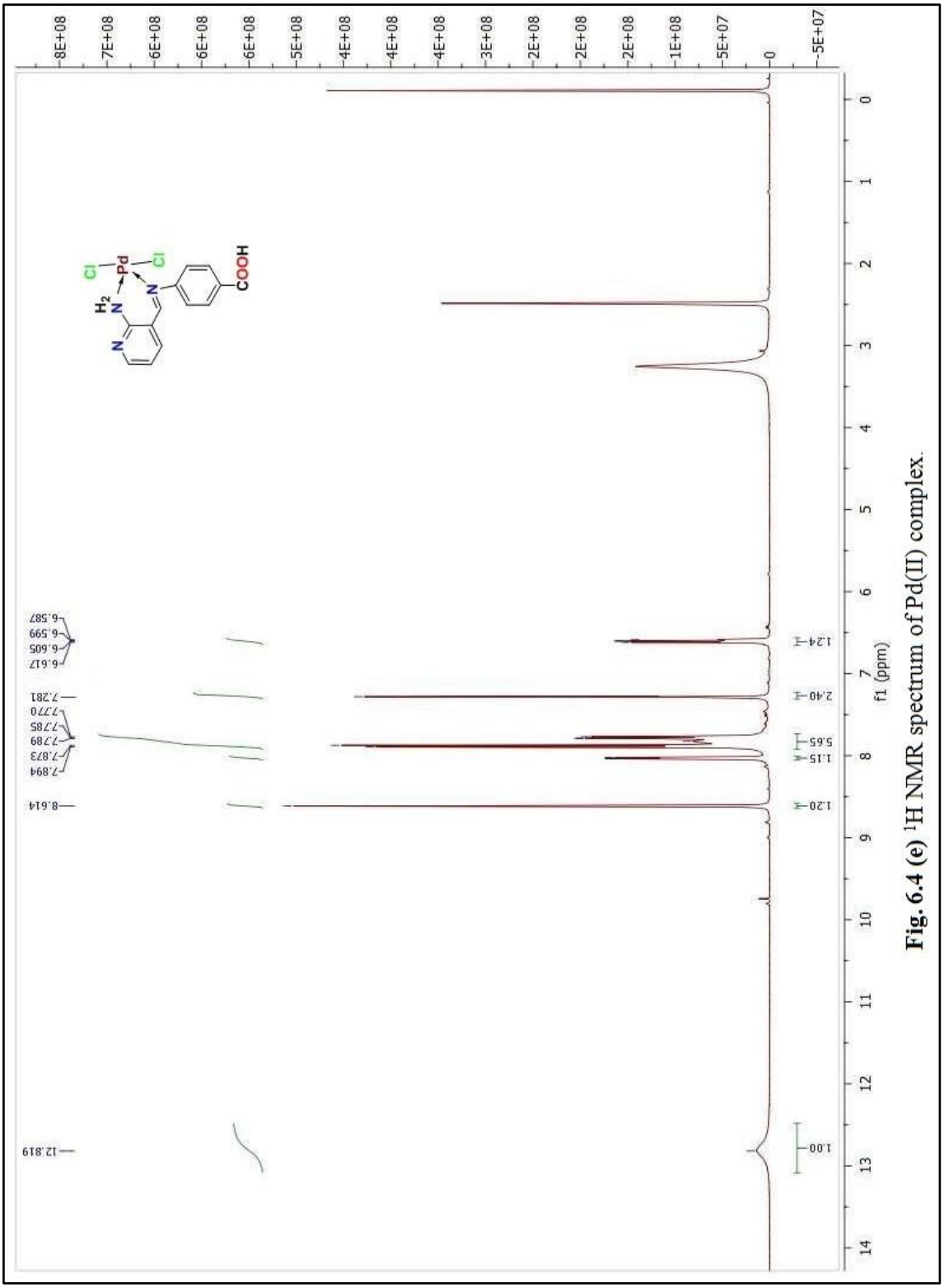

Fig. 6.4 (e) ^{1}H NMR spectrum of Pd(II) complex.

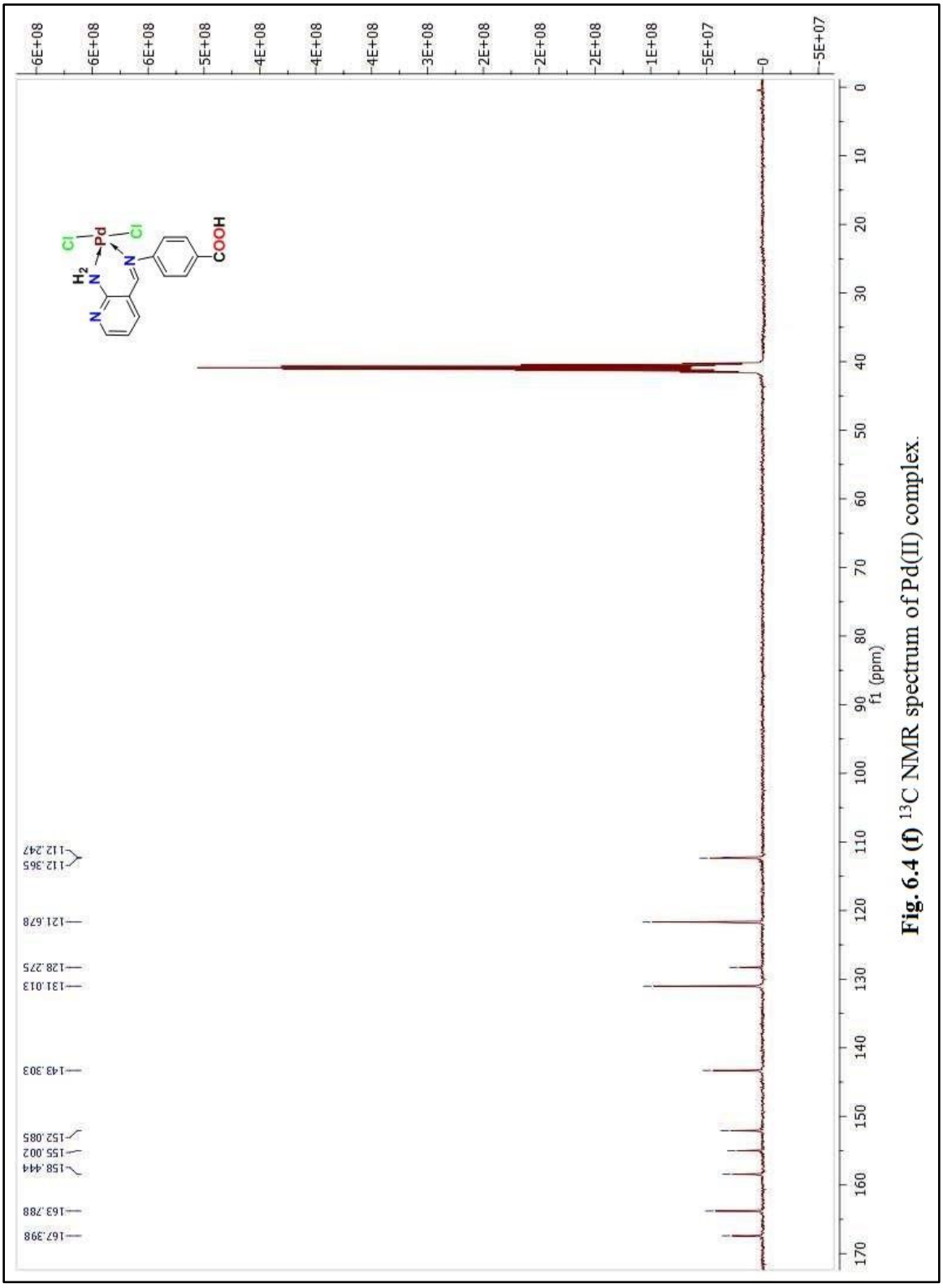

Fig. 6.4 (f) ^{13}C NMR spectrum of Pd(II) complex.

6.2 DFT Computations

The optimized molecular geometry for the ligand and its metal complexes are shown in Fig. 6.5. The results of bond angles, bond lengths and dihedral angles are

presented in Tables 6.5 and 6.6. On optimization of geometry, the observed global minimum energy of the compounds are -816.95688 Hartree (ANABZA), -2698.19907 Hartree [Co(II)], -2723.30339 Hartree [Ni(II)], -2749.76705 Hartree [Cu(II)], -2779.56640 Hartree [Zn(II)], -1865.00019 Hartree [Pd(II)] and -1904.886800 Hartree [Cd(II)] complexes, respectively.

Molecular electronic properties i.e. electron affinity (A), ionization potential (I), chemical potential (μ), global hardness (η), global electrophilicity power (ω) of ligand and its metal complexes were obtained from frontier molecular orbital energies comprising of HOMO and LUMO.

HOMO and LUMO are known as frontier molecular orbitals. They are important in quantum chemistry, as they determine the molecular reactivity of conjugated systems [53] and the ability of a molecule to absorb electromagnetic radiation. HOMO plays the role of an electron donor, whereas LUMO acts as electron acceptor [54,55] The results are presented in Table 6.7 and illustrated in Fig. 6.6. The complexes under investigation, the frontier molecular orbital energy gap were found in the order ANABZA > Zn(II) > Co(II) > Pd(II) > Ni(II) > Cu(II) > Pd(II). Generally, complexes with a small frontier orbital gap are readily polarizable and normally exhibit high chemical reactivity and low kinetic stability [56-58]. The frontier molecular orbital gap of metal complexes are small compared to the free ligand, hence the complexes are more polarizable than the ligand (Table 6.7). The chemical potential (μ) for the compounds being investigated are -7.31717 [(Co(II)], -6.71403 [(Ni(II))], -5.25906 [(Cu(II)], -6.76342 [(Zn(II)], -4.34001 [(Pd(II)] and -6.18355 [(Cd(II)], complexes respectively, where the negative values indicate the complexes are stable [59].

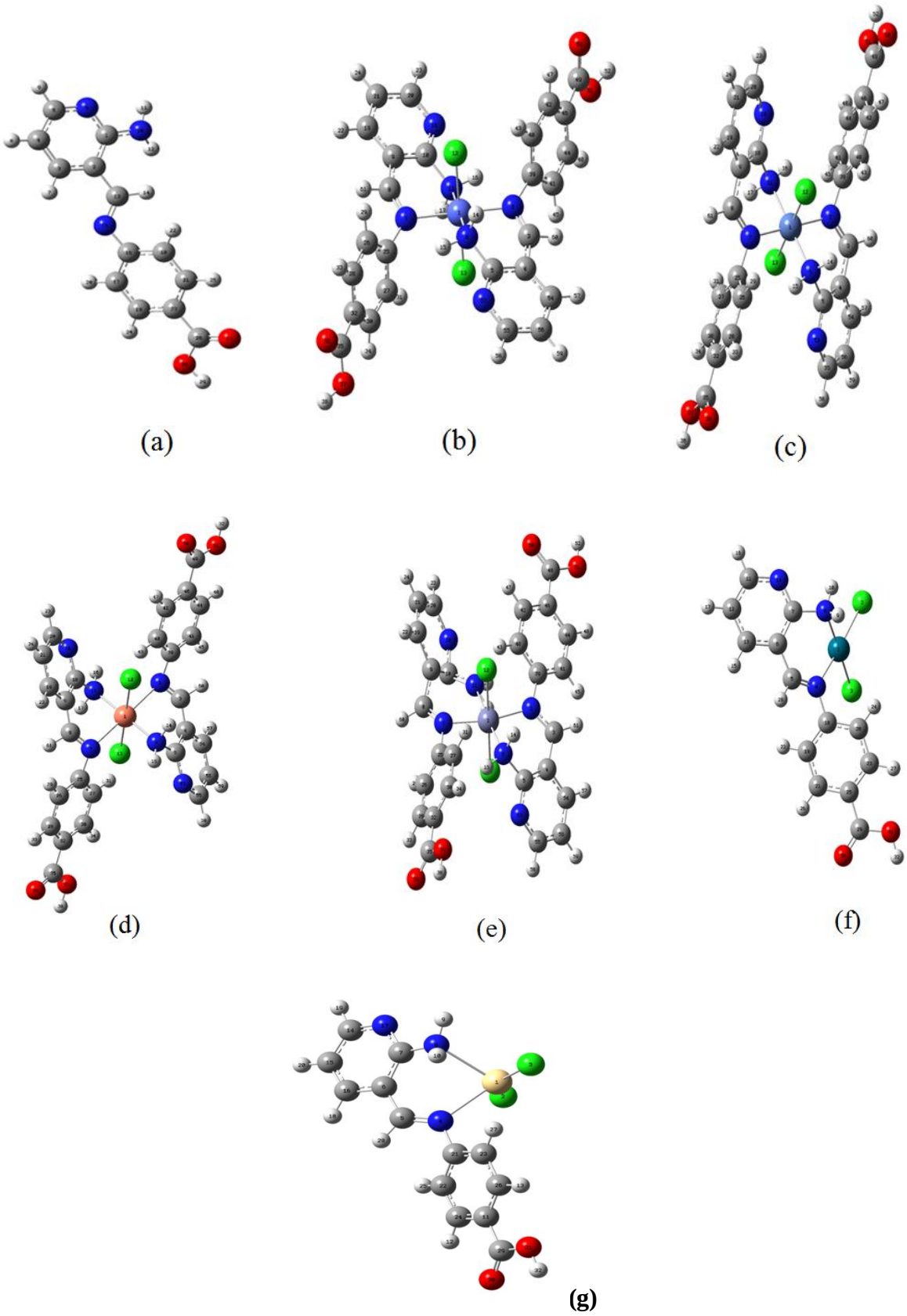

Fig. 6.5 Optimized structures along with atomic numbering of **(a)** ANABZA **(b)** Co(II) complex, **(c)** Ni(II) complex **(d)** Cu(II) complex, **(e)** Zn(II) complex, **(f)** Pd(II) complex and **(g)** Cd(II) complex.

Table 6.5 Optimized geometrical parameters of the ligand ANABZA

Bond length	Value (Å)	Bond angle	Value (°)	Dihedral angle	Value (°)
C1-C2	1.42122	C1-C2-C3	117.21480	C1-C2-C3-C4	−1.75184
C2-C3	1.39995	C2-C3-C4	120.27239	C2-C3-C4-C5	−0.45624
C3-C4	1.38588	C3-C4-C5	117.63683	C3-C4-C5-N6	1.91374
C4-C5	1.39556	C4-C5-N6	123.85376	C4-C5-C6-C1	−0.91487
C5-N6	1.33104	C5-N6-C1	118.55648	C5-N6-C1-C2	−1.54473
N6-C1	1.34098	N6-C1-C2	122.39875	N6-C1-C2-C3	2.84768
C3-H7	1.08346	C1-C2-C13	121.81121	C2-C3-C4-H7	−178.91721
C4-H8	1.08244	C2-C13-H14	116.88223	C3-C4-C5-H8	−179.00745
C5-H9	1.08661	C2-C13-N15	122.70621	C4-C5-N6-H9	179.66909
C1-N10	1.37990	C13-N15-C16	120.12913	C2-C1-N6-N10	178.14106
N10-H11	1.00981	N15-C16-C17	118.08140	C2-C6-N10-H12	31.02831
N10-H12	1.00683	C16-C17-C19	120.56235	N6-C1-N10-H11	−10.65379
C2-C13	1.46032	C17-C19-C23	120.28755	C1-C2-C13-N15	−169.38350
C13-H14	1.09707	C19-C23-C21	119.32780	C2-C13-N15-C16	−174.81323
C13-N15	1.28063	C23-C21-C18	120.51530	N15-C26-C17-C19	−179.71188
N15-C16	1.39967	C21-C18-C16	120.30906	C16-C17-C19-C23	1.51244
C16-C17	1.40447	C18-C16-C17	118.95816	C17-C19-C23-C21	0.12311
C17-C19	1.38617	C16-C17-H20	118.56143	C19-C23-C21-C18	−0.82620
C19-C23	1.40246	C17-C19-H24	120.10095	C23-C2-C18-C16	−0.10306
C23-C21	1.39970	C23-C21-H25	118.76452	C21-C18-C16-C17	1.70937
C21-C18	1.38711	C21-C18-H22	119.96215	C18-C16-C17-C19	−2.41612
C18−C16	1.40679	C19-C23-C26	122.40065	C16-C17-C19-H20	−179.35360
C17−H20	1.08330	C23-C26-O27	125.22327	C17-C19-C23-H24	179.43723
C19−H24	1.08215	C23-C26-O28	113.07488	C23-C21-C18-H25	179.45454
C21−H25	1.08323	C26-O28-H29	106.54015	C21-C18-C16-H22	177.90932
C18−H22	1.08387	O27-C26-O28	121.70174	C19-C2-C26-O28	0.62241
C23−C26	1.48157	H14-C13-N15	120.40763	C2-C23-C26-O27	−0.26012
C26-O27	1.21031	C2-C1-N10	122.49422	C23-C26-O28-H29	−179.96170
C26-O28	1.35995	C1-N10-H12	119.07478	-	-
O28-H29	0.96819	C1-N10-H11	113.62942	-	-

Table 6.6 Selected bond lengths and bond angles of the complexes

Co(II)		Ni(II)		Cu(II)		Zn(II)		Pd(II)		Cd(II)	
Bond length	**Value (Å)**	**Bond length**	**Value (Å)**	**Bond length**	**Value (Å)**	**Bond length**	**Value (Å)**	**Bond length**	**Value (Å)**	**Bond length**	**Value (Å)**
Co1-N2	2.03218	Ni1-N2	2.30606	Cu1-N2	2.35000	Zn1-N2	1.91254	Pd1-Cl2	2.35353	Cd1-Cl2	2.40394
N2-C3	1.25976	N2-C3	1.27349	N2-C3	1.11398	N2-C3	1.30598	Pd1-Cl3	2.35015	Cd-Cl3	2.43548
C3-C4	1.44058	C3-C4	1.46220	C3-C4	1.37670	C3-C4	1.46406	Pd1-N4	2.07926	Cd1-N4	2.45793
C4-C5	1.42907	C4-C5	1.42019	C4-C5	1.43970	C4-C5	1.41436	N4-C5	1.31025	N4-C5	1.30728
C5-N6	1.47725	C5-N6	1.45039	C5-N6	1.46491	C5—N6	1.54326	C5-C6	1.46658	C5-C6	1.46379
N6-Co1	2.00350	N6-Ni1	1.96345	N6- Cu1	1.92265	N6-Zn1	2.06224	C6-C7	1.42277	C6-C7	1.42981
Co1-N2	2.03915	Ni1—N7	2.31058	N7-Cu1	2.33000	N7- Zn1	2.45651	C7-N8	1.44905	C7-N8	1.41537
N7-C8	1.26117	N7-C8	1.27292	N7-C8	1.11757	N7-C8	1.52726	N8-Pd1	2.10592	N8-Cd1	2.46608
C8-C9	1.44408	C8-C9	1.46166	C8-C9	1.37729	C8-C9	1.61935	Bond angle	Value (°)	Bond angle	Value (°)
C9-C10	1.42799	C9-C10	1.42012	C9-C10	1.43970	C9-C10	1.45384	Cl2-Pd1-Cl3	93.43178	Cl2-Cd1-Cl3	148.69442
C10-N11	1.48072	C10-N11	1.45018	C10-N11	1.46706	C10-N11	1.48986	Cl3-Pd1-N4	92.73289	Cl3-Cd1-N4	104.60784
C11-Co1	2.00790	N11-Ni1	1.96451	N11- Cu1	1.93074	N11-Zn1	1.92163	Pd1-N4-C5	121.26035	Cd1-N4-C5	121.92251
Co1-Cl12	2.27016	Ni1-Cl12	2.29934	Cu1-Cl12	2.16467	Zn1-Cll2	2.29848	N4-C5-C6	125.87500	N4-C5-C6	126.03368
Co1- Cl13	2.28411	Ni1-Cl13	2.29944	Cu1-Cl13	2.16388	Zn1-Cll3	2.28958	C5-C6-C7	124.58417	C5-C6-C7	125.60388
Bond angle	Value (°)	Bond angle	Value (°)	Bond angle	Value (°)	Bond angle	Value (°)	C6-C7-N8	120.56767	C6-C7-N8	122.06983
Co1-N2-C3	111.64135	Ni1-N2-C3	119.58391	Cu1-N2-C3	100.05199	Zn1-N2-C3	123.34310	C7-N8-Pd1	112.52592	C7-N8-Cd1	112.57241
N2-C3-C4	142.99340	N2-C3-C4	126.55903	N2-C3-C4	138.89470	N2-C3-C4	123.78851	N8-Pd1-Cl2	85.61200	N8-Cd1-Cl2	114.37103
C3-C4-C5	115.68172	C3-C4-C5	124.07261	C3-C4-C5	123.35645	C3-C4-C5	128.93135	N8-Pd1-N4	88.21715	N8-Cd1-N4	73.41523
C4-C5-C6	119.35257	C4-C5-N6	121.01749	C4-C5-N6	121.34667	C4-C5-C6	121.95938				

C5-C6-Co1	118.62623	C5-N6-Ni1	119.20823	Cu1-N7-C8	100.29560	C5-N6-Zn1	109.94615				
Co1-N7-C8	111.65681	Ni1-N7-C8	119.45140	N7-C8-C9	138.75878	Zn1-N7-C8	99.63015				
N7-C8-C9	143.07162	N7-C8-C9	126.62006	C8-C9-C10	123.21746	N7-C8-C9	134.60675				
C8-C9-C10	115.57772	C8-C9-C10	123.92696	C9-C10-N11	121.23341	N8-C9-C10	98.91166				
C9-C10-N11	119.19665	C9-C10-N11	120.95988	C10-N11-Cu1	101.77903	C9-C10-N11	120.17000				
C10-N11-Co1	119.30108	C10-N11-Ni1	119.11235	N2-Cu1-Cl12	76.70180	C10-C11-Zn1	119.84187				
N2- Co1-Cl12	91.87577	N2- Ni1-Cl12	91.59393	N6-Cu1-Cl12	92.18965	N2-Zn1-Cl12	85.26809				
N6-Co1-Cl12	86.81401	N6- Ni1-Cl12	85.80806	N7-Cu1-Cl13	77.89497	N7-Zn1-Cl12	83.27208				
N7-Co1-Cl13	91.57108	N7-Ni1-Cl13	91.32768	N11-Cu1-Cl13	91.76743	N6-Zn1-Cl13	93.94000				
N11-Co1-Cl13	87.35005	N11-Ni1-Cl13	85.84111	-	-	N11- Zn-Cl13	81.34695				

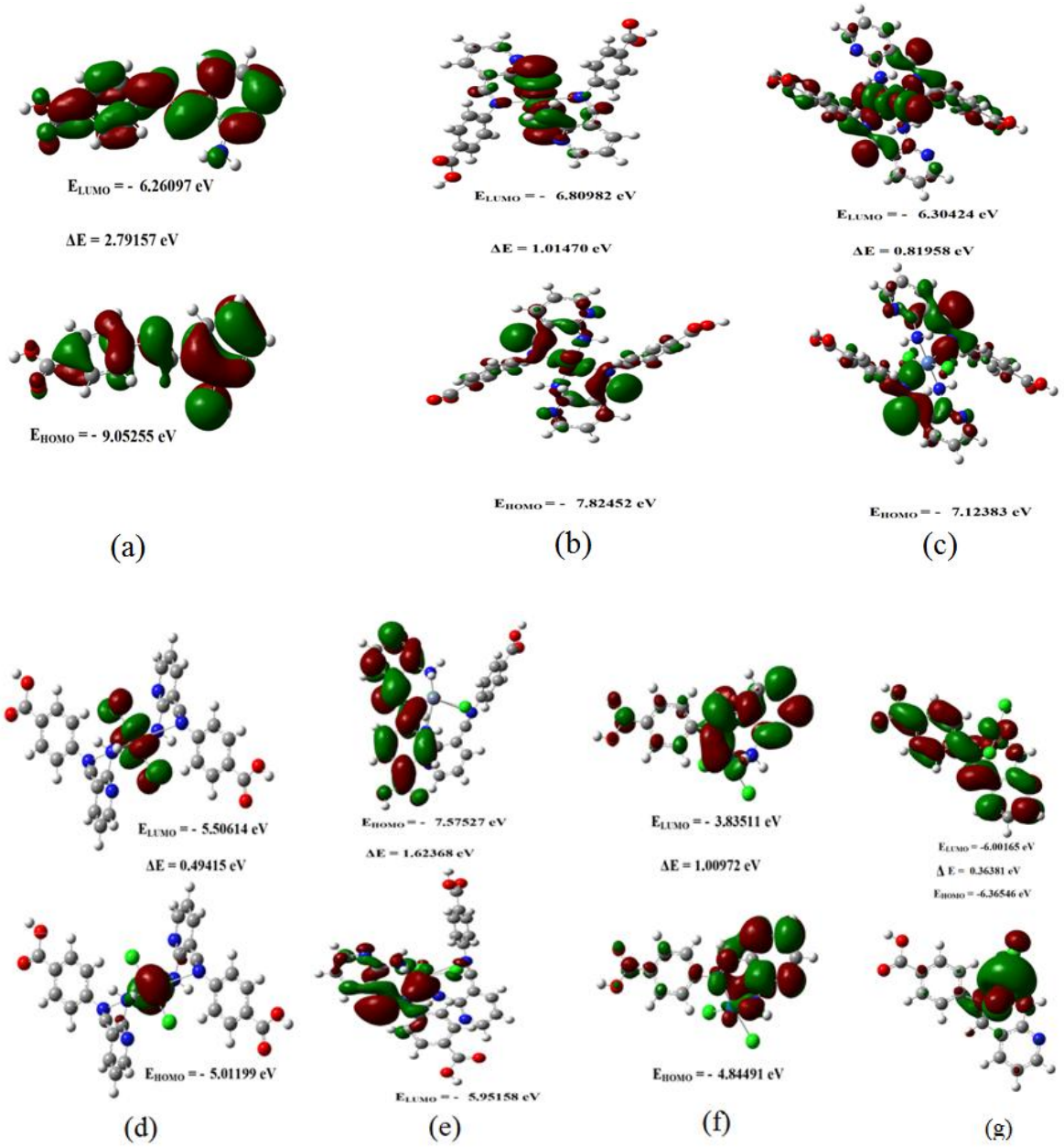

Fig. 6.6 Frontier molecular orbitals of **(a)** ANABZA, **(b)** Co(II), **(c)** Ni(II), **(d)** Cu(II), **(e)** Zn(II), **(f)** Pd(II) and **(g)** Cd(II) metal complexes.

Table 6.7 Frontier molecular orbital parameters of ligand and its metal complexes, values are expressed in (**eV**)

Frontier molecular Orbital parameter	Co(II)	Ni(II)	Cu(II)	Zn(II)	Pd(II)	Cd(II)	ANABZA
HOMO energy	-7.82452	-7.12383	-5.50614	-7.57527	-4.84491	-6.36546	-9.05255
LUMO energy	-6.80982	-6.30424	-5.01199	-5.95158	-3.83511	-6.00165	-6.26097
Frontier molecular orbital energy gap	1.01470	0.81958	0.49415	1.62368	1.00979	0.36381	2.79157
Ionization energy (I)	7.82452	7.12383	5.50614	7.57527	4.84491	6.36546	9.05255
Electron affinity (A)	6.80982	6.30424	5.01199	5.95158	3.83511	6.00165	6.26097
Global hardness (η)	0.50735	0.40979	0.24707	0.81184	0.504896	0.18190	1.39578
Chemical potential (μ)	-7.31717	-6.71403	-5.25906	-6.76342	-4.34001	-6.18355	-7.65676
Global electrophilicity power (ω)	52.76531	55.00158	55.96903	28.17294	18.65302	105.09961	21.00117

6.2.1 Non-linear optical (NLO) behaviour

For the most part, density functional theory based approaches are of considerable importance for investigating new non-linear molecular systems [60]. Theoretical approaches have been utilized for determination of polarizability (α_t), hyperpolarizabilities (β_t), total dipole moments (μ_t) and anisotropy of polarizability ($\Delta\alpha$) using density functional theory based on finite field approach and following Buckingham's definitions [61]. This method can reduce the cost and avoid synthesis work for measuring NLO properties. Generally, α_t and β_t were estimated for compounds in the presence of an applied electric field in order to predict cross section of various scattering process, molecular interactions and NLO properties of the system [62,63]. β_t is a third rank tensor hence, it was measured as a 3 x 3 x 3 matrix. From the basis of Kleinman symmetry [64], all the twenty seven components were condensed to ten components indicated as β_{xxx}, β_{xxy}, β_{xyy}, β_{yyy}, β_{xxz}, β_{xyz}, β_{yyz}, β_{xzz}, β_{yzz}, β_{zzz}. So, by using these components X,Y, Z we can calculate the μ_t, α_t and β_{tot} through the following equations.

$$\mu = \mu^2_x + \mu^2_y + \mu^2_z \qquad (1)$$

$$\alpha_o = \frac{\alpha_{xx} + \alpha_{yy} + \alpha_{zz}}{3} \quad (2)$$

$$\Delta\alpha = 2^{-1/2}[(\alpha_{xx} - \alpha_{yy})^2 + (\alpha_{yy} - \alpha_{xx})^2 + 6\alpha^2{}_{xx}]^{1/2} \quad (3)$$

$$\beta = (\beta^2{}_x + \beta^2{}_y + \beta^2{}_z)^{1/2} \quad (4)$$

$$\beta_x = \beta_{xxx} + \beta_{xyy} + \beta_{xzz} \quad (5)$$

$$\beta_y = \beta_{yyy} + \beta_{xxy} + \beta_{yzz} \quad (6)$$

$$\beta_z = \beta_{zzz} + \beta_{xxz} + \beta_{yyz} \quad (7)$$

Here, α_t, β_t and μ_t were calculated using DFT approach and the results are given in Table 6.8. It is a usual practice to determine the NLO behavior of compounds by comparing its μ_t and β_t with corresponding values of urea, which are 1.3732 Debye and 0.3728 x 10^{-30} cm^5/esu, respectively. The calculated β_t of the ligand is 16.962 × 10^{-30} cm^5/e.s.u, which is forty five times greater than urea. Hence, the ligand exhibits NLO properties. The complexes Ni(II), Cu(II) and Zn(II) showed more first order hyperpolarizability values compared to free ligand. The remaining complexes Co(II), Zn(II) and Cd(II) showed lower first order hyperpolarizability values than the ligand. The non-linear optical activity was associated with the intra-molecular charge transfer, obtained from the electron cloud movement, through resonance [65]. Hence, the ligand and its metal complexes Ni(II), Cu(II) and Zn(II) are strong ones for the expansion of NLO materials. The components of first order hyperpolarizability were also helpful to understand charge delocalization in the compounds.

Table 6.8 The values of dipole moment μ_t (in Debye); polarizability α_t and first order hyperpolarizability β_t (in 10^{-30}cm^5/e.s.u) of ligand and its metal complexes

Type of component	Co(II)	Ni(II)	Cu(II)	Zn(II)	Pd(II)	Cd(II)	ANABZA
β_{xxx}	35.1312	1412.5682	-437.8606	116.6001	-659.5690	228.25241	-2215.2291
β_{xxy}	-87.0246	-1177.8671	-241.1182	19.3886	737.6800	383.59359	-3.2906
β_{xyy}	39.0115	-624.5487	-1023.0287	-39.9696	51.2647	-214.37560	159.2177
β_{yyy}	-149.7493	-645.5117	-1755.5558	-5.5846	1793.0766	352.05626	-155.2760
β_{xxz}	-34.0008	-308.9618	31.8476	16.1393	-177.4568	-70.94831	-6.5763
β_{xyz}	-14.1808	-14.7839	19.7664	-14.5895	28.5835	-31.93086	-8.3224
β_{yyz}	36.1939	296.8233	447.3902	-9.1699	-114.7129	71.91038	-31.5628
β_{xzz}	0.7827	-37.6109	-16.9262	-8.3271	-127.2958	-26.42828	103.1029
β_{yzz}	0.5283	8.3044	89.1589	-7.4804	84.9524	67.61073	-42.6507
β_{zzz}	0.3429	-34.6800	65.0474	-18.8521	-201.0856	-110.24724	7.4817
β_t	2.141×10^{-30} cm^5/e.s.u	17.399×10^{-30} cm^5/e.s.u	21.347×10^{-30} cm^5/e.s.u	0.7048×10^{-30} cm^5/e.s.u	23.876×10^{-30} cm^5/e.s.u	7.0005×10^{-30} cm^5/e.s.u	16.962×10^{-30} cm^5/e.s.u
μ_x	0.4443	-4.3181	0.8809	-0.0019	-2.0877	-1.9209	1.7981
μ_y	-2.0118	-4.8734	-1.1144	-0.7539	12.0509	7.6770	-0.5068
μz	-1.1451	0.8624	-2.7097	-2.5866	-4.6024	-4.3357	-1.6375

μ_t	2.3571 Debye	6.5681 Debye	3.0595 Debye	2.6943 Debye	13.0676 Debye	9.0236 Debye	2.4848 Debye
α_{xx}	597.2192	576.2061	608.3871	672.9969	364.6869	355.46401	356.8497
α_{xy}	28.7435	-105.6276	-67.3388	17.6290	-25.5022	-32.35211	-4.4959
α_{yy}	545.8433	410.5628	526.1094	591.4939	242.7347	207.35461	170.6526
α_{xz}	-19.4824	22.6534	0.5215	10.0580	8.01807	3.80210	-5.0951
α_{yz}	32.9112	39.5342	-34.6070	-8.2554	23.4425	33.70313	-3.9852
α_{zz}	172.4103	259.2901	280.3167	274.8413	136.4581	139.41245	115.5721
α_t	438.480	286.040	471.5960	513.1060	247.953	234.07333	214.3530

6.3 Biological evaluations

6.3.1 Antimicrobial screening

Microorganisms used in this work were three gram negative bacteria like *Proteus vulgaris*, *Klebsiella pneumoniae* and *Pseudomonas aeruginosa*, two gram positive bacteria like *Staphylococcus aureus* and *Bacillus subtilis* and fungal strains such as *Aspergillus niger*, *Aspergillus flavus*, *Curvularia lunata*, *Rhizoctonia bataticola* and *Candida albicans* by disc diffusion method [66]. Streptomycin and Ketoconazole were chosen as the reference drugs for bacteria and fungi, respectively. The MIC values of the tested compounds and reference drugs were expressed in µg/mL. The results of antibacterial activity are presented in Table 6.9 and of antifungal activity are listed in Table 6.10. The antibacterial activity results revealed that Cu(II) complex exhibited excellent activity against S. *aureus* and *P. vulgaris* strains (MIC: 4.21 and 8.18 µg/mL, respectively) and it is also showed significant activity against *B. subtilis* (MIC: 5.13 µg/mL) and *P. aeruginosa* (MIC: 6.01 µg/mL). The Pd(II) complex exhibited broad spectrum activity against the strains with MIC values of 5.17 µg/mL (S. *aureus*), 7.69 µg/mL (*B. subtilis*), 10.54 µg/mL (*P. vulgaris*), 7.24 µg/mL (*K. pneumoniae*) and 7.25 µg/mL (*P. aeruginosa*), respectively. Moreover, Zn(II) complex against *B. subtilis* (MIC: 11.50 µg/mL), Ni(II) complex against *P. vulgaris* (MIC: 21.01 µg/mL), Cd(II) complex against *B. subtilis* (MIC: 13.89 µg/mL) and Co(II) complex against *P. aeruginosa* (MIC: 10.91 µg/mL) exhibited moderate activity compared to the reference drug. The fungi results showed that Ni(II) and Cu(II) complexes showed potent activity against *A. niger* (MIC = 3.94 µg/mL) and *R. bataticola* (MIC = 6.24 µg/mL), respectively compared to standard Ketoconazole. The Cu(II) and Pd(II) complexes exhibited significant activity against *A. niger* with MIC values of 4.17 and 4.03 µg/mL, respectively. The Co(II), NI(II) and Cu(II) complexes against *C. albicans* showed good activity with MIC values of 7.12, 7.99 and 8.18 µg/mL, respectively. In addition, Ni(II) complex against *A. flavus* (MIC = 10.77 µg/mL) and Zn(II) complex against *C. lunata* (MIC = 6.41 µg/mL) registered moderate activity. The remaining compounds showed poor activity against the tested microorganisms.

Table 6.9 MIC of the synthesized compounds against the growth of bacteria (μM)

Minimum Inhibitory Concentration (μg/mL)					
Compound	***S. aureus***	***B. subtilis***	***P. vulgaris***	***K. pneumoniae***	***P.aeruginosa***
Co(II)	21.87	25.79	>100	30.79	10.91
Ni(II)	18.15	14.35	21.01	>100	24.86
Cu(II)	**4.21**	**5.13**	**8.18**	8.27	**6.01**
Zn(II)	>100	11.50	29.28	31.40	29.63
Pd(II)	**5.17**	**7.69**	**10.54**	**7.24**	**7.25**
Cd(II)	35.46	13.89	>100	17.28	>100
ANABZA	50	>100	42.52	35.33	38.94
Streptomycin	3.42	3.15	6.25	3.15	4.27

Table 6.10 MIC of the compounds against the growth of fungi (μM)

Minimum Inhibitory Concentration (μg/mL)					
Compound	***A. niger***	***A. flavus***	***C. lunata***	***R. bataticola***	***C. albicans***
Co(II)	>100	17.25	50	50	7.12
Ni(II)	**3.94**	10.77	21.44	>100	7.99
Cu(II)	**4.17**	>100	26.45	**6.24**	8.18
Zn(II)	19.24	>100	6.41	>100	21.73
Pd(II)	**4.03**	18.72	>100	26.49	>100
Cd(II)	>100	15.43	>100	19.54	>100
ANABZA	>100	27.45	>100	35.29	21.05
Ketoconazole	2.92	3.85	2.16	4.57	3.26

6.3.2 Antioxidant activity

Antioxidant activity of the synthesized compounds have attracted a lot of interest and has been evaluated mostly in the *in vitro* systems [67,68]. The tested compounds were investigated for their antioxidant ability and these were carried out by using DPPH (1,1-diphenyl-2-picrylhydrazyl) radical as a reagent in the spectrophotometric test.

Ascorbic acid was used as a reference antioxidant. The compounds were performed in triplicate and was then calculated standard deviation [69]. The IC_{50} (µM) values are given in Table 6.11 and Fig. 6.7. It can be seen from the results that Zn(II) complex exhibited significant antioxidant activity with IC_{50} value of 6.11 ± 0.54 µM compared to the reference drug which showed IC_{50} value of 4.61 ± 0.93 µM. The Co(II) complex showed good activity with IC_{50} value of 7.63 ± 1.57 µM. Ni(II) and Cd(II) complexes exhibited moderate activity with IC_{50} value of 13.16 ± 0.85 µM and 17.16 ± 0.16 µM, respectively All the other complexes and ligand showed poor activity with IC_{50} values between 20.96 ± 1.82 µM to 29.47 ± 0.18 µM.

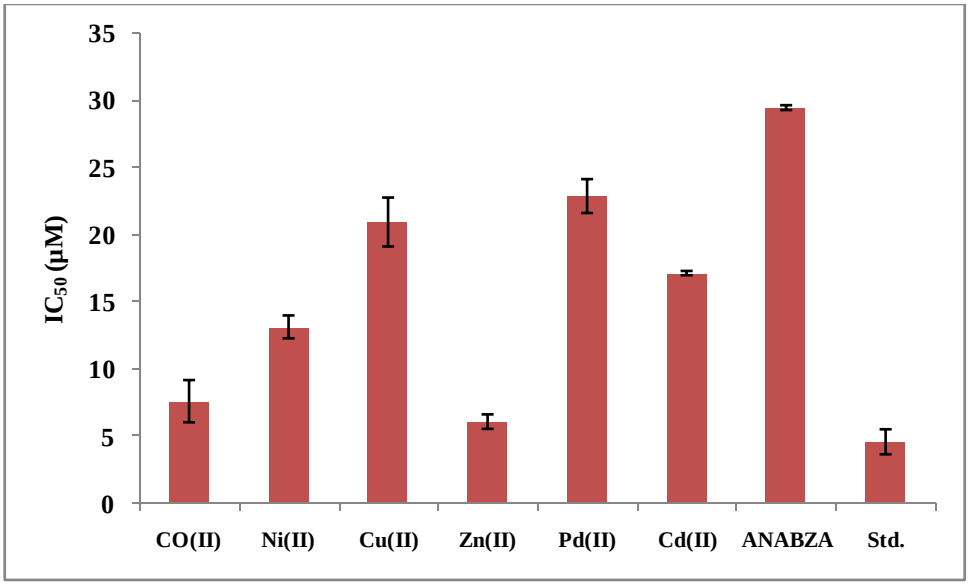

Fig. 6.7 Antioxidant activity of the ligand and its metal complexes.

Table 6.11 Antioxidant activity of compounds by DPPH radical scavenging assay

Compounds	IC_{50} (µM)
Co(II)	**7.63 ± 1.57**
Ni(II)	13.16 ± 0.85
Cu(II)	20.96 ± 1.82
Zn(II)	**6.11 ± 0.54**
Pd(II)	22.89 ± 1.26
Cd(II)	17.16 ± 0.16
ANABZA	29.47 ± 0.18
Ascorbic acid	**4.61 ± 0.93**

6.3.3 *In vitro* antiproliferative evaluation

Based on the successful evaluations and positive results of the antimicrobial and scavenging activity, it was also decided to examine the anticancer evaluation against different cancer cell lines, IMR-32 (neuroblastoma), HeLa (cervical), MCF-7 (breast), A549 (lung), HepG-2 (liver) and HEK293 (embryonic kidney) by using 3-(4,5-dimethylthiazol-2-yl)-2,5-diphenyltetrazolium bromide (MTT) method. The MTT assay results are shown in IC_{50}, and expressed in micromolar units and were summarized in Table 6.12. The percentage of cell viability *versus* concentration graphs are shown in Fig. 6.9. Cisplatin was used as reference drug. The results clearly indicate that Zn(II) complex showed excellent anti-proliferative activity against IMR-32, A549 and HepG-2 with IC_{50} value of 7.81 ± 0.52 µM, 6.18 ± 1.15 µM and 15.28 ± 1.26 µM, respectively. The values are close to standard cisplatin (IC_{50} = 5.78 ± 0.12 µM, 4.90 ± 0.31 µM and 10.52 ± 0.40 µM, respectively) and they showed good activity against MCF-7 (IC_{50} = 7.41 ± 0.32 µM) and HeLa (IC_{50} = 5.99 ± 0.23 µM). Similarly Co(II) complex was potent with a broad spectrum activity with IC_{50} values against HeLa (5.94 ± 1.13 µM), IMR-32 (8.51 ± 0.12 µM), HepG-2 (16.51 ± 1.18 µM), A549 (8.27 ± 0.38 µM) and MCF-7 (13.26 ± 0.19 µM). The observed higher efficiency of Co(II) and Zn(II) complexes are due to the presence of ligand coordinated to central cobalt and zinc metal ions. Also Ni(II) complex against HeLa (IC_{50} = 12.72 ± 0.27 µM) and ANABZA against A549 (IC_{50} = 19.38 ± 1.07 µM)

exhibited moderate activity. The other compounds exhibited least activity against the cell lines. In addition, we have also tested the cytotoxicity of Co(II) and Zn(II) complexes against HEK293 with IC_{50} values of 96.57 ± 0.42 µM and 81.37 ± 0.10 µM, respectively. None of the potent complexes [Co(II) and Zn(II)] interrupted the viability of the normal cell line, suggesting that the potent complexes are not toxic.

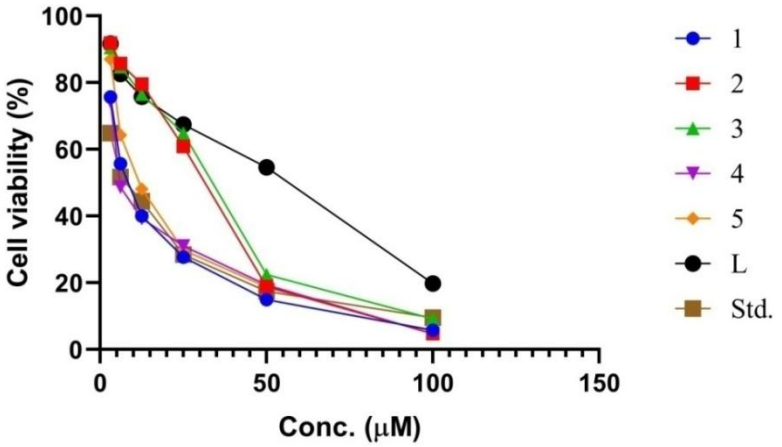

(a)

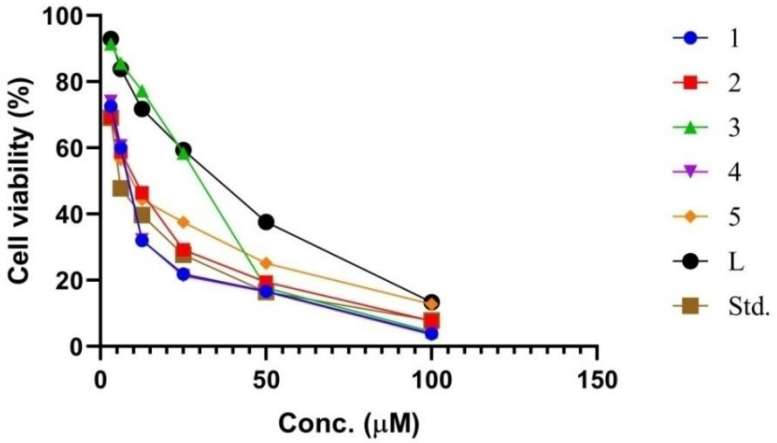

(b)

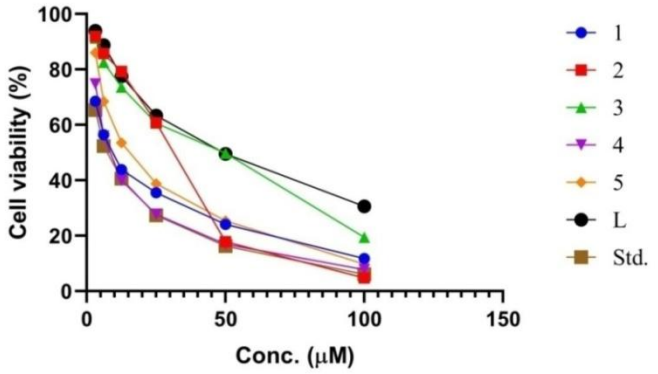

(c)

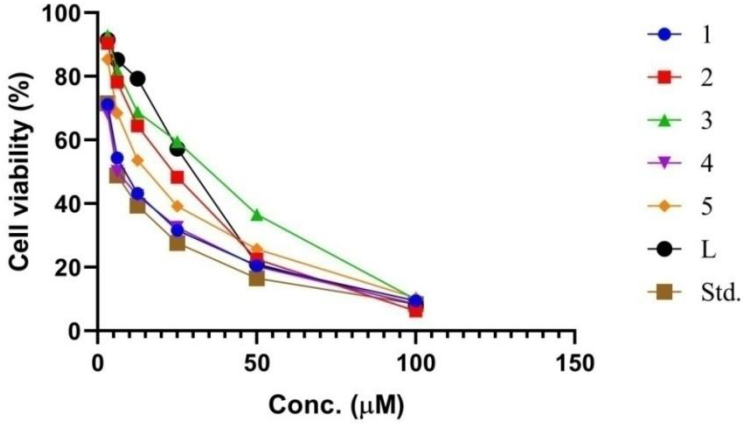

(d)

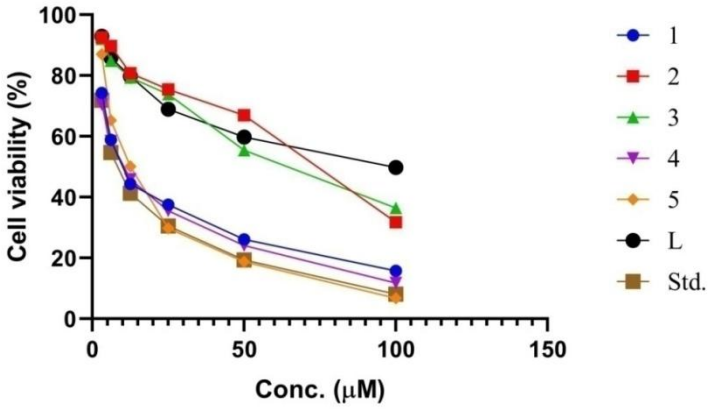

(e)

Fig. 6.8 Survival curves of cell lines (**a**) IMR-32, (**b**) HeLa, (**c**) MCF-7 and (**d**) A549 (**e**) HepG-2. **[**Here, **1** = Co(II), **2** = Ni(II), **3** = Cu(II), **4** = Zn(II), **5** = Pd(II) complexes and **L** = ANABZA, **Std.** = cisplatin**]**

Table 6.12 Cytotoxic activities of newly synthesized compounds on human cancer cell lines IMR-32, HeLa, MCF-7, A549 and HepG-2

Compound	IMR-32	HeLa	MCF-7	A549	HepG-2	HEK 293
Co(II)	**8.51 ± 0.12**	**5.94 ± 1.13**	10.26 ± 0.19	**8.27 ± 0.38**	**16.51 ± 1.18**	**96.57 ± 0.42**
Ni(II)	40.21 ± 1.25	12.72 ± 0.27	39.98 ± 1.34	34.87 ± 1.19	71.26 ± 1.92	ND
Cu(II)	42.08 ± 0.61	39.08 ± 0.13	51.52 ± 1.12	43.13 ± 0.15	69.94 ± 0.38	ND
Zn(II)	**7.81 ± 0.52**	**5.99 ± 0.23**	**7.41 ± 0.32**	**6.18 ± 1.15**	**15.28 ± 1.26**	**81.37 ± 0.10**
Pd(II)	29.35 ± 0.52	17.38 ± 1.05	28.31 ± 1.52	28.37 ± 0.16	52.75 ± 0.81	ND
Cd(II)	50.12 ± 0.13	35.81 ± 1.26	43.06 ± 0.53	48.64 ± 1.05	61.12 ± 1.12	ND
ANABZA	55.09 ± 0.81	45.35 ± 0.32	60.57 ± 0.27	19.38 ± 1.07	88.27 ± 0.28	ND
Cisplatin	5.78 ± 0.12	3.25 ± 0.23	4.63 ± 0.13	4.90 ± 0.31	10.52 ± 0.40	ND

Values are expressed in mean ± SD of three replicates. ND stands for not determine

6.3.4 Molecular docking

The *in silico* molecular docking analysis of the ligand and its metal complexes against human epidermal growth receptor (HER2) and epidermal growth factor (EGFR) was carried out to verify the relation between *in vitro* antiproliferative activity results and binding affinities of the inhibitors using auto dock programme. It plays a major role in the malignant growth from various origins [70]. It is expressed on the surfaces of most of the cell of human body [70] The over expression of HER2 involved in several cancers like breast cancer, adenocarcinoma of lungs, stomach cancer [71], ovarian cancer [72] and uterine cancer [71,72]. It is a suitable target for kinase inhibitors [70] on the other hand, EGFR is a prominent cell-surface receptor which belongs to the EGFR family [73]. The TKD (tyrosine kinase domain) and extracellular mutations of EGFR causes non small cell lung cancer and glioblastoma, respectively [74-76]. Its over expression also leads to epithelial tumors of the head, neck and anal cancer [77,78]. By considering the aforementioned reasons, we have chosen target protein receptors HER2 and EGFR for docking studies. Herein, the main aim is to explore the binding behaviour (in terms of binding energy) of the target compounds against HER2 and EGFR and their results are compared with well established inhibitors (*in vitro* and *in vivo*) such as Canertinib (HER2), Afatinib (HER2), Lapatinib (EGFR) and Gefitinib (EFGR) [79]. The comparative docking studies of the compounds and the reported inhibitors (Canertinib,

Afatinib, Lapatinib and Gefitinib) against proteins HER2 and EGFR along with their corresponding binding energies are listed in Table. 6.13. As shown in table 6.13, docking results revealed that Co(II) and Zn(II) complexes showed the least binding energies compared to other metal complexes against receptors HER2 and EGFR with their binding energies of -7.31 and -6.46 kcal/mol (for Co(II) complex); -8.02 and -7.35 kcal/mol (for Zn(II) complex), respectively. Hence HER2 and EGFR were taken as the target protein receptors for insightful discussion on Co(II) and Zn(II) complexes. The molecular docking results for Co(II) complex against HER2 exhibited four hydrogen bonds; one strong hydrogen bond between OH group of carboxylic acid moiety and the amino acid residue LYS875 with bond length 1.80 Å, one hydrogen bond between amino group of 2-aminopyridyl ring and amino acid residue SER720 with bond length 2.28 Å, one hydrogen bond between OH group of benzoic acid moiety and the amino acid residue ALA722 with bond length 2.90 Å and one carbon-hydrogen bond between –CH group of pyridyl ring and amino acid residue GLY724 with bond length 3.03 Å. The pyridyl ring interacts with amino acid residues ARG841 and CYS797 and the phenyl ring of the benzoic acid moiety interacts with amino acid residue ALA722 through hydrophobic interactions. In the related Co(II) complex against EGFR it exhibited eight hydrogen bonds; one strong hydrogen bond between -O- atom of carboxylic acid moiety and the amino acid residues ARG817 and GLY697 with bond length 1.87 Å and 3.28 Å respectively, one hydrogen bond between H-atom of the carboxylic acid moiety and amino acid residue ASP813 with bond length 2.14 Å, one hydrogen bond between carbonyl oxygen atom of the carboxylic acid group and the amino acid residue LYS721 with hydrogen bond length 3.04 Å, one hydrogen bond between amino group of 2-aminopyridyl ring and amino acid residue ARG817 with bond length 2.08 Å, one hydrogen bond between N-atom of pyridyl ring and the amino acid residue CYS773 with bond length 2.87 Å and one carbon-hydrogen bond between –CH group of pyridyl ring and amino acid residue ASP831 with bond length 3.16 Å, one hydrogen bond between N-atom of the imine group and the amino acid residue ARG817. The pyridyl ring interacts with the amino acid residues LEU820, ARG817 and VAL702 and the phenyl ring of the benzoic acid moiety interact with amino acid residue ARG817 through hydrophobic interactions. The hydrogen bonding interactions and hydrophobic interactions of the Co(II) complex are shown in Fig.s 6.9 and 6.10.

Zn(II) complex against HER2 exhibited five hydrogen bonds; one strong hydrogen bond between the –OH group of benzoic acid moiety and amino acid residue PRO877 with bond length 1.69 Å, one strong hydrogen bond between the –OH group of benzoic acid moiety and amino acid residue ASP837 with bond length 1.85 Å, one hydrogen bond between –CH group of imine moiety with amino acid residue ALA722 with bond length 3.56 Å, one hydrogen bond between –CH group of pyridyl moiety with amino acid residue GLY719 with bond length 3.69 Å and one hydrogen bond between carbonyl group of benzoic moiety with amino acid residue PRO877 with bond length 3.77 Å. The pyridyl ring interacts with the amino acid residues ARG841, LYS745 and VAL726 through hydrophobic interactions. In addition to this there was an electrostatic interaction between the pyridyl moiety with amino acid residues ASP855 and CYS797. In the related Zn(II) complex against EGFR it exhibited eight hydrogen bonds; three hydrogen bonds between carbonyl oxygen atom of the carboxylic acid group and the amino acid residue ARG779, LYS851 and LYS889 with hydrogen bond lengths 1.93 Å, 1.95 Å and 3.37 Å, respectively, one strong hydrogen bond between the –OH group of benzoic acid moiety and amino acid residue LYS889 with bond length 2.98 Å, two hydrogen bonds between amino group of 2-aminopyridyl ring and amino acid residue SER696 with bond length 1.61 Å, and 1.92 Å, one hydrogen bond between *N*-atom of pyridyl ring with amino acid residue GLY695 with bond length 3.57 Å and one Pi-donor hydrogen bond between pyridyl ring and amino acid residue SER696 with bond length 2.97 Å. The pyridyl ring interacts with the amino acid residues ARG817 through hydrophobic interactions. The hydrophobic interactions also played a vital role in increasing the affinity between the synthesized compounds and targeted proteins. The hydrogen bonding interactions and hydrophobic interactions of the Zn(II) complex are shown in Fig.s 6.15 and 6.16. Finally, the docking results clearly suggest that the affinity of the synthesized compounds towards the protein receptor HER2 is better than that of the protein receptor EGFR. The docking results were quite consistent with experimental anticancer activity. The best docking poses of the remaining complexes [Ni(II), Cu(II), Pd(II) and Cd(II)] against the proteins HER2 and EGFR are shown in Fig.s 11-20.

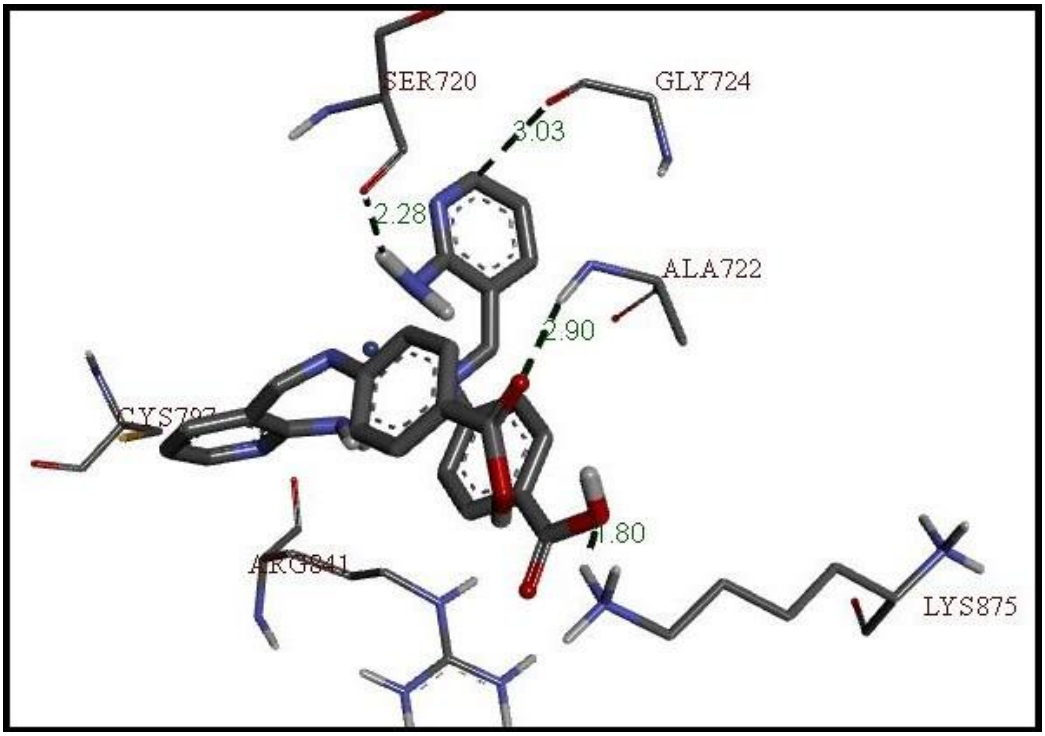

(a)

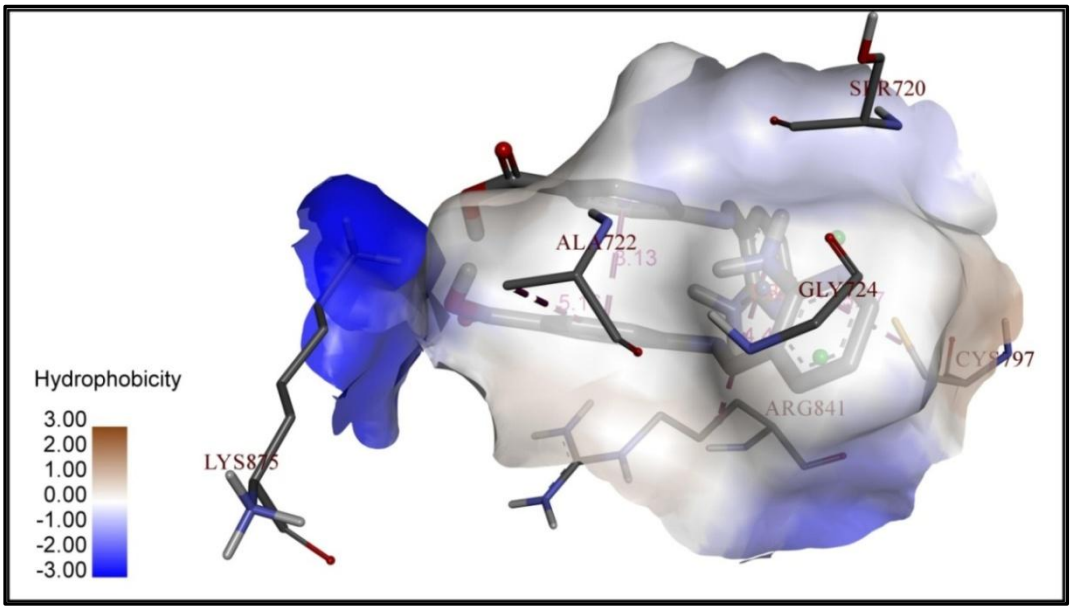

(b)

Fig. 6.9 The best docking pose of the Co(II) complex with HER2, **a)** hydrogen bond interactions, **b)** hydrophobic interactions.

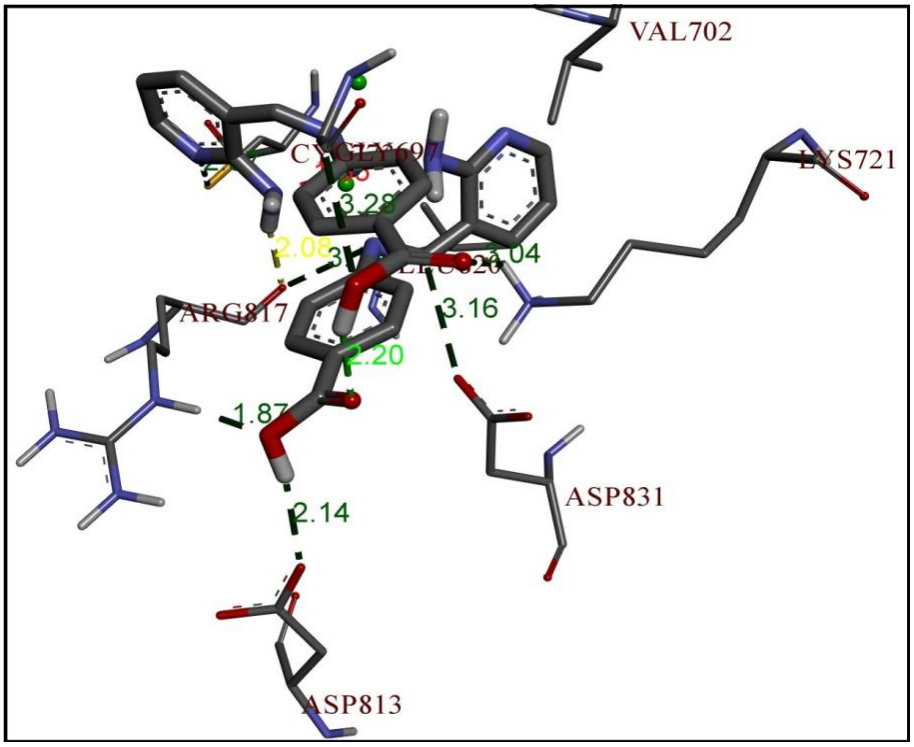

(c)

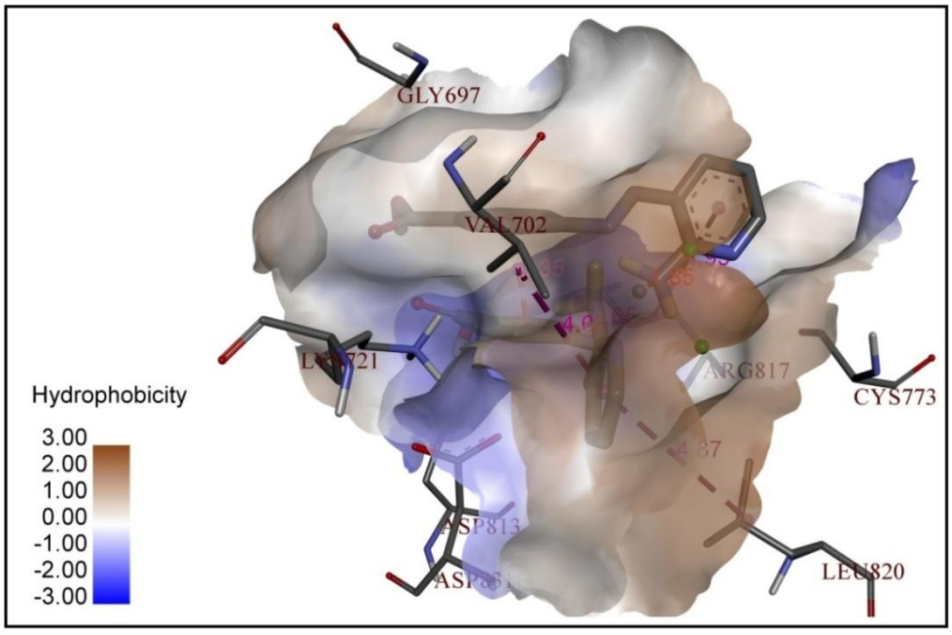

(d)

Fig. 6.10 The best docking pose of the Co(II) complex with EGFR, **c)** hydrogen bond interactions, **d)** hydrophobic interactions.

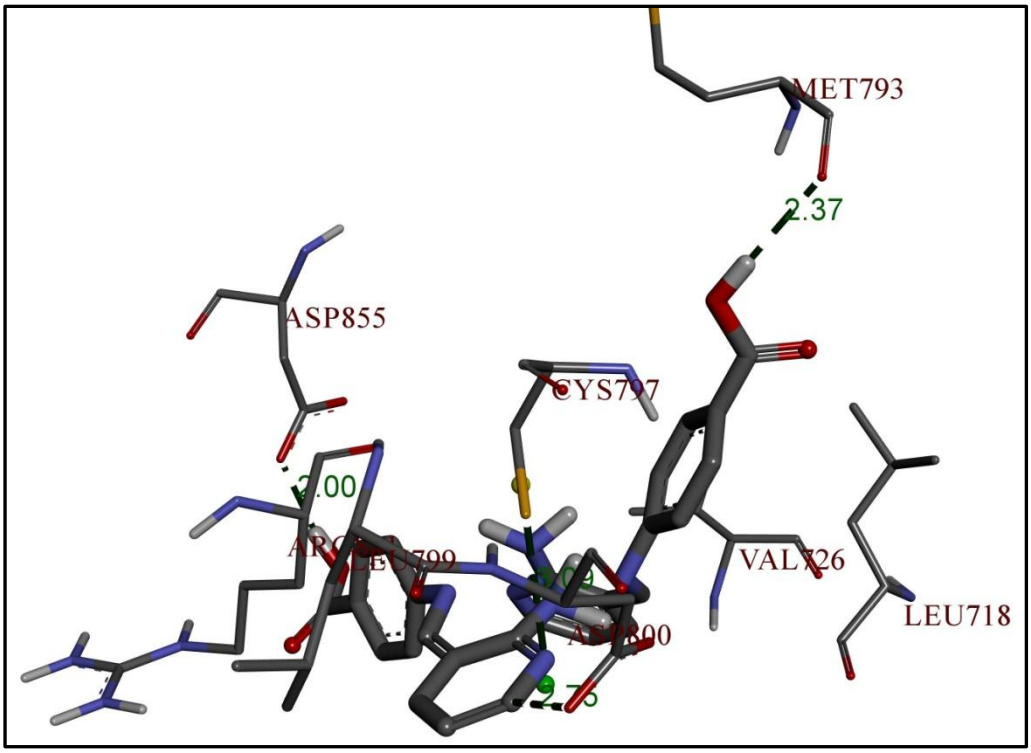

(e)

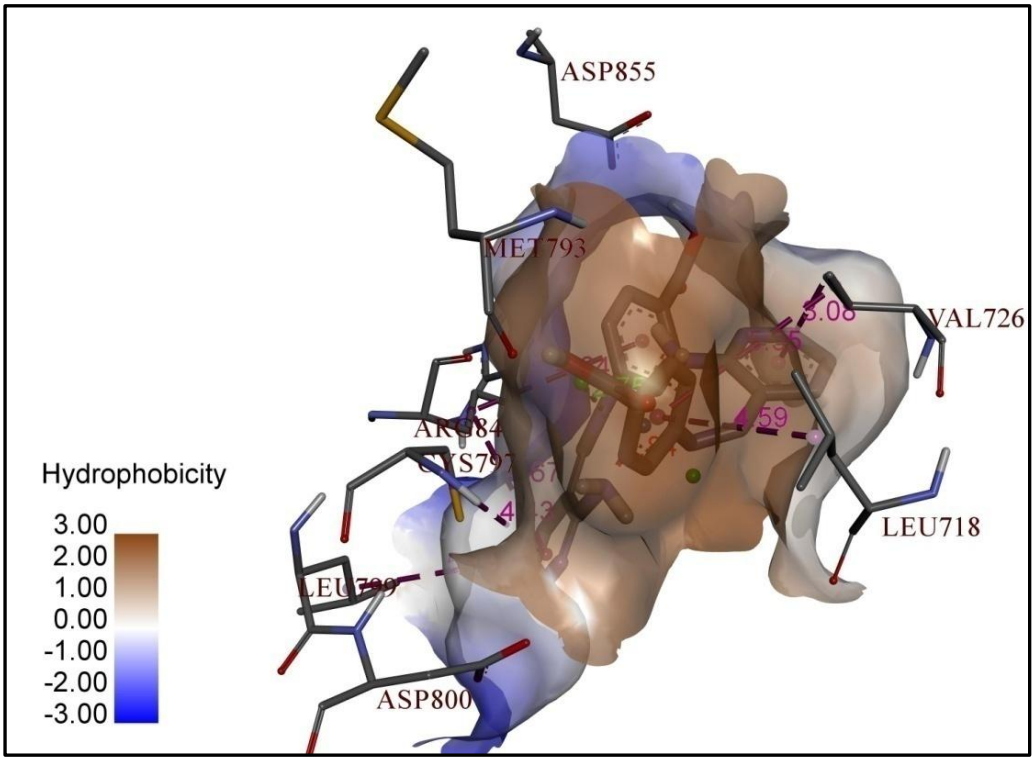

(f)

Fig. 6.11 The best docking pose of the Ni(II) complex with HER2, **e**) hydrogen bond interactions, **f**) hydrophobic interactions.

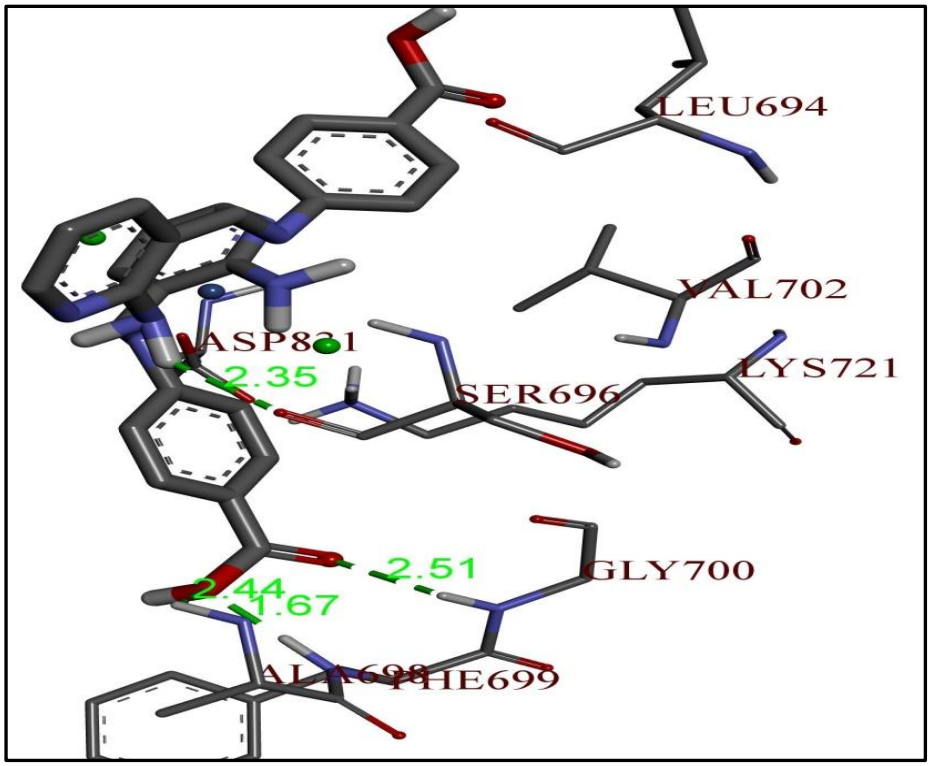

(g)

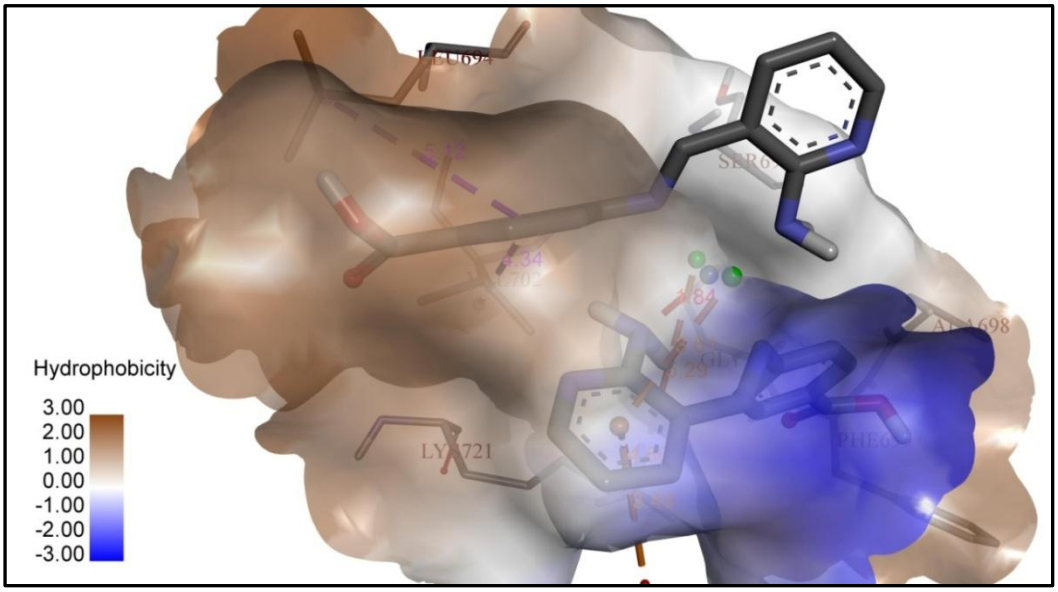

(h)

Fig. 6.12 The best docking pose of the Ni(II) complex with EGFR, **g)** hydrogen bond interactions, **h)** hydrophobic interactions.

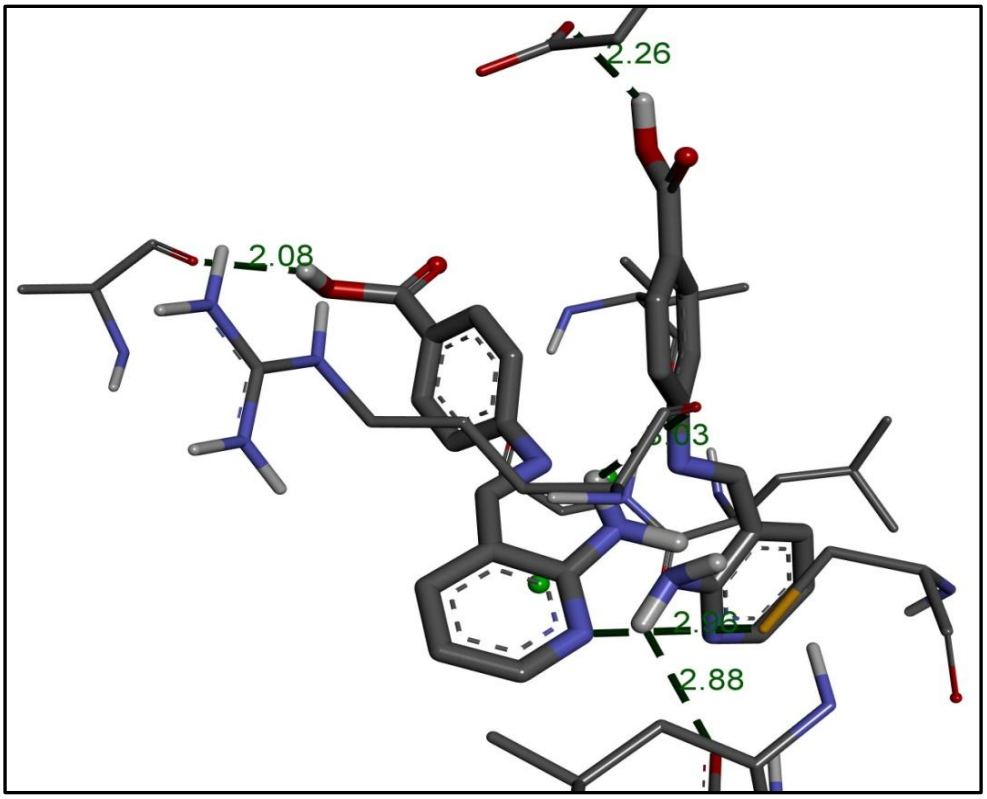

(i)

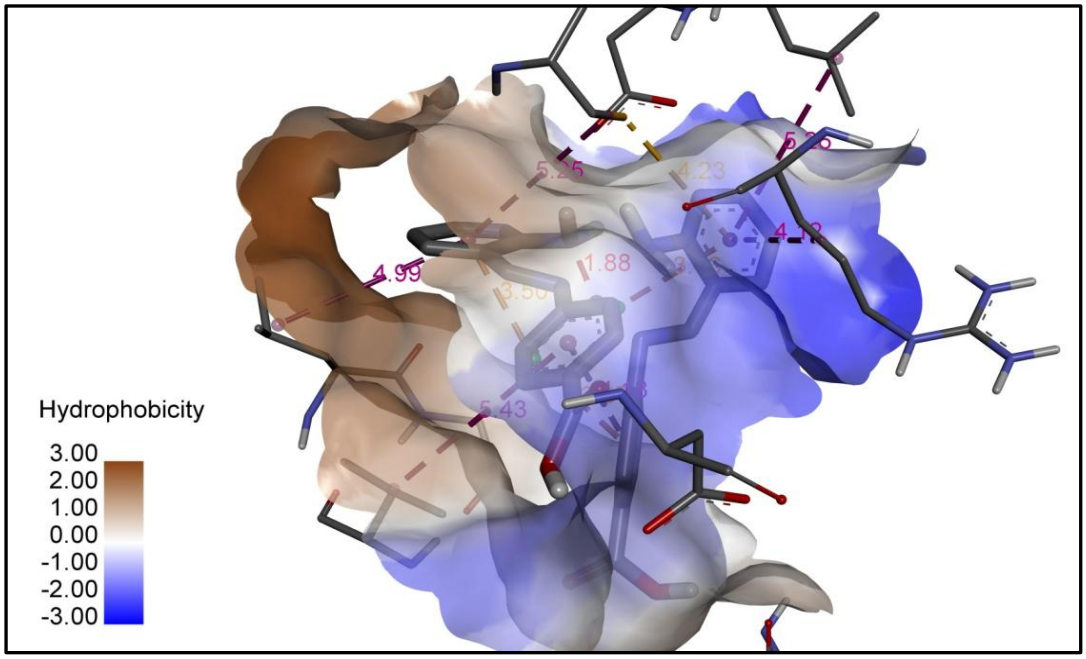

(j)

Fig. 6.13 The best docking pose of the Cu(II) complex with HER2, **i)** hydrogen bond interactions, **j)** hydrophobic interactions.

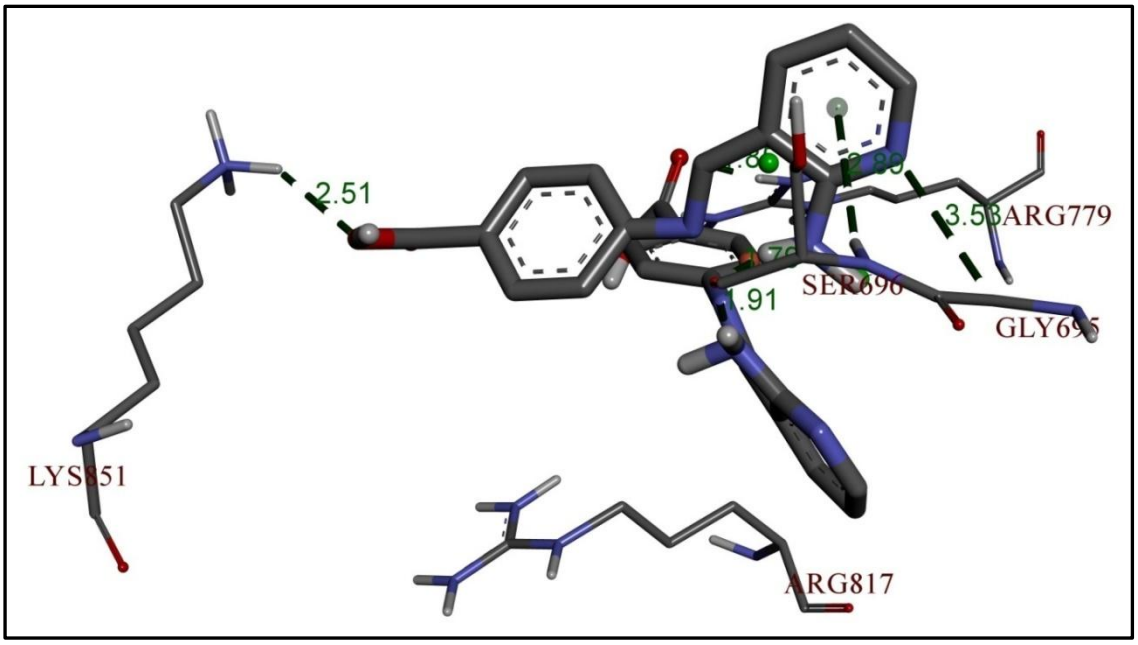

(k)

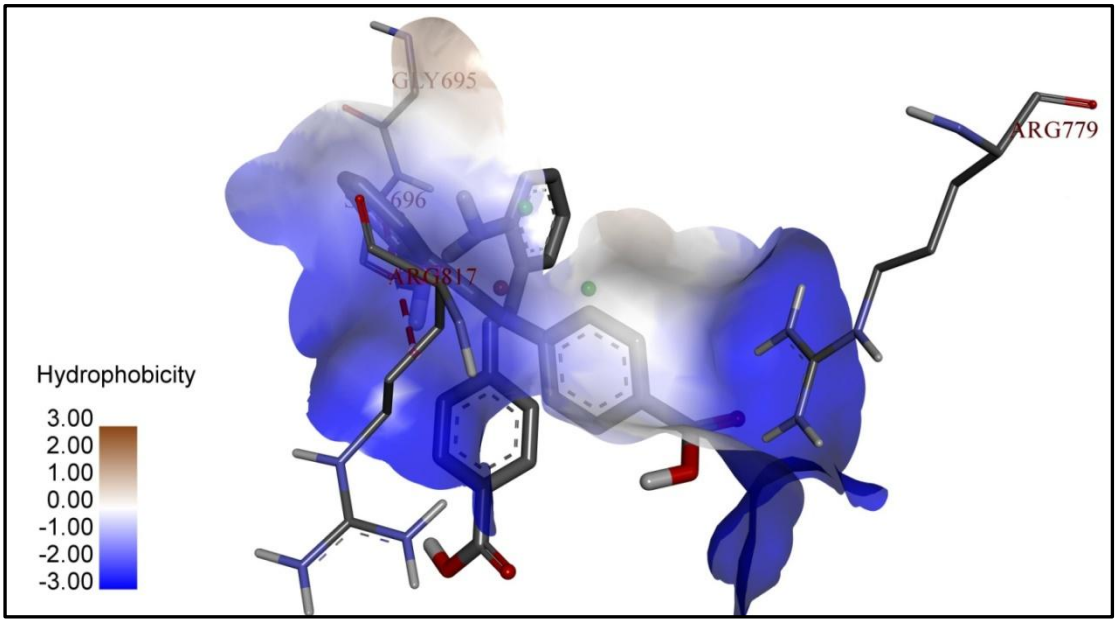

(l)

Fig. 6.14 The best docking pose of the Cu(II) complex with EGFR, **k**) hydrogen bond interactions, **l**) hydrophobic interactions.

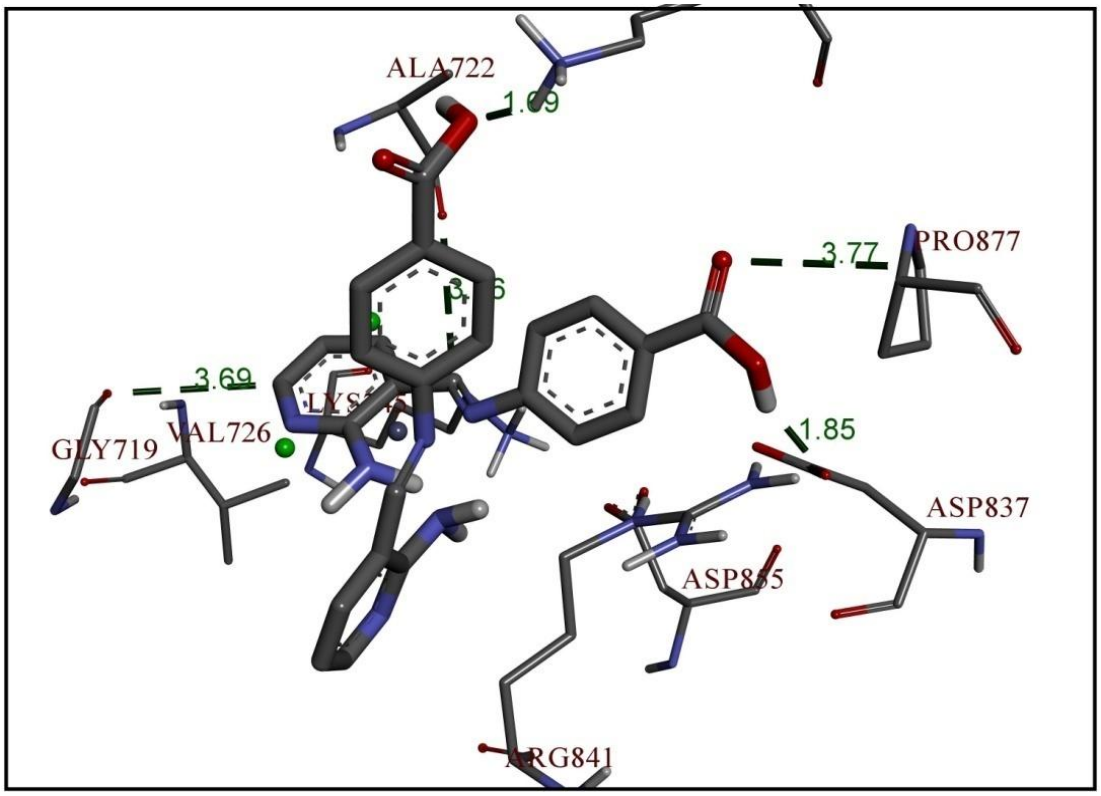

(m)

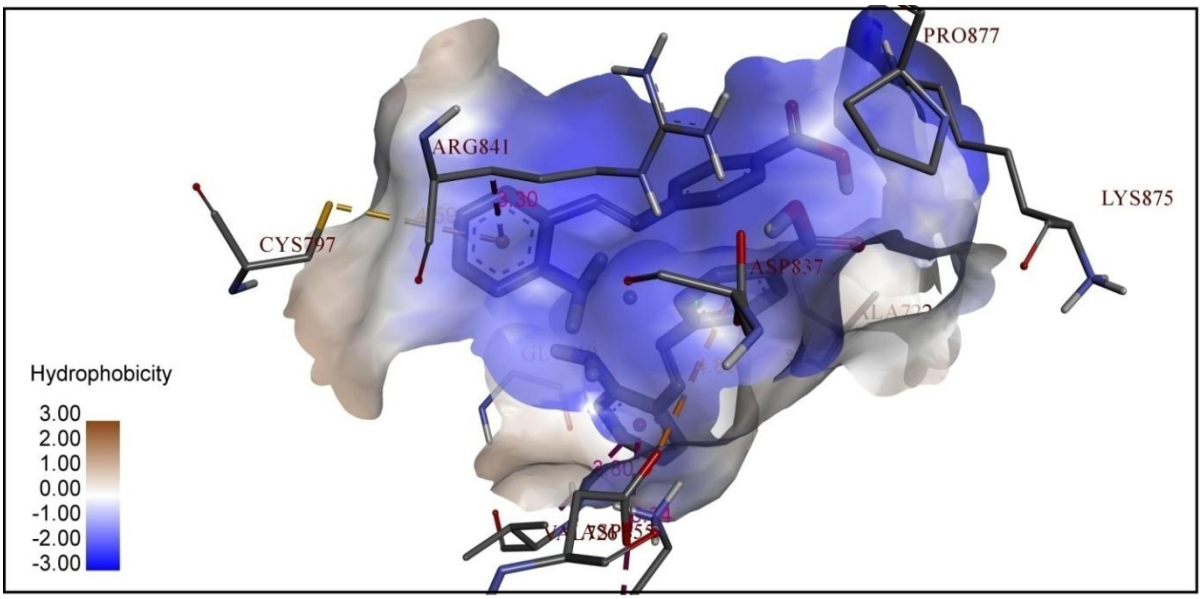

(n)

Fig. 6.15 The best docking pose of the Zn(II) complex with HER2, **m)** hydrogen bond interactions, **n)** hydrophobic interactions.

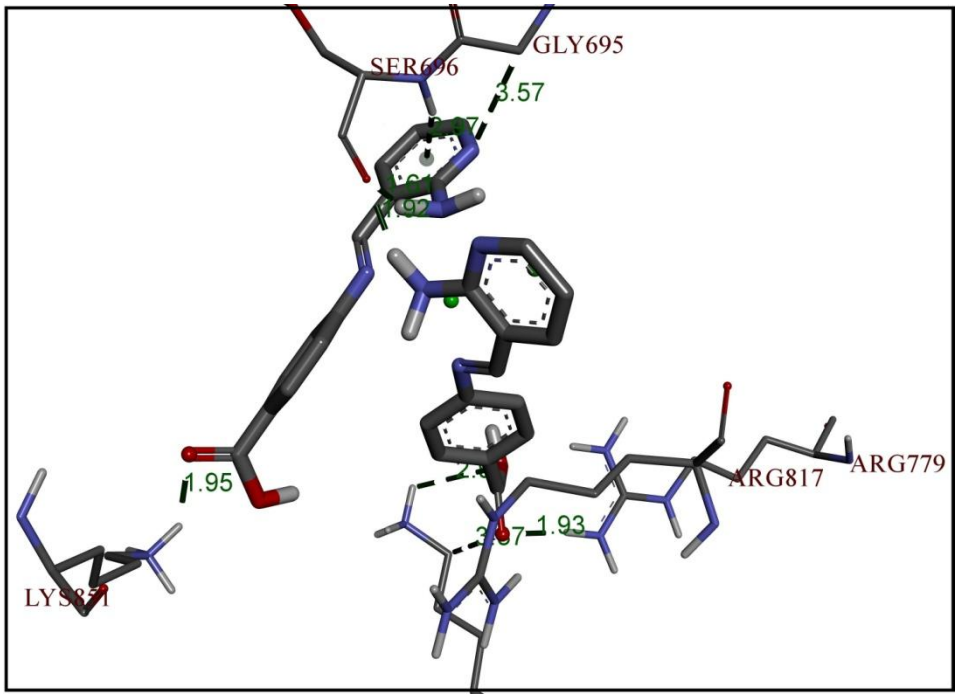

(o)

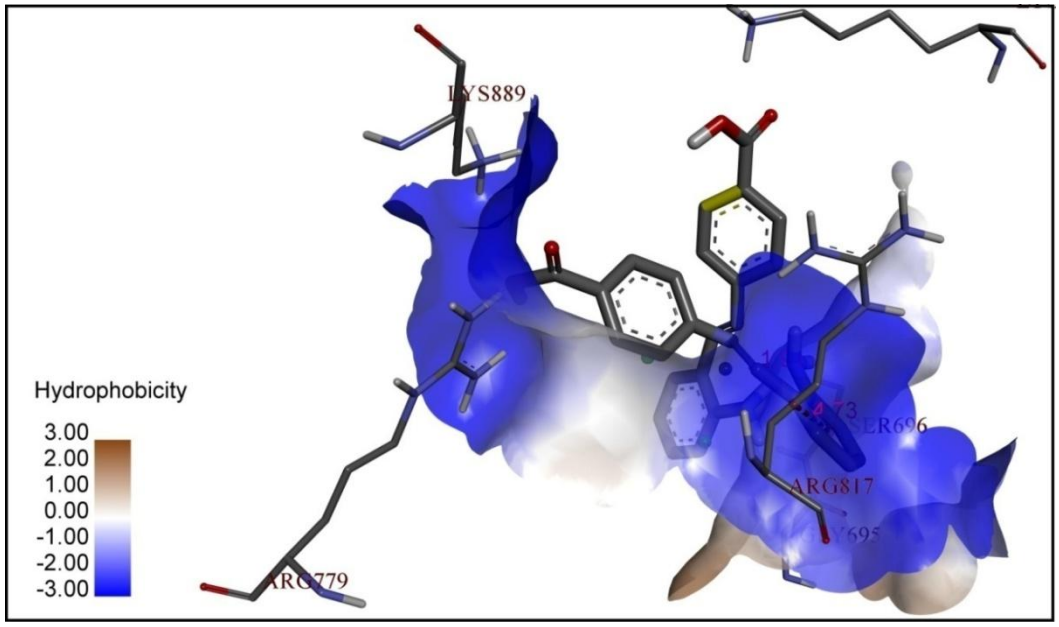

(p)

Fig. 6.16 The best docking pose of the Zn(II) complex with EGFR, **o)** hydrogen bond interactions, **p)** hydrophobic interactions.

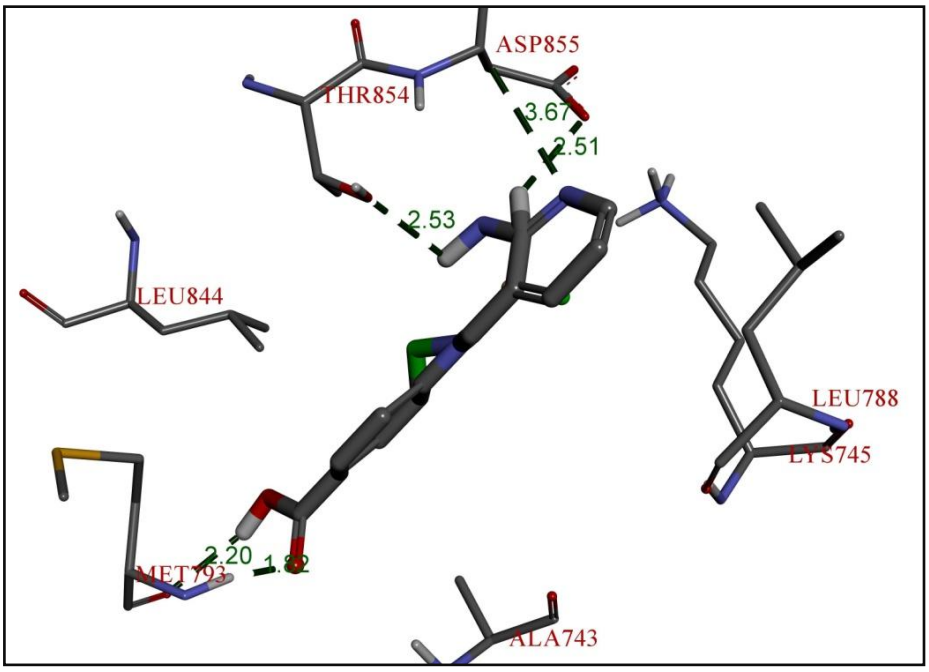

(q)

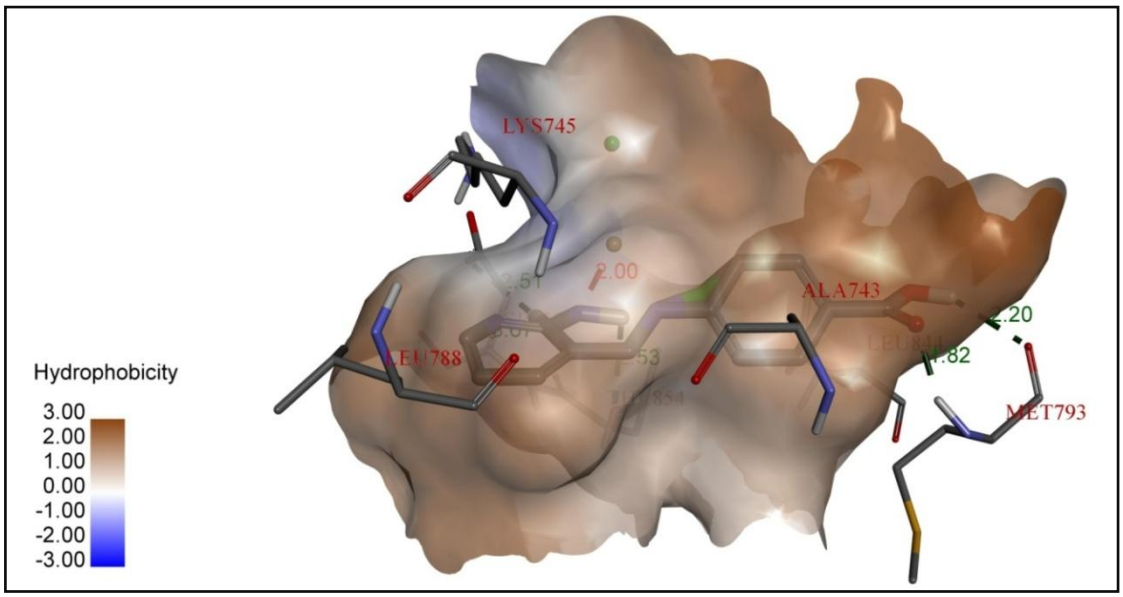

(r)

Fig. 6.17 The best docking pose of the Cd(II) complex with HER-2, **q)** hydrogen bond interactions, **r)** hydrophobic interactions.

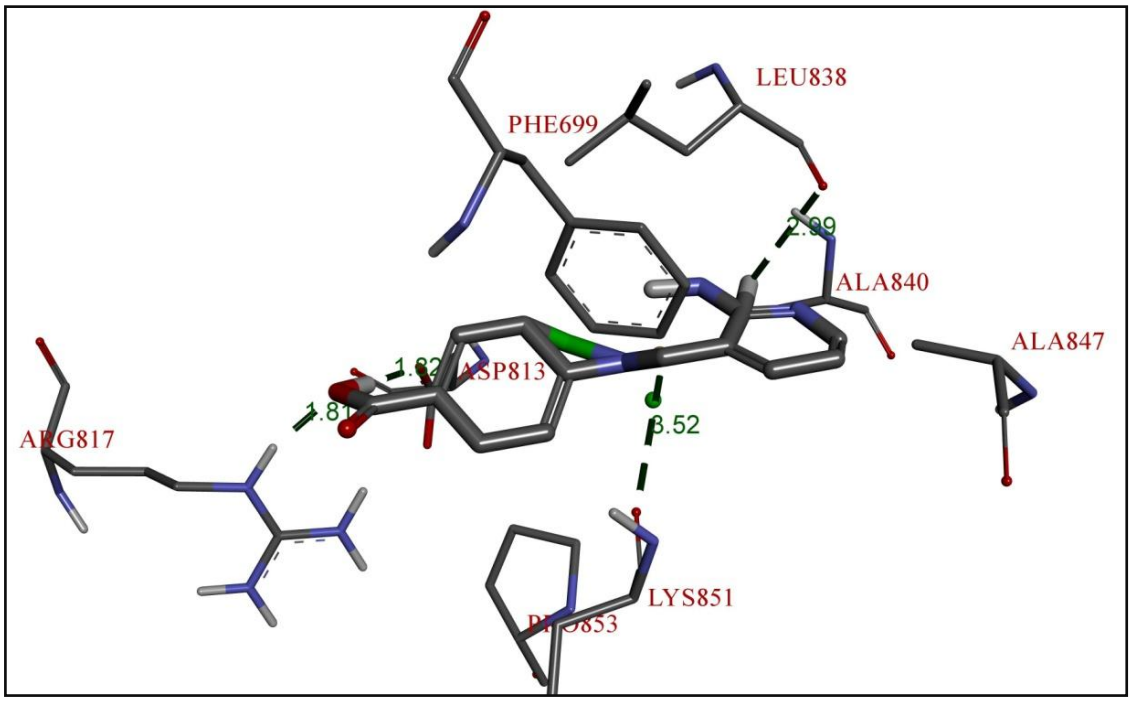

(s)

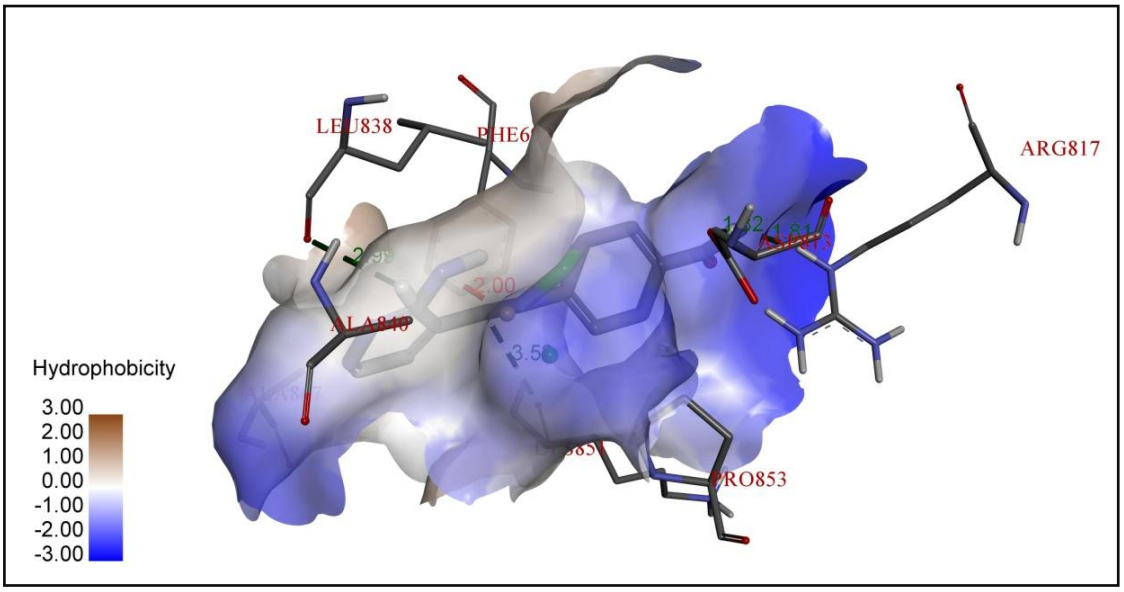

(t)

Fig. 6.18 The best docking pose of the Cd(II) complex with EGFR-2, **s)** hydrogen bond interactions, **t)** hydrophobic interactions.

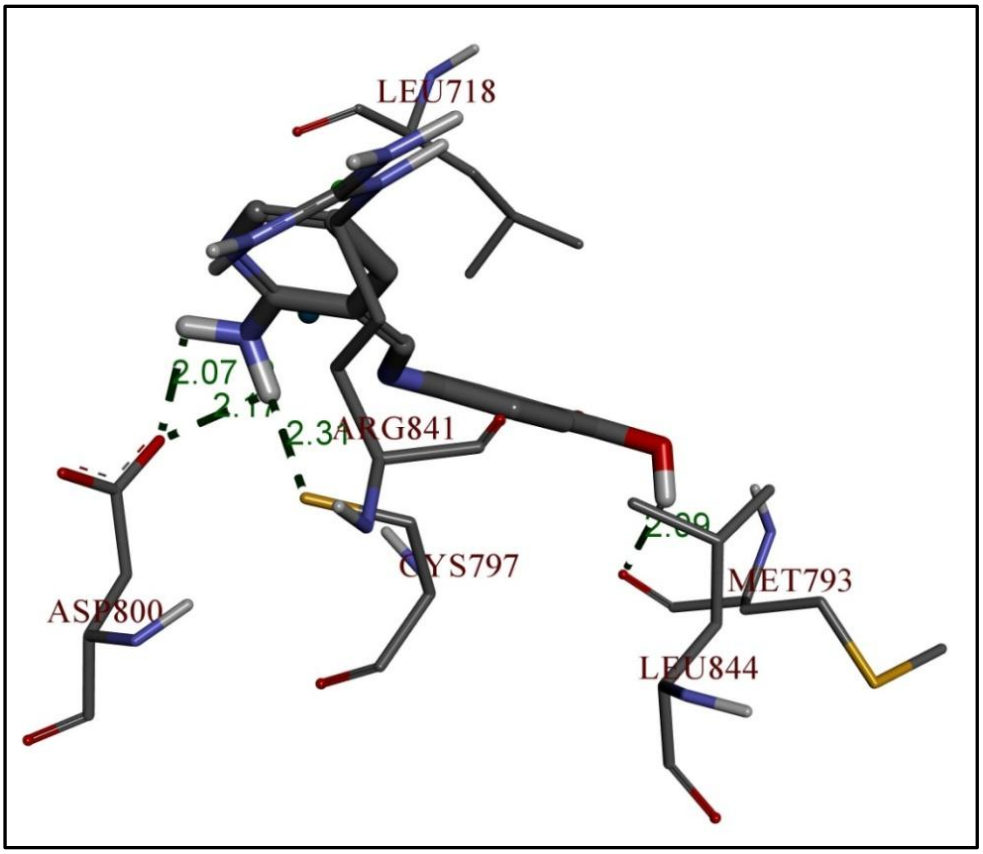

(u)

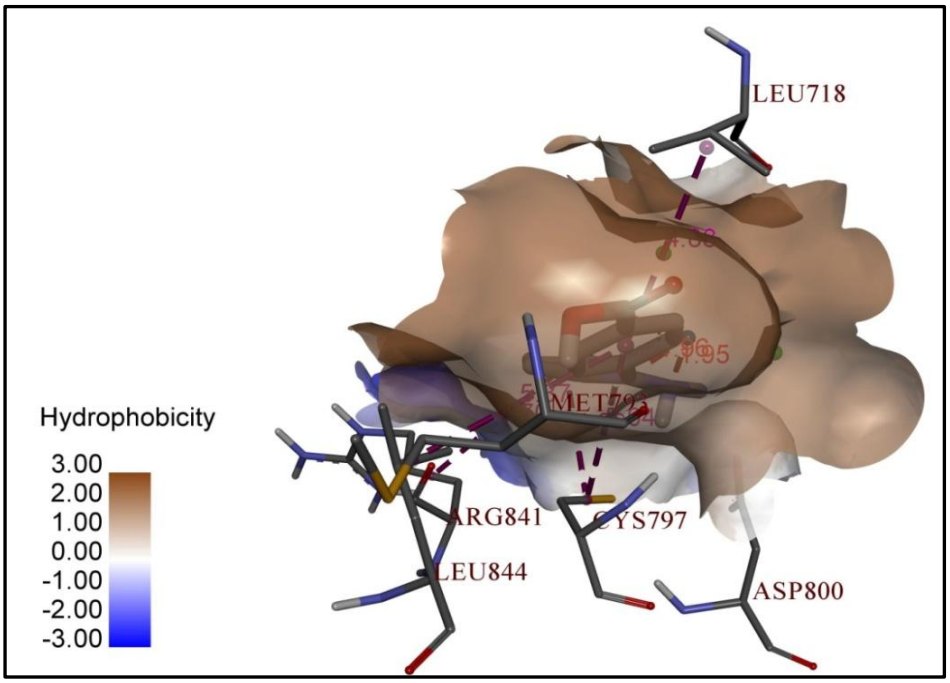

(v)

Fig. 6.19 The best docking pose of the Pd(II) complex with HER2, **u**) hydrogen bond interactions, **v**) hydrophobic interactions.

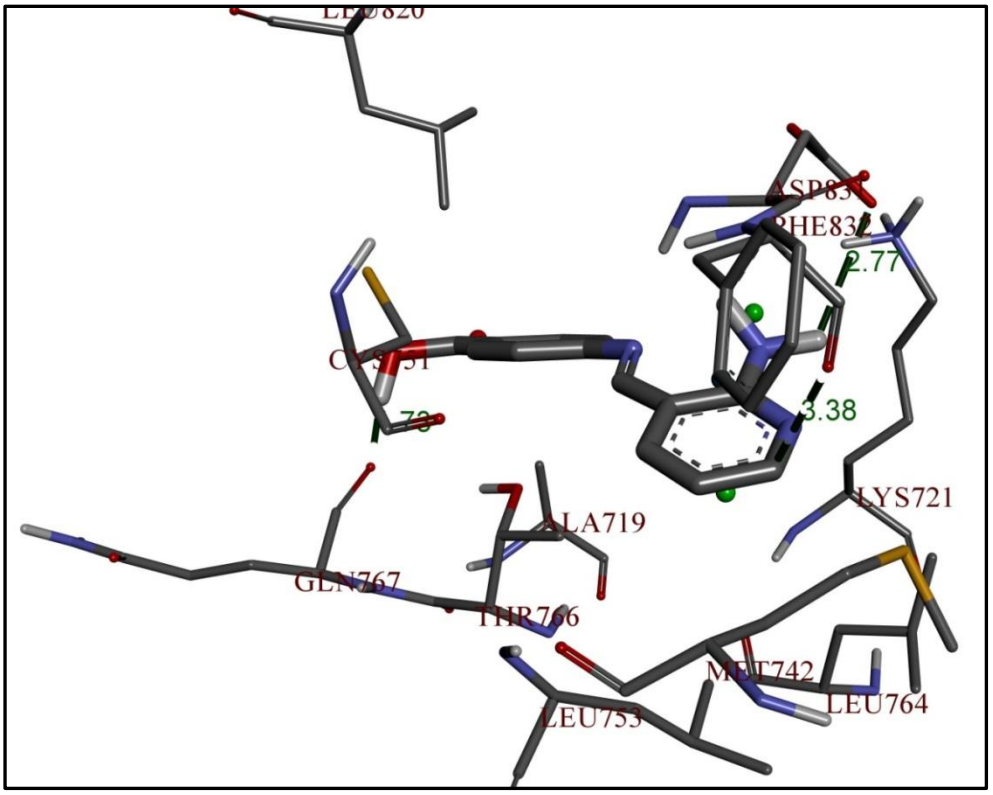

(w)

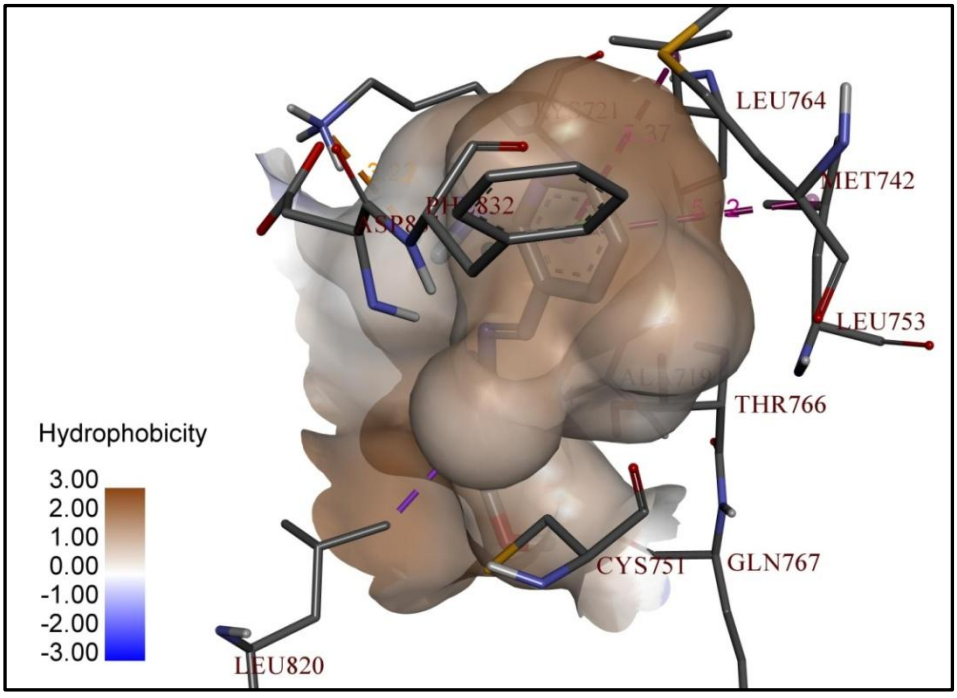

(x)

Fig. 6.20 The best docking pose of the Pd(II) complex with EGFR, **w**) hydrogen bond interactions, **x**) hydrophobic interactions.

.

Table 6.13 Binding energies of ligand and its metal complexes against protein receptors HER 2 and EGFR

HER2 (PDB ID: 3POZ)					EGFR (PDB ID: 4HJO)			
Compound	**Binding energy (kcal/mol)**	**No. of Hydrogen bonds**	**Amino acid residues involved in the hydrogen bonding**	**Hydrogen bond length (Å)**	**Binding energy (kcal/mol)**	**No. of Hydrogen bonds**	**Amino acid residues involved in the hydrogen bonding**	**Hydrogen bond length (Å)**
Co(II)	**-7.31**	**4**	**SER720, GLY724, ALA722, LYS875**	**1.80, 2.28, 2.90, 3.03**	**-6.46**	**8**	**ARG817, ASP813, ASP831, LYS721, CYS773, GLY697**	**1.87, 2.08, 2.14, 2.87, 3.04, 3.14, 3.16, 3.28**
Ni(II)	-7.08	4	MET793, ASP800, ASP855, CYS797	2.00, 2.37, 2.75, 3.09	-6.02	4	ALA698, PHE699, GLY700, SER696	1.67, 2.44, 2.51, 2.35
Cu(II)	-7.20	5	CYS797, ARG841, ASP800, ALA722, ASP855	2.08, 2.26, 2.88, 2.96, 3.02	-6.10	6	ARG779, LYS851, SER696, GLY695, SER696	1.79, 1.85, 1.91, 2.51, 2.89, 3.53
Zn(II)	**-8.02**	**5**	**LYS875, ASP837, PRO877, ALA722, GLY719**	**1.69, 1.85, 3.56, 3.69, 3.77**	**-7.35**	**8**	**ARG779, GLY695, LYS851, LYS889, SER696**	**1.61, 1.92, 1.93, 1.95, 2.97, 2.98, 3.37, 3.57**

Pd(II)	-6.37	4	CYS797, ASP800, MET793	2.07, 2.09, 2.17, 2.31	-6.42	3	ASP831, GLN767, PHE832	1.73, 2.77, 3.38
Cd(II)	-6.90	5	MET793, THR854, ASP855	1.82, 2.20, 2.51, 2.53, 2.67	-7.37	4	ARG817, ASP813, LYS851, LEU838	1.81, 1.82, 3.52, 2.99
ANABZA	-6.62	3	MET793, ASP855, GLN791	1.80, 1.84, 2.09	-5.56	5	LYS851, LYS721, ASN818	2.00, 2.65. 3.06 1.95
Canertinib	-7.73	2	ASN842, THR854	1.89, 3.36	-	-	-	-
Afatinib	-6.37	3	ASP800, ARG841, LYS745	2.71, 2.86, 2.56	-	-	-	-
Lapatanib	-	-	-	-	-5.94	3	CYS773, LYS721	3.08, 2.29, 2.95
Gefitinib	-	-	-	-	-6.60	6	ASP813, LYS721, ASP831, ARG817	3.03, 2.98, 2.85, 2.97, 1.82, 2.23

6.4 Conclusions

In summary, the complexes with Schiff base ligand have been designed, synthesized and characterized, with an aim to evaluate them for antioxidant, antimicrobial, cytotoxic activity, DFT calculations and HER2, EGFR target based *in silico* docking studies. The metal-ligand stoichiometry in the complexes of Co(II), Ni(II), Cu(II) and Zn(II) corresponds to 1:2, whereas in case of Pd(II) and Cd(II), 1:1 stoichiometry was observed, wherein the ligand behaves in a bidentate manner towards metals coordinating through azomethine nitrogen atom and the nitrogen of amine group. Based on DFT and spectral studies, octahedral geometry is assigned for Co(II), Ni(II) and Zn(II) complexes, distorted octahedral for Cu(II) complex, tetrahedral for Cd(II) and square-planar geometry for Pd(II) complex**.** All the complexes are non-electrolytic in nature in DMF. The evaluation of ESR parameters from the ESR spectrum confirms that the M-L bonds are covalent and out of plane π-bonded. From the antimicrobial activity results, it is known that metal complexes have better effect compared to the free ligand indicating that the metals are actually in action. Specifically, Cu(II) complex has shown excellent antimicrobial activity; likewise, Pd(II) complex exhibited a broad spectrum of antibacterial activity, and Ni(II) complex has shown superior antifungal activity compared to Streptomycin and Ketoconazole. Zn(II) complex has shown good antioxidant activity compared to reference drug ascorbic acid. In addition, complexes of Zn(II) and Co(II) have shown potent anti-proliferative activity against IMR-32 (IC_{50} = 7.81 ± 0.52, 8.51 ± 0.12 µM), A549 (IC_{50} = 6.18 ± 1.15, 8.27 ± 0.38 µM) and HepG-2 (IC_{50} = 15.28 ± 1.26 µM, 16.51 ± 1.18 µM), respectively. The docking results revealed that complexes Co(II) and Zn(II) exhibited the least binding energies against receptors HER2 and EGFR with their binding energies -7.31 and -6.46 kcal/mol (for Co(II) complex); -8.02 and -7.35 kcal/ mol (for Zn(II) complex), respectively compared to Canertinib (HER2), Afatinib (HER2), Lapatinib (EGFR) and Gefitinib (EFGR). From the results, it is clear that the complexes are strongly bound to HER2 and EGFR protein receptors. Interestingly, these compounds have shown most potent anticancer activity and minimum binding energies obtained by docking study. The results indicate that *in silico* molecular docking studies correlated well with the experimental anti-proliferative activity results.

References

[1] M. Salehi, M. Kubicki, M. Galini, M. Jafari, R.E. Malekshah, *J. Mol. Struct*. **2019**, *1180*, 595.

[2] I.B. Amali, M.P. Kesavan, V. Vijayakumar, N.I. Gandhi, J. Rajesh, G. Rajagopal, *J. Mol. Struct*. **2019**, *1183*, 342.

[3] S.M.E. Khalil, S.L. Stefan, K.A. Bashir, *Synth. React. Inorg. Met. Org. Chem*. **2001**, *31*, 927.

[4] E. Kwiatkowski, G. Romanowski, K. Suwin´ska, *Polyhedron* **2002**, *21*, 2071.

[5] G. Brewer, P. Kamaras, L. May, S. Prytkov, M. Rapta, *Inorganica Chim. Acta* **1998**, *279*, 111.

[6] M. Rahman, M.A. Mridha, M.A. Ali, *Transition Met*. Chem. **1994**, *19*, 237.

[7] S.J. Swamy, K. Suresh, P. Someshwar, D. Nagaraju, *Synth. Commun.* **2004**, *34*, 1847.

[8] S. Jyothi, K. Sreedhar, D. Nagaraju, S.J. Swamy, *Can. Chem. Trans.* **2015**, *3*, 368.

[9] A. Khamamkar, S. Gajula, V.R. Pallapothula, *Int. J. Pharm. Sci. Res.* **2016**, *7*, 3322.

[10] B. Swamy, J.R. Swamy, *Transition Met. Chem*. **1991**, 16, 35.-38

[11] Q. Albert, *Nature* **1953**, *9*, 370.

[12] R. Konakanchi, R. Mallela, R.Guda, L.R. Kotha, *Res. Chem. Intermed.* **2018**, *44*, 27.

[13] K. Ramaiah, K. Srishailam, K. Laxma Reddy, B. Venkatram Reddy, G. Ramana Rao, *J. Mol. Struct*. **2019**, *1184*, 405.

[14] K. Ramaiah, J. Prashanth, J. Haribabu, E. Srikanth, B.V. Reddy, R. Karvembu, K. Laxma Reddy, *J. Mol. Struct*. **2019**, *1175*, 769.

[15] R. Mallela, R. Konakanchi, R. Guda, N. Munirathinam, D. Gandamalla, N.R. Yellu, L.R. Kotha, *Inorganica Chim. Acta* **2018**, *469*, 66.

[16] W.H. Mahmoud, R.G. Deghad, M.M.I. El Desssouky, G.G. Mohamed, *Appl. Organomet. Chem*. **2018**, *33*, e4556.

[17] T. Thirunavukkarasu, H.A. Sparkes, K. Natarajan, V.G. Gnanasoundari, *Inorganica Chim. Acta* **2018**, *473*, 255.

[18] J. Devi, M. Yadav, D. Kumar, L.S. Naik, D.K. Jindal, *Appl. Organomet. Chem*. **2018**, *33*, e4693.

[19] R.P. Wernyj, P.J. Morin, *Drug Resist. Update* **2004**, *7*, 227.

[20] R.M. Ramadan, W.M. Elsheemy, N.S. Hassan, A.A. Abdel Aziz, *Appl. Organomet. Chem.* **2018**, *32*, e4180.

[21] H.P. Ebrahimi, J.S. Hadi, Z.A. Abdulnabi, Z. Bolandnazar, *Spectrochim. Acta A* **2014**, *117*, 485.

[22] A.K. Abu Al-Nasr, R.M. Ramadan, *Spectrochim. Acta A* **2013**, *105*, 14.

[23] R.M. Ramadan, A.K. Abu Al-Nasr, A.F.H. Noureldeen, *Spectrochim. Acta A* **2014**, *132*, 417.

[24] A.A. Abdel Aziz, S.H. Seda, *J. Fluoresc.* **2017**, *27*, 1051.

[25] A.A. Abdel Aziz, F.M. Elantabli, H. Moustafa, S.M. El-Medani, *J. Mol. Struct.* **2017**, *1141*, 563.

[26] G.R. Burns, *Inorg. Chem.* **1968**, *7*, 277.

[27] S. Jyothi, K. Sreedhar, D. Nagaraju, S.J. Swamy, *Can. Chem. Trans.* **2015**, *3*, 368.

[28] M. Saif, M.M. Mashaly, M.F. Eid, R. Fouad, *Spectrochim. Acta A* **2011**, *79*, 1849.

[29] F. Firdaus, K. Fatma, M. Azam, S.N. Khan, A.U. Khan, M. Shakir, *Spectrochim. Acta A* **2009**, *72*, 591.

[30] D. Shukla, L.K.Gupta, S. Chandra, *Spectrochim. Acta A* **2008**, *71*, 746.

[31] S. Chandra, *Spectrochim. Acta A* **2004**, *60*, 2153.

[32] J. Devi, M. Yadav, A. Kumar, *Chem. Pap.* **2018**, *72*, 2479.

[33] R. Konakanchi, J. Haribabu, J. Prashanth, N.V. Bharat, M. Ramachary, D. Gandamalla, R. Karvembu, B. Venkatram Reddy, N.R. Yellu, L.R. Kotha *Appl. Organomet. Chem.* **2018**, *32*, e4415.

[34] S. Nigam, M.M. Patel, A. Ray, *J. Phys. Chem. Sol.* **2000**, *61*, 1389.

[35] A.A. Saleh, *J. Coord. Chem.* **2005**, *58*, 255.

[36] D.M.L. Goodgame, M. Goodgame, *J. Chem. Soc.* **1963**, 207.

[37] N. Raman, S. Ravichandran, C. Thangaraja, *J. Chem. Sci.* **2004**, *116*, 215.

[38] K. Ganesan, P. Ponya Utthra, M. Dharmasivam, R. Natarajan, *Int. J. Biol. Macromol.* Press, 10.1016/j.ijbiomac.2018.09.116

[39] J. Devi, N. Batra, R. Malhotra, *Spectrochim. Acta A* **2012**, *97*, 397.

[40] P.L. Goggin, R.J. Goodfellow, F.J.S. Reed, *J. Chem. Soc. Dalton Trans.* **1972**, *12*, 1298.

[41] M.R. Gajendragad, U.C. Aggarwala, *J. Inorg. Nucl. Chem.* **1975**, *37*, 2429.

[42] M.M. Omar, G.G. Mohamed, *Spectrochim. Acta A* **2005**, *61*, 929.

[43] S.A. Patil, V.H. Kulkarni, *Polyhedron* **1984**, *3*, 21.

[44] A.E.M. Ramadan, *J. Mol. Struct*. **2012**, *1015*, 56.

[45] G.G. Mohamed, N.E.A. El-Gamel, F.A. Nour El-Dien, *Synth. React. Inorg. Met. Org. Chem*. **2001**, *31*, 347.

[46] F.A. Cotton, G. Wilkinson, C.A. Murillo, M. Bochmann, *Advanced Inorganic Chemistry, sixth ed.*, Wiley, New York, **1999**.

[47] P. Kavitha, K. Laxma Reddy, *Arabian J. Chem*. **2012**, *9*, 596.

[48] A. Sabastiyan, D. Venkappayya, *J. Indian Chem. Soc*. **1990**, *67*, 584.

[49] F.K. Kneubuhl, *J. Chem. Phys*. **1960**, *33*, 1074.

[50] P. Kavitha, M. Saritha, K. Laxma Reddy, *Spectrochim. Acta A 102*, **2013**, 159.

[51] D. Kivelson, R. Neiman, *J. Chem. Phys*. **1961**, *35*, 149.

[52] B.J. Hathaway, D.E. Billing, *Coord. Chem. Rev*. *1970*, *5*, 143.

[53] C.H. Choi, M. Kertez, *J. Phys. Chem A* **1997**, *101*, 3823.

[54] G. Gece, *Corros. Sci*. **2008**, *50*, 2981.

[55] K. Fukui, *Science* **1982**, *218*, 747.

[56] L. Sinha, O. Prasad, V. Naryan, S.R. Shukla, *J. Mol. Simul*. **2011**, *37*, 153.

[57] D.F.V. Lewis, C. Ioannides, D.V. Parke, *Xenobiotica* **1994**, *24*, 401.

[58] D. Kosar, C. Albayrak, *Spectrochim. Acta A* **2011**, *78*, 160.

[59] T.A. Koopmans, *Physica* **1933**, *1*, 104.

[60] P.N. Prasad, D.J. Williams, *Introduction to Nonlinear Optical Effects in Molecules and Polymers*, Wiley, New York, **1991**.

[61] A.D. Buckingham, *Adv. Chem. Phys*. **1967**, *12*, 107.

[62] F. Meyers, S.R. Marder, B.M. Pierce, J.L. Bredas, *J. Am. Ceram. Soc*. **1994**, *116*, 10703.

[63] F. Hinchliffe, R.W. Munn, John Wiley and Sons Ltd, Chichester, **1985**.

[64] D.A. Kleinman, *Phys Rev*. **1962**, *126*, 1977.

[65] M. Arivazhagan, S. Jeyavijayan, *Spectrochim. Acta* A **2011**, *79*, 376.

[66] T. Arun, S. Packianathan, M. Malarvizhi, R. Antony, N. Raman, *J. Photochem. Photobiol. B* **2015**, *149*, 93.

[67] P. Sathyadevi, P. Krishnamoorthy, E. Jayanthi, R.R. Butorac, A.H. Cowley, N. Dharmaraj, *Inorganica Chim. Acta* **2012**, *384*, 83.

[68] M. Mohanraj, G. Ayyannan, G. Raja, C. Jayabalakrishnan, *J. Photochem. Photobiol. B* **2016**, *158*, 164.

[69] M.Z. Gul, F. Ahmad, A.K. Kondapi, I.A. Qureshi, I.A. Ghazi, *Complem. Altern. Med*. **2013**, *13*, 53.

[70] C. Jost, J. Schilling, R. Tamaskovic, M. Schwill, A. Honegger, A. Pluckthun, *Structure* **2013**, *21*, 1979.

[71] N. Buza, D.M. Roque, A.D. Santin, *Arch. Pathol. Lab. Med.* **2014**, *138*, 343.

[72] A.D. Santin, S. Bellone, J.J. Roman, J.K. McKenney, S. Pecorelli, *Int. J. Gynecol. Obstet.* **2008**, *102*, 128.

[73] J. Sebastian, R.G. Richards, M.P. Walker, J.F. Wiesen, Z. Werb, R. Derynck, Y.K. Hom, G.R. Cunha, R.P. Di Augustine, *Cell Growth Differ.* **1998**, *9*, 777.

[74] N. Foloppe, A.D. MacKerell, *J. Comput. Chem.* **2000**, *21*, 86.

[75] C.M. Breneman, K.B. Wiberg, *J. Comput. Chem.* **1990**, *11*, 361.

[76] F. Walker, L. Abramowitz, D. Benabderrahmane, X. Duval, D. Descatoire, D. Hénin, T. Lehy, T. Aparicio, *Hum. Pathol.* **2009**, *40*, 1517.

[77] T.J. Lynch, D.W. Bell, R. Sordella, S. Gurubhagavatula, R.A. Okimoto, B.W. Brannigan, P.L. Harris, S.M. Haserlat, J.G. Supko, F.G. Haluska, D.N. Louis, D.C. Christiani, J. Settleman, D.A. Haber, *Engl. J. Med.* **2004**, *350*, 2129.

[78] A.M. Davis, S.J. Teague, *Angew. Chem. Int. Ed.* **1999**, *38*, 736.

[79] R.L. Schroeder, C.L. Stevens, J. Sridhar, *Molecules* **2014**, *19*, 15196.

LIST OF PUBLICATIONS

List of Publications

[1] **Ramaiah K,** Ramachary M, Ramu G, Laxma Reddy K, Synthesis, characterization, biological screening and molecular docking studies of 2- aminonicotinaldehyde and its metal complexes, ***Research on Chemical Intermediates***, **2018**, *44*, 27-53.

[2] **Ramaiah K,** Haribabu J, Prashanth J, Ramachary M, Saikumar M, Durgaiah G, Ramasamy R, Venkatram Reddy B, Narsimha Reddy Y , Laxma Reddy K, Synthesis, Structural, Biological Evaluation, Molecular Docking, DFT Studies of Co(II), Ni(II), Cu(II), Zn(II), Cd(II), Hg(II) and Pd(II) Complexes bearing Heterocyclic Thiosemicarbazone ligand, ***Applied Organometallic Chemistry,*** **2018**, *32*,e4415.

[3] **Ramaiah K**, Shravan Kumar K, Laxma Reddy K, Zinc-catalysed multicomponent reactions: Facile synthesis of fully substituted pyridines, ***Synthetic communications,*** **2018,** *48,* 1777-1785.

[4] **Ramaiah K,** Shravan Kumar K, Laxma Reddy K, $Zn(ANA)_2Cl_2$ complex as efficient catalyst for the synthesis of dihydropyrano *[2,3-c]* pyrazoles in aqueous medium via one-pot multicomponent reaction: A green approach, ***Synthetic communications, 2018,*** *48,* 2642-2651.

[5] Ramachary M, **Ramaiah K,** Ramu G, Munirathinam N, Durgaiah G, Narsmiha Reddy Y, Laxma Reddy K, ***Inorganica Chemica Acta,*** **2018**, *469,* 66-75.

[6] **Ramaiah K,** Prashanth J, Haribabu J, Sreekanth KE, Venkaram Reddy B, Karvembu R, Laxma Reddy K, Vibrational spectroscopic (FTIR, FT-Raman), anti-inflammatory, docking and molecular characteristic studies of Ni(II) complex of 2-aminnicotinaldehyde using theoretical and experimental methods, ***Journal of Molecular Structure, 2019,*** *1175,* 769-781.

[7] **Ramaiah K**, Ramesh G, Laxma Reddy K, NaF catalyzed efficient one-pot synthesis of dihydropyrano *[2,3-c]* pyrazoles under ultrasonic irradiation *via* MCR approach, ***Synthetic communications, 2018,*** *48,* 2642-2651.

[8] **Ramaiah K,** Srishailam K, Laxma Reddy K, Venkatram Reddy B, Ramana Rao G, Synthesis, crystal and molecular structure, and characterization of 2-(2-aminopyridin-3-yl)methylene)-*N*-ethylhydrazinecarbothioamide using spectroscopic (^{1}H and ^{13}C NMR, FT-IR, FT-Raman, UV-Vis) and DFT methods and evaluation of its anticancer activity, ***Journal of Molecular Structure, 2019,*** *1184,* 405-417.

[9] **Ramaiah K[1],** Munikumari G[2], Ramesh G, Laxma Reddy K, Chandrasekhar K.B, Ramachandraiah C, Palladium(II) complexes of 5-substituted isatin

thiosemicarbazones: Synthesis, spectroscopic characterization, biological evaluation and *in silico* docking studies, ***Synthetic Communications*, 2019,** *49,* 146-158. **[1,2 Equal Contribution]**

[10] **Ramaiah K[1, $],** Eswar Srikanth K[2, $], Prabhakara Rao K[3], Laxman naik J[4], Veeraiah A[2], Prashanth J[5*], Experimental and theoretical analyzes on structural (monomer and dimeric form), spectroscopic and electronic properties of an organic semiconductor 2,6-dimethoxyanthracene, ***Indian Journal of physics,* 2019. [$: Equal Contribution]**

[11] **Ramaiah K[1],** Sreekanth KE[2], Prashanth J, A Combined Experimental (FT-IR) and Computational Studies of 9-Chloroanthracene, ***Asian Journal of Chemistry,* 2019,** *31,* 1332-1342. **[1,2 Equal Contribution]**

[12] Rohini G, **Ramaiah K,** Sreekenth A, Naphthalene dianhydride based selective detection targetable fluorescent probe for monitoring exogenous Iron in living cells, ***Tetrahedron Letters*, 2018,** *59,* 3858-3862.

[13] Srividya S, Haribabu J, Naveen Kumar K, **Ramaiah K,** Nithya B, Bhuvanesh N, Karvembu, Synthesis and Anticancer Activity of [$RuCl_2(\eta^6$-arene)(aroylthiourea)] Complexes-High Activity against the Human Neuroblastoma (IMR-32) Cancer Cell Line, ***ACS Omega,* 2019,** *4,* 6245-6256.

[14] Rohini G, **Ramaiah K,** Aneesrahman K.N, Aryasenan M.C, Bhuvanesh N.S.P. Laxma Reddy K, Sreekanth, Biological evaluation, DNA/protein-binding aptitude of novel dibenzosuberene appended palladium(II)-thiourea complexes, ***Applied Organometallic Chemistry*, 2018,** *32,* e4567.

[15] Rohini G, **Ramaiah K**, Prashanth J, Bhuvanesh NSP, Sreekenth A, Unusual coordination mode of aroyl/acyl thiourea ligands and their π-arene ruthenium(II) piano-stool complexes: Synthesis, molecular geometry, theoretical studies and biological applications, ***Applied Organometallic Chemistry*, 2018,** *33,* e4899.

[16] Rohini G, Haribabu J, Aneesrahman K.N, **Ramaiah K,** Bhuvanesh NSP, Karvembu R Sreekanth A, Half-sandwich Ru(II)(η^6-*p*-cymene) complexes bearing *N*-dibenzosuberenyl appended thiourea for catalytic transfer hydrogenation and in vitro anticancer activity, ***Polyhedron,* 2019,** *152,* 147-154. **[Review Paper]**

[17] Babji P, Ramesh T, Vijendar Reddy K, **Ramaiah K,** Nageswara Rao P, Gobi KV, Identification and Characterisation of Rucaparib Degradation Products and Their Comparison with Known Impurities, ***Chromatographia,* 2019,** *82,* 591-604.

[18] Aneesrahman KN, **Ramaiah K,** Rohini G, Stefy GP, Bhuvanesh NSP, Sreekanth A, Synthesis and characterisations of copper(II) complexes of 5-methoxyisatin

thiosemicarbazones: Effect of N-terminal substitution on DNA/protein binding and biological activities, ***Inorganica Chemica Acta*, 2019,** *492,* 131-141.

[19] Prashanth J, **Ramaiah K,** Venkatram Reddy B, Barrier potentials, Molecular structure, force filed calculations and quantum chemical studies of some bipyridine di-carboxylic acids using the experimental and theoretical using (DFT, IVP) approach, ***Molecular Simulation,*** DOI: 10.1080/08927022.2019.1634807

[20] Sanjeeva T, Soumya P, Navven A, **Ramaiah K**, Sateesh V, Hariprasad K, An efficient Pd(II)-(2-aminonicotinaldehyde) complex as complementary catalyst for the Suzuki-Miyaura coupling in water, ***Tetrahedron Letters,*** DOI: https://doi.org/10.1016/j.tetlet.2019.06.051

BRIEF CURRICULUM VITAE

Mr. Konakanchi Ramaiah was born on 12th June 1989 in Gunjaloor, Suryapet, India. He did B.Sc. Chemistry in Osmania University (OU), Hyderabad and M.Sc. Inorganic Chemistry in Kakatiya University (KU) campus, Warangal, India. After completing her post-graduation, he has joined as a research scholar under the guidance of Dr. K. Laxma Reddy, Professor, Department of Chemistry, National Institute of Technology, Warangal in June 2014.